3.2.1 Linear polarisation of a Pb electrode in $Pb(NO_3)_2$ solutions containing selected addition agents.

All potentiodynamic experiments reported in this Section were carried out at 25°C by polarising a Pb working electrode in a negative direction at a sweep rate of 1 mV sec^{-1}, in a stock solution of 0.1M $Pb(NO_3)_2$ + 0.1M HNO_3.

E vs log i curves for the stock solution free from organic addition agents and for this solution containing butyne 1,4 diol and 1,4 naphthoquinone are shown in Fig. 61. The presence of a diffusion limited current is clearly visible as is an increase in overpotential before the onset of rapid dendritic growth.

The most interesting effect of certain additives is the increase in overpotential prior to dendritic growth. This phenomenon was most pronounced with the addition of particular surface active agents, (see Fig. 62), whilst with other surface active agents, this was not so noticeable (see Fig. 63).

In view of the large number of addition agents screened for their effect on the E vs log i curves for Pb deposition, the results of this work are expressed in a tabulated rather than graphical form (see Appendix).

The results are given in terms of the overpotential necessary to produce a given current density when a Pb electrode was polarised at a sweep rate of 1 mV sec^{-1} in the stock solution containing selected additives.

Some of the chemicals investigated would not be suitable for use in the simultaneous electrodeposition of Pb and PbO_2 because of their liability to be oxidised at the anode. Experiments were nevertheless conducted to see how these additives affected the Pb deposition process. From the Appendix it can be seen that those additives that are normally used as addition agents for Pb deposition in conventional plating solutions i.e gelatin, hydroquinone and resorcinol, have a negligible effect on the E

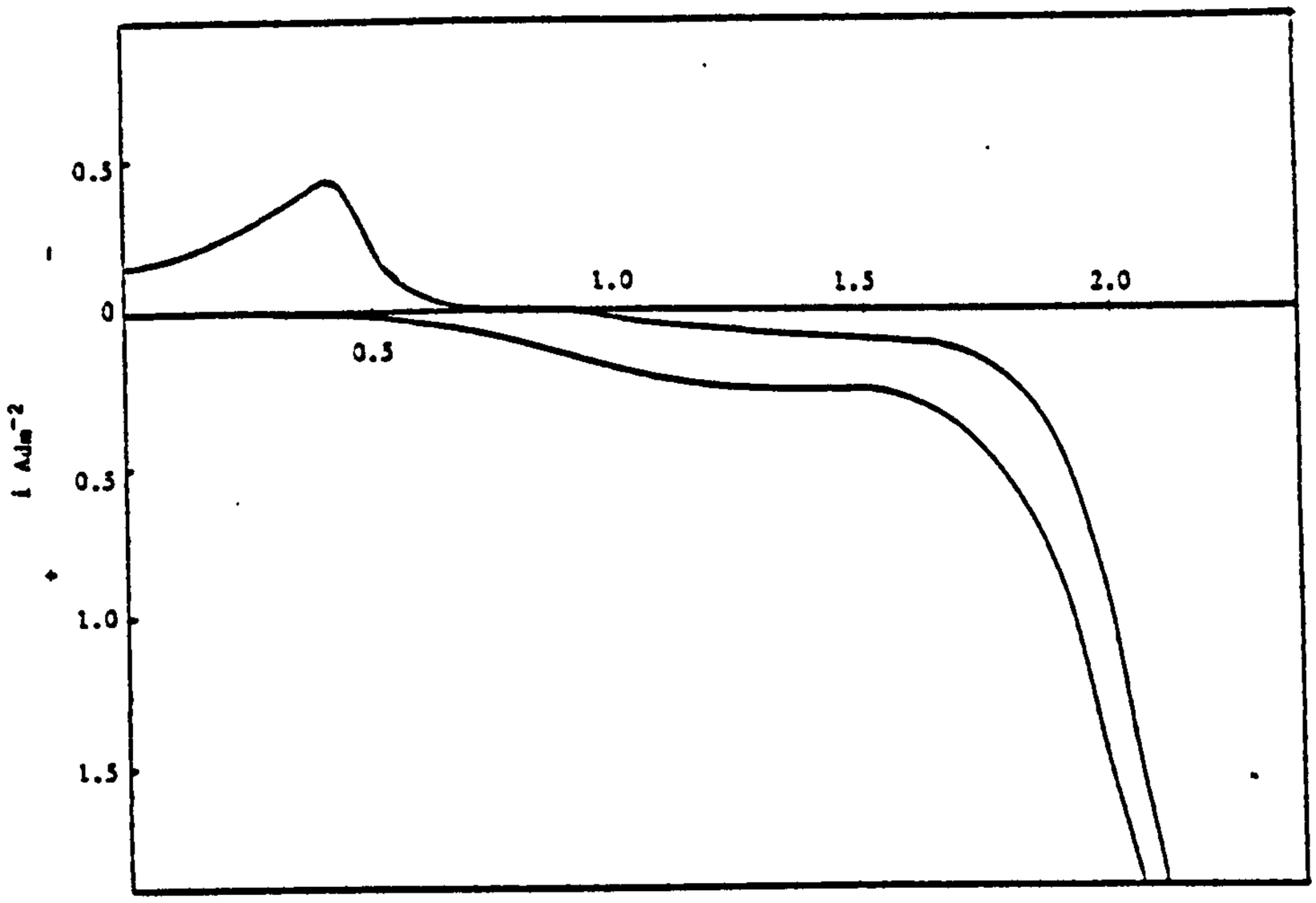

A cyclic voltammogram for a Pt electrode polarised at a sweep rate of 100mV sec^{-1} , in a solution of 0.2 M Na_2SO_4 plus 5 gl^{-1} Tannic acid.

FIGURE 60

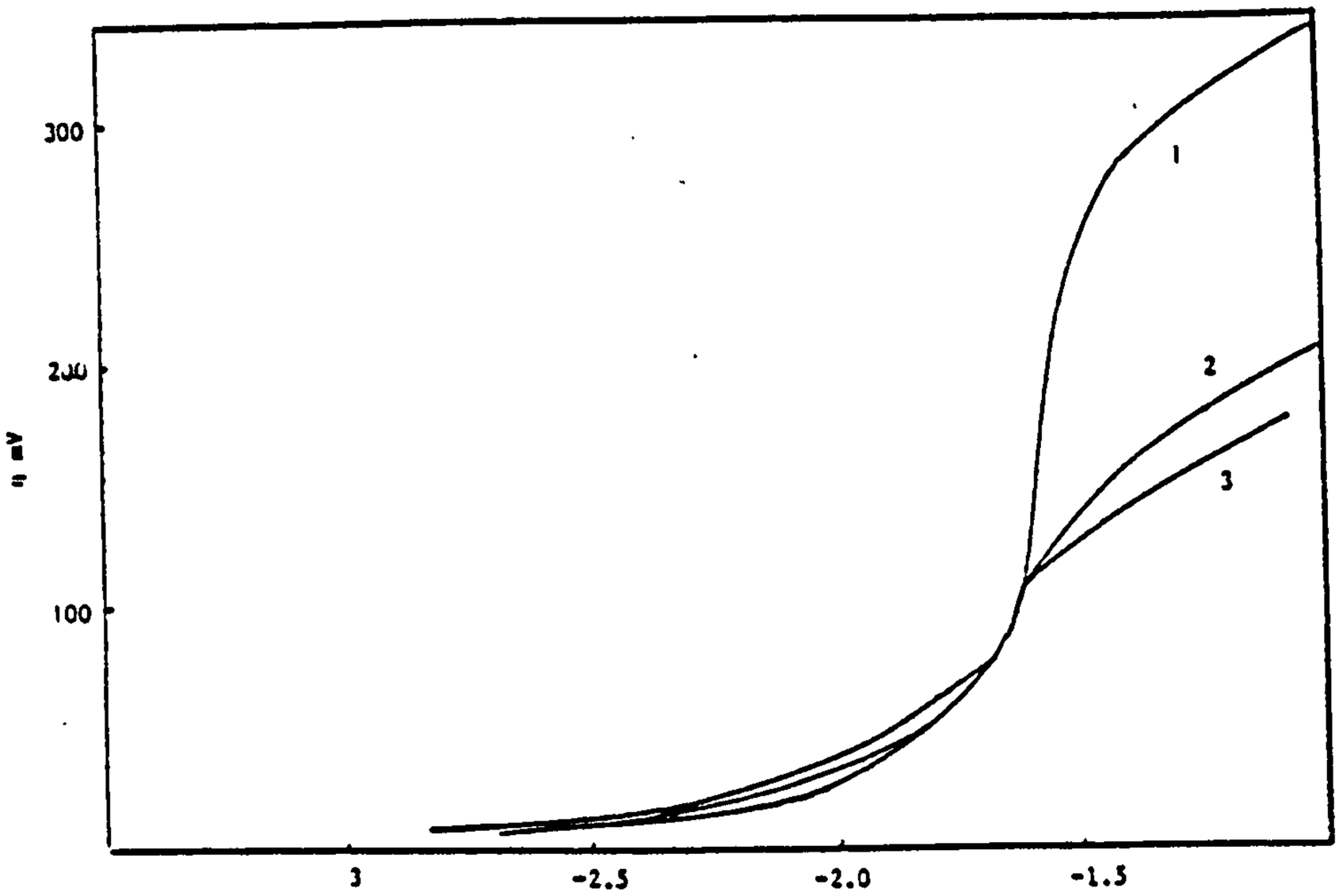

E vs log i curve for Pb deposition onto a Pb electrode from a stock solution of 0.1M $Pb(NO_3)_2$ + 0.1M HNO_3 containing selected surface active agents. The electrode polarised at a sweep rate of 1mV sec^{-1} .

1 = stock solution plus 0.5 gl^{-1} 1,4 naphthoquinone
2 = stock solution plus 2 gl^{-1} butyne 1,4 diol
3 = stock solution without addition agent.

FIGURE 61

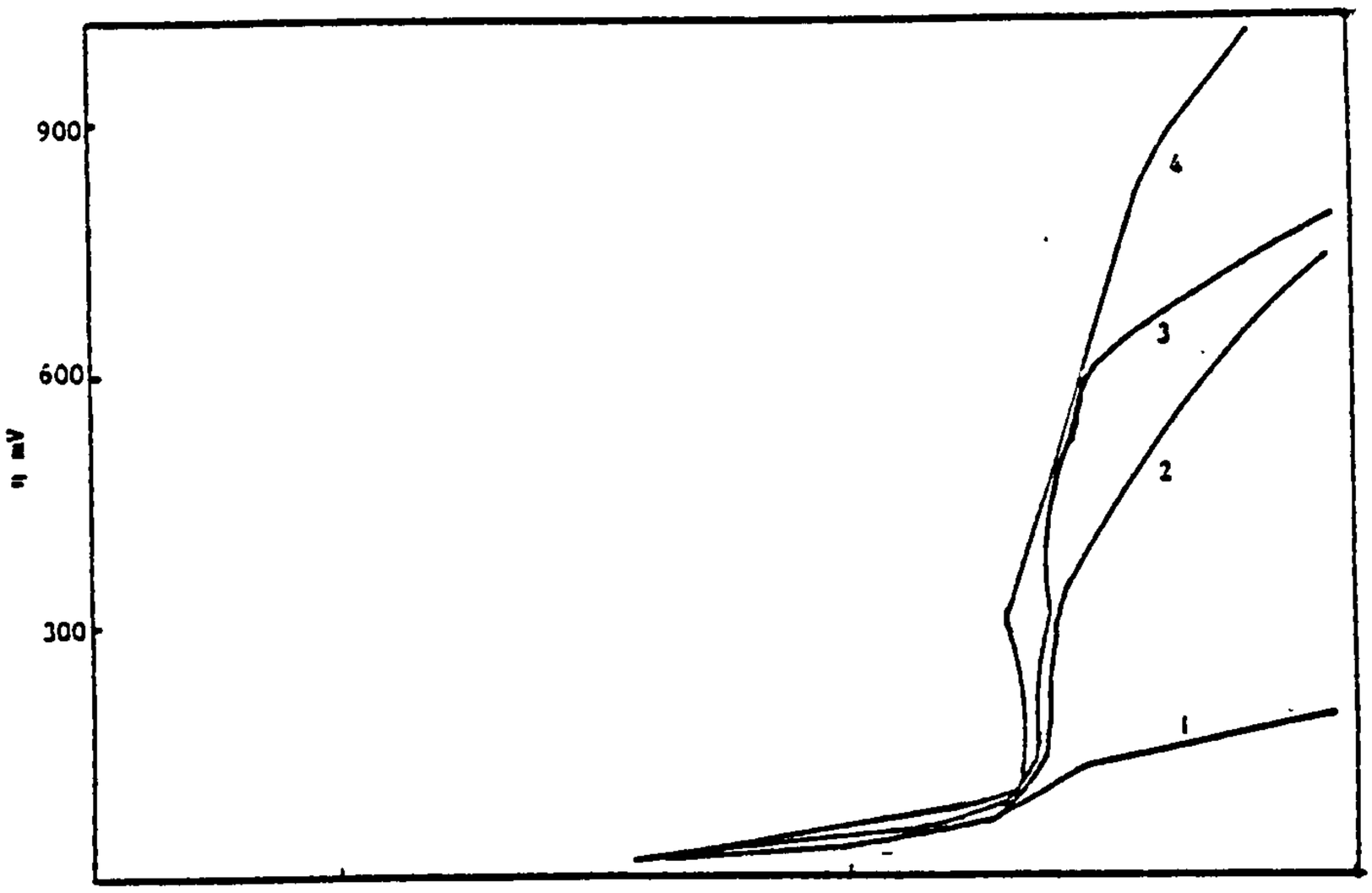

η vs log i curve for a Pb electrode cathodically polarised at a sweep rate of 1mV sec^{-1} in a solution of 0.1M $Pb(NO_3)_2$ + 0.1M HNO_3 with and without selected addition agents.

1 = No additives
2 = stock solution plus 0.5 gl^{-1} BRIJ 35
3 = stock solution plus 0.5 gl^{-1} Triton X100
4 = stock solution plus 0.3 gl^{-1} Pluronic L64

FIGURE 62

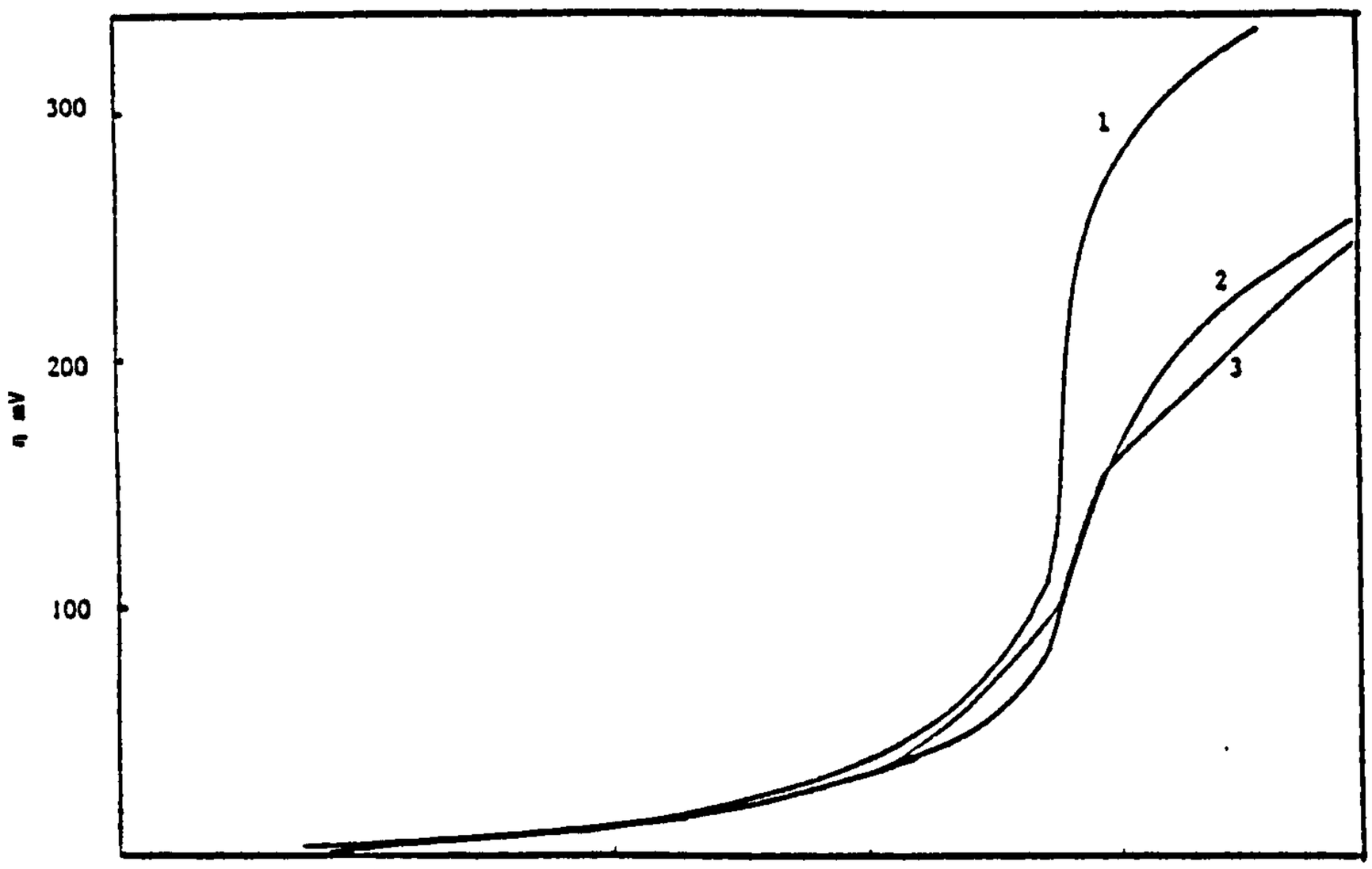

E vs log i curve for Pb deposition onto a Pb electrode from a stock solution of 0.1M $Pb(NO_3)_2$, 0.1M HNO_3 containing selected surface active agents.

1 = stock solution plus 0.5g l^{-1} Hyamine
2 = stock solution plus 0.5g l^{-1} Polyoxyethylene oxide
3 = stock solution plus 0.5g l^{-1} Pluronic F68.

FIGURE 63

vs i curves obtained, when compared to the non additive $Pb(NO_3)_2$ solution. The additives that showed the highest increases in polarisation were considered to be worthy of further investigation using other techniques.

The most successful additive combination in $Pb(NO_3)_2$ solutions was found to be Triton X100 and anthraquinone-2-mono sulphonic acid. A typical polarisation curve for which is shown in Fig. 64.

3.2.2 Studies on Pb deposition from $Pb(NO_3)_2$ solutions, using a rotating disc electrode

The effect of rotational speed on the cathodic polarisation of a Pb electrode immersed in 0.1M $Pb(NO_3)_2$ in a supporting electrolyte of 1M KNO_3, plus 0.1M HNO_3 can be seen from Fig. 65. Under static conditions a "limiting c.d." is clearly visible and an overpotential of approximately 90 mV is necessary at a sweep rate of 0.5 mV sec^{-1}, before the onset of a rapid increase in current. Further increases in the rotational speed do result in an increase in the current at a given overpotential, although no "limiting c.d." was observed. The change in current at a given overpotential is not large and above 200 rpm, the polarisation curve obtained at say 300 rpm was not greatly different from that obtained at 1000 rpm. The rest potential of the Pb electrode in this electrolyte was found to be -0.19V vs SHE.

The effect of certain additives on the linear polarisation characteristics of a Pb electrode in 0.1M $Pb(NO_3)_2$, 0.1M HNO_3 plus 1M KNO_3 at given rotational speeds is shown in Figs. 66-72. Other additives were investigated but did not show any significant inhibiting effect.

The surface active agents BRIJ 35, Triton X100, Pluronic L64 whilst producing limiting currents in 0.1M $Pb(NO_3)_2$ solutions under static conditions showed no strong inhibiting effect at higher rotational speeds (see Figs 66-78).

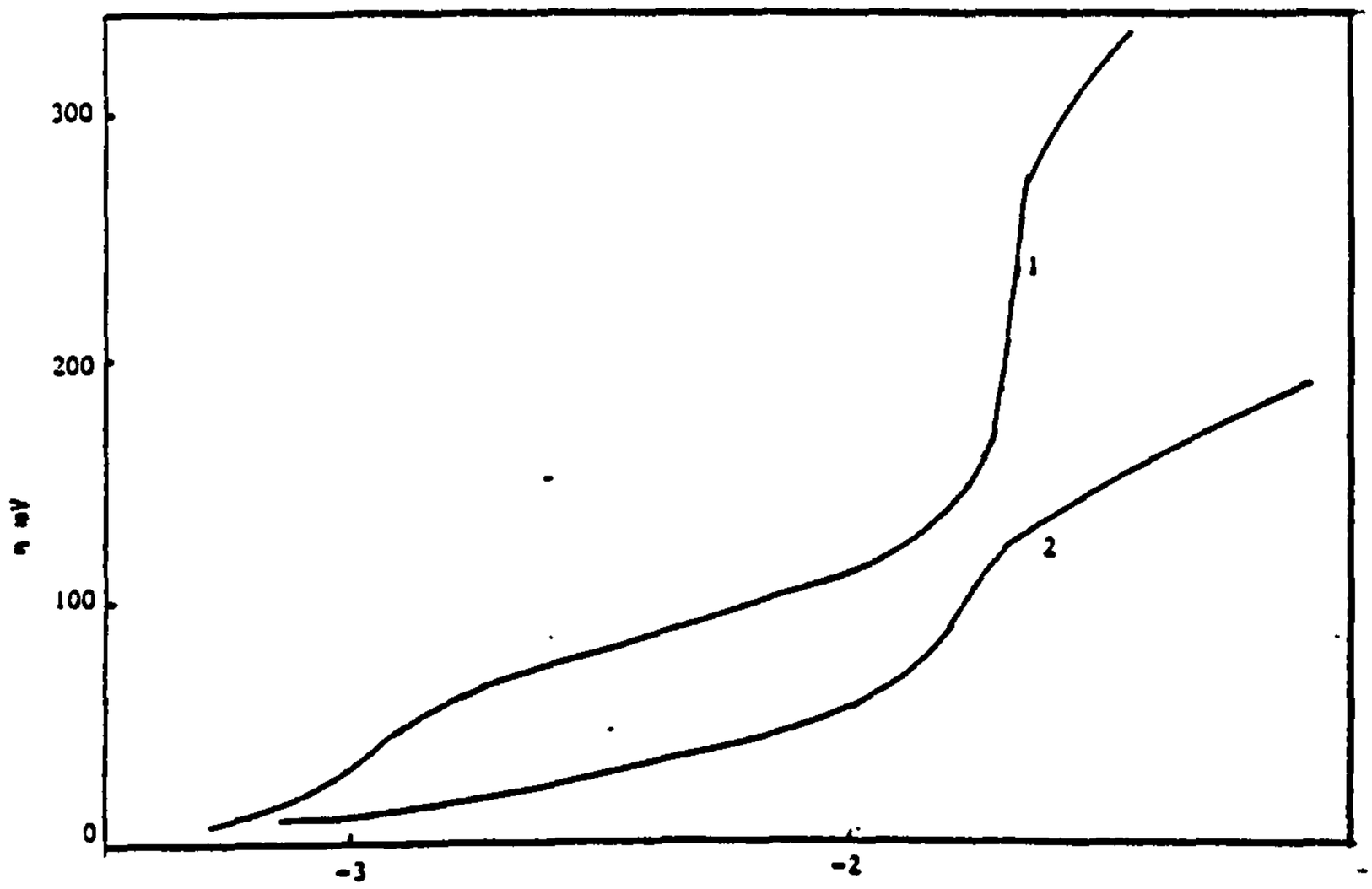

η vs i for a Pb electrode cathodically polarised at a sweep rate of 5mV sec^{-1} from rest potential in a stock solution of 0.1M $Pb(NO_3)_2$ + 0.5M KNO_3 with and without selected addition agents.

1 = No addition agents. 2 = stock solution plus 1 gl^{-1} Triton X100 0.1 gl^{-1} anthraquinone-1-monosulphonic acid.

FIGURE 64

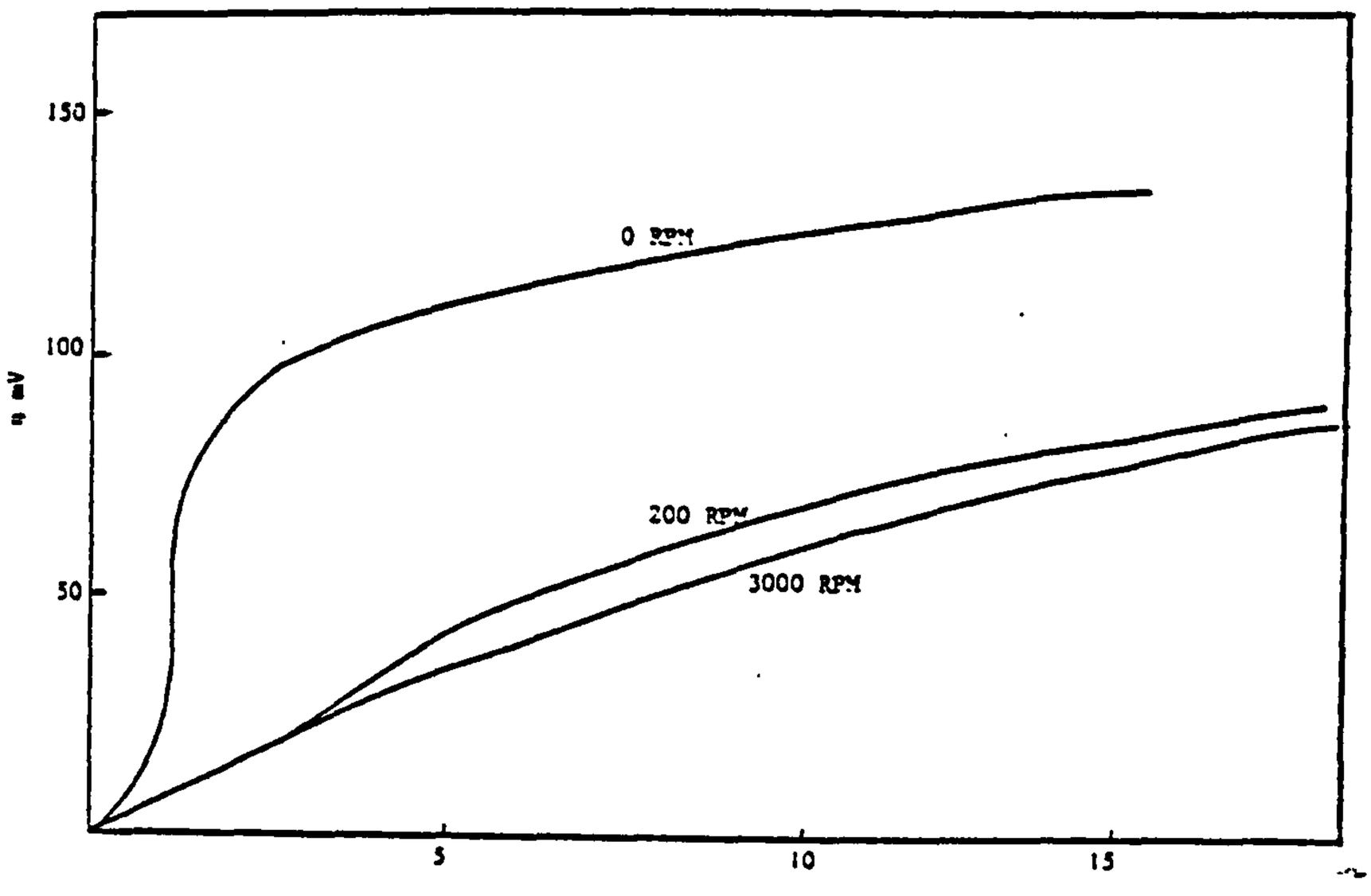

A graph of η versus i at selected rotational speeds for a Pb electrode cathodically polarised at a sweep rate of 0.5mV sec^{-1} in a solution of 0.1M $Pb(NO_3)_2$, 1M KNO_3 + 0.1M HNO_3 at 25°C

FIGURE 65

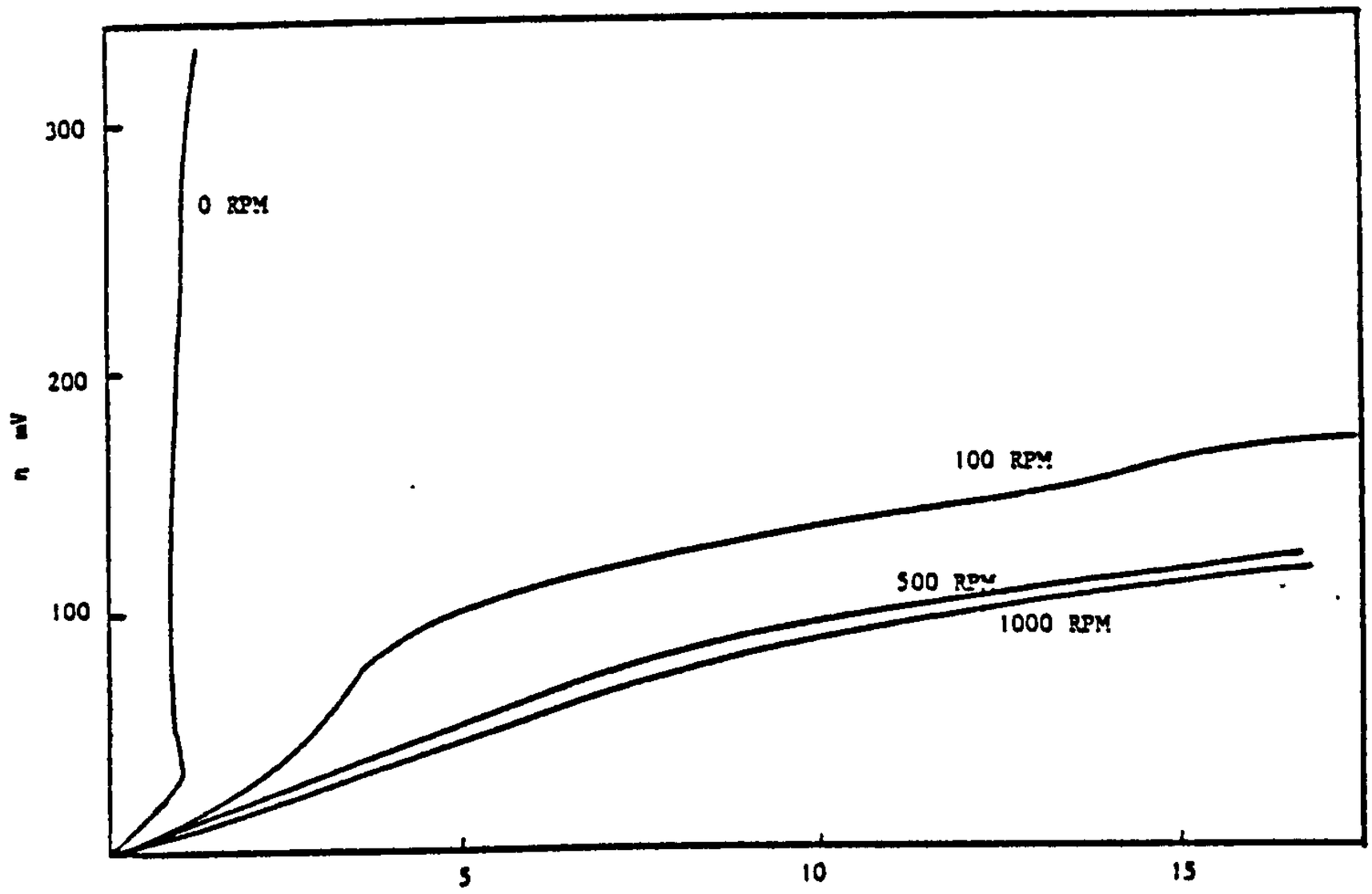

A graph of η vs i at selected rotational speeds for a Pb electrode cathodically polarised at a sweep rate of 0.5mV sec^{-1} in a solution of 0.1M $Pb(NO_3)_2$. 1M KNO_3, 0.1M HNO_3 plus 1 gl^{-1} BRIJ 35 at 25°C.

FIGURE 66

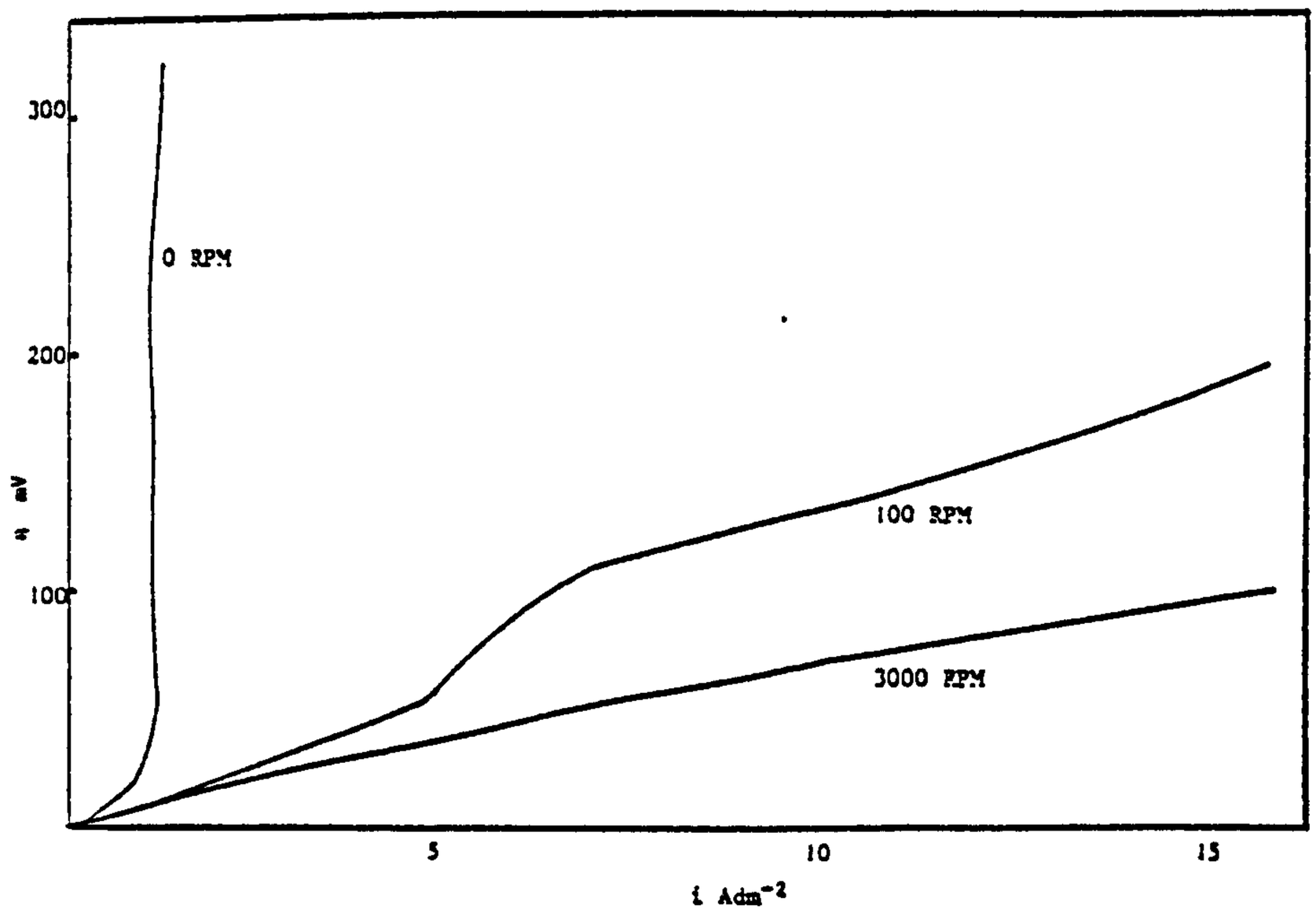

A graph of η versus i at selected rotational speeds for a Pb electrode cathodically polarised at a sweep rate of 0.5mV sec^{-1} in a solution of 0.1M $Pb(NO_3)_2$, 1M KNO_3 , 0.1M HNO_3 plus 1 gl^{-1} Triton X100 at 25°C.

FIGURE 67

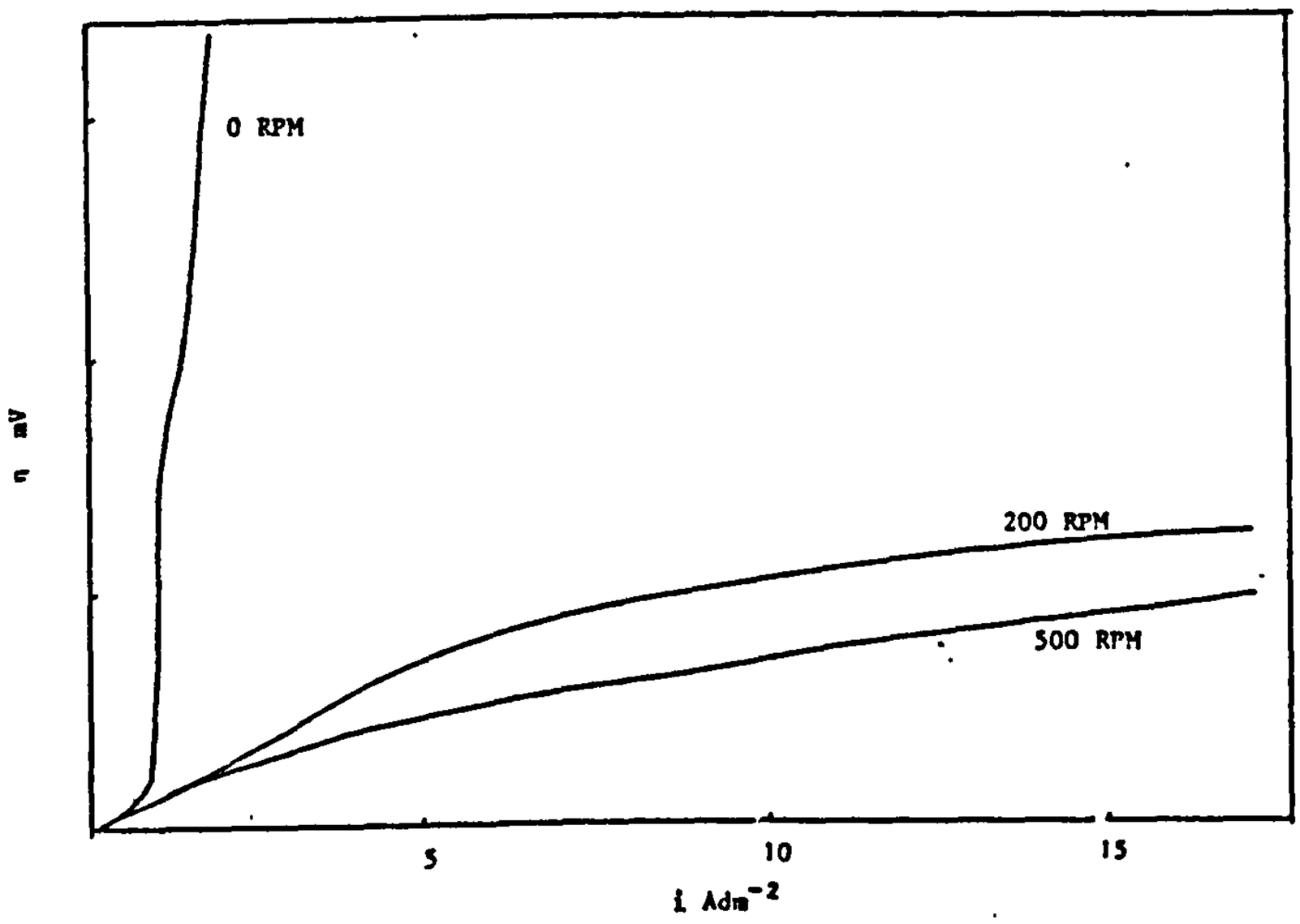

A graph of η vs i at selected rotational speeds for a Pb electrode cathodically polarised at a sweep rate of 0.5 mV sec^{-1} in a solution of 0.1M $Pb(NO_3)_2$, 1M KNO_3 , 0.1M HNO_3 plus 1 gl^{-1} Pluronic L64 at 25°C.

FIGURE 68

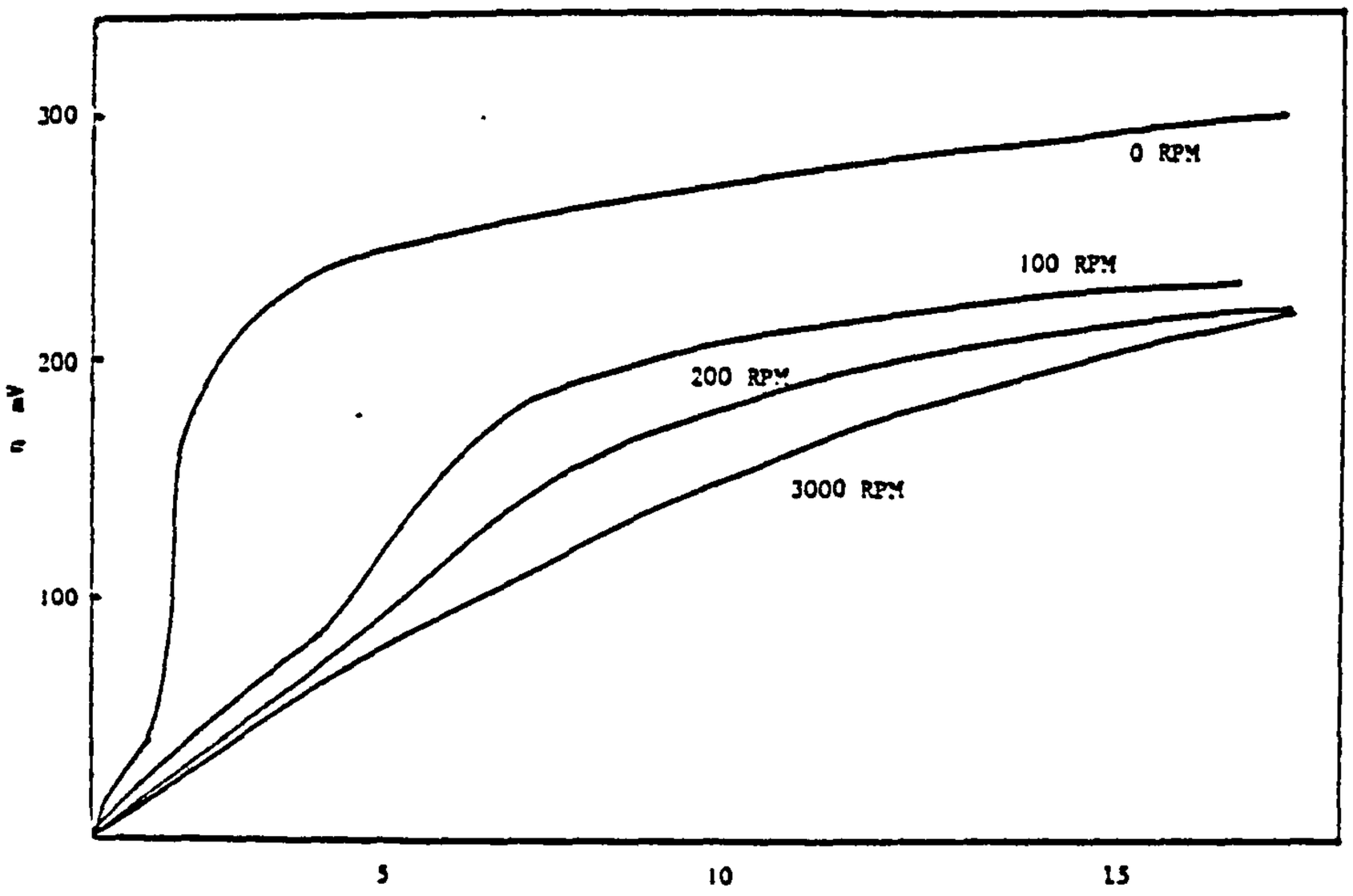

A graph of η versus i at selected rotational speeds for a Pb electrode anodically polarised at a sweep rate of 0.3mV sec^{-1} in a solution of 0.1 M $Pb(NO_3)_2$, 1M KNO_3, 0.1M HNO_3 plus 0.5 gl^{-1} Hyamine at 25°C.

FIGURE 69

The effect of Hyamine on the polarisation curves can be seen in Fig. 69 whilst the strongest inhibiting effect of any additive as seen from Fig. 70 was shown by tannic acid. Fig. 71 shows that anthraquinone-2-monosulphonic acid has a greater inhibiting effect than its' disulphonic acid derivative anthraquinone-2,6-disulphonic acid (Fig. 72).

In the case of additions of 1 gl^{-1} BRIJ 35, Pluronic L64 and Triton X100 to the 0.1M $Pb(NO_3)_2$ solution a limiting c.d. was observed at zero rpm, that showed only a slight tendency to increase at high overpotentials as is evident from Table 42.

TABLE 42

The c.ds. obtained at high overpotentials when a Pb electrode is polarised at 0.5 mV sec^{-1} from its rest potential in 0.1 M $Pb(NO_3)_2$ + 1M KNO_3 + 0.1M HNO_3 containing 1 gl^{-1} of selected addition agents under static conditions.

Overvoltage mV	Current density (Adm^{-2})		
	BRIJ 25	Triton X100	Pluronic L64
400	1.18	1.31	1.69
500	1.45	1.45	2.08
600	1.89	1.73	2.61
700	2.50	2.15	3.21
800	3.32	3.17	3.99
900	4.27	5.57	5.56

Under static conditions an overpotential of 300 mV had to be applied before any rapid increase in current density could be observed for the stock solutions plus 1 gl^{-1} tannic acid. The magnitude of the overpotential necessary to result in a rapid increase in current density was dependent upon the nature of

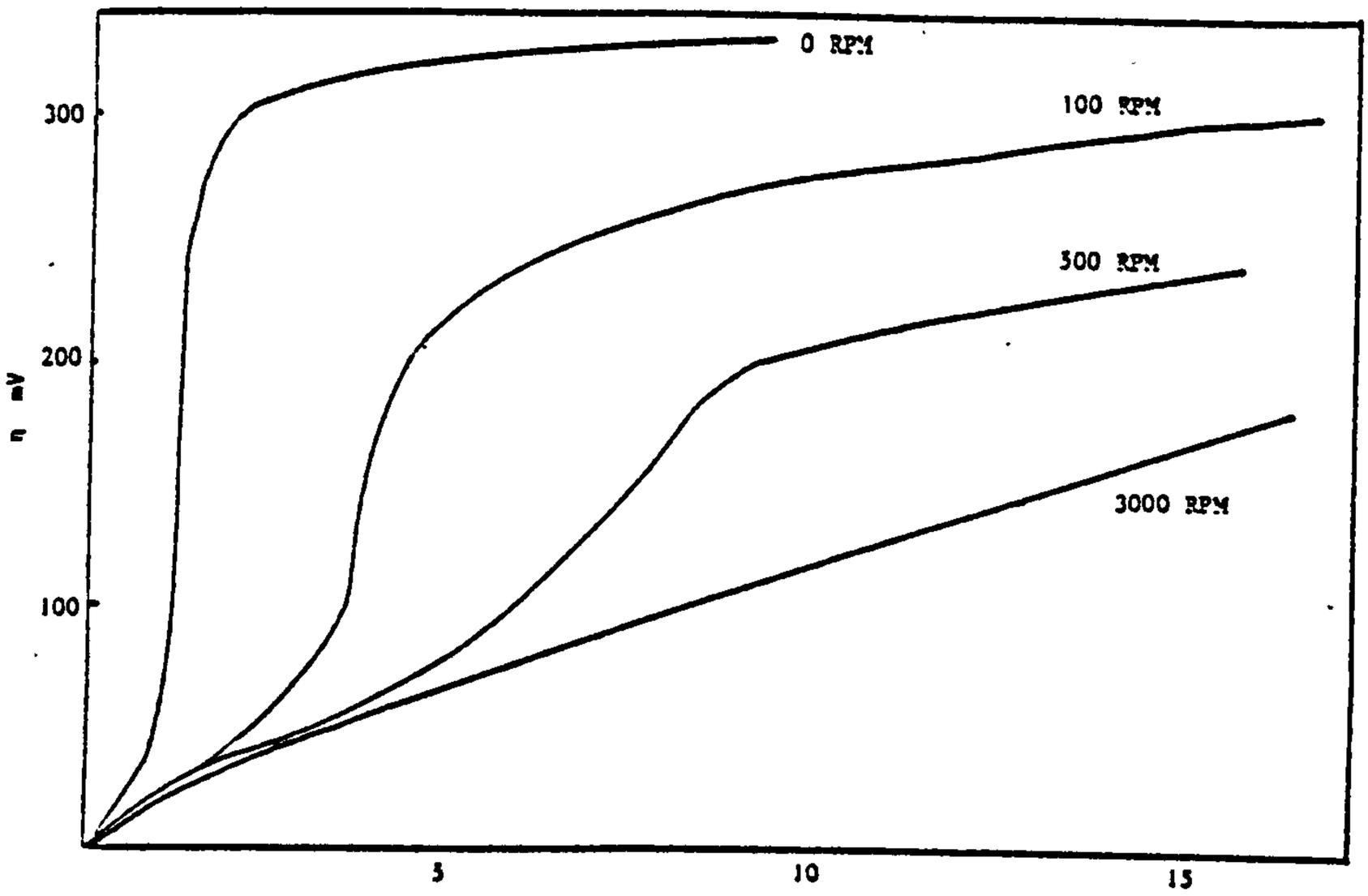

A graph of η versus i at selected rotational speeds for a Pb electrode cathodically polarised at a sweep rate of 0.5mV sec^{-1} in a solution of 0.1M $Pb(NO_3)_2$, 1M KNO_3, 0.1M HNO_3 plus 1 gl^{-1} tannic acid at 25°C.

FIGURE 70

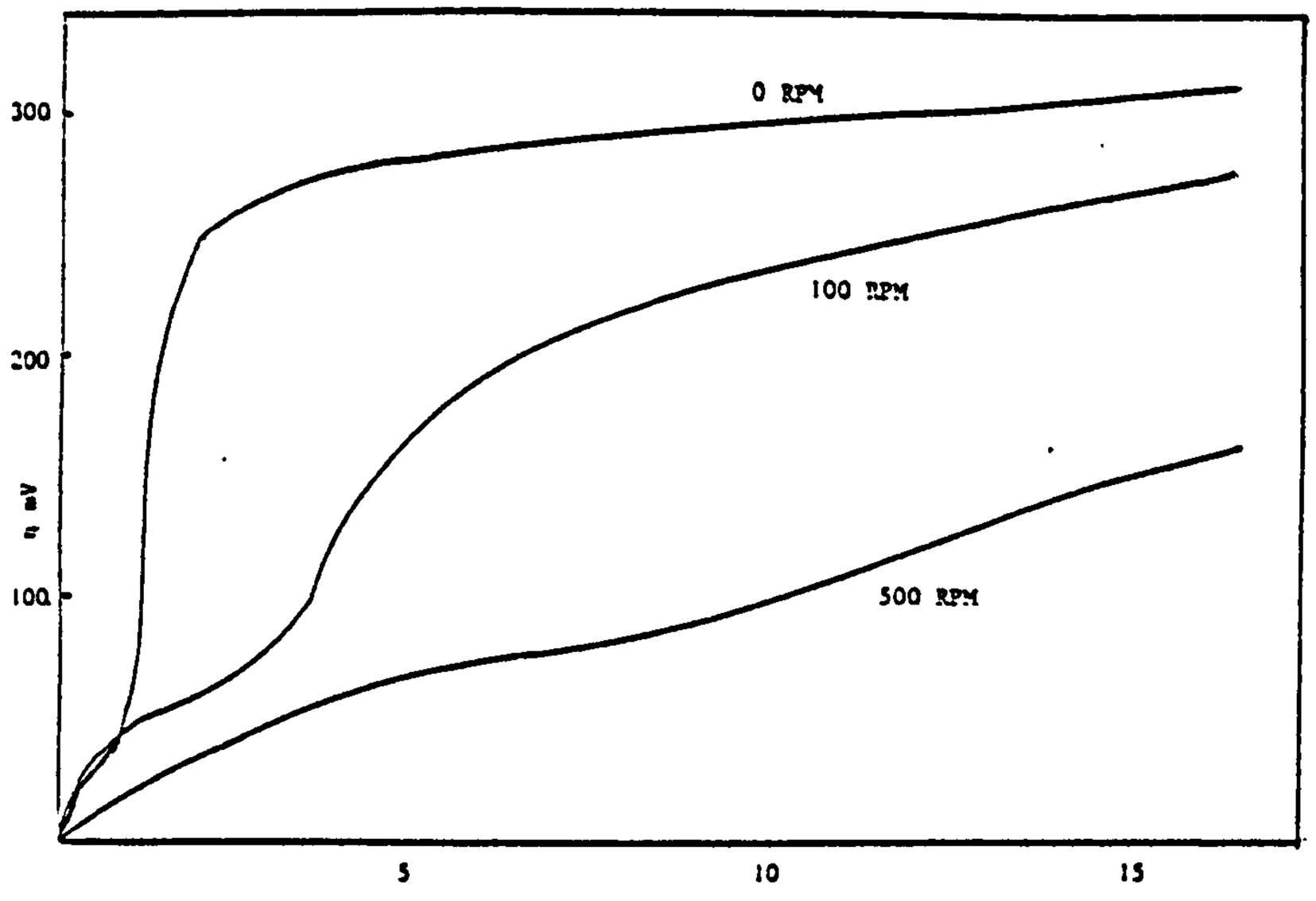

A graph of η vs i at selected rotational speeds for a Pb electrode cathodically polarised at a sweep rate of 0.5mV sec^{-1} in a solution of 0.1M $Pb(NO_3)_2$, 1M KNO_3, 0.1M HNO_3 plus 0.1 gl^{-1} anthraquinone-2-monosulphonic acid at 25°C.

FIGURE 71

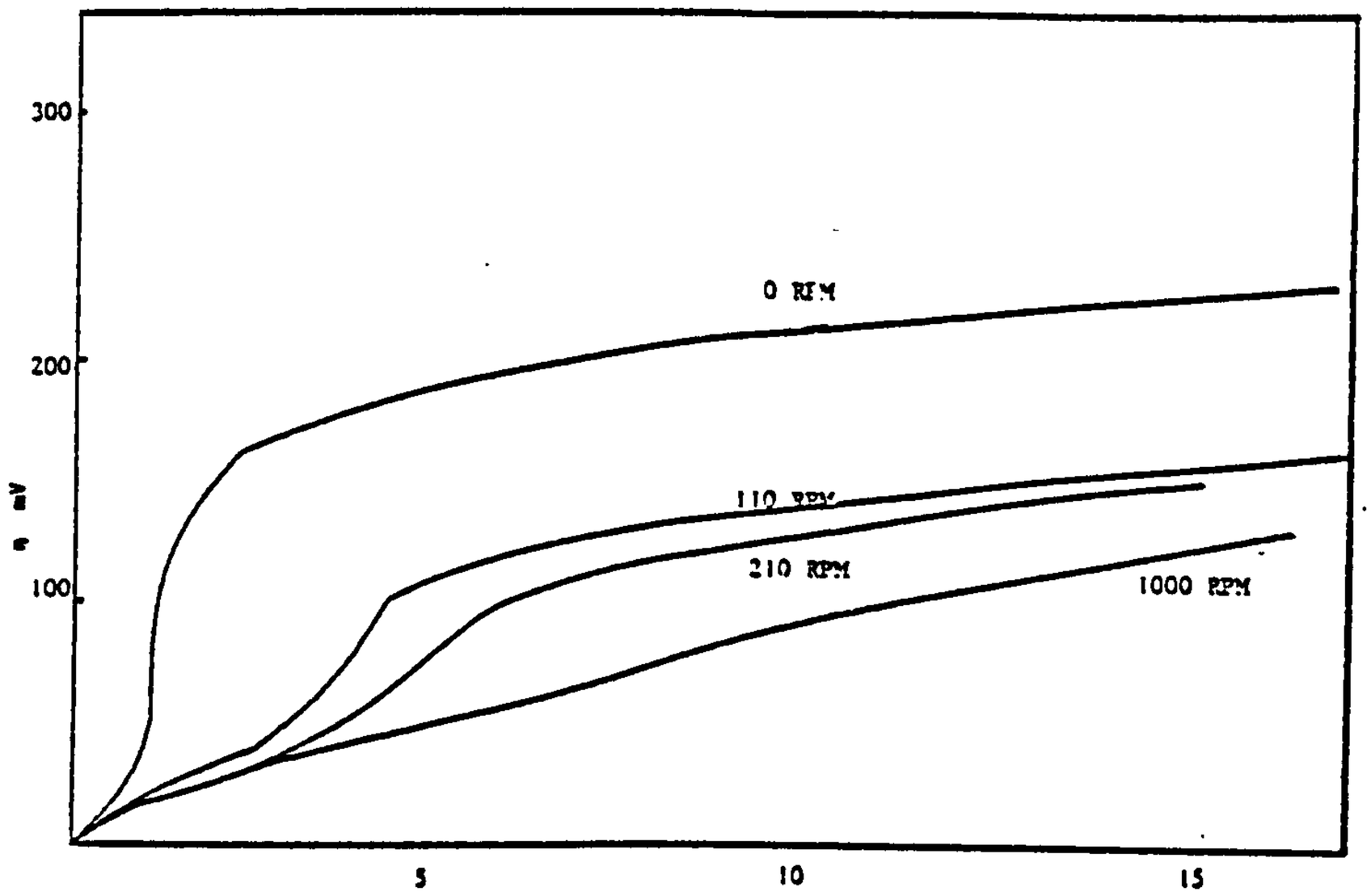

A graph of η versus i at selected rotational speeds for a Pb electrode cathodically polarised at a sweep rate of 0.5mV sec^{-1} in a solution of 0.1 M $Pb(NO_3)_2$, 1M KNO_3, 0.1M HNO_3 plus 0.1 gl^{-1} anthraquine-2,6-disulphonic acid at 25°C.

FIGURE 72

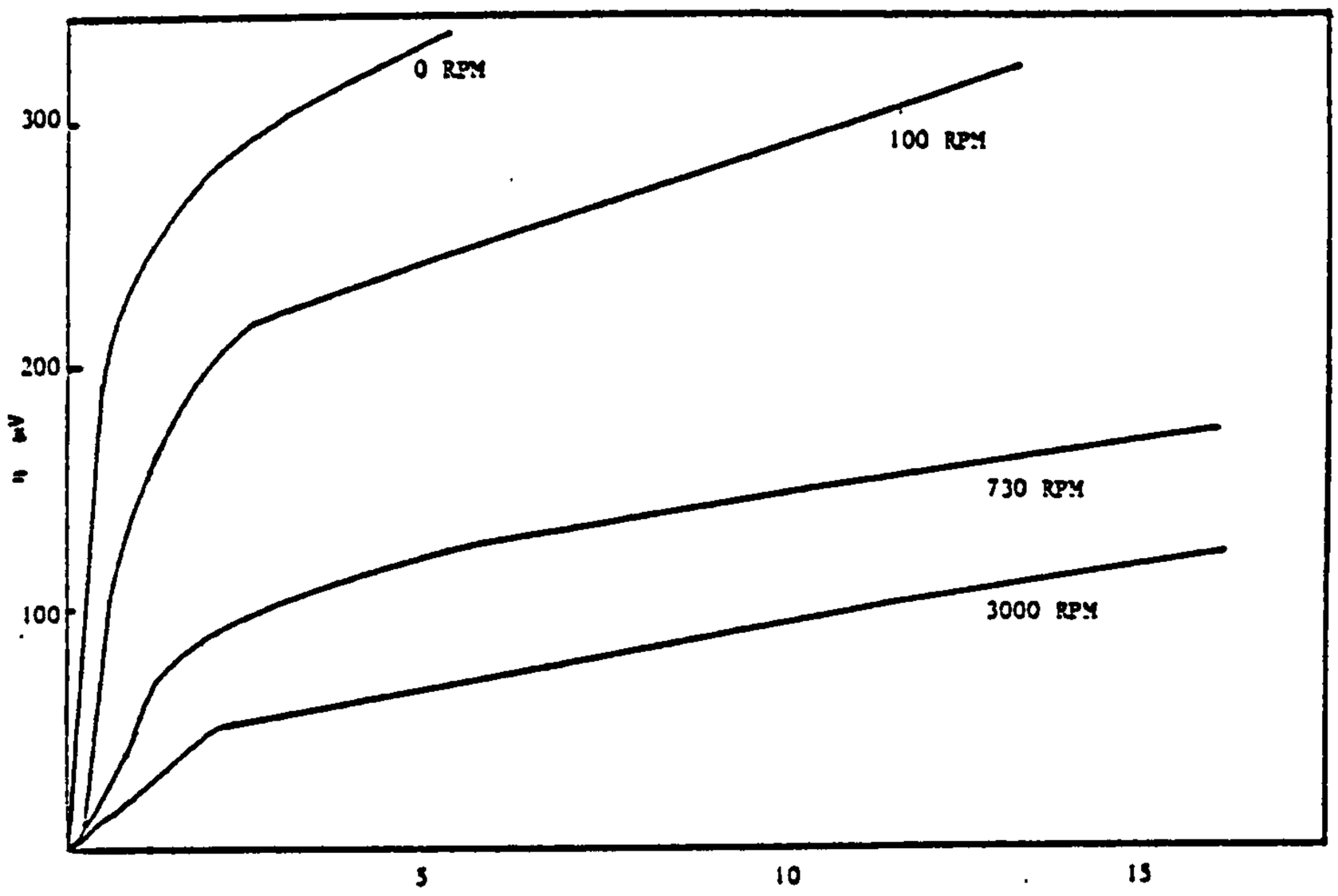

A graph of η vs i at selected rotational speeds for a Pb electrode cathodically polarised at a sweep rate of 0.5mV sec^{-1} in a solution of 0.01M $Pb(NO_3)_2$, 1M KNO_3, 0.1M HNO_3 with no additives at 25°C.

FIGURE 73

the addition agent added to the stock solution e.g with 0.1 gl^{-1} anthraquinone-2,6-disulphonic acid under the same conditions the value was 250 mV, 0.1 gl^{-1} anthraquinone-2-sulphonic acid 150 mV and with 0.5 gl^{-1} Hyamine 100 mV.

For both the additive and non additive solutions, a large difference in the E vs i curve was observed for a small increase in the rotational speed in the range from zero to 100 rpm. Unfortunately the rotating disc unit used for the present studies was unable to maintain a constant rotational speed in this range and therefore no meaningful data could be obtained.

TABLE 43

Overpotential (mV) necessary to result in a selected c.d. when a Pb electrode was rotated at 500 rpm and cathodically polarised at a sweep rate of 0.5 mV sec^{-1} in 0.1M $Pb(NO_3)_2$ + 0.1M HNO_3 + 1M KNO_3 containing selected addition agents

Additive concentration gl^{-1}	Overpotential (mV) at selected current densities (Adm^{-2})				
	1	3.5	5	7	10
No additive	8	28	41	54	70
Hyamine (0.5 gl^{-1})	11	38	43	75	97
Triton X100 (1 gl^{-1})	9	29	43	62	91
BRIJ 35 (1 gl^{-1})	12	37	54	72	92
Pluronic L64 (1 gl^{-1})	12	39	48	58	73
anthraquinone-2- sulphonic acid (0.1 gl^{-1})	17	56	66	79	104
tannic acid (1 gl^{-1})	25	56	82	133	221

The overpotential obtained at a selected current density for certain additive-containing solutions when a Pb electrode was rotated at 500 rpm and polarised at 0.5 mV sec^{-1} is given in Table 43. The degree of inhibition was assessed by the over-potential necessary to result in a given current density.

The effect of selected additives on the nature and shape of the E vs i curves in a 0.01M $Pb(NO_3)_2$ solution is shown in Figs.74-78. At this Pb^{2+} concentration the inhibitive effect of different additives is visible, the reproducibility of results good and differences in the E vs i curves at high rotational speeds easily discernable.

Again, the nature of the curves obtained in the presence of the surfactants BRIJ 35, Pluronic L64 and Triton X100 (Figs.74-76 respectively) was similar, with Pluronic L64 and Triton X100 appearing to have a strong inhibitive effect when compared to the solution without any additives (Fig. 73). The onset of a rapid current increase with overpotential was only apparent with BRIJ 35 and even then, only at high rotational speeds.

The effect of the addition of 1 gl^{-1} tannic acid and 0.1 gl^{-1} anthraquinone-2-monosulphonic acid is shown in Figs. 77 and 78 respectively, indeed at zero rpm the effect of the addition of tannic acid is similar to that with other surface active agents i.e a limiting current density was observed.

3.2.2.1 The effect of $Pb(NO_3)_2$ concentration on the E vs i curves for a Pb deposition at a constant rotational speed

The effect of varying the concentration of $Pb(NO_3)_2$ dissolved in a stock solution of 1M KNO_3 + 0.1M HNO_3 on the E vs i curves for Pb^{2+} deposition at 300 rpm is shown in Fig. 79.

The addition of 1 gl^{-1} Triton X100 (Fig. 80) and 1 gl^{-1} tannic acid (Fig. 81) to this solution can be seen to effect the Pb deposition process.

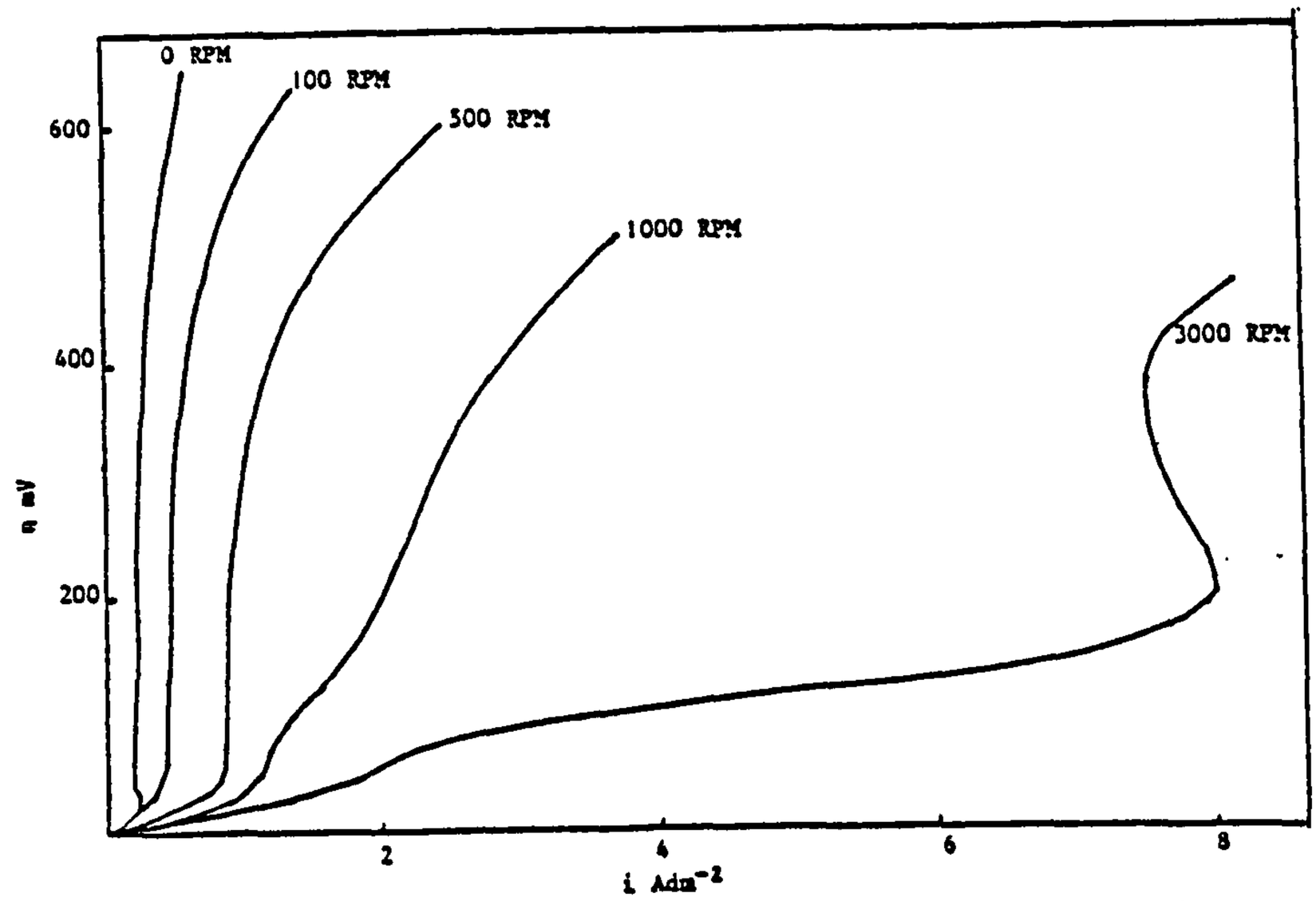

η vs i curves for a Pb electrode rotated at selected rotational speeds and cathodically polarised at a sweep rate of 0.5 mV sec^{-1} in a solution of 0.01 M $Pb(NO_3)_2$, 1M KNO_3 , 0.1 M HNO_3 plus 1 gl^{-1} BRIJ 35.

FIGURE 74

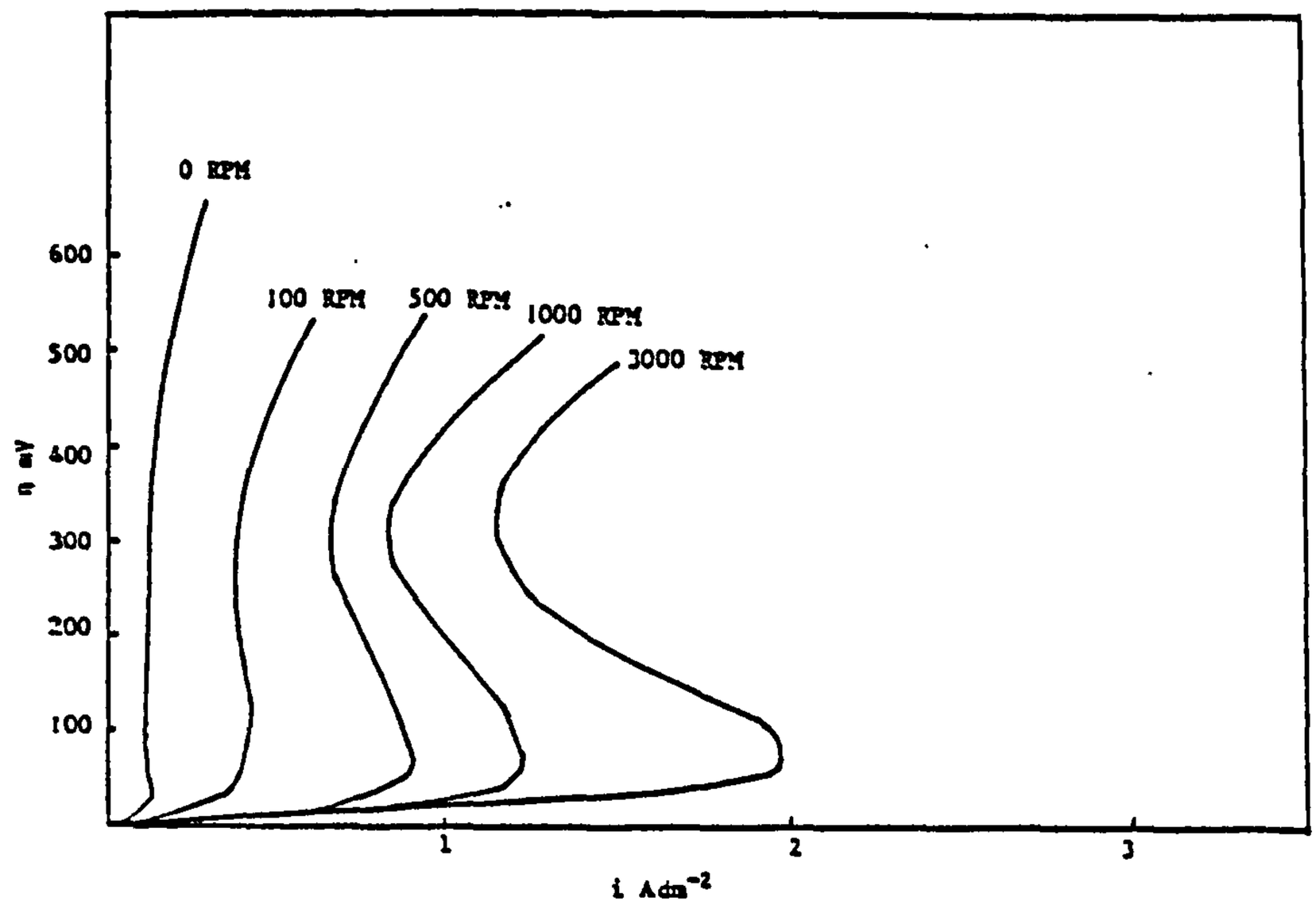

η vs i curves for a Pb electrode rotated at selected rotational speeds and cathodically polarised at a sweep rate of 0.5mV sec^{-1} in a solution of 0.01M $Pb(NO_3)_2$, 1M KNO_3 , 0.1M HNO_3 plus 1 gl^{-1} Triton X100.

FIGURE 75

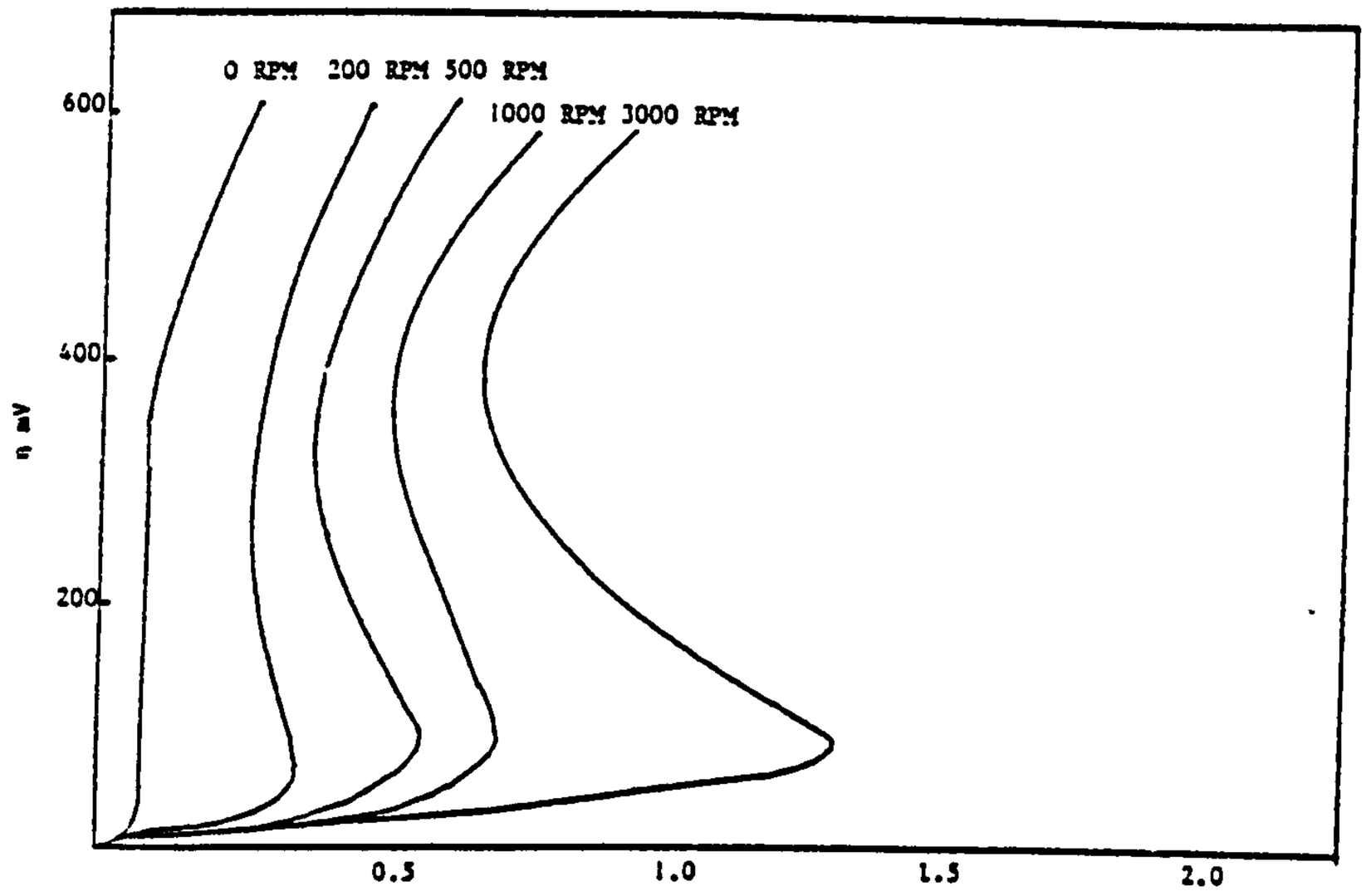

A graph of η versus i at selected rotational speeds for a Pb electrode cathodically polarised at a sweep rate of 0.3mV sec^{-1} in a solution of 0.01M $Pb(NO_3)_2$, 1M KNO_3 0.1M HNO_3 plus 1 gl^{-1} Pluronic L64 at 25°C.

FIGURE 76

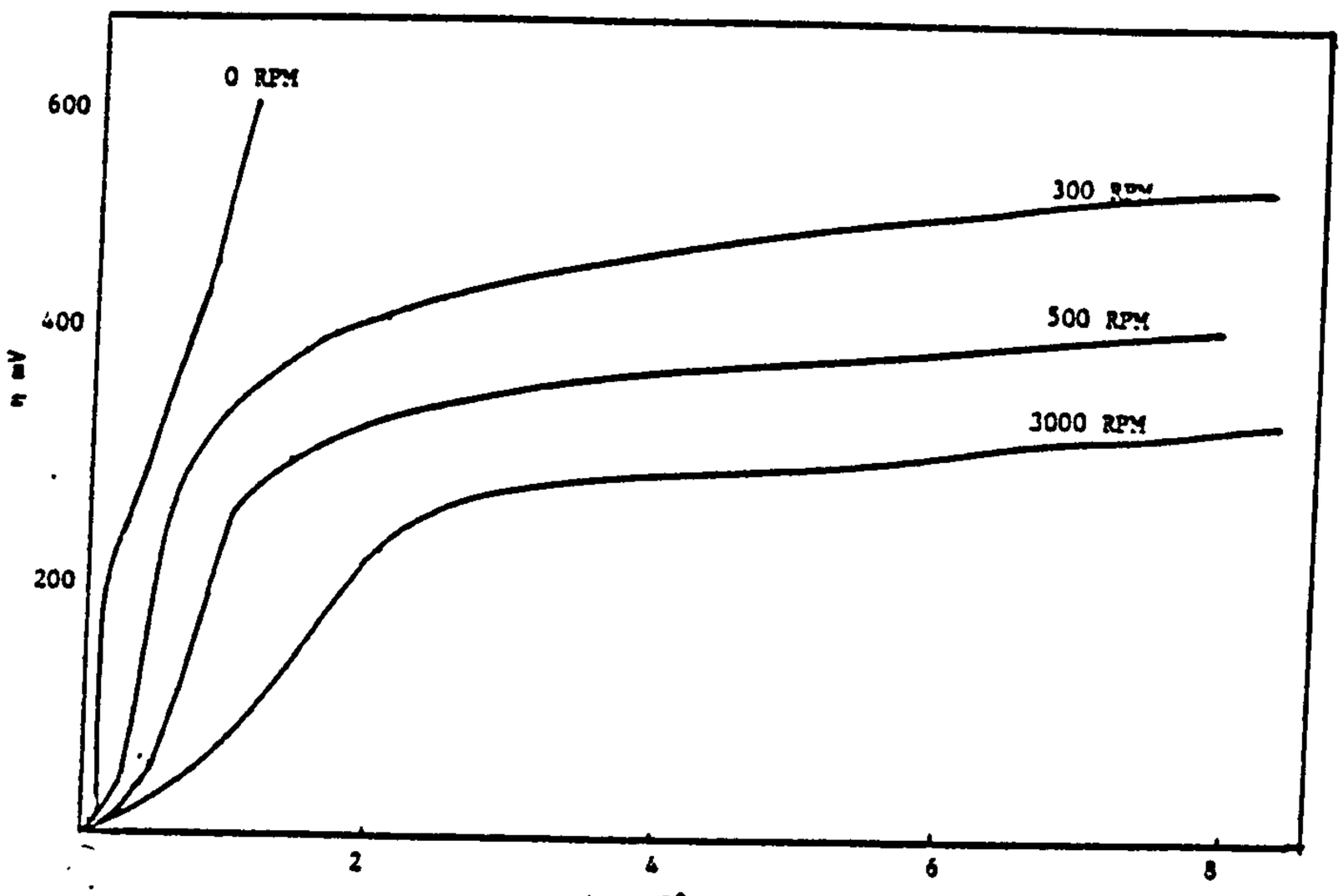

η vs i curves for a Pb electrode rotated at selected rotational speeds and cathodically polarised at a sweep rate of 0.5mV sec^{-1} in a solution of 0.01M $Pb(NO_3)_2$, 1M KNO_3 , 0.1M HNO_3 plus 1 gl^{-1} tannic acid.

FIGURE 77

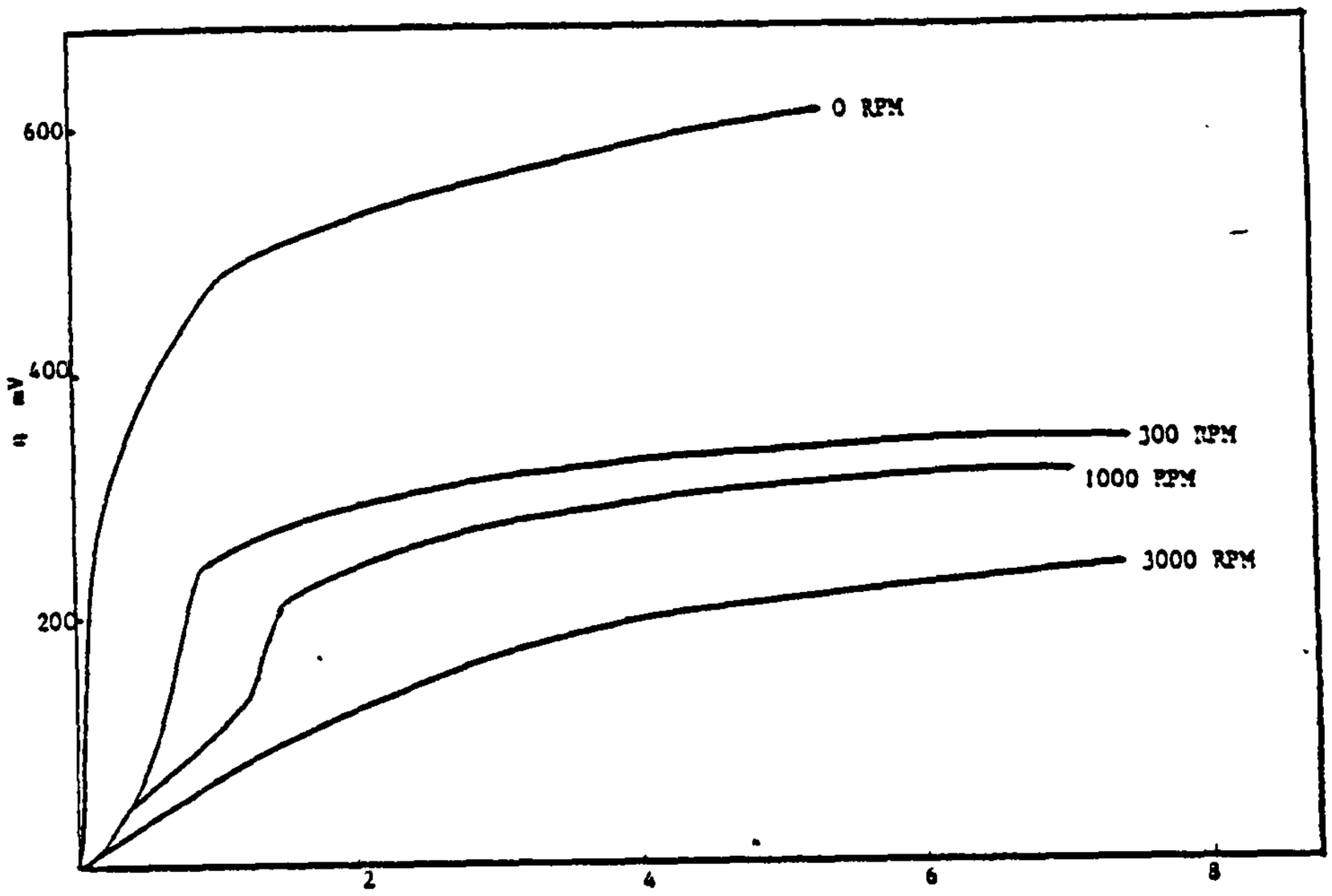

A graph of η versus i at selected rotational speeds for a Pb electrode cathodically polarised at a sweep rate of 0.5mV sec^{-1} in a solution of 0.01M $Pb(NO_3)_2$ & 1M KNO_3, 0.1M HNO_3 plus 0.1 gl^{-1} anthraquinone-2-monosulphonic acid at 25°C.

FIGURE 78

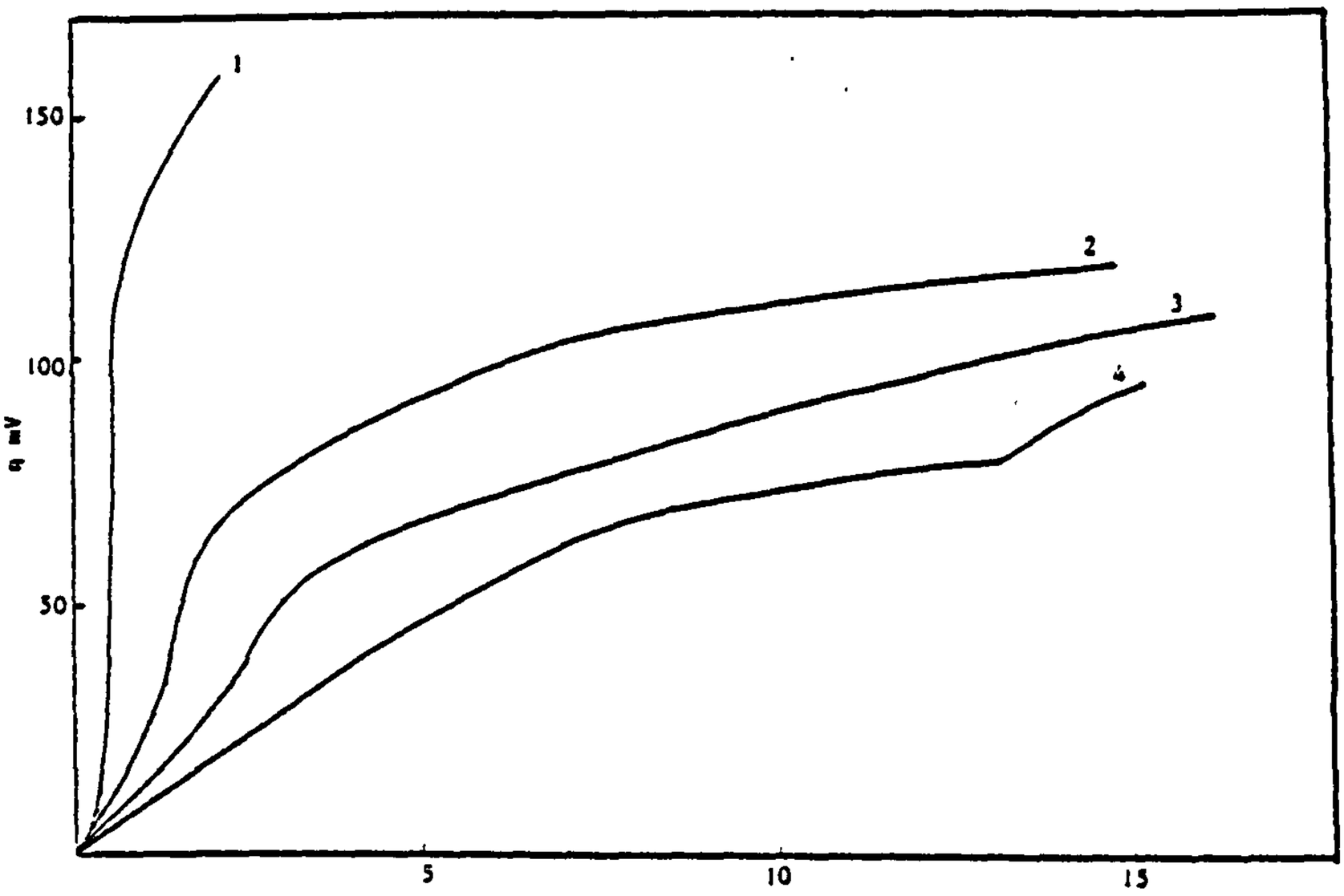

A graph of η versus i for a Pb electrode rotated at 300 RPM and cathodically polarised at a sweep rate of 0.5mV sec^{-1} in a solution of 1M KNO_3 , 0.1M HNO_3 at different $Pb(NO_3)_2$ concentrations.

1 = 0.005M $Pb(NO_3)_2$ 2 = 0.024M $Pb(NO_3)_2$

3 = 0.05M $Pb(NO_3)_2$ 4 = 0.1M $Pb(NO_3)_2$

FIGURE 79

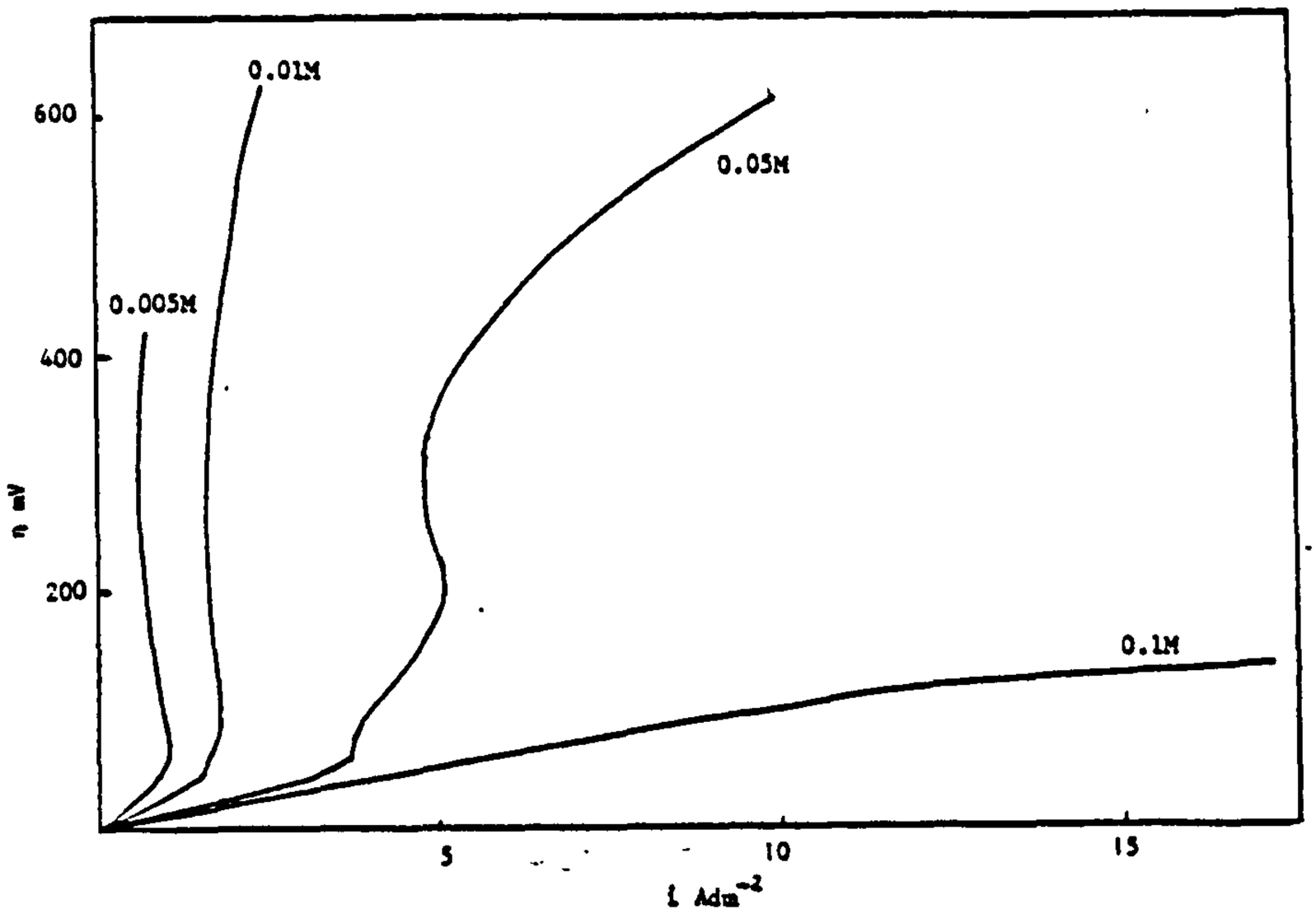

η vs i curves for a Pb electrode rotated at 300 RPM and cathodically polarised at a sweep rate of 0.5mV sec^{-1} in a stock solution of 1M KNO_3 , 0.1M HNO_3, 1 gl^{-1} Triton X100 containing different $Pb(NO_3)_2$ concentrations.

FIGURE 80

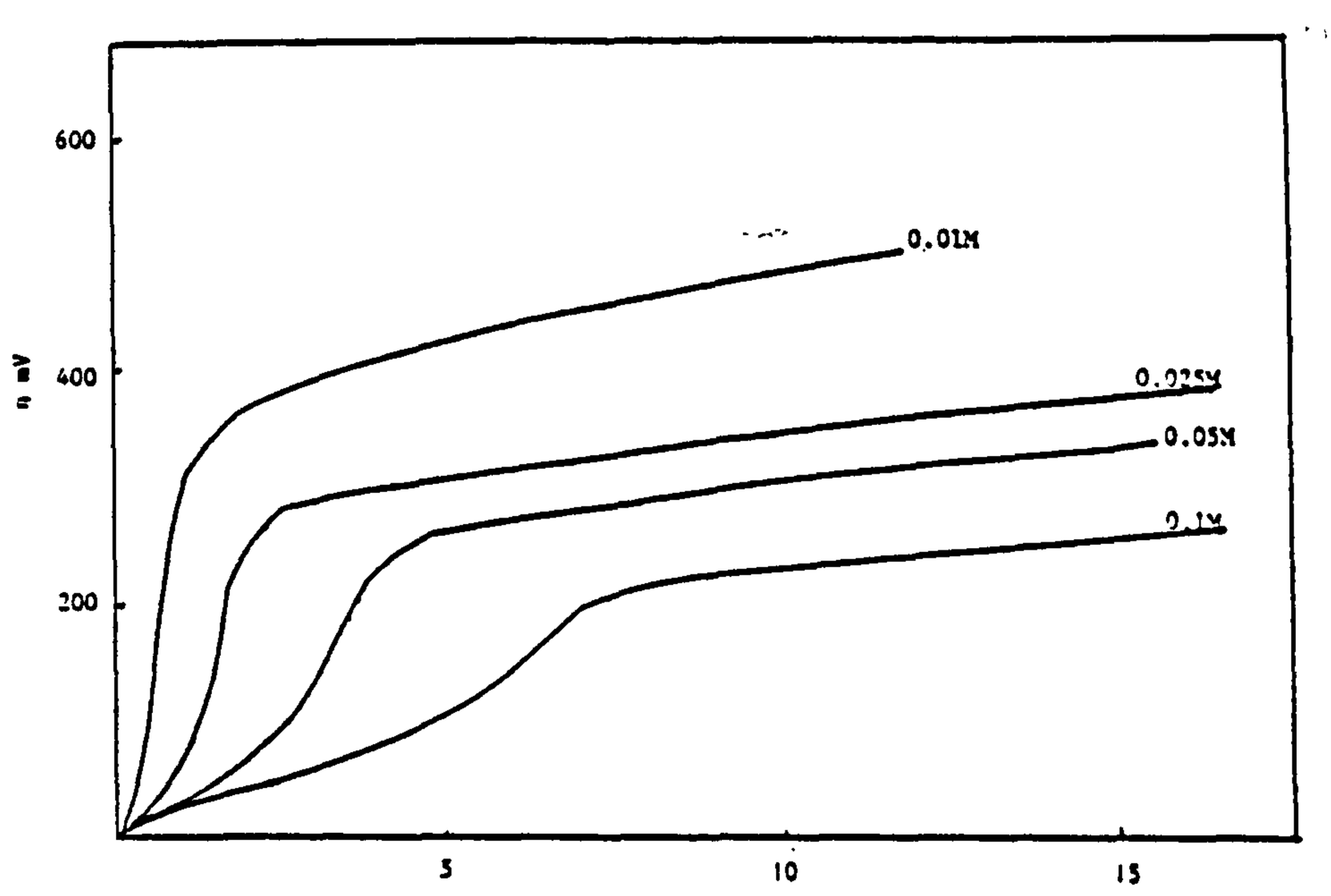

η vs i curves for a Pb electrode rotated at 300 RPM and cathodically polarised at a sweep rate of 1mV sec^{-1} in a solution of 1M KNO_3 , 0.1M HNO_3 , 1 gl^{-1} tannic acid containing different $Pb(NO_3)_2$ concentrations.

FIGURE 81

In 0.1M $Pb(NO_3)_2$ solutions tannic acid appears to have a greater inhibiting effect than Triton X100. However, at a concentration of 0.05M $Pb(NO_3)_2$ and below it is the Triton X100 that has the greater effect.

Triton X100 and tannic acid were the only additives selected for this study since separate plating experiments have shown that these were the most effective additives for Pb deposition from $Pb(NO_3)_2$ solutions.

3.2.2.3 Calculation of diffusion coefficients

The relationship between totally mass transfer limited current and the rotational speed of a rotating disc electrode, at a given potential is given by the Levich equation.

$$i_d = 0.62\ n\ F\ D^{2/3}\ \ v^{-1/6}\ w^{1/2}\ C_b$$

Where D = diffusion coefficient ($cm^2\ sec^{-1}$)
v = Kinematic viscosity ($cm^2\ sec^{-1}$)
w = rotational speed (rad sec^{-1})
C_b = bulk concentration (moles cm^{-3})
F = Faradays number
n = no of electrons involves in the deposition reaction
i_d = diffusion current (Acm^{-2})

From the above equation it can be seen that a plot of i_d vs $w^{1/2}$ at a constant potential will enable the diffusion coefficient to be calculated provided of course that v, n, and C_b are known.

The viscosity of all the solutions used was measured with an Ostwald Viscometer at 25°C and the kinematic viscosity was calculated from the density of the stock solution by the relationship :

$$\text{Kinematic viscosity} = \frac{\text{solution viscosity } (\eta)}{\text{solution density } (d)}$$

The kinematic viscosities of a stock solution of 0.1M $Pb(NO_3)_2$ plus 1M KNO_3 and 0.1M KNO_3 and the stock solution plus additives are listed in Table 44.

TABLE 44

The kinematic viscosity of 0.1M $Pb(NO_3)_2$, 1M KNO_3 + 0.1M HNO_3 at 25°C containing different surface active agents

Solution	Kinetic Viscosity $cm^2\ sec^{-1}$
0.1M $Pb(NO_3)_2$ stock solution	1.04×10^{-2}
" + Triton X100 1 gl^{-1}	5.44×10^{-3}
+ Pluronic L64 1 gl^{-1}	4.80×10^{-3}
+ BRIJ 35 1 gl^{-1}	6.36×10^{-3}
+ tannic acid 1 gl^{-1}	6.30×10^{-3}
+ anthraquinone-2-sulphonic acid 0.1 gl^{-1}	5.80×10^{-3}

A plot of i vs $w^{1/2}$ for 0.1M $Pb(NO_3)_2$ at selected overpotentials is shown in Fig. 82, the slope of which is potential dependent. The potential range was limited to only 30 mV above the rest potential, since at greater overpotentials the current did not remain constant at a given rotational speed. This was attributed to dendritic growth of Pb on the working electrode surface during the course of the experiment producing a non uniform surface area.

The effect the addition of 1 gl^{-1} Triton X100, to a solution of 0.1M $Pb(NO_3)_2$ on the i_d vs $w^{1/2}$ plot is shown in Fig. 83. The slope of these plots at a given overpotential is again potential dependent, as is the intercept at $w^{1/2} = 0$.

The values for the apparent diffusion coefficients for Pb^{2+} in 0.1M $Pb(NO_3)_2$ with and without certain addition agents, calculated from the i_d vs $w^{1/2}$ plots are given in Table 45.

Ideally determinations of the diffusion coefficient should be carried out at high overpotentials so that the concentration of metal ions at the electrode surface is zero. This was not possible in the present studies because of the production of dendritic Pb deposits at high overpotentials. The values of diffusion coefficient were therefore calculated assuming both zero Pb^{2+} concentration at the electrode surface and the thermodynamic value for Pb^{2+} concentration at a given over-potential (calculated from the Nernst equation).

As can be seen from Figs. 82 and 83, the i_d versus $w^{1/2}$ plots are not linear, as would be obtained for a totally diffusion controlled process, but are what would be expected if a kinetic step is involved.

The linear portion of these plots is limited to approximately 800 rpm and below, above this rotational speed the i_d vs $w^{1/2}$ relationship was not linear.

A plot of i_d vs $w^{1/2}$ for the stock electrolyte containing 0.01M $Pb(NO_3)_2$ is shown in Fig. 84, whilst plots of i_d vs $w^{1/2}$ for additive containing $Pb(NO_3)_2$ solutions are shown in Figs. 85 and 86. The values for the diffusion co- efficient of Pb^{2+} in 0.01M $Pb(NO_3)_2$ solutions, in the absence and presence of certain organic addition agents were calculated from the i_d vs $w^{1/2}$ plots (see Table 46).

The slopes of the i_d vs $w^{1/2}$ plots were overpotential dependent, however the intercept at $w^{1/2} = 0$ appeared to be overpotential independent. This was indeed the case with a 0.01M $Pb(NO_3)_2$ solution containing 1 gl^{-1} BRIJ 35 (Fig. 85) and 0.1gl^{-1} anthraquinone-2-monosulphonic acid (Fig. 86).

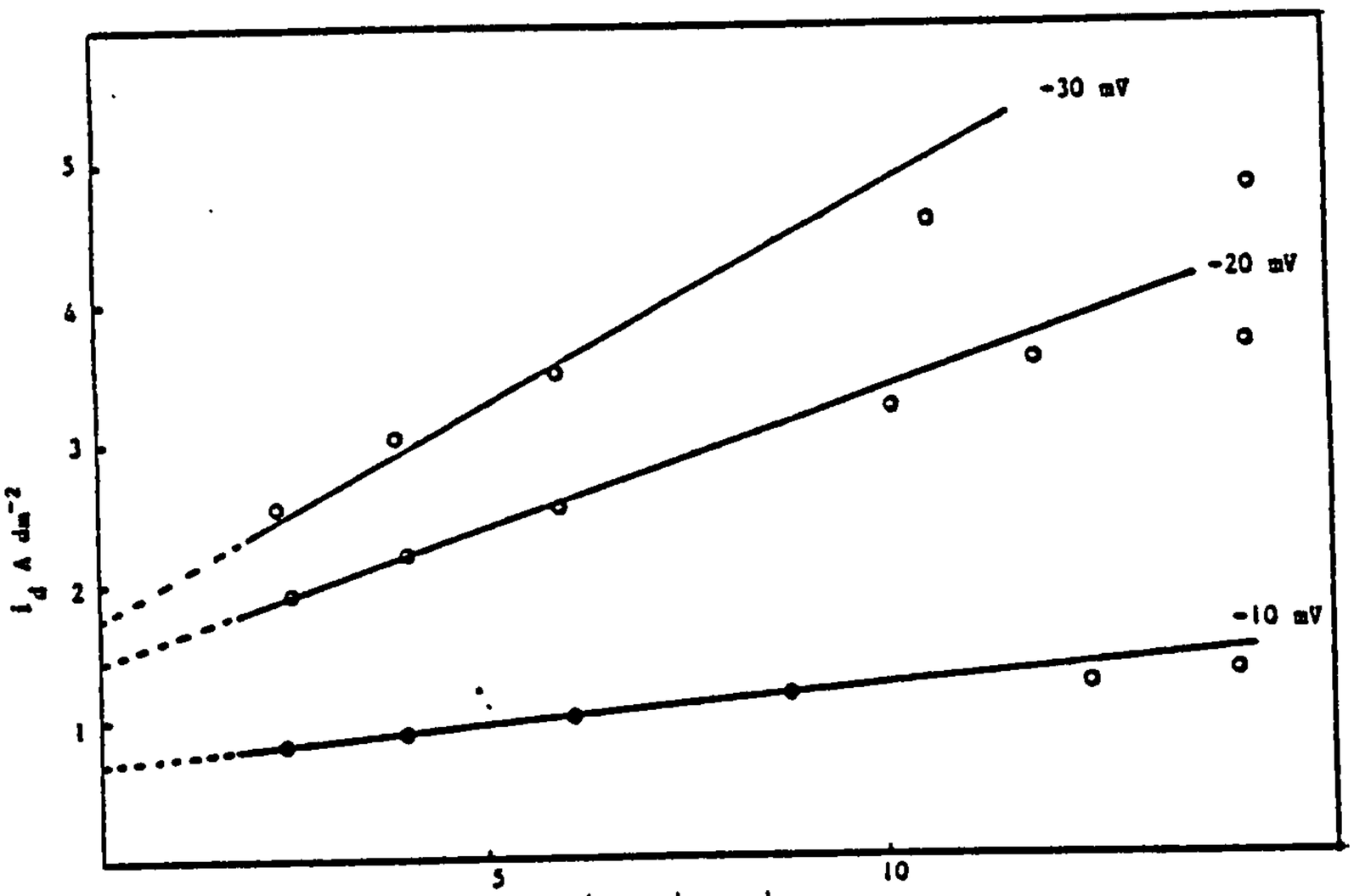

A graph of i_d vs $w^{\frac{1}{2}}$ for a Pb electrode held at fixed overpotential in a solution of 0.1M $Pb(NO_3)_2$, 1M KNO_3 , 0.1M HNO_3 without selected addition agents.

FIGURE 82

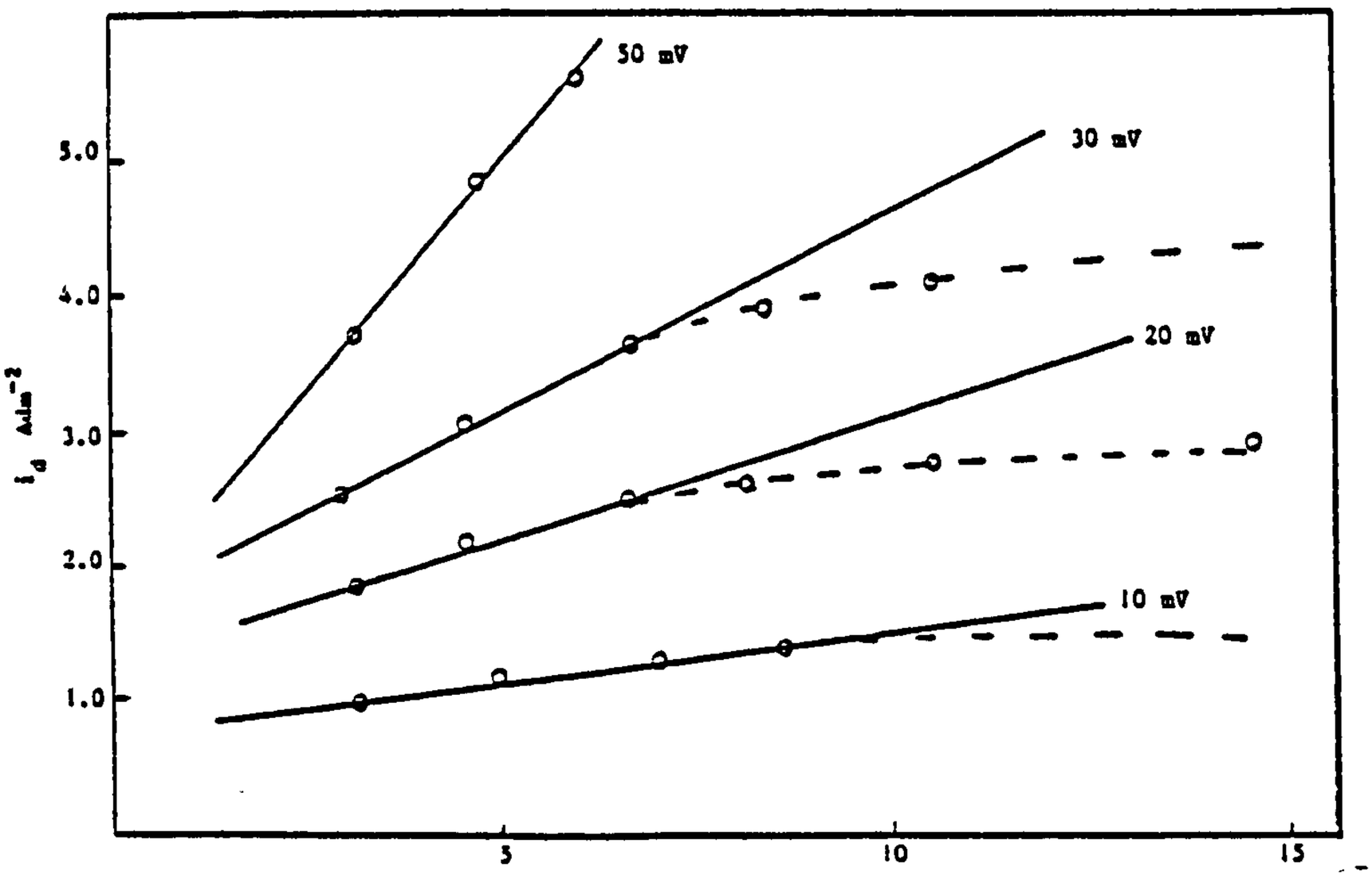

A graph of i_d versus $w^{\frac{1}{2}}$ for a Pb electrode held at selected overpotentials in a solution of 1M $Pb(NO_3)_2$, 1M KNO_3 , 0.1M HNO_3 plus 1 gl^{-1} Triton X100 at 25°C.

FIGURE 83

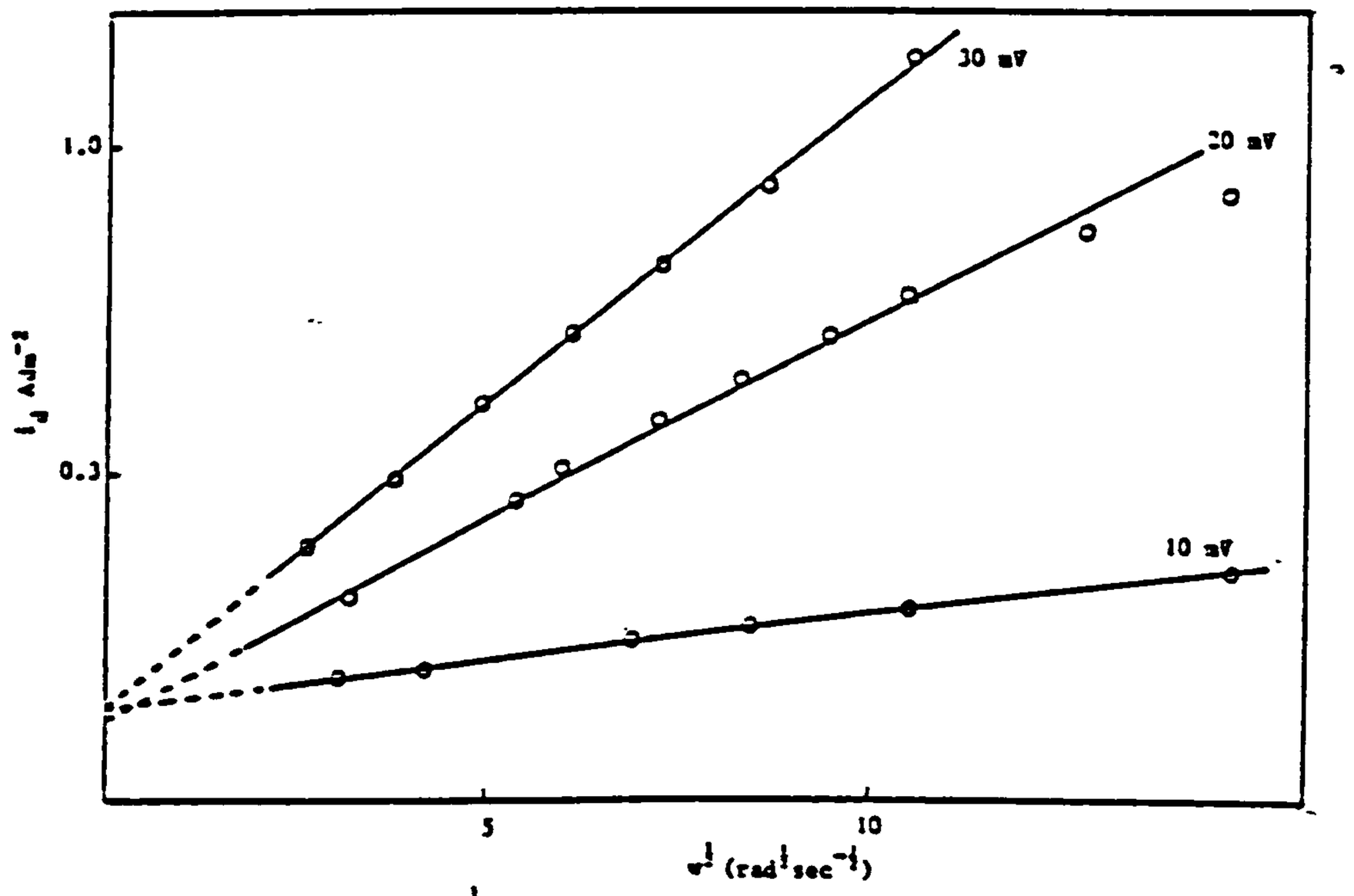

A graph of i_d versus $w^{\frac{1}{2}}$ for a Pb electrode held at selected cathodic over-potentials from -0.219V in a solution of 0.01M $Pb(NO_3)_2$, 1M KNO_3 , 0.1M HNO_3 at 25°C.

FIGURE 84

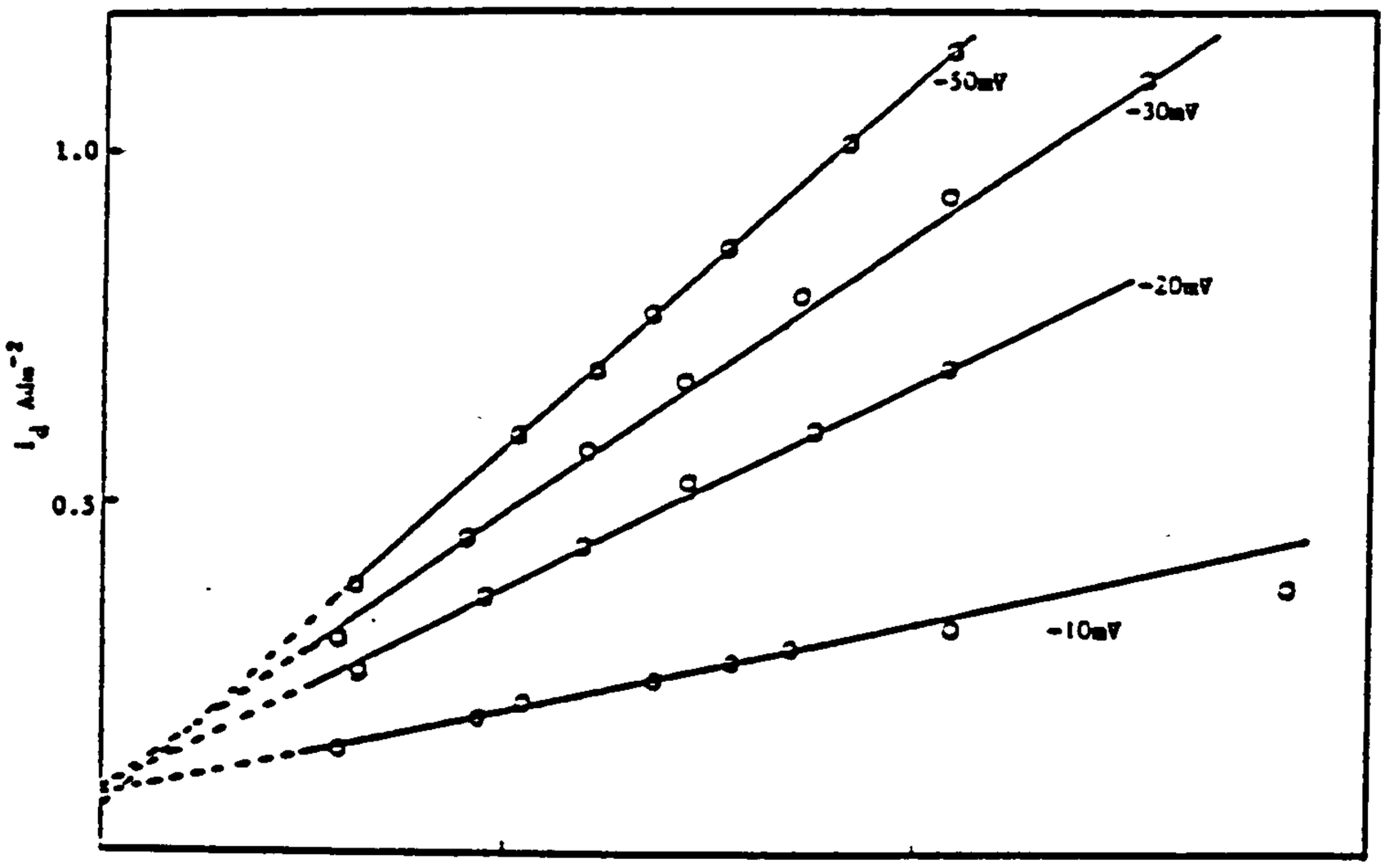

A graph of i_d vs $w^{\frac{1}{2}}$ for Pb deposition onto a Pb electrode, held at a fixed potential from the rest potential in a solution of 0.01M $Pb(NO_3)_2$, 1M KNO_3, 0.1M HNO_3 plus 1 gl^{-1} BRIJ 35.

FIGURE 85

TABLE 45

"Apparent" diffusion coefficients for Pb^{2+} ($cm^2 sec^{-1}$) in 0.1M $Pb(NO_3)_2$ + 0.1M HNO_3 + 1M KNO_3 with and without selected addition agents. The Pb electrode was rotated at 3000 rpm and polarised at selected overpotentials from -0.19V.
The figures outside the brackets are the values for the diffusion coefficient assuming a surface Pb^{2+} concentration of zero, whilst those within the brackets are based on the thermodynamic Pb^{2+} concentration at a given overpotential

Additive	Diffusion coefficient cm^2 sec^{-1} at a given overpotential from -0.190V		
	10 mV	20 mV	30 mV
None	9.8×10^{-8} (1.8×10^{-7})	8.9×10^{-7} (1.1×10^{-6})	1.81×10^{-6} (2.0×10^{-6})
1 gl^{-1} BRIJ 35	3.2×10^{-8} (5.9×10^{-8})	5.1×10^{-7} (6.5×10^{-7})	1.18×10^{-6} (1.31×10^{-6})
1 gl^{-1} Pluronic L64	9.8×10^{-8} (1.8×10^{-7})	4.2×10^{-7} (5.3×10^{-7})	1.25×10^{-6} (1.38×10^{-6})
1 gl^{-1} Triton X100	1.2×10^{-7} (2.2×10^{-8})	5.1×10^{-7} (6.5×10^{-7})	1.05×10^{-6} (1.16×10^{-6})

The range over which the i_d vs $w^{1/2}$ plots was linear in 0.01M $Pb(NO_3)_2$ solutions was extended (up to 2000 rpm) and the overpotential range over which measurements could be made, before a rising current was observed (at a given rotational speed and a fixed potential) was extended to 50 mV.

The values of diffusion coefficients for Pb^{2+} in 0.01M $Pb(NO_3)_2$ in a stock solution of 1M KNO_3 plus 0.1M HNO_3 in the absence and presence of certain organic addition agents, calculated from the i_d vs $w^{1/2}$ plots are presented in Table 46.

TABLE 46

"Apparent" diffusion coefficient (cm^2 sec^{-1}) for Pb^{2+} in a solution of 0.01M $Pb(NO_3)_2$ + 1M KNO_3 + 1M HNO_3 at selected overpotentials from the rest potential of -0.22V.

All measurements conducted at 25°C and at an electrode rotational speed of 3000 rpm. The figures outside the brackets are the diffusion coefficients calculated on a surface Pb^{2+} concentration of zero, whilst those inside the brackets are the thermodynamic values for Pb^{2+} concentration at a given overpotential

Stock Solution of 0.01M $Pb(NO_3)_2$ plus selected additives	Diffusion coefficient for Pb^{2+} at a given overpotential from -0.220 V			
	10 mV	20 mV	30 mV	50m V
No additive	7.7×10^{-8} (1.9×10^{-7})	7.1×10^{-7} (1.0×10^{-6})	1.3×10^{-6} (1.5×10^{-6})	2.1×10^{-6} (2.2×10^{-6})
Pluronic L64 $1gl^{-1}$	5.2×10^{-8} (1.3×10^{-7})	3.9×10^{-7} ($5.5 \times 1-^{-7}$)	8.4×10^{-7} (9.8×10^{-7})	1.1×10^{-6} (1.1×10^{-6})
BRIJ 35 1 gl^{-1}	1.2×10^{-7} (7.7×10^{-7})	4.7×10^{-7} (6.7×10^{-7})	7.7×10^{-7} (8.9×10^{-7})	1.1×10^{-6} (1.1×10^{-6})
anthraquinone-2-sulphonic acid 0.1 gl^{-1}	2.5×10^{-8} (6.3×10^{-8})	- -	1.3×10^{-7} (1.5×10^{-7})	7.7×10^{-7} (7.9×10^{-7})
Triton X100 1 gl^{-1}	1.1×10^{-8} (8.8×10^{-8})	8.4×10^{-8} (9.8×10^{-8})	1.0×10^{-7} (1.2×10^{-7})	3.0×10^{-7} (3.1×10^{-7})

3.2.2.4 Effect of certain additives on the kinetics of the Pb^{+2} deposition reaction

The current under diffusion controlled conditions where the bulk concentration C_b does not equal the surface concentration C_s is given by :

$$i = n F D_o \frac{(C^b - C^s)}{\delta} \qquad 1)$$

where D_o = diffusion coefficient for the oxidised species.
δ = diffusion layer thickness.

It can also be shown that :

$$\delta = 1.16 D^{1/3} \nu^{1/6} w^{-1/2} \qquad 2)$$

$$i = 0.62 nF D^{2/3} w^{1/2} \nu^{-1/6} (C_b - C_s) \qquad 3)$$

The limiting current under diffusion control (i_d) when the surface concentration is equal to zero is given by :

$$i = 0.62 nFD^{2/3} w^{1/2} \nu^{-1/6} C_b \qquad 4)$$

For a first order reaction the nett current, assuming a negligible reverse current at a fixed potential is given by :

$$i = nF k_f C_b \quad \text{at a fixed potential}$$

From equation 3 it can be shown that the current (i) when the surface concentration C_s does not equal zero is :

$$i = nF k_f C_s \left(1 - \frac{i}{i_d}\right) \qquad 5)$$

The current in the absence of any diffusion (i_k) is defined as $i_k = nF k_f C_b$ and equation 5 can be rearranged to give

$$\frac{1}{i} = \frac{1}{i_k} + \frac{1}{0.62 nF C_b D^{2/3} \nu^{-1/6} w^{1/2}} \qquad 6)$$

Therefore a plot of 1/i vs $1/w^{1/2}$ will be a straight line, which when extrapolated to $1/w^{1/2} = 0$ will give an intercept of $1/i_k$ at a given potential.

The above equation applies to reactions with a low exchange current density where the rate of the reverse reacton K_b is negligible. Where the reverse reaction is not negligible at low overpotentials and by similar deductive reasoning taking into account the reserve current one obtains :

$$\text{where } \frac{1}{i} = \frac{1}{nF(k_f C_b - k_b C_b)} + \frac{(k_f/B_o + K_b/Br)}{(K_f C_b - K_b C_b)w^{1/2}}$$

k_b = rate constant for the reverse reaction

B_o = $0.62\ nF\ D^{2/3}v^{-1/6}$

A plot of 1/i vs $1/w^{1/2}$ for 0.1M $Pb(NO_3)_2$ in the stock solution is shown in Fig. 87, and at overpotentials greater than 30mV intercepts on the $1/w^{1/2}$ axis were observed in this solution. This was thought to be due to the dendritic growth of Pb changing the nature of the electrode surface, particularly at high rotational speeds. A plot of 1/i vs $1/w^{1/2}$ for the same solution containing 1 gl^{-1} Triton X100 is shown in (Fig. 88) and that for a solution containing BRIJ 35 in Fig. 89.

The values of the intercepts at $1/w^{1/2}=0$ for the current in the absence of diffusion control for Pb deposition from 0.1M $Pb(NO_3)_2$ solutions with and without different addition agents and at selected overpotentials are given in Table 47.

The values of the intercept at $1/w^{1/2} = 0$ for the plots of 1/i vs $1/w^{1/2}$ for 0.01M $Pb(NO_3)_2$ solutions with and without selected addition agents at given overpotentials are given in Table 48.

TABLE 47

Values of the intercept on the 1/i axis from a graph of $1/i$ vs $1/w^{1/2}$ for a Pb electrode rotated at 3000 rpm in a solution of 0.1M $Pb(NO_3)_2$ with and without selected addition agents, at 25°C.

Stock solution of 0.1M $Pb(NO_3)_2$ plus selected additives at 1 gl^{-1}	Intercept at given overpotential (A^{-1} cm^2) from the rest potential of -0.190 V		
	10 mV	20 mV	30 mV
No additive	68.9	23.5	15.6
Triton X100	60.1	29.5	19.3
Pluronic L64	68.9	27.8	16.4
BRIJ 35	108	33.7	19.8
Tannic acid	91	46.5	21.9

TABLE 48

The values of the intercept obtained from plots of $1/i$ vs $1/w^{1/2}$ for a Pb electrode maintained at selected overpotentials in a solution of 0.01M $Pb(NO_3)_2$ with and without selected addition agents

Stock solution of 0.1M $Pb(NO_3)_2$ plus selected addition agent	Intercept at selected overpotentials ($A^{-1}cm^2$) from the rest potential of -0.220 V vs SHE			
	10mV	20mV	30mV	50mV
No additive	145	43	26	-
Triton X100 1 gl^{-1}	608	221	167	102
0.1 gl^{-1} anthraquinone-2-monosulphonic acid	275	-	142	44
Pluronic L64 1 gl^{-1}	196	51	29	15
BRIJ 35 1 gl^{-1}	146	39	22	9

TABLE 47A

Diffusion coefficients for Pb^{2+} in a 0.1M $Pb(NO_3)_2$ + 1M KNO_3 + 0.1M HNO_3 solution at selected overpotentials from the rest potential - 0.19V at 25°C. The values calculated from a plot of 1/i vs $1/w^{1/2}$ and from the Nernstian value of Pb^{2+} concentration at a given overpotential

Stock solution of 0.1M $Pb(NO_3)_2$ plus selected additives	Diffusion coefficient for Pb^{2+} (cm^2 sec^{-1}) at a given overpotential			
	10mV	20mV	30mV	50mV
No additives	8.4×10^{-6}	1.42×10^{-5}	1.48×10^{-5}	-
1 gl^{-1} BRIJ 35	7.85×10^{-6}	1.02×10^{-5}	1.01×10^{-5}	-
1 gl^{-1} Pluronic L64	6.8×10^{-6}	1.04×10^{-5}	1.27×10^{-5}	-
1 gl^{-1} Triton X100	1.11×10^{-5}	1.38×10^{-5}	1.74×10^{-5}	-
1 gl^{-1} tannic acid	-	7.99×10^{-6}	1.29×10^{-5}	1.25×10^{-5}

TABLE 48A

Diffusion coefficient for Pb^{2+} in a solution of 0.01M $Pb(NO_3)_2$ + 1M KNO_3 + 0.1M HNO_3 at selected overpotentials from the rest potential of -0.22V at 25°C.

The value calculated from a plot of 1/i vs $1/w^{1/2}$ and from the Nernstian value of Pb^{2+} concentration at a given overpotential

Stock solution of 0.1M $Pb(NO_3)_2$ plus selected additives	Diffusion coefficient for Pb^{2+} ($cm^2 sec^{-1}$) at a given overpotential			
	10mV	20mV	30mV	50mV
No additives	8.36×10^{-6}	1.11×10^{-5}	1.22×10^{-5}	1.25×10^{-5}
1 gl^{-1} BRIJ 35	4.94×10^{-6}	8.83×10^{-6}	9.32×10^{-6}	9.21×10^{-6}
1 gl^{-1} Triton X100	4.83×10^{-6}	6.29×10^{-6}	1.14×10^{-5}	1.31×10^{-5}
1 gl^{-1} Pluronic L64	1.77×10^{-5}	1.45×10^{-5}	1.45×10^{-5}	1.36×10^{-5}
0.1 gl^{-1} anthraquinone-2-sulphonic acid	1.61×10^{-6}	-	3.74×10^{-6}	8.31×10^{-6}

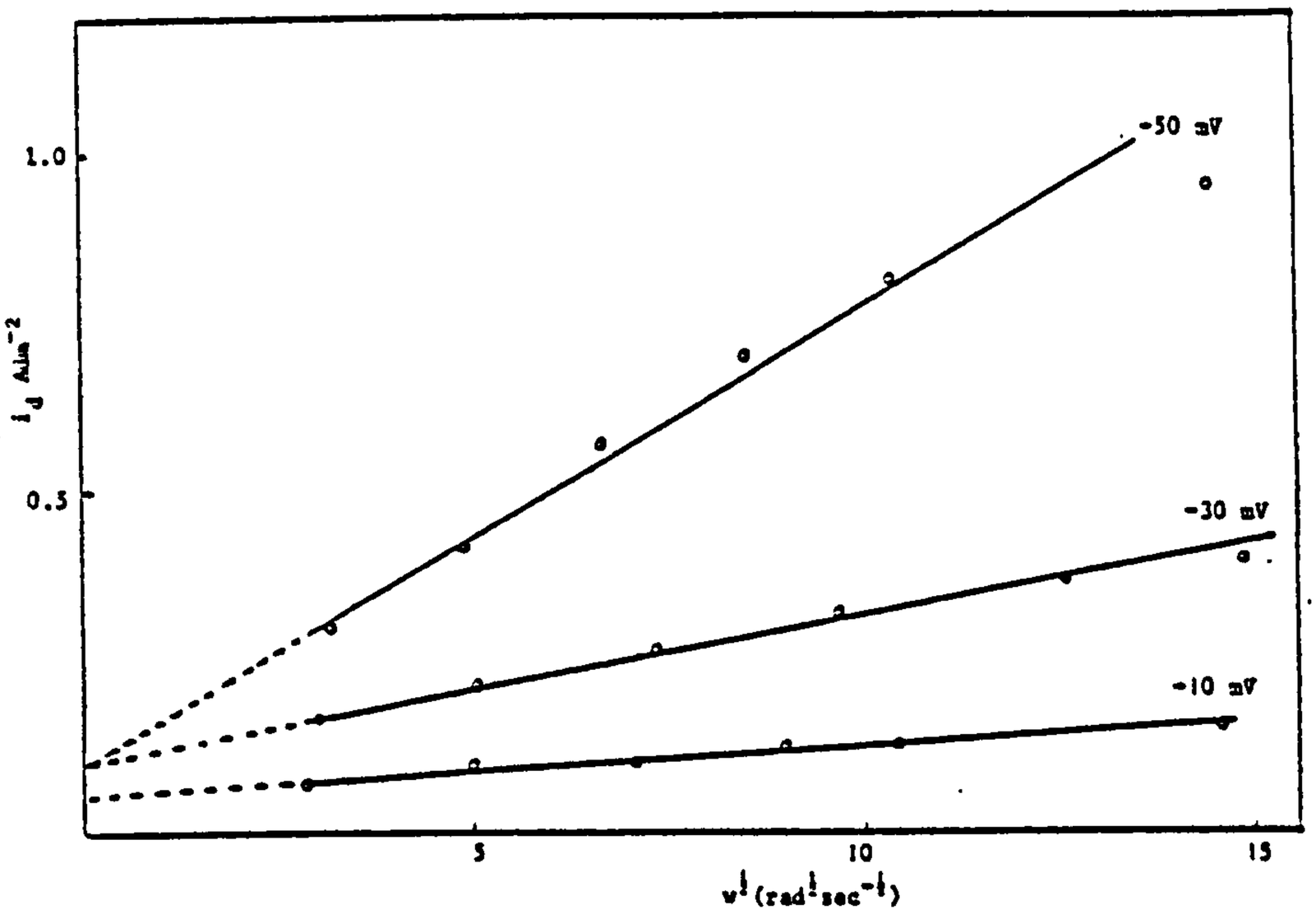

A graph of i_d versus $w^{\frac{1}{2}}$ for a Pb electrode held at a selected cathodic over-potential from E_{rest} in a solution of 0.01M $Pb(NO_3)_2$, 1M KNO_3 , 0.1M HNO_3 plus 0.1 gl^{-1} anthraquinone-2-monosulphonic acid.

FIGURE 86

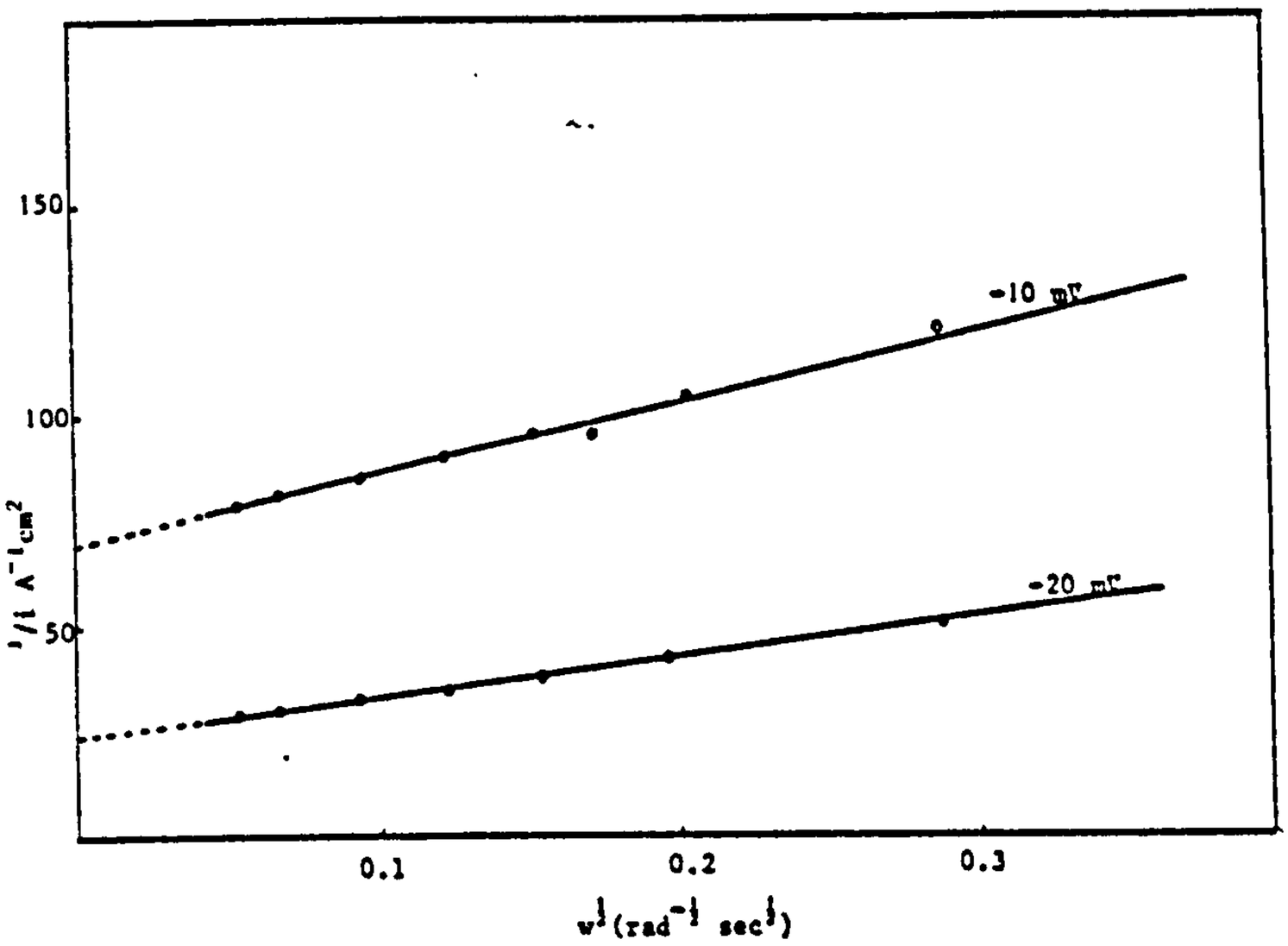

A graph of $^1/i$ vs $w^{-\frac{1}{2}}$ for a Pb electrode held at a fixed cathodic overpotential from the rest potential in a solution of 0.1M $Pb(NO_3)_2$, 1M KNO_3 , 0.1M HNO_3 without any addition agents.

FIGURE 87

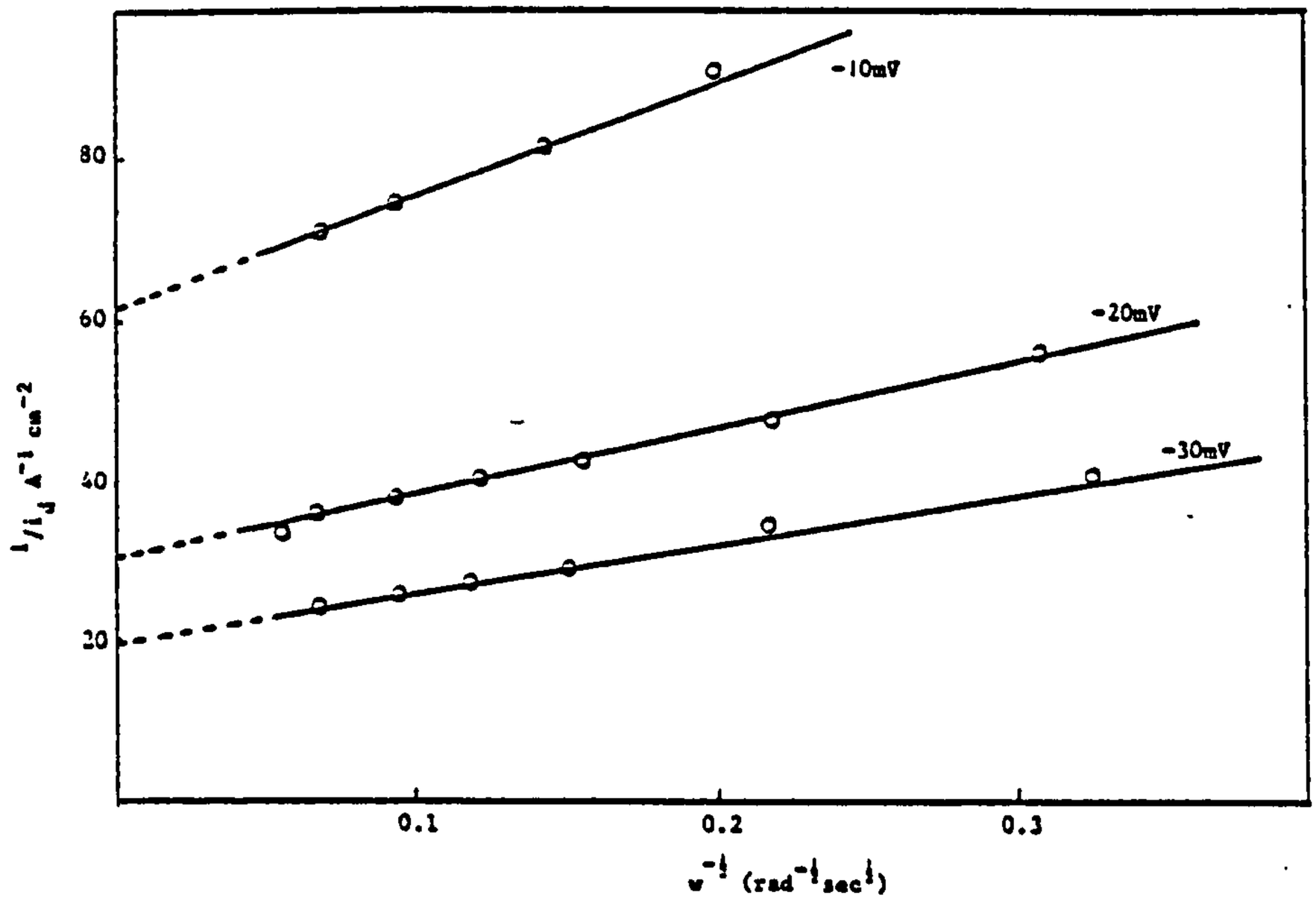

A graph of $^1/i_d$ versus $w^{-\frac{1}{2}}$ for a Pb electrode held at a selected overpotential from E_{rest} in a solution of 0.1M $Pb(NO_3)_2$, 1M KNO_3 , 0.1M HNO_3 plus 1 gl^{-1} Triton X100 at 25°C.

FIGURE 88

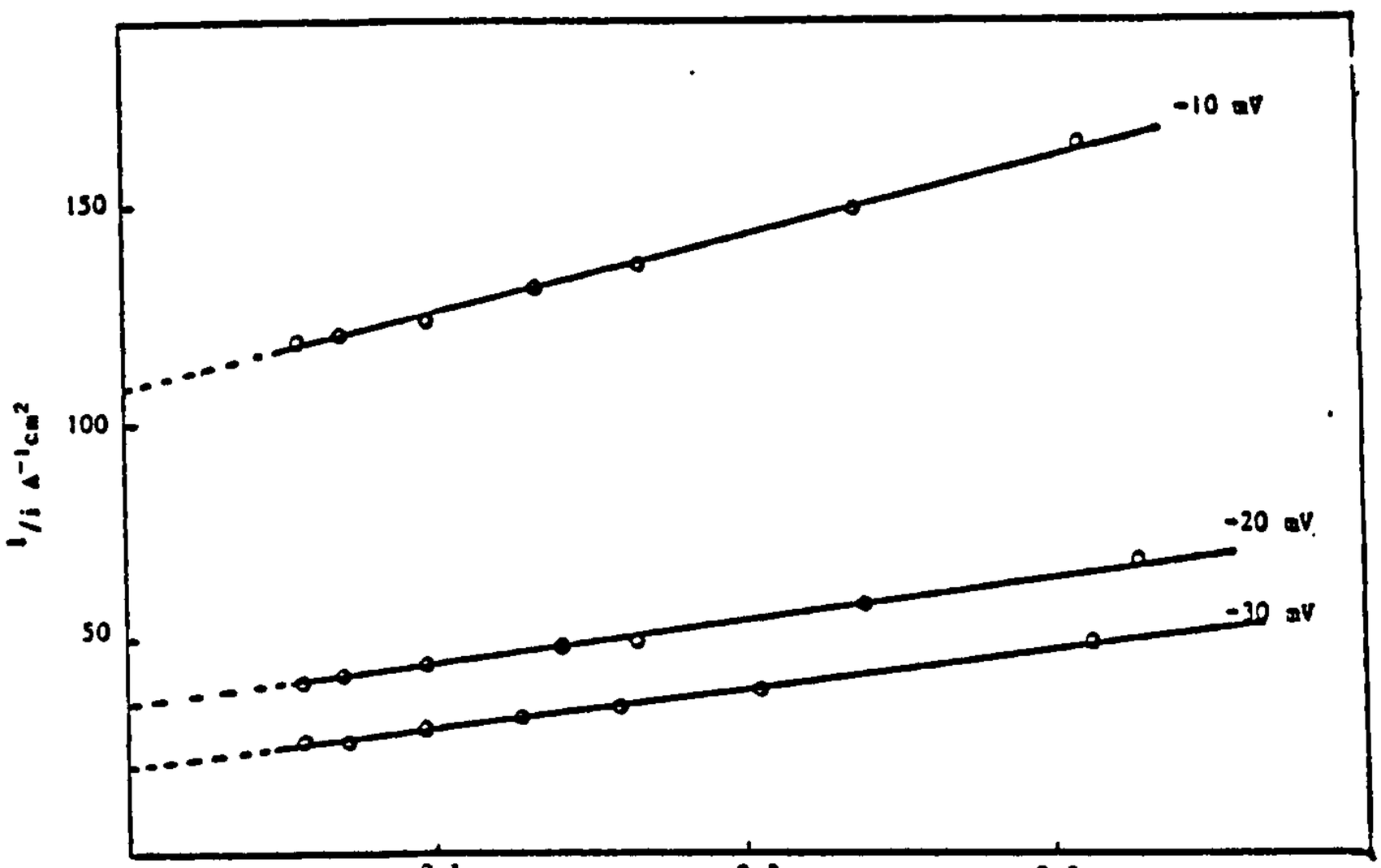

A graph of $^1/i$ vs $w^{-\frac{1}{2}}$ for a Pb electrode held at fixed overpotential from the rest potential in a solution of 0.1M $Pb(NO_3)_2$, 1M KNO_3 , 0.1M HNO_3 plus 1 gl^{-1} BRIJ 35.

FIGURE 89

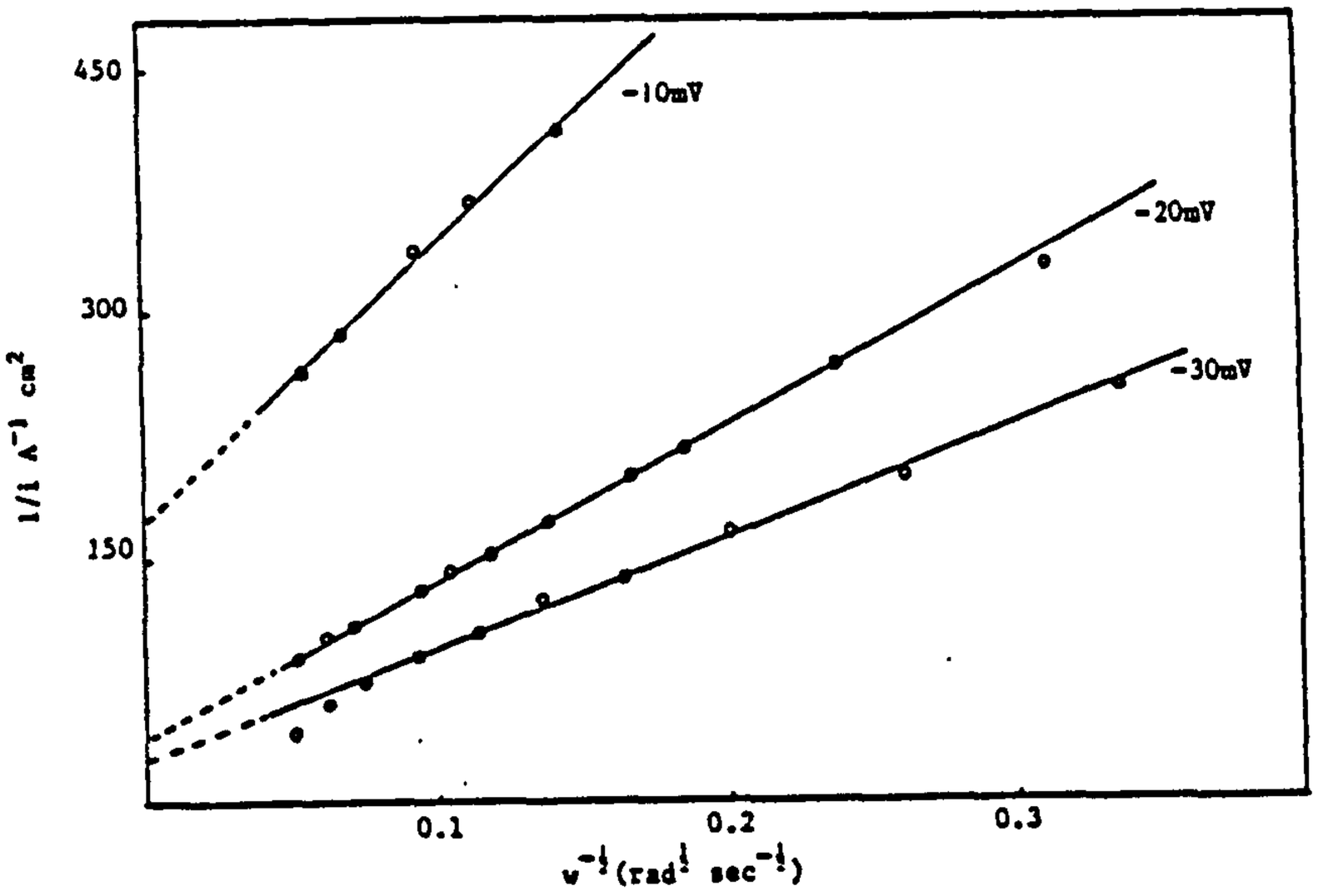

A graph of $1/i_d$ versus $w^{-\frac{1}{2}}$ for a Pb electrode held at a selected cathodic overpotential from the rest potential in a solution of 0.01M $Pb(NO_3)_2$, 1M KNO_3, 0.1M HNO_3 without any additives.

FIGURE 90

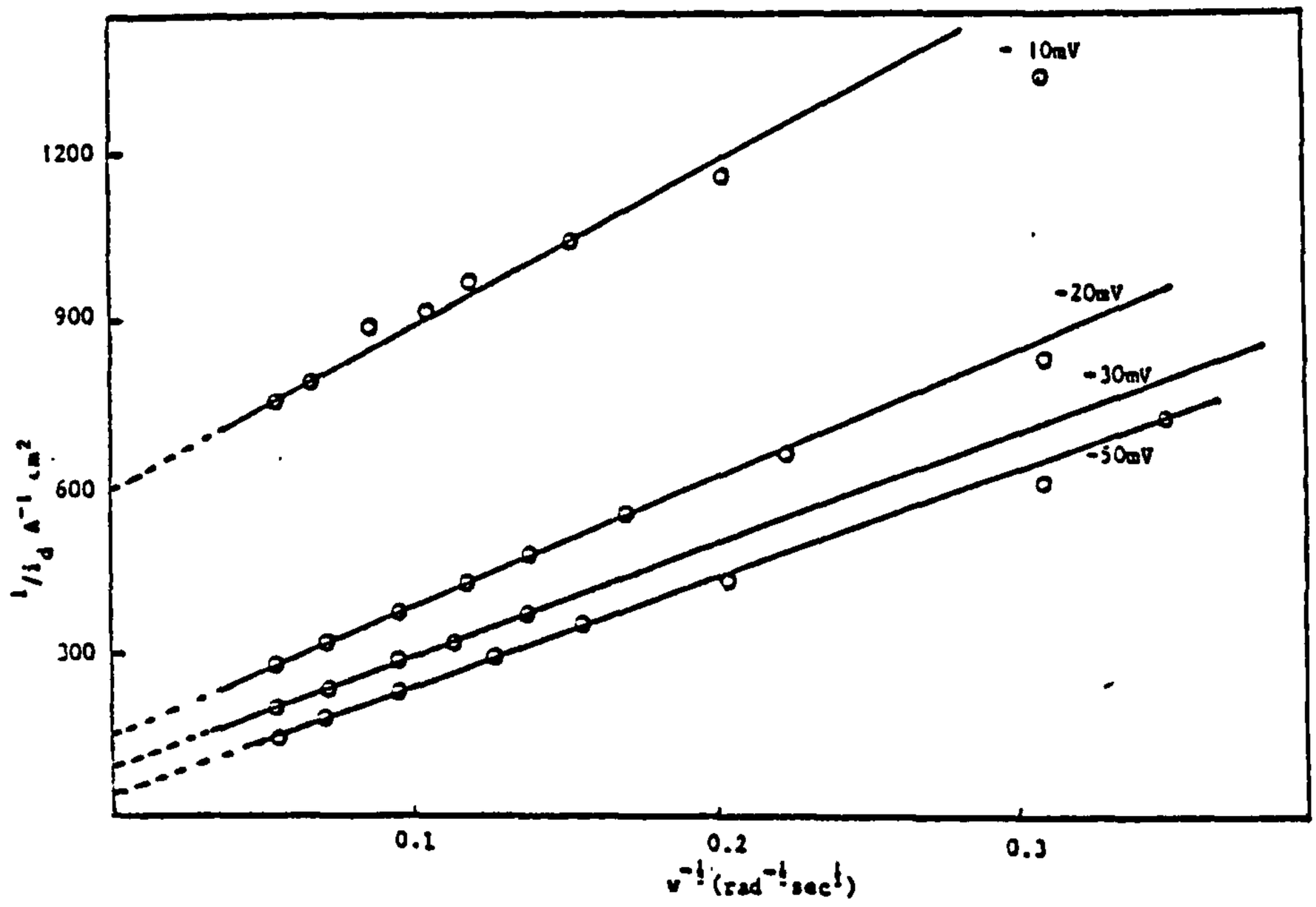

A graph of $1/i_d$ versus $w^{-\frac{1}{2}}$ for a Pb electrode held at a selected overpotential from the rest potential in a solution of 0.01M $Pb(NO_3)_2$, 1M KNO_3, 0.1M HNO_3 plus 1 gl^{-1} Triton X100 at 25°C.

FIGURE 91

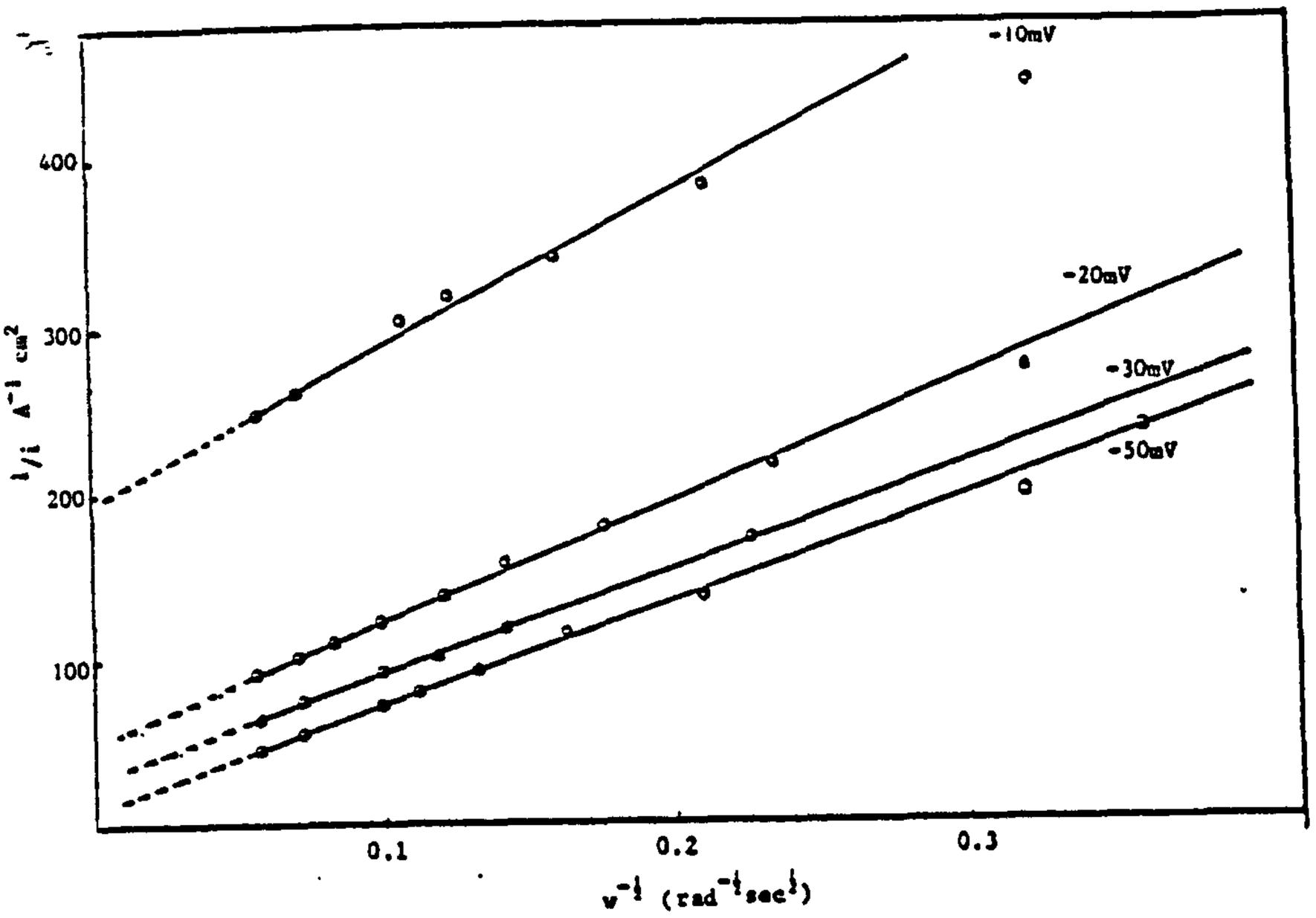

A graph of $^1/i$ vs $w^{-\frac{1}{2}}$ for Pb deposition onto a Pb electrode from a solucion of 0.01M $Pb(NO_3)_2$, 1M KNO_3 , 0.1M HNO_3 plus 1 gl^{-1} Pluronic L64.

FIGURE 92

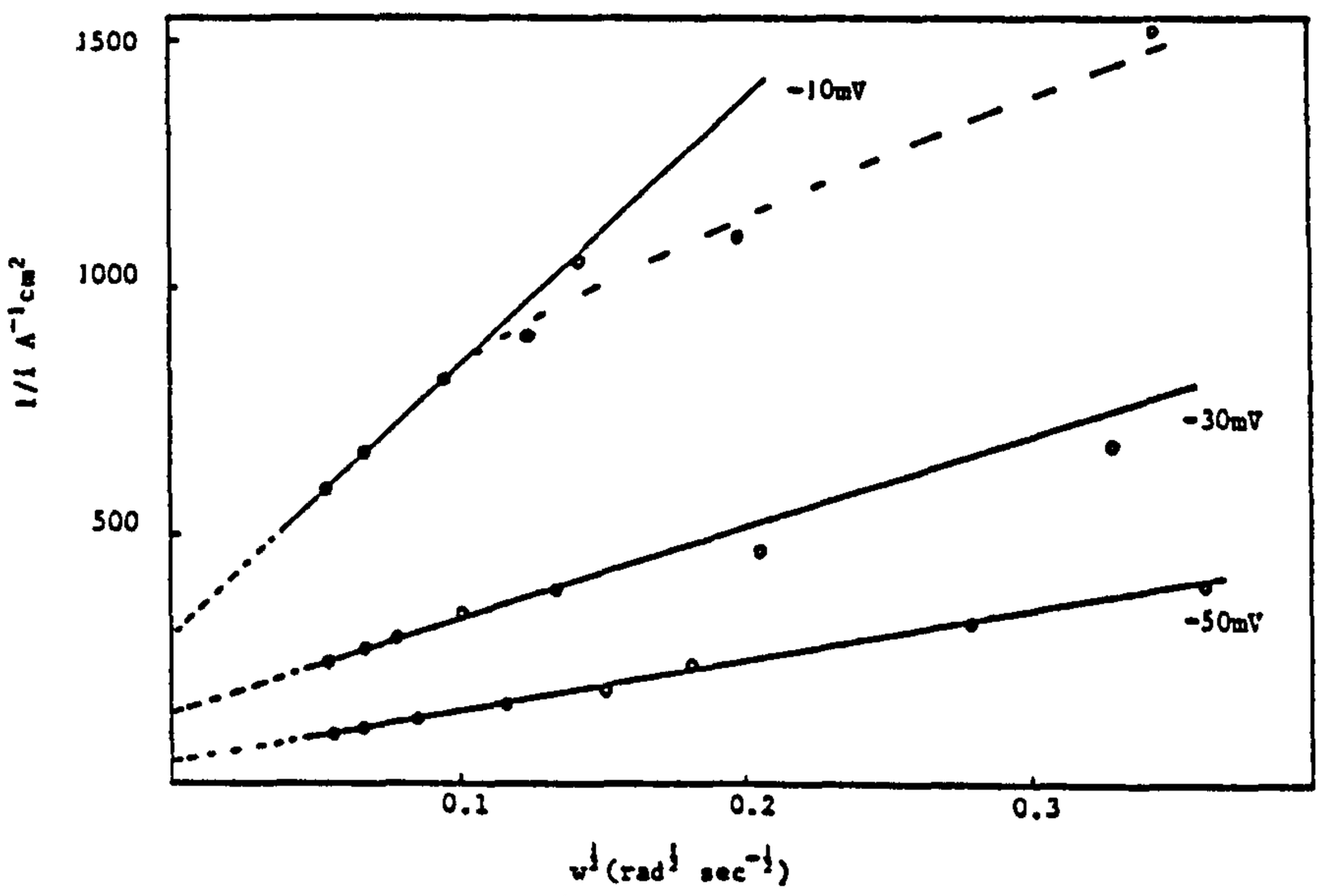

A graph of i/i_d vs $w^{-\frac{1}{2}}$ for Pb deposition onto a Pb electrode maintained at a fixed cathodic overpotential from a solution of 0.01M $Pb(NO_3)_2$, 1M KNO_3, 0.1M HNO_3 plus 0.1 gl^{-1} anthraquinone-2-monosulphonic acid.

FIGURE 93

3.2.2.5 Exchange current density (i_o) measurements

A graph of log i_o vs log $[Pb^{2+}]$ for a solution of $Pb(NO_3)_2$ in 1M KNO_3 + 0.1M HNO_3 without any additives is shown in Fig. 94. This figure shows two separate straight line plots, because the values for i_o at each concentration were determined by two separate methods. Line 1 shows the values for i_o obtained by extrapolation of the linear portion of the E vs log i curve to zero overpotential and Line 2 the values i_o obtained from the slope of the η vs i curve, near the reversible potential.

The slope of line 1 is 0.39 and that of line 2 is 0.48, these are the respective values of β for Pb^{2+} deposition i.e the symmetry factor.

$$\frac{d \log i_o}{d \log [Pb^{2+}]} = \beta$$

A value of 0.5 for β has been reported in the literature for the Pb deposition in nitrate solutions (202). There is as can be seen from Fig. 94 a difference between the i_o values obtained by the two separate methods. Nevertheless, the results from these methods were in general, in relatively close agreement with each other.

The values of i_o for Pb^{2+} deposition from 0.1M $Pb(NO_3)_2$ solutions were determined at different temperatures and a graph of $^1/T$ vs log i_o plotted to determine the activation energy for this process (see Fig. 95). The values obtained are given in Table 49.

The value for the activation energy determined in this way is 7 kJ $mole^{-1}$.

Typical values of the i_o for 0.1M $Pb(NO_3)_2$ solution with and without selected addition agents, at room temperature determined by extrapolation of the linear portion of the E vs log i curve to zero overpotential were as follows :

0.1M $Pb(NO_3)_2$	i_o = 0.016 A cm^{-2}
" + 1 gl^{-1} Pluronic L64	i_o = 0.011 A cm^{-2}
" + 1 gl^{-1} tannic acid	i_o = 0.012 A cm^{-2}
" + 1 gl^{-1} BRIJ 35	i_o = 0.016 A cm^{-2}
" + 1 gl^{-1} Triton X100	i_o = 0.017 A cm^{-2}

TABLE 49

The variation of i_o for Pb deposition from a solution of 0.1M $Pb(NO_3)_2$ + 1M KNO_3 + 0.1M HNO_3

Temperature ^oC	i_o A cm^{-2}
25	0.016
36	0.018
45	0.022
54	0.025
65	0.030

The variation in the values of i_o for solutions of 0.1M $Pb(NO_3)_2$ with different addition agents at selected temperatures are given in Table 50. The values for the non additive solution are included for comparision and the values of the activation energy for Pb^{2+} deposition calculated from these results also given in Table 50.

TABLE 50

Values of the exchange current density for Pb deposition at different temperatures for solutions 0.1M $Pb(NO_3)_2$ + 1M KNO_3 + 0.1M HNO_3 with and without selected addition agents.

All values determined by extrapotation of the linear portion of the E vs log i curve, for a Pb electrode rotated at 3000 rpm.

Temperature	Values of i_o (Acm^{-2}) for a solution of 0.1M $Pb(NO_3)_2$ plus selected additives			
^oC	No additive	Triton X100	anthraquinone-2-sulphonic acid	tannic acid
35	0.018	0.021	0.012	0.015
45	0.022	0.023	0.016	0.020
55	0.025	0.026	0.019	0.023
65	0.030	0.028	0.021	0.027
Activation energy kJ $mole^{-1}$	7	4.5	7.2	6.2

The above results should be treated with care, as they are the result of only one individual determination (in the case of additive solutions). Nevertheless, whilst not being absolute values they are believed to be representative and indicative of apparent trends.

In the case of anthraquinone-2-monosulphonic acid it can be seen that this additive has a pronounced effect on the value of i_o, with tannic acid also having a slight inhibitive effect. In the case of Triton X100 the values of i_o obtained near room temperature appear to indicate that this additive actually increases, the value of i_o from that obtained in the non additive solution.

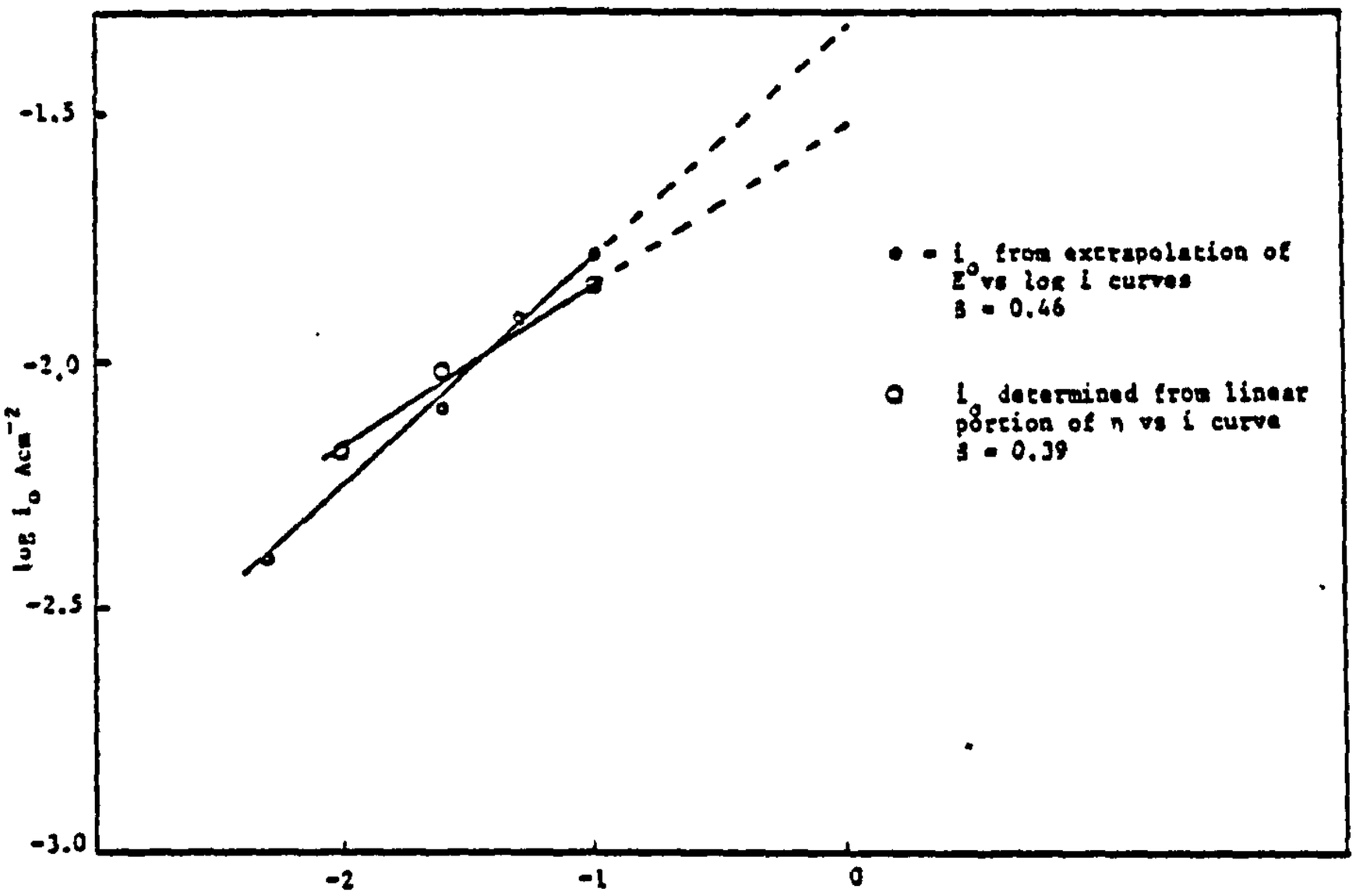

A graph of log i_o for Pb deposition versus $Pb(NO_3)_2$ concentration values of i_o determined by two different methods.

FIGURE 94

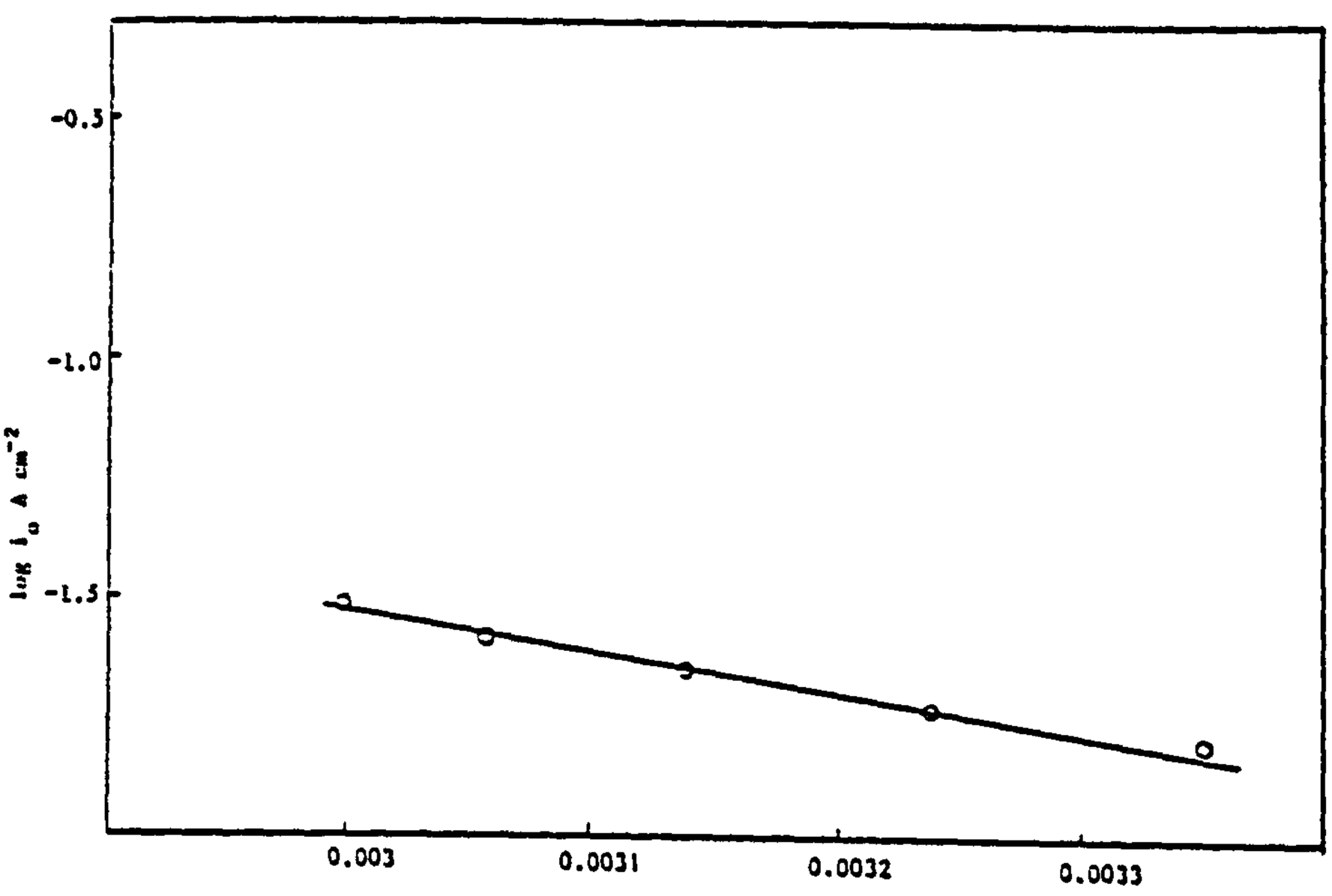

A graph of log i_o vs $^1/T$ for the electrodeposition of Pb onto a Pb electrode from a solution of 0.1M $Pb(NO_3)_2$. 1M KNO_3 plus 0.1M HNO_3 .

FIGURE 95

An interesting effect was also observed on a Pb electrode cathodically polarised in a 0.1M $Pb(NO_3)_2$ solution containing 0.1 gl^{-1} anthraquinone-2-monosulphonic acid, in that at the change over between an anodic to cathodic current, when the Pb electrode was polarised 150 mV above and below the rest potential, a narrow potential range was visible before the linear portion of the (η) vs i plot was obtained. This 'onset potential' i.e potential before a normal E vs i curve is observed was greater for this additive than any of the other additives investigated. This deviation from the expected behaviour is shown in Fig. 96. This 'onset potential' was also found to be temperature dependent e.g for anthraquinone-2-monosulphonic acid at 25°C it was 6.8 mV whilst at 46°C it was 3.3 mV.

3.2.2.6 Studies on the nitrate reduction reaction at a Pb cathode

Fig. 97 shows the polarisation characteristics for a Pb electrode polarised at a given sweep rate in a solution of 1M KNO_3, pH 3.9. A "peak" current was observed in the oxygenated solution. The rest potential for the Pb electrode was -0.275V and the pH chosen as 3.9, since it is that of the $Pb(NO_3)_2$ solution used for the production of PbO_2 from commercial plating baths.

The effect of oxygen on the polarisation characteristics of a Pb electrode in the same solution but at a different pH is also shown in Fig. 98. No peak current was observed indicating that the appearance of this peak is a function of pH, as is the magnitude of the current at a given overpotential. The higher current density in oxygenated solutions is due to both the oxygen and nitrate reduction reactions occuring at the same potential. The effect of pH on the polarisation characteristics of a Pb electrode in an oxygen free solution of 1M KNO_3 is shown in Fig. 99. This shows that an increase in pH increases the current density at a given overpotential.

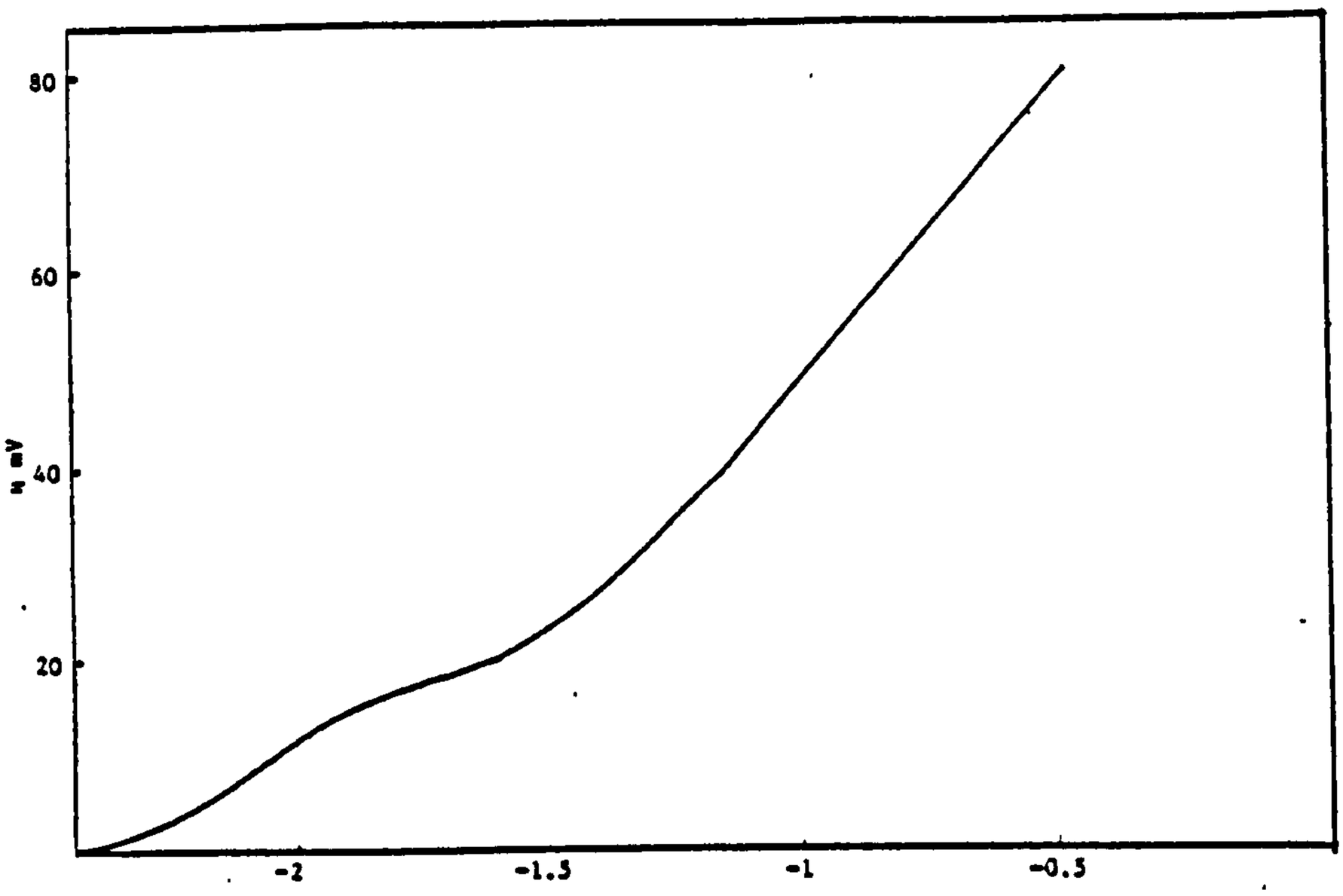

A graph of η versus log i for Pb deposition on a Pb electrode polarised at 0.5mV sec^{-1} in a solution of 0.1M $Pb(NO_3)_2$, 1M KNO_3 , 0.1M HNO_3 plus 0.1 gl^{-1} anthraquinone-2-monosulphonic acid at 25°C.

FIGURE 96

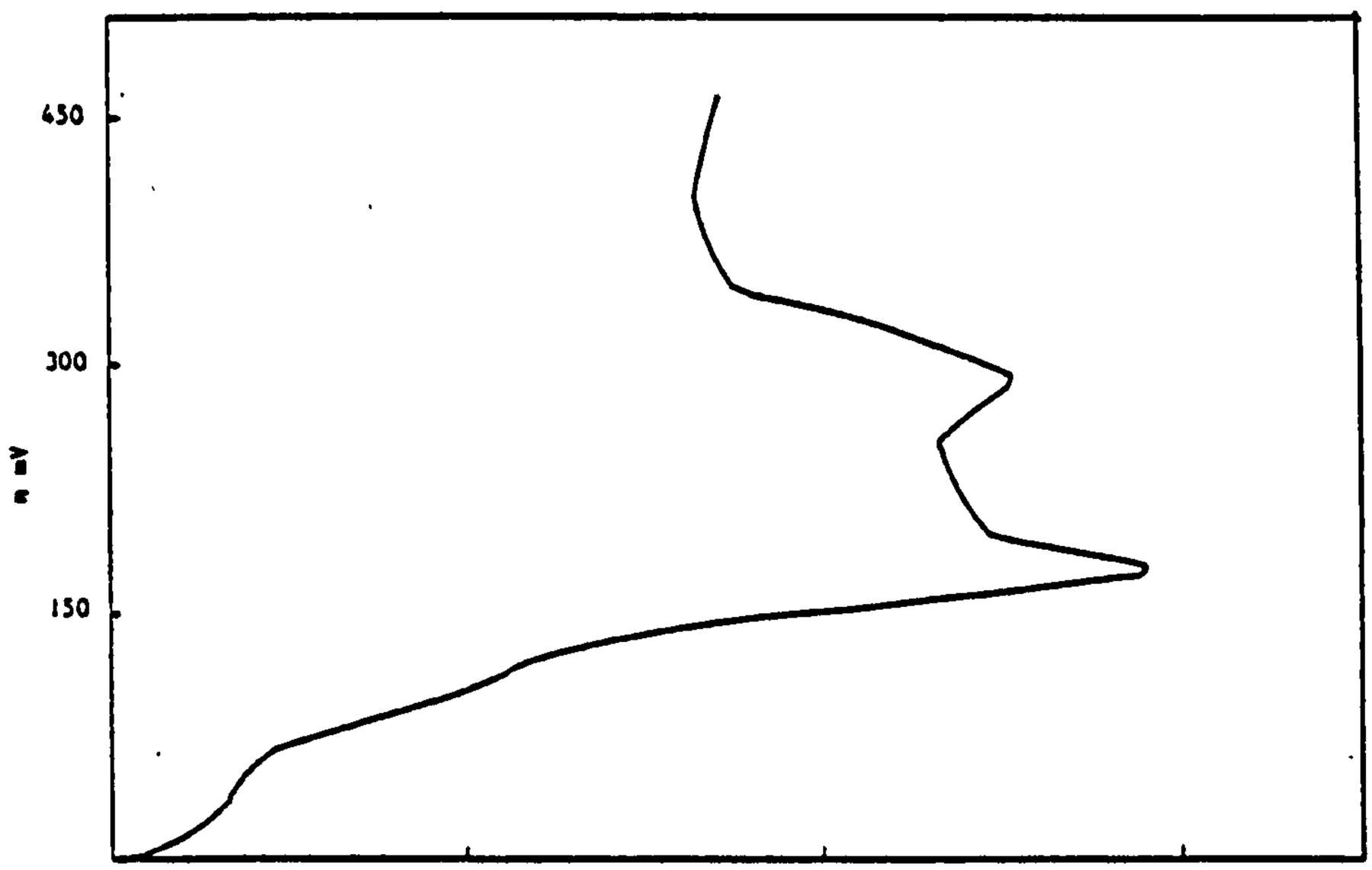

A graph of η vs i for a Pb electrode cathodically polarised at a sweep rate of 1 mV sec^{-1} in a solution of 1M KNO_3 pH 3.9. Experiment conducted at 0 RPM and in a deoxygenated solution.

FIGURE 97

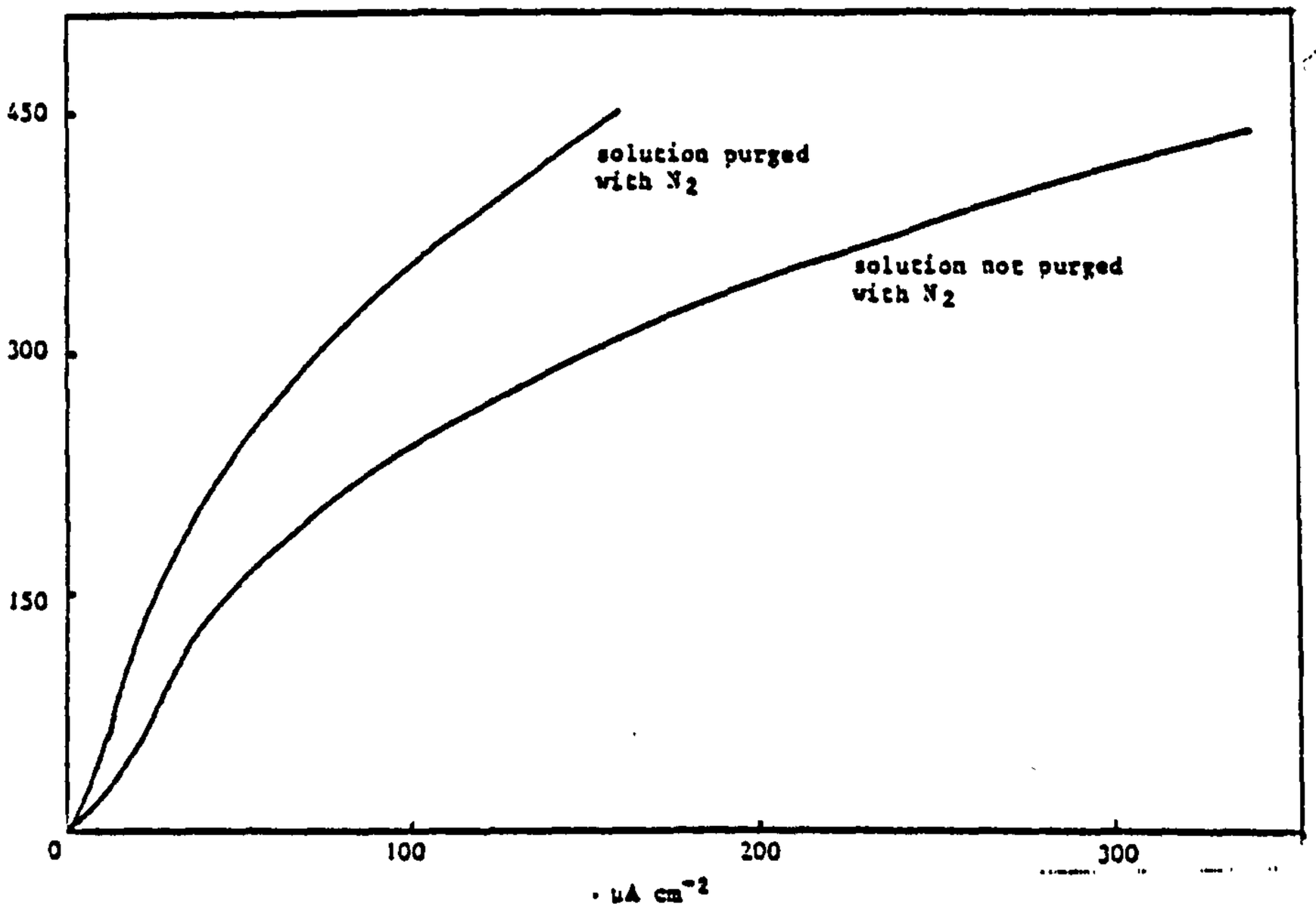

A graph of η vs i for a Pb electrode rotated at 200 RPM in a solution of 1M KNO_3 pH 2.0. The electrode polarised at a sweep rate of 1 $mV\ sec^{-1}$.

FIGURE 98

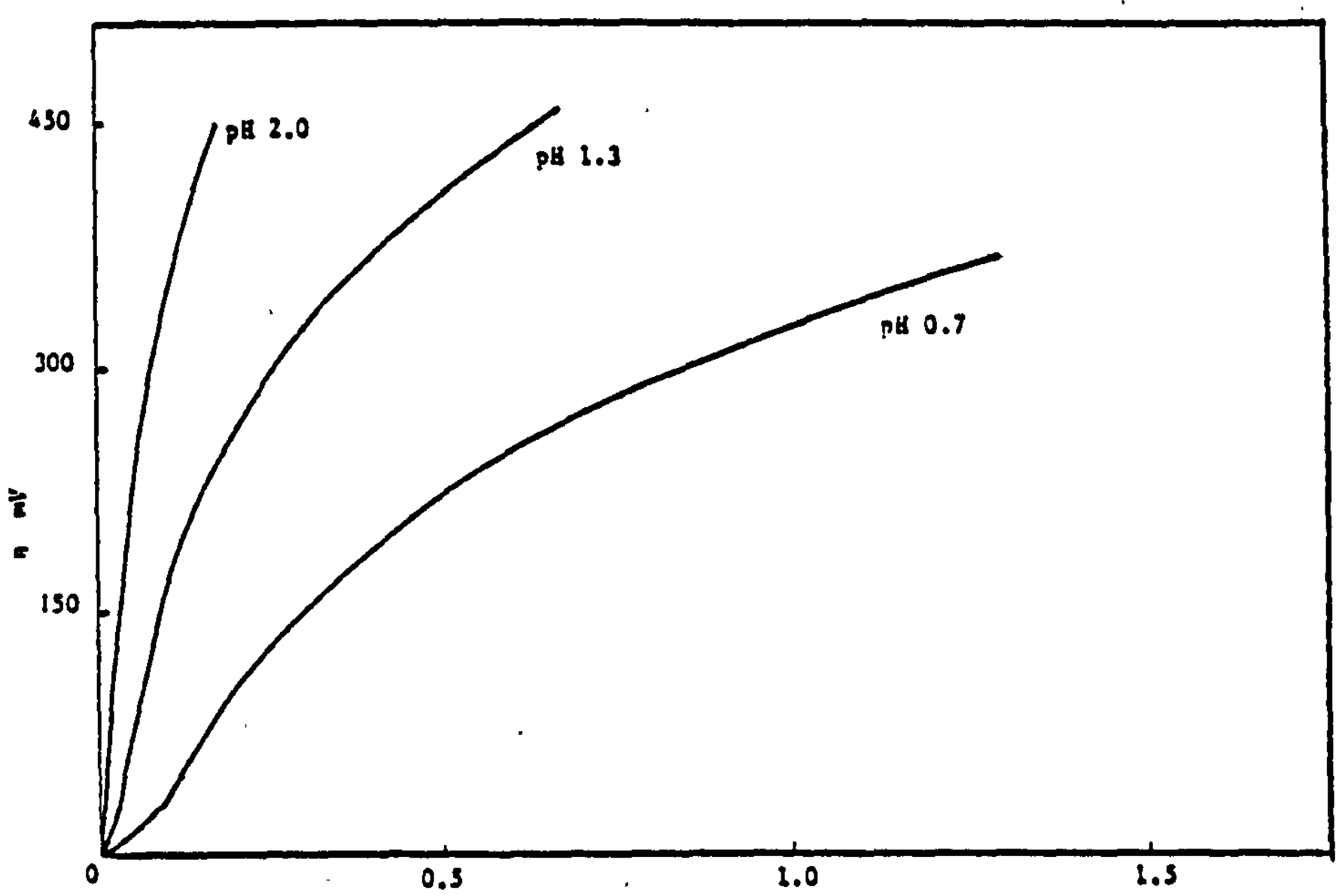

A graph of η vs i for a Pb electrode rotated at 200 RPM in a solution of 1M KNO_3 at different pH, pH adjusted with HNO_3 . The Pb electrode polarised at 1 mV sec^{-1} .

FIGURE 99

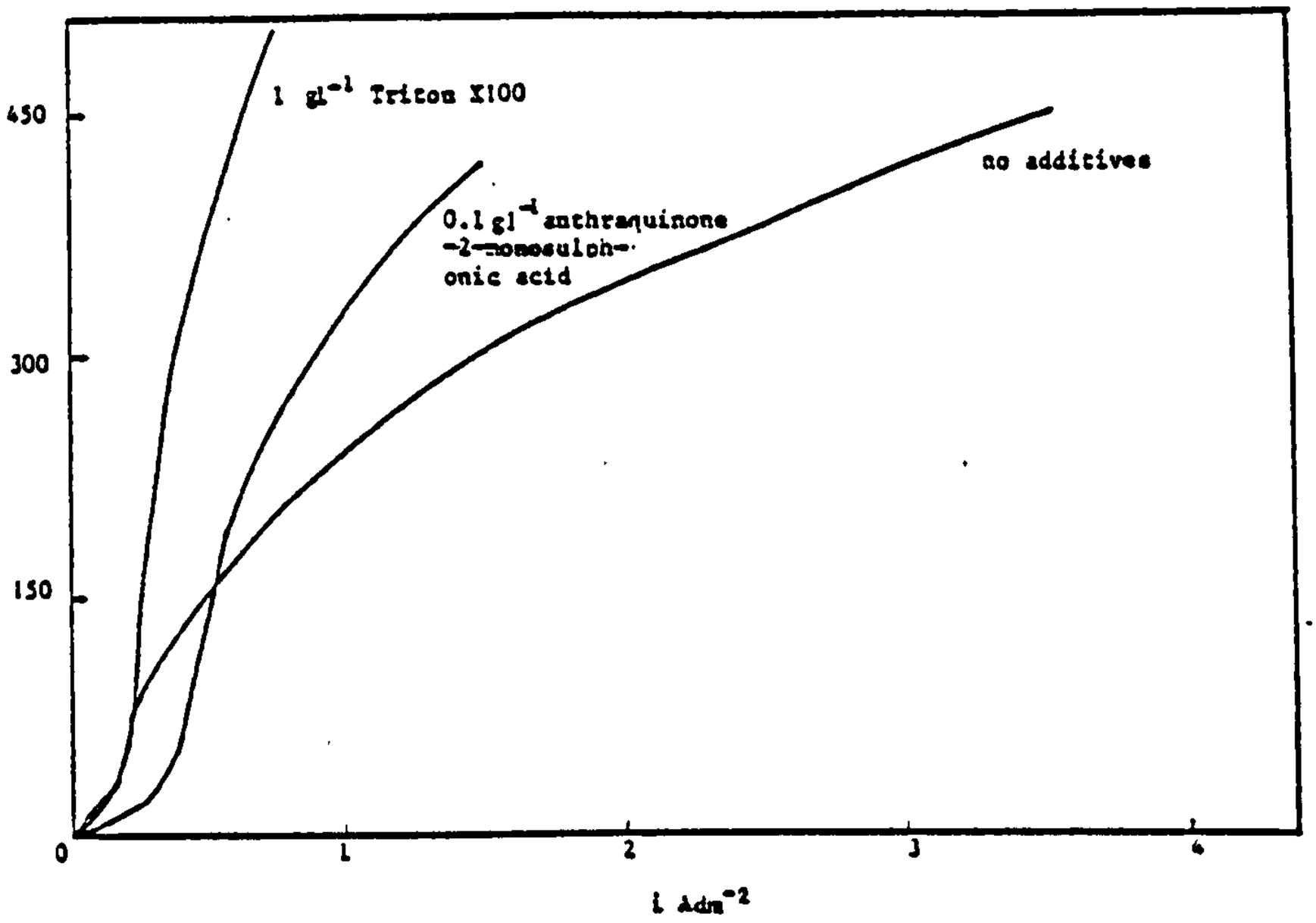

A graph of η vs i for a Pb electrode rotated at 200 RPM and polarised at a sweep rate of 1 mV sec^{-1} in a solution of 1M KNO_3 pH 2.0 with and without selected addition agents.

FIGURE 100

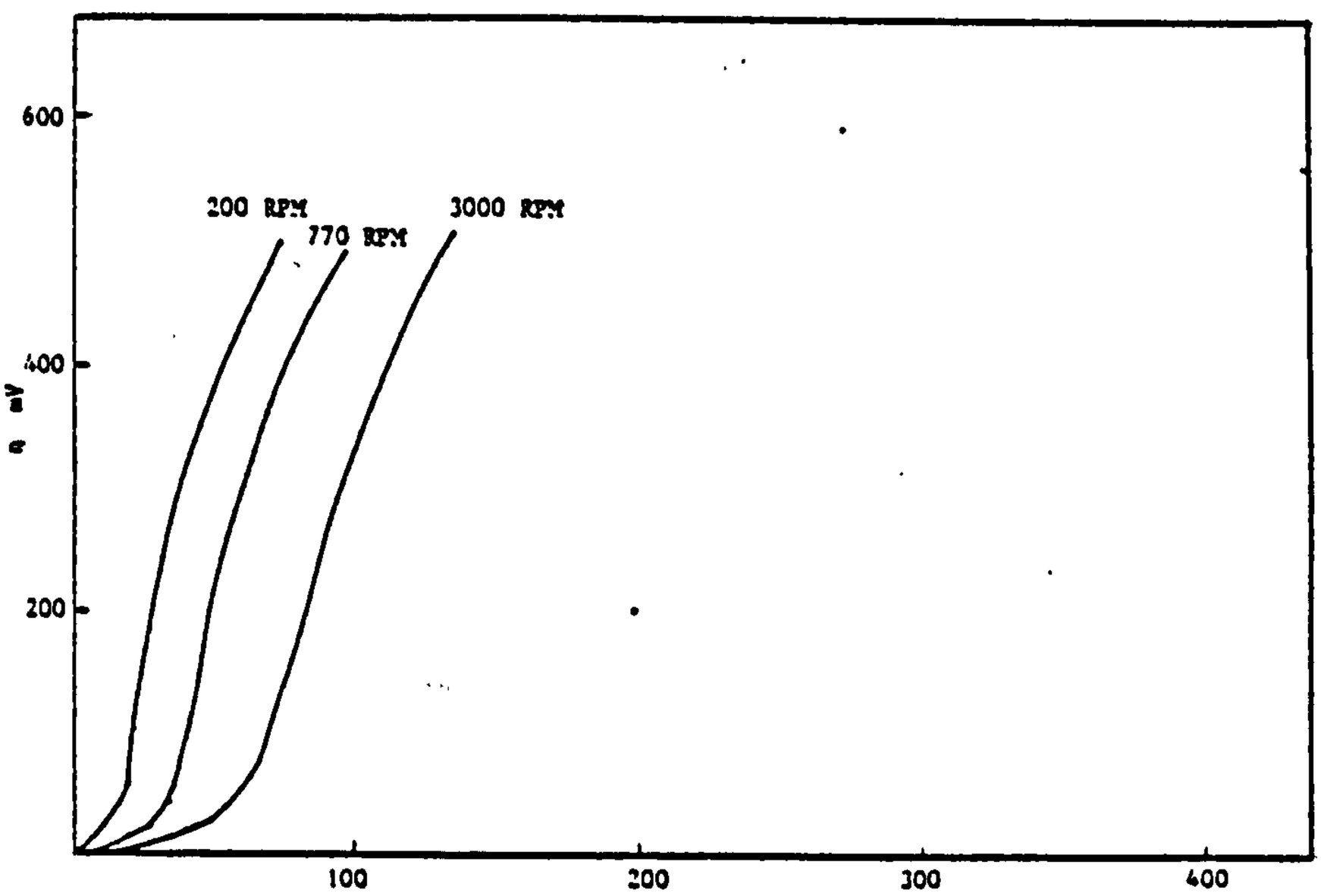

A graph of η vs i for a Pb electrode cathodically polarised at a sweep rate of 1 mV sec^{-1} in a solution of 1M KNO_3 pH 2.0 plus 1 gl^{-1} Triton X100 at different rotational speeds.

FIGURE 101

The most interesting effect was the addition of Triton X100 on the polarisation characteristics of a Pb electrode in 1M KNO_3, (Fig, 100). This additive has a pronounced inhibiting effect on both the nitrate and oxygen reduction reactions. Anthraquinone 2 sulphonic acid additions to 1M KNO_3 solutions have an inhibiting effect at high overpotentials but at low over-potentials higher c.ds. are observed than in the additive free 1M KNO_3 solutions. This may be attributed to one of two possible cathodic reactions a) reduction of the additive or b) re-deposition of dissolved Pb^{2+}.

The rest potentials adopted by a Pb electrode immersed in 1M KNO_3 and 1M KNO_3 + 1 gl^{-1} Triton X100 was - 0.265V whilst in 1M KNO_3 + 1 gl^{-1} anthraquinone-2-sulphonic acid the value was -0.280V.

The effect of rotational speed on the polarisation curves for nitrate reduction in an oxygenated solution of 1M KNO_3, pH 2.0 plus 1 gl^{-1} Triton X100 is shown in Fig. 101. The effect of rotational speed in the non additive case is not so marked. In general it was observed that in the high pH solutions rotational speed had a greater effect than in the low pH solutions, and at pH 0.7 it hardly had any effect over the ranges studied (200 rpm and 770 rpm). Fig. 102 shows the effect of rotational speed on the polarisation characteristics of a 1M KNO_3 solution pH 2.9

These results show how small the nitrate reduction current is in comparison to the Pb^{2+} reduction process.

3.2.3 Cyclic voltammetry studies on Pb deposition from $Pb(NO_3)_2$

The reduction of Pb^{2+} in nitrate solutions, with and without selected addition agents was investigated using cyclic voltammetry, the aim of which was to supplement electrochemical studies carried out using other techniques.

A detailed theoretical analysis of the results obtained using this technique is complicated by the rapidly changing nature of the electrode surface, as a result of the formation of dendritic deposits of Pb.

The voltammograms obtained for some of the additive and non additive containing solutions are given in Figs. 103 to 110.

Fig. 103 shows the voltammogram for an additive-free 0.1M $Pb(NO_3)_2$ solution and a peak current (i_p) due to the diffusion limited supply of Pb^{2+} is observed at a potential (E_p), followed by a rapidily rising current due to the production of Pb dendrites which were clearly visible at the surface of the Pt electrode, after each scan at low sweep speeds. The tendency towards dendritic growth is also clearly exhibited with solutions containing 1 gl^{-1} butyne 1,4 diol (Fig. 104), 1 gl^{-1} Wafex (Fig. 105) and 0.1 gl^{-1} anthraquinone-2-monosulphonic acid (Fig. 106). The tendency towards dendritic growth is more pronounced at low sweep speeds (20 mV sec^{-1}) since insufficient charge passes at high sweep speeds to enable large dendrites to form.

The nature of the voltammograms obtained for Pb deposition from the stock solution containing either 1 gl^{-1} BRIJ 35, 1 gl^{-1} Triton X100 or 1 gl^{-1} tannic acid (Figs. 107 to 109) are all similar in appearance. The diffusion limited supply of Pb is visible at high sweep speeds and only at low sweep speeds is there a rising current indicating dendritic growth.

Other additive containing solutions were also investigated in this way with the exact appearance of the voltammogram dependent upon the particular additive under investigation.

In the case of a reversible deposition process, the value of E_p should be independent of sweep rate, with the value of $E_p - E_{p/2} = 0.056.5/n$ ($E_{p/2}$ is the potential at 1/2 the peak height). In the present studies the values of E_p and $E_{p/2}$ were found to vary with sweep rate, and typical values for both additive and non-additive solutions are given in Tables 53 to 55.

For an irreversible process the value of E_p is dependent upon the logarithm of the sweep rate (v). A plot of E_p vs log v for two additive-containing solutions is shown in Fig. 110. This plot deviates from linearity at high sweep rates. A plot of E_p vs $v^{1/2}$ for the same solutions was however found to be linear over the sweep speed range studied i.e up to 140mV sec^{-1} (see Fig. 111), for solutions of 0.1 M $Pb(NO_3)_2$ containing different additives. At sweep rates greater than 100 mV sec^{-1} for the non additive containing solutions and 140 mV for additive containing solutions the plot deviates from linearity. Values of E_o for certain solutions obtained by extrapolation of the E_p vs $v^{1/2}$ plots to zero sweep rate (see Fig. 111) are given in Table 51.

TABLE 51

Values of E^o for solutions of 0.1M $Pb(NO_3)_2$ containing different addition agents

Solution	E^o Volts
0.1M $Pb(NO_3)_2$	-0.275
" " + 1 gl^{-1} butyne 1,4 diol	-0.228
" " + 1 gl^{-1} BRIJ 35	-0.242
" " + 1 gl^{-1} Triton X100	-0.248
" " + 1 gl^{-1} Pluronic L64	-0.238

The test for reversibility of metal deposition used by Berzins and Delahay (311) is to plot E vs log $(i_p - i)$ which should approach linerarity over the range 0.5-0.9 i_p and be of a slope 2.2nF/RT; such a plot is shown in Figs. 112 and 113.

The slope of E vs log $(i_p - i)$ for 0.1M $Pb(NO_3)_2$ polarised at 20 mV sec^{-1}, over the range 0.5 to 0.9p was found to be 14.2 which results in a value of n of 0.17, whilst a similar plot of results obtained at 100 mV sec^{-1} yields a value for n of 0.14. These low values for n indicate that this method of analysis does not apply to this particular system.

The plots of i_p vs $v^{1/2}$ for 0.1M $Pb(NO_3)_2$ solutions containing selected addition agents are essentially linear (see Figs. 114 to 115) and enable the apparent diffusion coefficient for Pb^{2+} to be calculated.

In the case of three-dimensional growth of electrodeposits the relationship between peak current and sweep rate is given by :

$$i_p = 3.67 \times 10^5 \; n^{3/2} \; D^{1/2} \; v^{1/2} \; C^b_{M+}$$

in which the symbols have already been defined.

A plot of i_p vs $v^{1/2}$ will enable D to be calculated, provided all the other parameters are known. The values of D for certain additive-containing solutions determined in this way are listed in Table 52.

The value for the exchange current density for Pb deposition in non-agitated solutions at a sweep rate of 140 mV sec^{-1} from a non additive solution was 0.015 Acm^{-2} whilst at 20 mV sec^{-1} a value of 0.004 Acm^{-2} was recorded.

TABLE 52

Values of diffusion coefficient for Pb^{2+} in 0.1M $Pb(NO_3)_2$ solutions containing selected addition agents at 25°C

Solution of 0.1M $Pb(NO_3)_2$ + 1M KNO_3 + 0.1M HNO_3	Diffusion Coefficient for Pb^{2+} $cm^2\ sec^{-1}$
No addition agent	7.2×10^{-7}
$1gl^{-1}$ tannic acid	9.7×10^{-7}
$1gl^{-1}$ butyne 1,4 diol	1.0×10^{-6}
$1gl^{-1}$ Pluronic L64	1.12×10^{-6}
$1gl^{-1}$ BRIJ 35	1.57×10^{-6}
$1gl^{-1}$ Triton X100	1.67×10^{-6}

TABLE 53

"Selected parameters obtained from cyclic voltammetry studies on Pb deposition from 0.1M $Pb(NO_3)_2$ solutions with and without addition agents"

1) 0.1M $Pb(NO_3)_2$ + 1M KNO_3 + 0.1M HNO_3 without any addition agents

E_p Volts	$Ep_{/2}$ Volts	$E_p - Ep_{/2}$ Volts	i_{P_2} Adm^2	V $V\ sec^{-1}$	$v^{1/2}$ sec^{-1}
0.325	0.252	0.073	2.24	0.010	0.1
0.330	0.253	0.077	2.17	0.020	0.141
0.360	0.268	0.092	2.83	0.050	0.224
0.400	0.283	0.117	3.57	0.100	0.314
0.512	0.315	0.197	5.04	0.140	0.374

NB. E_p was not always clearly definable.

TABLE 54

2) 0.1M $Pb(NO_3)_2$ + 1M KNO_3 + 0.1M HNO_3 + 1 gl^{-1} butyne 1,4 diol

E_p Volts	$Ep_{/2}$ Volts	$E_p - Ep_{/2}$ Volts	i_{P_2} Adm^2	V V sec^{-1}	$v^{1/2}$ sec^{-1}
0.280	0.233	0.047	2.06	0.010	0.1
0.294	0.240	0.054	2.57	0.020	0.141
0.318	0.253	0.065	3.42	0.050	0.224
0.345	0.263	0.082	4.26	0.100	0.314
0.375	0.279	0.096	5.0	0.140	0.374

TABLE 55

3) 0.1M $Pb(NO_3)_2$ + 1M KNO_3 + 0.1M HNO_3 + 1 gl^{-1} Triton X100

E_p Volts	$Ep_{/2}$ Volts	$E_p - Ep_{/2}$ Volts	i_{p} Adm^{-2}	V V sec^{-1}	$v^{1/2}$ sec^{-1}
0.280	0.252	0.028	2.21	0.010	0.1
0.305			2.72	0.020	0.141
0.325	0.285	0.040	3.82	0.050	0.224
0.340	0.289	0.051	4.48	0.075	0.274
0.363	0.303	0.060	5.33	0.100	0.316
0.386	0.315	0.071	5.81	0.141	0.374

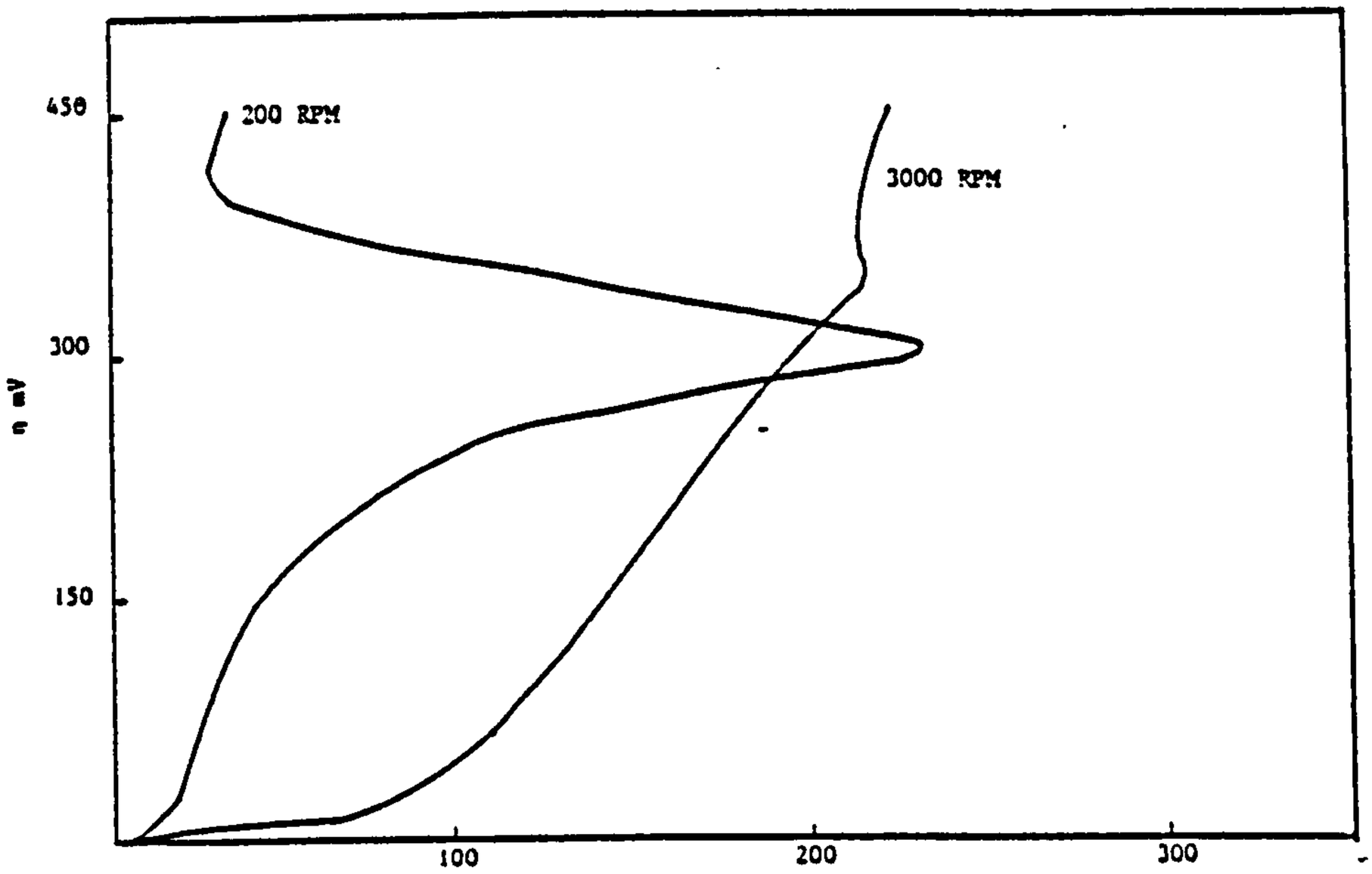

A graph of η vs i for a Pb electrode cathodically polarised at 1 mV sec from rest potential in a solution of 1M KNO_3 pH 2.9, the solution not purged with nitrogen prior to polarisation.

FIGURE 102

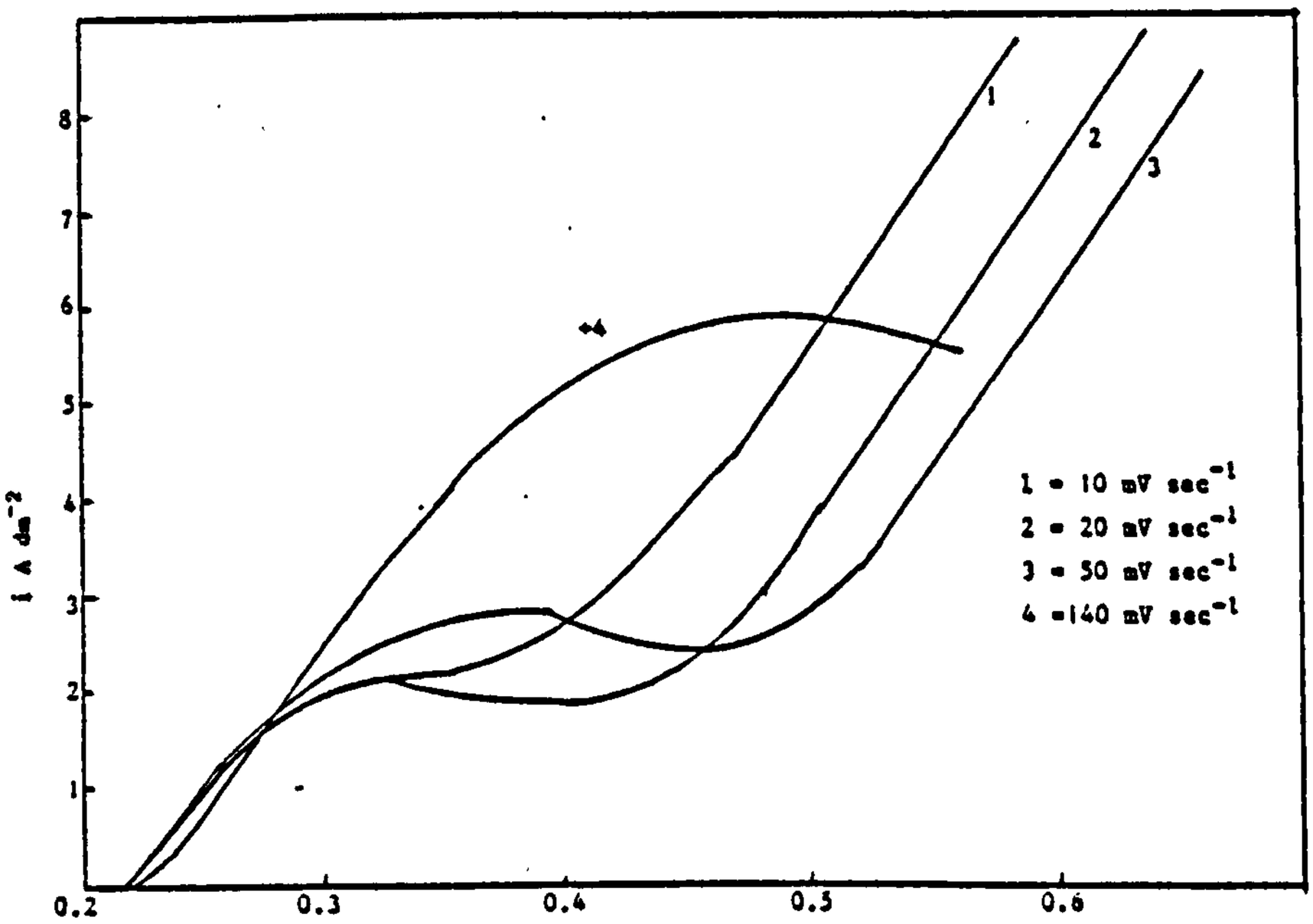

E vs i curves for a Pt electrode cathodically polarised at a different sweep rate in a solution of 0.1M $Pb(NO_3)_2$, 1M KNO_3 , 0.1M HNO_3 without any addition agents.

FIGURE 103

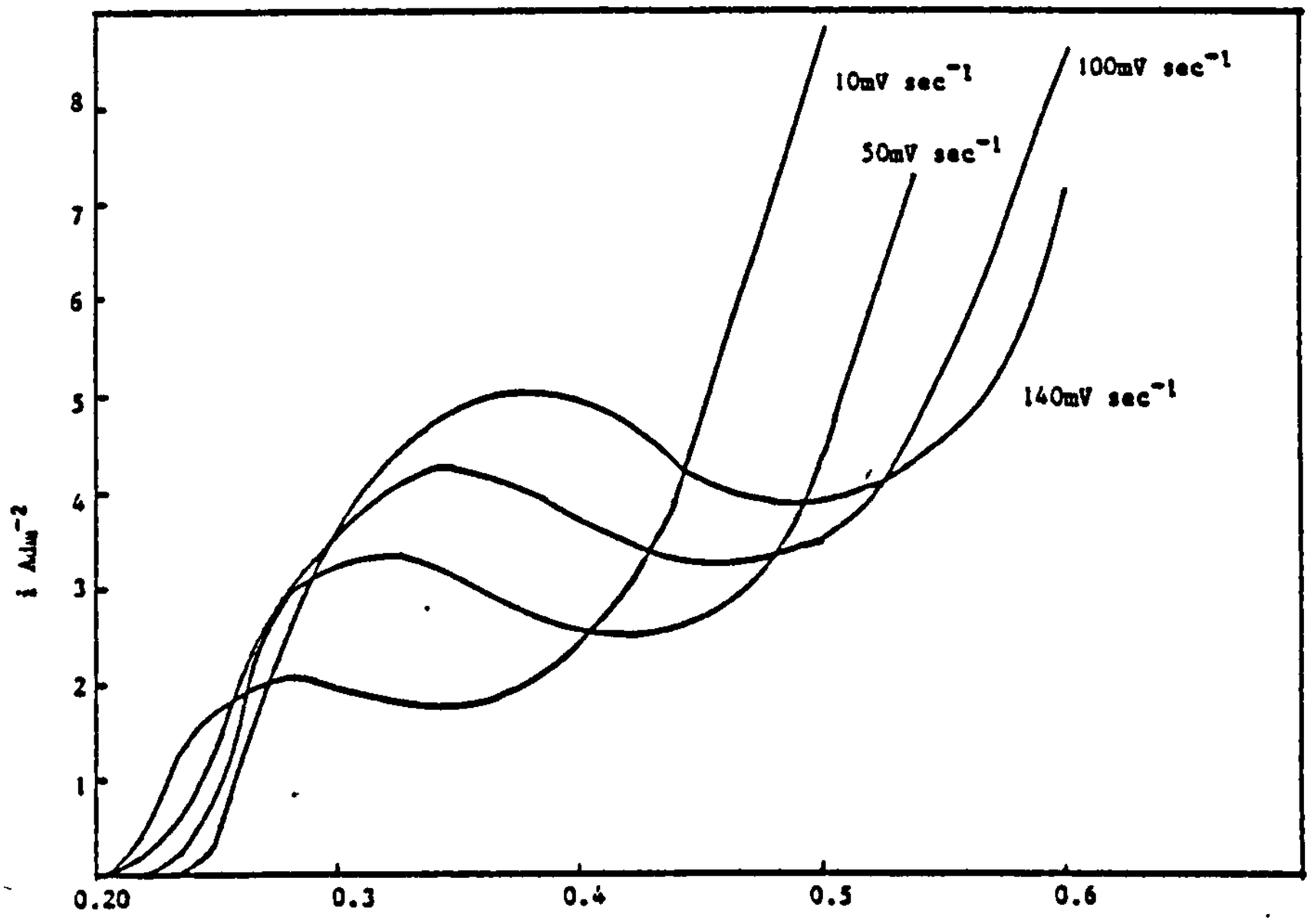

E vs i curves for a Pt electrode cathodically polarised at different sweep rates in a solution of 0.1M $Pb(NO_3)_2$,1M KNO_3, 0.1M HNO_3 plus 1 gl^{-1} butyne 1,4 diol.

FIGURE 104

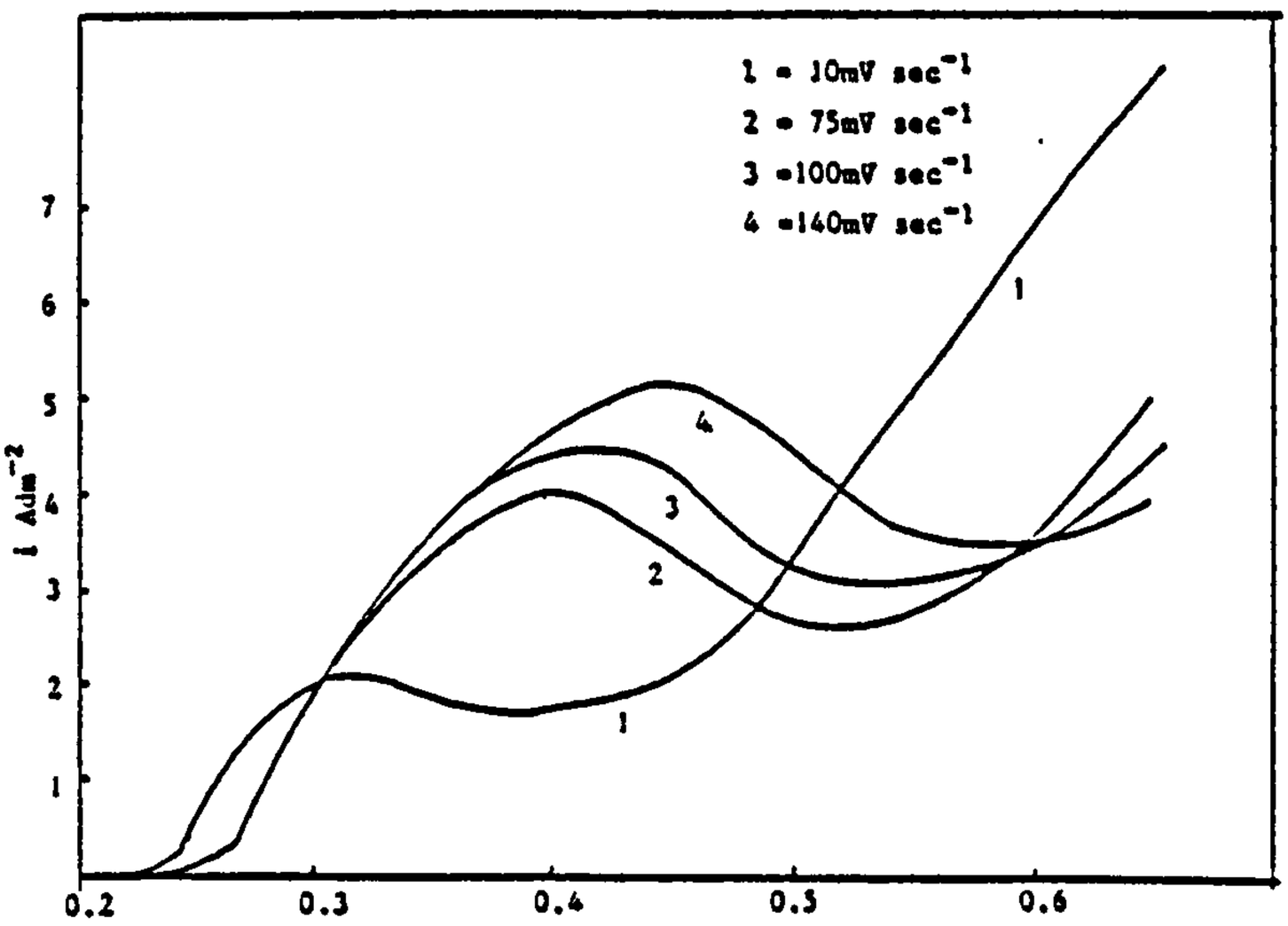

E vs i curves for a Pt electrode cathodically polarised at different sweep rates in a solution of 0.1M $Pb(NO_3)_2$, 1M KNO_3 , 0.1M HNO_3 plus 1 gl^{-1} Hafex.

FIGURE 105

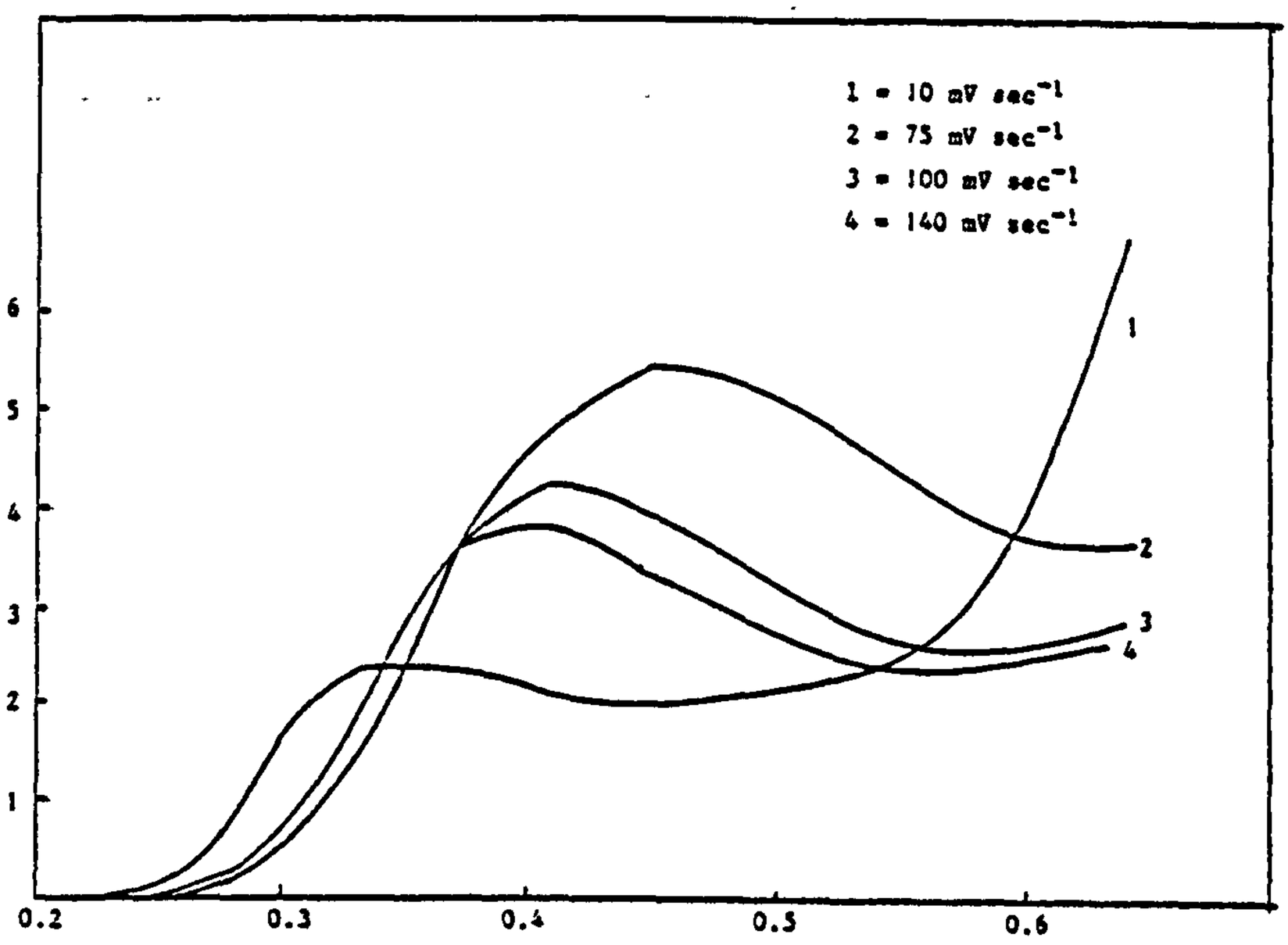

E vs i curves for a Pt electrode cathodically polarised at different sweep rates in a solution of 0.1M $Pb(NO_3)_2$, 1M KNO_3 , 0.1M HNO_3 plus 0.1 gl^{-1} anthraquinone monosulphonic acid.

FIGURE 106

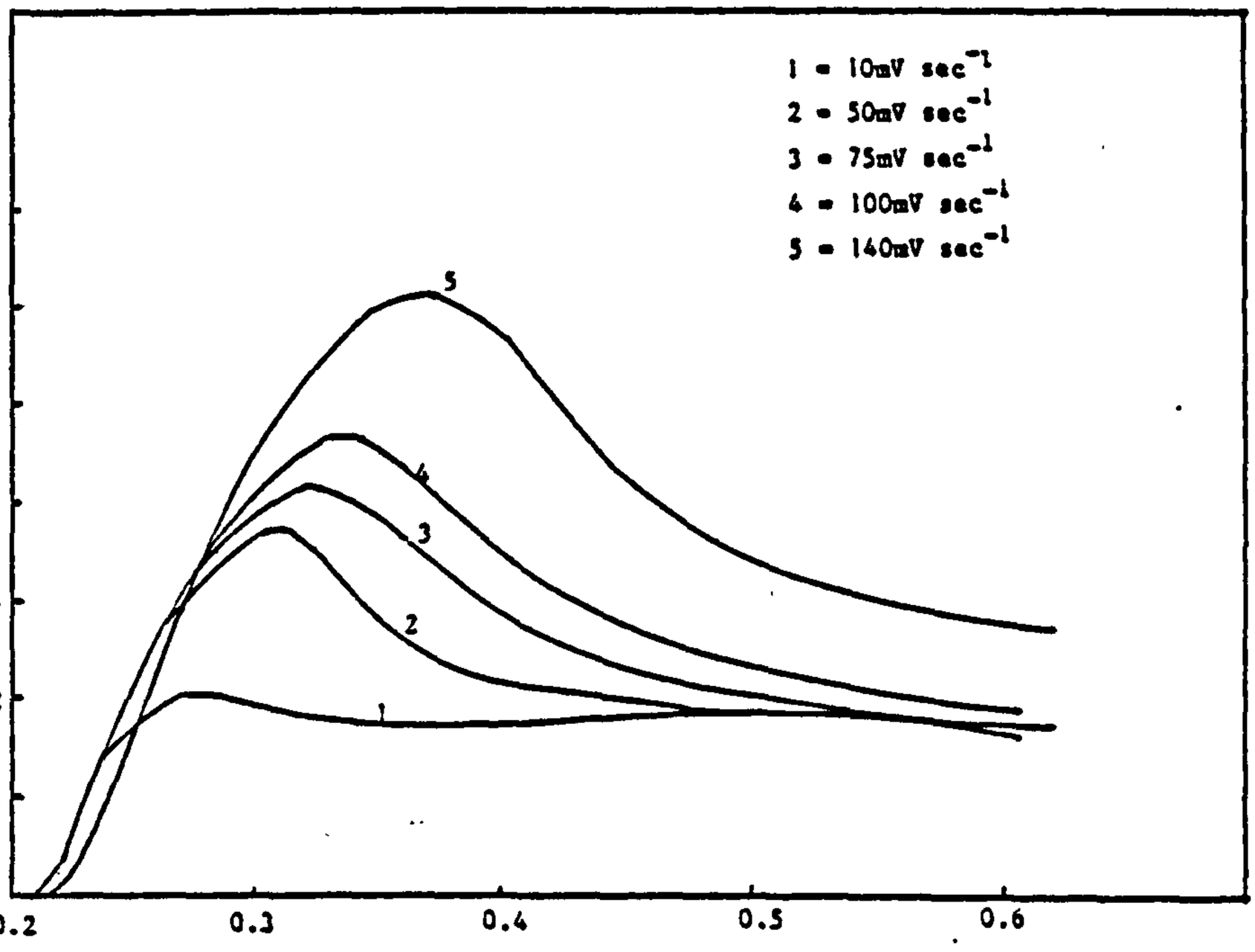

A graph of E vs i for a Pt electrode cathodically polarised at different sweep rates in a solution of 0.1M $Pb(NO_3)_2$, 1M KNO_3, 0.1M HNO_3 plus 1 gl^{-1} BRIJ 35.

FIGURE 107

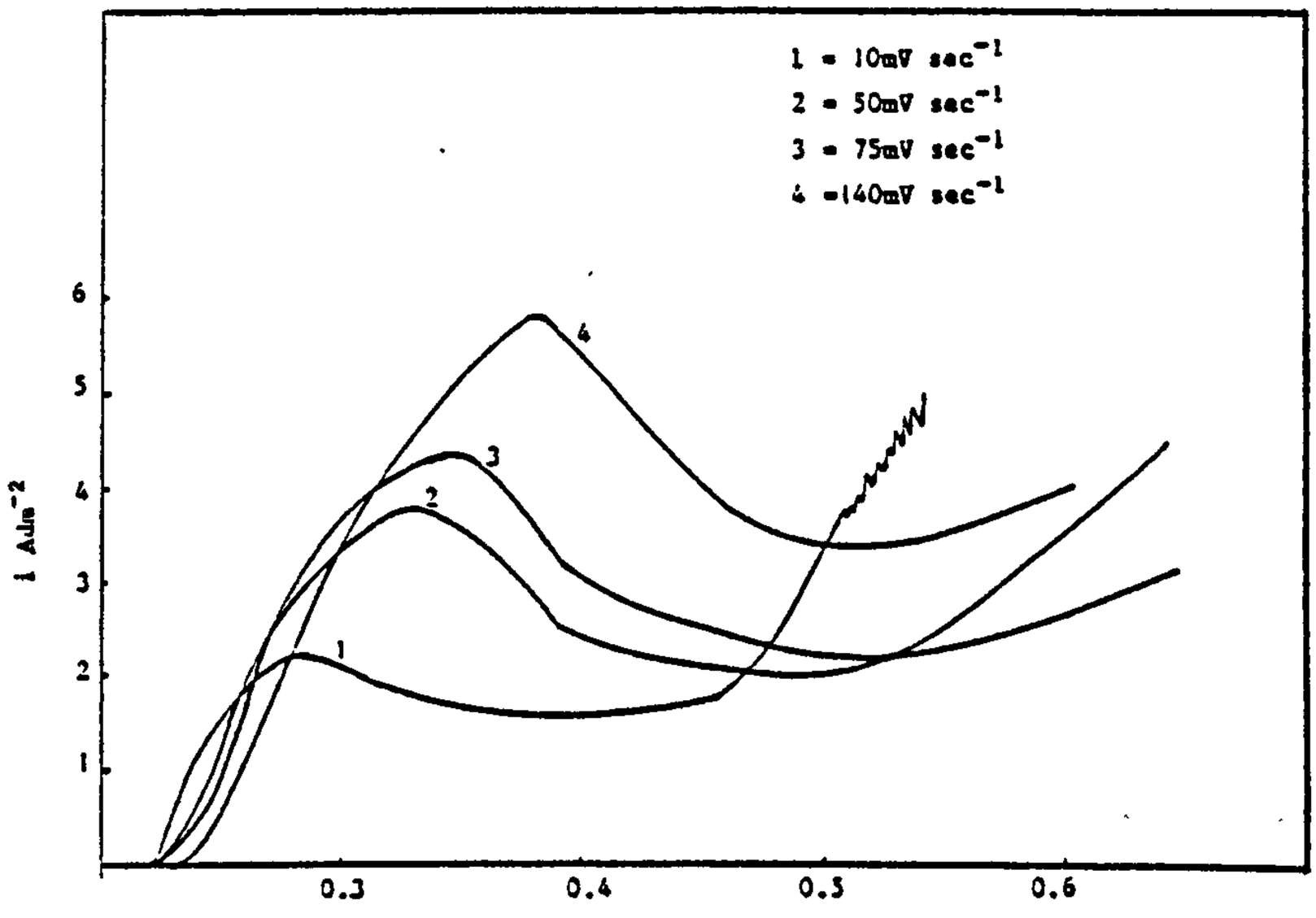

E vs i curve for a Pt electrode cathodically polarised in a solution of 0.1M $Pb(NO_3)_2$, 1M KNO_3 , 0.1M HNO_3 plus $1gl^{-1}$ Triton X100 at different sweep rates.

FIGURE 108

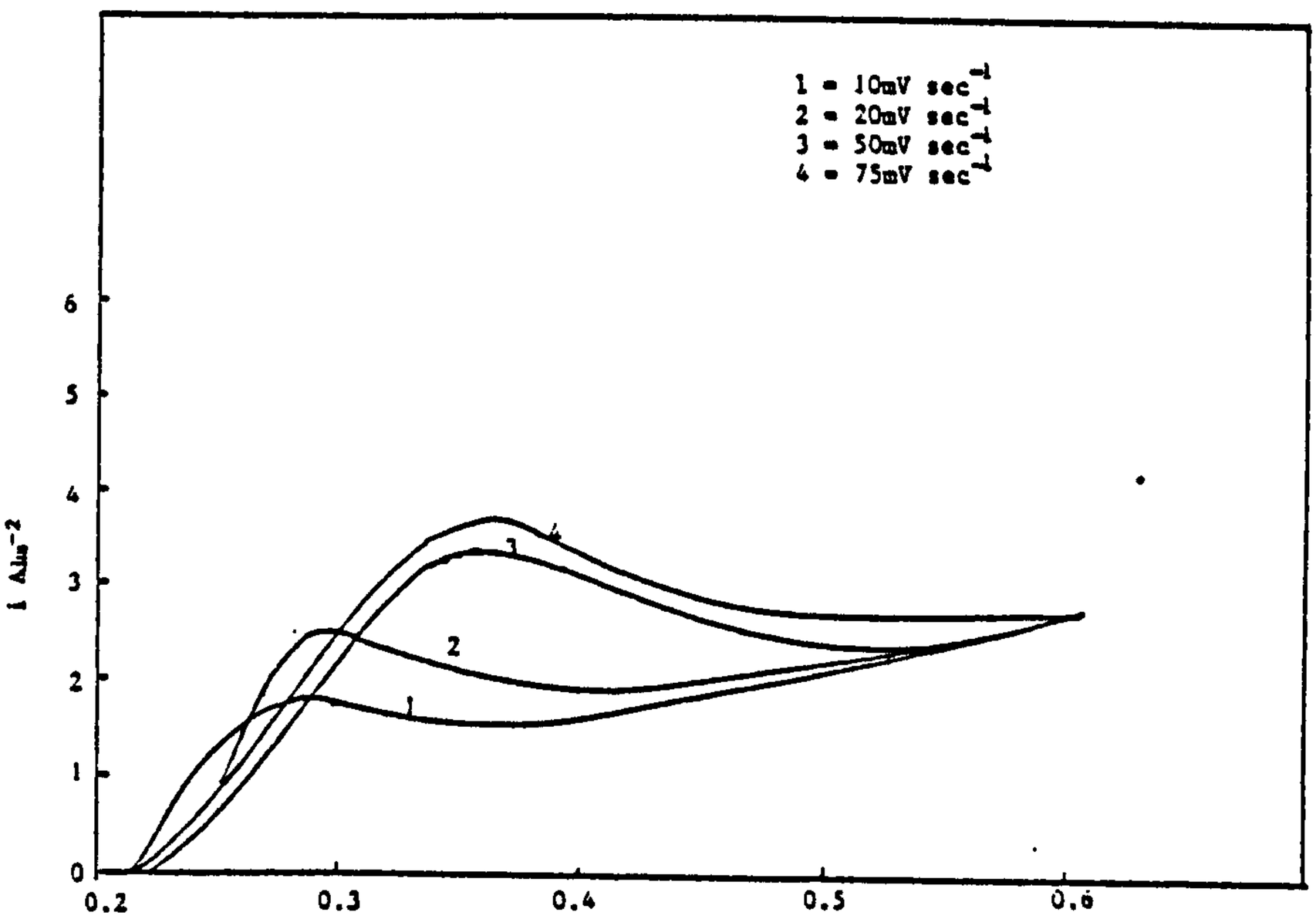

E vs i curves for a Pt electrode cathodically polarised at different sweep rates in a solution of 0.1M $Pb(NO_3)_2$, 1M KNO_3 , 0.1M HNO_3 plus 1 gl^{-1} tannic acid.

FIGURE 109

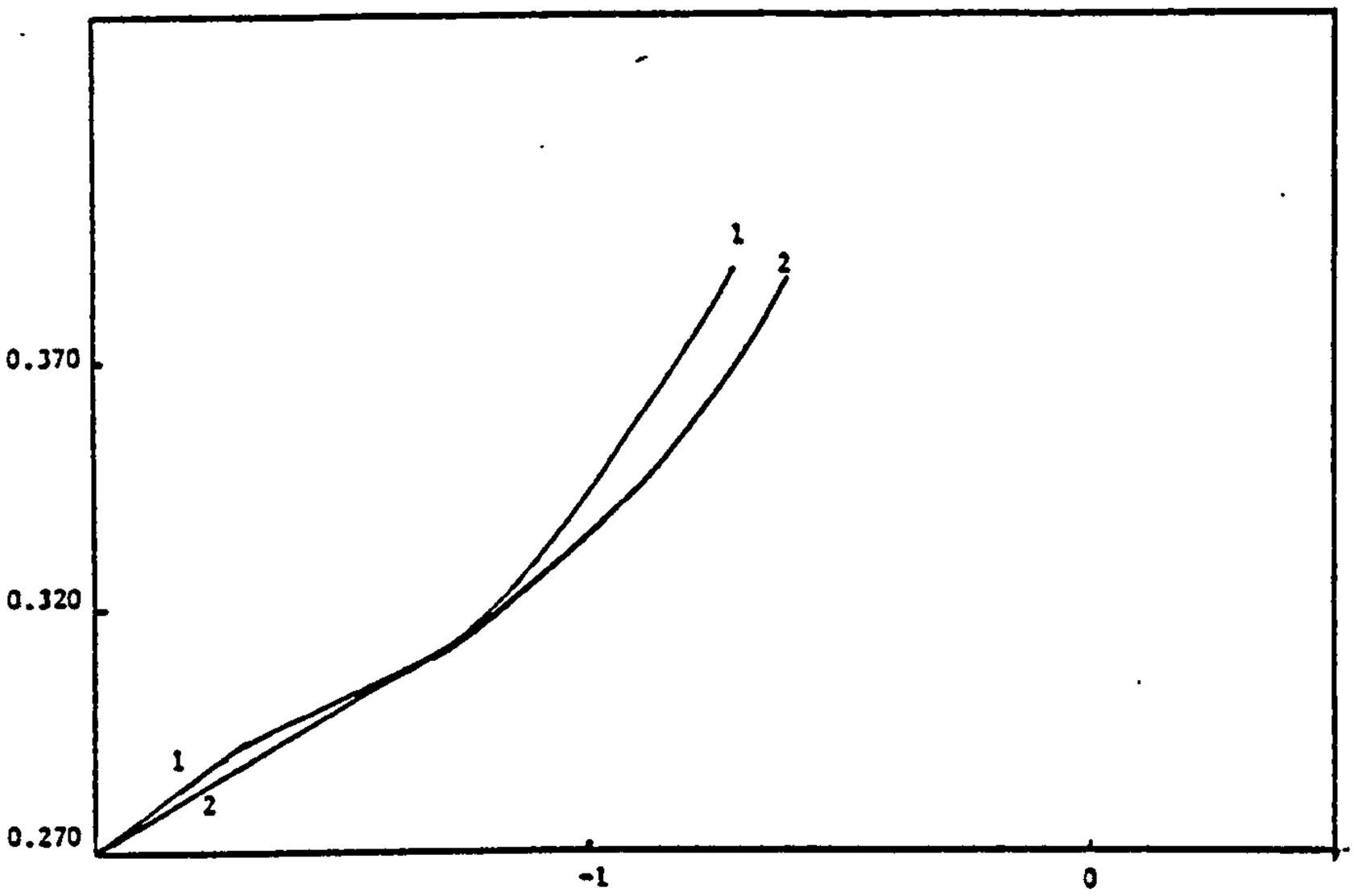

A graph of E_p vs log V for Pb deposition onto a Pt electrode from a stock solution of 0.1M $Pb(NO_3)_2$, 1M KNO_3 , 0.1M HNO_3 plus different surface active agents.

1 = stock solution plus 1 gl^{-1} Pluronic L64.
2 = stock solution plus 1 gl^{-1} BRIJ 35.

FIGURE 110

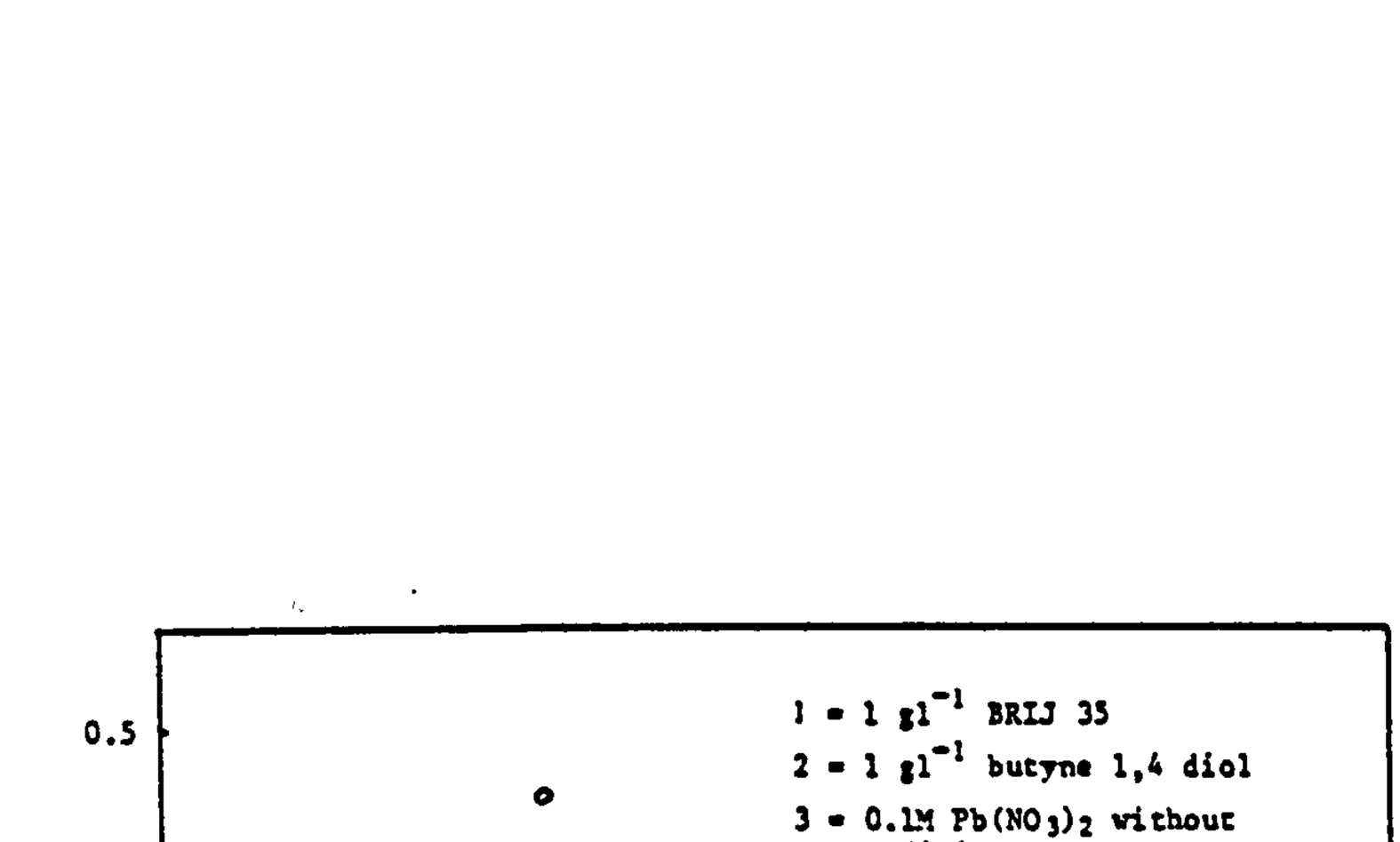

A graph of E_p versus $v^{\frac{1}{2}}$ (sweep rate)$^{\frac{1}{2}}$ from a Pt electrode cathodically polarised in a solution of 0.1M $Pb(NO_3)_2$ + 1M KNO_3 + 0.1M HNO_3 containing selected addition agents.

FIGURE 111

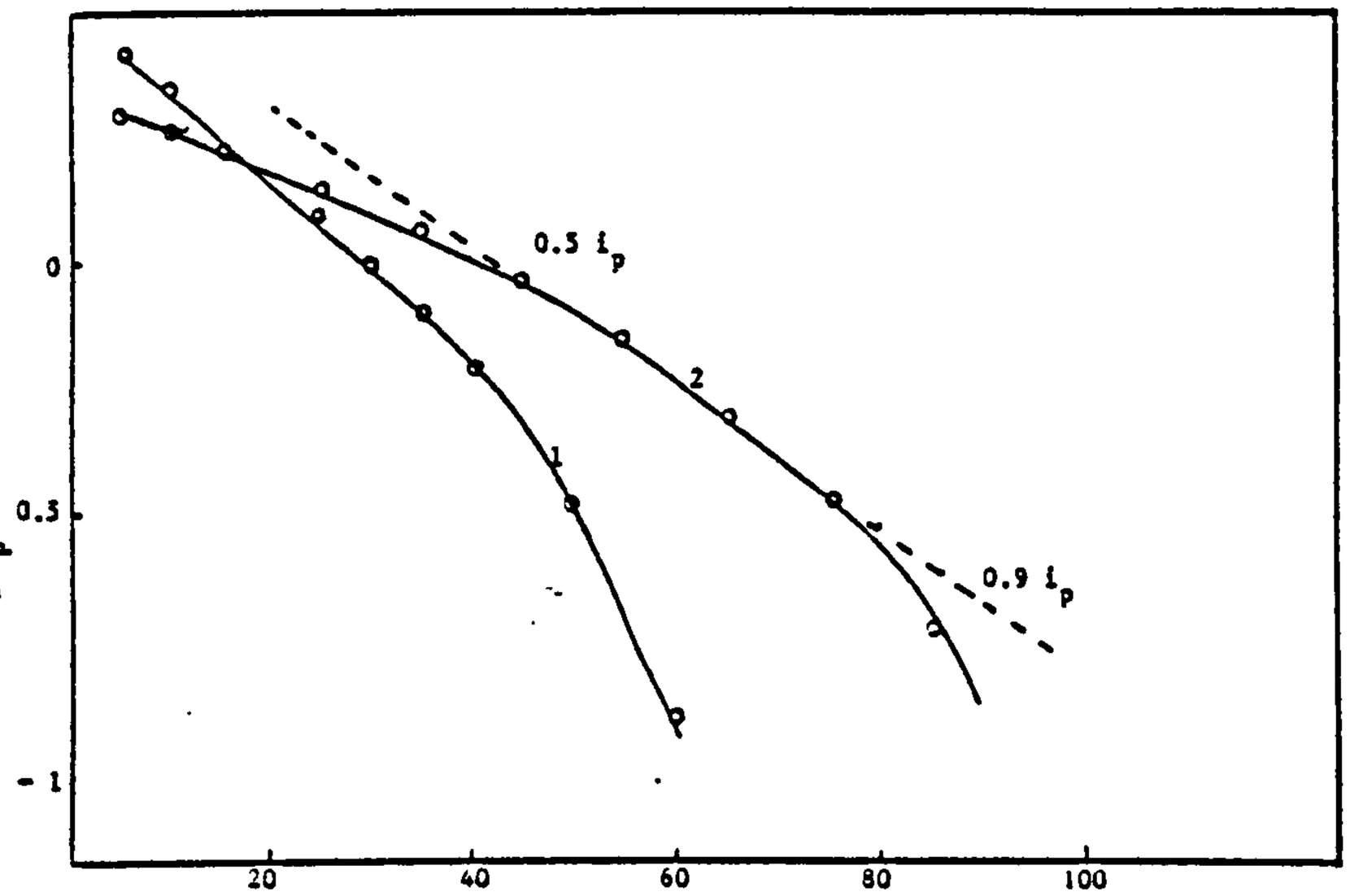

A plot of i_p - i vs η for the electrodeposition of Pb onto a Pt electrode, at a sweep rate of 20 mV sec^{-1} from a stock solution of 0.1M $Pb(NO_3)_2$, 1M KNO_3 , 0.1M HNO_3 , with and without 1 gl^{-1} BRIJ 35.

1 = curve with 1 gl^{-1} BRIJ 35 2 = curve for stock solution without BRIJ 35.

FIGURE 112

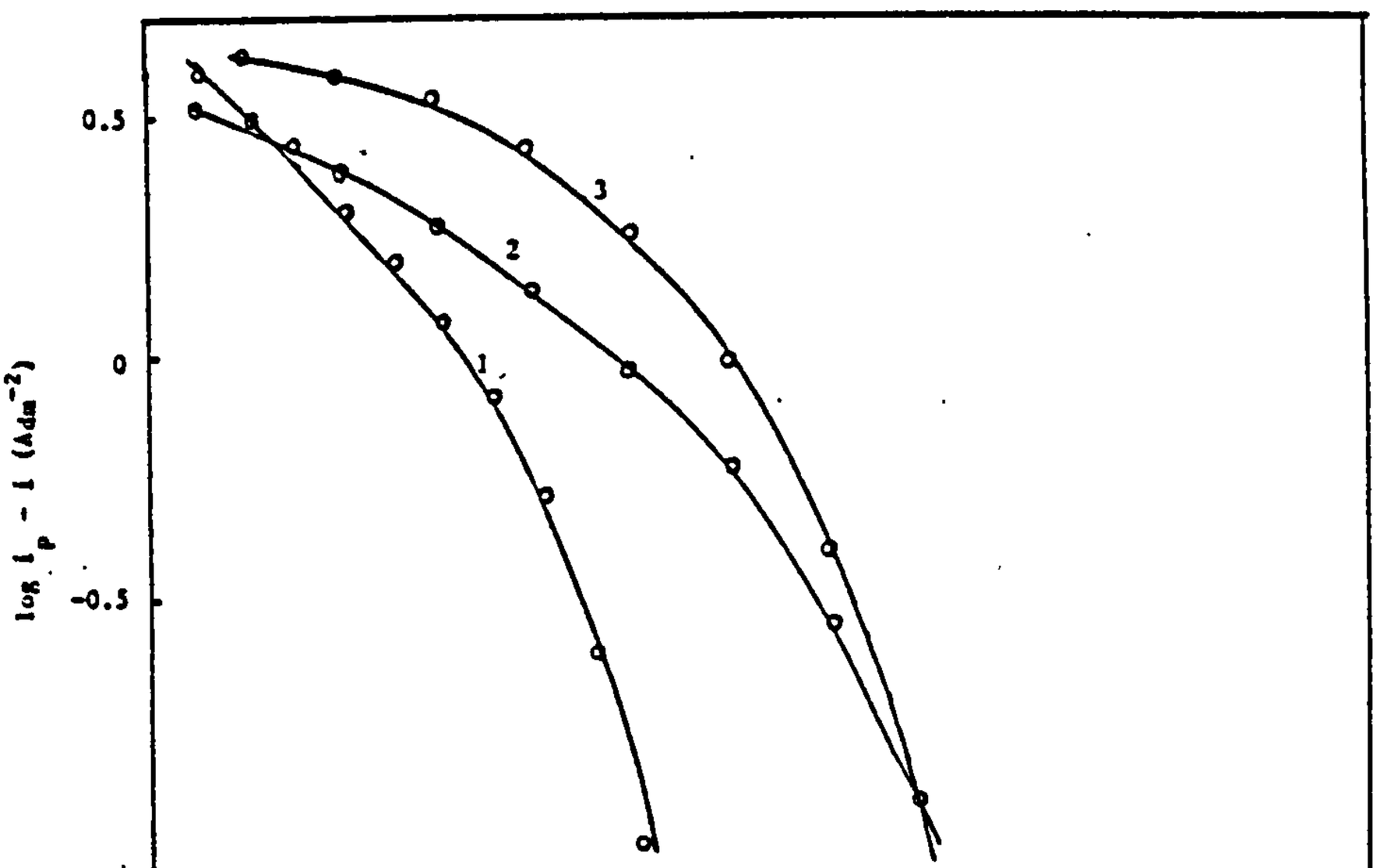

A graph of log i_p - i vs η for the electrodeposition of Pb onto a Pt electrode at a sweep rate of 100 mV sec^{-1} from a stock solution of 0.1M $Pb(NO_3)_2$, 1M KNO_3 , 0.1M HNO with and without selected addition agents.

1 = stock solution plus 1 gl^{-1} BRIJ 35
2 = stock solution without addition agents
3 = stock solution plus 0.1 gl^{-1} anthraquinone-2- monosulphonic acid.

FIGURE 113

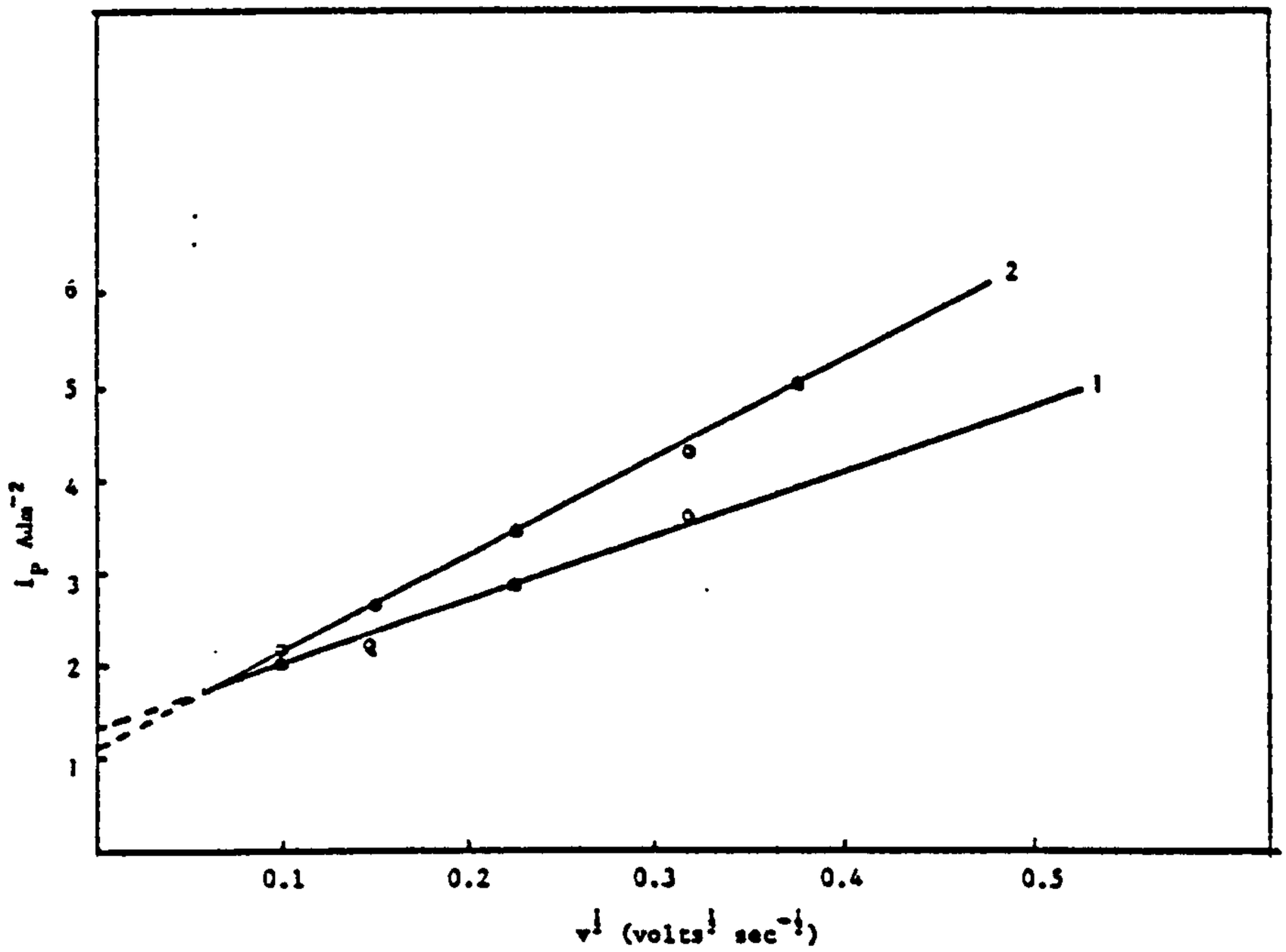

A plot of i_p vs $v^{\frac{1}{2}}$ for Pb electrodeposition onto a Pt electrode from a stock solution of 0.1M $Pb(NO_3)_2$, 1M KNO_3 , 0.1M HNO_3 plus selected organic addition agents.

1 = Stock solution without addition agents.
2 = Stock solution plus 1 gl^{-1} butyne 1,4 diol.

FIGURE 114

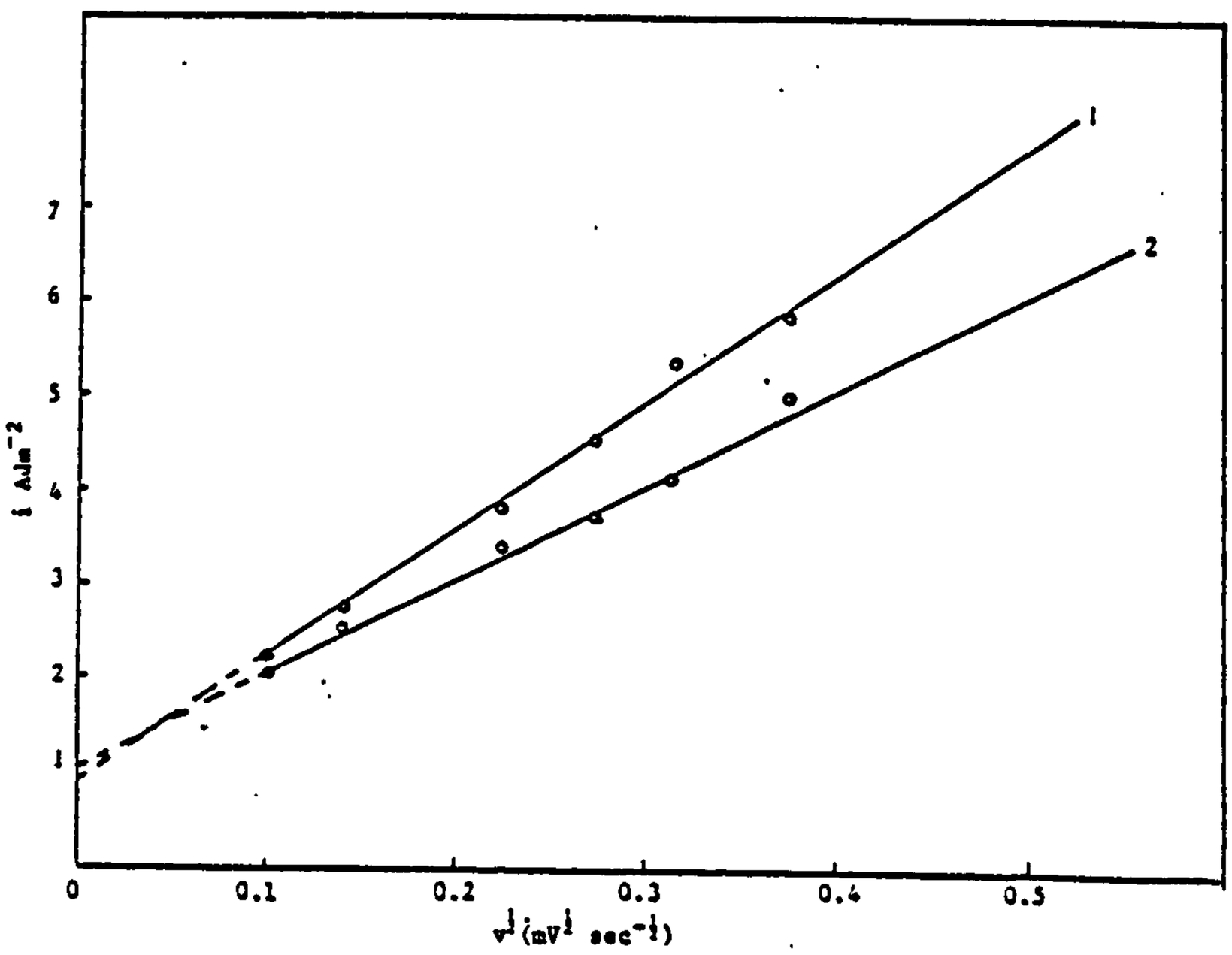

A graph of i_p vs $v^{\frac{1}{2}}$ (sweep rate)$^{\frac{1}{2}}$ for Pb deposition onto a Pt electrode from a stock solution of 0.1M $Pb(NO_3)_2$, 1M KNO_3, 0.1M HNO_3 plus different surface active agents.

1 = stock solution plus 1 gl^{-1} Triton X100
2 = stock solution plus 1 gl^{-1} Tannic acid

FIGURE 115

3.2.4 Pulse potentiostatic studies on Pb deposition

All the work in the literature on the study of the nucleation of Pb by the pulse potentiostatic technique has been conducted in low concentration solutions. In the present investigations where the Pb^{2+} concentration was high, good reproducibility of results was found to be a problem. Nevertheless, the results obtained were representative of the general trends, especially as the pulse potentiostatic work was only intended as a brief attempt to investigate the nucleation and growth process for Pb deposition from practical plating solutions.

Fig. 116 shows the current transients for Pb deposition from a solution of 0.1M $Pb(NO_3)_2$ + 0.5M KNO_3 on nickel at selected potentials, whilst Fig. 117 shows the current transients at -0.200V for a solution 0.1M $Pb(NO_3)_2$ + 0.5M KNO_3 with and without selected addition agents. The pronounced affect of the additive combination 1 gl^{-1} Triton X100 plus 0.1 gl^{-1} anthraquinone-2-sulphonic acid on the growth process is clearly visible at a constant potential (see Fig. 117).

A plot of i vs $t^{1/2}$ for the current transient for Pb deposition from the non-additive bath (Fig. 118) shows a linear relationship at low overpotentials but deviations from this curve, occur at high overpotentials. This relationship is consistent with instantaneous nucleation followed by three dimensional growth (212). The effect of selected addition agents on the i vs $t^{1/2}$ curve for Pb deposition from $Pb(NO_3)_2$ solutions can be seen in Figs. 119 and 120.

The initially high peak current shown in Figs. 118, 119 is attributed to charging of the double layer, followed by subsequent decay. The decay transient was observed in the intial 200 μS after application of the potential pulse and was seen to be a function of $t^{-1/2}$ (see Fig. 121), indicative of a diffusion-dependent nucleation process. The effect of additives on this process is small since no real change in slope between

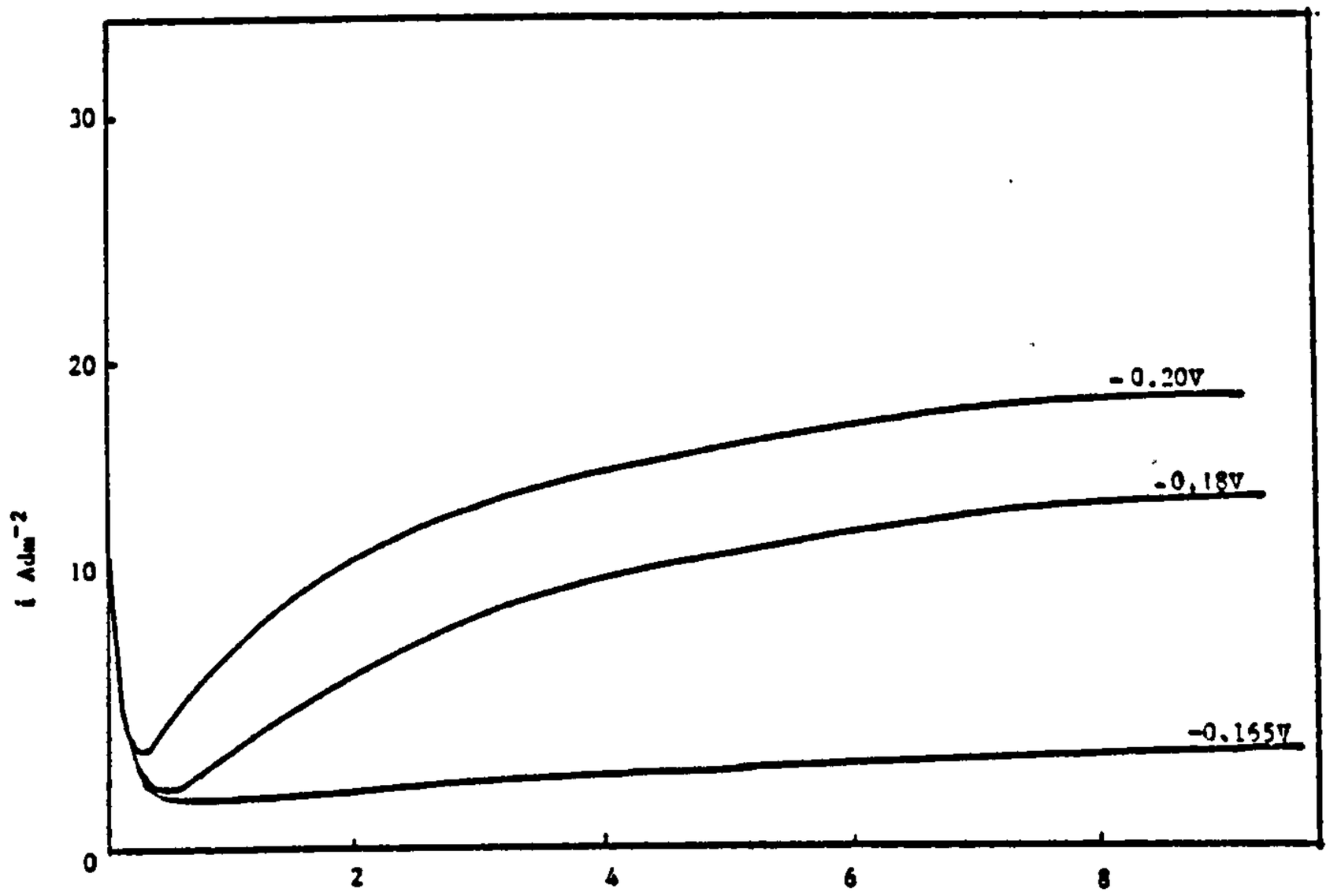

i vs t curve for a Ni electrode pulsed to a fixed potential vs SHE in a solution of 0.1M $Pb(NO_3)_2$, plus 1M KNO_3 .

FIGURE 116

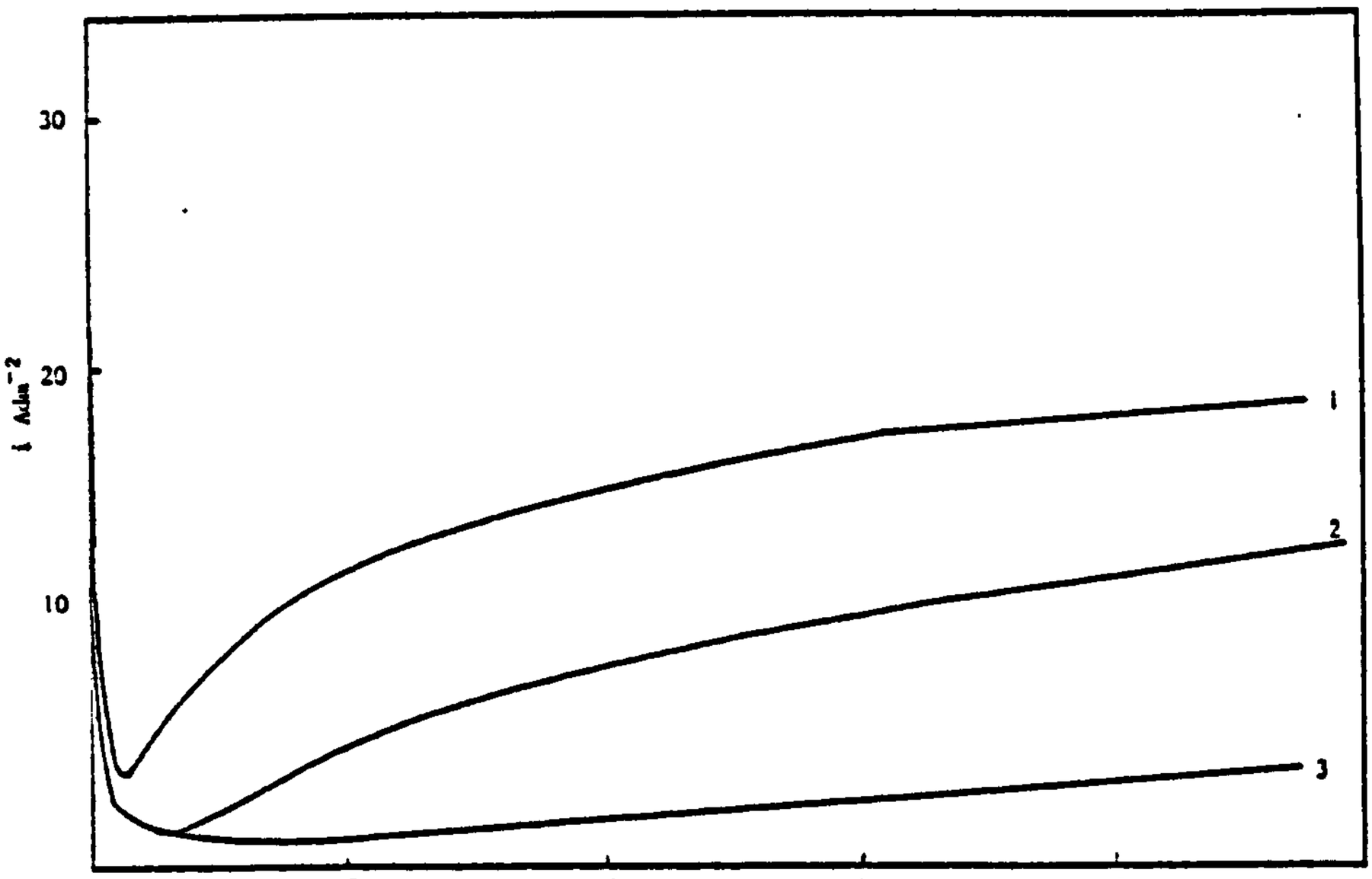

i vs t for a Ni electrode pulsed to -0.200 volts vs SHE in a solution of 0.1M $Pb(NO_3)_2$ 1M KNO_3 plus selected addition agents.

1 = no additives.

2 = stock solution plus 0.5 gl^{-1} cacyl trimethyl ammonium bromide.

3 = stock solution plus 1 gl^{-1} Triton X100, 0.1 gl^{-1} anthraquinone-2-monosulphuric acid.

FIGURE 117

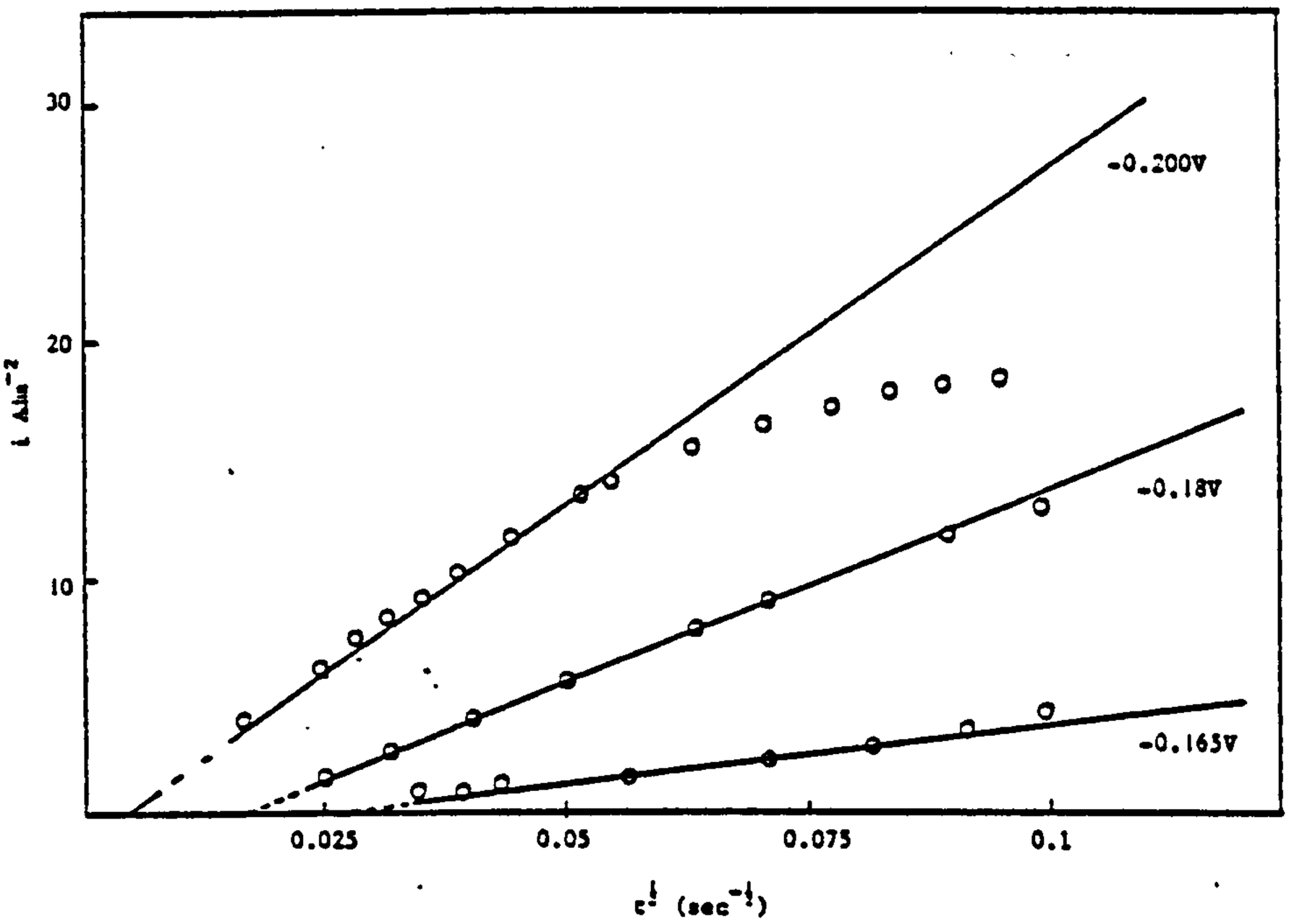

A graph of i vs $t^{\frac{1}{2}}$ for a Ni electrode pulsed to a fixed potential in a solution of 0.1M $Pb(NO_3)_2$, 1M KNO_3 .

FIGURE 118

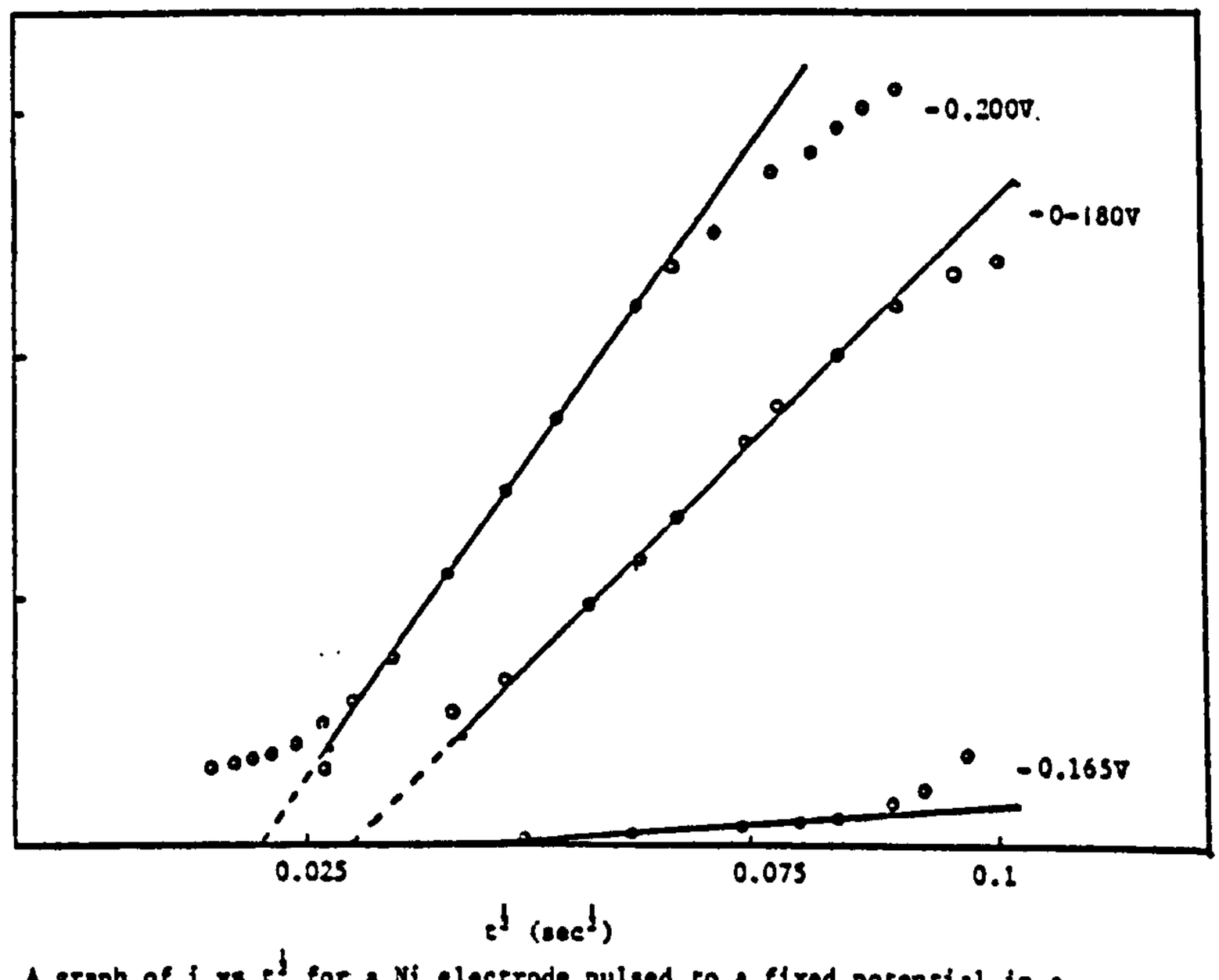

A graph of i vs $t^{\frac{1}{2}}$ for a Ni electrode pulsed to a fixed potential in a solution of 0.1M $Pb(NO_3)_2$, 1M.KNO_3 plus 0.5 gl^{-1} Wafex.

FIGURE 119

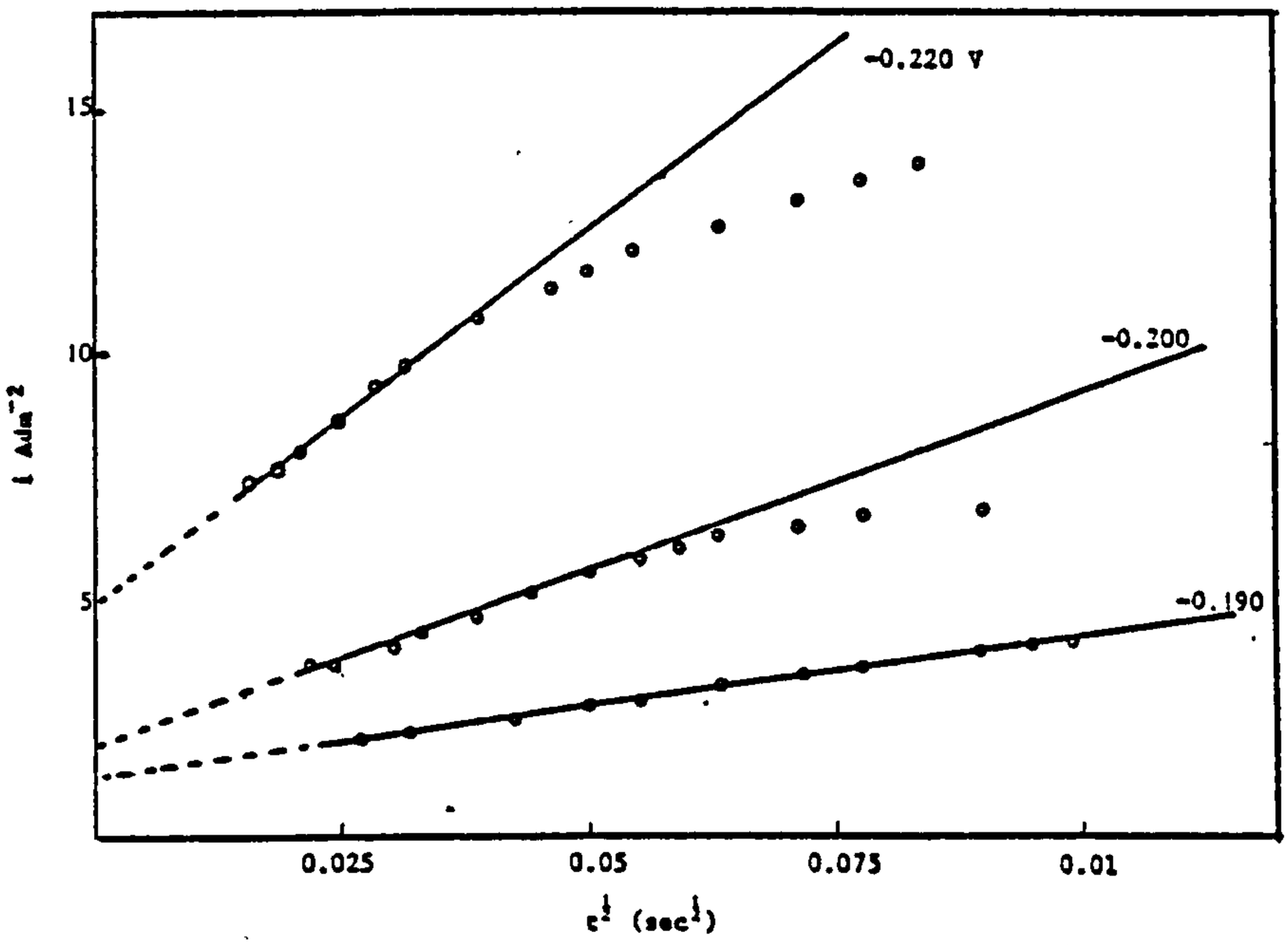

i vs $t^{\frac{1}{2}}$ for a Ni electrode pulsed to a fixed potential in a solution of 0.1M $Pb(NO_3)_2$, 1M KNO_3 plus 1 gl^{-1} Triton X100, 0.1 gl^{-1} anthraquinone-2-monosulphonic acid.

FIGURE 120

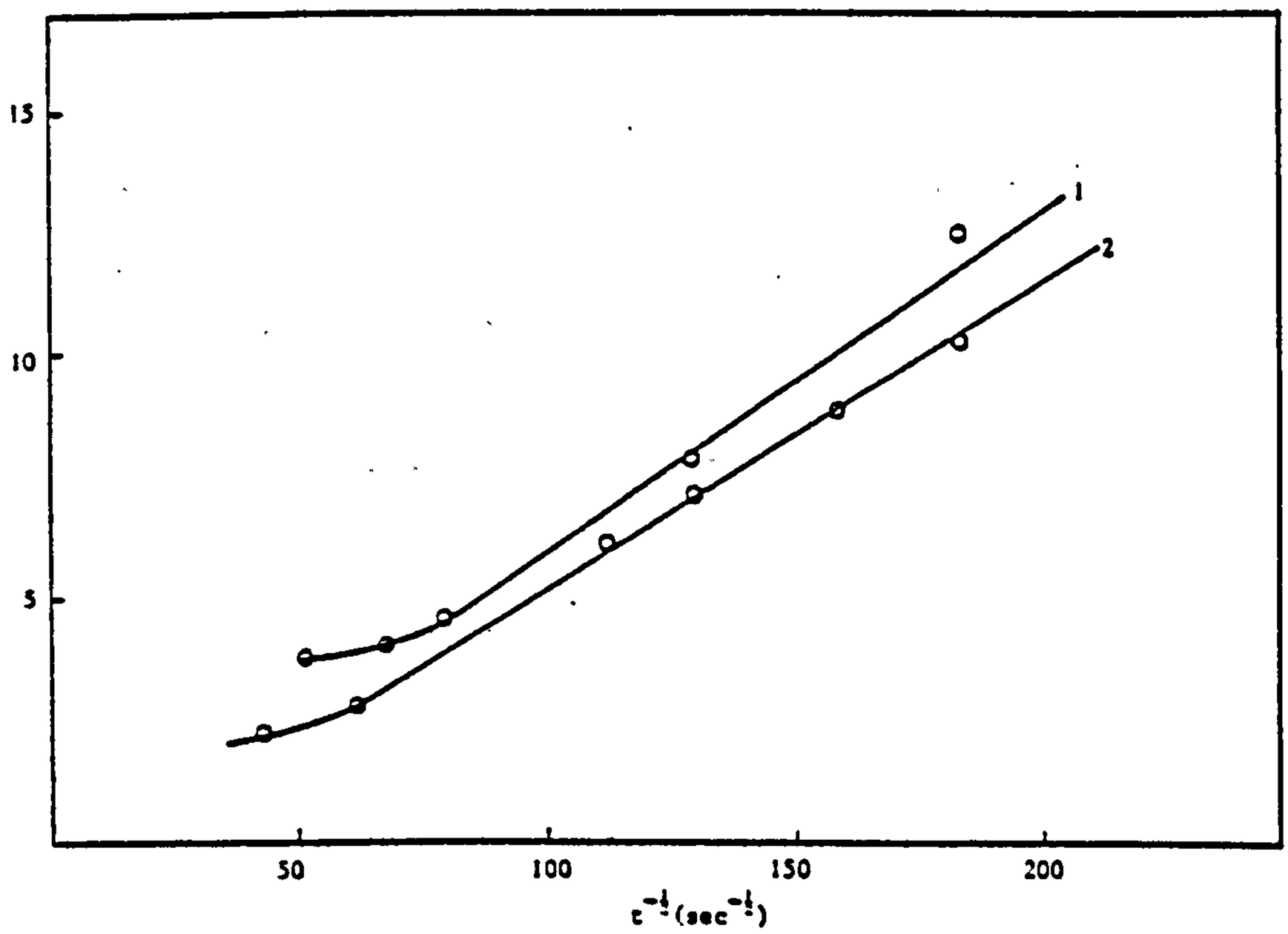

A graph of i vs $t^{-\frac{1}{2}}$ for a Ni electrode held at
in a stock solution of 0.1 M $Pb(NO_3)_2$ plus 1 M KNO_3 containing selected addition agents.

1 = stock solution without additives.

2 = stock solution plus 1g l^{-1} Triton X100, 0.1g l^{-1} 2 anthraquinone mono-sulphonic acid.

FIGURE 121

the non additive and additive combination of Triton X100 plus 0.1 gl^{-1} anthraquinone-2-monosulphonic acid is observed. However, the time before the growth process current becomes significant is greater in the case of an additive containing $Pb(NO_3)_2$ solution. This is represented by the deviation from the straight line portion of the graph.

The most striking differences in the i vs $t^{1/2}$ characteristics were for a 0.1M $Pb(NO_3)_2$ + 0.5M KNO_3 + 1 gl^{-1} Triton X100 + 0.1 gl^{-1} anthraquinone-2-sulphonic acid solution. In this case a linear relationship was observed for a plot of i vs $t^{1/2}$ but the intercept of this graph was on the current and not the time axis as would be expected. The slope of the i vs $t^{1/2}$ plot for this additive-containing solution is lower than for the non additive solution at a given overpotential (see Fig. 121).

3.2.5 Electrochemical impedance determinations

The work carried out using the impedance analyser was not undertaken as a separate study but merely to verify data obtained from conventional techniques. The results from this work were divided into two sections (a) studies of Pb deposition from a 0.05M $Pb(NO_3)_2$ solution and (b) studies on both Pb and PbO_2 electrodes in HBF_4 solutions (see Section 3.4.4)

3.2.5.1 Pb deposition from $Pb(NO_3)_2$ solutions

A plot of Z_{real} versus $Z_{imaginary}$ for a polished Pb electrode in a solution of 0.05M $Pb(NO_3)_2$ + 1 M KNO_3 at E_{rest} is shown in Fig. 122.

The value of R_{ct} obtained from this plot is 0.17 ohm cm^2 which corresponds to a value for of i_o of 0.076 Acm^{-2} at 25°C. Assuming β = 0.5, this gives a value of i_o for 0.1M $Pb(NO_3)_2$ of 0.11 Acm^{-2} and 0.340 Acm^{-2} for 1M $Pb(NO_3)_2$.

A plot of Z" vs w for the high frequency range yields a double layer capacitance of 16.5 $\mu F\ cm^{-2}$ at the rest potential of -0.222V with a value of 500 Hz for w_{max}.

Reproducibility of results in this system was found to be difficult as Fig. 123 shows. The highest value of R_{ct} for this solution at E_{rest} was 0.12 ohm cm^2 which corresponds to a value for i_o of 0.107A cm^{-2} in 0.05M $Pb(NO_3)_2$, 0.15 Acm^{-2} in 0.1M $Pb(NO_3)_2$ and 0.47 Acm^{-2} in 1M $Pb(NO_3)_2$ again assuming a value for β of 0.5. The value of C_{dl} was found to be 16 $\mu F\ cm^{-2}$.

A diffusion limited slope is clearly visible in the low frequency range for Z' vs Z" of slope approximately 45^o. A plot of Z" vs $1/w^{1/2}$ is given in Fig. 124 and a slope of approxi- mately 0.205 was obtained using the equation.

$$\sigma = \frac{RT}{n^2 F^2 A \sqrt{2}} \left(\frac{1}{D_o^{1/2} C_o^*} + \frac{1}{D_R^{1/2} C_R^*} \right)$$

From the above equation a value for D of 2.1 x 10^{-5} $cm^2\ sec^{-1}$ was obtained.

Decreasing the potential of the Pb electrode to -0.260 V resulted in a Z' vs Z" plot that exhibited no discernable high frequency semi-circle (Fig. 125) but showed a diffusion limited impedance plot. The value of D at this potential was found to be 8 x 10^{-7} $cm^2\ sec^{-1}$ from a plot of Z' vs $1/w^{1/2}$. Addition of 1 gl^{-1} Triton X100 to the test solution produced a Z' vs Z" plot as shown in Fig. 126 in which the diffusion limited low frequency region exhibited considerable scatter. The value for i_o of 0.075 Acm^{-2} in this solution is not noticeably different from that of a non-additive solution. The value of the double layer capacitance C_{dl} in this solution was 14 $\mu F\ cm^{-2}$ at E_{rest}.

A Nyquist plot for a solution of 0.05M $Pb(NO_3)_2$, 1M KNO_3 plus 1 gl^{-1} Triton X100 and 0.1 gl^{-1} anthraquinone-2-mono

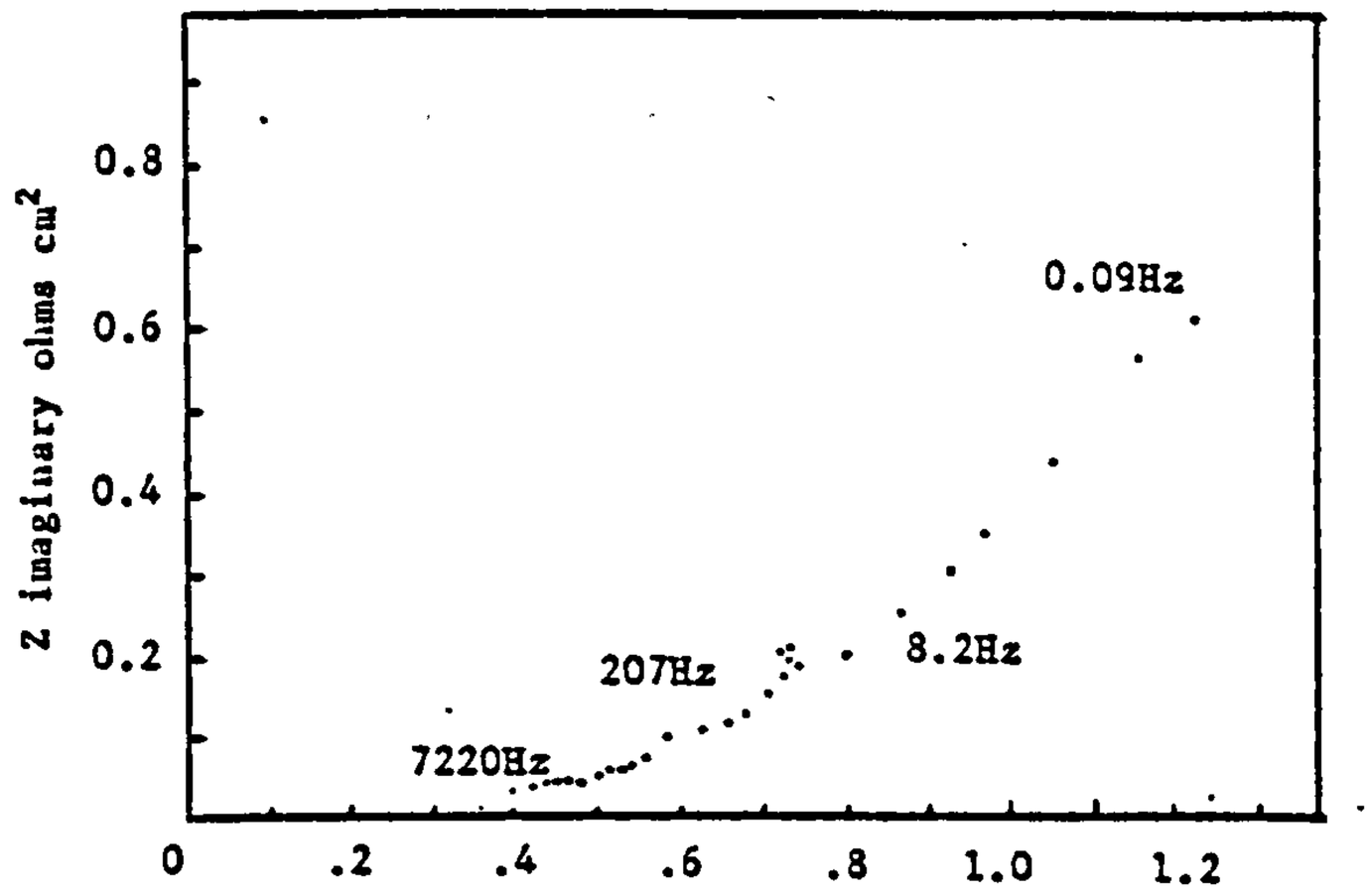

Z real vs Z imaginary for a Pb electrode held at a potential of -0.222 Volts vs SHE in a solution of 0.05M $Pb(NO_3)_2$, 1M KNO_3 without addition agents.

FIGURE 122

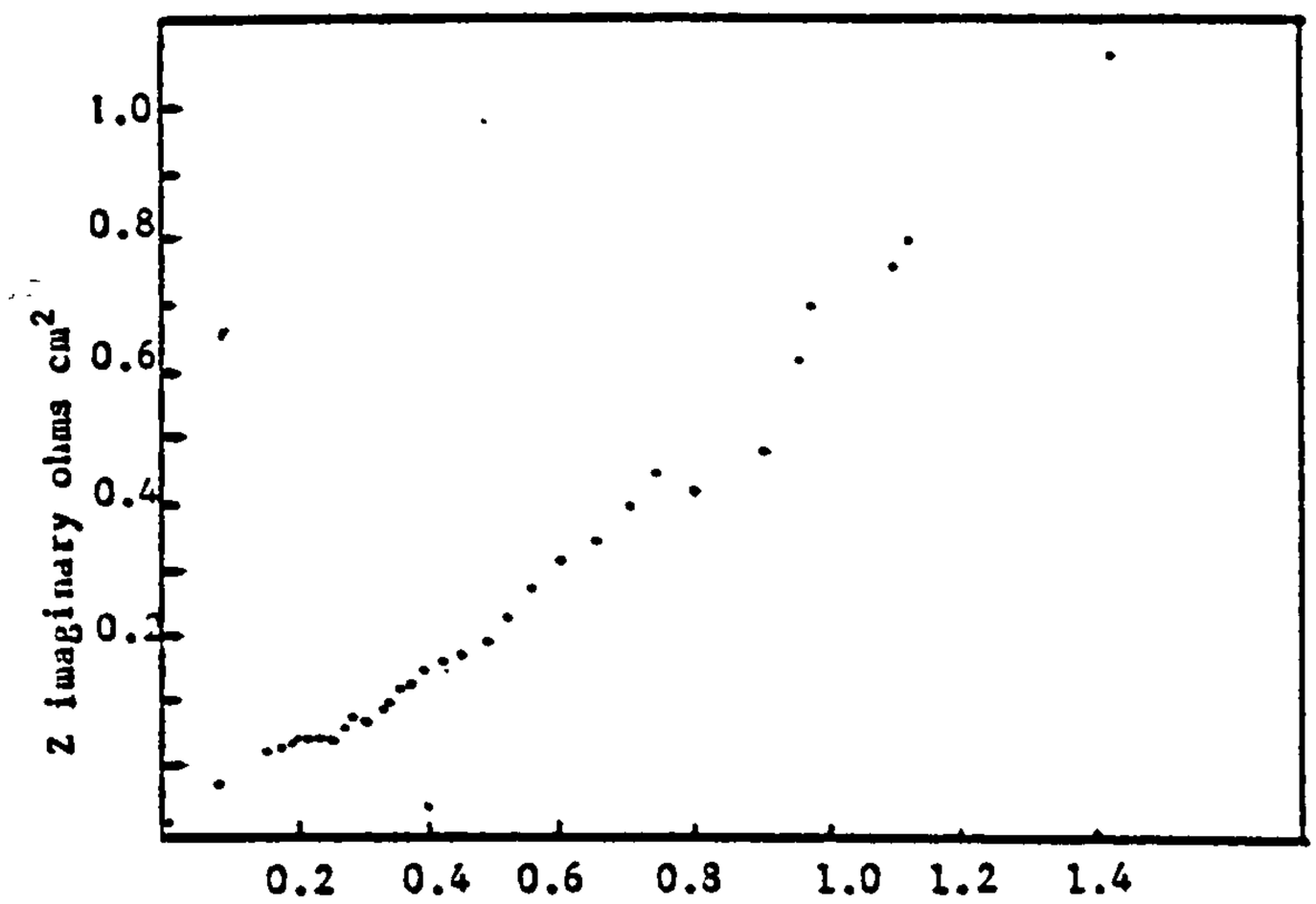

Z real vs Z imaginary for a Pb electrode held at its rest potential of -0.204V vs SHE in a solution of 0.05M $Pb(NO_3)_2$ + 1M KNO_3 free of addition agents.

FIGURE 123

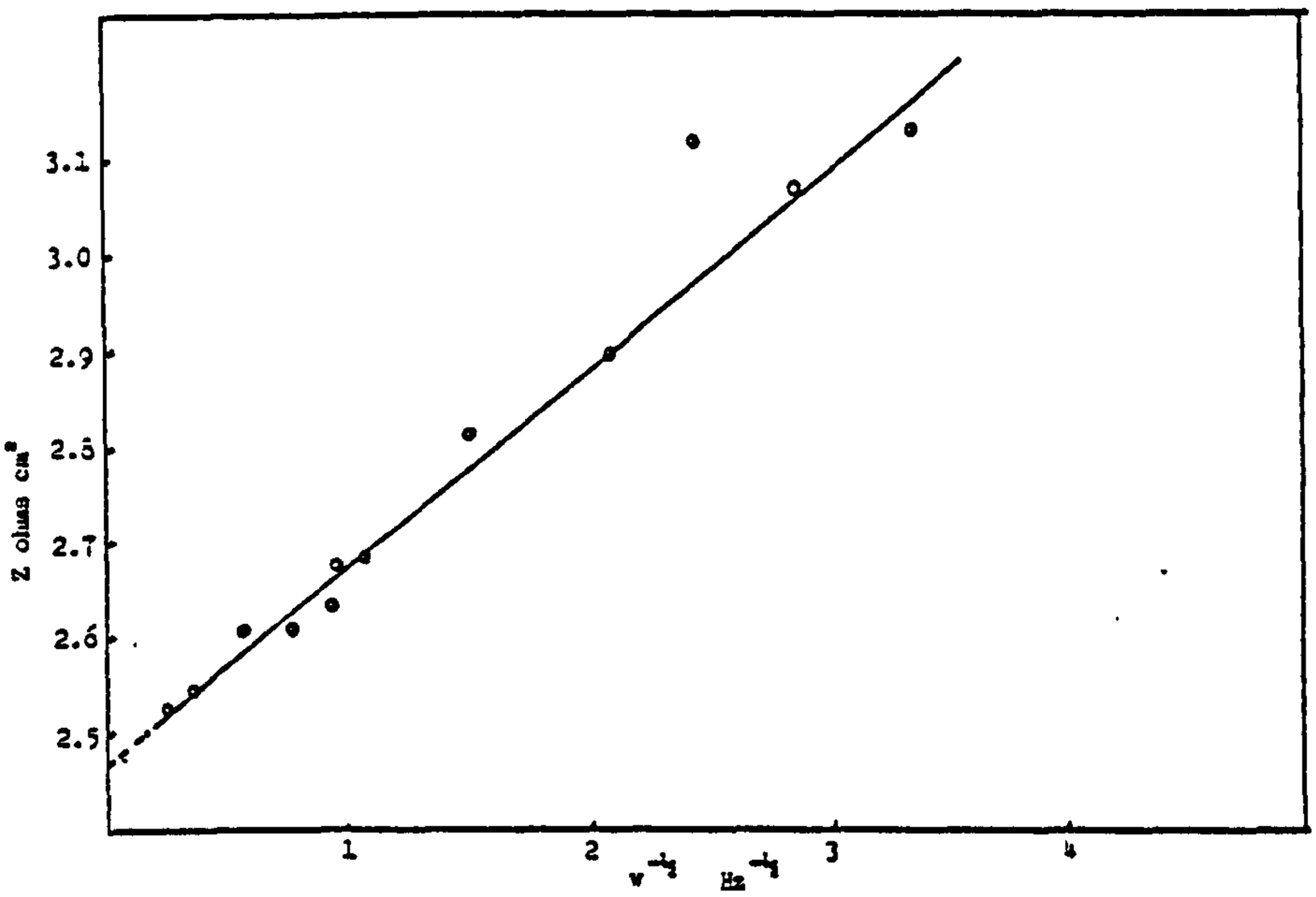

A plot of Z' vs $w^{-\frac{1}{2}}$ for the low frequency region of a Pb electrode immersed in solution of 0.05M $Pb(NO_3)_2$ + 1M KNO_3

FIGURE 124

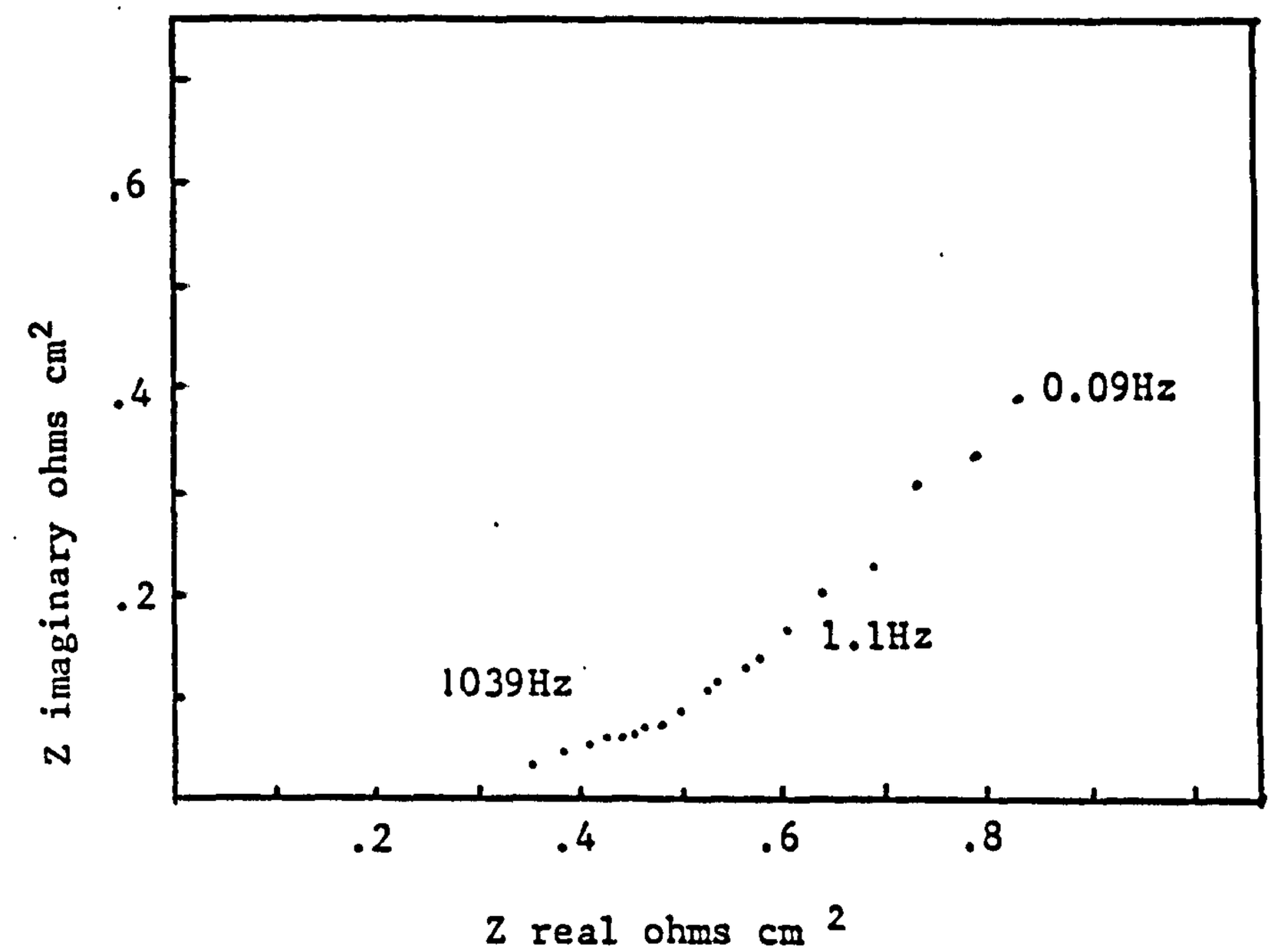

Z real vs Z imaginary for a Pb electrode held at -0.260 Volts vs SHE in a 0.05M $Pb(NO_3)_2$, 1M KNO_3 solution.

FIGURE 125

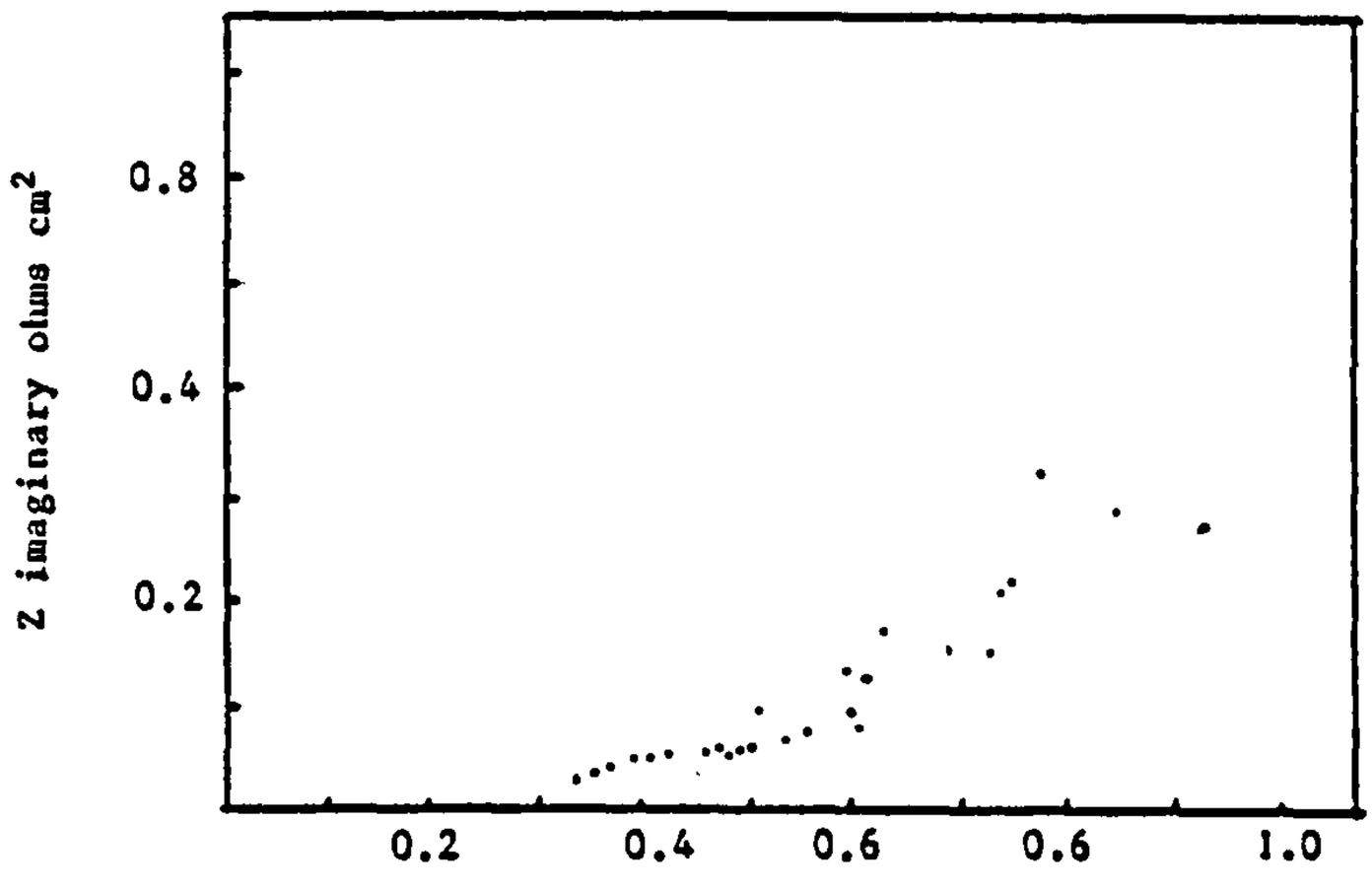

Z real vs Z imaginary for a Pb electrode held at its rest potential of -0.22 V, in a solution of 0.05M $Pb(NO_3)_2$, $1MKNO_3$ + $1gl^{-1}$ Triton X100.

FIGURE 126

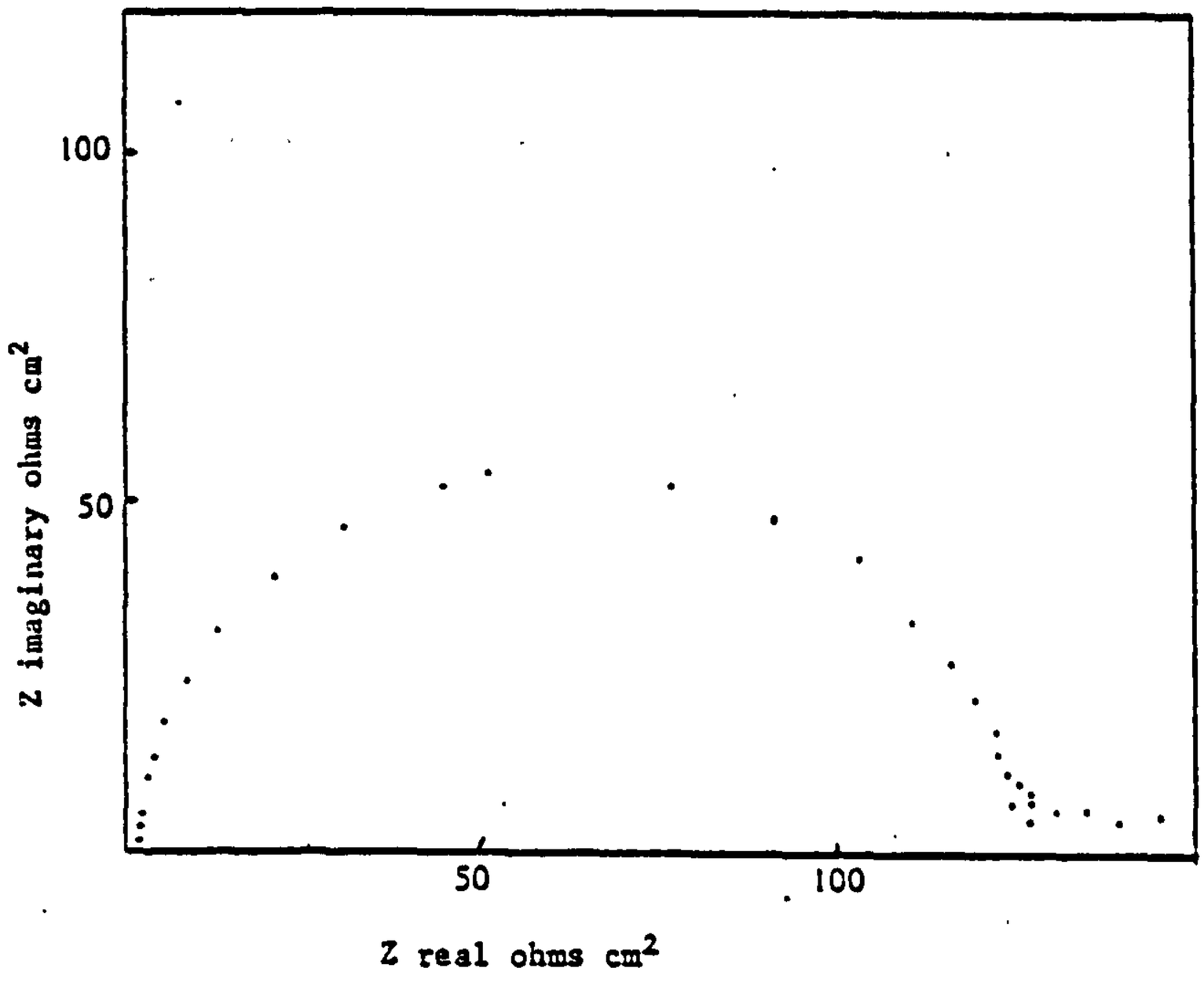

Z real versus Z imaginary for a Pb electrode at E_{rest} -0.204V vs SHE in a solution of 0.05M $Pb(NO_3)_2$, 1M KNO , 1 gl^{-1} Triton X100 plus 0.1 gl^{-1} anthraquinone-2-monosulphonic acid.

FIGURE 127

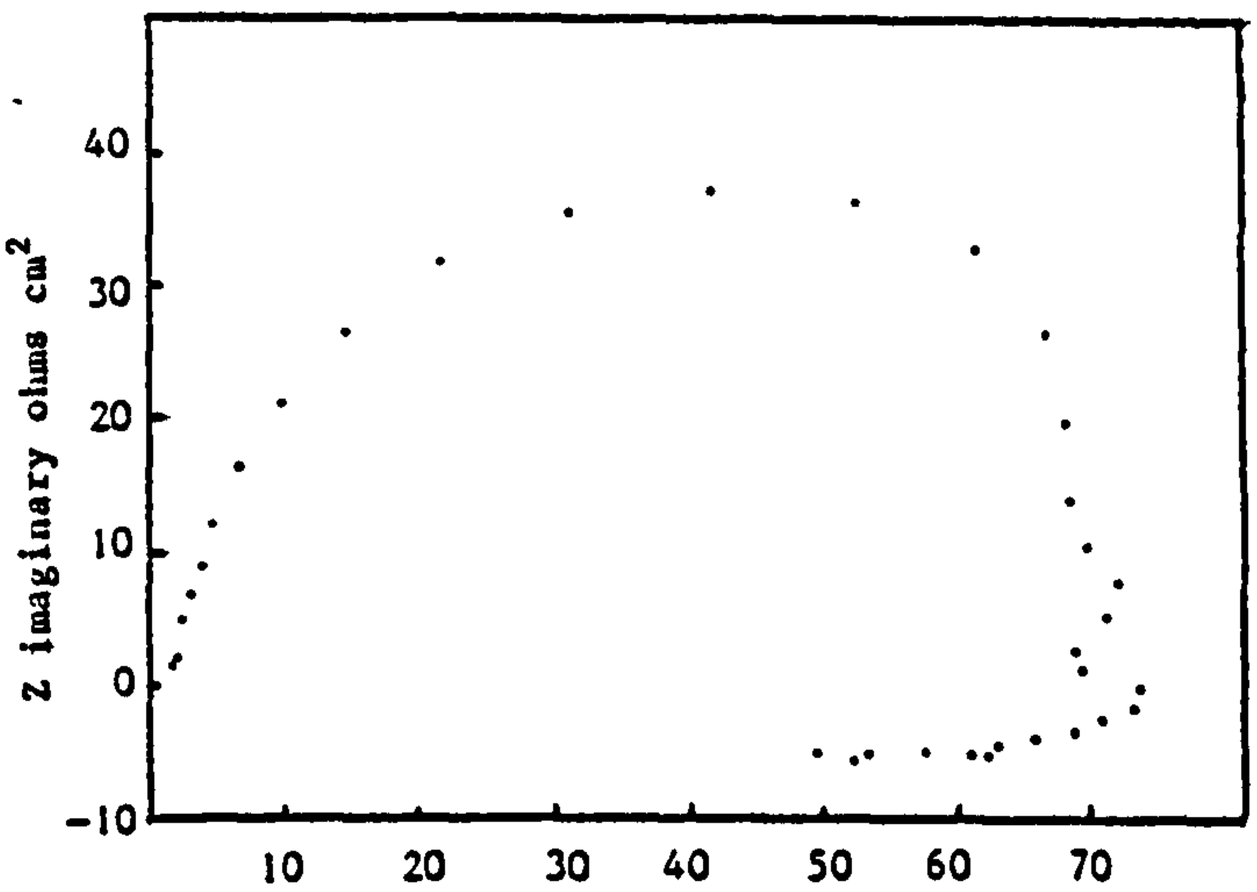

Z real vs Z imaginary for a Pb electrode held at a potential of -0.260V vs SHE in a solution of 0.05M $Pb(NO_3)_2$ + 1M KNO_3 + 1 gl^{-1} Triton X100 + 0.1 gl^{-1} anthraquinone 2-sulphonic acid.

FIGURE 128

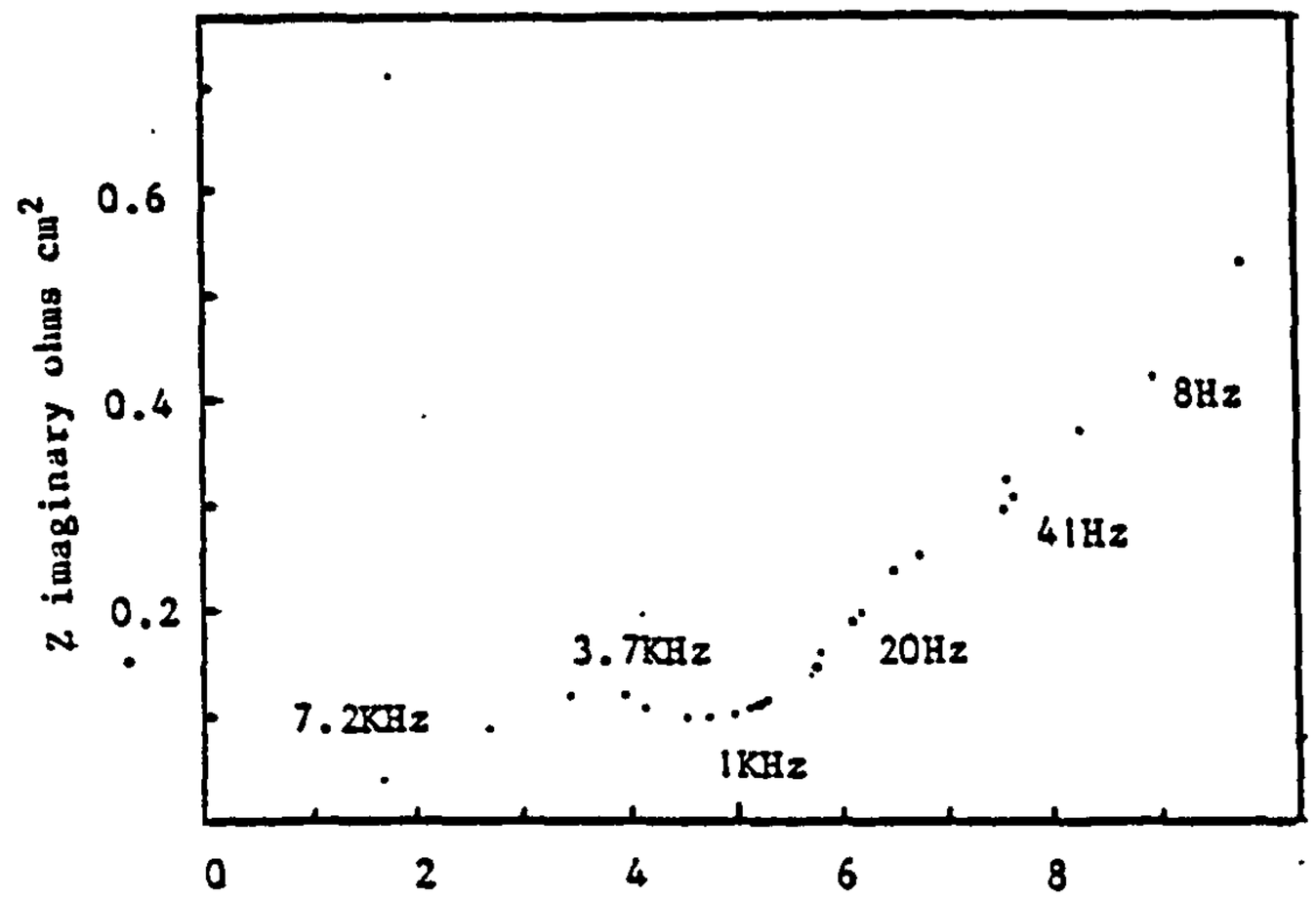

Z real vs Z imaginary for a Pb electrode held at -0.260 Volts vs SHE in a 0.05M $Pb(NO_3)_2$+1M KNO_3 solution plus 1 gl^{-1} Triton X100.

FIGURE 129

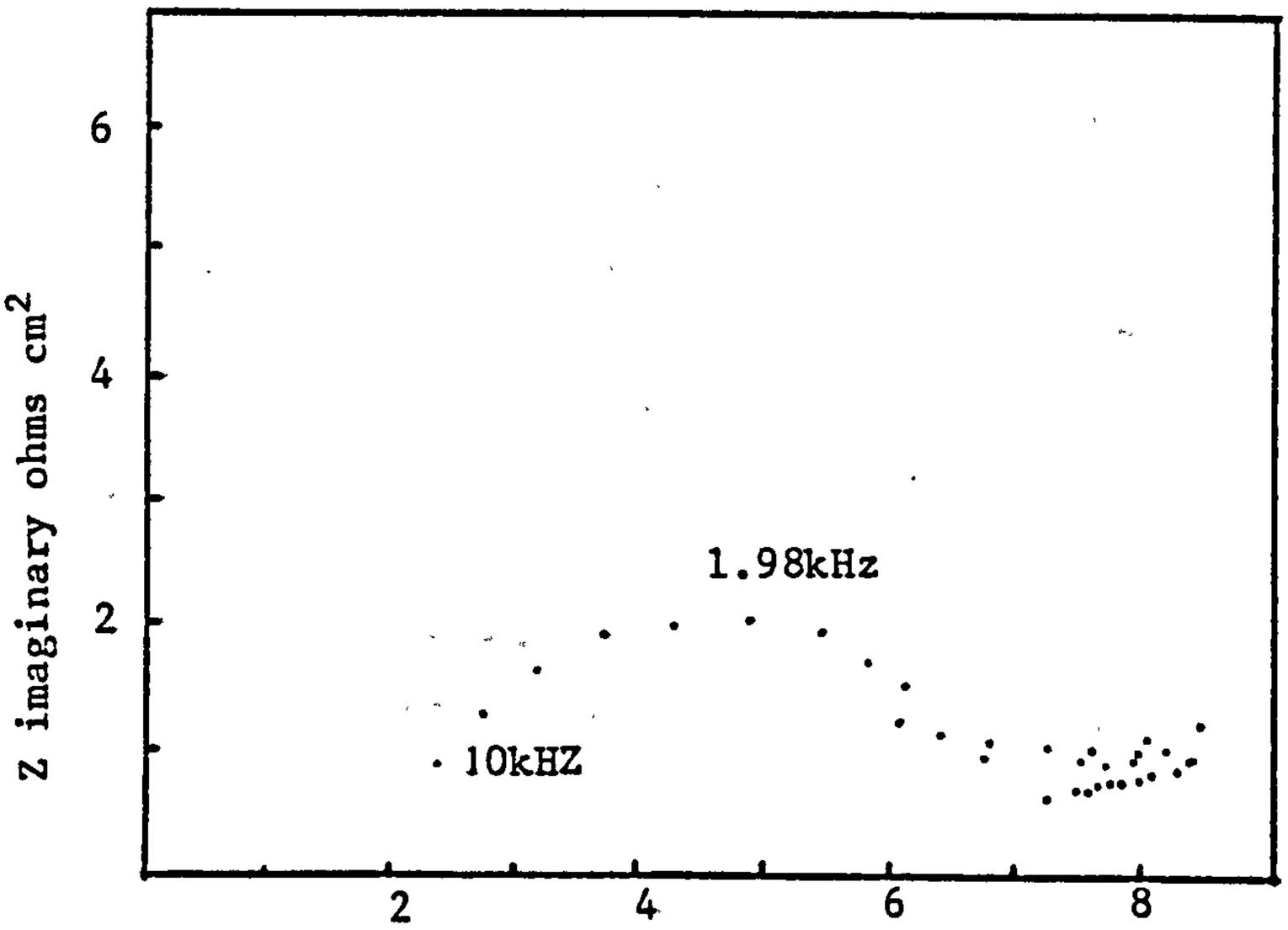

Z real vs Z imaginary for a Pb electrode held at a potential of -0.202 Volts vs SHE in a 0.05M $Pb(NO_3)_2$+1M KNO_3 ; 1 gl^{-1} tannic acid solution.

FIGURE 130

sulphonic acid is shown in Fig. 127. The Z' vs Z" curve in the presence of the additive anthraquinone-2-monosulphonic acid is different to that in the non additive solution i.e. no diffusion limited process is visible. The value of R_{ct} at E_{rest} from the high frequency semi-circle was found to be 107 ohm cm^2 which corresponds to an i_o value of 1.2×10^{-4} Acm^{-2}. The value of C_{dl} measured at w_{max} of 108 Hz was 170 $\mu F\ cm^{-2}$ whilst measurement of C_{dl} from a plot of Z" vs w over the frequency range 7,000 to 2,500 Hz yields a value of 720μ F cm^{-2} for C_{dl}. For a Pb electrode in the same solution yet held at -0.260V and at a c.d of 0.08 Adm^{-2} a similar Z' vs Z" curve was obtained except that an inductive loop appeared in the high frequency region (see Fig. 128). The value of R_{ct} was 65 ohm cm^2 with a value of C_{dl} at w_{max} (149 Hz), 180 $\mu F\ cm^{-2}$.

For a Pb electrode in the stock solution + 1 gl^{-1} Triton X100 held at -0.260 V (see Fig. 129) a Warbug coefficient of 0.91 was obtained. A value of D of 1.07×10^{-6} $cm^2\ sec^{-1}$ was obtained from the Warburg equation.

The effect of the addition of 1 gl^{-1} tannic acid to the stock solution of 0.05M $Pb(NO_3)_2$, 1M KNO_3, 0.1M HNO_3 can be seen in Fig. 130. The value of R_{ct} obtained at the rest potential is 4.47 ohm cm^2, which corresponds to a value for i_o of 0.0029A cm^{-2} in 0.05M $Pb(NO_3)_2$. The value of C_{dl} at E_{rest} was evaluated as 29.7 $\mu F\ cm^{-2}$ from a plot of Z" vs w, with the value of w_{max} found to be 1983 Hz. No diffusion limited slope is visible the plot of Z' vs Z", which was similar in appearance to that seen in Fig. 128 for a solution of 0.05M $Pb(NO_3)_2$, 1M KNO_3, 0.1M HNO_3 + 1 gl^{-1} Triton X100 + 0.1 gl^{-1} anthraquinone-2-monosulphonic acid.

3.2.6 PbO_2 deposition from $Pb(NO_3)_2$ solutions

A typical voltammogram for the anodic polarisation of a Pt electrode in a 0.1M $Pb(NO_3)_2$ solution in a supporting electrolyte of 0.5M KNO_3 and 0.1M HNO_3 is shown in Fig.131.

Three peaks were clearly discernible. and are due to (a) the nucleation of PbO_2 on the inert Pt electrode, (b) nucleation of PbO_2 on previously formed PbO_2, this peak was obtained on re-cycling of the electrode and (c) the reduction of PbO_2.

The E vs i curves for PbO_2 formation obtained at a sweep rate of 50 mV sec^{-1} from the stock solution, containing selected addition agents are shown in Figs. 132-139.

In the case of additions of 1 gl^{-1} BRIJ 35 (Fig. 132) and 1 gl^{-1} Pluronic L64 similar voltammograms were obtained, the only difference being the slightly higher value of i_p for the BRIJ 35 solution. The effect of the addition of 1 gl^{-1} Triton X100 (Fig. 133) on the voltammogram for PbO_2 deposition onto Pt can be seen in Fig. 133. The value of i_p in this instance of 4.26 Adm^{-2} is also greater than that of the non-additive solution of 2.88 Adm^{-2}, at a sweep speed of 50 mV sec^{-1}. E_p is also moved in a more positive direction + 1.96V compared to the value of +1.84V for the non-additive solution.

The addition of butyne 1,4 diol (Fig. 134) did not significantly alter the value of i_p (3.23 Adm^{-2}) from that of the non-additive solution nor effect the value of E_p, 1.85 V, though it did appear to increase the oxygen overvoltage e.g at +2.14V the instantaneous current recorded at this sweep rate was 4.4 Adm^{-2} compared to 3.7 Adm^{-2} for the non-additive solution.

Other plating additives were also found to alter the nature of the E vs i curves, with CETB having a prounced influence on the nucleation process, moving E_p to 2.0V and reducing the current at 2.14V to 2.7 Adm^{-2} (Fig. 135); tannic acid had an even more pronounced effect on the nucleation process (see Fig. 136). A similar effect was observed for both peptone and diphenylamine at a concentration of 0.5 gl^{-1} in the test electrolyte (see Fig. 137).

The effect of the additives anthraquinone-2-monosulphonic acid and 'Wafex' on the E vs i curves for PbO_2 deposition at low sweep speeds can be seen by examination of Figs. 138 and 139.

The results of the linear polarisation at 5 mV sec^{-1} of a Pt electrode in the stock solution with and without certain addition agents on the E vs i curves are given in Figs. 140-142.

The reproducibility of the linear sweep voltammograms (LSV's) at sweep rates greater than 20mV sec^{-1} was good, whilst at lower sweep rates the reproducibility was poor. Fig. 143 shows the reproducibility of the E vs i curves for a solution of 0.1M $Pb(NO_3)_2$, 0.5M KNO_3 and 0.1M HNO_3 containing 1 gl^{-1} Triton X100, and it shows that the initial stages of PbO_2 nucleation are the most difficult to reproduce. The most interesting effect observed at low sweep speeds (5 mV sec^{-1}) in the presence of certain additives is the increase in over-voltage necessary before nucleation of PbO_2 occurs. This is best exemplified by the addition of tannic acid (see Fig. 140). The potential before the onset of nucleation, was obtained by extrapolation of the initial linear portion of the E vs i curve to the potential axis (see Fig. 141).

Typical values for this potential in certain additives containing solutions are given in Table 56.

The LSV's of additive-containing solutions obtained at a higher sweep rate (140 mV sec^{-1}) are shown in Figs. 144-150, whilst the voltammograms at even higher sweep rates (250 mV sec^{-1}) for the non additive containing $Pb(NO_3)_2$ solution and the stock solution plus 1 gl^{-1} tannic acid are shown in Figs. 151 and 152 respectively. In the case of the tannic acid solution at this high sweep rate no discernable nucleation peak is visible on the first sweep, with the initial reduction peak also moved in a more cathodic direction. This effect was also observed with 0.5 gl^{-1} peptone as the addition agent i.e the first PbO_2 nucleation peak almost completely disappears.

As a general observation it can be seen that additives that produce highly-stressed PbO_2 deposits show little or no nucleation peaks at high sweeps rates (250 mV sec^{-1}) e.g peptone and diphenylamine (Fig. 153).

TABLE 56

Potential before the onset of nucleation of PbO_2 onto a Pt electrode, at a sweep rate of 5 mV sec^{-1} in a solution of 0.1M $Pb(NO_3)_2$, 0.5M KNO_3 + 0.1M HNO_3

Additive	Potential before the onset of nucleation (V)
No additive	+1.63
Hyamine	+1.64
Pluronic L64	+1.65
Triton X100 1 gl^{-1}	+1.66
BRIJ 35 1 gl^{-1}	+1.68
Butyne 1,4 diol 1 gl^{-1}	+1.71
CETB 0.1 gl^{-1}	+1.72
Wafex 1 gl^{-1}	+1.73
Tween 80 1 gl^{-1}	+1.74
Tannic acid 1 gl^{-1}	+1.84

In the case of the addition of certain additives it was easy to discern the nucleation peak formed on the first sweep, however with others it was not so easy namely, tannic acid, CETB, and diphenylamine. For the non additive solution a linear relationship was found between i_p and $v^{1/2}$ see Figs. 154 to 155, whilst other parameters are listed in Table 57.

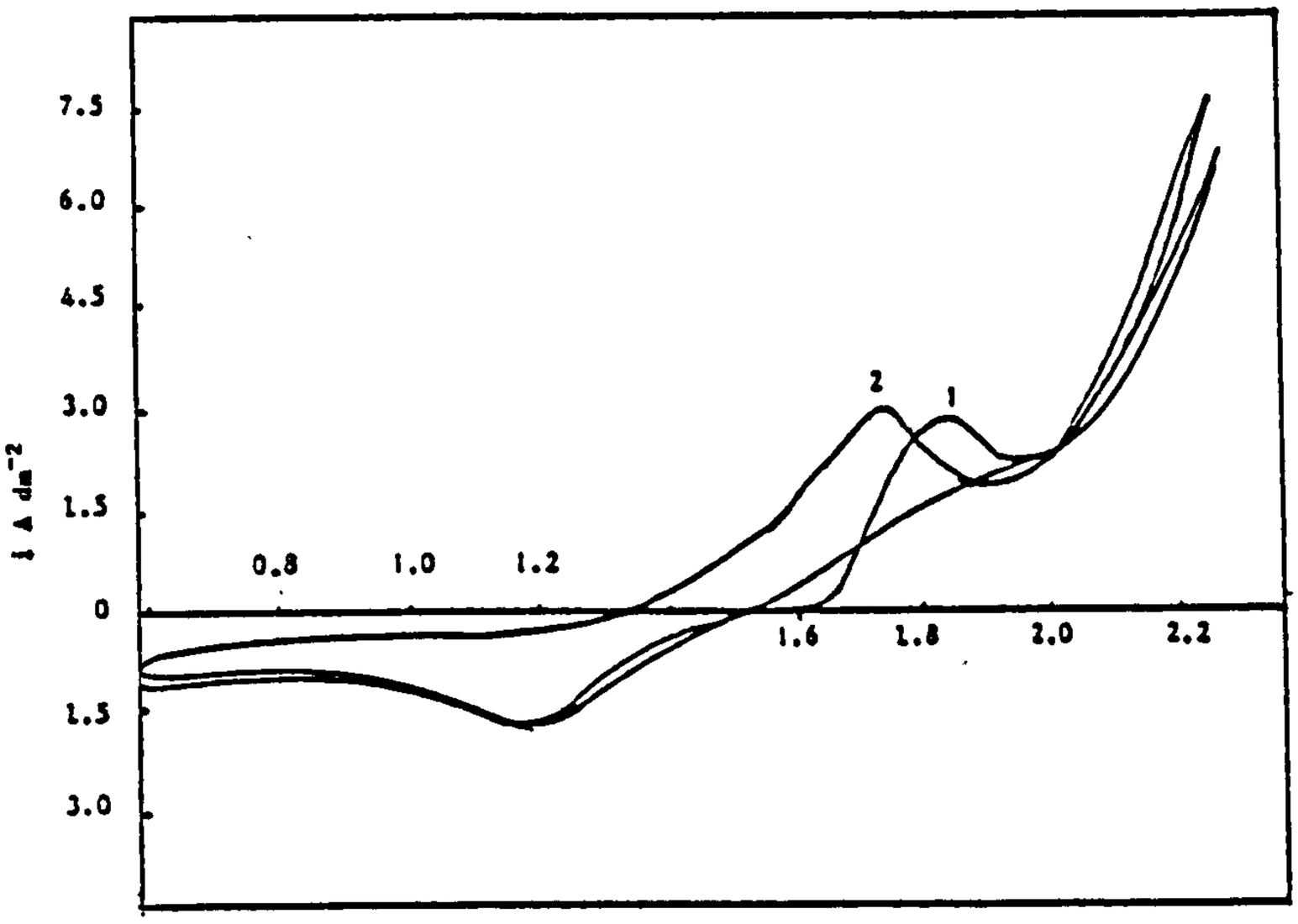

Cyclic voltammogram for a Pt electrode polarised at a sweep rate of 50mV sec^{-1} in a solution of 0.1M $Pb(NO_3)_2$, 1M KNO_3 , 0.1M HNO_3 without any surface active agents.

FIGURE 131

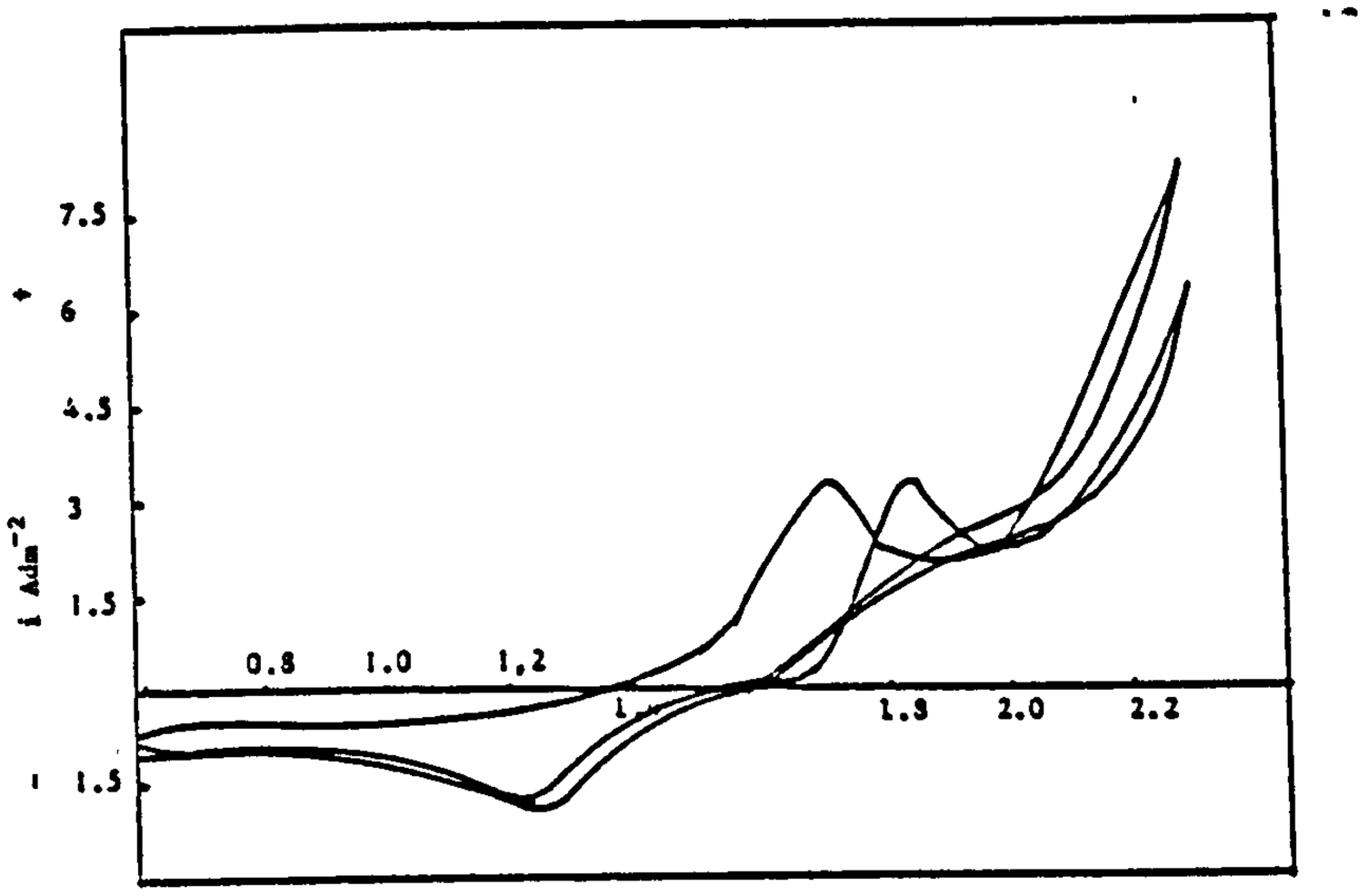

Cyclic voltammogram for a Pt electrode polarised at a sweep rate of 50 mV sec^{-1} in a stock solution of 0.1M $Pb(NO_3)_2$, 1M KNO_3, 0.1M HNO_3 plus 1 gl^{-1} BRIJ 35.

FIGURE 132

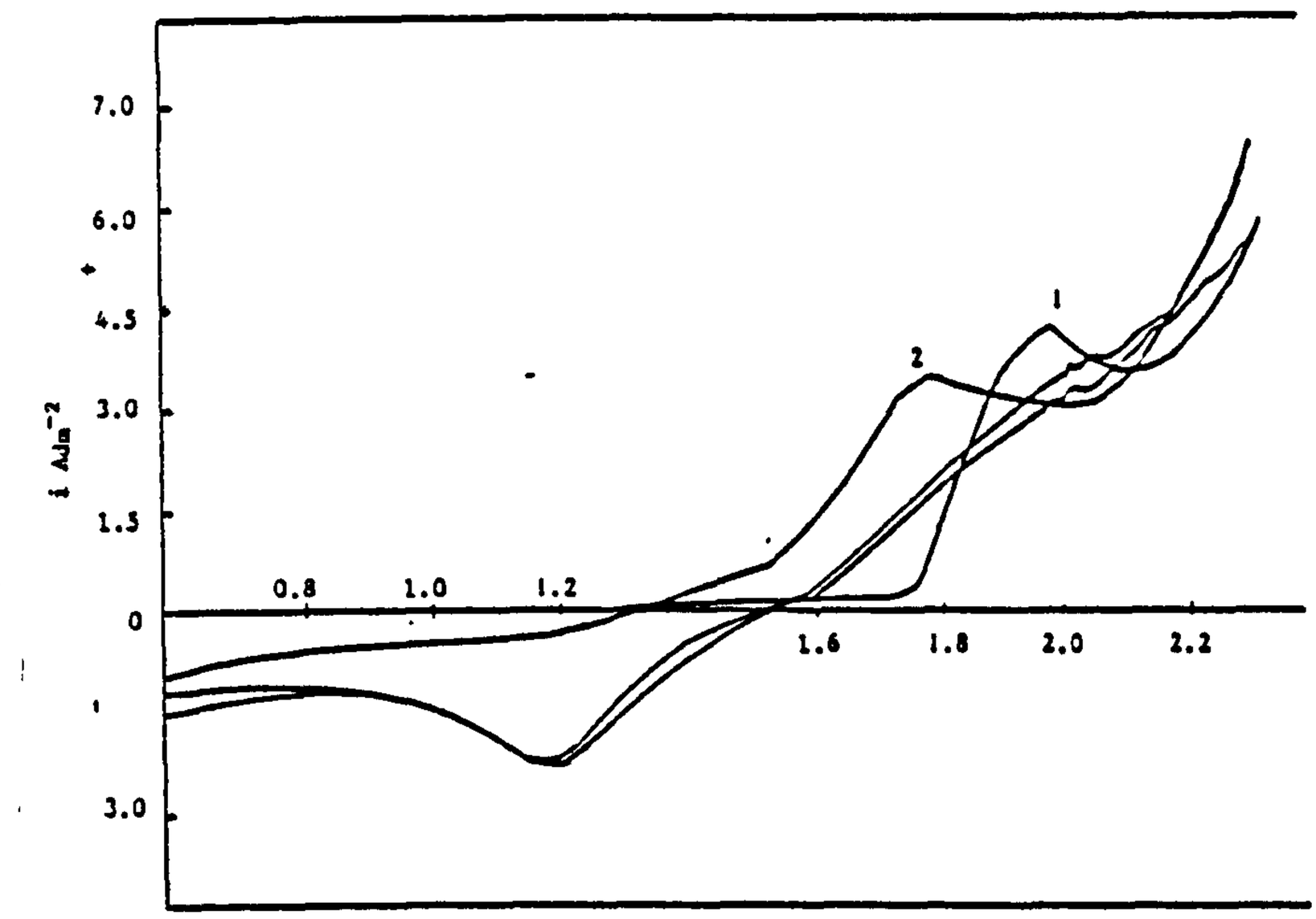

E vs SHE (Volts)

Cyclic voltammorram of a Pt electrode polarised at a sweep rate of 50mV sec^{-1} in a stock solution of 0.1M $Pb(NO_3)_2$, 1M KNO_3 , 0.1M HNO_3 plus 1 gl^{-1} Triton X100.

1 = 1st scan 2 = 2nd scan

FIGURE 133

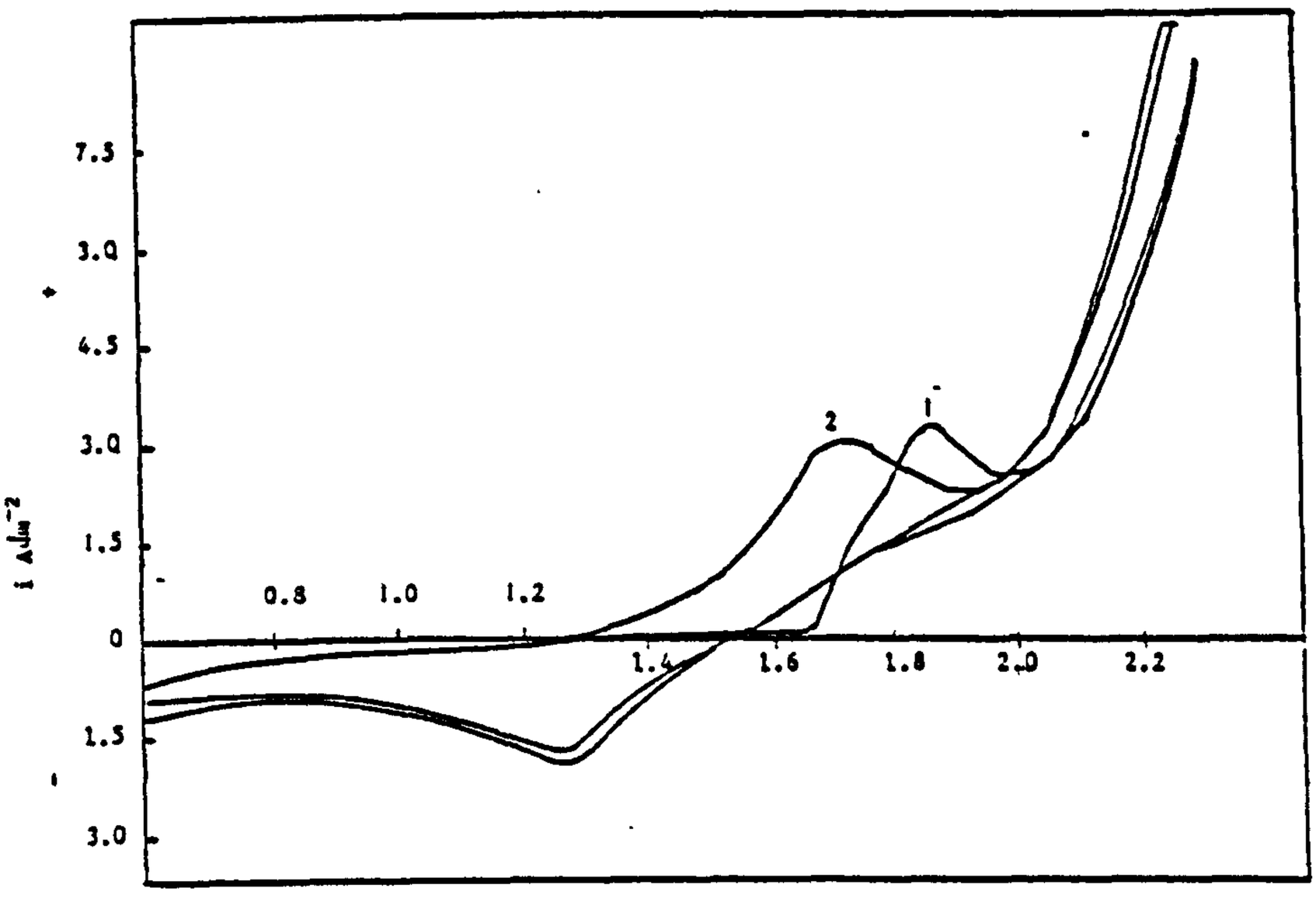

E vs SHE (Volts)

Cyclic voltammogram for a Pt electrode polarised at a sweep rate of 50mV sec^{-1} in a solution of 0.1M $Pb(NO_3)_2$, 1M KNO_3, 0.1M HNO_3 plus 1 gl^{-1} butyne 1,4 diol.

1 = 1st scan 2 = 2nd scan

FIGURE 134

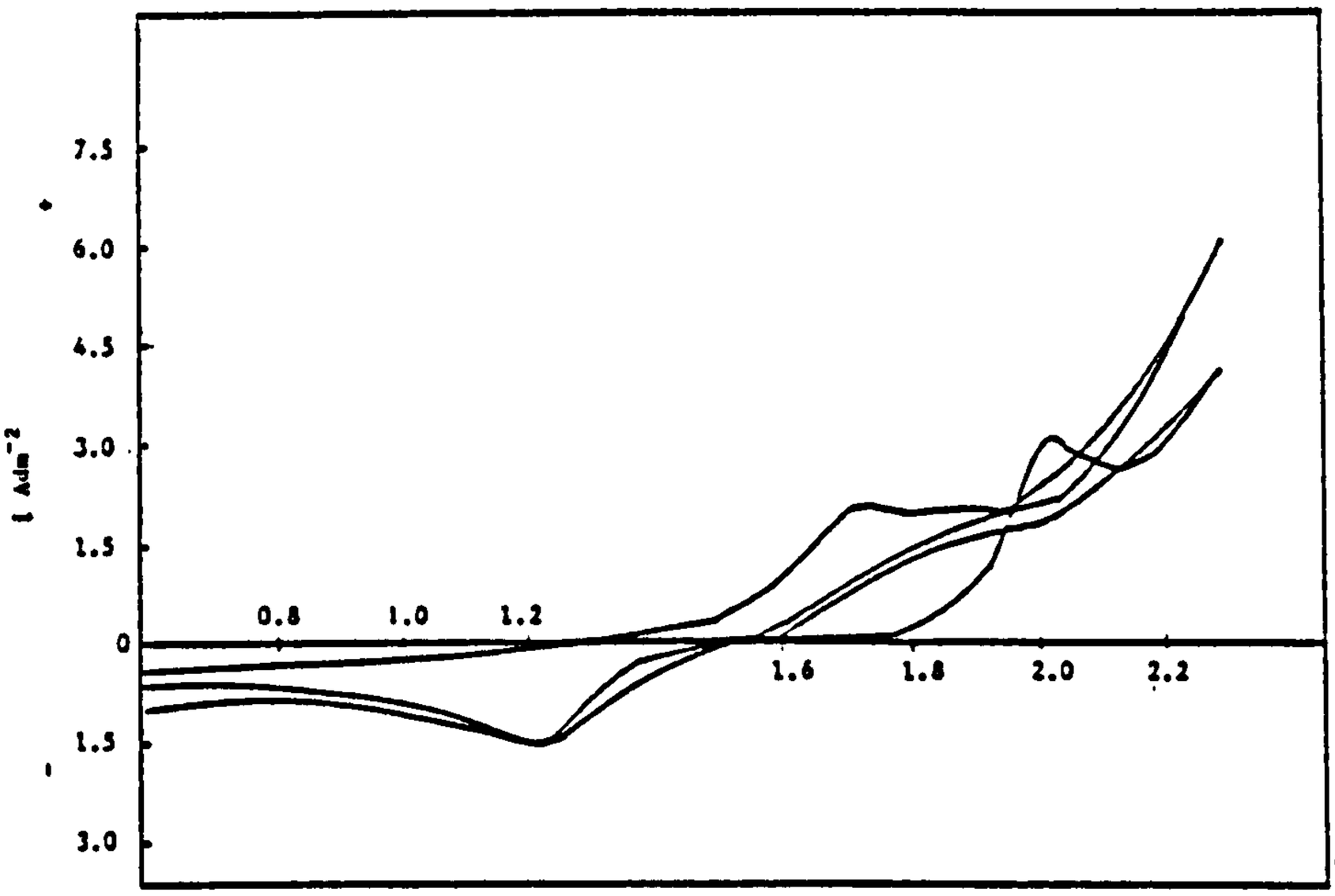

Cyclic voltammogram for a Pt electrode polarised at a sweep rate of 50mV sec^{-1} in a solution of 0.1M $Pb(NO_3)_2$, 1M KNO_3 , 0.1M HNO_3 plus 0.1 gl^{-1} cetyl trimethyl ammonium bromide.

1 = 1st scan 2 = 2nd scan

FIGURE 135

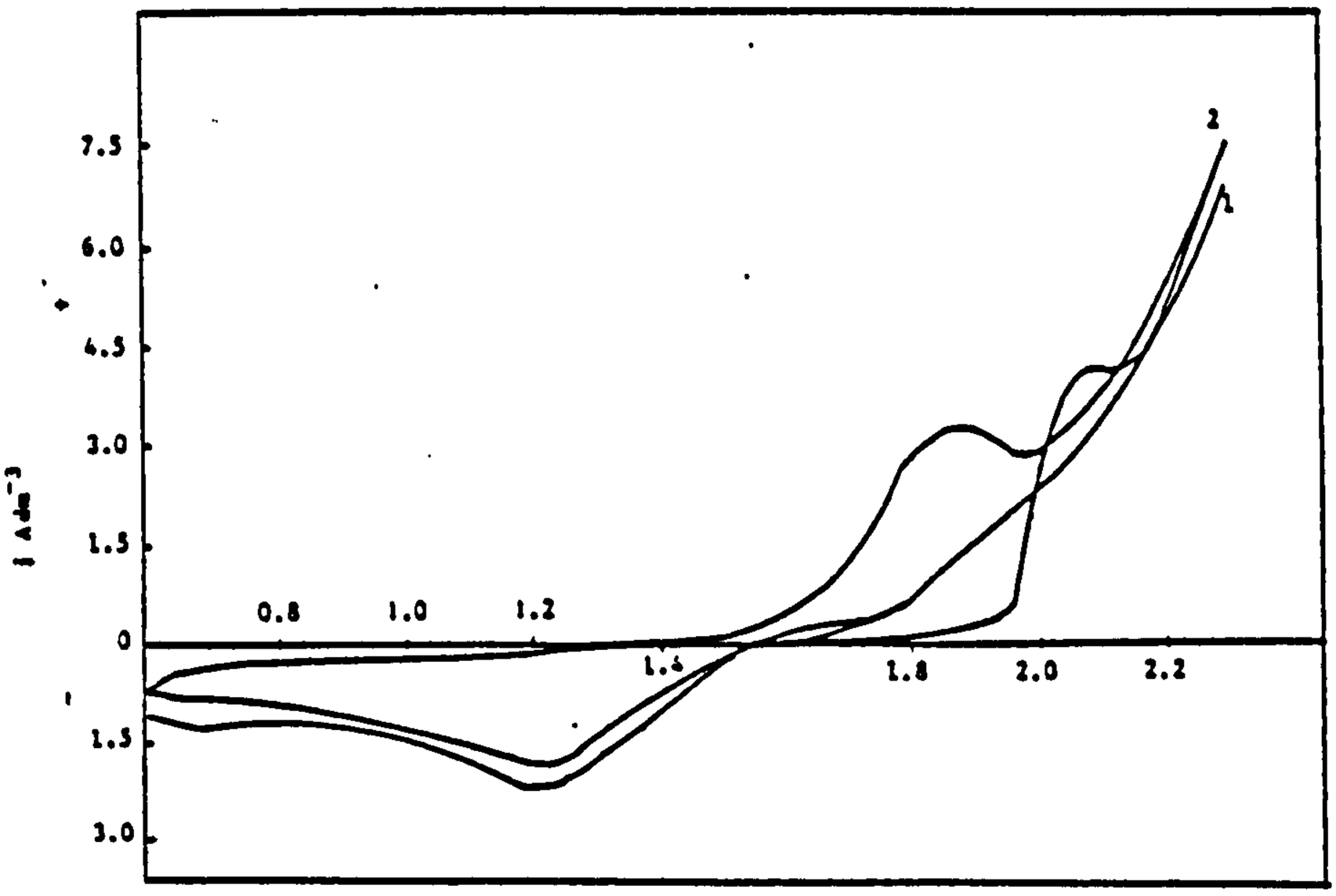

Cyclic voltammogram for a Pt electrode polarised at a sweep rate of 50mV sec^{-1} in a solution 0.1M $Pb(NO_3)_2$, 1M KNO_3 , 0.1M HNO_3 plus 1 gl^{-1} tannic acid.

1 = 1st scan 2 = 2nd scan

FIGURE 136

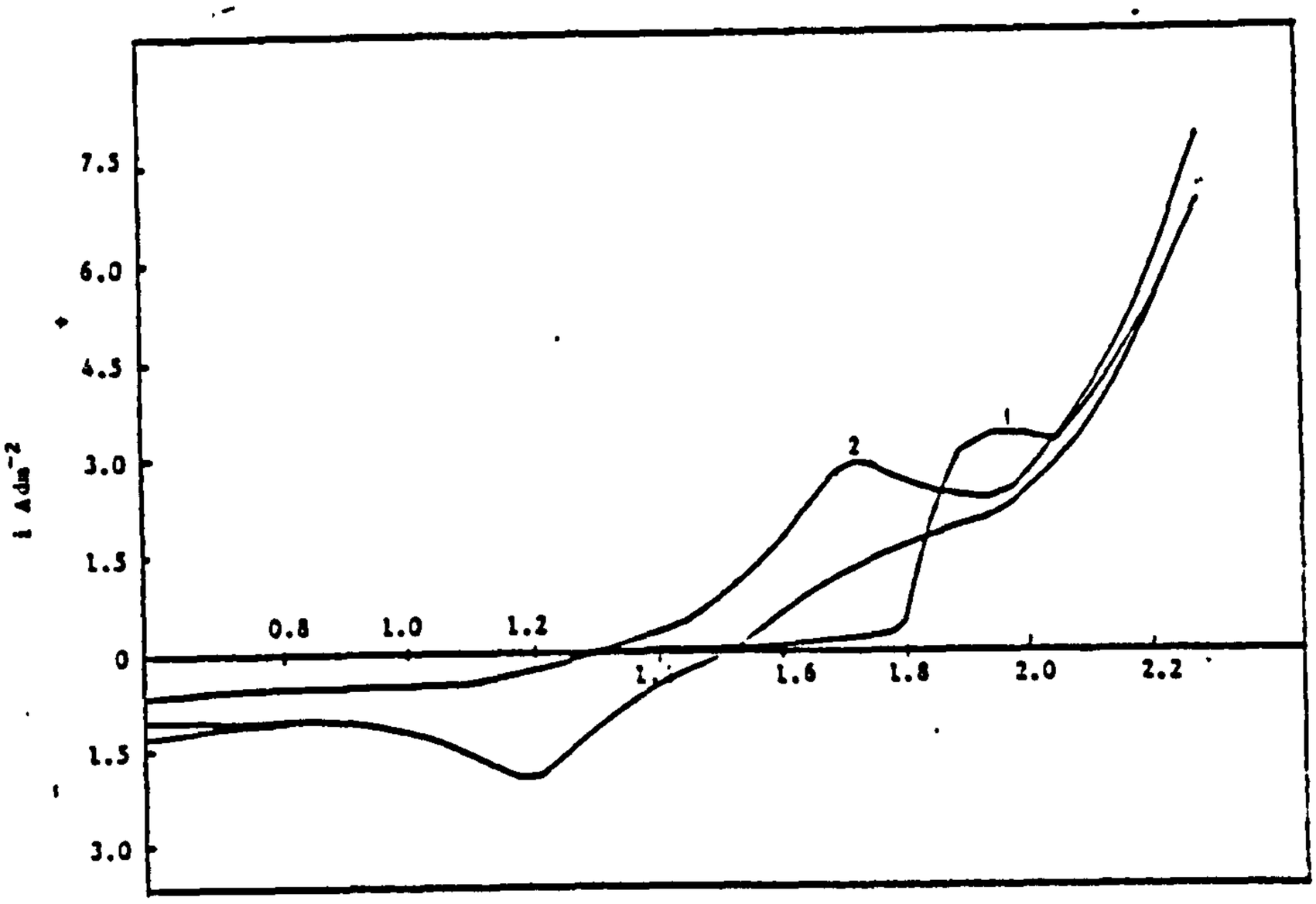

Cyclic voltammogram for a Pt electrode scanned at a sweep rate of 50 mV sec^{-1} in a stock solution of 0.1M $Pb(NO_3)_2$, 1M KNO_3, 0.1M HNO_3 plus 0.5 gl^{-1} diphenylamine.

1 = 1st scan 2 = 2nd scan

FIGURE 137

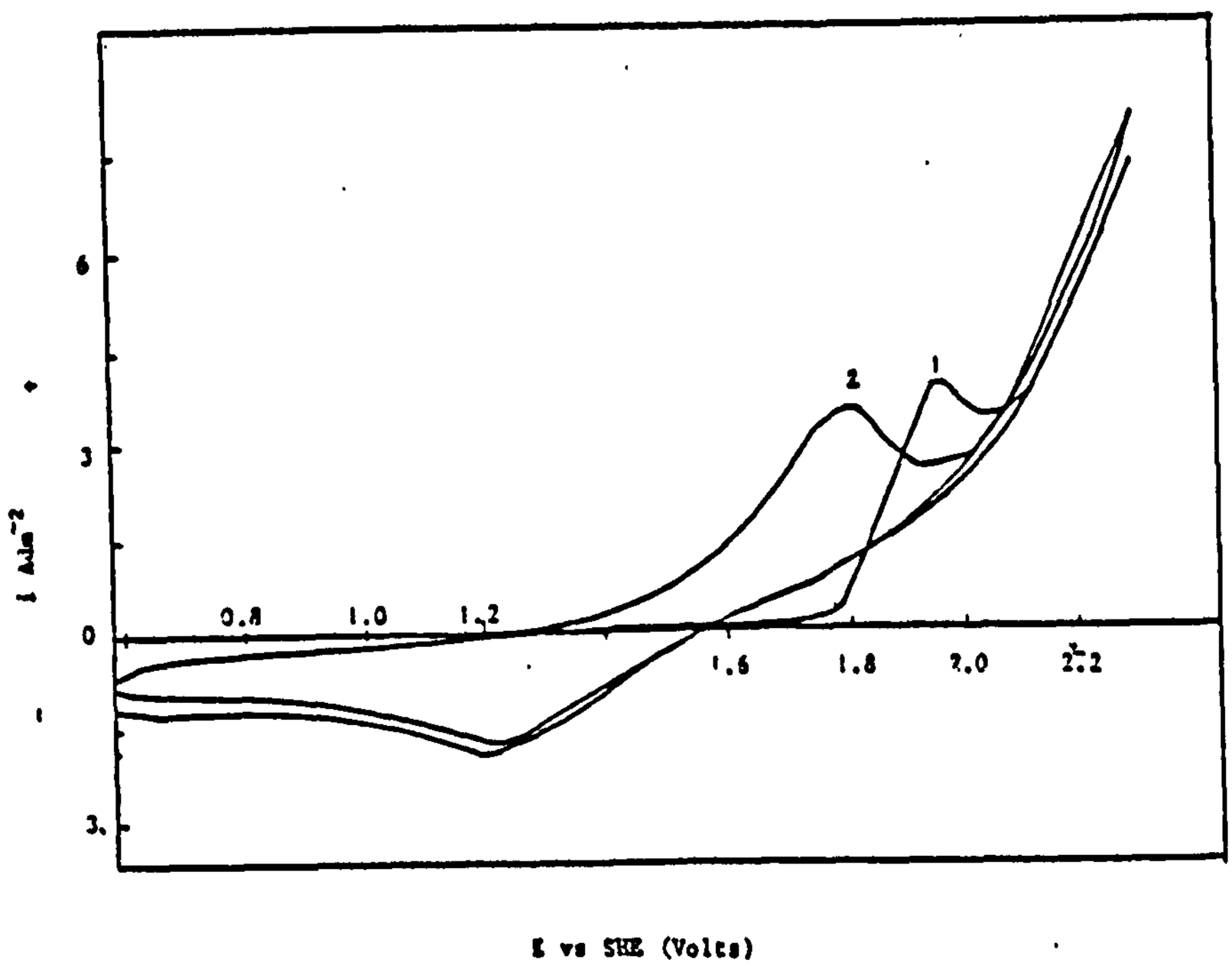

Cyclic voltammogram for a Pt electrode polarised at a sweep rate of 50mV sec^{-1} in a solution of 0.1M $Pb(NO_3)_2$, 1M KNO_3 , 0.1M HNO_3 plus 1 gl^{-1} Wafax.

FIGURE 138

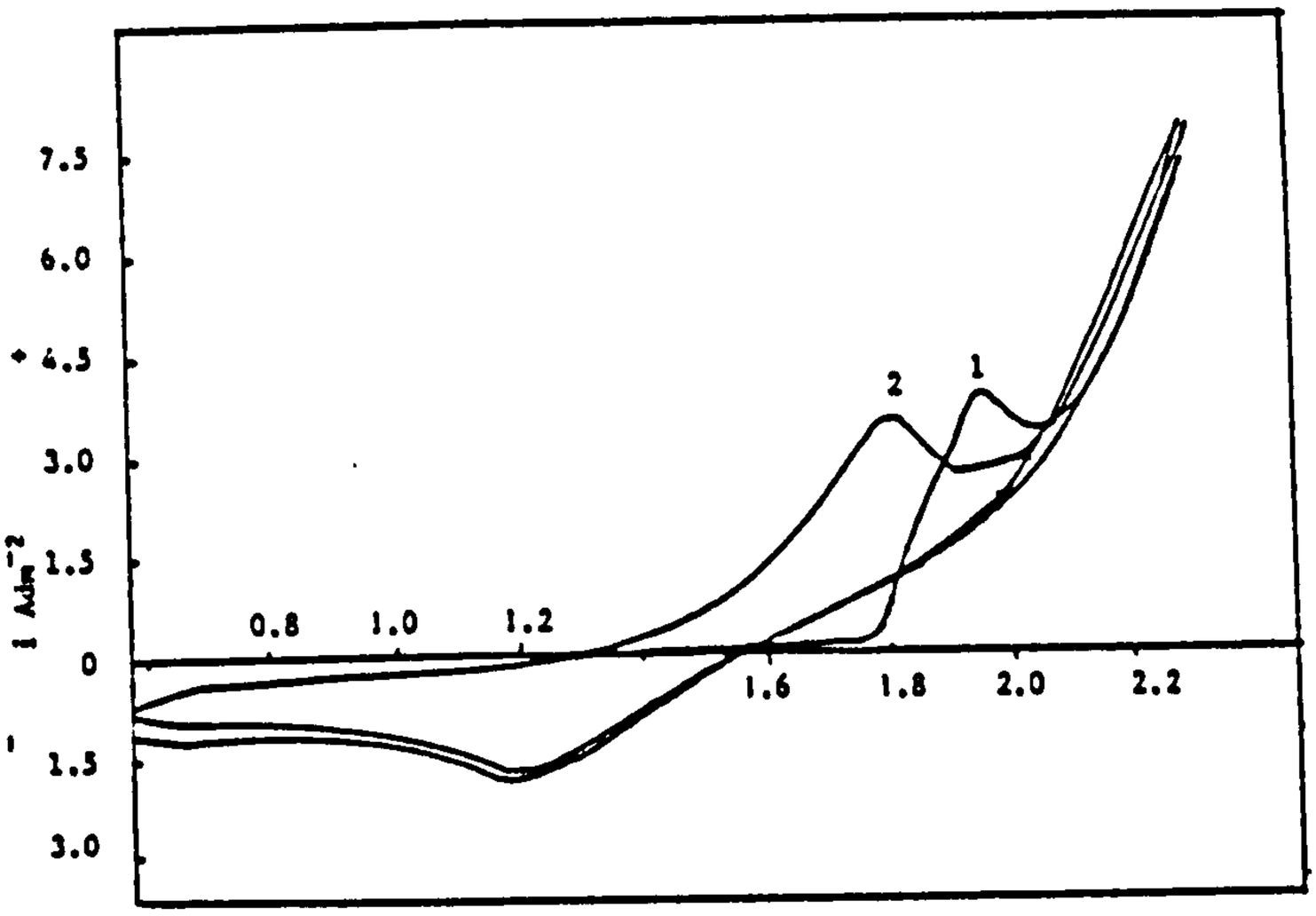

E vs SHE (Volts)

Cyclic voltammogram for a Pt electrode scanned at a sweep rate of 50 mV sec^{-1} from 0.6 volts in a stock solution of 0.1M $Pb(NO_3)_2$, 1M KNO_3, 0.1M HNO_3 , plus 0.1 gl^{-1} anthraquinone-2-monosulphonic acid.

1 = 1st scan 2 = 2nd scan.

FIGURE 139

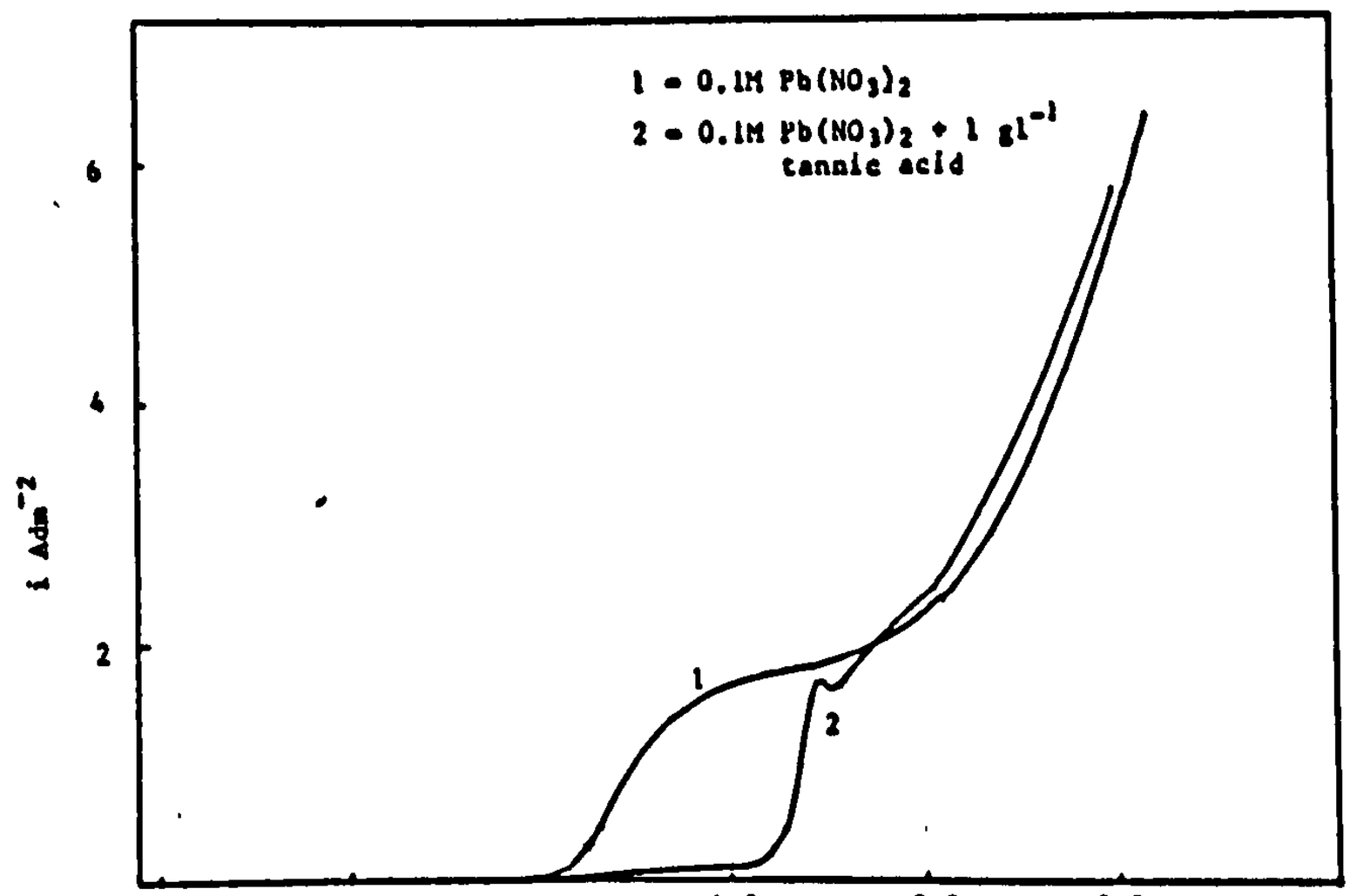

E vs SHE (Volts)

E vs i curve for a Pt electrode anodically polarised at a sweep rate of 5 mV sec^{-1} in 0.1M $Pb(NO_3)_2$, 1M KNO_3 , 0.1M HNO_3 with and without 1 gl^{-1} tannic acid.

FIGURE 140

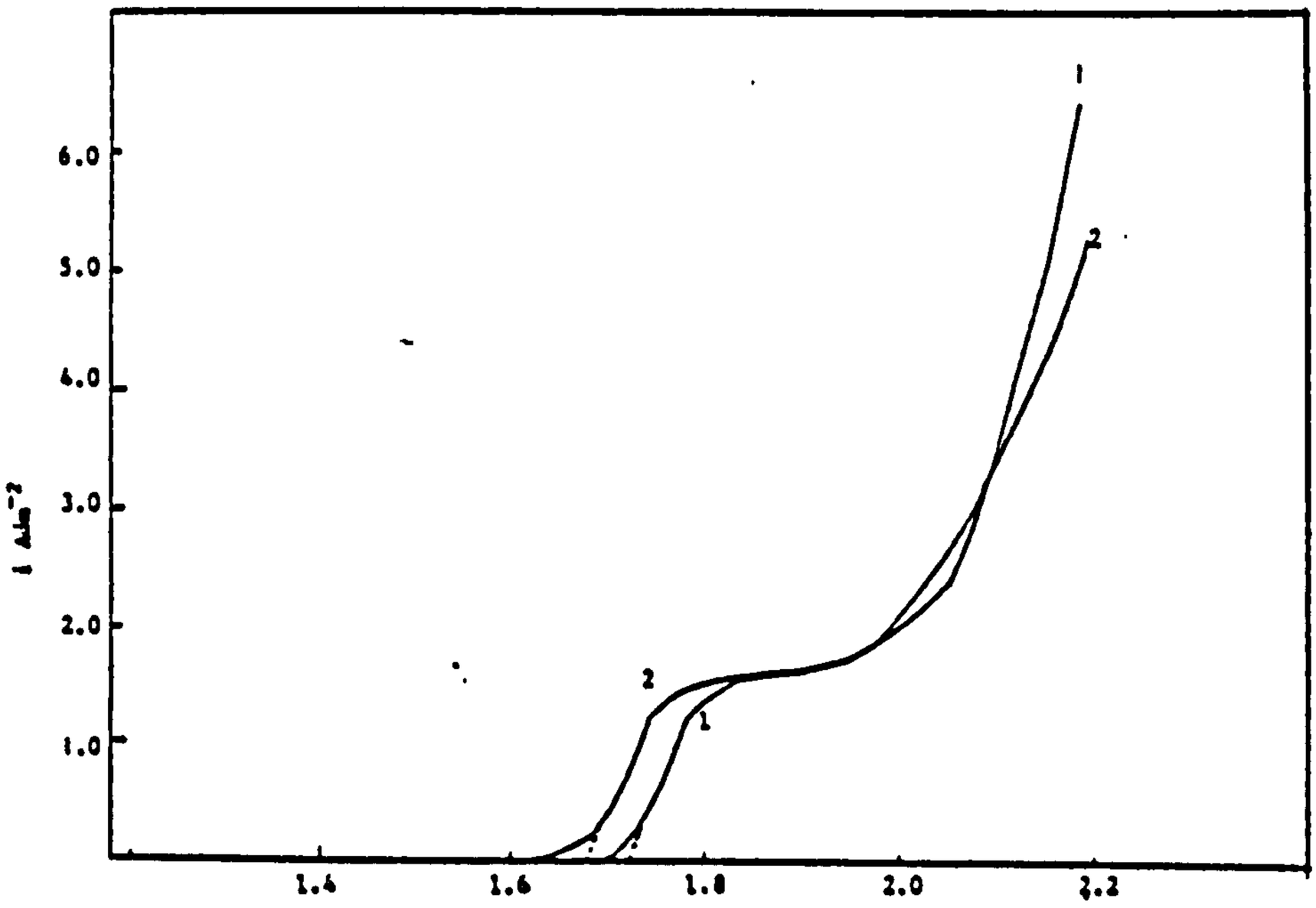

E vs i curve for a Pt electrode polarised at a sweep rate of 5mV sec^{-1} in a stock solution of 0.1M $Pb(NO_3)_2$, 1M KNO_3 , 0.1M HNO_3 plus selected addition agents.

1 = stock solution plus 1 gl^{-1} butyne 1,4 diol
2 = " " " 1 gl^{-1} Pluronic L64

FIGURE 141

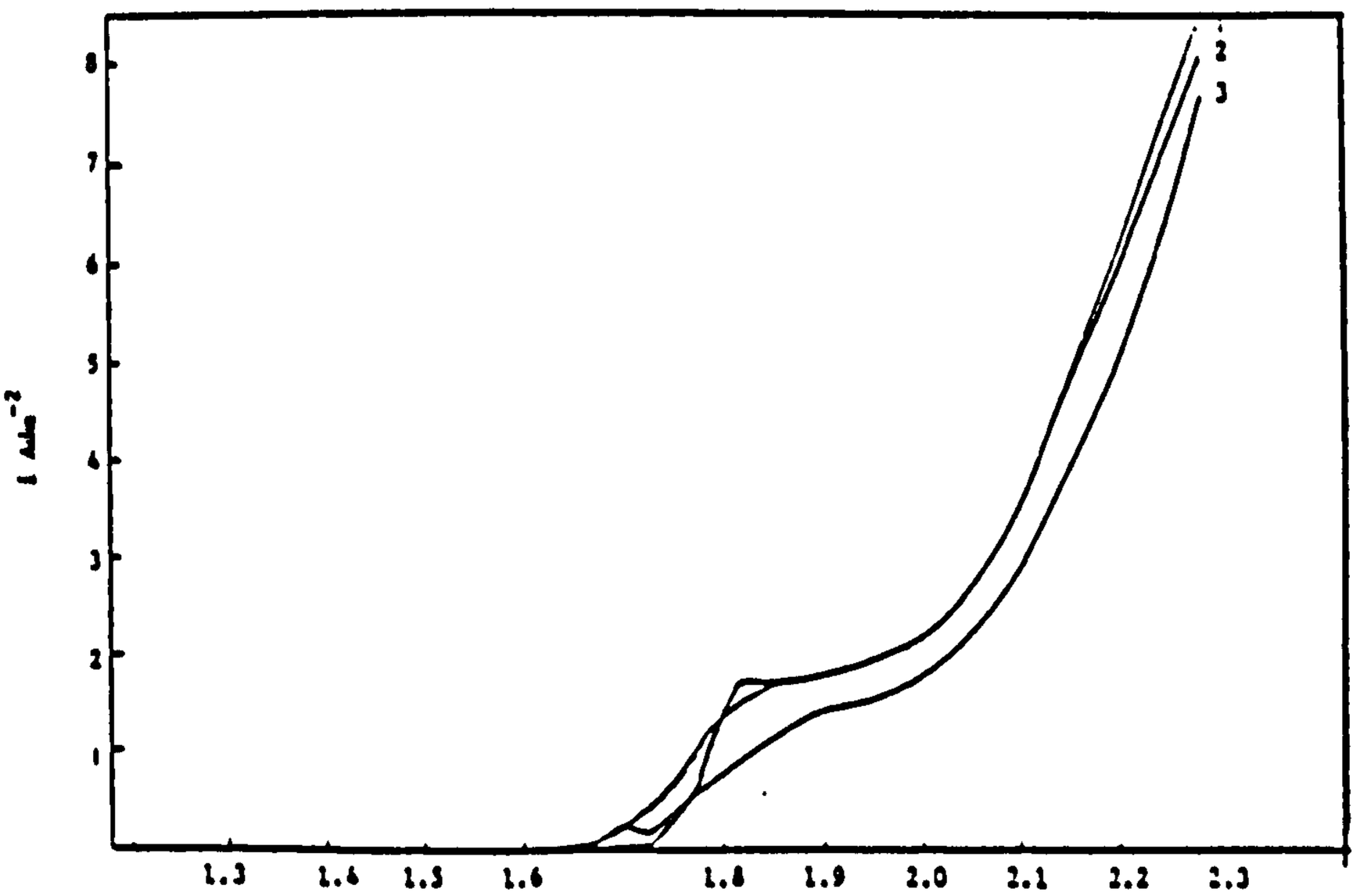

E vs i curve for a Pt electrode anodically polarised at a sweep rate of 5 mV sec^{-1} in a stock solution of 0.1M $Pb(NO_3)_2$, 1M KNO_3, 0.1M HNO_3 plus selected addition agents.

1 = stock solution plus 1 gl^{-1} Hyamine
2 = " " " 1 gl^{-1} Wafax
3 = " " " 0.1 gl^{-1} Cetyl trimethyl ammonium bromide.

FIGURE 142

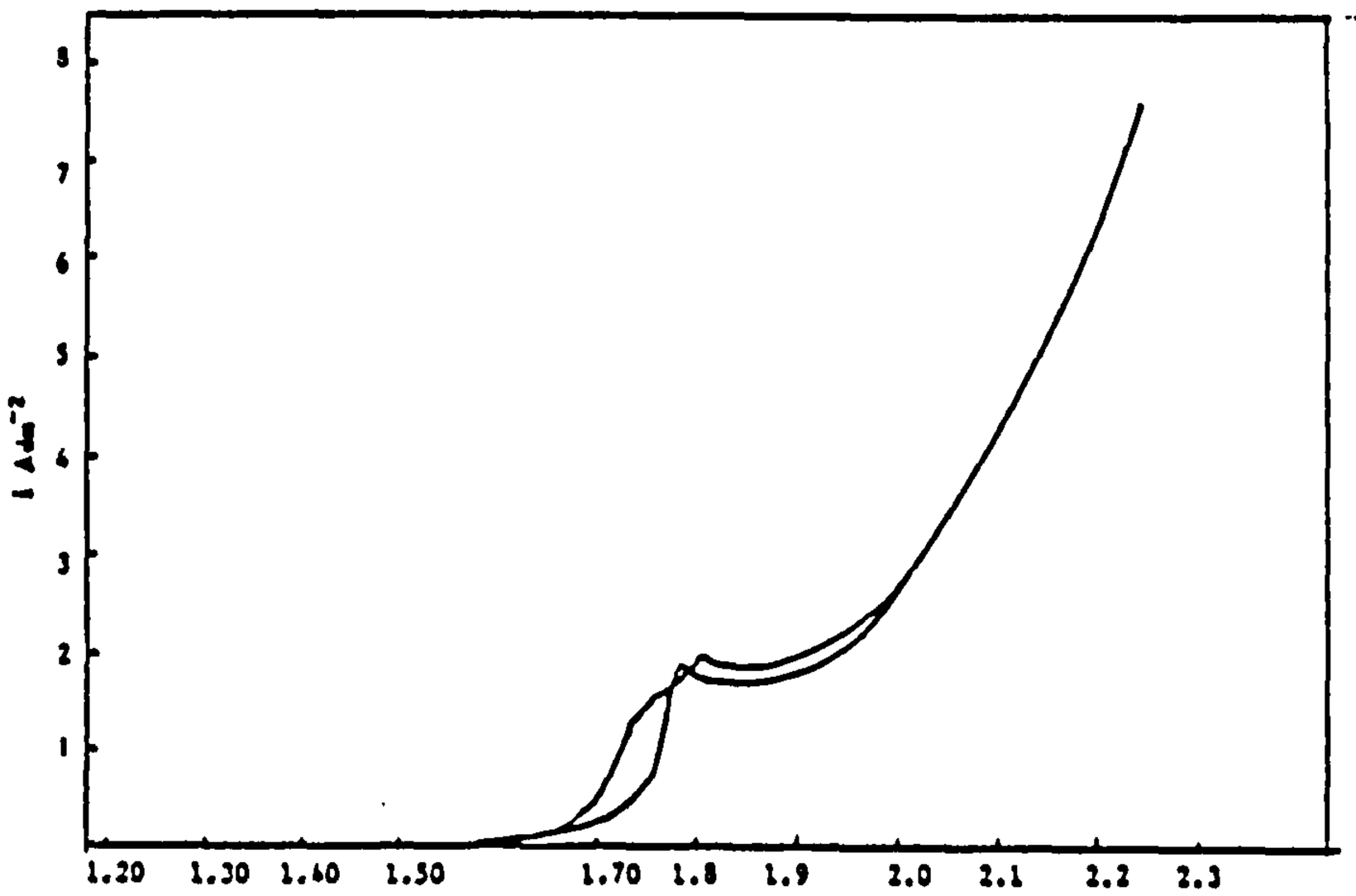

A graph of E vs i for a Pt electrode anodically polarised at a sweep rate of 5mV sec^{-1} in a solution of 0.1M $Pb(NO_3)_2$. 1M KNO . 0.1M HNO_3 plus 1 gl^{-1} Triton X100. The graph shows the reproducibility of two different scans.

FIGURE 143

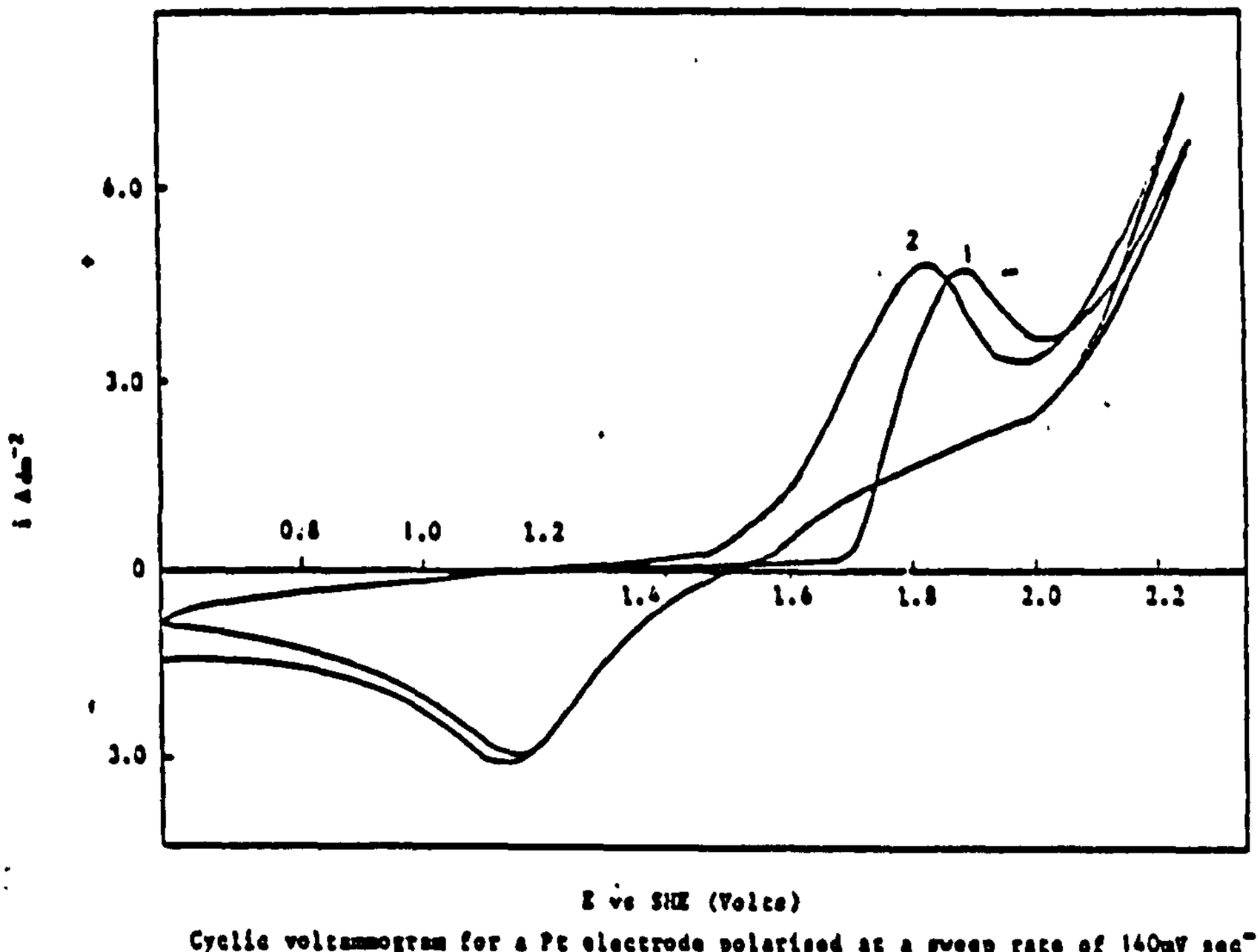

Cyclic voltammogram for a Pt electrode polarised at a sweep rate of 140mV sec^{-1} in a solution of 0.1M $Pb(NO_3)_2$, 1M KNO_3 plus 0.1M HNO_3 .

1 = 1st scan 2 = 2nd scan

FIGURE 144

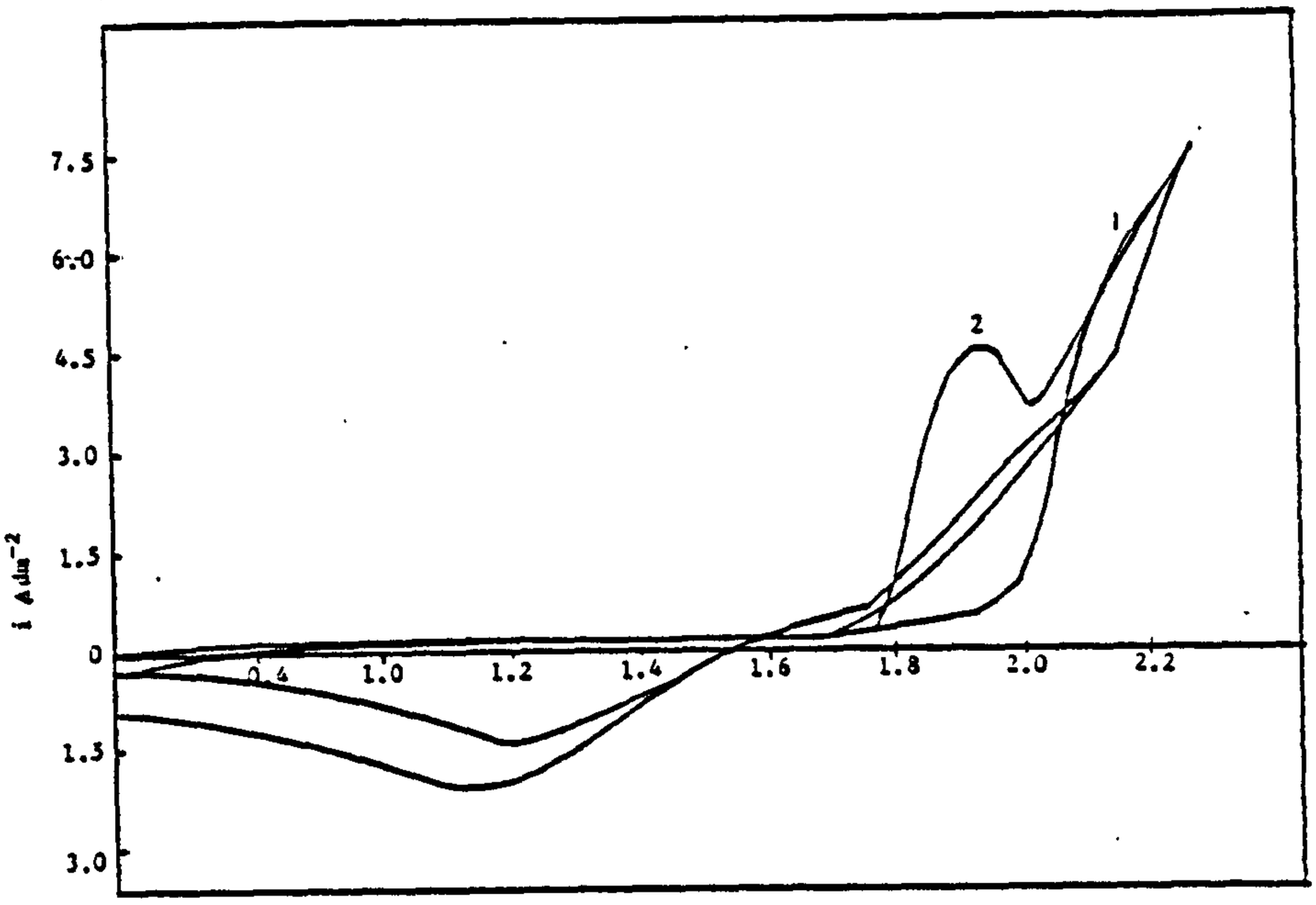

E vs SHE (Volts)

Cyclic voltammogram for a Pt electrode polarised at a sweep rate of 140mV sec^{-1} from volts in a solution of 0.1M $Pb(NO_3)_2$, 1M KNO_3 , 0.1M HNO_3 plus 1 gl^{-1} tannic acid.

1 = 1st scan 2 = 2nd scan

FIGURE 145

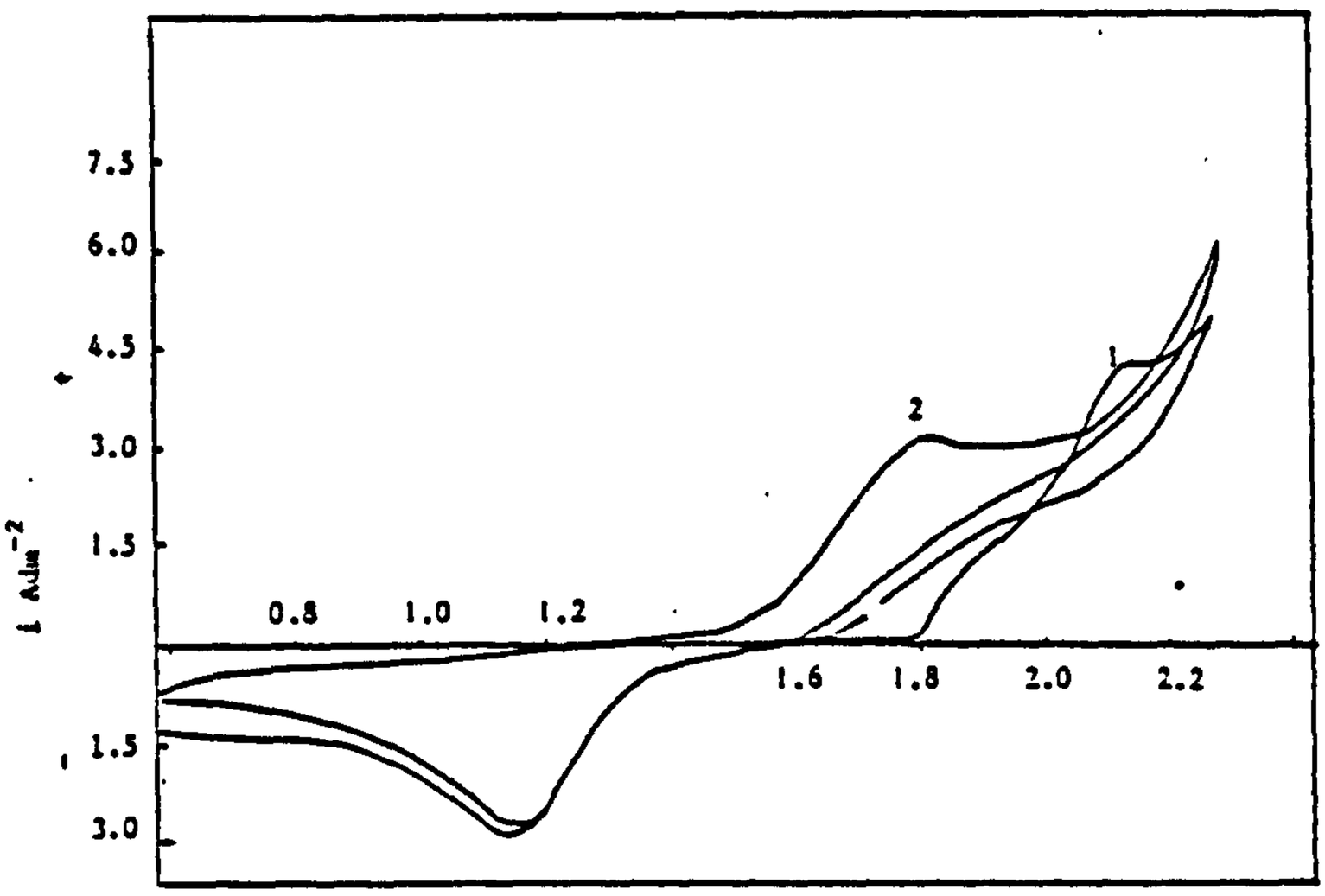

E vs SHE (Volts)

Cyclic voltammogram for a Pt electrode anodically polarised at a sweep rate of 140 mV sec^{-1} in a solution of 0.1M $Pb(NO_3)_2$, 1M KNO_3 , 0.1M HNO_3 plus 0.1 gl^{-1} cetyltrimethylammonium bromide.

1 = 1st scan 2 = 2nd scan.

FIGURE 146

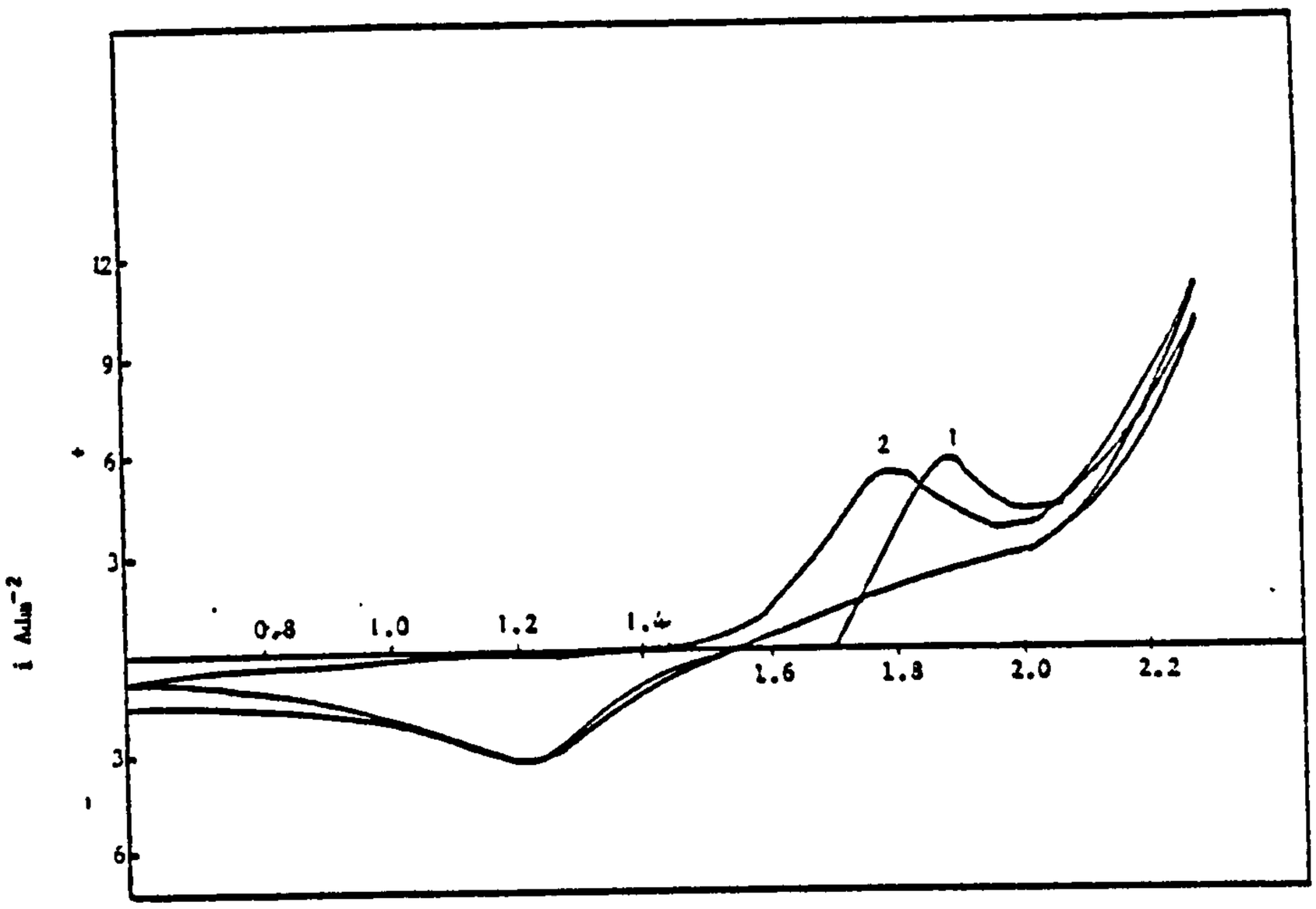

A cyclic voltammogram for a Pt electrode anodically polarised at a sweep rate of 140mV sec^{-1} in a 0.1M $Pb(NO_3)_2$, 0.5M KNO_3, 0.1M HNO_3 solution plus 1 gl^{-1} butyne 1,4 diol.

1 = 1st scan 2 = 2nd scan

FIGURE 147

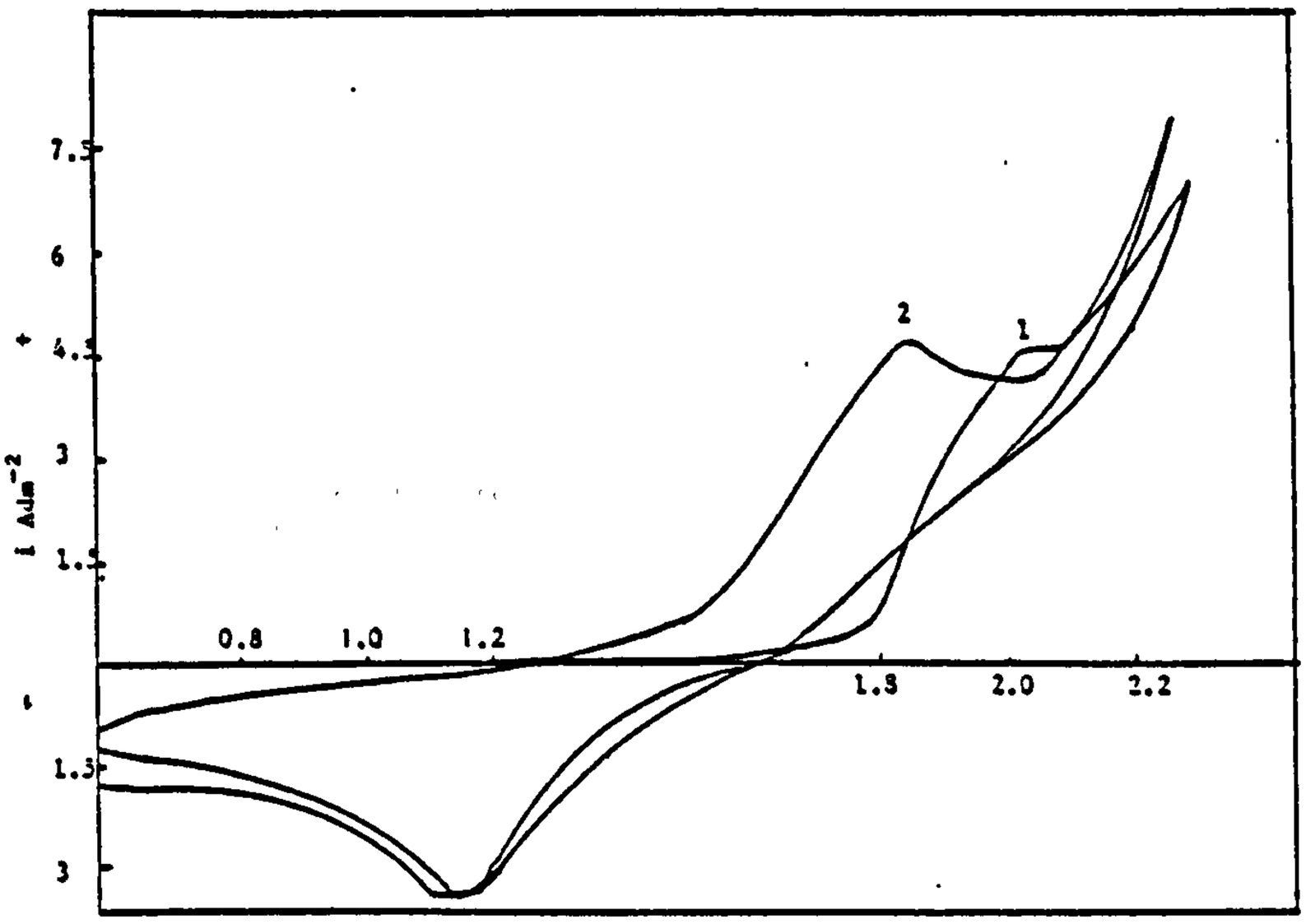

Cyclic voltammogram for a Pt electrode anodically polarised at a sweep rate of 140 mV sec^{-1} in a solution of 0.1M $Pb(NO_3)_2$, 1M KNO_3 , 0.1M HNO_3 plus 0.1 gl^{-1} of Hyamine.

FIGURE 148

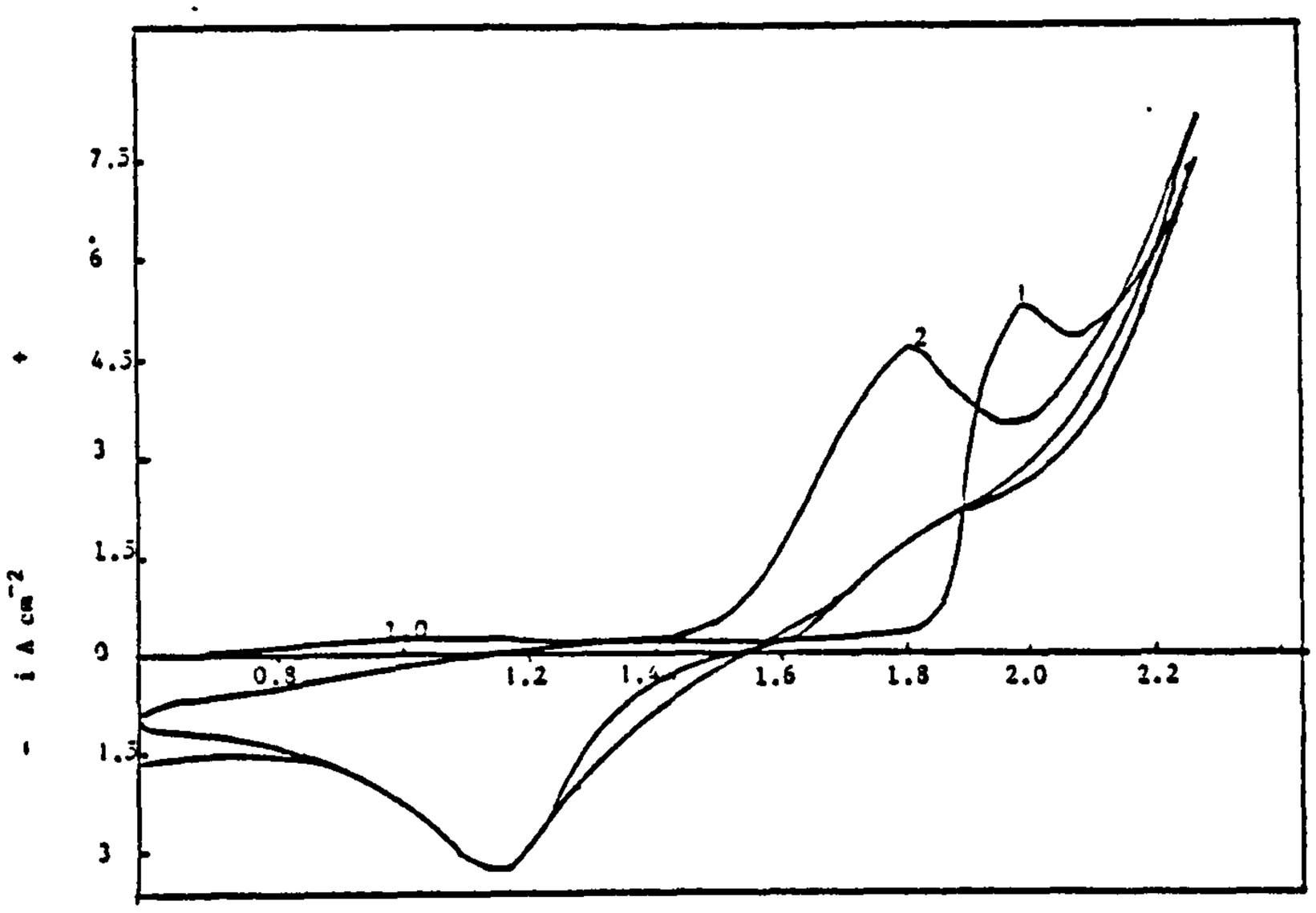

E vs SHE (Volts)

Cyclic voltammogram for a Pt electrode polarised at a sweep rate of 140 mV sec^{-1} in a solution of 0.1M $Pb(NO_3)_2$, 1M KNO_3, 0.1M HNO_3 plus 0.5 gl^{-1} diphenylamine.

FIGURE 149

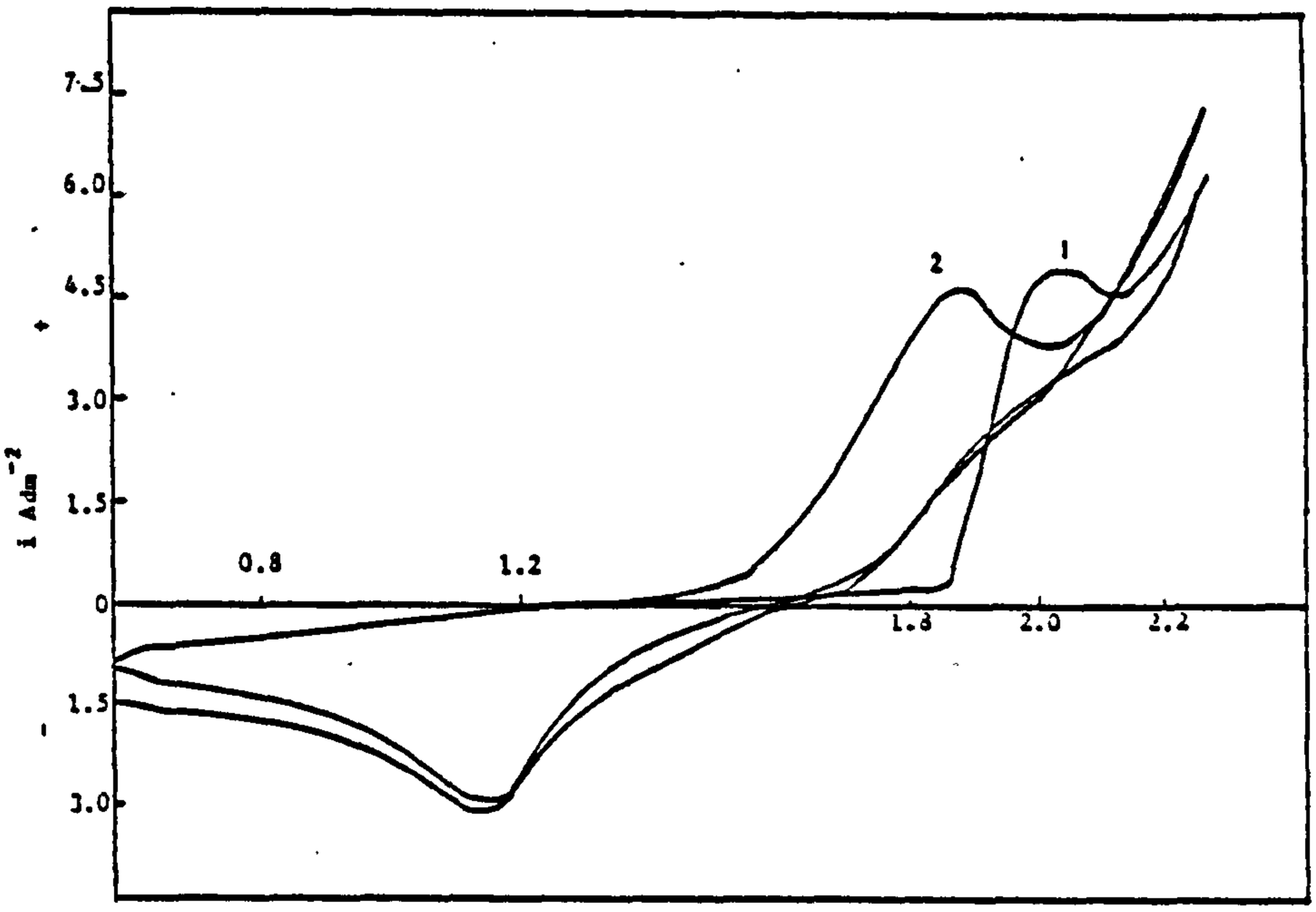

E vs SHE (Volts)

Cyclic voltammogram for a Pt electrode scanned at a sweep rate of 140mV sec^{-1} in a solution of 0.1M $Pb(NO_3)_2$, 1M KNO_3 , 0.1M HNO_3 plus 1 gl^{-1} Wafex.

1 = 1st scan 2 = 2nd scan

FIGURE 150

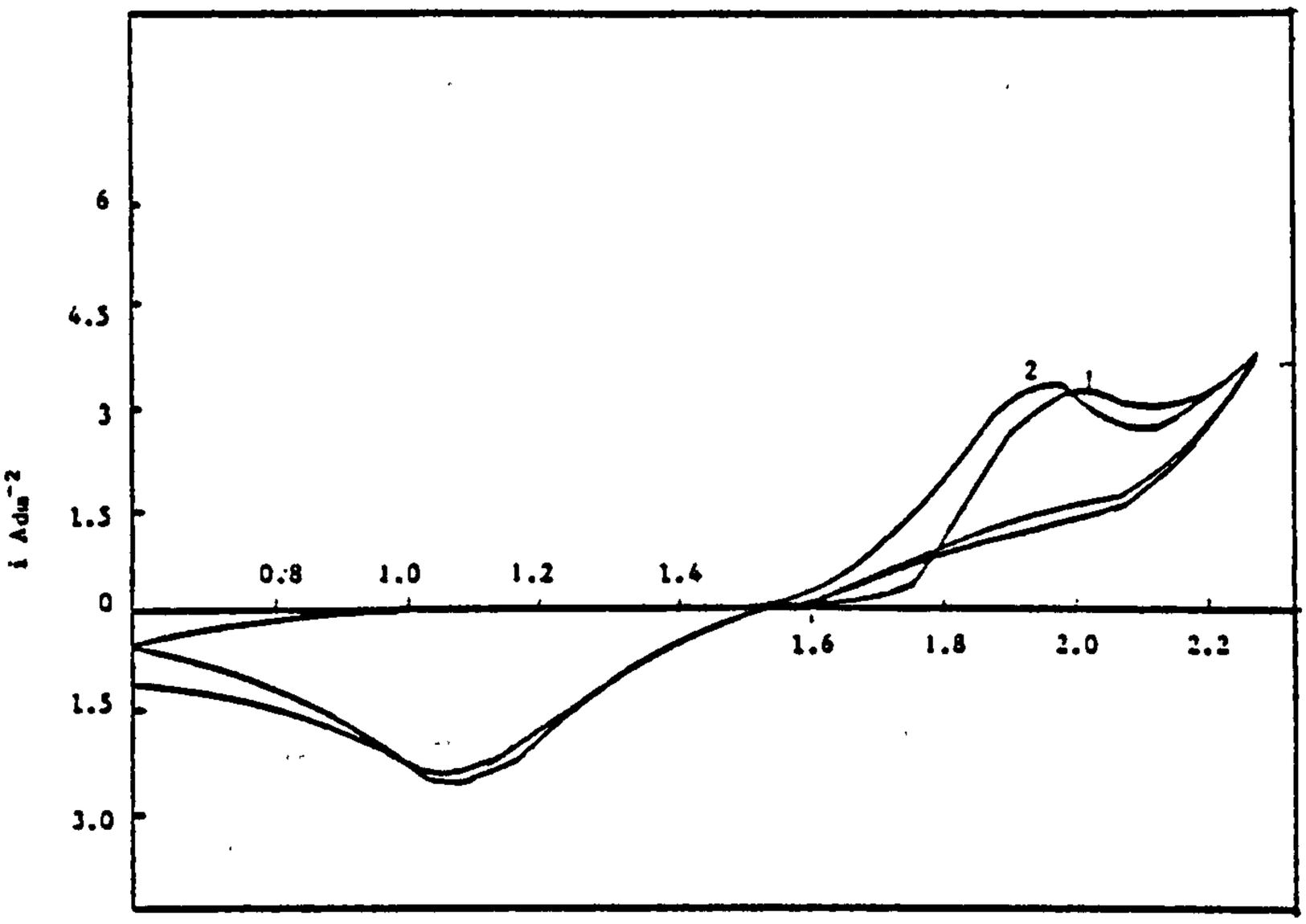

Cyclic voltammogram for a Pt electrode scanned at a sweep rate of 250 mV sec^{-1} from a solution of 0.1M $Pb(NO_3)_2$, 1M KNO_3 0.1M HNO_3 .

1 = 1st scan 2 = 2nd scan

FIGURE 151

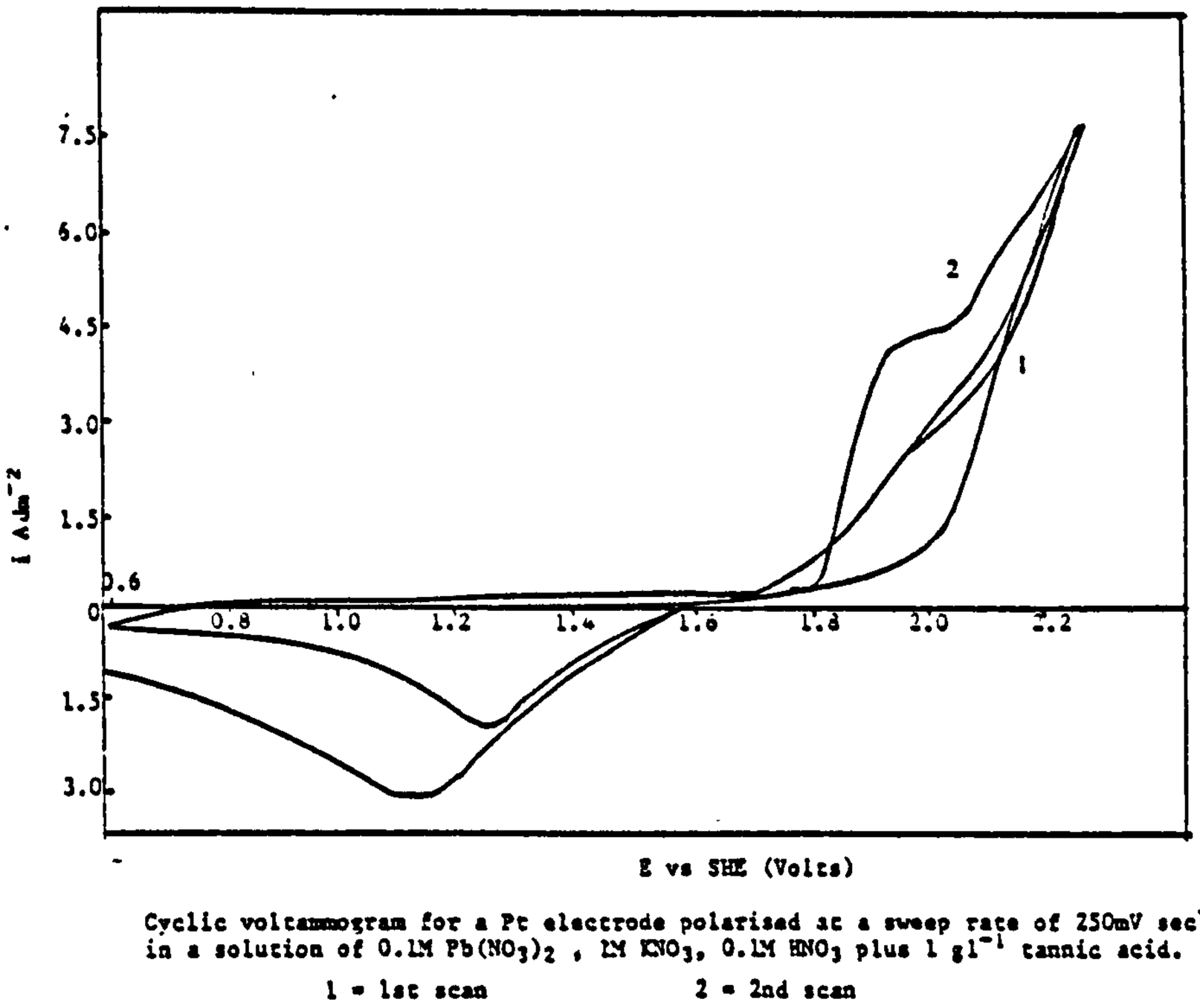

Cyclic voltammogram for a Pt electrode polarised at a sweep rate of 250mV sec^{-1} in a solution of 0.1M $Pb(NO_3)_2$, 1M KNO_3, 0.1M HNO_3 plus 1 gl^{-1} tannic acid.

1 = 1st scan 2 = 2nd scan

FIGURE 152

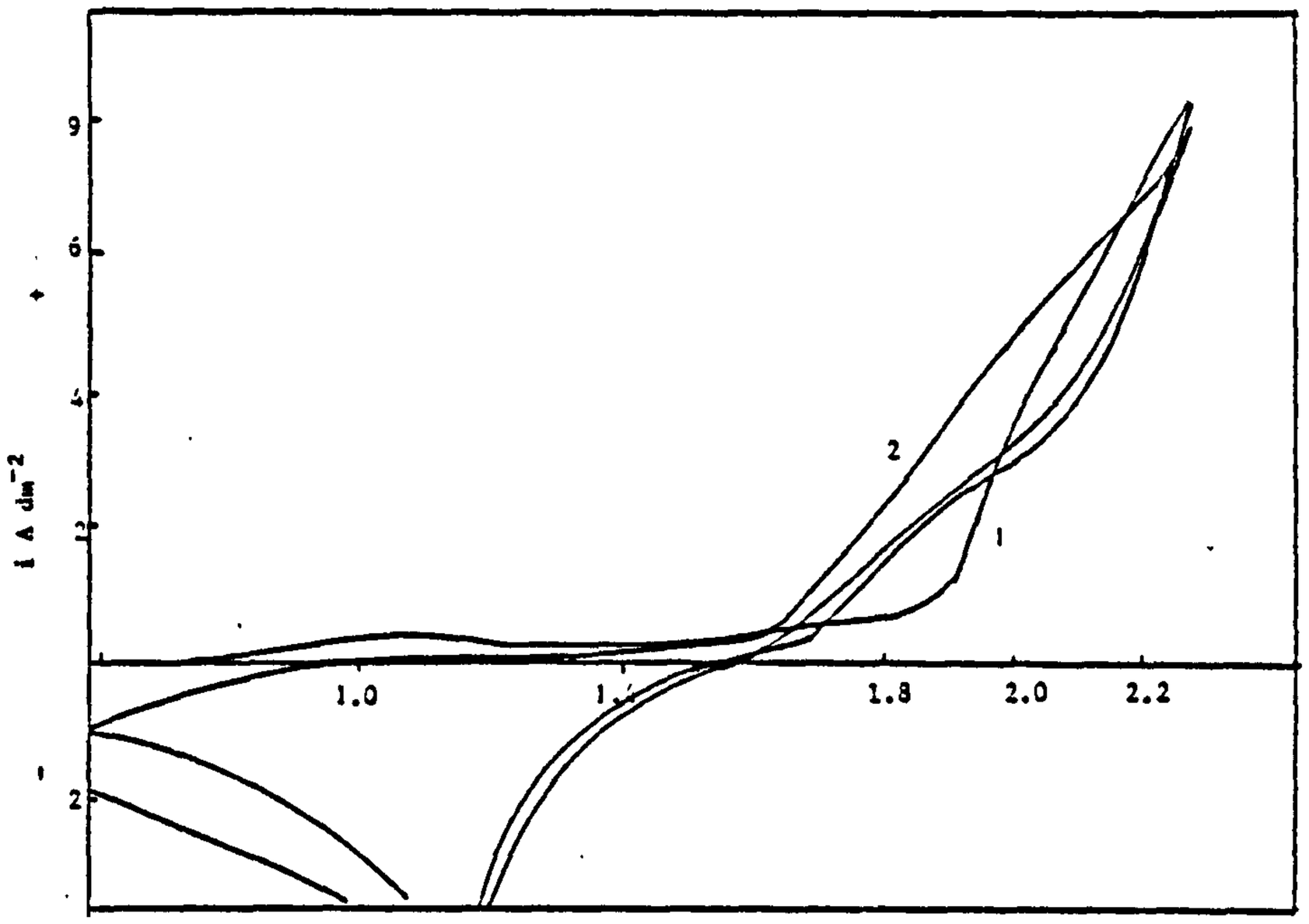

Cyclic voltammogram for a Pt electrode polarised at a sweep rate of 250 mV sec^{-1} in a solution of 0.1M $Pb(NO_3)_2$, 1M KNO_3, 0.1M KNO_3 plus 0.5 gl^{-1} diphenylamine.

1 = 1st scan 2 = 2nd scan

FIGURE 153

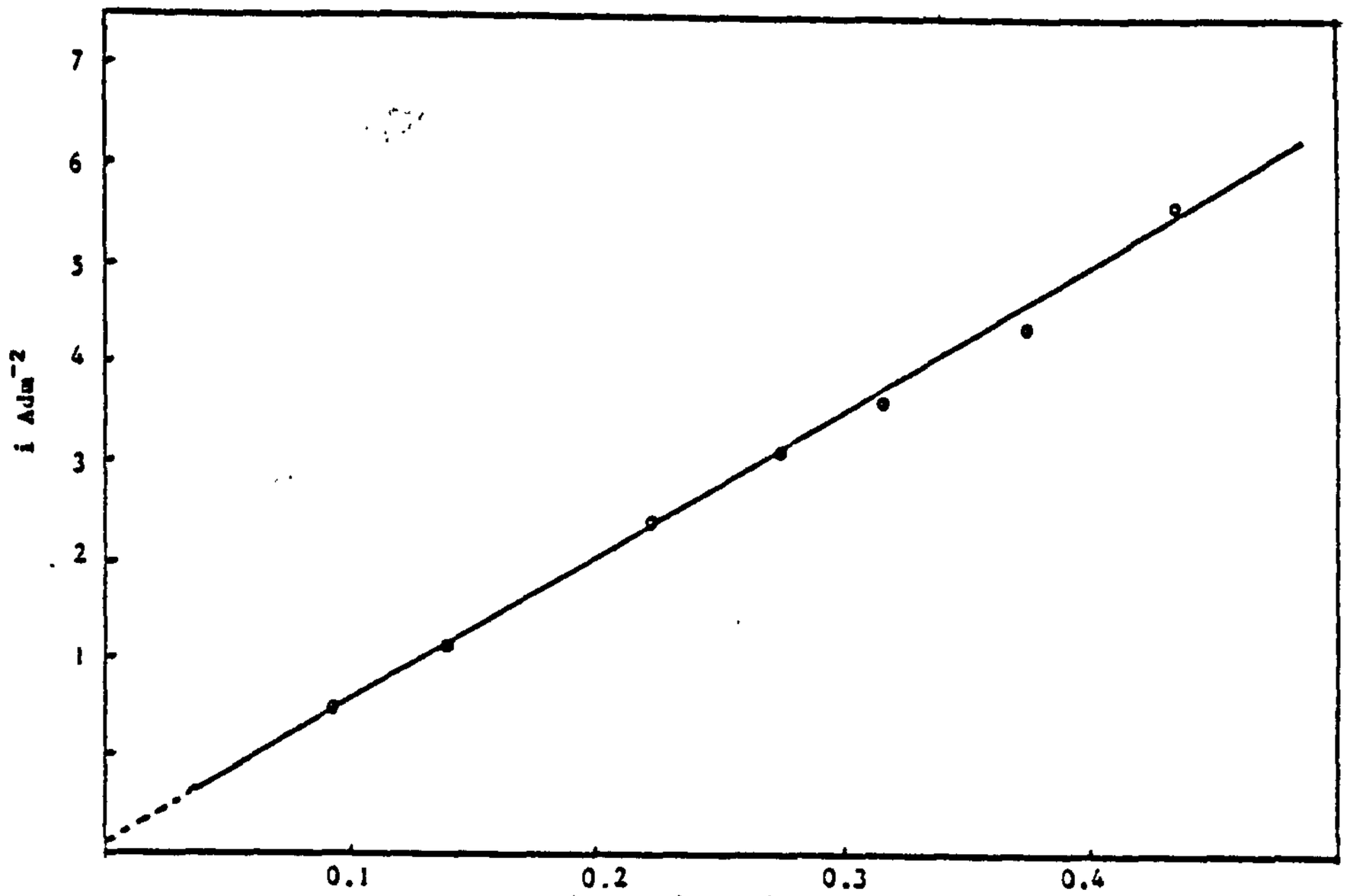

A graph of i_p vs $V^{\frac{1}{2}}$ for the electrodeposition of PbO_2 from a solution of 0.1M $Pb(NO_3)_2$ + 0.5M KNO_3 + 0.1M HNO_3 on a Pt electrode.

FIGURE 154

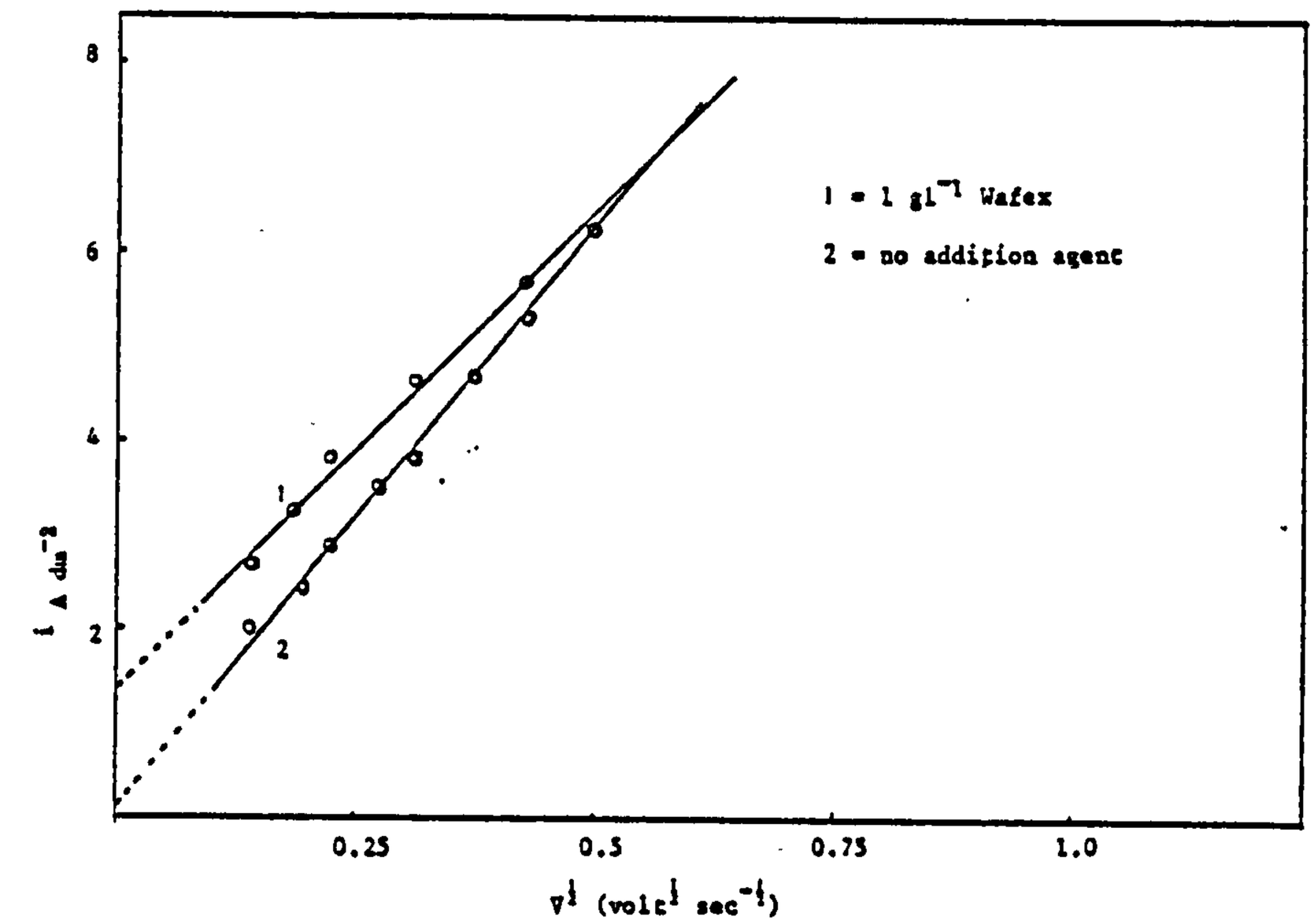

i_p vs $V^{\frac{1}{2}}$ for Pt electrode anodically polarised at difference sweep rates in a solution of 0.1M $Pb(NO_3)_2$ + 0.5M KNO_3 + 0.1M HNO_3 with and without 1 gl^{-1} Wafex.

FIGURE 155

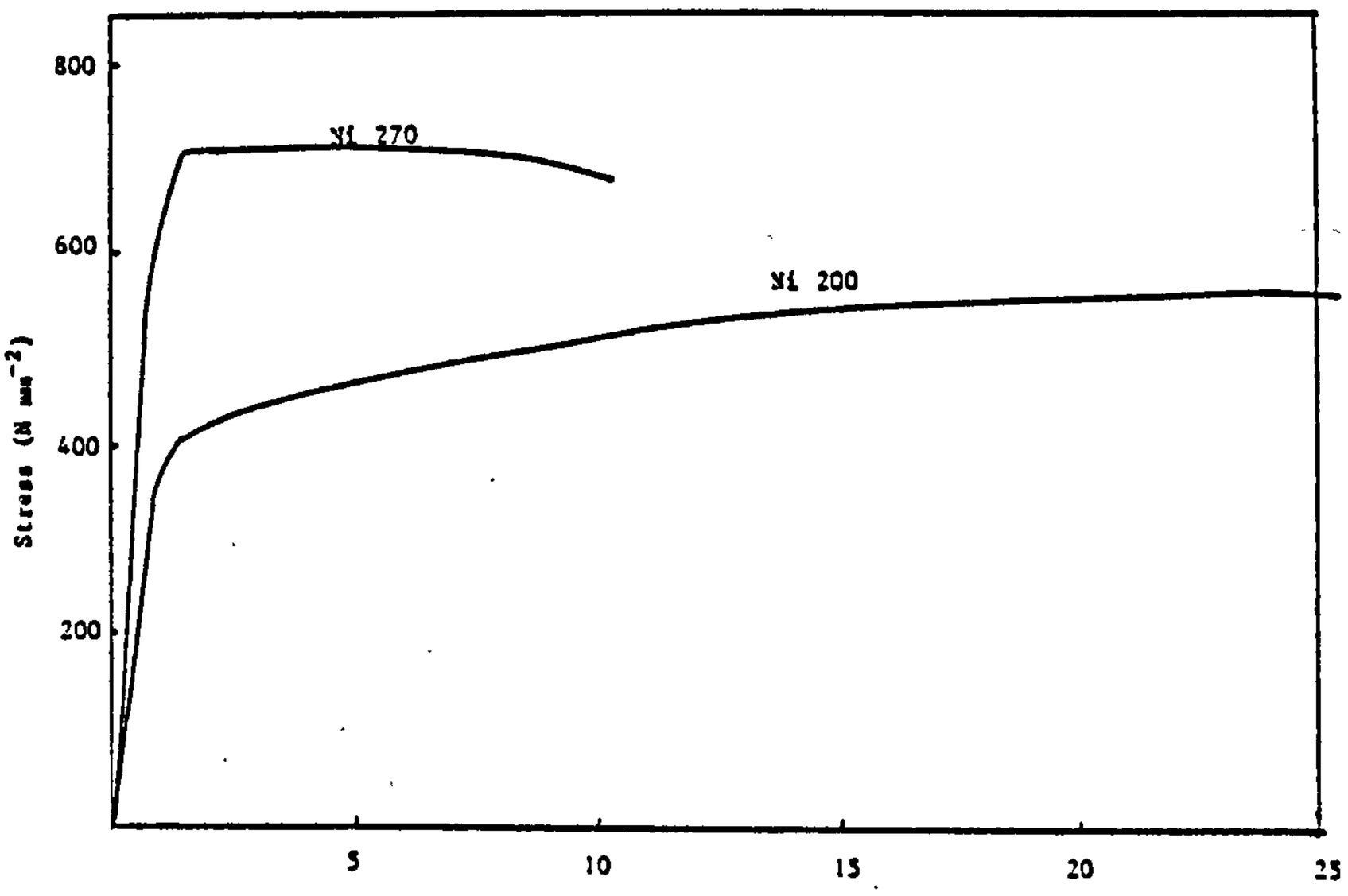

A graph of stress vs % elongation for a sample of Ni270 and a sample of Ni200 foil. The Ni270 foil thickness = 125 um, Ni200 foil thickness = 200 µm.

FIGURE 156

TABLE 57

Value of E_p, and i_p for the anodic polarisation of a Pt electrode in the stock solution at selected sweep speeds

E_p Volts	$E_{p/2}$ Volts	$E_p - E_{p/2}$ Volts	i_{p_2} Adm	v $mVsec^{-1}$	$v^{1/2}$ $mV^{1/2}sec^{-1/2}$
1.8	1.687	0.113	1.98	20	0.141
1.843	1.726	0.117	2.87	50	0.223
1.890	1.777	0.113	3.51	75	0.274
1.902	1.787	0.115	3.79	100	0.316
1.910	1.793	0.117	4.71	140	0.374
1.933	1.801	0.132	5.29	190	0.436
1.983	1.832	0.151	6.18	250	0.50
2.120	1.917	0.203	7.79	500	0.707

TABLE 58

Stock solution + 1 gl^{-1} Wafex

E_p Volts	$E_{p/2}$ Volts	$E_p - E_{p/2}$ Volts	i_{p_2} Adm	v $mVsec^{-1}$	$v^{1/2}$ $mV^{1/2}sec^{-1/2}$
1.933	1.851	0.082	2.65	20	0.141
1.956	1.847	0.109	3.82	50	0.223
2.027	1.925	0.102	4.63	100	0.316
2.066	1.941	0.125	5	140	0.374
2.089	1.964	0.125	5.66	190	0.436
2.144	1.992	0.152	6.54	250	0.50

TABLE 59

Stock solution + 1 gl^{-1} BRIJ 35

E_p Volts	$E_{p/2}$ Volts	$E_p - E_{p/2}$ Volts	i_{p_2} Adm	v $mVsec^{-1}$	$v^{1/2}$ $mV^{1/2}sec^{-1/2}$
1.808	1.738	0.070	2.06	20	0.141
1.847	1.781	0.066	3.42	50	0.224
1.871	1.802	0.069	4.15	75	0.274
1.894	1.820	0.074	4.6	100	0.316
1.910	1.827	0.082	5.35	140	0.374
1.941	1.820	0.121	6.62	190	0.436

3.3 The Adhesion of β-PbO_2 onto Ni Foils

3.3.1 Chemical analysis of Ni foil

The results of the atomic absorption analysis for individual impurity elements in samples of Ni foil from different sources are given in Table 60.

The nominal chemical compositions for Ni alloy foils are listed in Table 61, whilst the composition of typical Ni200 and Ni270 samples supplied by Henry Wiggins and Co and used as the substrates for the electrodeposition of both Pb and PbO_2 is given in Table 62.

The results of the atomic absorption anaylsis show that the sample of 'good' adhesion foil conforms to the specification for Ni200 given in BS 3073, whilst all samples of 'bad' adhesion foil meet the specification for Ni270, except in respect of the Si content.

TABLE 60

Impurity levels in different Ni foils determined by atomic absorbtion (values in ppm)

Element	Good adhesion Ni source RARDE	Bad adhesion Ni source Ionic Plating 125 µm thick	Bad adhesion Ni source Ionic Plating 200 µm thick	Bad adhesion Source RARDE 200 µm thick	Bad adhesion source RARDE annealed at 800°C 200 µm thick
Si	670	290	230	250	250
Fe	1200	268	91	140	140
Cu	270	30	3	2	2
Mn*	1700	66	1	1	1
Cr*	120	2	1	1	1
Mo	-	40	18	50	50

*The detection limit for Mn and Cr in the foil samples was 1ppm

Table 61

Nominal chemical composition of Ni alloys taken from BS 3073.

(All Values given in %)

Nickel Alloy	Element												
	Ni	C	Mn	Fe	S	Si	Cu	Cr	Co	Mo	Al	Ti	others
Ni200	99.5	0.08	0.18	0.2	0.0005	0.18	0.13	-	-	-	-	-	-
Ni201	99.5	0.01	0.18	0.2	0.0005	0.18	0.13	-	-	-	-	-	-
Ni205	99.5	0.08	0.18	0.10	0.0004	0.08	0.08	-	-	-	-	0.03	Mg 0.05
Ni212	97.7	0.10	2.0	0.05	0.0005	0.05	0.03	-	-	-	-	-	-
Ni222	99.5	0.01	0.02	0.04	0.0025	0.01	0.01	0.01	0.06	-	0.01	0.01	Mg 0.08
Ni270	99.98	0.01	0.003	<0.001	<0.001	<0.001	<0.001	<0.001	<0.001	-	-	<0.001	Mg 0.001

Table 62

Typical values for the chemical composition of Ni200 and Ni270 foil supplied by Henry Wiggins and Co. Ltd., used as substrates for the electrodeposition of Pb and PbO_2

(All Values given in %)

Nickel Alloy	Element												
	C	Si	Cu	Fe	Mn	Mg	Cr	Ti	Al	Co	Mo	Ni	S
Ni200	0.012	0.05	0.037	0.12	0.19	0.12	-	0.25	-	0.069	-	99.4	0.003
Ni270	.012	<0.001	<0.001	.006	<0.001	<0.001	<0.001	<0.001	-	<0.001	-	Bal	<0.001

The results of the XRFS analysis confirm the analysis obtained using atomic absorption for the good adhesion foil, with the following elements detected, Mn 0.3%, Fe 0.1-0.5% and Ti 0.1-0.5%. Trace amounts of K and Cl were also detected (0.01%). A sample of Ni270 foil 200 microns thick supplied by the Ionic Plating Co Ltd, that produced a randomly etched surface after anodic etching in 30% H_2SO_4 was examined using XRFS. This was carried out to see if there were any differences in the surface composition of the Ni in the etched and unetched areas. One observable difference was that a high S current was found in the well etched areas of the Ni. The Fe content of this foil was found to be about 0.01%, and trace amounts of K, Cl,P were also detected. The Cr content of the etched area was also lower than for the unetched area. A high Si content was not detected using XRFS.

3.3.2 Anodic etching of Ni foils in 30 wt% H_2SO_4

One immediate observation after the anodic etching of Ni foils in 30% by wt H_2SO_4 at 50°C and at a current density of 2.7 Adm^{-2} was the uneven random etch pattern found on all samples of the bad adhesion foils.

In fact, large areas of the Ni270 specimens were found to be completely unaffected by the etching solution as can be seen in Fig. 75P. The etch pattern was found to be completely random and varied from sample to sample. This uneven etch was only observed for Ni270 foils. The samples of Ni200 etched in the same manner, all showed an evenly etched surface with no apparent tendency for certain areas to be unaffected by the etching solution (see Fig. 74P). The pre-treatment carried out on all samples has been described in Section 2.1.

Samples of a Ni270 foil that exhibited a random etch pattern were annealed in a hydrogen atmosphere at 500°C and also under vacuum at 800°C. In both cases the heat treatment was carried out for 30 mins. The samples heated to 500°C still exhibited

a randomly etched surface after anodic etching in 30% by wt H_2SO_4. However, the samples heated to 800°C all showed a smooth-faceted evenly etched surface with all areas of the foil affected by the etching process.

Variations in the etch current density from 1 to 10 Adm^{-2} did not have any effect on the uneven etching of Ni270 foils, neither did an increase in the time of cathodic pre-treatment from 10 to 60 mins at 5 Adm^{-2} prior to the etching operation. No other parameters of the etching solution composition or pre-treatment scheme were investigated since these have been examined in some detail elsewhere (192).

3.3.3 Hardness determinations on Ni foils

The hardness of the Ni foils under investigation was measured on a Vickers microhardness tester and the results were as follows :

'Good' adhesion Ni200 (source RARDE (125 μm)) hardness 180HV
'Bad' adhesion Ni270 (source Ionic Plating Ltd (125 μm)) hardness 163HV
'Bad' adhesion Ni270 (source Ionic Plating Ltd (200 μm)) hardness 180HV.

Each hardness result is the average of 20 separate determinations over the foil area. It should be noted that the value of hardness for a typical Ni200 foil, cold rolled in the quarter hard condition given by the manufacturers of the foil Henry Wiggin is 140 HV, whilst that for Ni270 cold rolled foil in the hard condition the value is 150 HV.

Table 63 shows the values for hardness of Ni200 foils after different rolling treatments (values obtained from BS 3073).

3.3.4 Tensile Tests

A typical stress vs strain curve for samples of Ni200 and Ni270 foils is shown in Fig. 156, with the mean value of the results for six separate tensile test specimens on each foil, given on Table 64.

TABLE 63

The variation of hardness for Ni200 foils with extent of cold rolling

Ni foil Condition	Hardness Value (HV) Minimum	Maximum
Cold rolled skin hard	110	130
Cold rolled quarter hard	125	150
Cold rolled half hard	145	175
Cold rolled three quarter hard	165	195
Cold rolled hard	185	215
Cold rolled spring hard	215	-

TABLE 64

Physical properties of samples of Ni200 and Ni270 foils, that exhibited good and bad adhesion of PbO_2

Sample	Yield Strength Nmm^{-2}	1% Proof stress Nmm^{-2}	UTS Nmm^{-2}	Elongation before failure %	Youngs Modulus Nmm^{-2}
Ni200 125 μm thick (good adhesion)	293	367	518	24.6	629
Ni270 200 μm thick (bad adhesion)	527	648	690	10.2	1170

3.3.5 Capacitance determinations on etched Ni foils

The mean value for the double layer capacitance for specimens of Ni200 anodically etched in 30% H_2SO_4, at 2.7 Adm^{-2} for 10 mins was found to be 37 $\mu F\ cm^{-2}$ (± 3 $F\ cm^{-2}$) at -0.16 V. This foil was known to give good adhesion of PbO_2 onto nickel and after removal from the etching solution appeared to be uniformly etched.

The double layer capacitances for two samples of foil that exhibited bad adhesion of β-PbO_2 both Ni270, one 125 μm thick the other 200 μm thick were also measured.

In the case of the 125 μm foil the mean double layer capacitance at -0.16V was found to be 29 $\mu F\ cm^{-2}$ ($\pm 1\ \mu F\ cm^{-2}$). However it should be pointed out that even after the anodic etching treatment used above, large areas of all the Ni270 foils tested were clearly unaffected by the etching process. The etch pattern on the 200 m thick Ni270 foil was even more difficult to reproduce as some samples had a few unetched areas whilst others had noticeably more. In the case of a well etched Ni270 specimen the capacitance was 50 $\mu F\ cm^{-2}$ whilst for a poorly etched specimen it was 39 $\mu F\ cm^{-2}$ at -0.16V.

The value for the double layer capacitance for an unetched sample of Ni200 at -0.16 V was 24.1 $\mu F\ cm^{-2}$ whilst that for unetched Ni270 was 25.1 $\mu F\ cm^{-2}$.

3.4.6 Auger analysis of Ni foils

The results of the XPS analysis on the 'as received' samples of Ni200 and Ni270 indicate that the oxide thickness on Ni270 is greater than that on Ni200 as given by the relative intensities of the oxygen peak for the respective samples, (see Figs 157 and 158 respectively).

Argon ion beam etching of the Ni200 foil for 1 min removed most of the oxide contamination, although a total of 5 mins etching

was required to ensure complete removal of the oxide film. The sputtering rate of the ion beam was estimated to be 40 A^{o} min^{-1} and this corresponds to an estimated oxide film thickness of 200 A^{o} for the Ni200 foil.

In the case of the Ni270 sample, after ion beam etching for 1 min the oxide peak is still significant and even etching for 5 mins failed to remove all the oxide, complete removal only being achieved after a total of 10 mins etching, which corresponds to an estimated oxide film thickness of 400 A^{o}.

The presence of C was also detected on the 'as received' samples however this is not thought to be significant and may be as a result of surface contamination during handling, residual lubricating oils or in the case of Ni200 as a constituent of the foil..

The XPS spectra of etched Ni200 after 1 min Ar etching is shown in Fig. 159, some oxide contamination was still visible and Cu and S were also detected. The XPS spectra for a sample of Ni270 containing both unetched and etched areas of Ni is shown in Fig.160. and a significant oxide peak is still apparent and also a low level of S, Cu and C contamination.

To enable a closer examination of the surface of the etched and unetched areas of Ni270 two further samples of a well-etched section of Ni270 and of unetched Ni270 were examined using A.E.S. The A.E.S spectra from these samples were recorded after ion-beam etching for 30 sec to clean the surface. The peak to peak heights of the trace elements were calculated as ratios of the principal Ni LLM peak and these results are set out in Table 61.

Slightly higher oxygen levels are shown in the etched areas, though there appears to be no other detectable differences between the two areas. The Cl peak was recorded for only one sample. Typical A.E.S spectra for the etched and unetched sections are shown in Figs. 161 and 162 respectively.

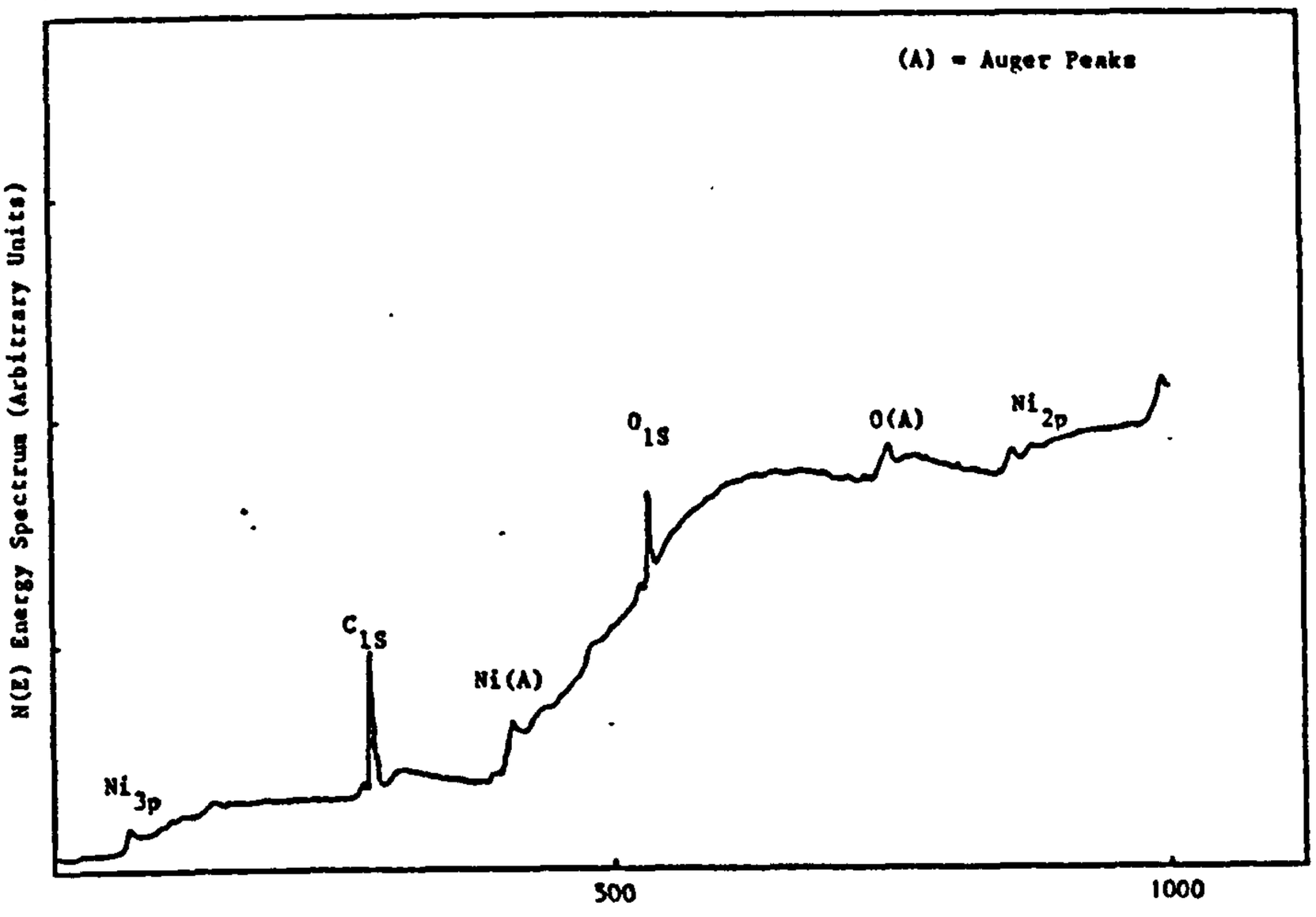

XPS spectra for as received sample of Ni 200 that exhibited good adhesion for electrodeposited PbO using Mg K_α radiation setting 12 kV at 20mA.

FIGURE 157

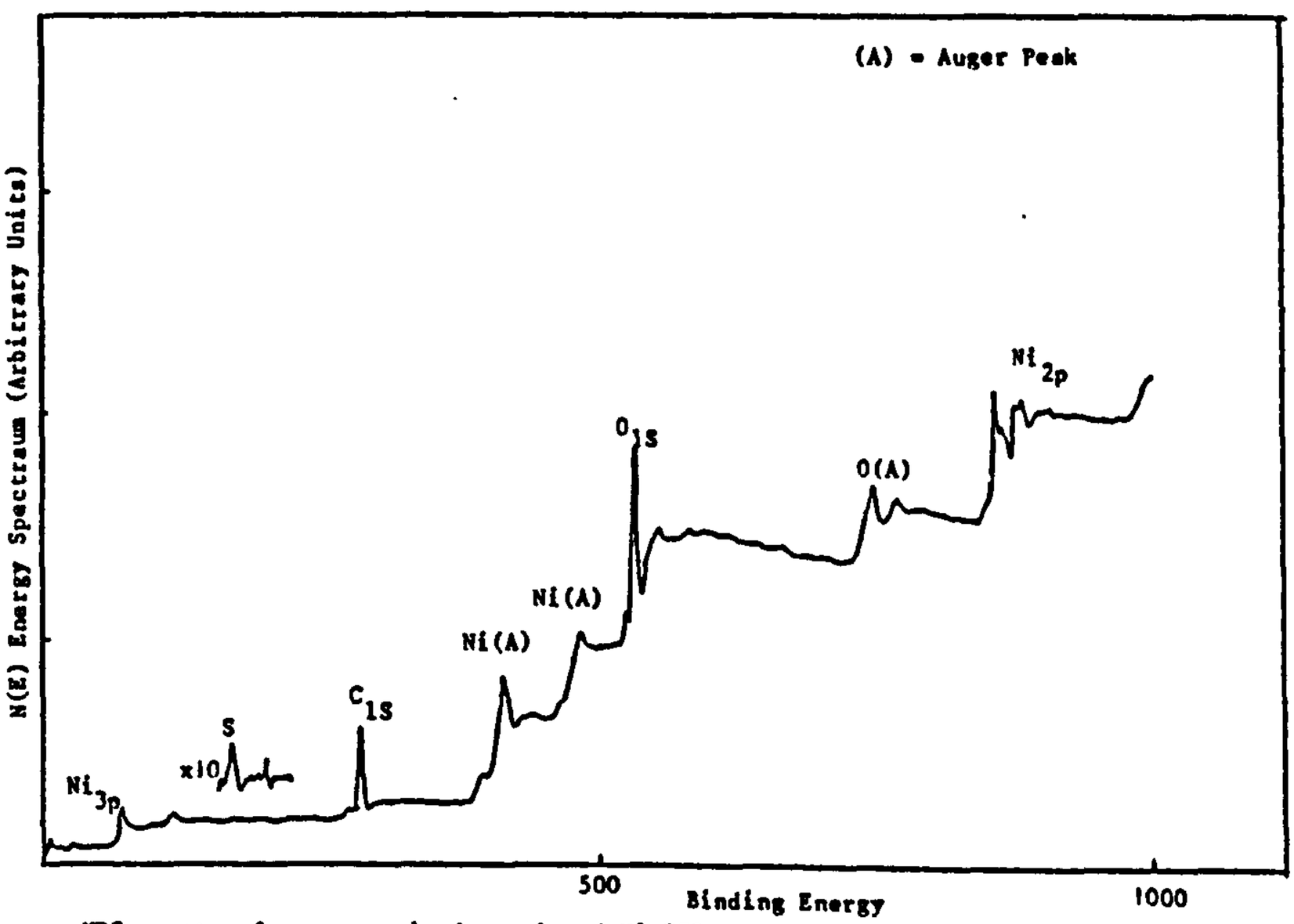

XPS spectra for as received sample of Ni 270 that exhibited bad adhesion for electrodeposited PbO_2 using Mg K_α radiation setting 12 kV, 20mA.

FIGURE 158

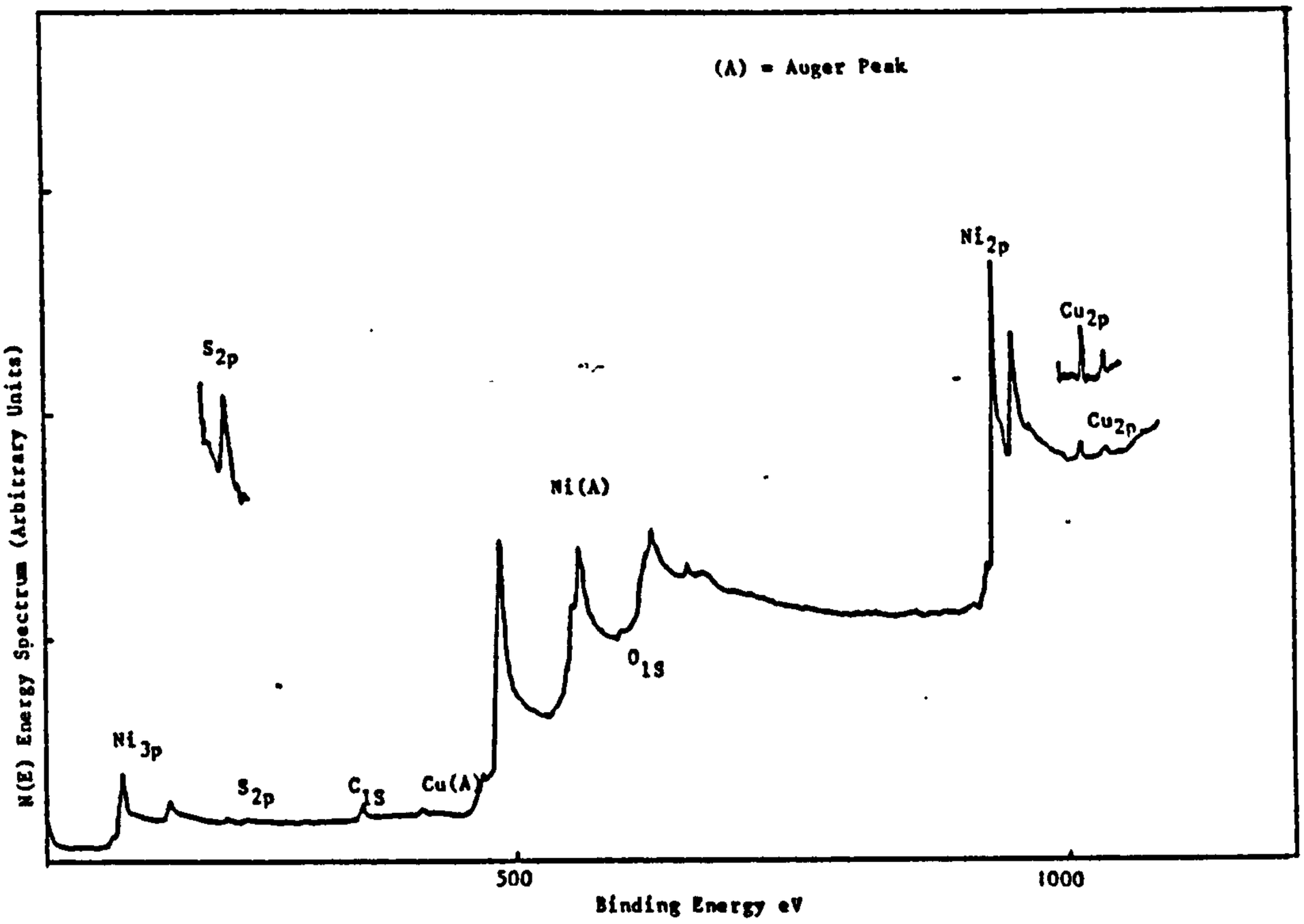

XPS spectra for sample of etched Ni 200 that exhibited good adhesion for electrodeposited PbO_2, 10kV, 20mA.

FIGURE 159

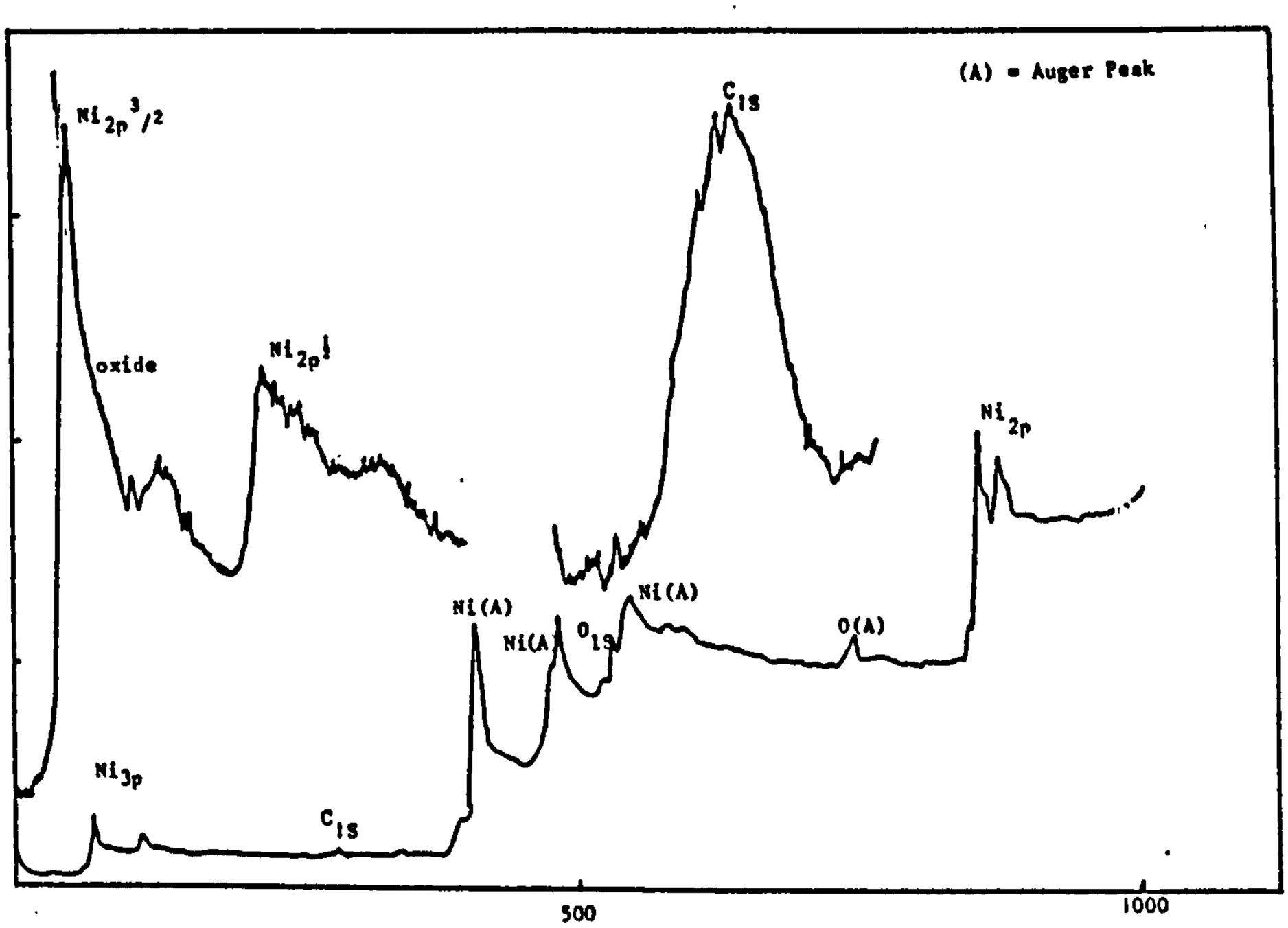

XPS Spectra for etched Ni 270 foil that exhibited bad adhesion of electrodeposited PbO_2 at 10 kV, 20 mA.

FIGURE 160

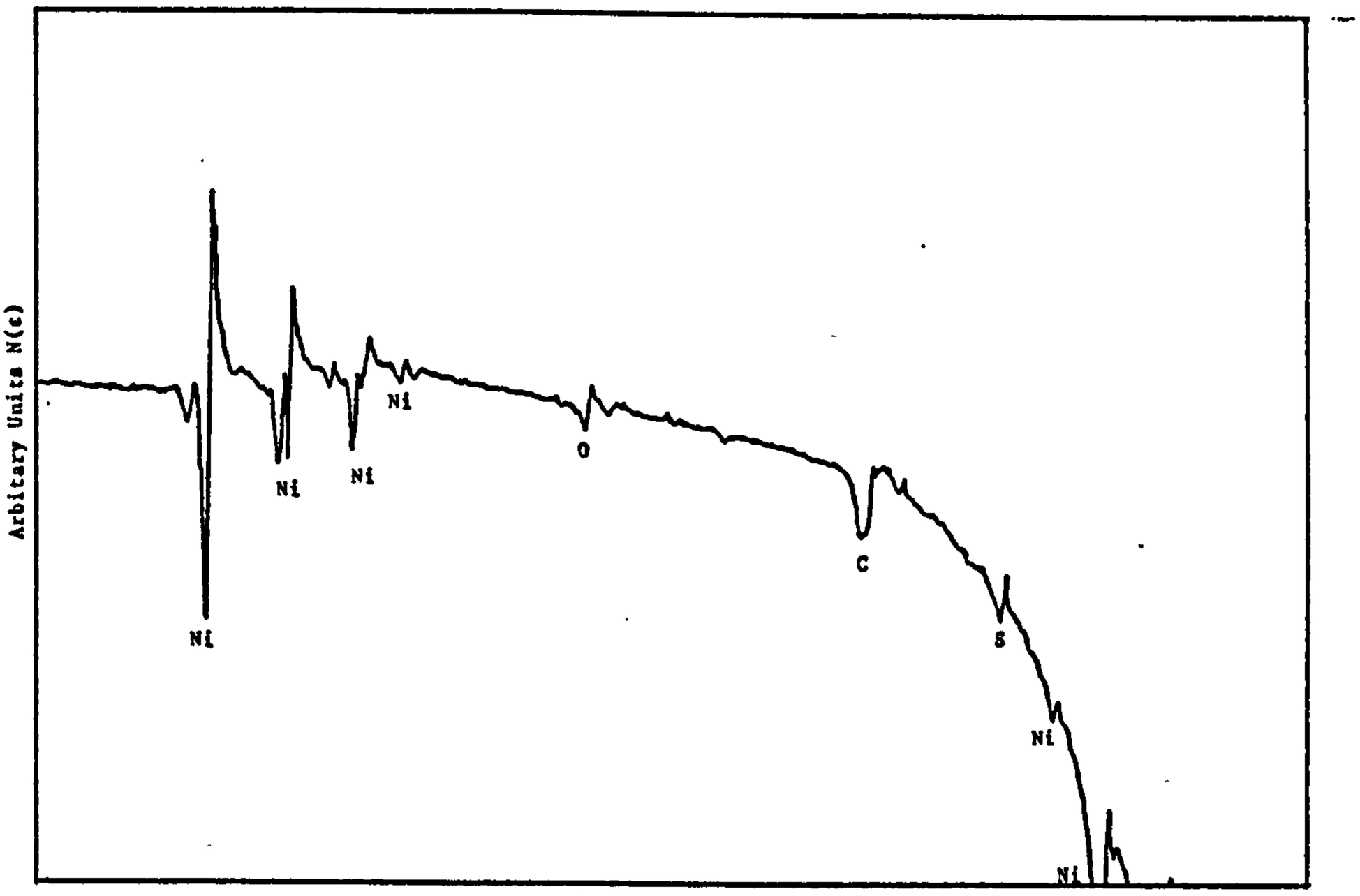

Auger spectrum of the unetched area of Ni 270 obtained after a bulk sample of Ni 270 was anodically etched at 2.7 A dm^{-2} in 30% H_2SO_4 at 50°C.

FIGURE 161

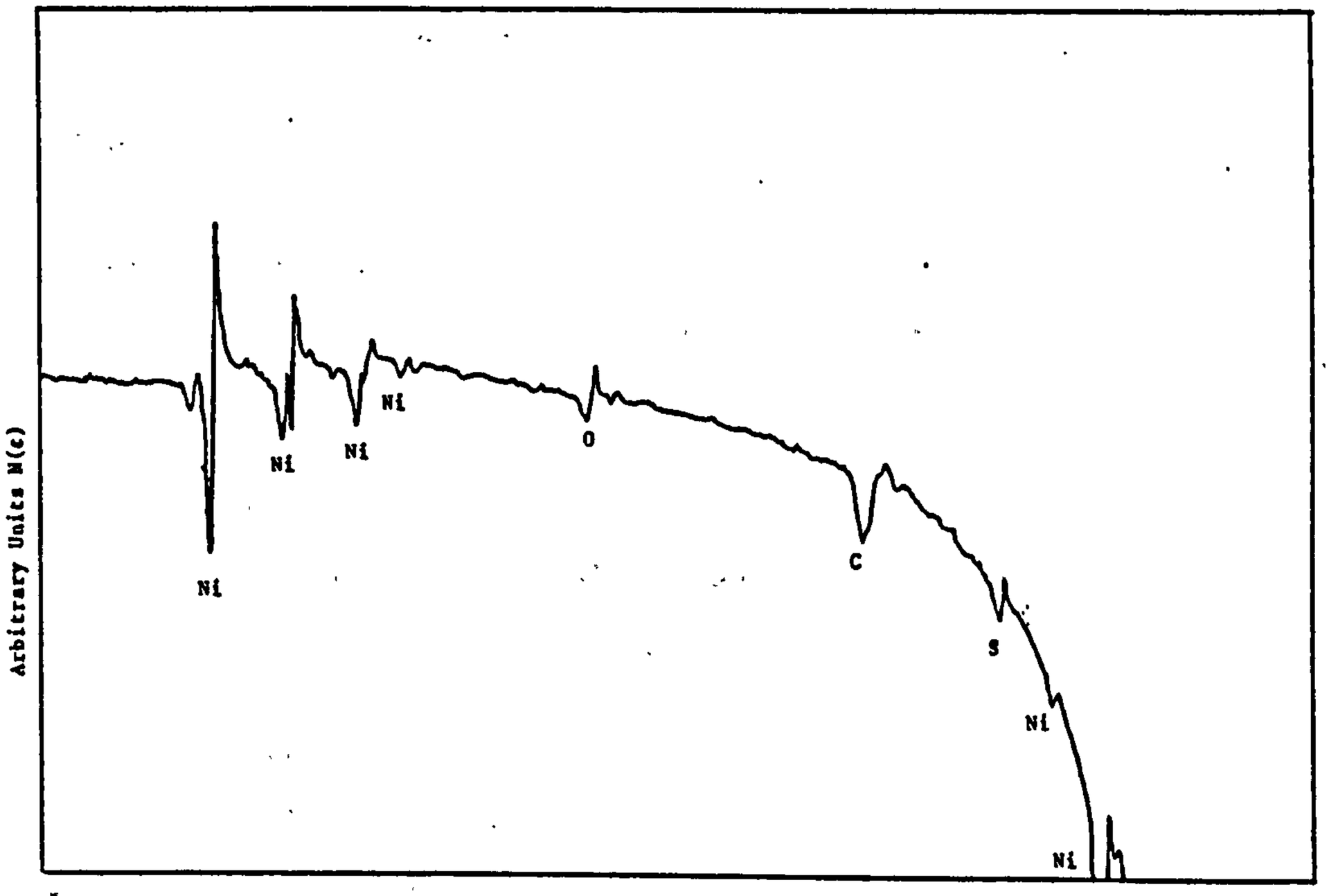

Auger spectrum for the etched area of Ni 270 after a bulk sample of Ni 270 was anodically etched at 2.7 A dm^{-2} in a solution of 30% H_2SO_4 at 50°C.

FIGURE 162

TABLE 65

Peak to Peak Height Ratios for different impurity elements expressed as a ratio of the Ni LLM peak

Sample	Region examined	Ratio : Ni LLM C	Cl	S	O
N1270 (a)	unetched	.23	.06	.29	.04
	unetched	.08	-	.07	.11
	etched	.12	.04	.12	.17
	etched	.14	.04	.13	.19
N1270 (b)	unetched	.22	-	.38	.09
	unetched	.16	-	.11	.10
	etched	.20	-	.14	.16
	etched	.24	-	.22	.20

3.3.7 Electrochemical Studies

The electrochemical properties of Ni foils in H_2SO_4 and $Pb(NO_3)_2$ solutions were investigated to discover if there were any discernable differences in electrochemical properties between the 'good' and 'bad' adhesion materials.

3.3.7.1 Studies on Ni dissolution in 30% H_2SO_4

Reproducibility of results was found to be a problem owing to the nature of the surface under investigation.

The Ni foils were not subjected to any surface treatment prior to any investigation, other than vapour degrease in trichlorethylene followed by cathodic degreasing in a solution of 50 gl^{-1} NaOH, 50 gl^{-1} Na_2CO_3 and 5 gl^{-1} Na_2SO_4 at 5 Adm^{-2} for 10 mins. The pre-treatment afforded to each sample was that used in the commercial production of etched foil for the Pb/PbO_2 primary battery (see Section 2.1). No mechanical polishing of the foil specimens was attempted, primarily because of the need to simulate the actual surface condition of Ni foils prior to anodic etching.

The two extremes of the E vs log i curves for samples of the same Ni270 foil anodically polarised in 30% H_2SO_4 at 20°C are shown in Fig. 163 indicating the level of reproducibility of the results. All the subsequent results reported are representative values of the polarisation curves recorded for a number of different samples.

The E vs log i curves, for a sample of Ni200 foil that exhibited good adhesion of β-PbO_2, in 30% H_2SO_4 at 20 and 50°C are given in Fig. 164, whilst Figs. 165 and 166 are examples of the E vs log i curves for different samples of Ni270.

The mean values of E_{rest}, E_{pp}, i_{pp} and i_{pass} recorded from various Ni200 and Ni270 foils are given in Table 66.

As can be seen from Table 66, i_{pass} is higher for Ni200 than Ni270 foils in all cases, whilst similar values of i_{pp} for both Ni200 and Ni270 were observed.

The values of E_{pp} for Ni200 were essentially the same at 20 and 50°C (see Fig. 164), unlike the Ni270 foils studied where the potential range over which dissolution occurred was found to increase with increase in temperature (see Figs. 165 and 166). The Tafel constant for Ni dissolution at 50°C on Ni200 was found to be approximately 30mV per decade whilst for Ni270 at the same temperature it was found to be approximately 60 mV per decade for one sample of Ni270 and 48mV per decade for a sample of Ni270 from a different source. A direct comparison of the E vs log i curve for a sample of Ni200 and Ni270 is given in Fig. 167.

Samples of Ni270 foils that showed an unevenly etched surface after anodic dissolution in the H_2SO_4 etching solution were cut so as to obtain samples of the unetched material. These samples were then polarised at 5 mV sec^{-1} in 30% H_2SO_4 to see if these areas exhibited any markedly different polarisation characteristics. Differences in the E vs log i curves were detected with the values of i_{pp} being lower than the bulk

TABLE 66

Values of E_{rest}, E_{pp}, i_{pp} and i_{pass} for different samples of Ni foil polarised at 5 mV sec^{-1} in 30% H_2SO_4 at 20 and 50°C

Foil	E_{rest} (Volts)		E_{pp} (Volts)		i_{pp} (Adm^{-2})		i_{pass} (Adm2-)	
	20°C	50°C	20°C	50°C	20°C	50°C	20°C	50°C
Ni200 'good' adhesion	0.075	0.070	0.510	0.520	17.8	47.8	1.85×10^{-2}	8.2×10^{-2}
Ni270 Ionic	0.090	0.120	0.445	0.545	13.5	45.3	1.45×10^{-2}	5.08×10^{-2}
Ni270 RARDE	0.100	0.055	0.463	0.530	19.0	45.8	1.43×10^{-2}	5.73×10^{-2}
Ni270 RARDE annealed	0.135	0.104	0.400	0.550	5.5	47.0	1.4×10^{-2}	5.6×10^{-2}

N.B i_{pass} has been taken as the minimum current observed in the passive region.

unetched samples e.g a typical value of i_{pp} for this sample was 29 Adm^{-2}, at 50°C compared to 45.3 Adm^{-2} for a bulk sample of unetched Ni270.

The values of E_{pp} were +0.455V for the poorly etched foils compared to +0.545V for the bulk sample.

The E vs log i curve for a sample of Ni270 annealed under vacuum for 30 mins at 800°C (see Fig. 168) shows two distinct potential arrests are visible, one at +0.490V and the other at +0.55V. This phenomenon was observed at both 20 and 50°C on a number of separate specimens with a Tafel slope of 59 mV per decade recorded for Ni dissolution.

3.3.7.2 Pit nucleation of Ni foil etched in 30% H_2SO_4

In order to investigate the rates of pit nucleation and growth specimens of Ni foil where held at a constant anodic potential of + 0.27V and the resultant current versus time transients recorded over a period of 500 sec. Fig. 169 shows the i vs t curve for two as received samples of Ni200 held at + 0.27V. Reproducibility of results was again found to be a problem with the curves shown in Figure 169 representing the extremes of the i vs t curves, obtained from 5 separate samples. The same trend was shown for all Ni200 samples studied in this way i.e an initial decrease in current, followed by a sharp rise in current until a peak is reached when the current then decreases exponentially. A similar trend was observed for a sample of Ni270 annealed under vacumm for 30 minutes (see Fig. 170) although the rate of decay after the peak current was reached, was lower.

The i vs t curves for samples of Ni270 from different sources (Figs 171 to 173) were all found to be essentially the same, yet different from those of samples of Ni200, with an initial decay of current over the first 5 to 10 sec followed by a continuing increase in dissolution current.

3.3.8. Electrochemical studies on Ni passivity in $Pb(NO_3)_2$ solutions

Slow potential sweep, cyclic voltammetry and galvanostatic polarisation experiments were conducted on samples of Ni200 that exhibited 'good adhesion' and samples of Ni270 foils that

exhibited 'bad adhesion'. A solution of 360 gl^{-1} $Pb(NO_3)_2$, pH 3.5 was placed in the electrochemical cell shown in Fig. 8 and heated to 50°C. The specimen under investigation was then inserted into the electrochemical cell and 5 mins allowed for a stable rest potential to be attained.

3.3.8.1 Slow potential sweep experiments

The E vs log i curves for samples of Ni200 polarised at 5 mV sec^{-1} in 360 gl^{-1} $Pb(NO_3)_2$ solutions of varying pH's is shown in Fig. 174 whilst an E vs log i curve for samples of Ni270; that exhibited bad adhesion of PbO_2 when polarised under the same conditions is shown in Fig. 175.

In the case of both Ni200 and Ni270 foils the potential at which passivation occurs (E_{pp}) and the current density necessary for passivation i_{pp} are pH dependent. Indeed a logarithmic relationship was observed between pH and i_{pp} (see Fig. 176) with Ni200 foils having a higher value of i_{pp} at a given pH and sweep rate, than Ni270 in a 360 gl^{-1} $Pb(NO_3)_2$ solution. The following relationships was observed :

$$\log i = KpH + \log i_o, \text{ in which}$$

For Ni270 $K = -0.78$ and $\log i_o = -0.88$

For Ni200 $K = -0.73$ and $\log i_o = -0.76$

($\log i_o$ = the value of i_{pp} at pH = 0 in Acm^{-2})

At pH 3.7 two distinct potential arrests one at +0.185V and a second at +0.30 V were recorded for Ni200 samples but only one was observed for Ni270, whilst the values of i_{pass} were dependent on potential but essentially independent of pH.

The potential at which nucleation of PbO_2 occurs was found to be pH dependent. At pH 3.7 no nucleation peak was observed for the Ni270 sample although at other pH's the potential at which

nucleation of PbO_2 occurred and the value of the nucleation current peak were the same for both N1200 and N1270. The values of $E_{nucleation}$ were + 1.3 and +1.4 V at pH's 1.8 and 0.8, respectively.

3.3.8.2 Cyclic voltammetry

A typical cyclic voltammogram for N1200 and N1270 foils polarised at a sweep rate of 700 mV sec^{-1}, in a solution of 360 gl^{-1} $Pb(NO_3)_2$ at 50°C and pH 3.5 is shown in Fig. 179. This work was conducted to investigate the nature of the passive film formed when a Ni electrode is rapidly polarised, as would be the case in a commerical PbO_2 plating solution based on $Pb(NO_3)_2$. Two distinct potential maxima were observed. In the case of N1200 one at +0.31V and the other at +0.55V whilst for the N1270 bad adhesion foil the first one was observed at +0.29V and the second peak at +0.53V. The relative intensities of the two peaks varied from different samples with the second peak always of greater magnitude.

The N1200 samples always exhibited the higher peak dissolution currents when compared to N1270 samples. The results were found difficult to reproduce for both foil samples and the result shown in Fig. 177 is representative of typical experiments.

3.3.8.3 Galvanostatic studies

Work was also undertaken to determine the current density necessary for passivation of a Ni electrode in a 360 gl^{-1} $Pb(NO_3)_2$ solution of varying pH. A sample of 'good' adhesion N1200 foil and a sample of 'bad' adhesion N1270 foil 200 m thick, supplied by RARDE was used for this purpose.

In order to obtain reproducible results the rate of increase in current density was maintained at the same value for all experiments i.e.at 156 Acm^{-2} sec^{-1}.

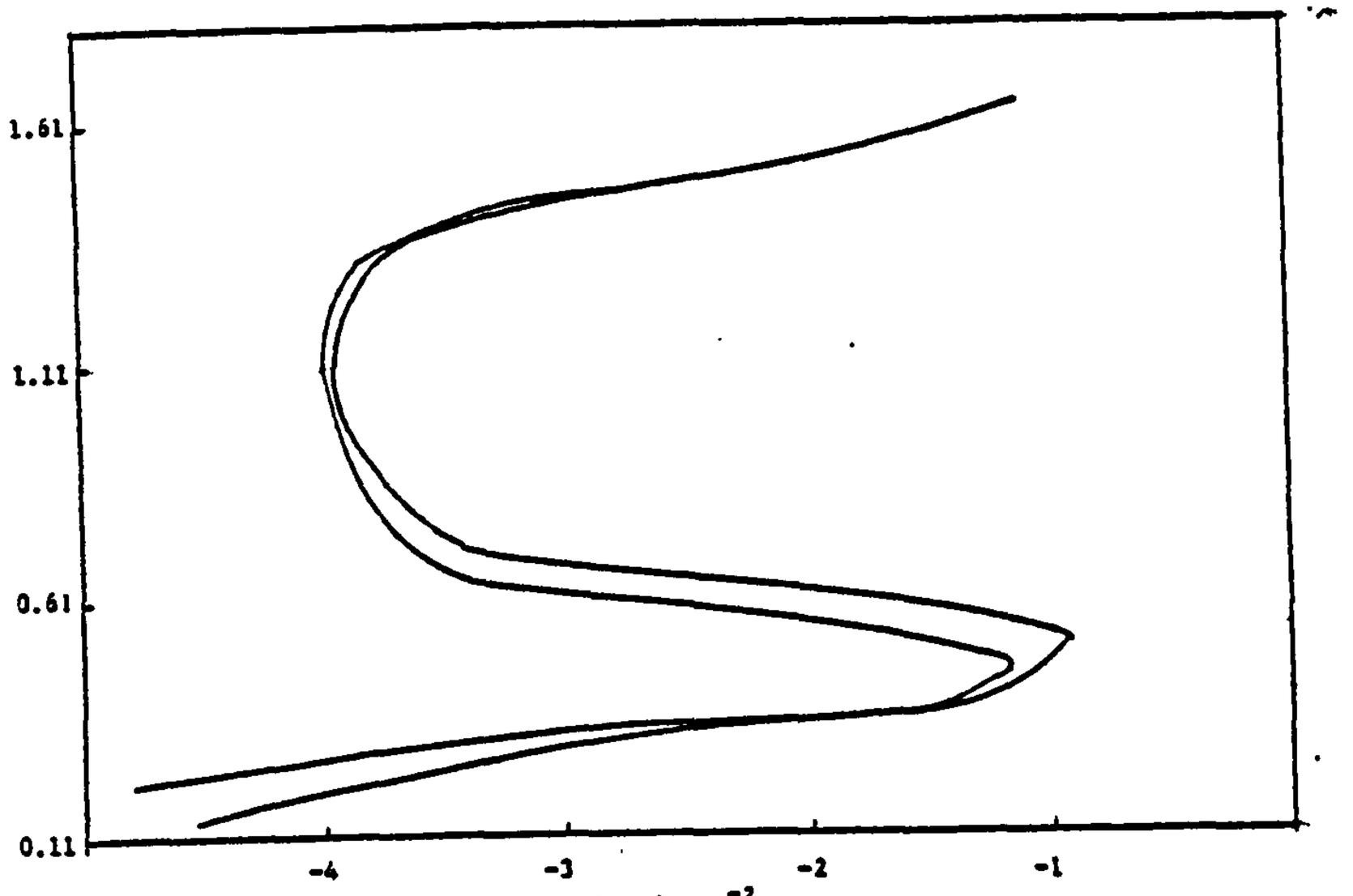

E vs log i curves for two different samples of Ni270 foil 200 um thick from the same source. The Ni foil anodically polarised at 5mV sec^{-1} from its rest potential in a 30% H_2SO_4 solution at 20°C.

FIGURE 163

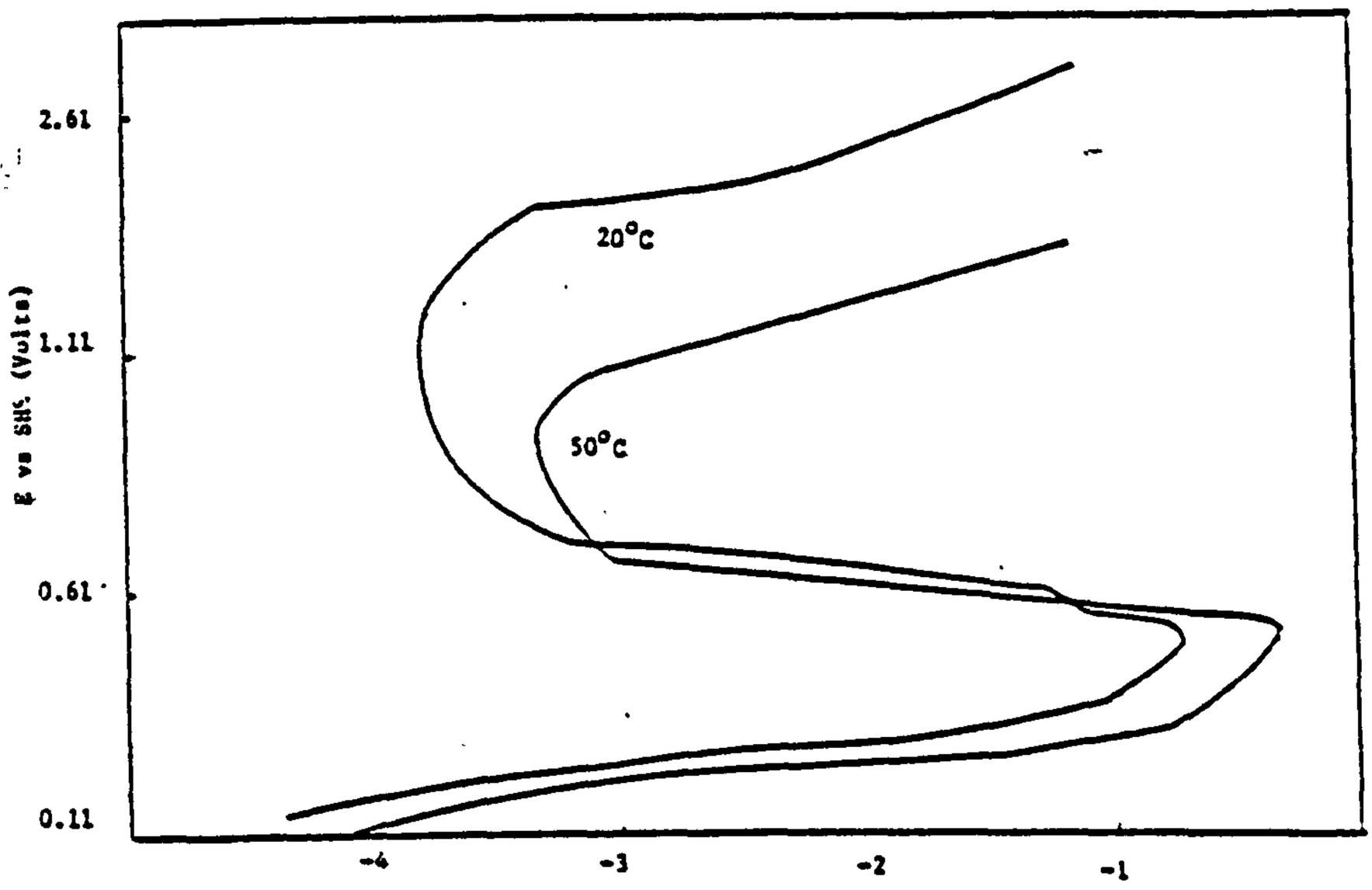

E vs log i curve for Ni200 foil 200 um thick that exhibited good adhesion for electrodeposited βPbO_2. The foil anodically from rest potential polarised at a sweep rate of 5mV sec^{-1} in 30% H_2SO_4 at 20°C and 50°C.

FIGURE 164

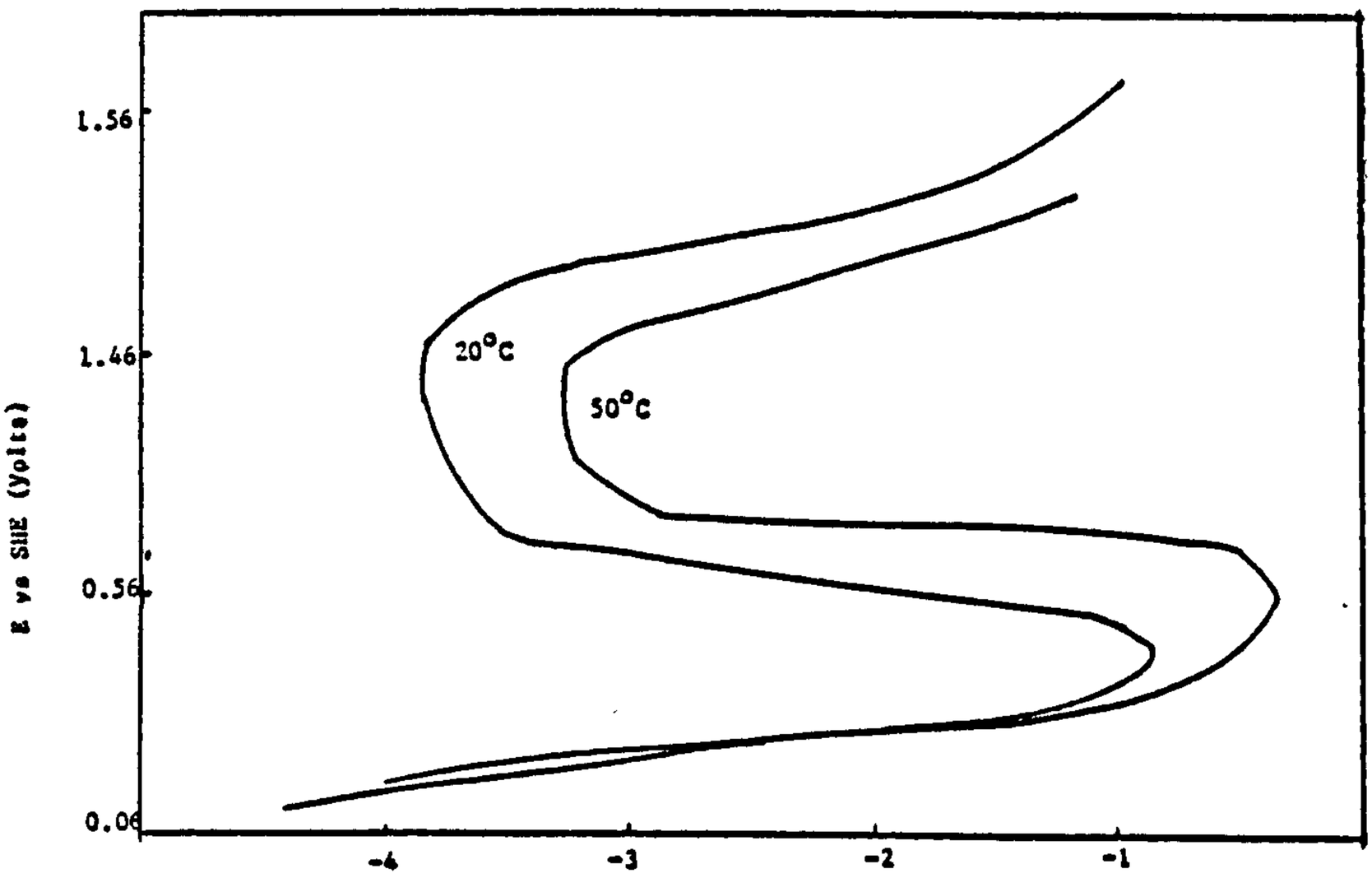

E vs log i curves for a sample of Ni270 200 um thick that exhibited bad adhesion of βPbO_2 . The Ni foil polarised from rest potential at a sweep rate of 5mV sec^{-1} in a solution of 30% H_2SO_4 .

FIGURE 165

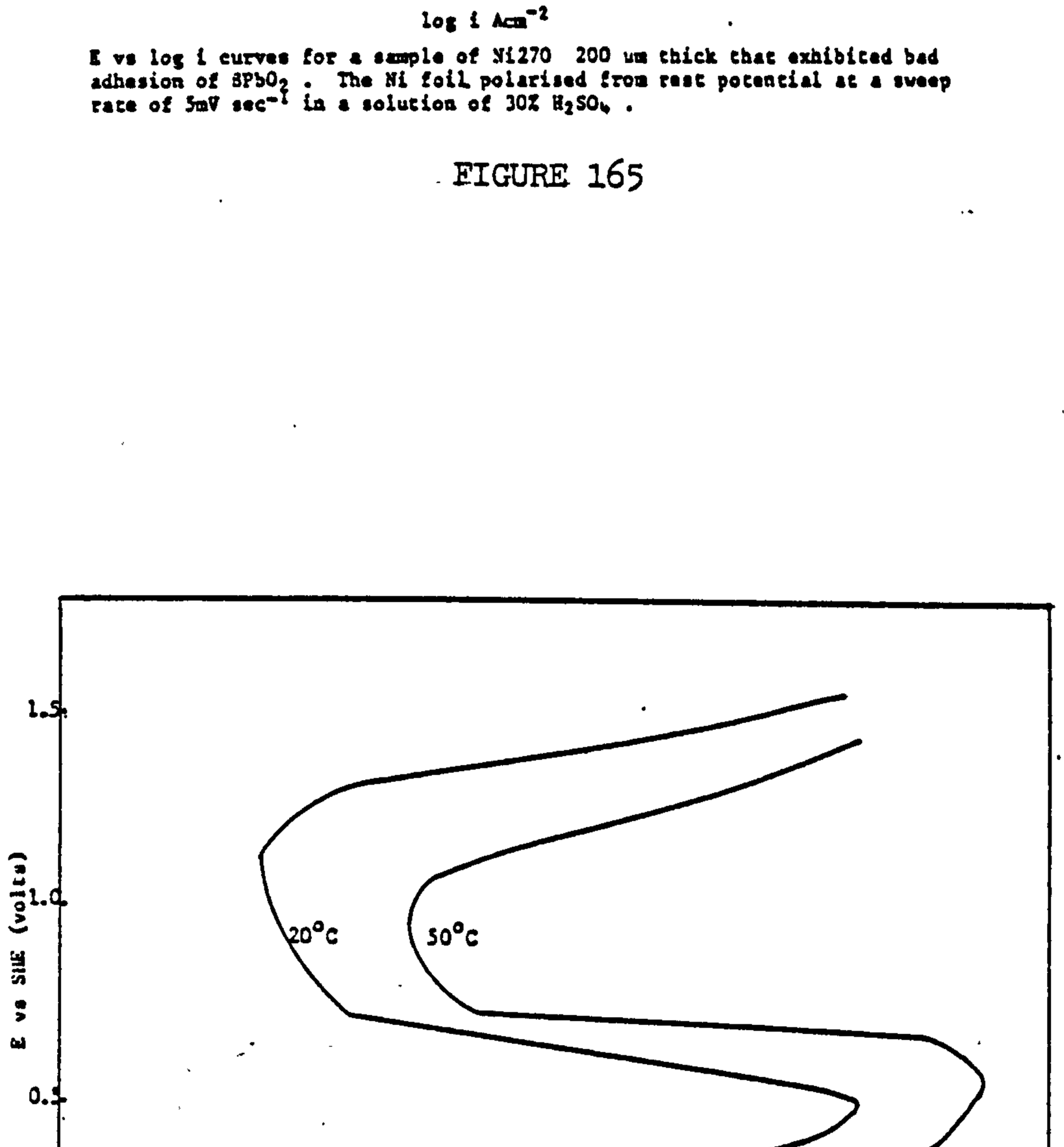

A graph of E vs log i for Ni 270 foil 200 um thick that exhibited bad adhesion for electrodeposited βPbO_2 . The foil anodically polarised from its rest potential at a sweep rate of 5 mV sec^{-1} .

FIGURE 166

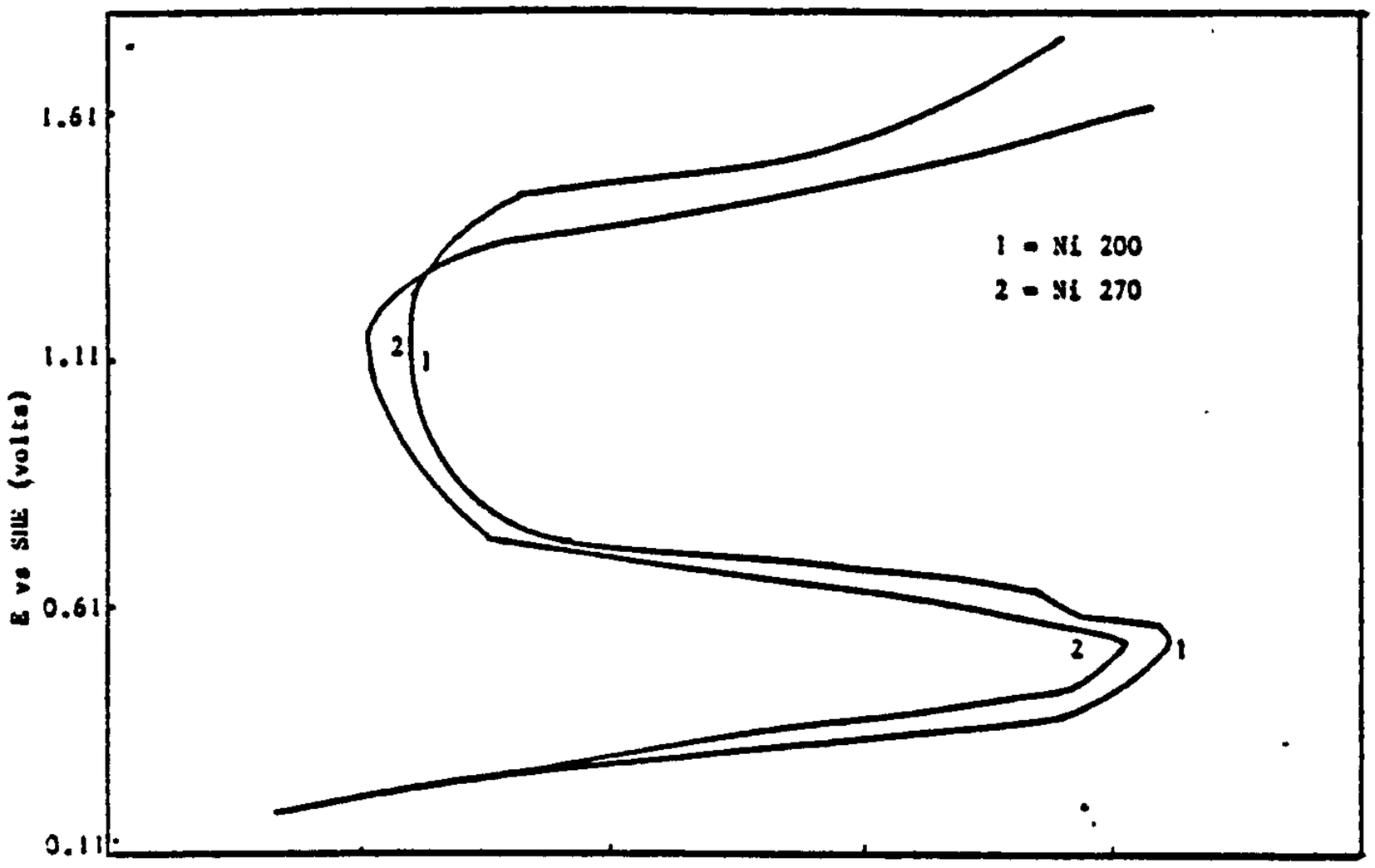

E vs log i curve for Ni 200 and Ni 270 samples anodically polarised from the rest potential in 30% H_2SO_4 at 4 mV sec^{-1} . The electrolyte temperature maintained at 20°C .

FIGURE 167

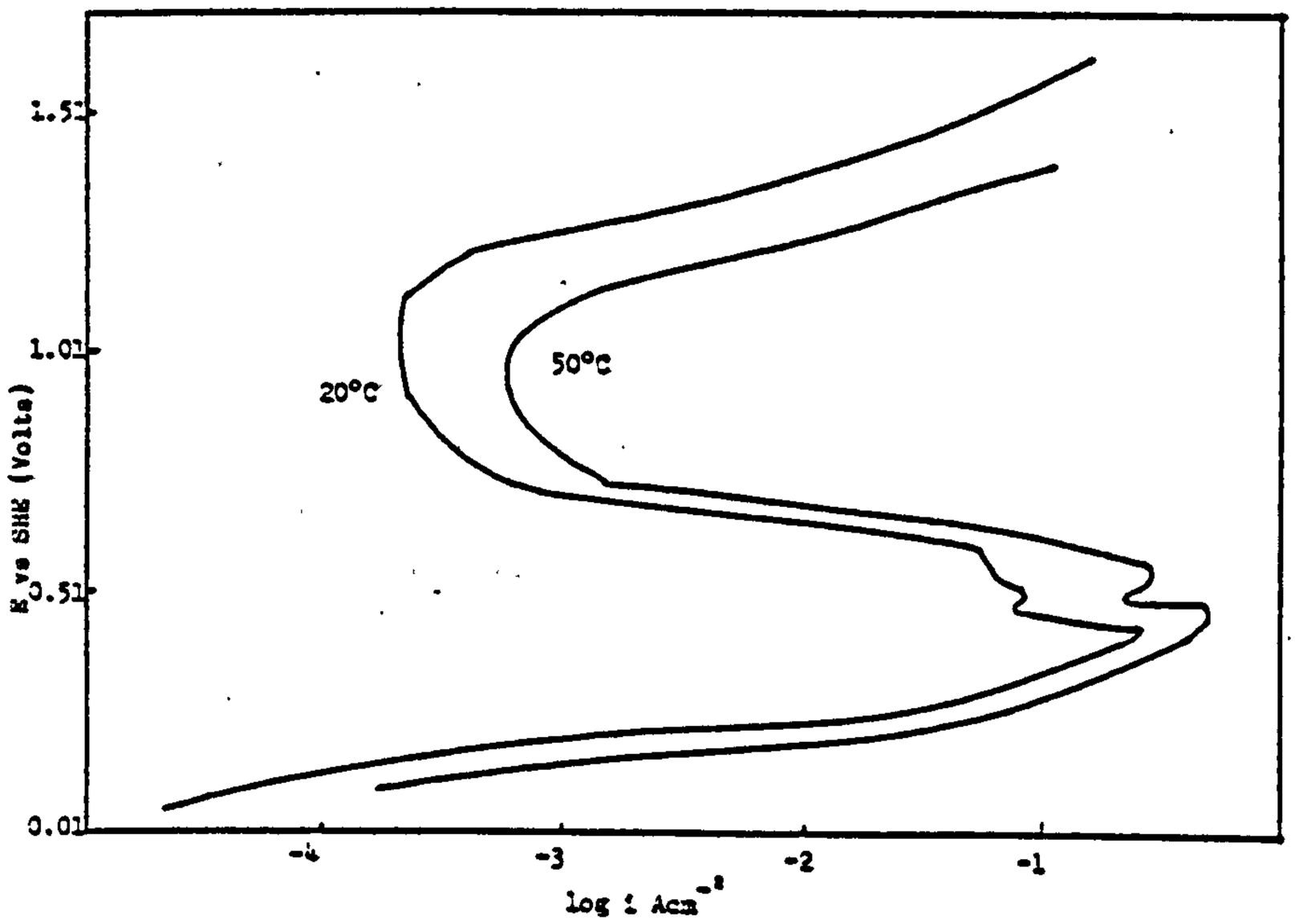

E vs log i curve for sample of Ni 270 annealed under vacuum at 300°C for ½hr. then anodically polarised at a sweep rate of 5mV sec^{-1} in a solution of 30% H_2SO_4

FIGURE 168

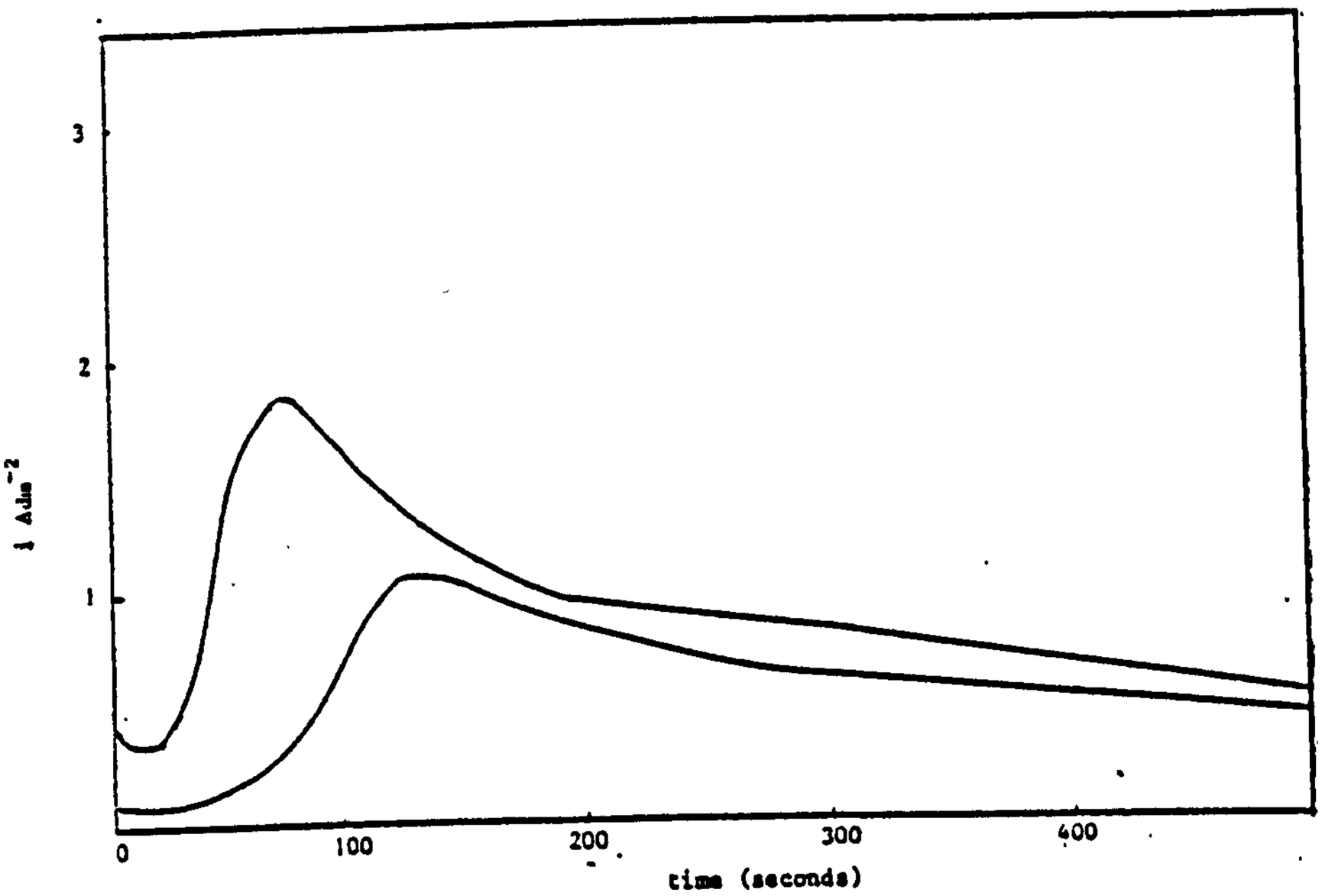

A graph of i vs t for Ni200 electrodes held at a fixed potential of +0.27 volts vs SHE.

FIGURE 169

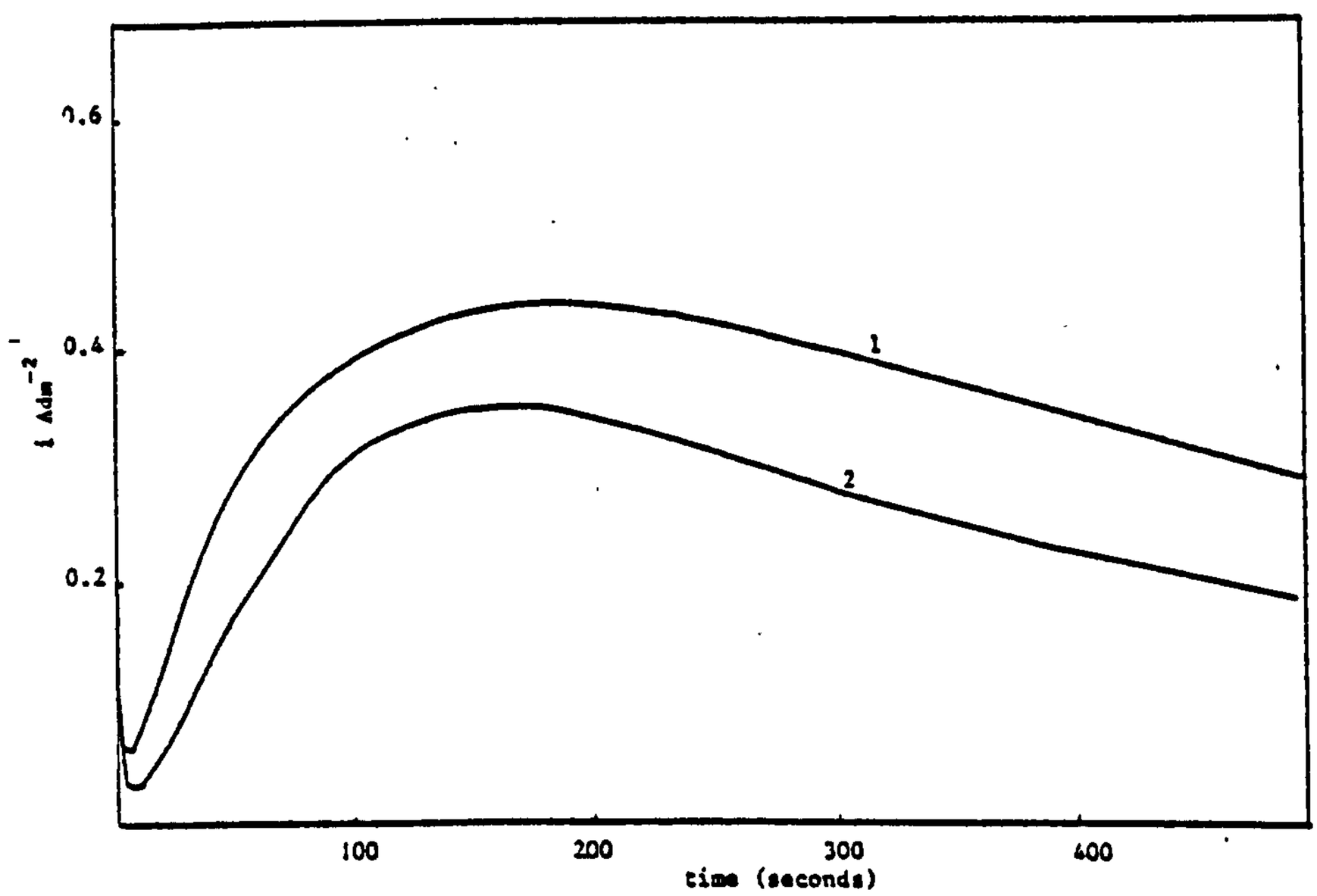

i vs t curve for samples of Ni270, 200 um thick annealed under vacuum at 900°C for ½ hour, then held at a fixed potential of +0.27 volts vs SHE.

FIGURE 170

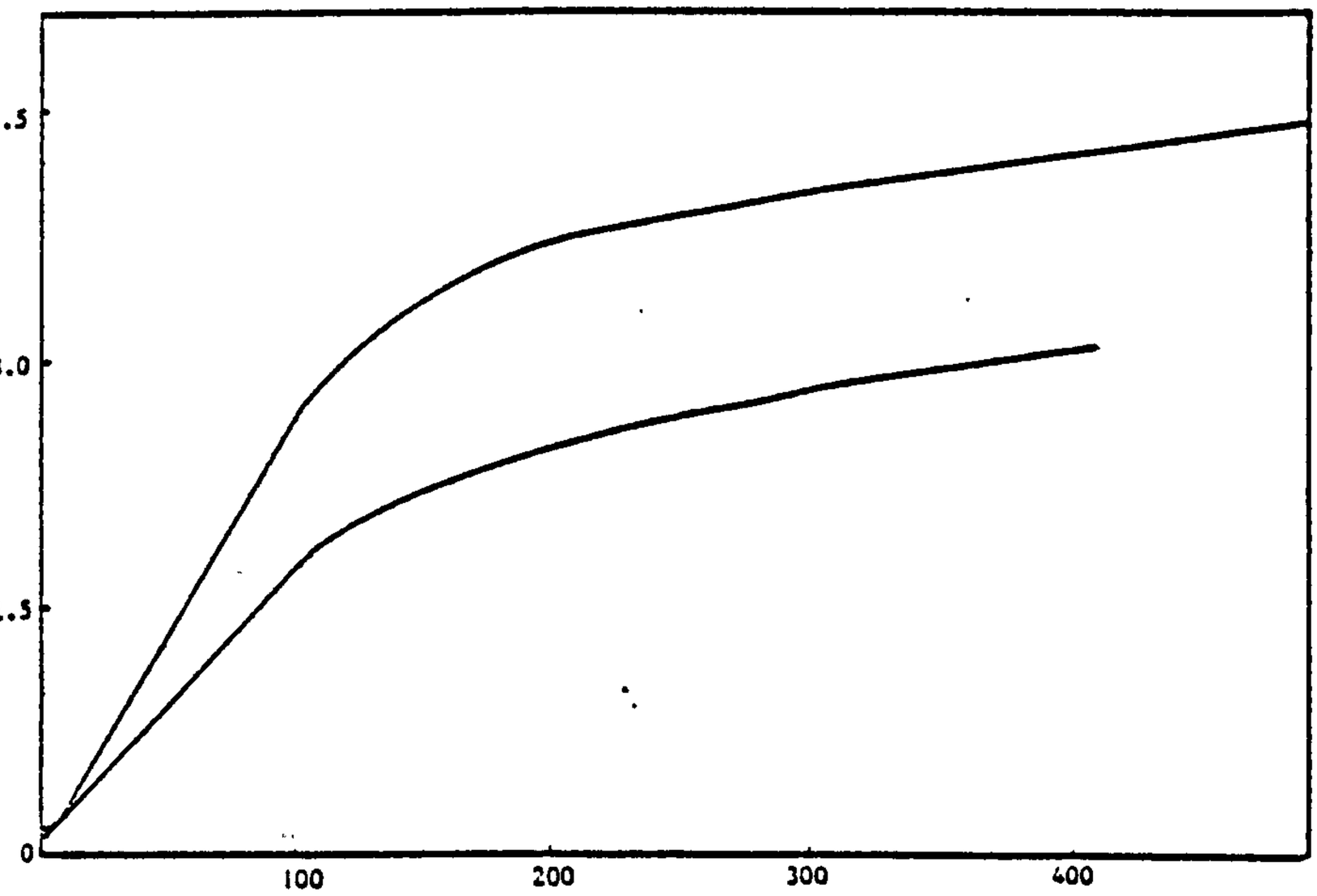

A graph of i vs t for different samples of Ni270 foil 125 um thick held at a potential of +0.270 volts vs SHE in a 30% H_2SO_4 solution.

FIGURE 171

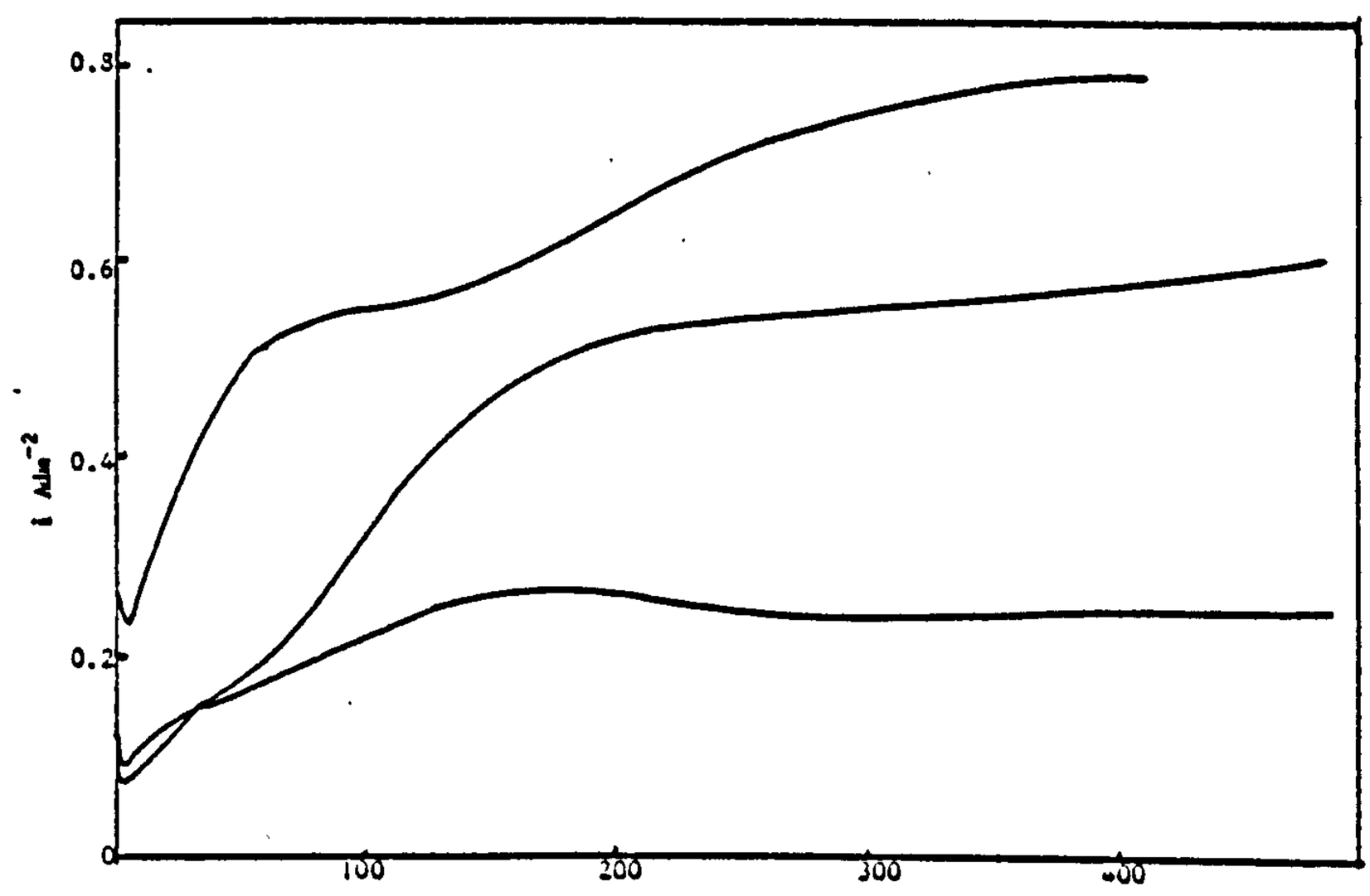

i vs t curves for samples of Ni270 200 um thick supplied by the Ionic Plating Co Ltd. The Ni foil samples held at a potential of +0.270 volts vs SHE.

FIGURE 172

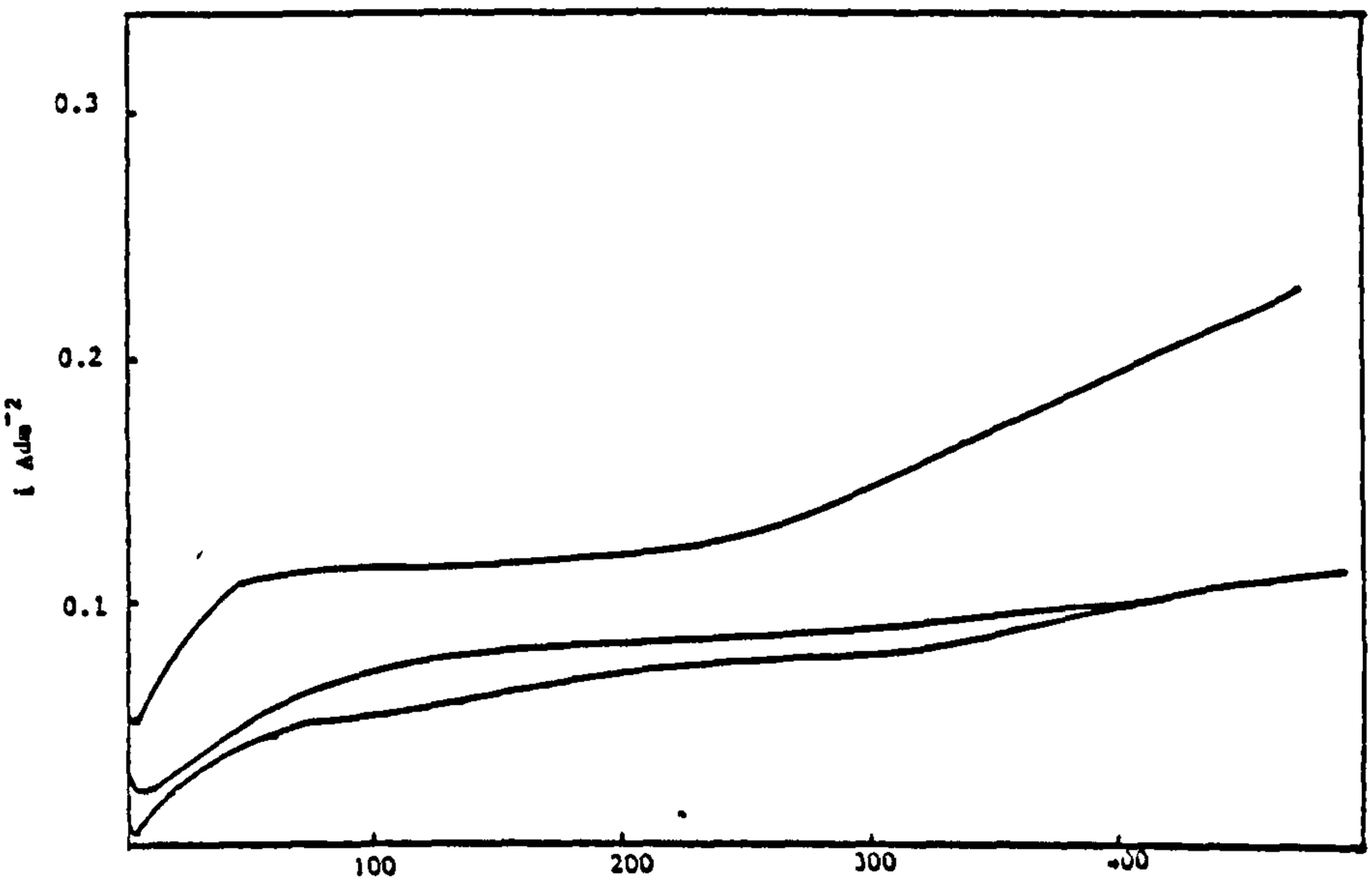

i vs t curves for different samples of Ni270 foil 200 um thick (source RARDE) sample unannealed. The Ni foil held at a fixed potential of +0.27 volts vs SHE.

FIGURE 173

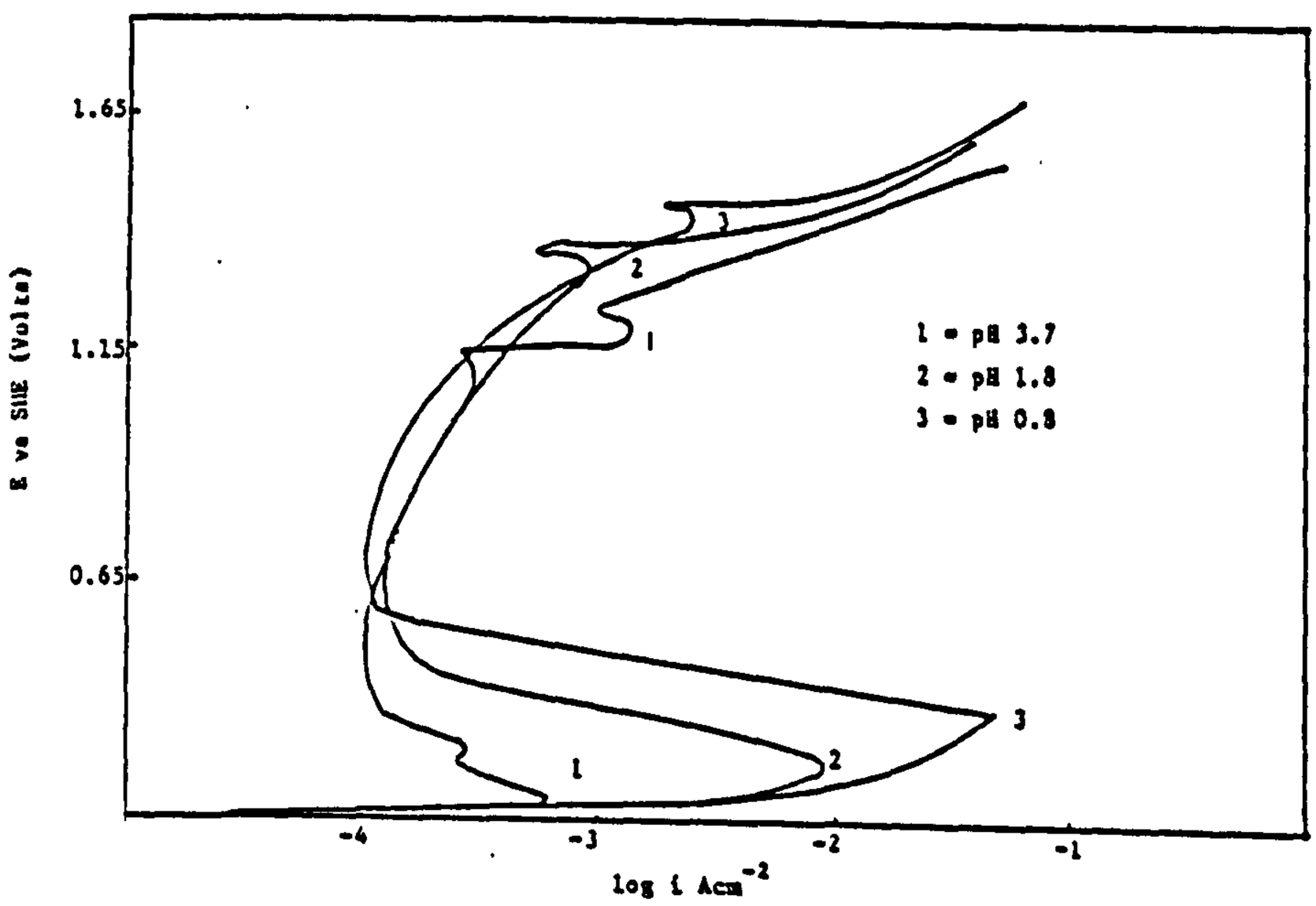

E vs log i curves for samples of Ni 200 foil anodically polarised at a sweep rate of 5 mV sec^{-1} in a solution of 360 gl^{-1} $Pb(NO_3)_2$ of varying pH, at 50°C.

FIGURE 174

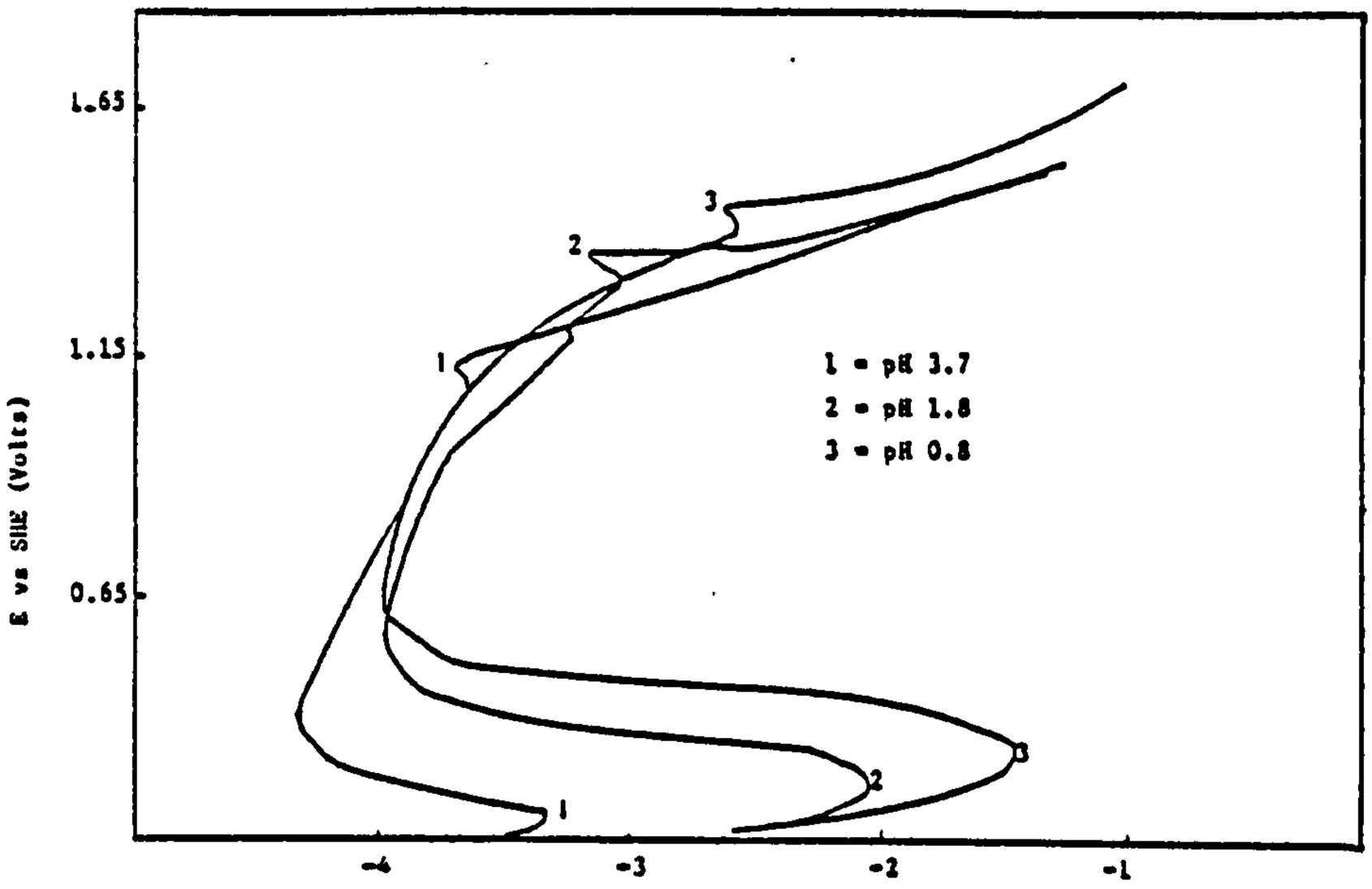

E vs log i curve for sample of Ni270 foil anodically polarised at a sweep rate of 5mV sec^{-1} in a solution of 360 gl^{-1} $Pb(NO_3)_2$ of varying pH, at 50°C, (pH adjusted with HNO_3).

FIGURE 175

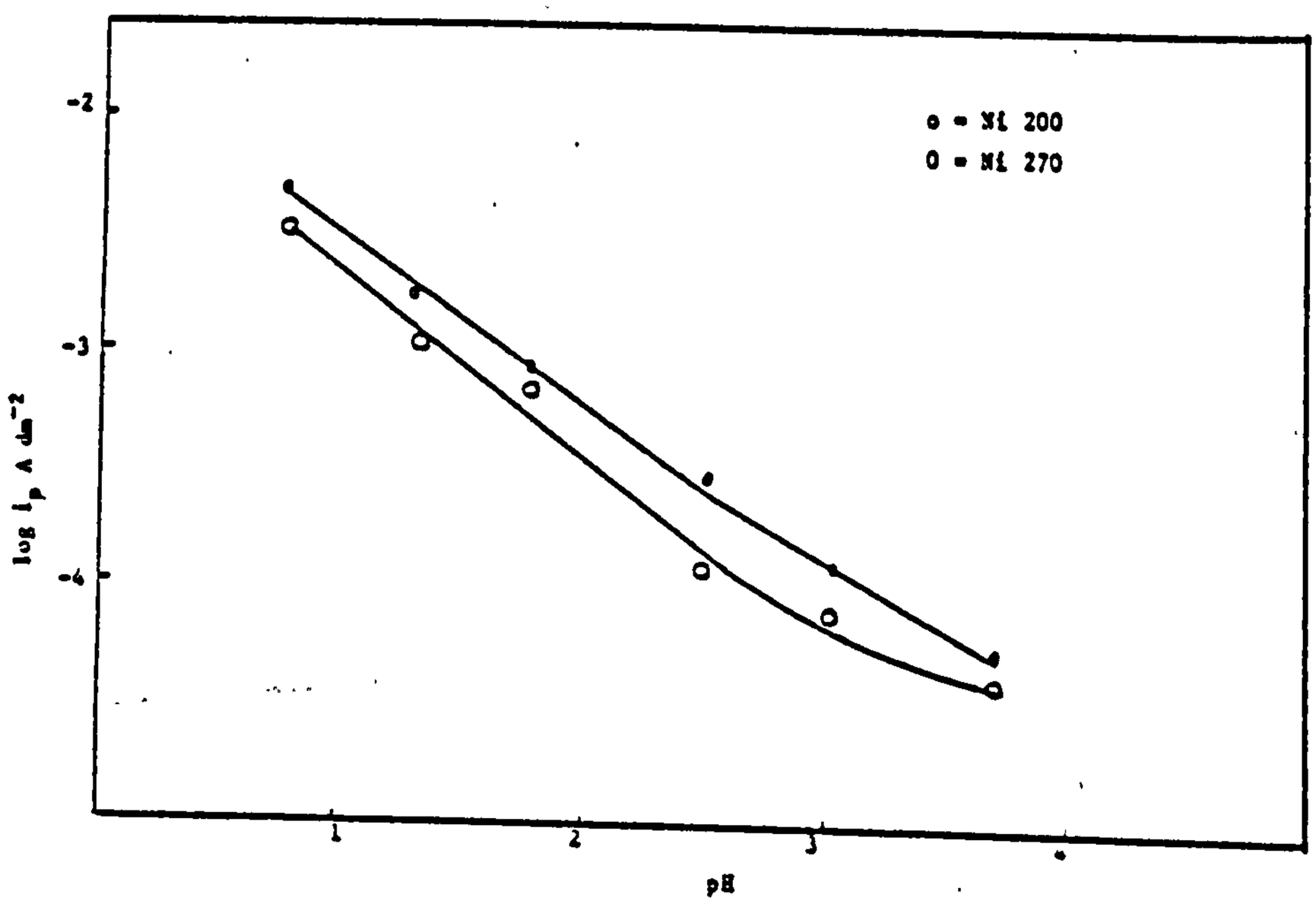

A graph of log i_p vs pH for samples of Ni200 and Ni270 foil anodically polarised at 5mV sec^{-1} in a solution of

FIGURE 176

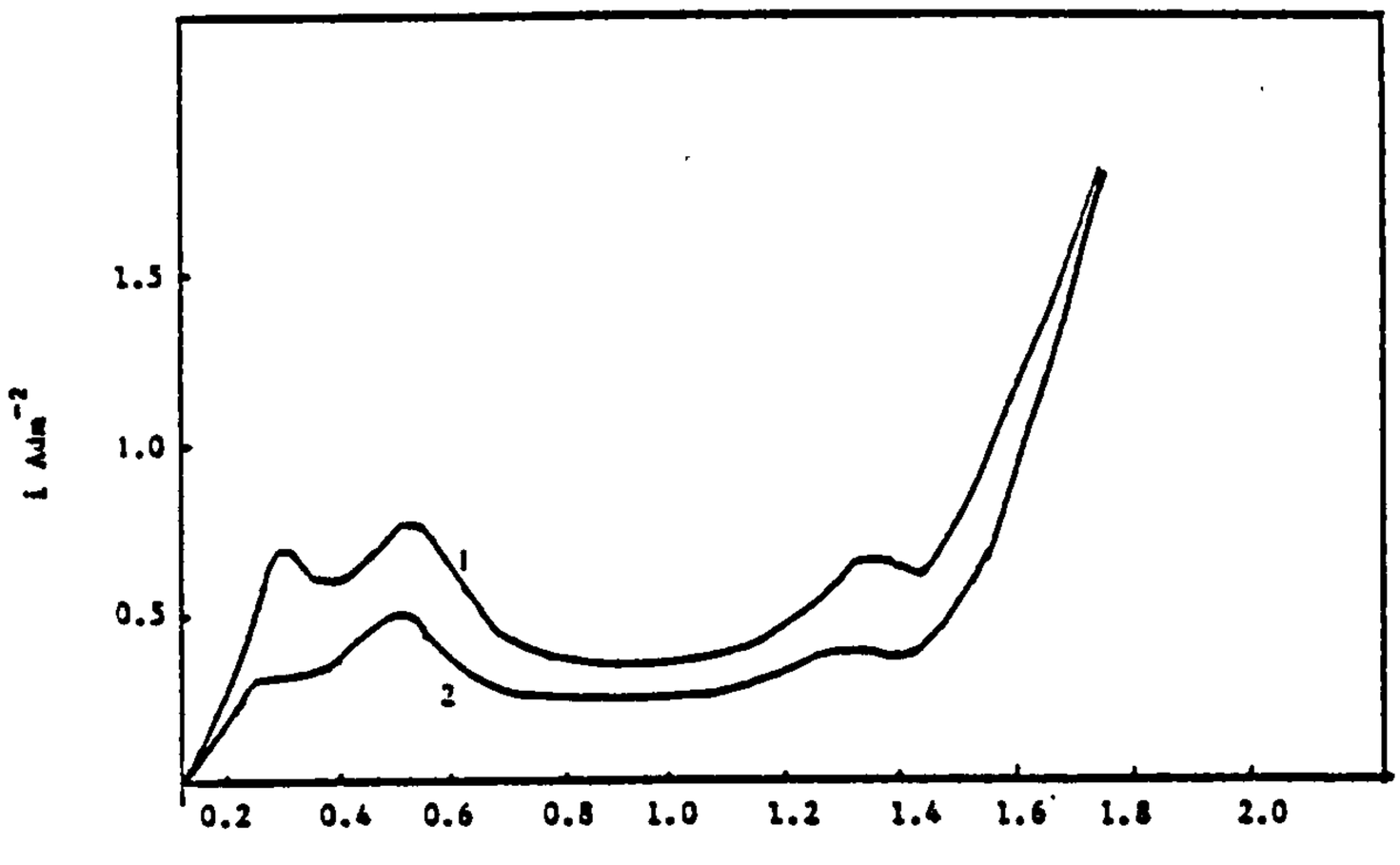

E vs i curve for a sample of Ni200 (curve 2) and Ni270 (curve 1) polarised at a sweep rate of 700mV sec^{-1} from the rest potential in a 360 gl^{-1} $Pb(NO_3)_2$ solution pH 3.5 at 25°C

FIGURE 177

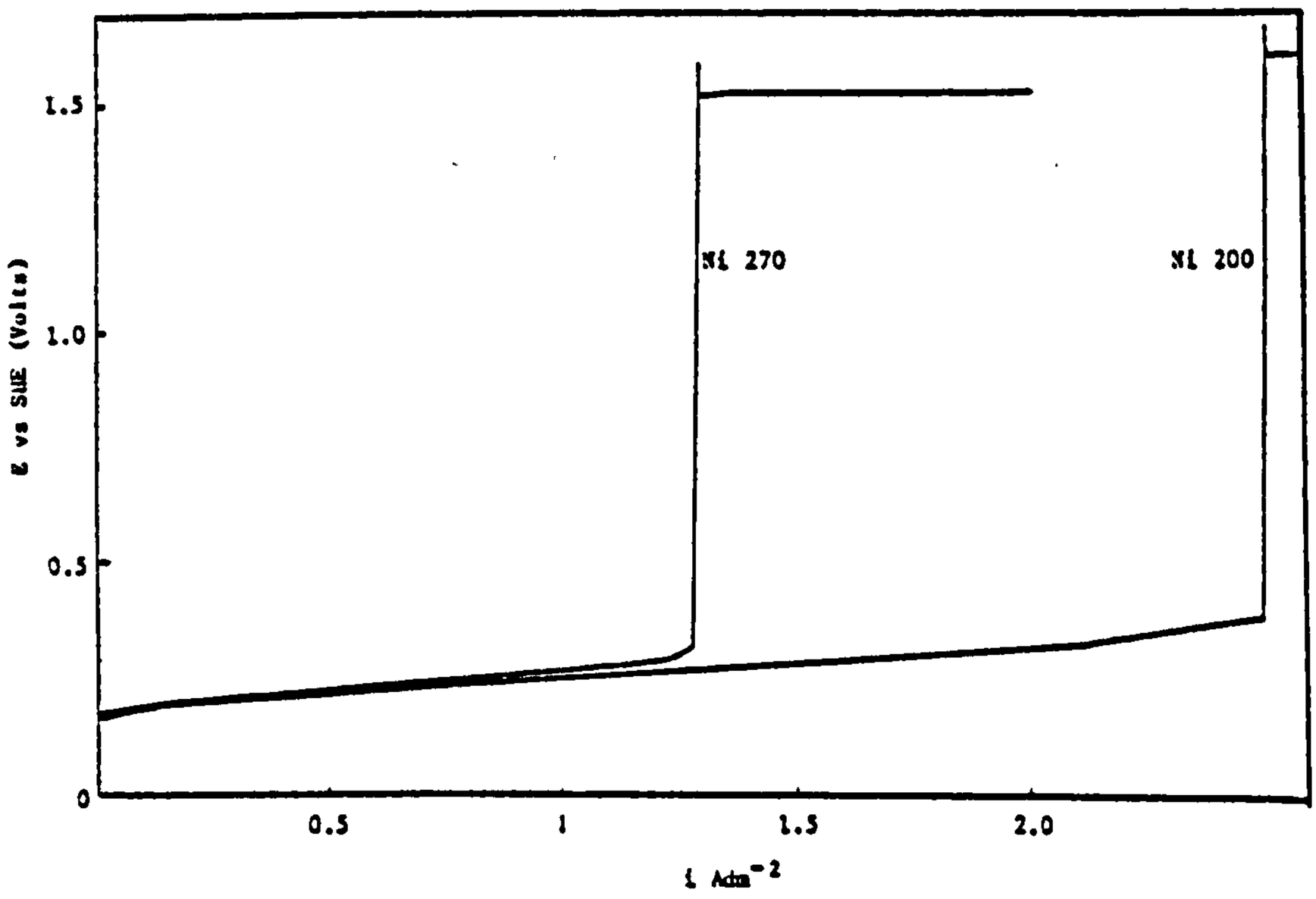

E vs i curves for a sample of Ni200 and Ni270 galvanostatically polarised at 15.6 μ A dm^{-2}sec^{-1} from rest potential in a solution of 360 g l^{-1} $Pb(NO_3)_2$ pH 1.0 at 30°C.

FIGURE 178

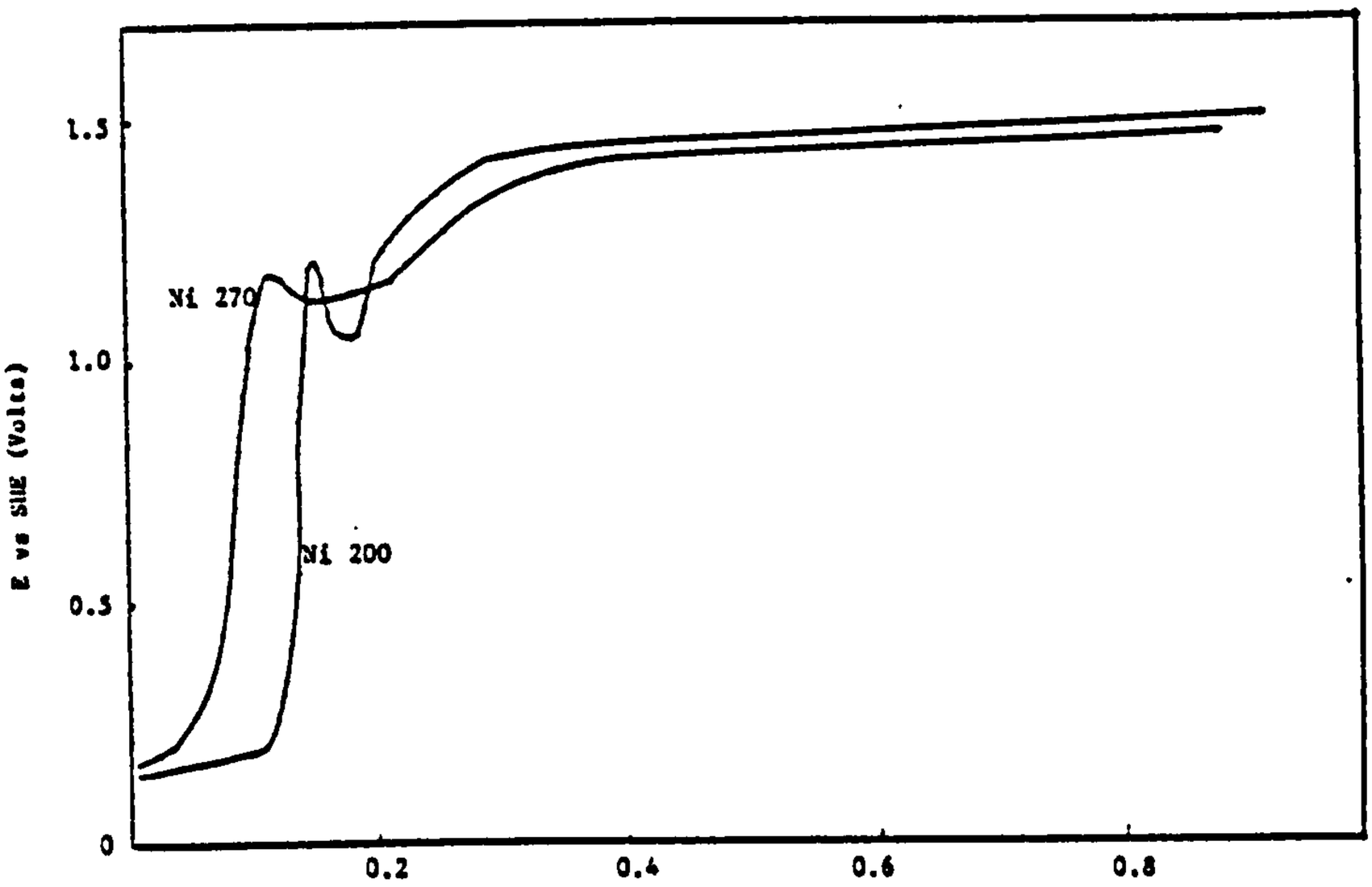

E vs i for a sample of Ni200 and Ni270 polarised at 15.6 uA dm^{-2} sec^{-1} from rest potential in a solution of 360 g l^{-1} $Pb(NO_3)_2$ pH 2.0 at 50^{o}C.

FIGURE 179

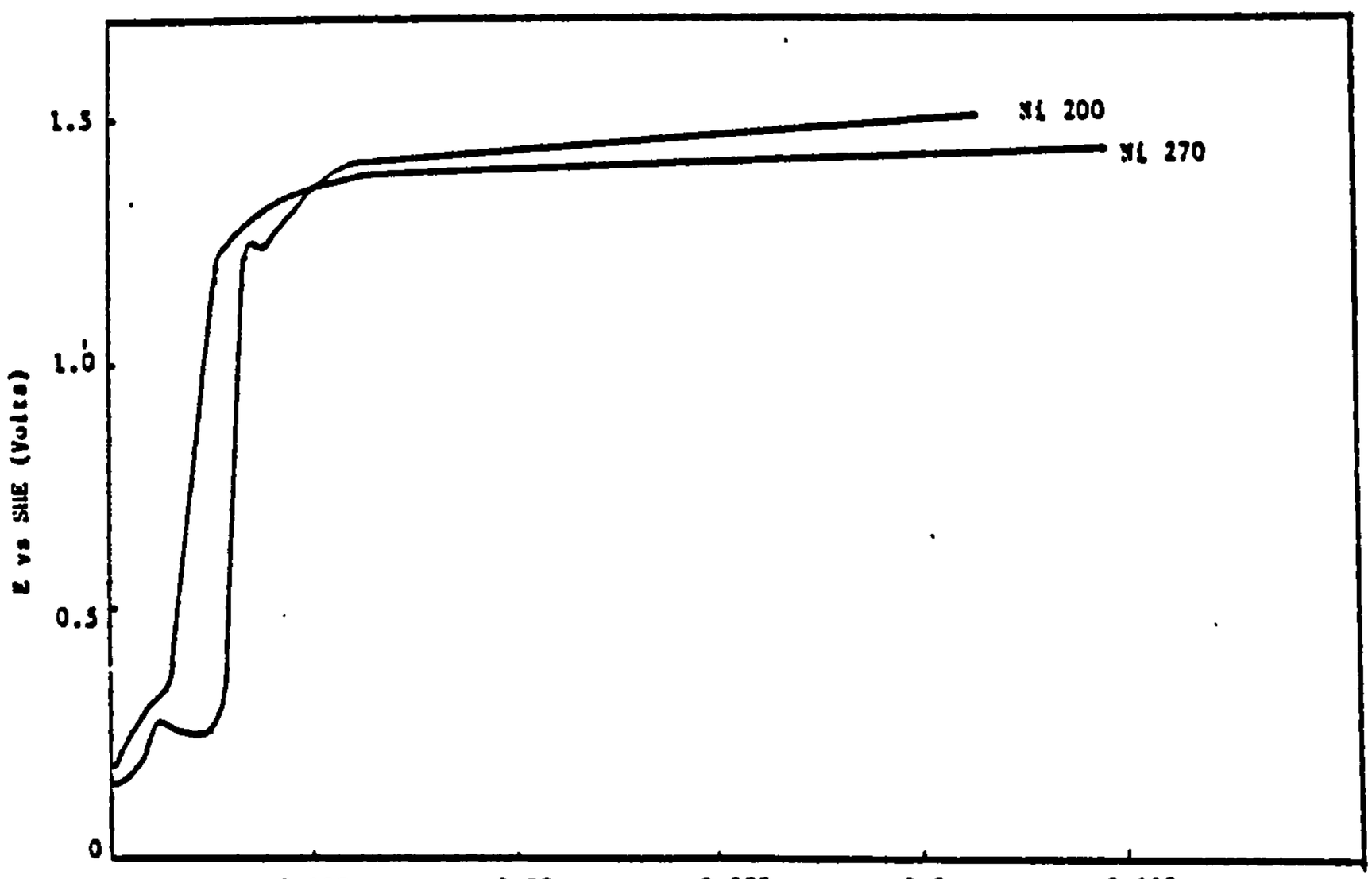

A graph of E vs i for a sample of Ni200 and Ni270 foil galvanostatically polarised at 15.6 uA dm^{-2} sec^{-1} from the rest potential in a solution of 360 gl^{-1} $Pb(NO_3)_2$ pH 2.7 at 50^{o}C.

FIGURE 180

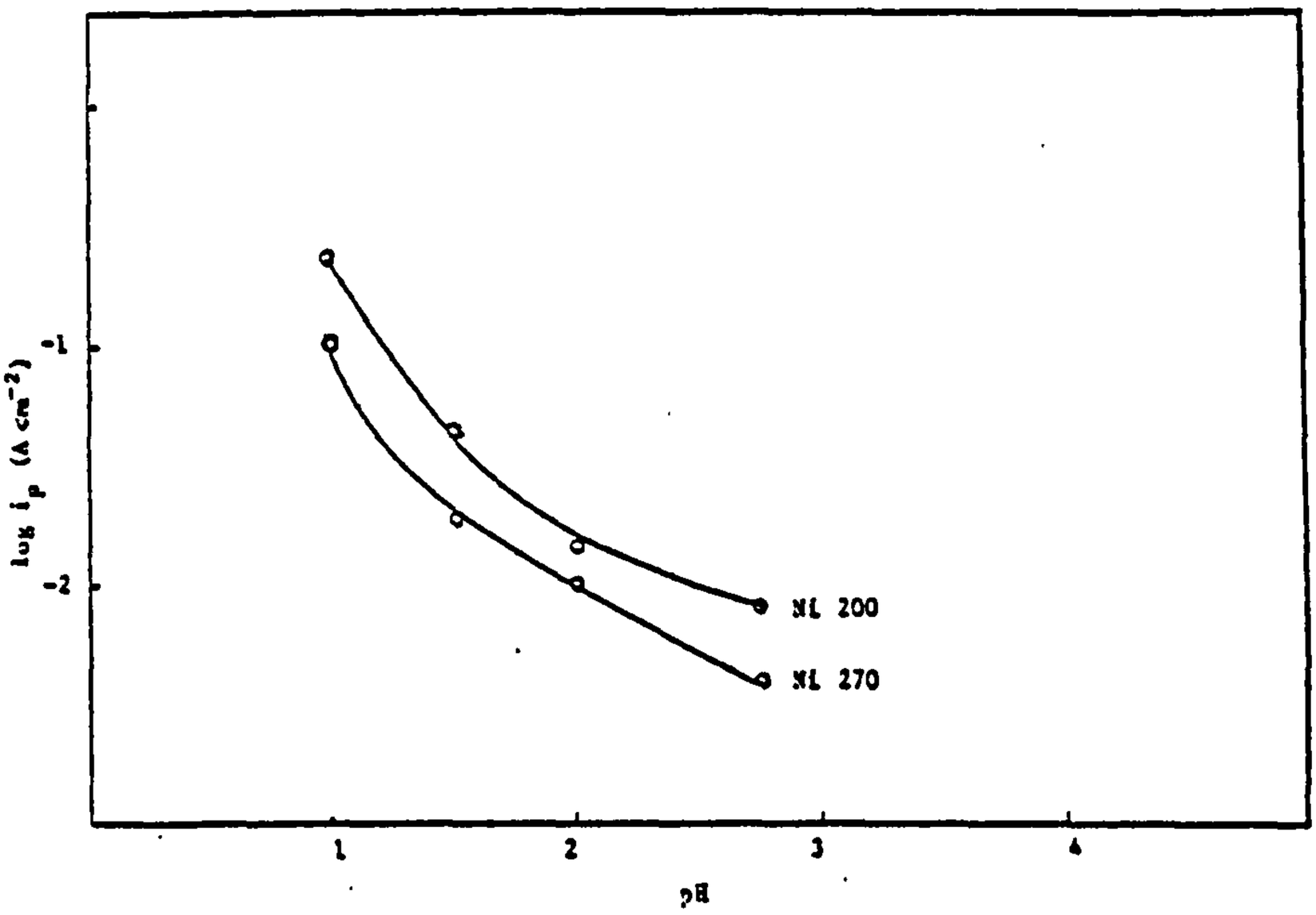

A graph of log i_p (current density required for passivation) vs pH for samples of Ni200 and Ni^{P}270 foil galvanostatically polarised at a 15.6μA dm^{-2} sec^{-1} in a 360 gl^{-1} $Pb(NO_3)_2$ solution.

FIGURE 181

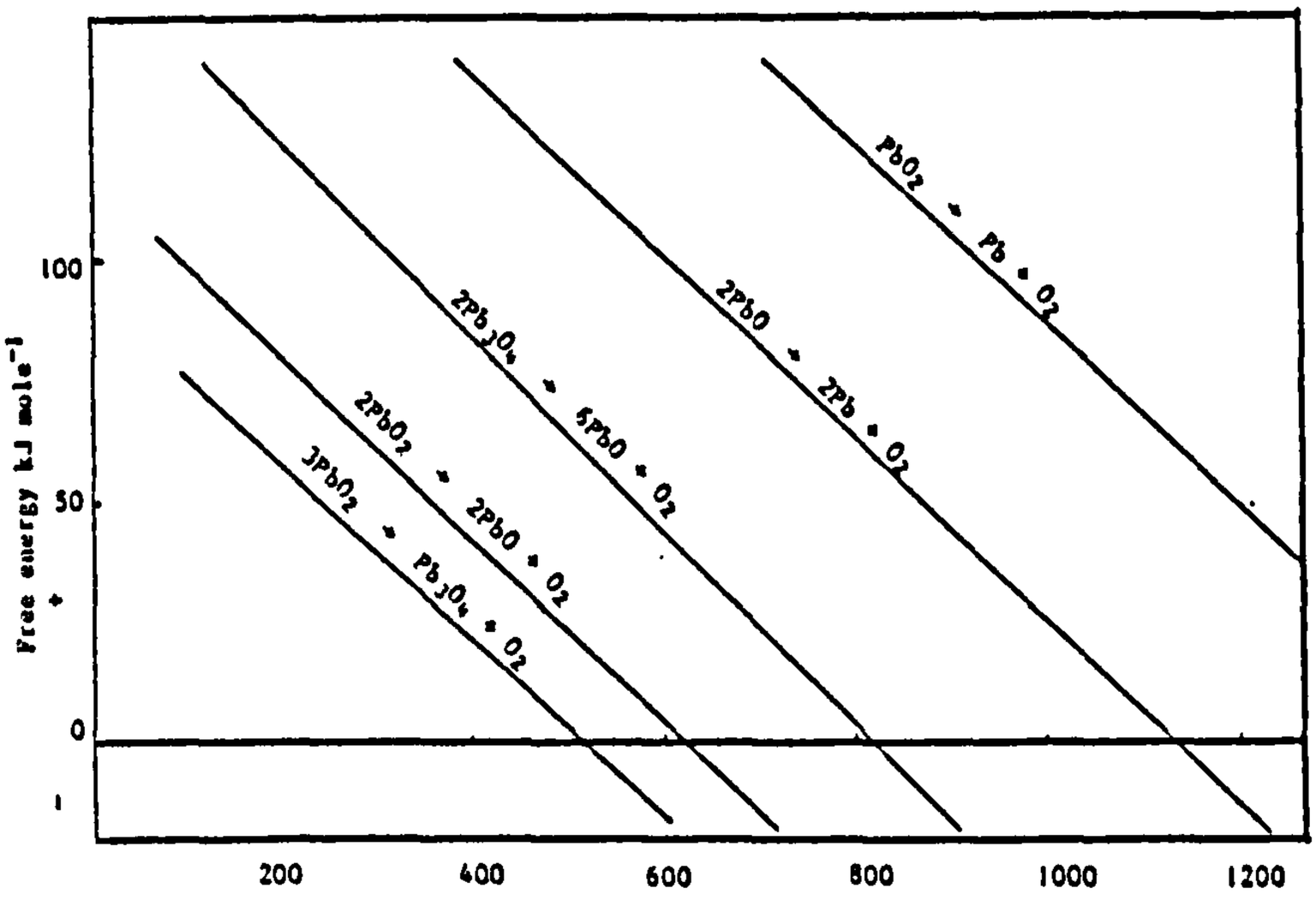

A graph of free energy versus temperature for the thermal decomposition of different lead oxides.

FIGURE 182

Typical potential versus current density curves for Ni200 and Ni270 samples at selected pH's are given in Figs.178 to 180. A plot of pH against the logarithm of the current density for passivation is shown in Fig. 181. As can be seen from these results all Ni200 samples required a greater current density to effect passivation than did the Ni270 samples at a given pH. Indeed in a $Pb(NO_3)_2$ solution of pH 1, Ni200 would clearly be unsuitable for the electrodeposition of PbO_2, since Ni dissolution would be the only reaction that would occur at the current density used for PbO_2 deposition i.e. 2 Adm^{-2}

3.3.9 Scanning Electron Microscope Examinations

3.3.9.1 Studies on the adhesion of PbO_2 onto Ni

Figs. 63P and 64P show the tips of two different bend test adhesion failure specimens. The area over which the coating has been detached is clearly visible and extends either side of the centre of the bend. Indeed, on one of the specimens under investigation (Fig. 63P) some plastic deformation of the Ni substrate was detected at the centre of the bend, although this is not easily visible in (Fig. 63P).

The centre of the tip of a bend test adhesion failure specimen is shown in Fig. 65P. No exposed Ni surface is visible, as would be expected from a visual examination of the failure specimen where coating had obviously become detached and what appear to be cracks in the remaining PbO_2 deposit can be seen. The cracks run parallel to the centre of the bend, with the spacing between each line of cracks, increasing with the distance from the centre of the bend.

Higher magnification views of the surface at the centre of an adhesion failure specimen can be seen in Figs. 66P and 67P. The failure appears to be cohesive in the PbO_2 layers close to the Ni/PbO_2 interface not adhesive with no exposed Ni visible even at high magnifications.

A view inside one of the surface cracks can be seen in Fig. 68P, no Ni was visible only what appeared to be small crystals of PbO_2. EDAX (Energy Dispersive X-ray Analysis) confirmed Pb and O were present.

The boundary between the detached and undetached PbO_2 was found to be essentially linear (ses Fig. 69P) and run parallel to the centre of the bend. Some cracks were visible in the remaining PbO_2 deposit (see Fig. 70P) yet these did not result in detachment of the PbO_2 deposit. The edge of the failure can also be seen to coincide with the direction of the cracks visible on the PbO_2/Ni interface (see Fig. 70P).

Samples that exhibited good adhesion were also subjected to the adhesion bend test outlined in (Section 2.1.8) and examined on the S.E.M.

Figs. 71P and 72P show the tip of a bend on a specimen found to exhibit good adhesion. The presence of surface cracks on the PbO_2 can be detected (see Fig. 72P) but these have not resulted in detachment of the coating. The cracks in the PbO_2 deposit were only found at or in the region of the centre of the bend (see Fig. 71P).

A sample of Ni270 was heated under vacumm at 800°C for 30 minutes then subjected to an anodic etch in 30% H_2SO_4 as described in Section 2.1. A small section of this foil was coated with electrodeposited PbO_2 and tested using the adhesion bend test. All samples, failed the adhesion bend test but when examined under the S.E.M, the failure was found to be adhesive occuring at the PbO_2/Ni interface with the etched Ni surface clearly visible at the centre of the adhesion failure (see Fig. 73P).

3.3.9.2 S.E.M examination of etched Ni foil

Samples of different Ni foils with different pre-treatments and chemical composition were examined after electrochemical etching in 30 wt% H_2SO_4. The prime object of which was to examine

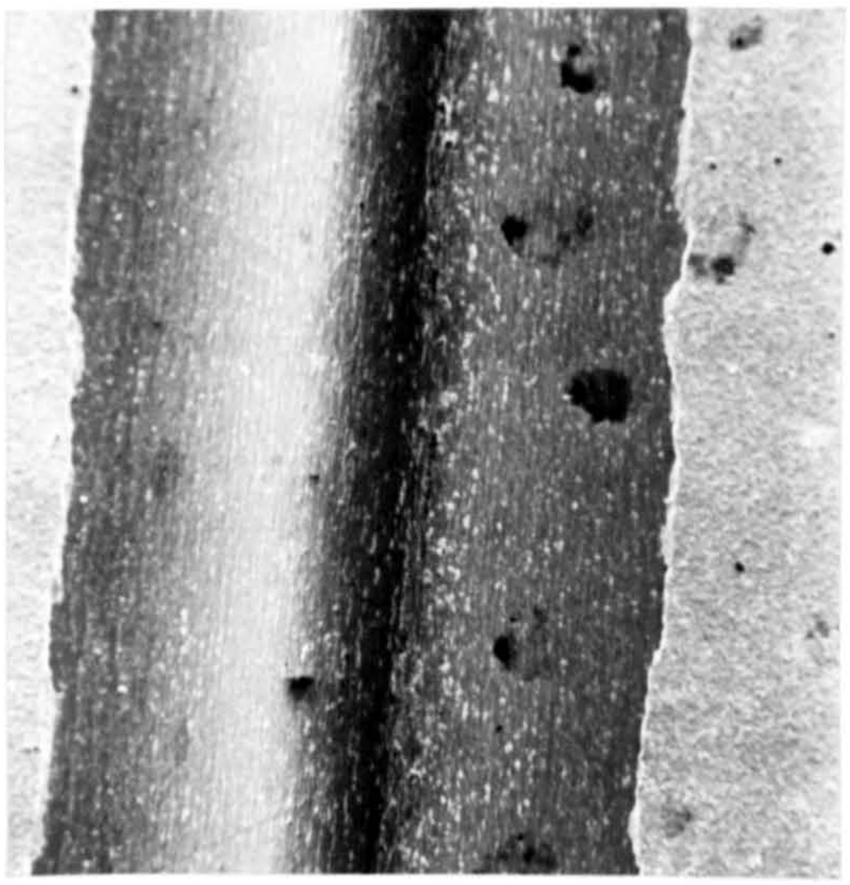

FIGURE 63P

The tip of a bend test adhesion failure specimen for PbO_2 electrodeposited onto Ni270

(Magnification 50X)

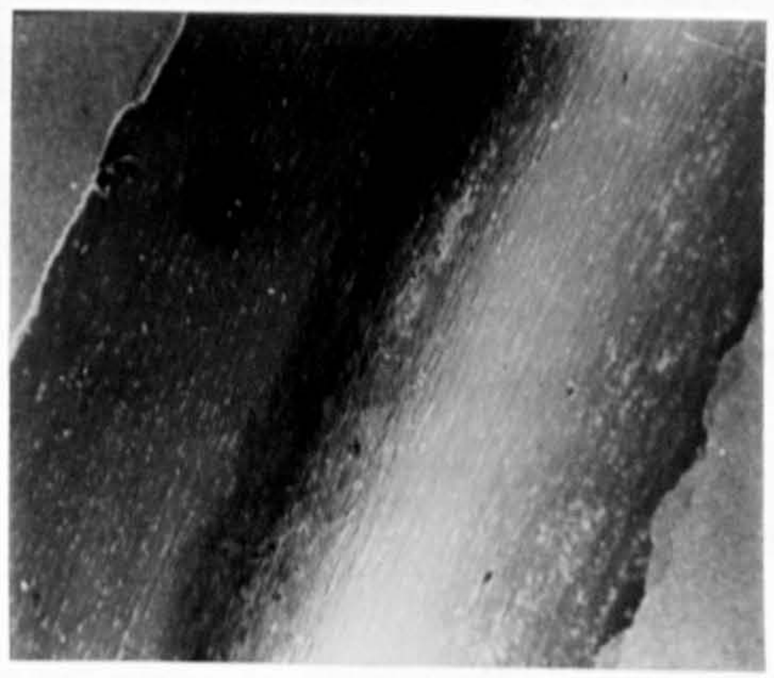

FIGURE 64P

The tip of a bend test adhesion failure specimen for PbO_2 electrodeposited onto Ni270 (from a different source)

(Magnification 50X)

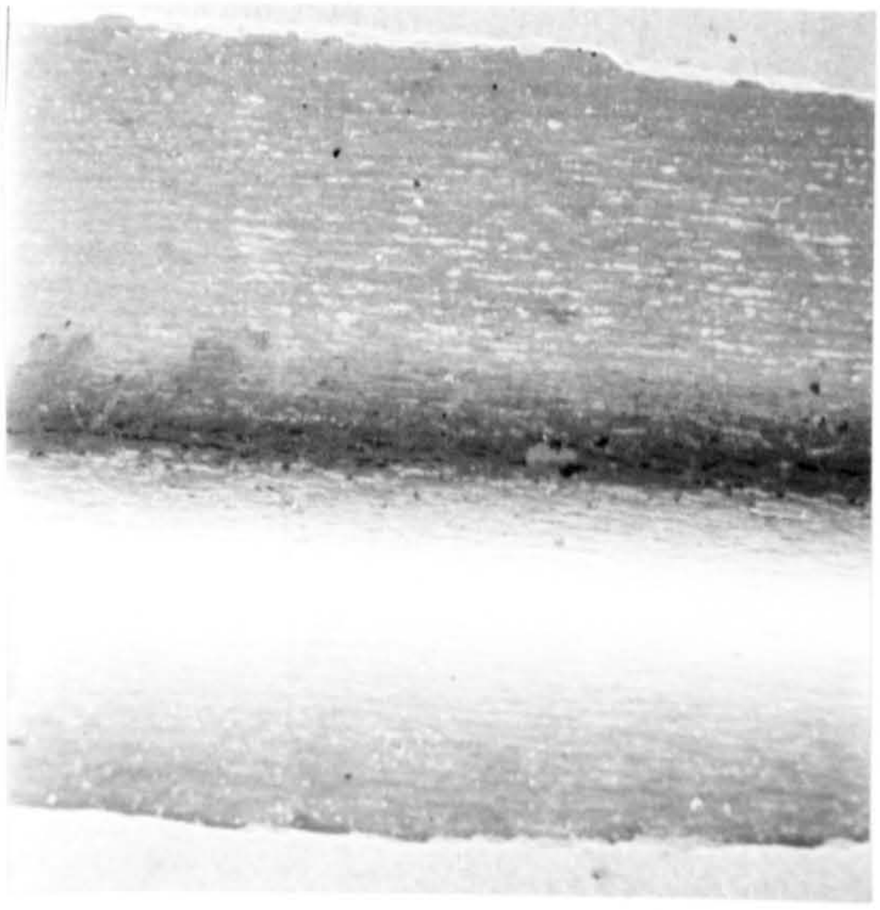

FIGURE 65P

The centre of the bend test adhesion specimen shown in Figure 64P

(Magnification 250X)

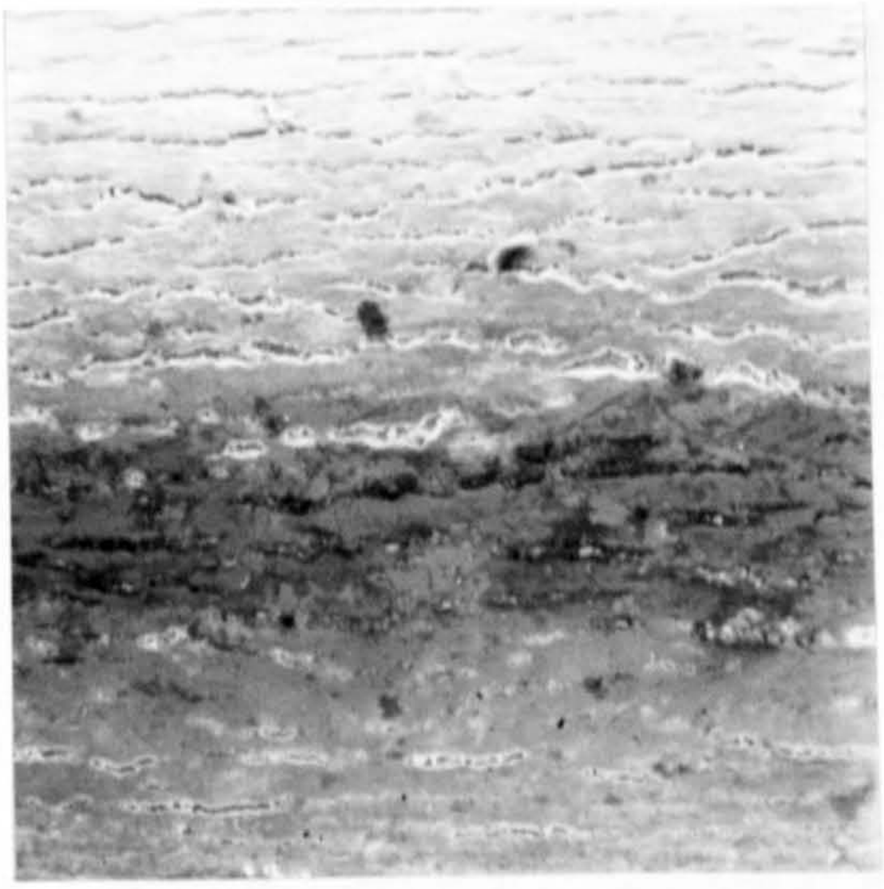

FIGURE 66P

The centre of the bend test adhesion failure specimen shown in Figure 64P

(Magnification 1000X)

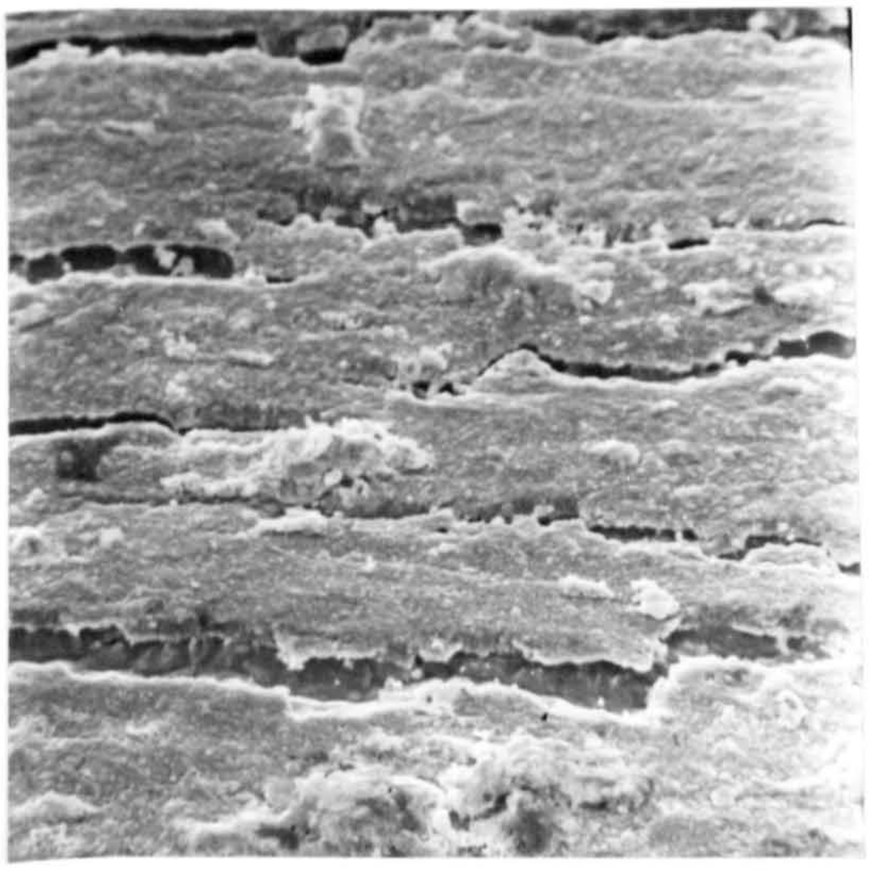

FIGURE 67P

The tip of the bend test adhesion failure specimen shown in Figure 63P

(Magnification 1000X)

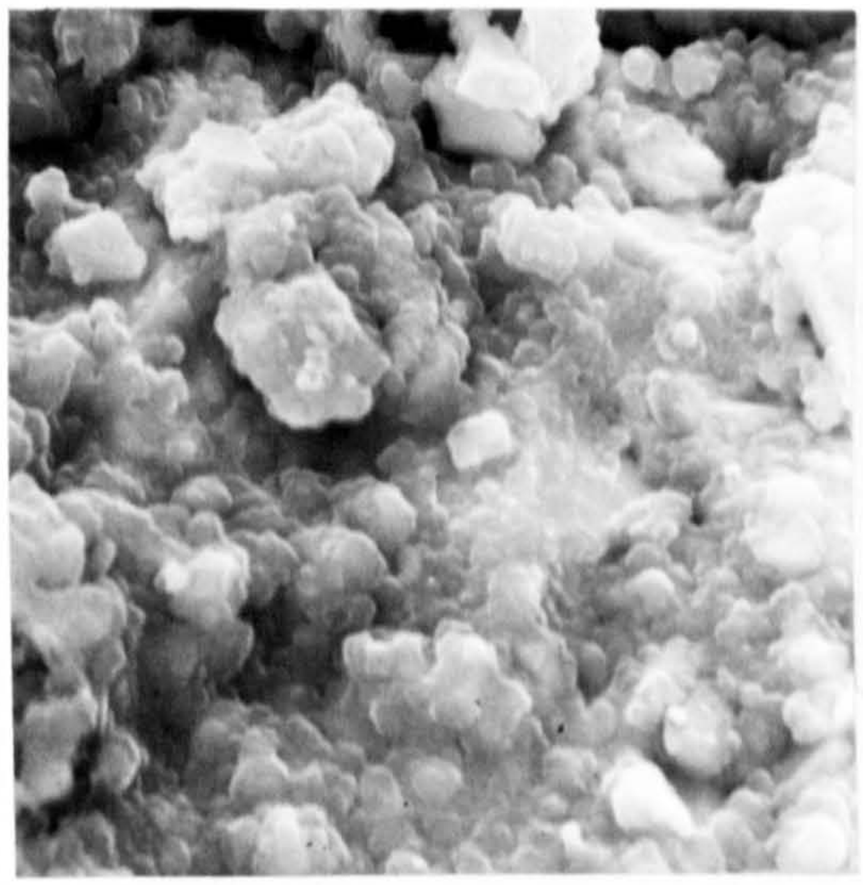

FIGURE 68P

View inside a surface crack as seen in Figure 67P for a bend test adhesion failure specimen

(Magnification 5000X)

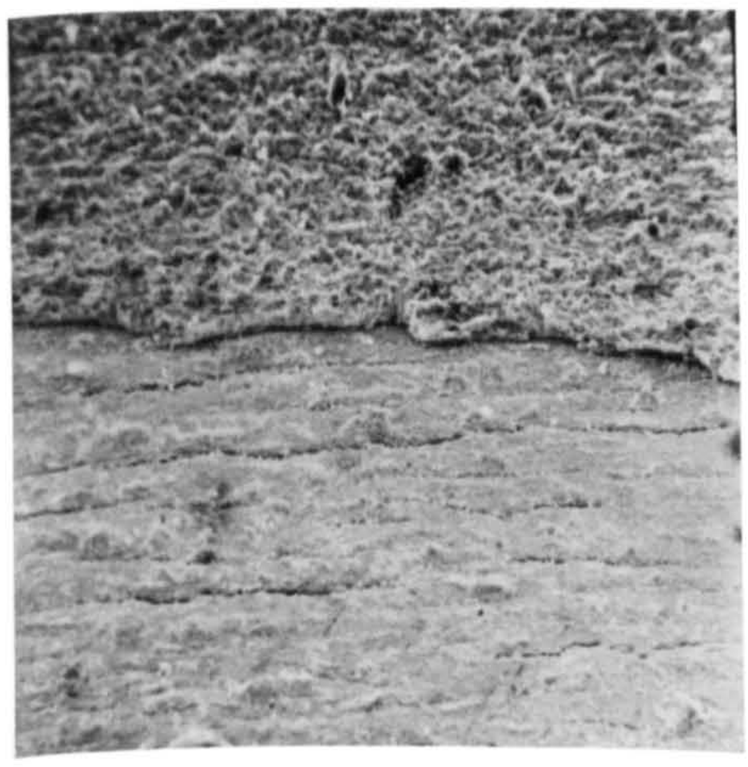

FIGURE 69P

The boundary between detached and un-detached PbO_2 on a bend test failure specimen

(Magnifiation 200X)

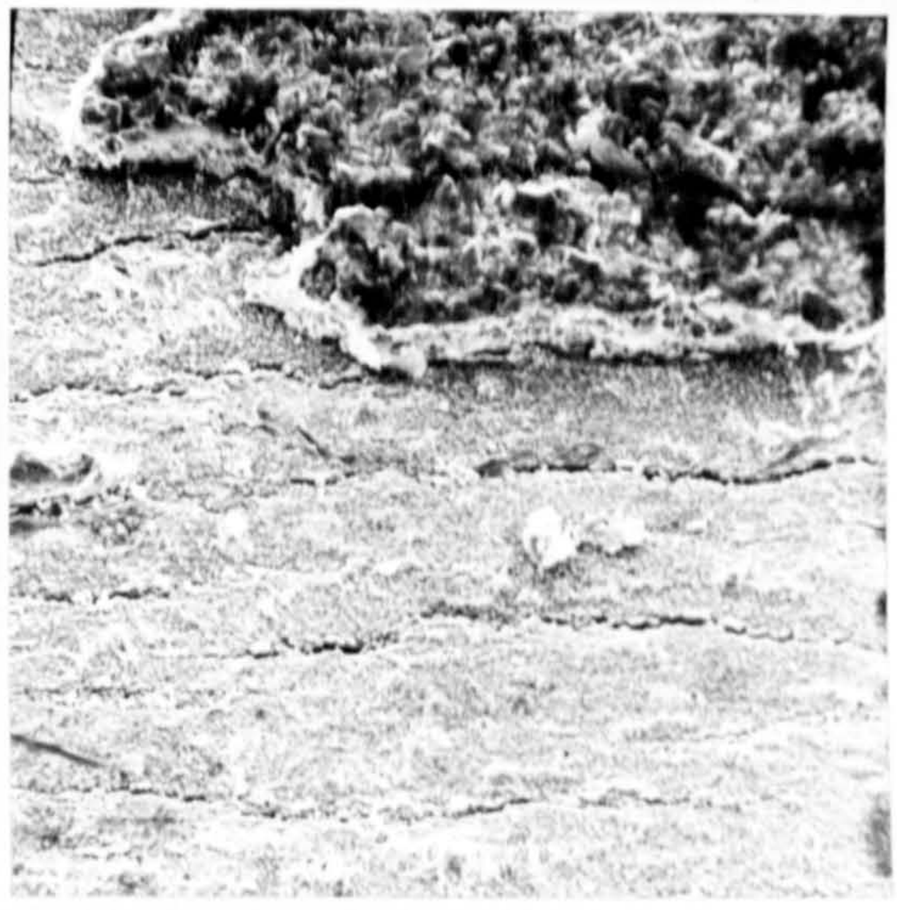

FIGURE 70P

Boundary between detached and un-detached PbO_2 on bend test failure specimen

(Magnification 500X)

FIGURE 71P

Tip of the bend on a specimen of PbO_2 electrodeposited onto Ni that exhibited good adhesion in the bend test

(Magnification 100X)

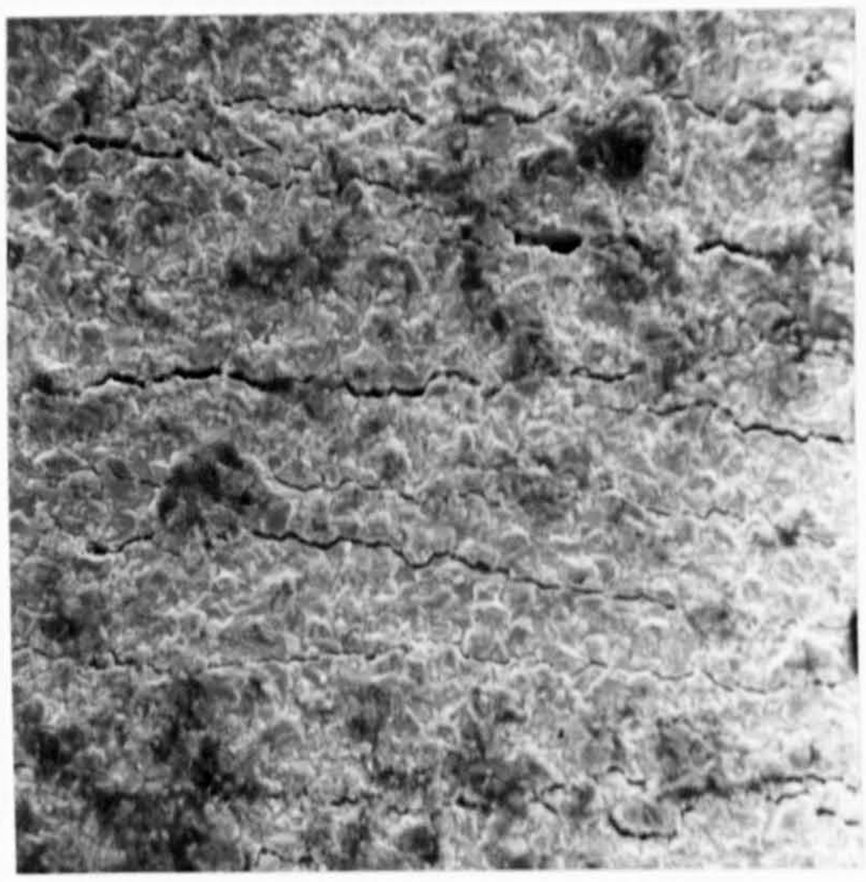

FIGURE 72P

Tip of a bend on a specimen of PbO_2 electrodeposited onto Ni for a specimen that exhibited good adhesion in the adhesion bend test

(Magnification 500X)

FIGURE 73P

Edge of adhesion failure on a specimen of Ni270, heated under vacuum at 800° C for a $\frac{1}{2}$ hour, then plated with PbO_2

(Magnification 1000X)

the surface topography of etched Ni foils and discover if any relationship existed between surface finish and the adhesion of PbO_2 onto Ni. In addition an explanation for the variation in etch pattern on certain types of Ni270 foils was also sought.

Fig. 74P shows a photograph of a sample of Ni200 (4 cm x 3.5 cm) after anodic etching in 30% H_2SO_4 at 50°C and 2 Adm^{-2}, whilst Fig. 75P shows a sample of Ni270 etched under identical conditions. The Ni270 foil (Fig. 75P) exhibited areas that appeared to be completely unaffected by the etching operations.

The Ni200 samples all produced a uniformly etched surface, on anodic etching with no unetched areas visible. Indeed, all samples of Ni200 were subsequently found to exhibit 'good' adhesion for electrodeposited PbO_2 whilst the randomly etched Ni270 samples exhibited 'bad' adhesion for PbO_2.

Fig. 76P shows a low magnification view of the surface of Ni200 after anodic etching in H_2SO_4. The etch pits are all elongated in the direction of rolling. The area around the etch pit appears to be unaffected by the etching operation (Fig. 77P and Fig. 78P), whilst inside the etch pit well etched crystallographic faces of Ni are visible. A sample of Ni200 from a different source, when etched in 30wt % H_2SO_4 also exhibited a similar etched surface, see Figs. 80P-82P. The pits were elongated and in the direction of rolling and the Ni surface in the immediate vicinity of the pit was unaffected. However, some undermining of Ni surface by pits radiating out sideways from the initial pit can be detected. These can in fact be seen as the dark areas in Figs. 80P-82P. A sample of Ni270 (125 m thick) supplied by The Ionic Plating Co Ltd, when etched in 30% H_2SO_4 showed areas that were hardly affected by the etching process (see Fig. 83P). Etch pits elongated in the direction of rolling were visible and the Ni surface in the vicinity of the pits hardly attacked. Yet other areas on the same sample of foil were well etched (see Fig. 84P). No areas of the Ni foil appeared to be completely unaffected by the anodic etching process. The etch pits appeared to be un-

directional i.e in the direction of rolling. The etch pits seen in Figs. 85P and 86P are different to those obtained for samples of Ni200 They are rounded and do not show areas of Ni that are unaffected by the etching process. The etch pattern observed on Ni270 foils appears to be dependent upon the rolling history of the foil and is different for different samples of Ni270. Fig. 87P to 88P shows the results of anodic etching in 30% H_2SO_4 on a sample of Ni270 (200 μm thick). Areas on the same sample that were etched to different extents are visible (see Fig. 87P). The nature of the etch pits is however different to those on Ni200 samples. No preferred orientation in the direction of rolling could be seen (Figs. 88P-89P).

Heating a sample of Ni270 to 500°C in an atmosphere of hydrogen for 1/2 hour, prior to anodic etching in H_2SO_4, failed to eliminate the uneven etch pattern observed (see Figs. 90P and 91P). Although the surface topography in the etched areas of Ni heated to 500°C was different from that on the un-heat treated foil, as is evident from Fig. 91P. Samples of the same Ni270 foil were heated to 800°C under vacuum for 30 minutes, then subjected to the same anodic etching procedure described earlier. In this instance the surface of the Ni foil was found to be uniformly etched with no unetched areas or etch pits visible (see Fig. 92P). The nickel grain size was also found to increase, presumably due to grain recrystallisation. Fig. 93P shows what appears to be the presence of a triple point and this is seen in greater detail in Fig. 94P. The triple point is also stepped possibly as a result of preferential etching along a certain crystal plane.

The etch pattern in other areas in the foil can be seen in Fig. 95P. The presence of facets can be seen which is further evidence of preferential etching.

3.3.10 Back Scatter X-ray diffraction on Ni foils

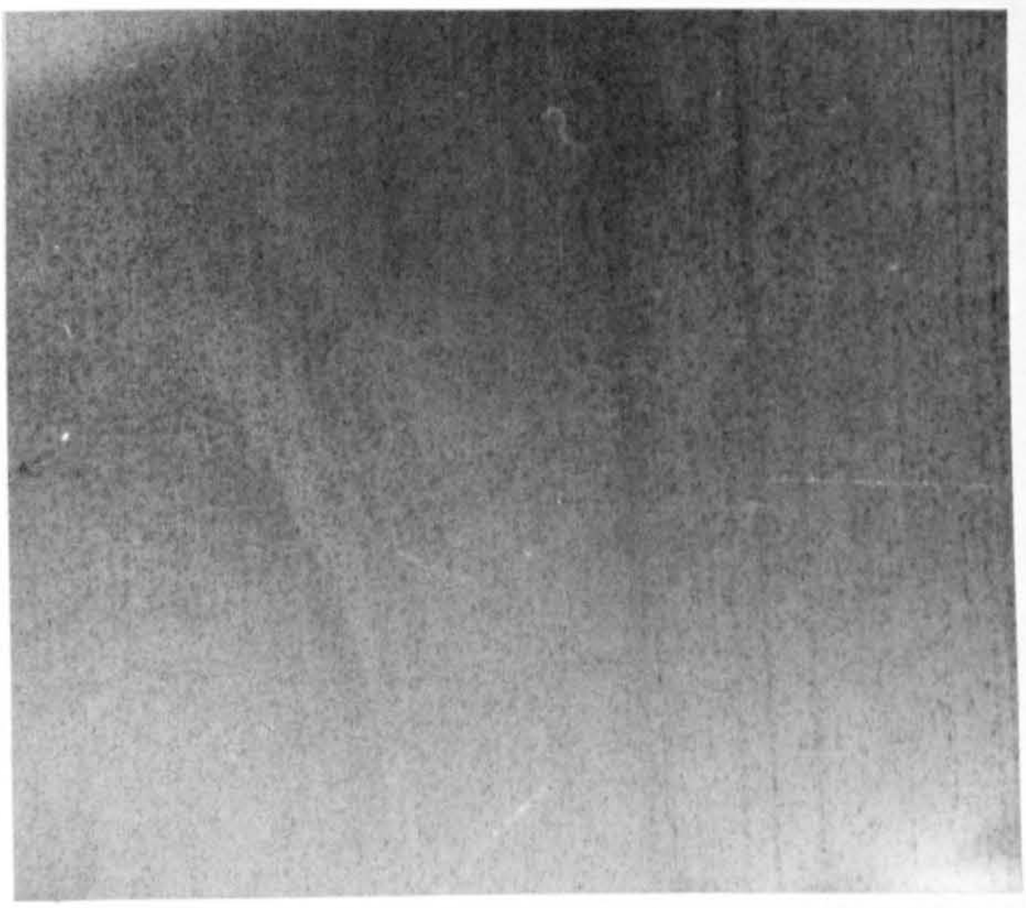

FIGURE 74P

Sample of Ni200 etched at 2 Adm^{-2}

in 30% H_2SO_4 at 50°C

(Magnificiation 1X)

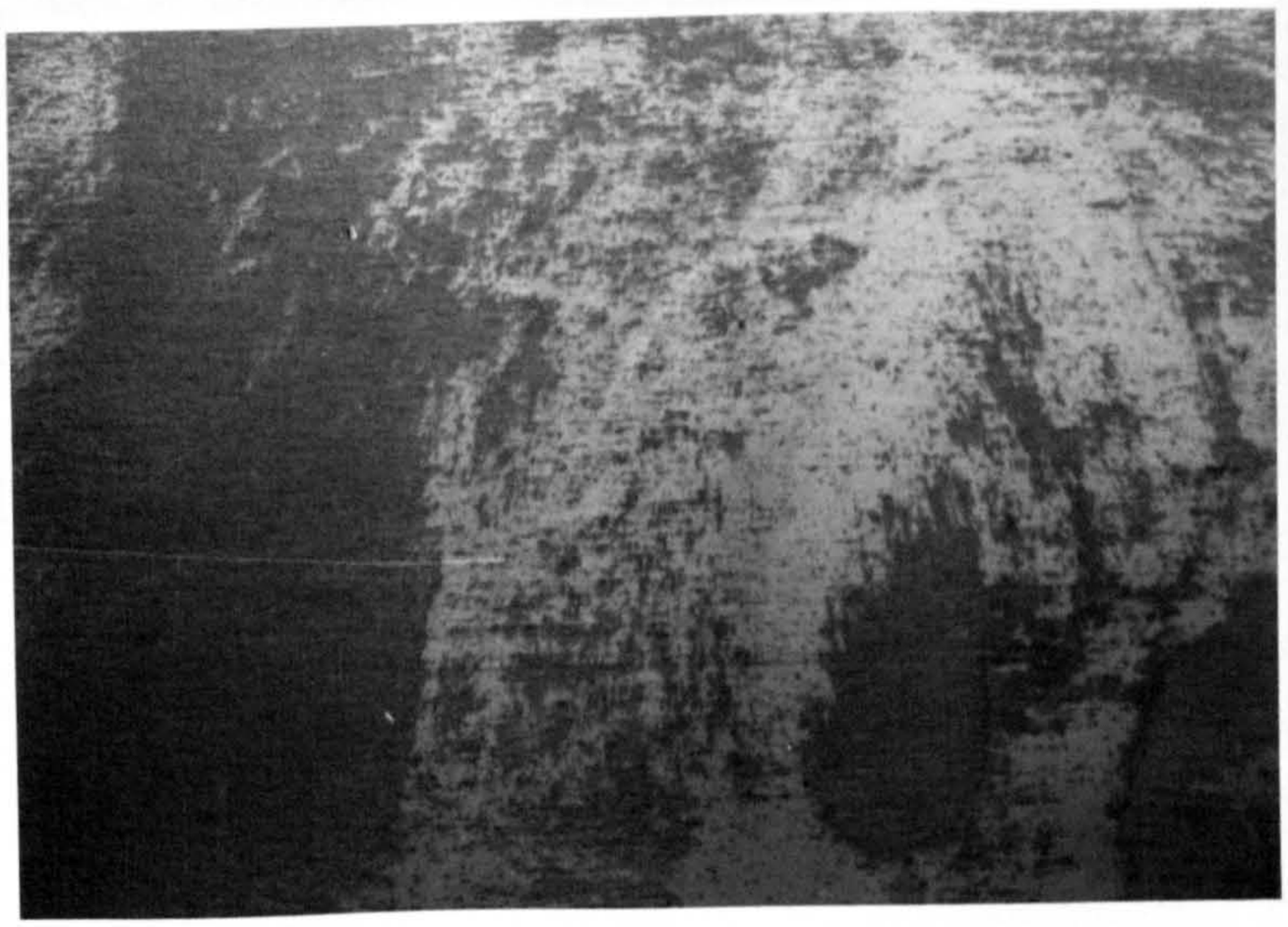

FIGURE 75P

Sample of Ni270 showing an uneven etch pattern after

anodic etching at 2 Adm^{-2} in 30% H_2SO_4 at 50°C

(Magnification 1X)

FIGURE 76P

Sample of Ni200 after an anodic etch at 2 Adm^{-2} in 30 wt % H_2SO_4 at 50°C for 10 minutes

(Magnification 100X)

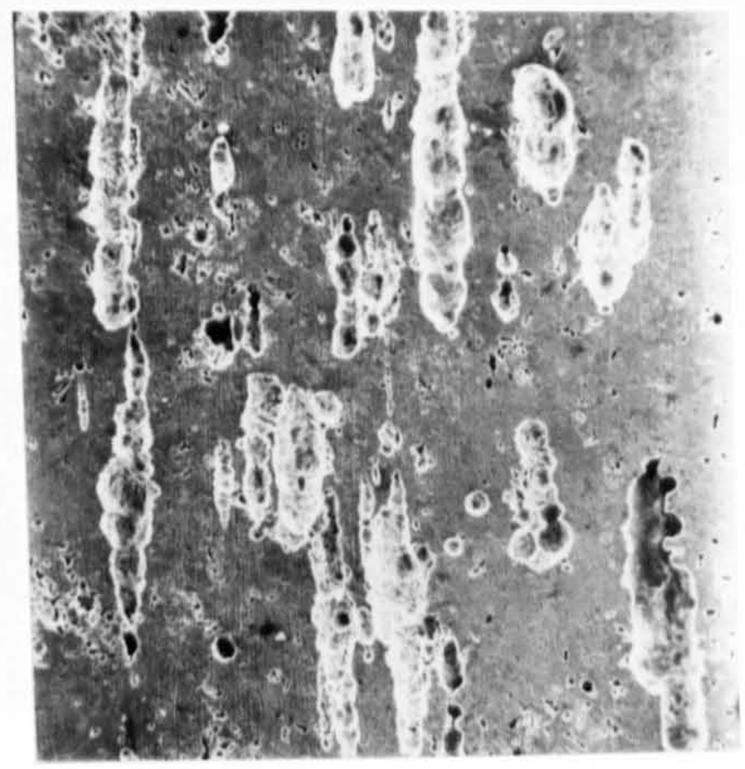

FIGURE 77P

View of etch pits on a sample of Ni200 after an anodic etch at 2 Adm^{-2} in 30 wt % H_2SO_4 at 50° C for 10 minutes

(Magnification 250X)

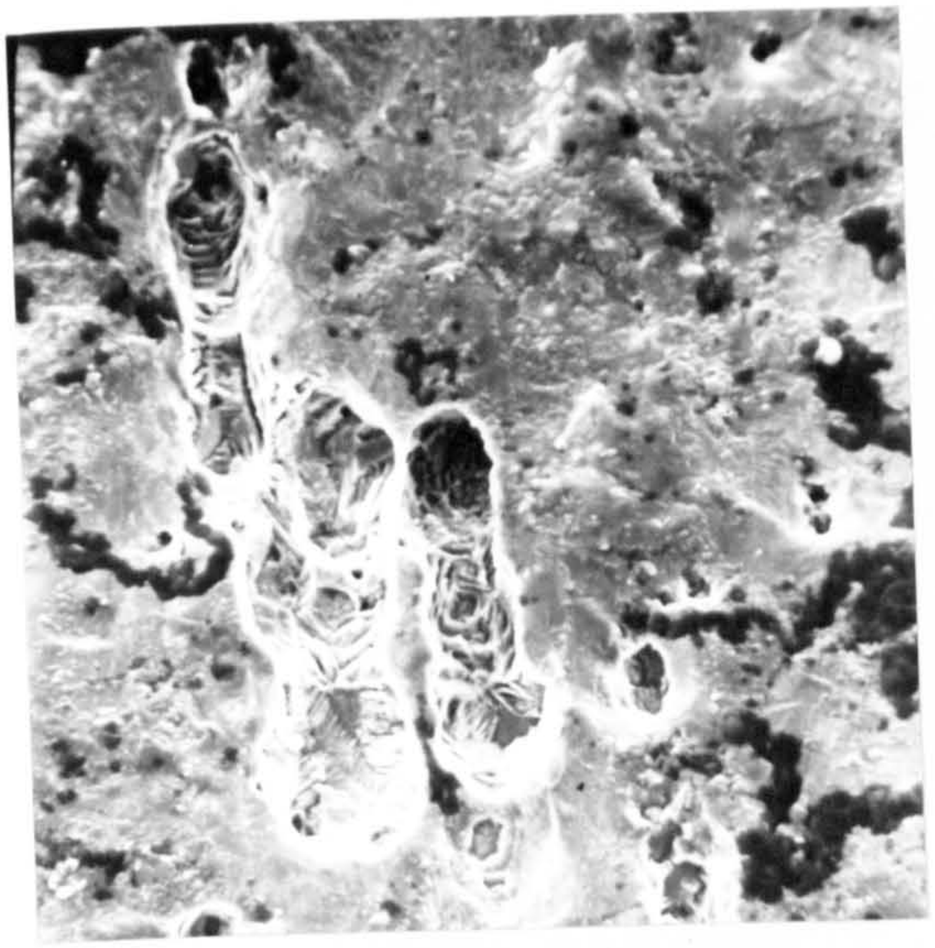

FIGURE 78P

View of etch pit on Ni surface shown in Figure 77P

(Magnification 1000X)

FIGURE 79P

Higher magnification view of etch pits shown in Figure 78P

(Magnification 2000X)

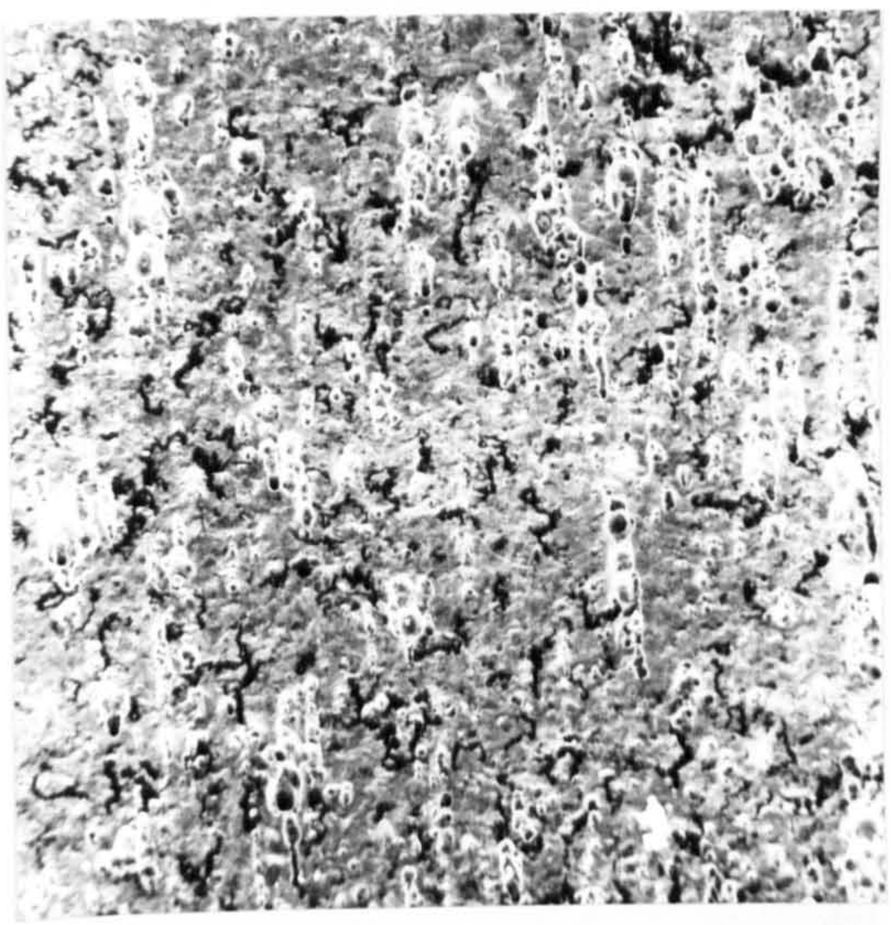

FIGURE 80P

Surface of Ni200 after anodic etching at 2 Adm^{-2} in 30 wt% H_2SO_4 at 50°C for 10 minutes
(Ni200 from a different source)

(Magnification 150X)

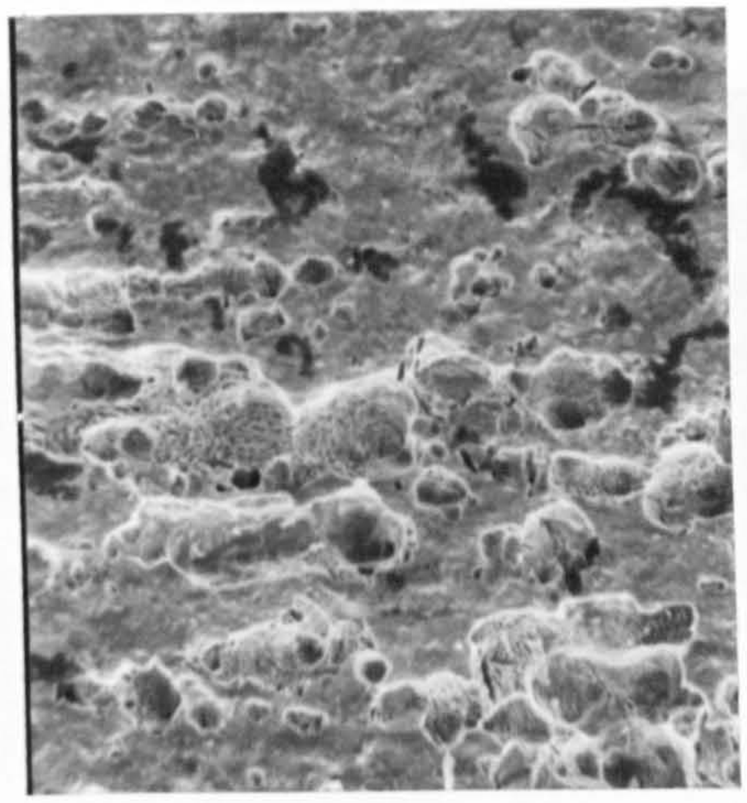

FIGURE 81P

View of etch pits for same sample as shown in Figure 80P

(Magnification 500X)

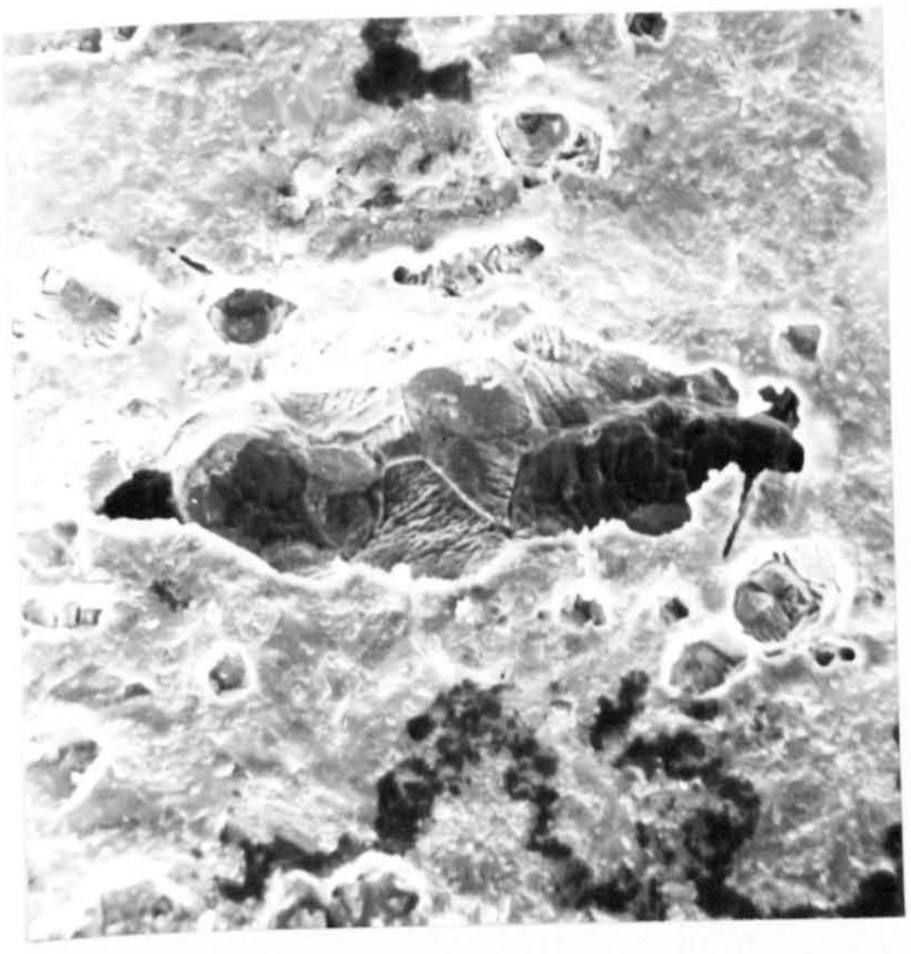

FIGURE 82P

View of etch pit found in Figure 81P

(Magnification 1000X)

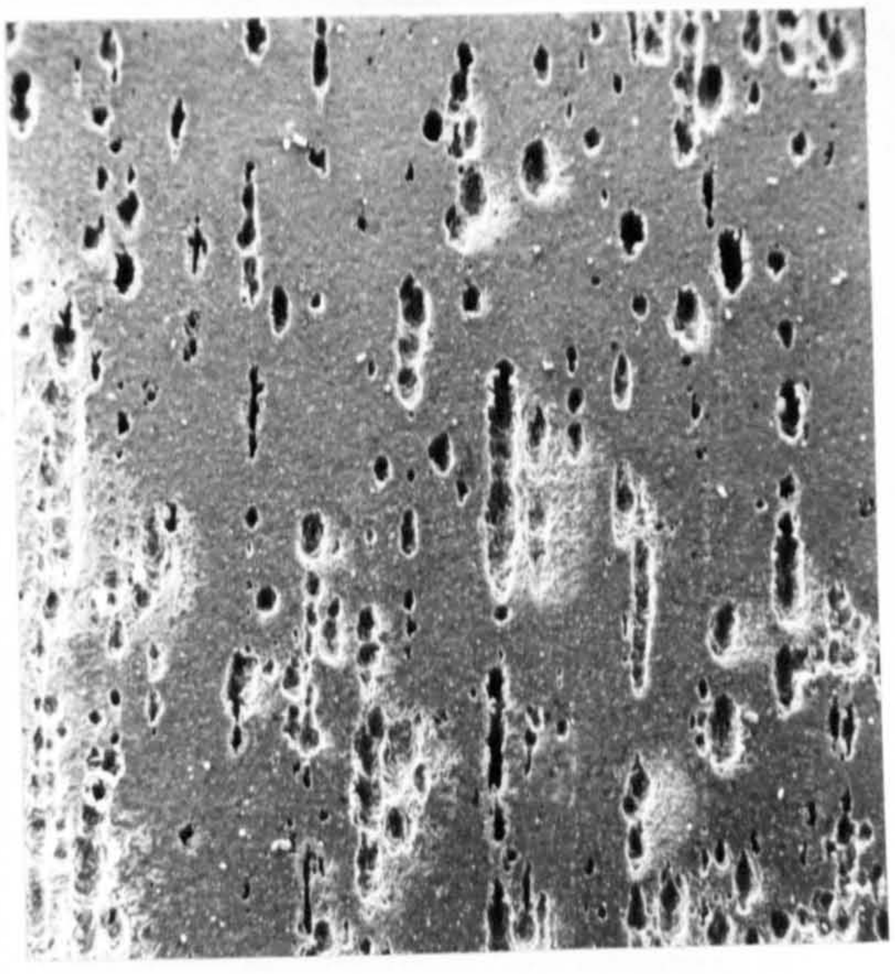

FIGURE 83P

Sample of Ni270 125 µm thick anodically etched at 2 Adm^{-2} in 30 wt% H_2SO_4 at 50°C for 10 minutes.
View of poorly etched area

(Magnification 50X)

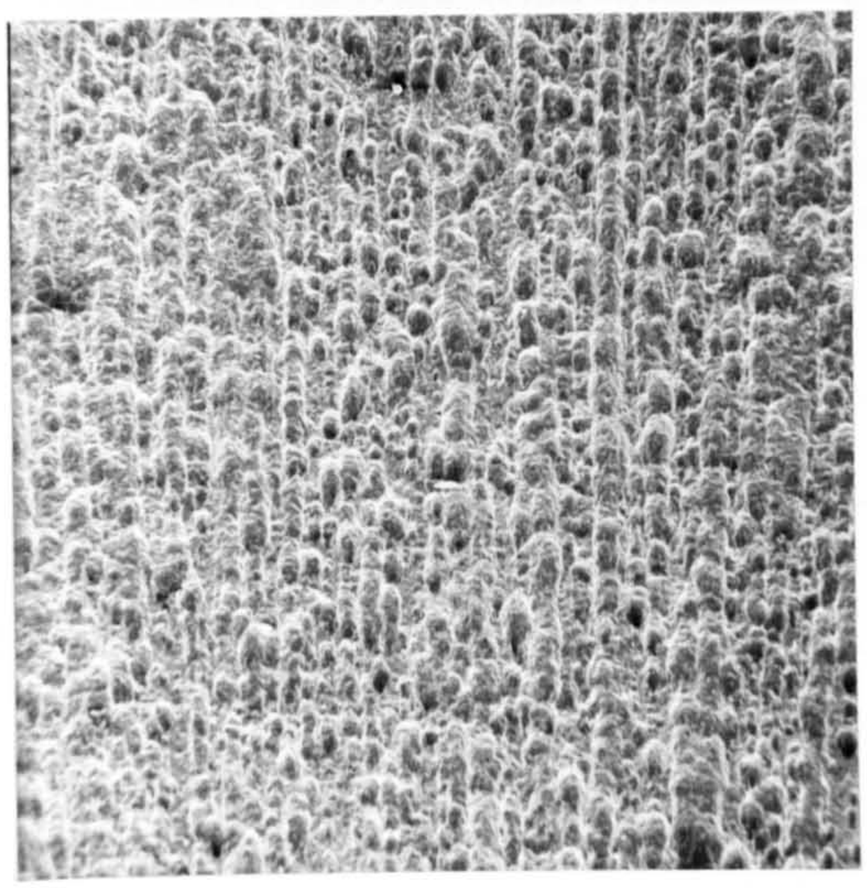

FIGURE 84P

Sample of Ni270 (125μm thick) anodically etched at 2 Adm^{-2} in 30 wt% H_2SO_4 at 50°C.
View of well etched area on sample

(Magnification 50X)

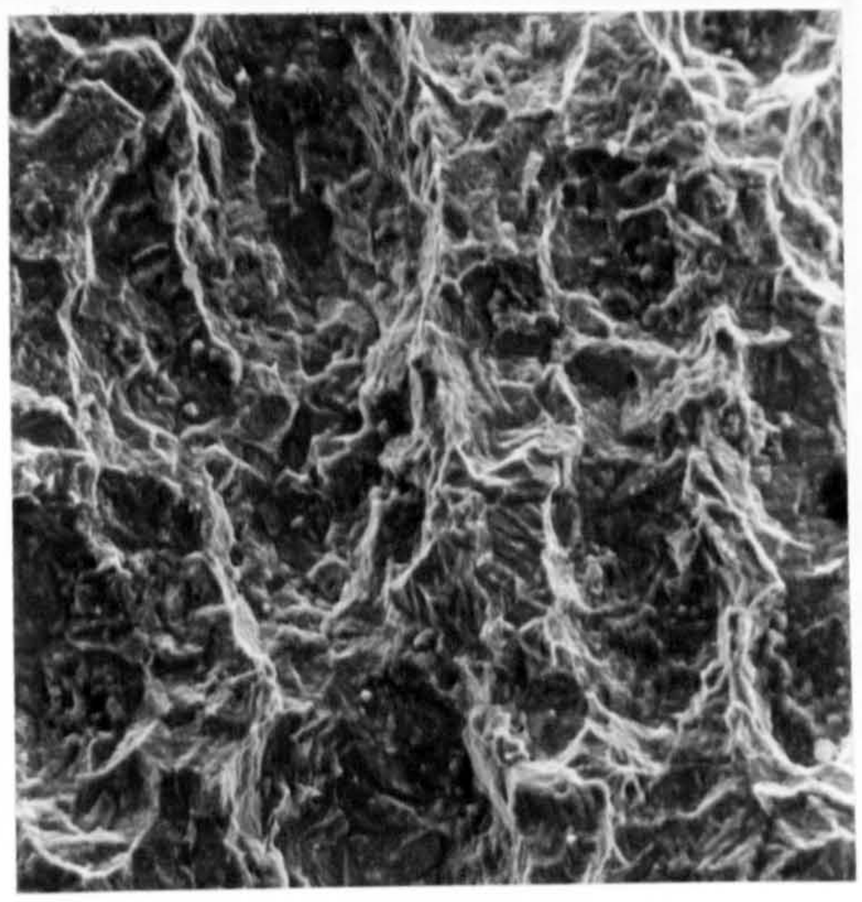

FIGURE 85P

Higher magnification view of well etched area on Ni270 sample seen in Figure 84P

(Magnification 250X)

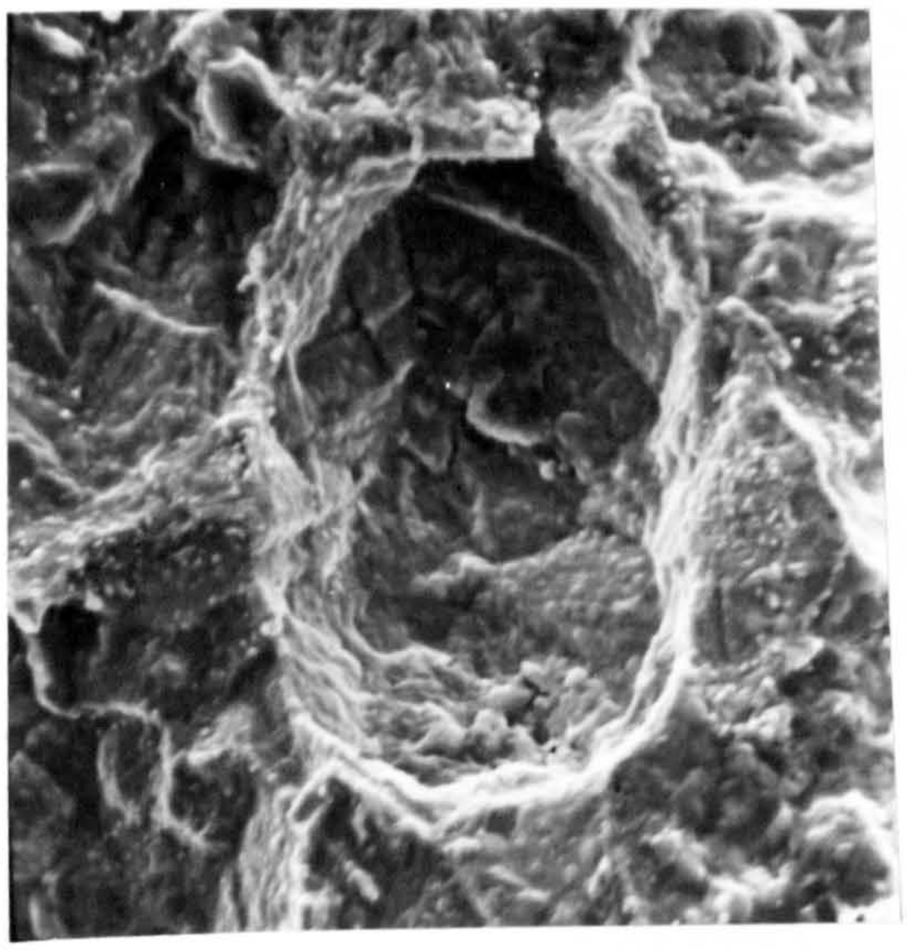

FIGURE 86P

View of etched pit on well etched area shown in Figure 84P

(Magnification 1000X)

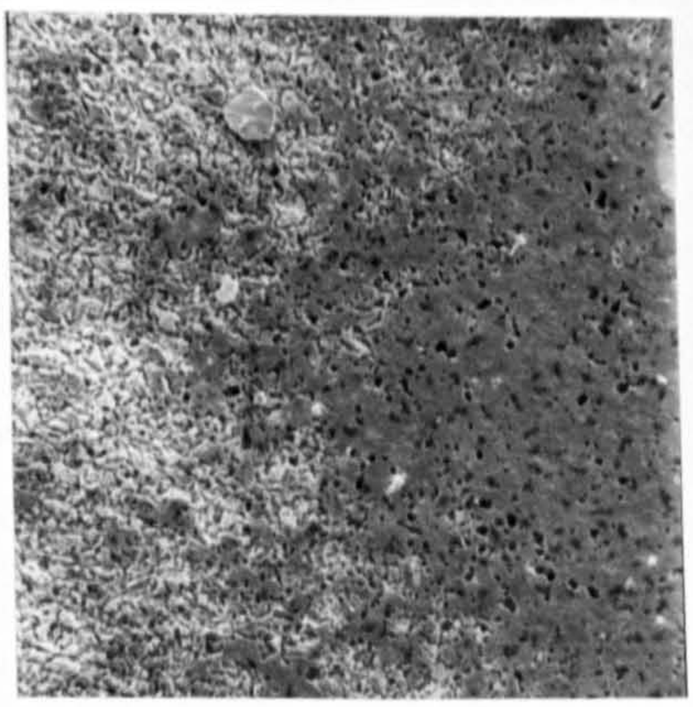

FIGURE 87P

Sample of Ni270 (200μm thick) anodically etched at 2 Adm^{-2} in 30 wt% H_2SO_4 50°C.
View showing both etched and unetched areas

(Magnification 100X)

FIGURE 88P

View of the well etched area of the specimen shown in Figure 87

(Magnification 500X)

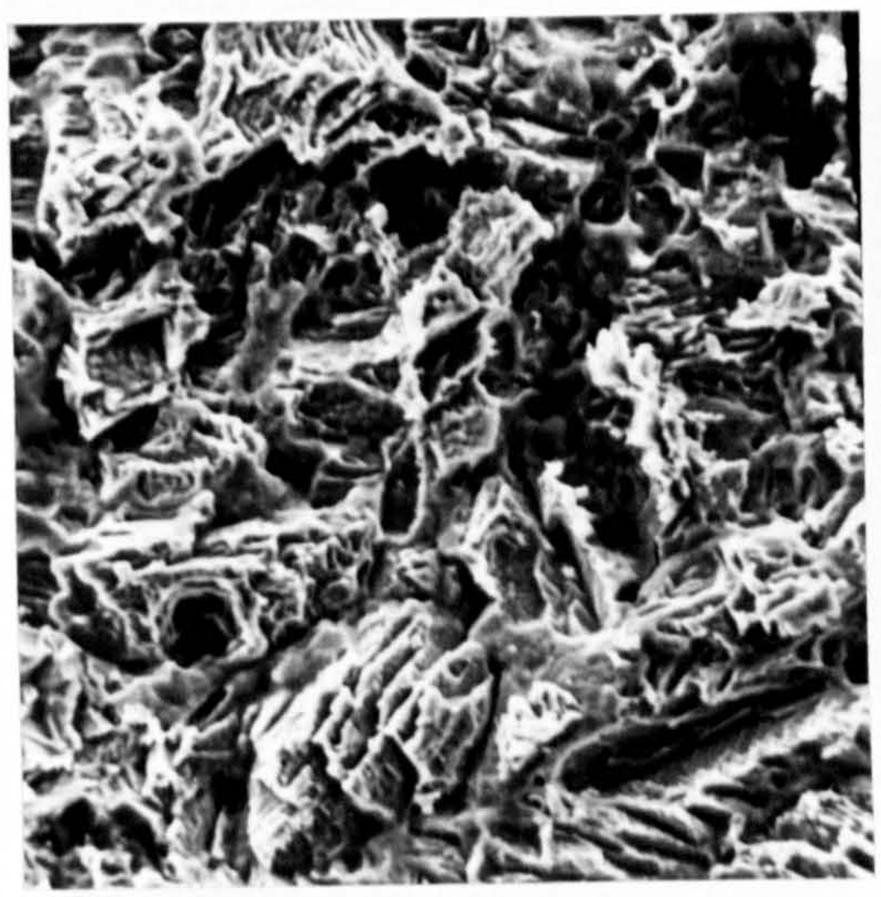

FIGURE 89P

View of etch pit on well etched area of Ni270, shown in Figure 87P

(Magnification 1000X)

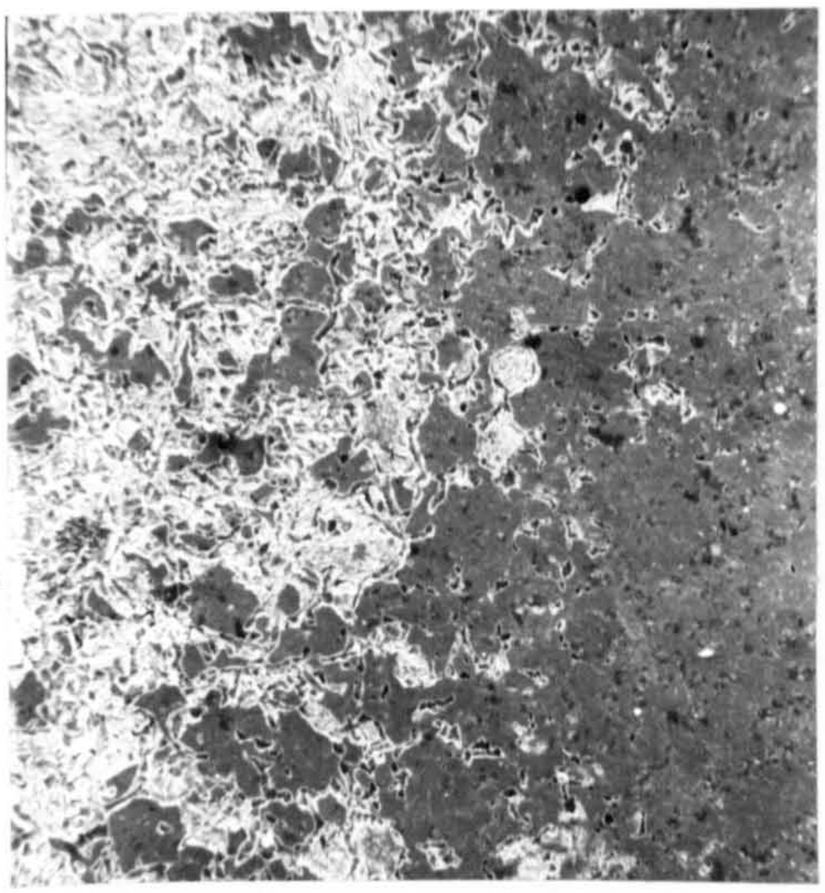

FIGURE 90P

Sample of Ni270 heated to 500°C under H_2 for $\frac{1}{2}$ hour prior to etching in 30 wt% H_2SO_4 at 2 Adm^{-2} and at 50°C.

View of etched and unetched areas of same foil

(Magnification 100X)

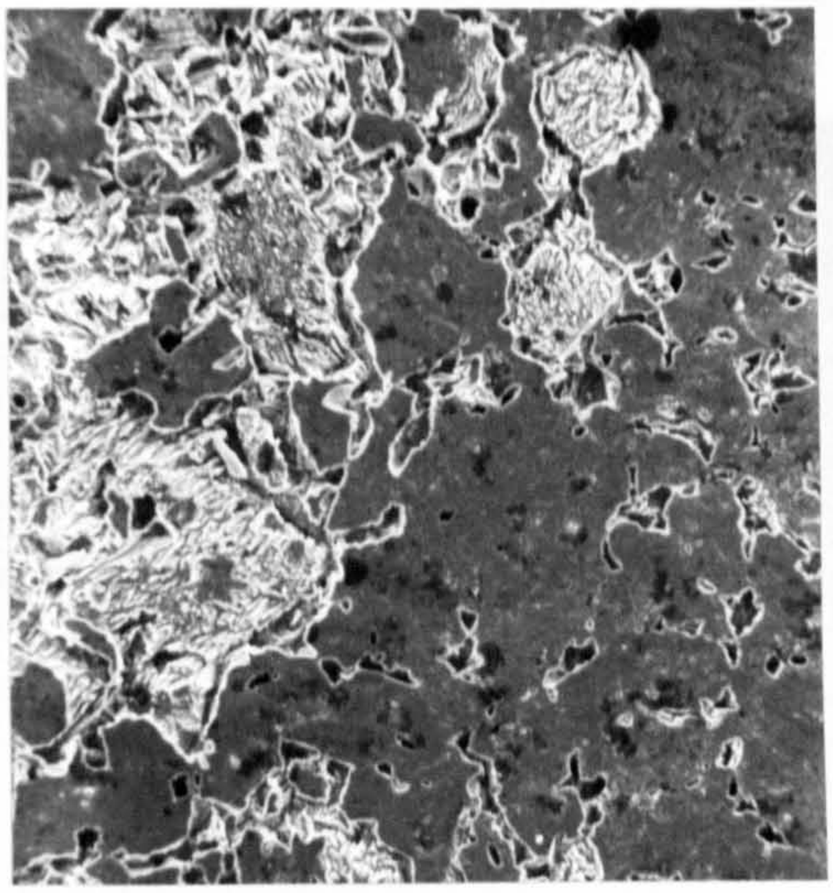

FIGURE 91P

View of unetched area shown in Figure 90P

(Magnification 250X)

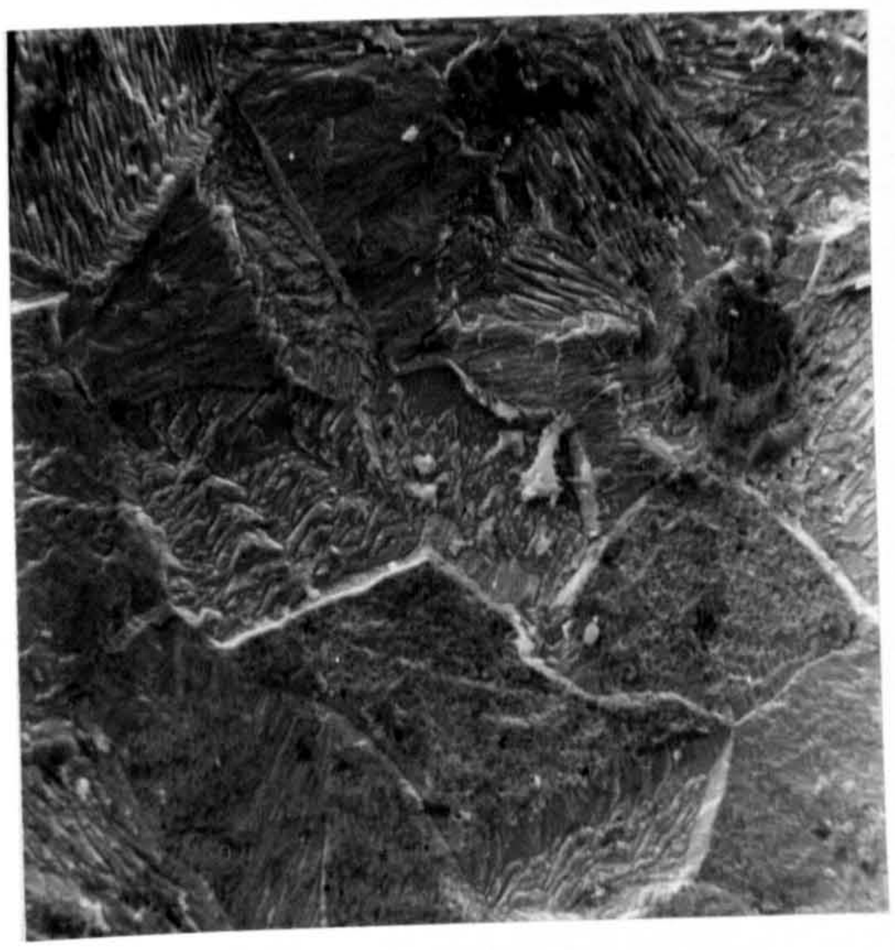

FIGURE 92P

Ni270 annealed under vacuum for $\frac{1}{2}$ hour at 800°C then etched in 30 wt% H_2SO_4 at 2 Adm^{-2} and 50°C.

View of etched surface

(Magnification 500X)

FIGURE 93P

Different area on the same sample as shown in Figure 92P.

(View of triple point)

(Magnification 1000X)

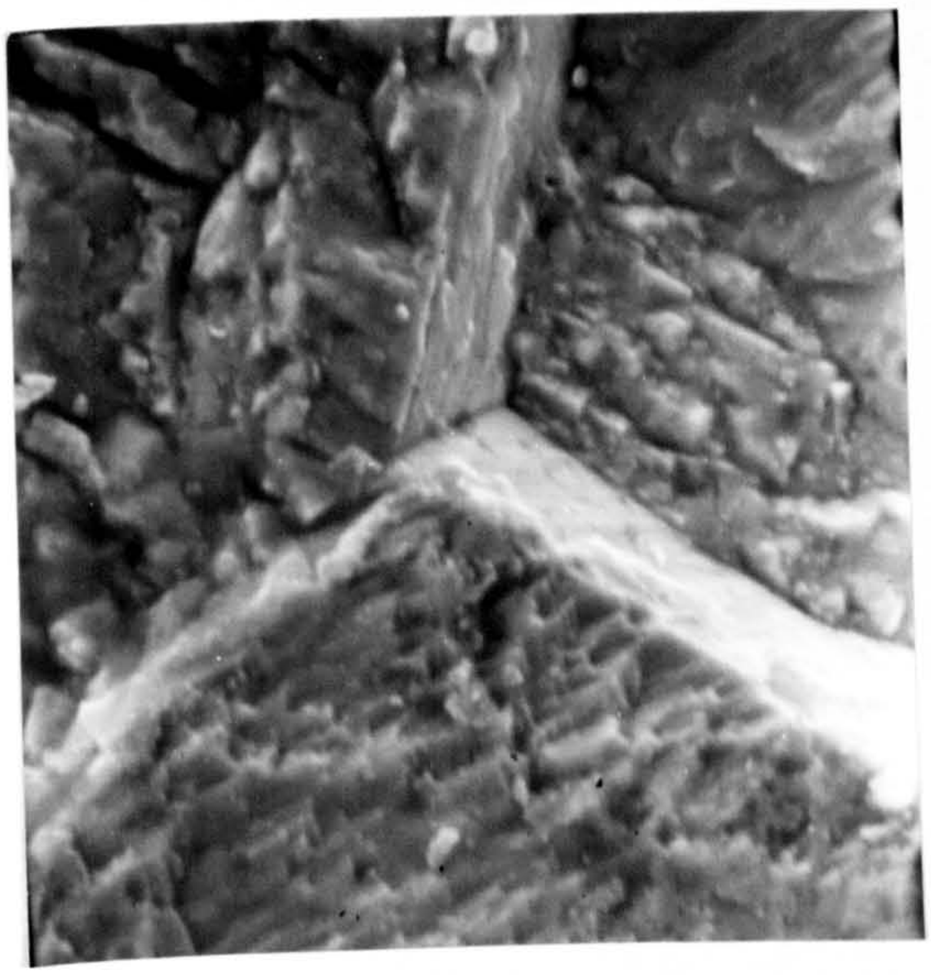

FIGURE 94P

Higher magnification view of the triple point shown in Figure 93P

(Magnification 4000X)

FIGURE 95P

View of etched area of Ni foil shown in Figure 92P

(Magnification 2500X)

The X-ray diffraction pattern for samples of Ni foil that exhibited both good and bad adhesion of electrodeposited PbO_2 were recorded. No evidence of preferred orientation could be detected. Similar measurements were conducted on well etched and poorly etched sections of Ni foil after anodic etching. No evidence of preferred orientation was detected on these samples.

3.4 Studies on the factors that affect the voltage rise time and discharge properties of β-PbO_2 in 48% HBF_4

3.4.1 The thermodynamics for the thermal decomposition of PbO_2

PbO_2 will revert to one of its more thermodynamically stable lower valent oxides on heating. The temperature at which decomposition of PbO_2 occurs can be calculated from thermodynamic data for the different oxides and elements, values of which are given in the Table 68. A number of different reactions are possible for the thermal decomposition of PbO_2 and for which thermodynamic data is available, these are listed below :

(a) $3\ PbO_2 \longrightarrow Pb_3O_4 + O_2$

(b) $2\ PbO_2 \longrightarrow 2\ PbO(yellow) + O_2$

(c) $2\ PbO_2 \longrightarrow 2\ PbO\ (red) + O_2$

(d) $2\ Pb_3O_4 \longrightarrow 6\ PbO + O_2$

(e) $2\ PbO \longrightarrow 2\ Pb + O_2$

(f) $PbO_2 \longrightarrow 4\ Pb + O_2$

The free energy for each reaction at a given temperature can be calculated from the data listed in Table 68. This data was used to plot a graph of free energy versus temperature for each of the above reactions. The values for free energy of each reaction can be calculated as shown for the following reaction :

$$3\ PbO_2 \qquad Pb_3O_4 + O_2.$$

$$\Delta H = \quad H^{o} \ (\text{products}) - \quad \Delta H^{o} \ (\text{reactants})$$

$$= -734.7 + 0 - 3 \times (-276.6)$$

$$= 95.1\ kJ\ mole^{-1}$$

$$\Delta G = \quad \Delta G^{o} \ (\text{products}) - \quad \Delta G^{o} \ (\text{reactants}$$

$$= -617.5 - 3 \times (-218.9)$$

$$= 39.2\ kJ\ mole^{-1}$$

$$\Delta S = \quad \Delta S^{o} \ (\text{products}) - \ \Delta S^{o} \ (\text{reactants})$$

$$= 20.5.02 + 211 - 3 \times 76.5$$

$$= 186.55\ kJ^{-1}\ mole^{-1}$$

The same reasoning can be applied to calculate the values of ΔG, ΔH and ΔS for each possible reaction for the thermal decomposition of PbO_2 and can be used to plot a graph of free energy versus temperature for the particular reaction under consideration, see Fig. 182.

All possible reactions for the thermal decomposition of PbO_2 have a positive value of free energy at $298^{o}K$ and therefore the thermal decomposition of PbO_2 is not favoured at this temperature. Only when the value of ΔG for the reaction is less than zero can the reaction proceed. The temperature at which the decomposition of PbO_2 can theoretically occur has been calculated and is given in Table 67.

All the calculations for free energy are based on a unit partial pressure of oxygen i.e 1 atmosphere, However the partial pressure of oxygen in air at atmospheric pressure is only

0.21 atm and this must be taken into account when determining the dissociation temperature for any metal oxide in air. Consider a reaction involving the decomposition of a pure solid oxide to produce a pure metal as :

$$2\ MO_{(s)} \rightarrow 2M_{(s)} + O_2(g)$$

Equilibrium will be established between M, MO and O_2 at a certain value of pO_2.

The equilibrium constant for the reaction may be written as :

$$K = \frac{[M]^2\ [O_2]}{[MO]}$$

Since both [M] and [MO] equal unity the equilibrium constant is therefore directly related to the partial pressure of oxygen.

At equilibrium $\Delta G = 0$ and it can be shown that

$$G^o = RT \ln K$$

$$G^o = RT \ln pO_2$$

It can also be shown that :

$$\frac{d\ (\ln K_p)}{dt} = \frac{\Delta H^o}{RT^2}$$

$$\ln K_p = \Delta H^o + \underline{\text{constant}}$$
$$RT$$

A plot of $\ln K_p$ versus 1/T will be a straight line of slope $-\ \Delta H^o/R$. It is possible therefore to determine the temperature at which $K_p = 0.21$ and thus the dissociation temperature in air for the various reaction schemes. These values are given in Table 67.

If the ambient partial pressure of oxygen is greater than the equilibrium value, then dissociation will not take place. Conversely if the ambient pO_2 value is less than the equilibrium value at a given temperature dissociation will occur. These calculations show that decomposition of PbO_2 is theoretically possible at temperatures in excess of 204°C. Thus heating electrodeposited β-PbO_2 to 250°C should theoretically result in its' dissociation.

TABLE 68

Thermodynamic Values for Pb and Pb oxides at 25°C (322)

Substance	H^o kJ mole^{-1}	G^o kJ mole^{-1}	S^o J K^{-1}mole^{-1}	C_p J K$_{-1}$mole^{-1}
Pb	0	0	64.89	26.8
O_2	0	0	205.02	29.35
PbO_2	-276.6	-218.9	76.5	64.4
PbO (yellow)	-217.8	-188.4	69.4	48.53
Pb_3O_4	-734.7	-617.5	211	147
PbO	-219.2	-188.8	65.3	45.77

3.4.1.1 The kinetics for PbO_2 decomposition

The loss in weight of PbO_2 with time at a constant temperature was recorded over the temperature range 250°C to 500°C and the results of this work are shown in Fig. 183. The loss in weight was expressed as milligrams of oxygen per gram of PbO_2. This corresponds to a maximum theoretical oxygen weight loss of 44.6 mg per of gram PbO_2 for the thermal decomposition of PbO_2 to Pb_3O_4, whilst for decomposition to PbO it is 66.9 mg per gram of PbO_2 and for decomposition to Pb, 133.9 mg per gram of PbO_2.

Table 68

Values for the dissociation temperature for
lead oxides and other thermodynamic parameters

Reaction	G° kJ mole $^{-1}$	H° kJ mole $^{-1}$	S° Jk $^{-1}$ mole $^{-1}$	Dissociation Temperature °C $P^{0}2$ = 1 atm	Dissociation Temperature °C $P^{0}2$ = 0.21 atm
$3PbO_2 - Pb_3O_4 + O_2$	39.2	95.1	186.55	237	204
$2PbO_2 - PbO$ (Yellow) $+ O_2$	61	117.6	190.82	343	304
$2PbO_2 - 2PbO$ (Red) $+ O_2$	60.2	114.8	182.62	356	314
$2PbO_4 - 6PbO + O_2$	104.6	162.6	199.42	542	493
$2PbO - 2Pb + O_2$	188.4	217.8	196	838	768
$PbO_2 - Pb + O_2$	218.9	276.6	193.41	1,157	1,064

N.B. All Values for G°, H° and S° are at 25°C

At 250°C an initial weight loss was recorded, thought this may be partly attributable to loss of absorbed water (not removed by pre-heating) followed by a slow but steady weight loss with time e.g after 2.5 min a loss of 0.31 mg per gram of PbO_2 was recorded which increased to 0.66 mg per gram after 10 min and to only 0.92 mg per gram after 1400 min exposure. The weight loss was approximately linear after 30 min exposure and corresponded to a weight loss of 1.1×10^{-4} mg gram per gram of PbO_2 per min. This equates to a total Pb_3O_4 content of 2% in the PbO_2 after 1500 min exposure at 250°C.

A similar curve was observed at 300°C except that the weight loss with time only became linear after 60 min exposure and was 2.3×10^{-3} mg per gram of PbO_2 per min. At 350°C the weight loss was essentially linear after 400 min exposure. For temperatures in excess of 350°C, the nature of the weight loss vs time curve was found to be different. The thermal decomposition of PbO_2 tended to proceed until a maximum value was reached, the valve of which was temperature dependent.

The thermal decomposition of PbO_2 was found to follow neither a 1st nor 2nd order reaction scheme. A determination of the order of reaction from the initial rate of reaction showed that only the initial decomposition process is 1st order, as a plot of K versus t shows (see Fig. 184), the subsequent decomposition process does not follow any particular relationship. The thermal decomposition of PbO_2 is also complicated by the fact that a number of different reactions are possible, all of which can theoretically occur in the temperature range between 250 and 500°C. Variation in the PbO_2 particle size would also have an effect on reproducibility of the results obtained, although this was not investigated in the present studies.

A plot of the initial rate of decomposition versus 1/T could not be produced with any degree of accuracy to enable an accurate value of the activation energy for the thermal decomposition of PbO_2 to be determined.

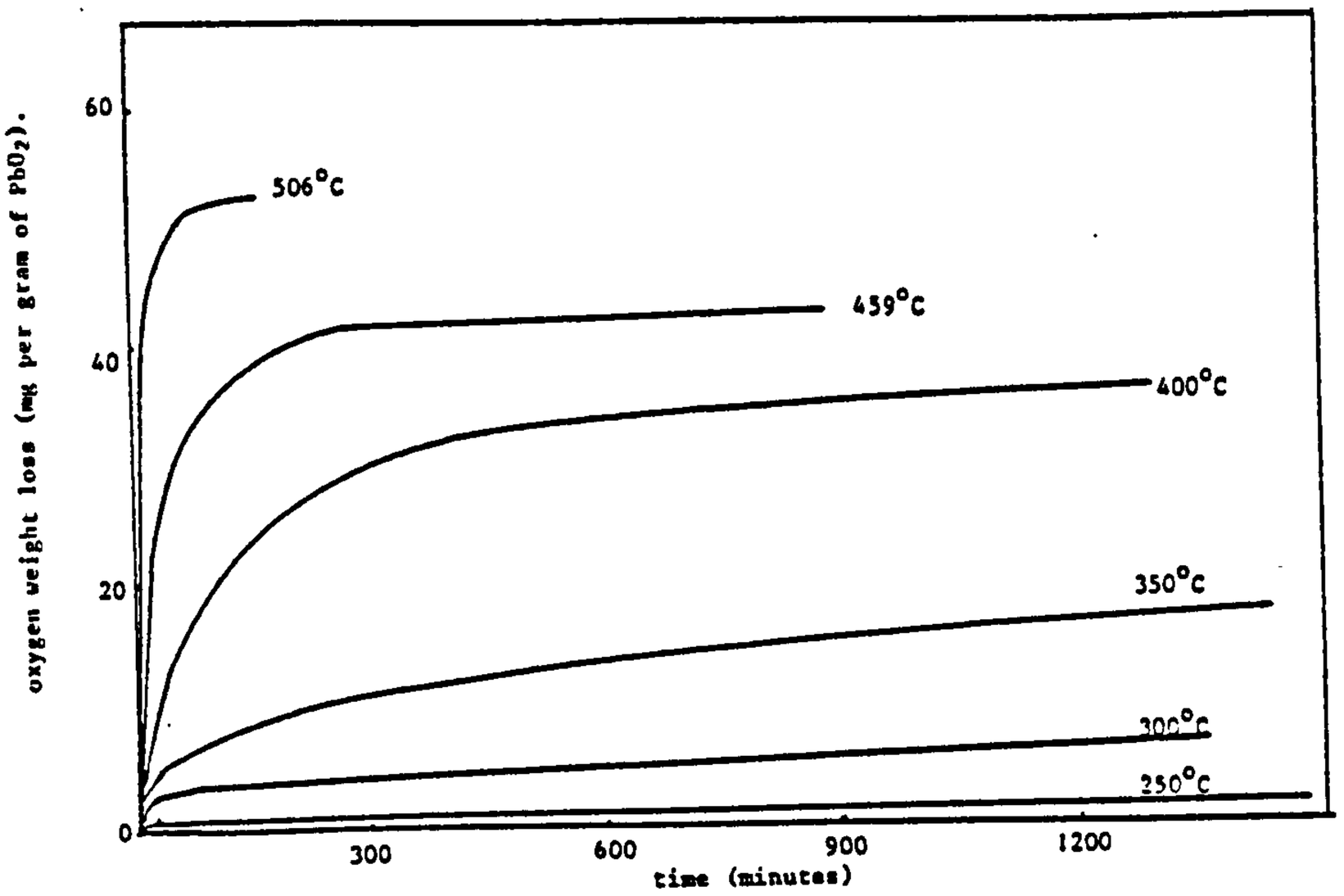

weight loss vs time for a sample of PbO_2 at selected constant temperatures.

FIGURE 183

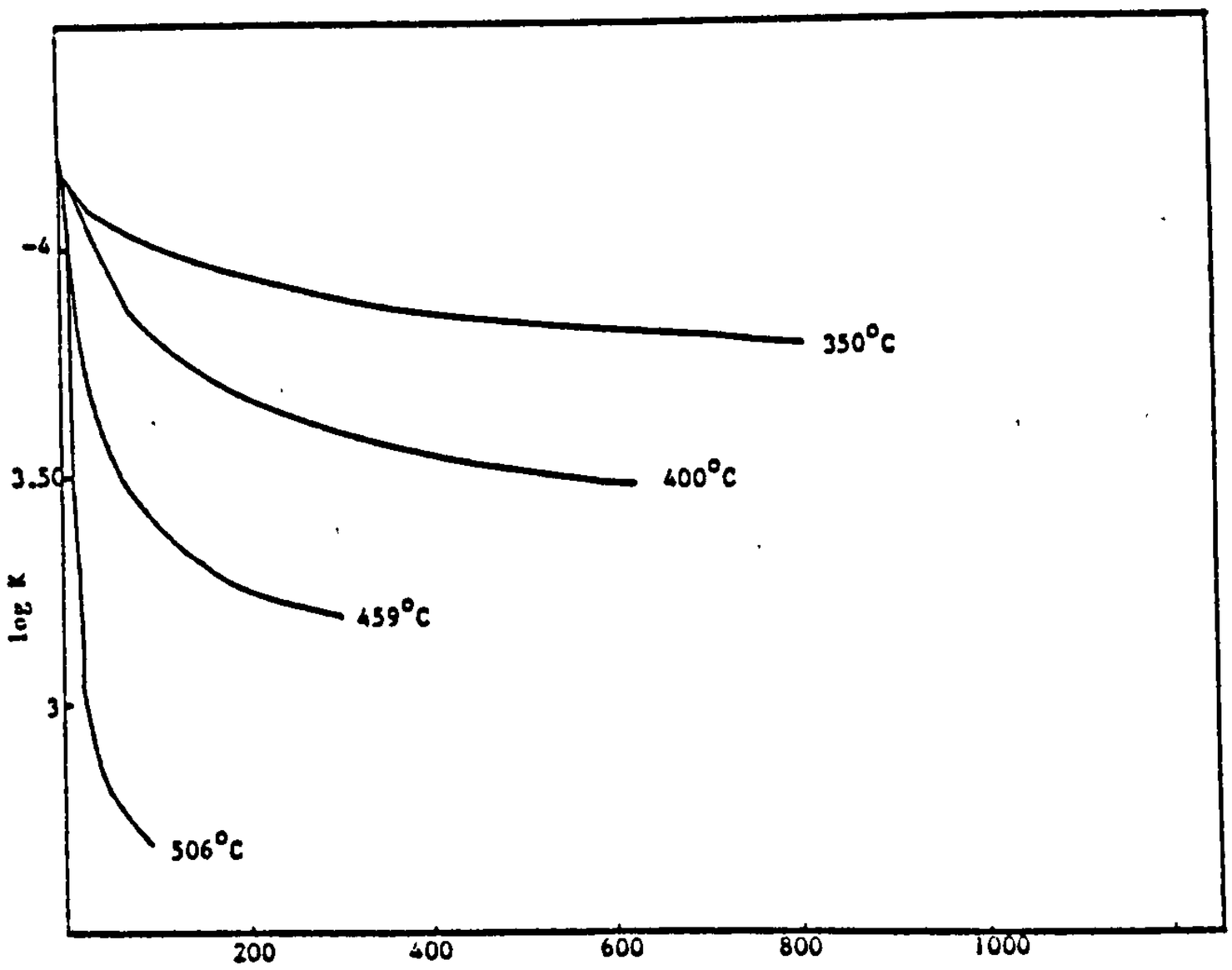

A graph log K vs time for the thermal decomposition of PbO_2 at different temperatures, for a 1st order decomposition process.

FIGURE 184

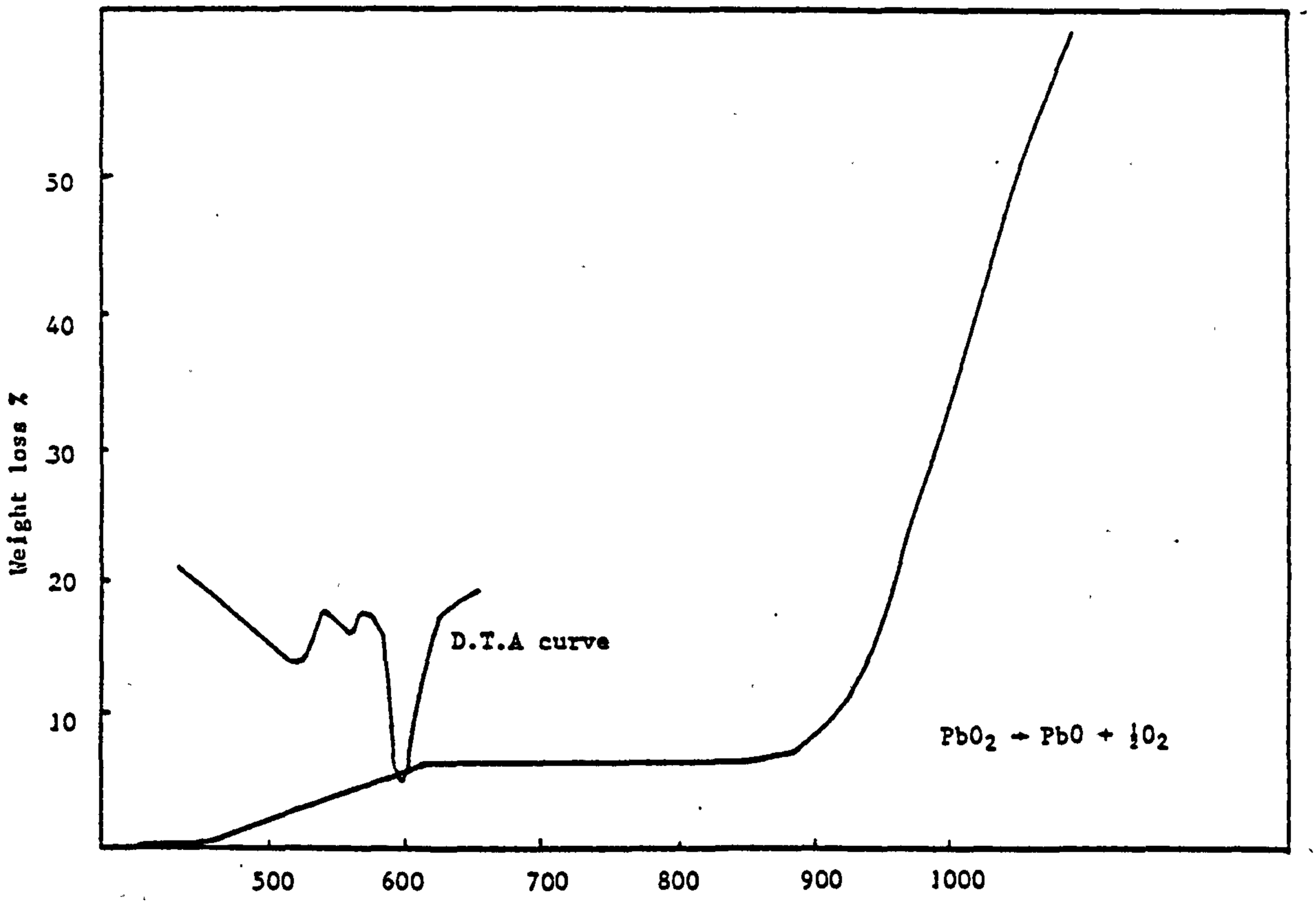

A graph of weight loss versus temperature for a sample of $5PbO_2$ heated at 5°C per minute, together with a differential thermal analysis trace.

FIGURE 185

3.4.1.2 D.T.A analysis on the thermal decomposition of PbO_2

A separate experiment was conducted to determine the temperature at which phase transformation or thermal decomposition of PbO_2 occurs using the technique of differential thermal analysis (DTA). The results of this work can be seen in Fig. 185 for a sample of PbO_2 heated in air at 5^oC per min.

The first loss of weight commences at 400^oC and proceeds at a slow rate up to 460^oC, after which temperature a rapid loss of weight occurs until a temperature of 620^oC is reached. No further loss in weight occured until 870^oC when a second rapid loss in weight was recorded. The complimentary DTA trace indicates a major transformation peak at 600^oC, which commences at 400^oC. The rapid loss in weight above 870^oC is associated with the decomposition of PbO to Pb, whilst the plateau recorded between 600^oC and 870^oC corresponds to the expected % weight loss, if all the PbO_2 decomposed to PbO.

3.4.2 X-ray diffraction studies on heat treated electrodeposited β-PbO_2

Studies were undertaken to see what effect, if any, heat treatment of electrodeposited PbO_2 had on the X-ray diffraction pattern for PbO_2. This work was undertaken to try and identify a possible explanation for the improved activation times of heat treated PbO_2 deposits.

The diffraction pattern for samples of β-PbO_2 electrodeposited onto Ni at 2 Adm^{-2} for 15 min were recorded, then the samples heated to 250^oC for 30 min and the X-ray diffraction pattern measured over the same specimen area, (see Figs. 186 - 187). No marked difference in the diffraction pattern could be detected and neither could the appearance of any new reflection peaks. A small variation in the relative intensities of the various reflections was however noted (see Table 69). The relative intensities of the reflections varied for different samples depending upon the degree of preferred orientation. The same specimen area was always re-examined after heat treatment.

Indeed heat-treatment of electrodeposited PbO_2 for 24 hours at 250°C was not found to effect the nature of the diffraction pattern obtained, with no new reflection peaks detected.

A similar effect was observed on heating samples of electrodeposited β-PbO_2 to 300°C in that only a small variation in the relative peak intensity was observed with time (see Figs. 188 to 189) and no new reflection peaks were recorded.

Only on heating to 350°C for extended periods was any observable variation in the diffraction pattern with time observed (see Figs. 190 to 194).

TABLE 69

Variation of relative intensity for selected angular reflections on samples of PbO_2 before and after heat-treatment at 250°C for 30 min

Reflection Angle (degrees)	Relative intensity for an unheat treated sample of PbO_2 %	Relative intensity for a sample of PbO_2 heat treated for 30 min at 250°C %
12.8	100	100
14.35	21	29
16.0	17	17
17.55	52	47
24.5	30	29
26.05	16	16

A reduction in intensity of the PbO_2 reflection at 3.48 A^o with time was recorded, as was an increase in the intensity for the β-PbO_2 reflection at 3.11A^o (111). The latter reflection is also attributable to the (200) plane of Pb_3O_4 and it is this reflection that is considered to explain the increase in intensity of this peak.

Some β-PbO_2 still exists even after heating for 24 hours at 350^oC and the decrease in intensity for the (100) peak with time is shown in Table 70.

New reflections at 2.70, 1.93, 1.92 and 1.63 A^o were recorded and these are thought to be associated with the formation of Pb_3O_4. Samples of electrodeposited PbO_2 on Ni could not be heat treated to temperatures above 350^oC without the PbO_2 deposit detaching itself from the surface of the Ni foil.

TABLE 70

Decrease in intensity for the (100) plane of PbO_2 with time at 350^oC

Time at 350^oC (hrs)	Intensity cps x 100	% PbO_2
0	60	100
0.5	51.6	86
8	32.5	54
24	12.2	20

3.4.3 The effect of heat treatment of electrodeposited PbO_2 at 250^oC on the voltage rise time of the $Pb/HBF_4/PbO_2$ battery

A sample of commercially prepared PbO_2 was electrodeposited onto a nickel foil substrate 300 x 150 mm, from a solution of 360 gl^{-1} $Pb(NO_3)_2$ pH4 then cut into a number of sections 40 x 20 mm. Half of these samples were heated to 250^oC for 30

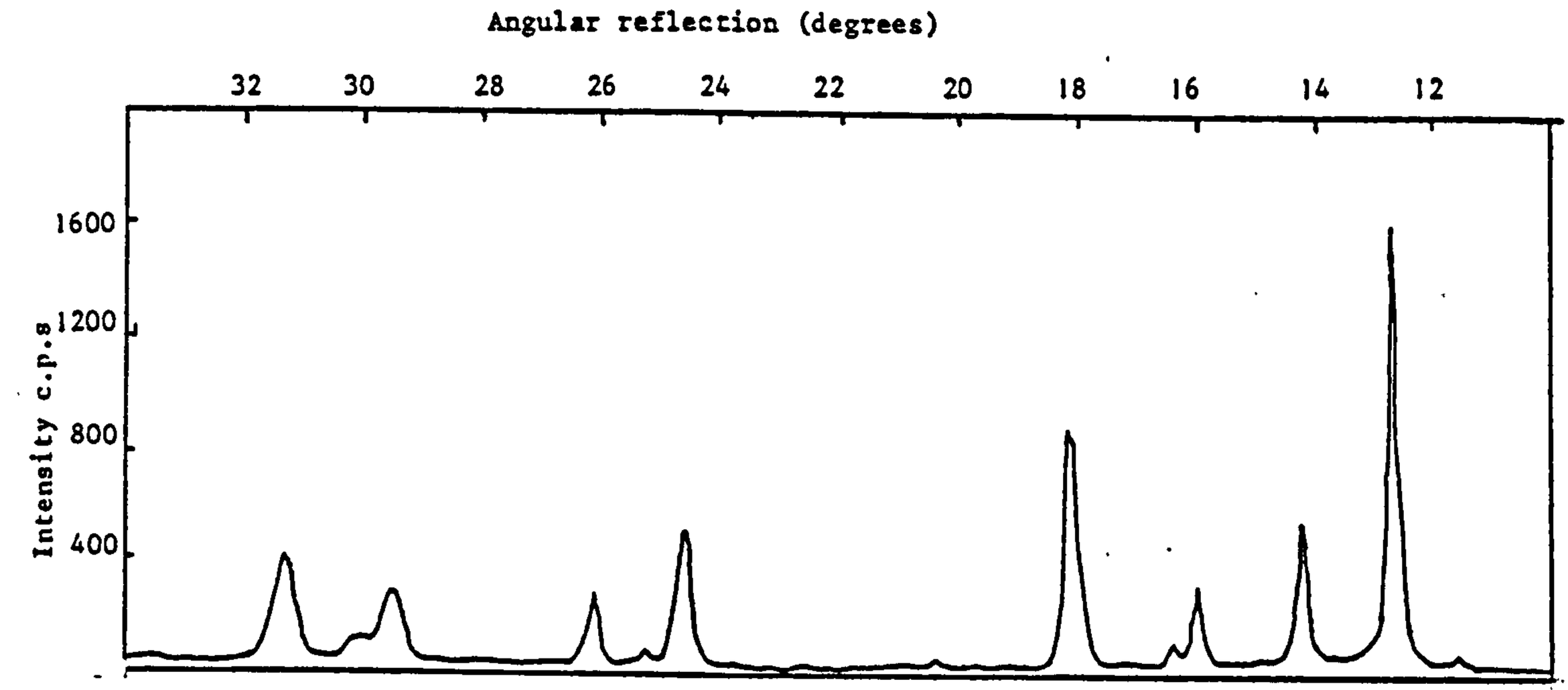

X-ray diffraction pattern for PbO_2 electrodeposited on Ni at 2 A dm^{-2} from a 360 gl^{-1} $Pb(NO_3)_2$ solution at 50°C.

FIGURE 186

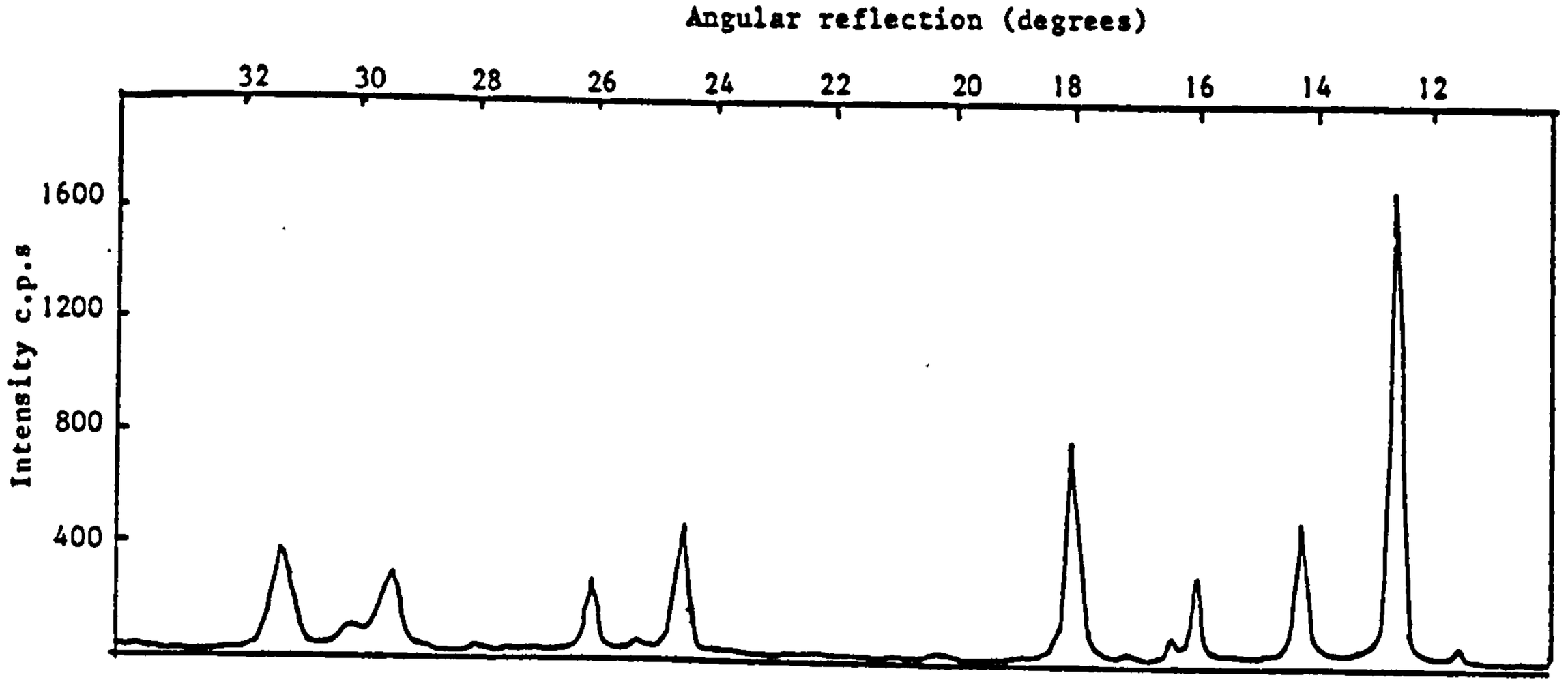

X-ray diffraction pattern for PbO_2 electrodeposited onto a Ni substrate at 2 A dm^{-3} from a 360 gl^{-1} $Pb(NO_3)_2$ solution at 50°C. The sample then heated at 250°C for ½ an hour.

FIGURE 187

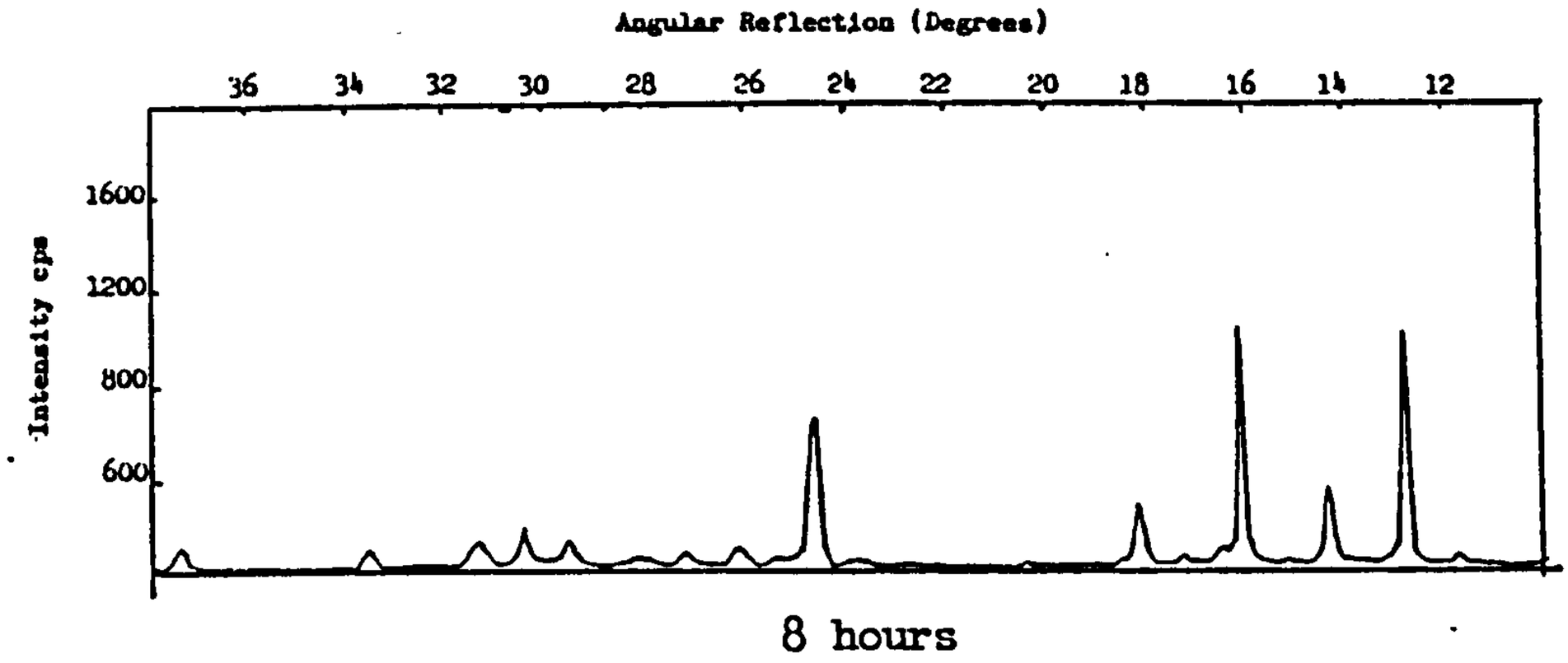

8 hours

FIGURE 188

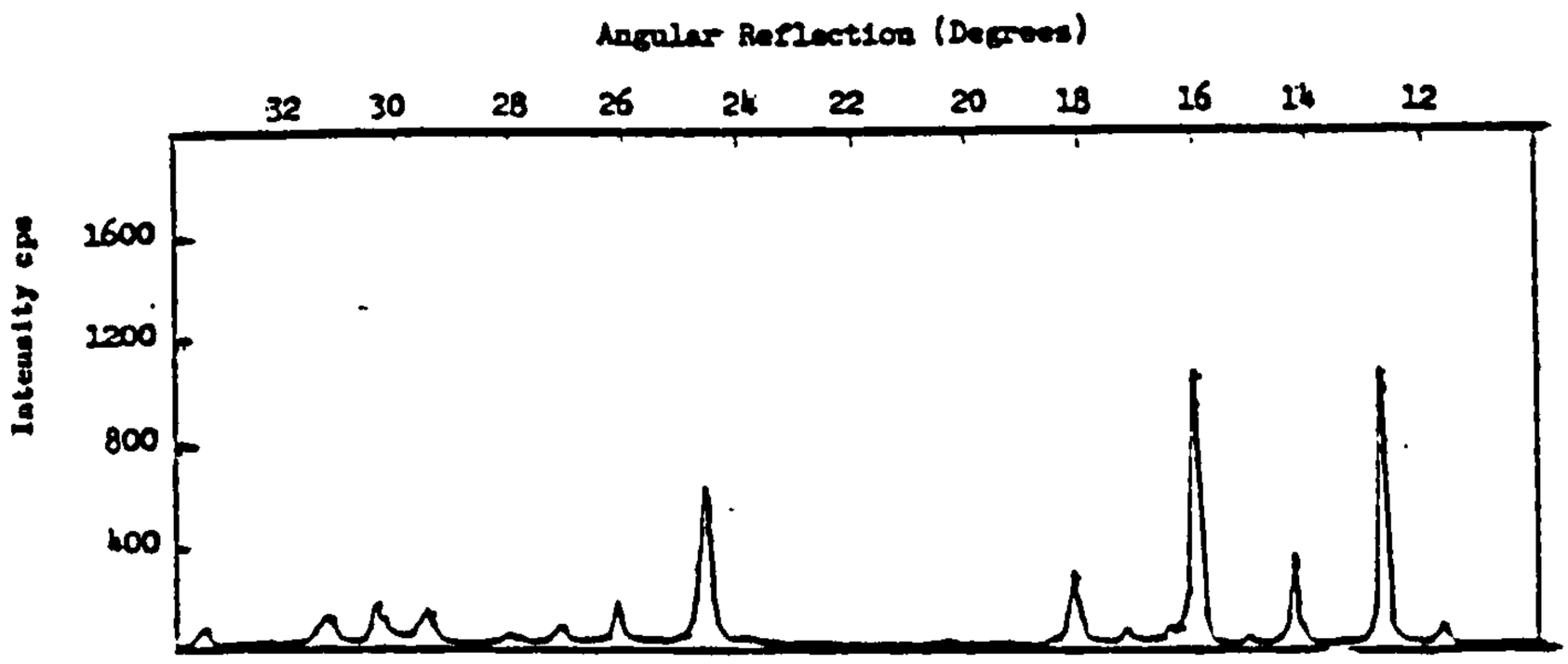

2 hours

FIGURE 189

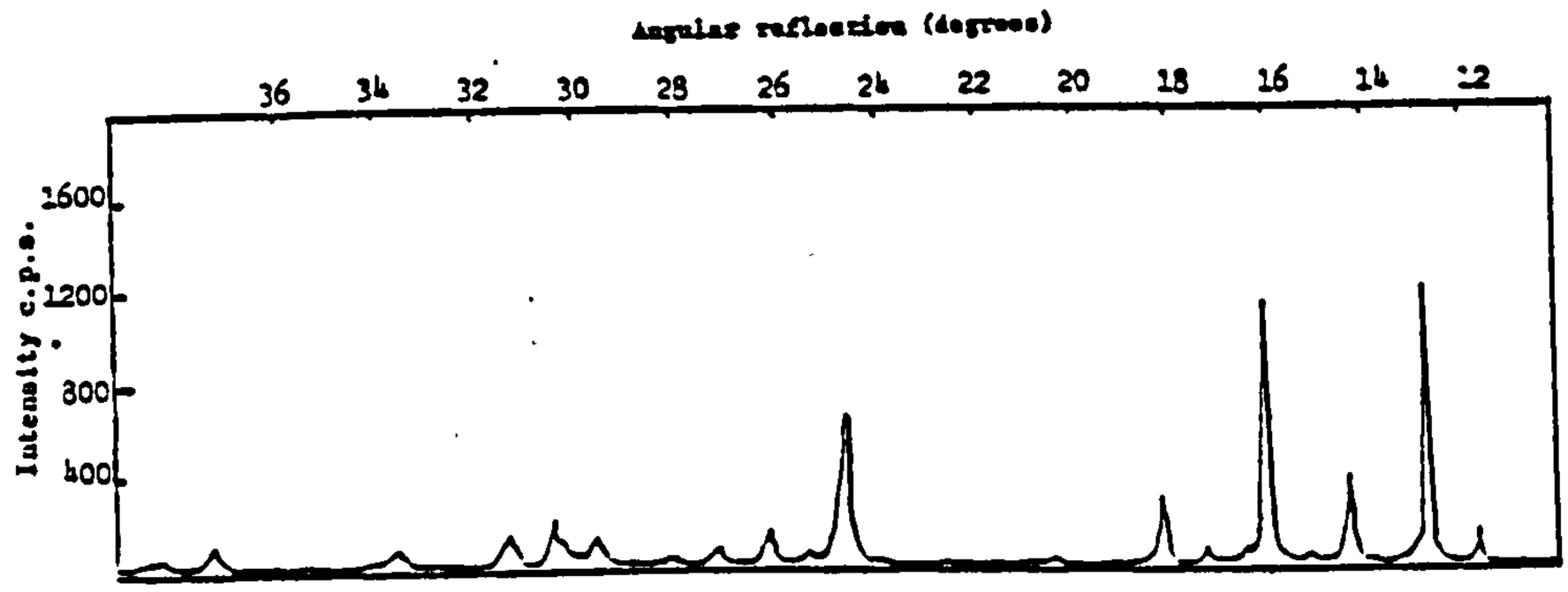

0 hours

FIGURE 190

X-ray diffraction pattern for PbO_2 electrodeposited at $2Adm^{-2}$ from a $360gl^{-1}$ $Pb(NO_3)_2$ solution, heated at 300°C for different times.

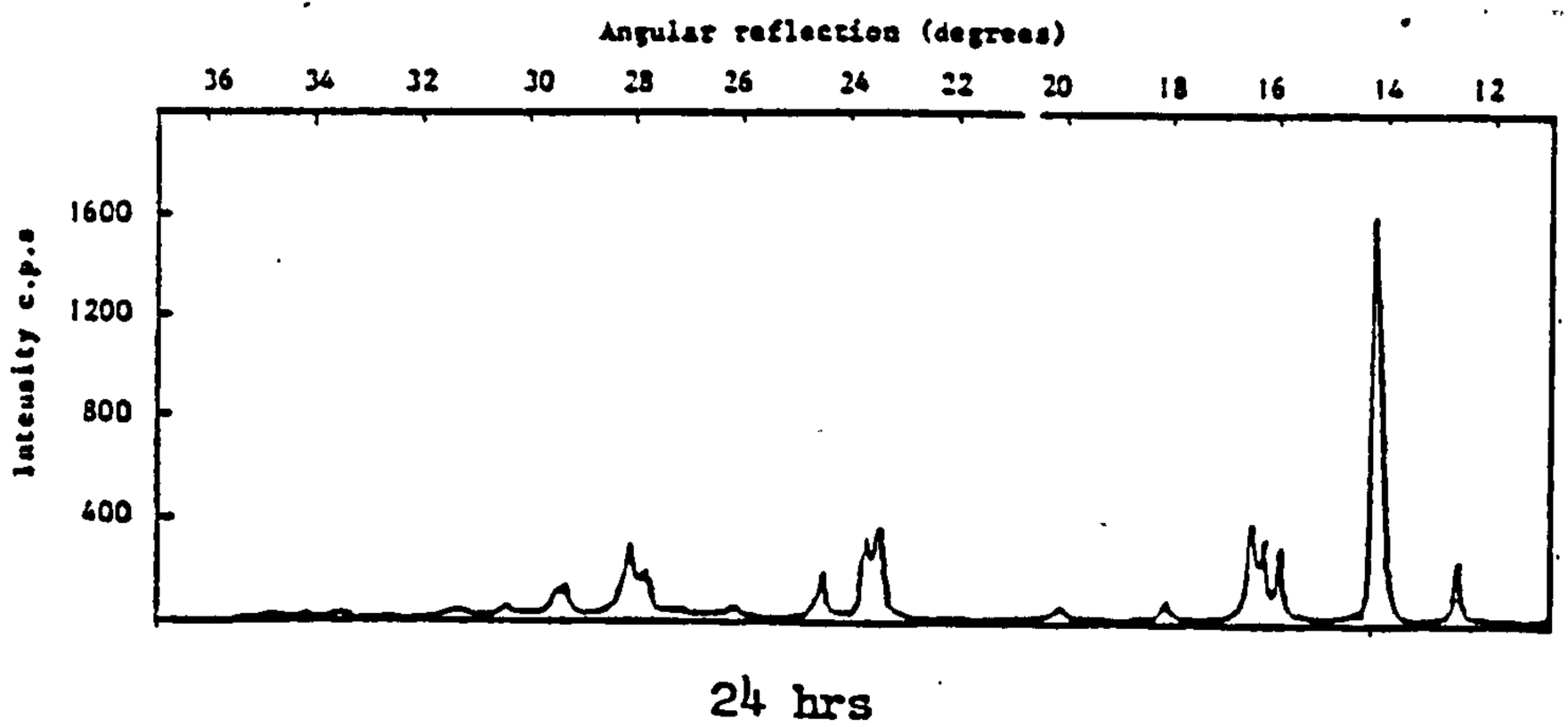

FIGURE 194

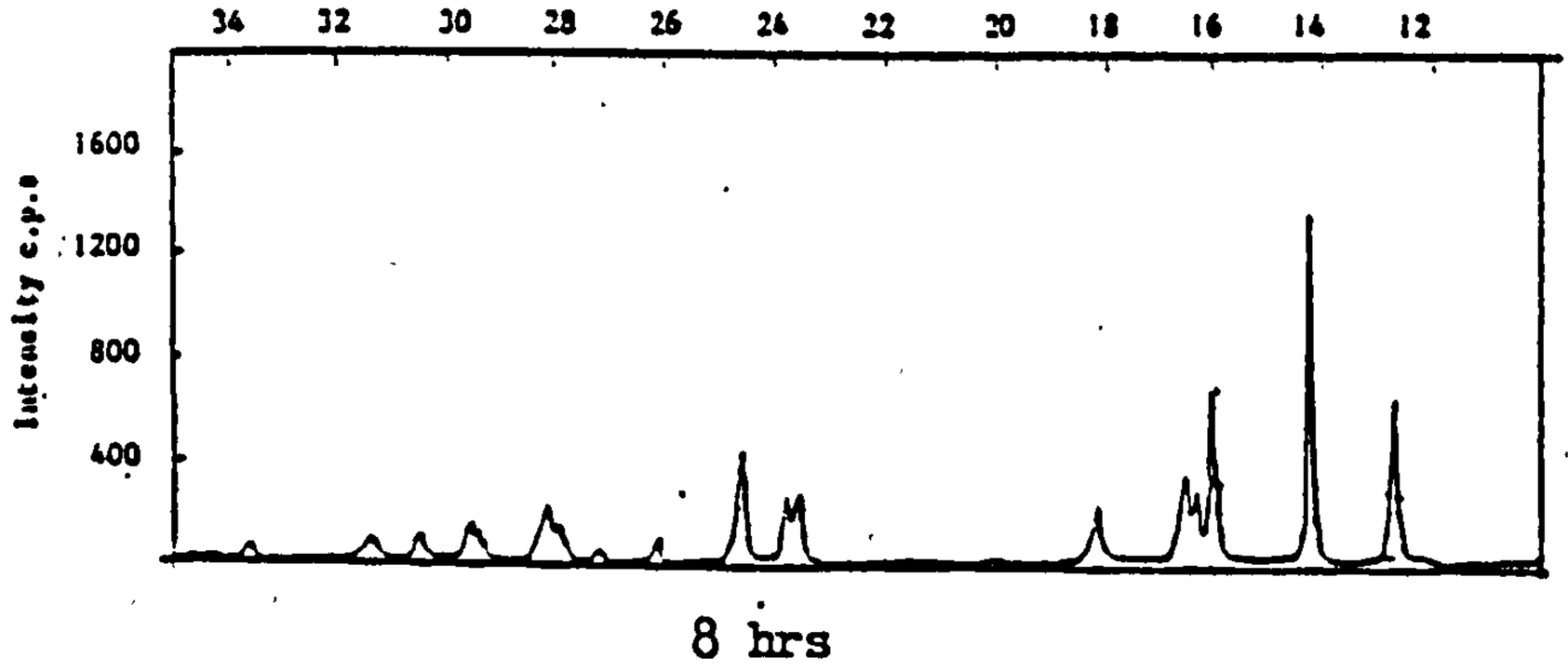

FIGURE 193

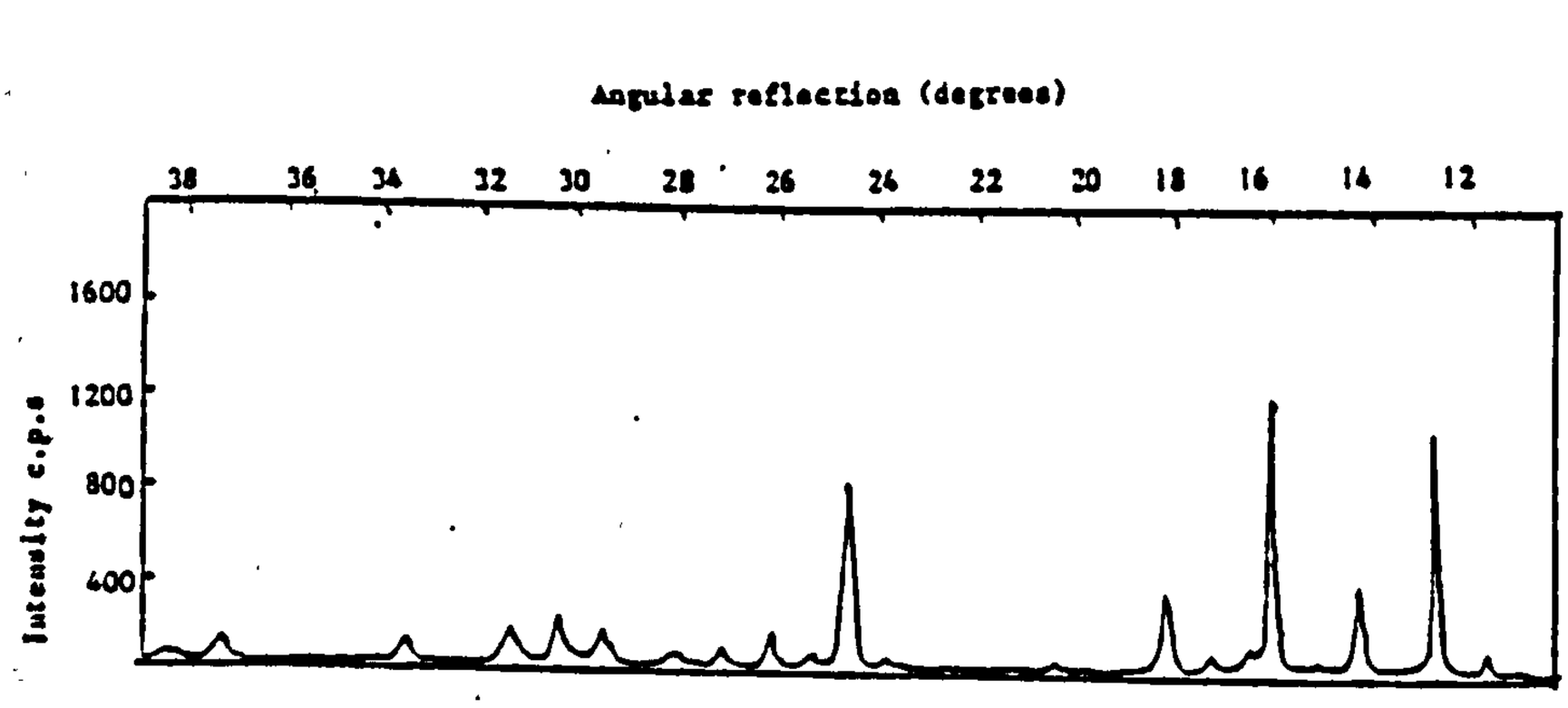

FIGURE 192

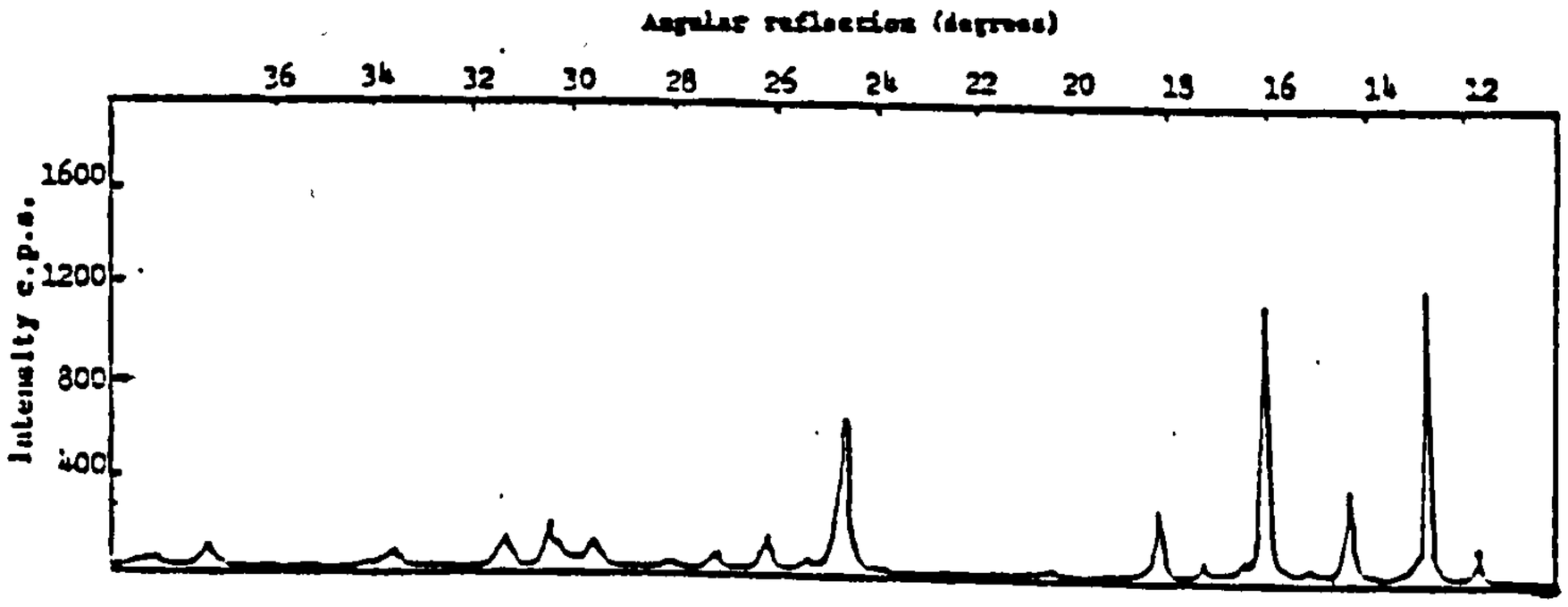

FIGURE 191

X-ray diffraction pattern for PbO_2 electrodeposited at 2 Adm onto a Ni foil substrate and heated for various times at 350°C

min and the voltage rise time recorded. The voltage rise time for the unheat-treated samples was also measured as a comparison. The results of this work are shown in a graphical form in Fig. 195. An improvement in activation time upon heating the PbO_2 deposit was recorded, however it should be pointed out that the unheat-treated samples of β-PbO_2 would be unacceptable as battery plate material, since the measured voltage after 100 ms was less than the required value of 1.18 Volts. Samples of this foil were then subjected to electrochemical impedance measurements (see Section 3.4.4).

3.4.3.1 The effect of agitation of the $Pb(NO_3)_2$ plating solution on the voltage rise time of electrodeposited PbO_2

Samples of β-PbO_2 were electrodeposited onto a Ni foil substrate from a 360 gl^{-1} $Pb(NO_3)_2$ solution pH4, at selected rotational speeds. The anode used was 80 mm diameter nickel foil which was rotated at selected rotational speeds, whilst deposition of PbO_2 took place. The voltage rise time curves for the resultant PbO_2 deposits are given in Fig. 195. Increase in the rotational speed up to 500 rpm improved the voltage rise time charateristics of the deposit. However increase in the anode rotational speed above this value resulted in a reduced activation time. The PbO_2 deposit formed at 1000 rpm was not smooth but consisted of nodular deposits which were easily removed. It is the detachment of the nodular PbO_2 deposits formed during the initial stages of activation which is thought to account for the decrease in cell voltage observed on the voltage rise time curve for these samples after 20 milliseconds (see Fig. 196).

3.4.4 The anodic dissolution of Pb in 48% HBF_4

(a) Linear Polarisation

The E vs log i curve for a Pb electrode, anodically polarised in 48% HBF_4, at a sweep speed of 0.5 mV sec^{-1} at different temperatures is shown in Fig 197. At room temperature

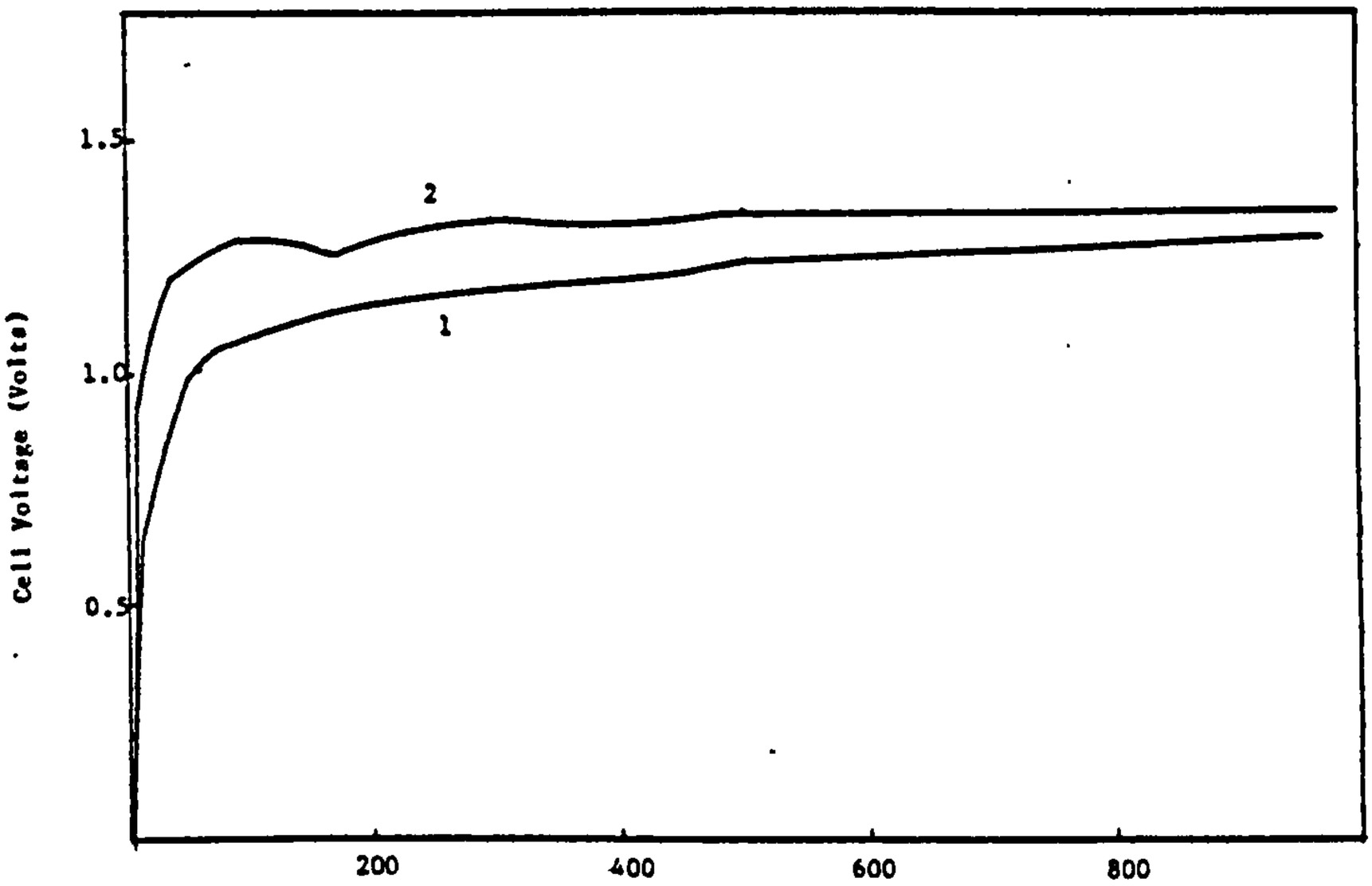

Voltage vs time of immersion in 48% HBF_4 at -33°C for different samples of commercial battery plate material.

1 = Commercially produced βPbO_2 battery plate material.

2 = The same commercially produced βPbO_2 battery plate material but heated to 250°C for ½ an hour prior to immersion.

FIGURE 195

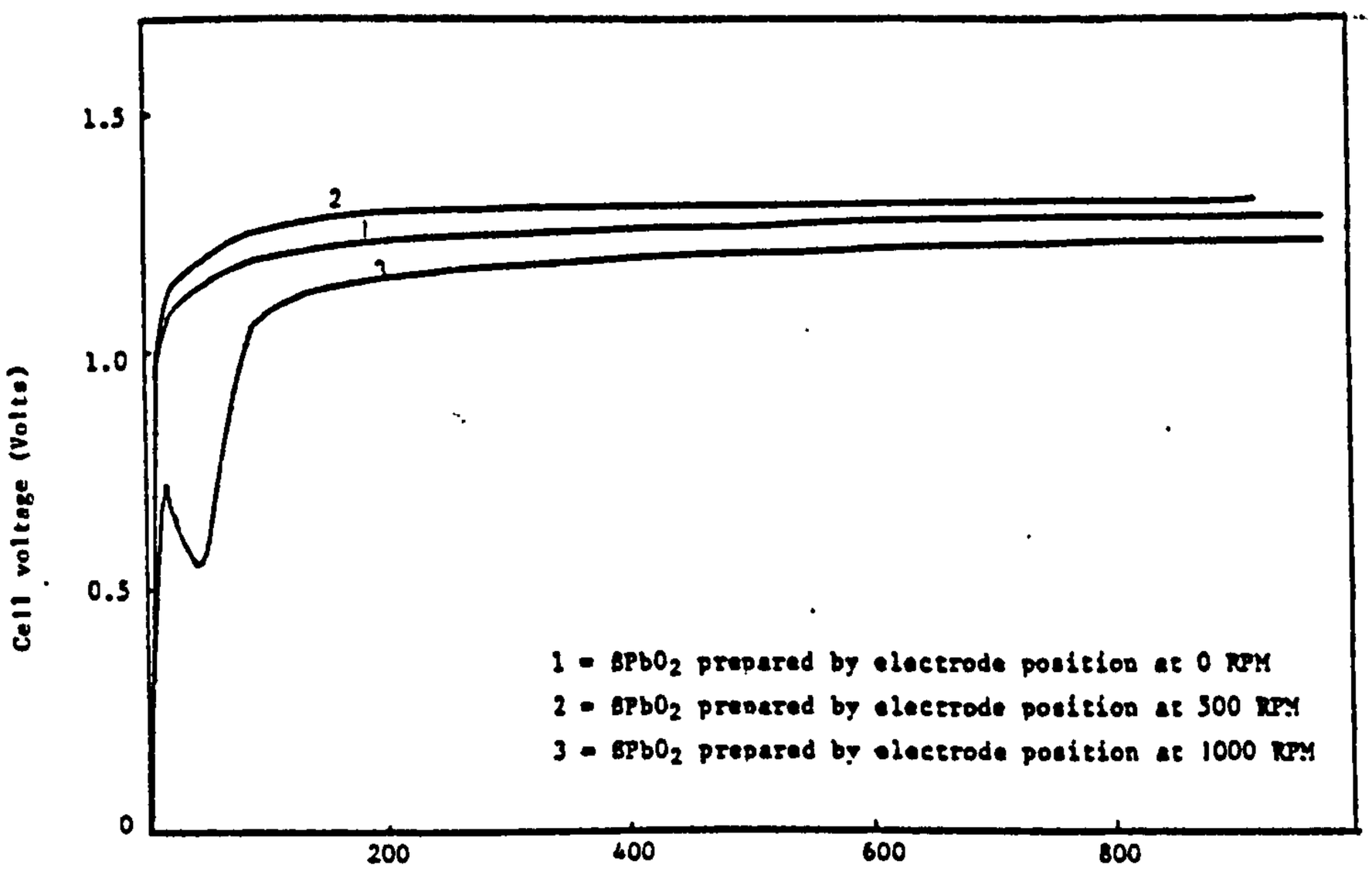

A graph of voltage vs time of immersion in a 48% HBF_4 solution at -29°C for samples of βPbO_2 electrodeposited onto a Ni foil substrate at selected rotational speeds, from a 360 gl^{-1} $Pb(NO_3)_2$ solution at 2 Adm^{-2}

FIGURE 196

passivation of the Pb electrode occured at a current density of 26 Adm^{-2}, although at higher temperatures no passivation was observed at this sweep speed.

The value of E_{rest} for Pb in 48% HBF_4 at 23°C was found to be - 0.265V.

The values of i_o for Pb dissolution in 48% HBF_4 obtained by extrapolation of the E vs log i curves are given in Table 71 with the braketed figures the values for i_o predicted from the linear relationship between i and η near the reversible potential.

No easily discernable Tafel region was visible for Pb dissolution in HBF_4 and extrapolation of the E vs log i curve to zero overpotential was therefore difficult. Alternative values of i_o for Pb dissolution were therefore sought using the electrochemical impedance measurements (see Section 3.4.4).

TABLE 71

The variation of i_o with temperature for Pb dissolution in 48% HBF_4, for a Pb electrode polarised at 0.5 mV sec^{-1}

Temperature °C	Exchange current density for Pb dissolution in 48% HBF_4 (Acm^{-2})	
23	1.6×10^{-3}	(1.1×10^{-3})
38	2.8×10^{-3}	(2.1×10^{-3})
61	5.6×10^{-3}	(3.5×10^{-3})

The calculated activation energy for Pb dissolution was found to be 27.4 kJ $mole^{-1}$ from the values of i_o obtained by extrapolation of the E vs log i curves and 26 kJ $mole^{-1}$ using the values of i_o obtained from the linear portion of the η vs i curve.

3.4.4.1 The cathodic reduction of β-PbO_2 in 48% HBF_4

The E vs log i curve for β-PbO_2 cathodically polarised in 48% HBF_4 at a sweep rate of 0.5 mV sec^{-1}, at selected temperatures is shown in Fig. 198.

The rest potential adopted by β-PbO_2 in this electrolyte was found to vary with time which could be associated with porosity of the PbO_2 deposit on the Ni substrate and the resultant self corrosion of the deposit.

The values of i_o for the reduction of β-PbO_2 in 48% HBF_4 obtained by extrapolation of the linear portion of the E vs log i curve to zero overpotential are given in Table 72, whilst the figures in brackets are the values of i_o obtained from the linear relationship between η and i near the reversible potential.

TABLE 72

The variation of i_o with temperature for the reduction of β-PbO_2 in 48% HBF_4

Temperature ^oC	i_o A cm^{-2}	
23	2.5×10^{-4}	(5×10^{-4})
41	5.9×10^{-4}	(1.6×10^{-3})
51	8.9×10^{-4}	-
61	1.48×10^{-3}	(3.5×10^{-3})

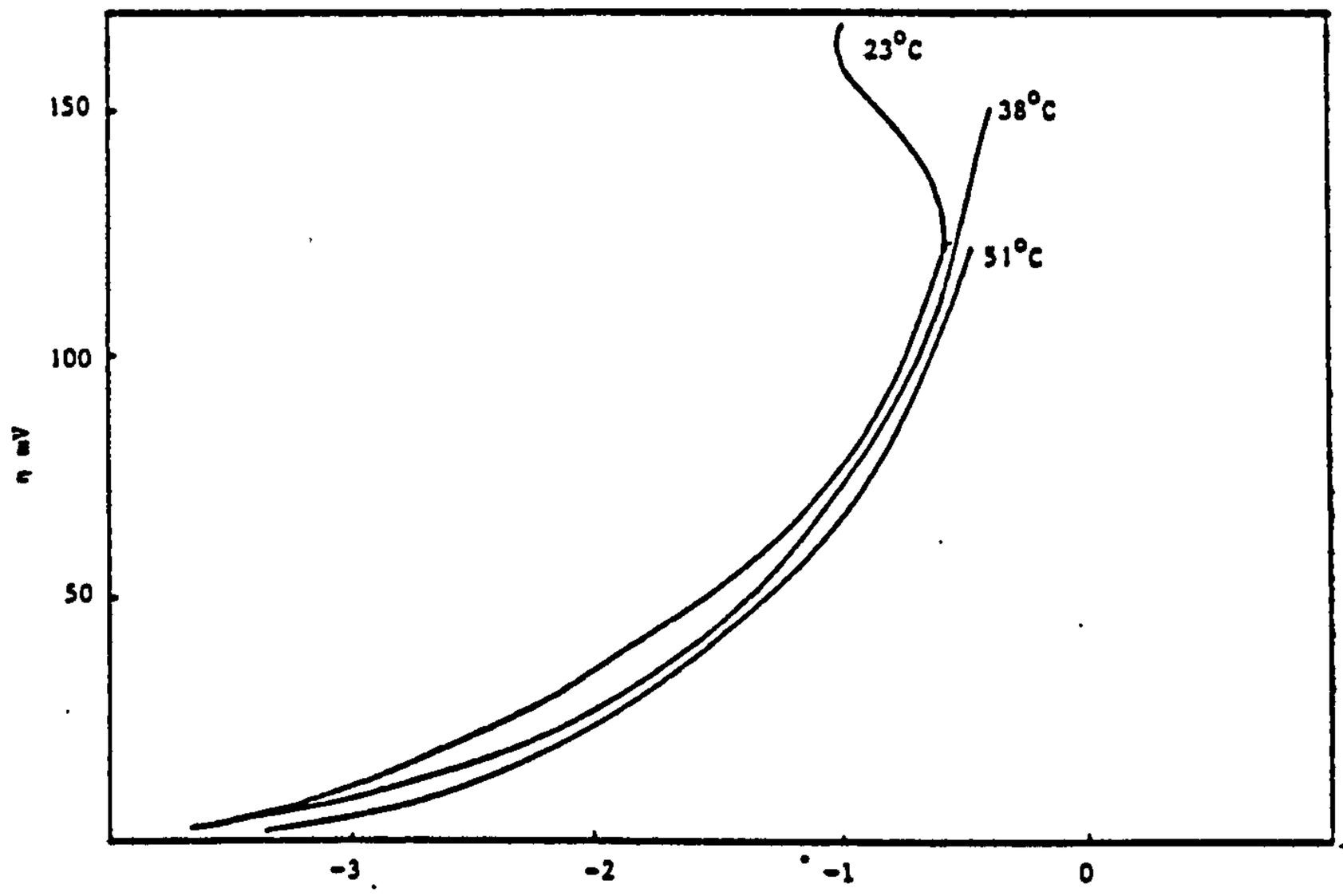

E vs log i for a Pb electrode anodically polarised at a sweep rate of 0.5 mV sec^{-1} in a solution of 48% HBF_4 at different temperatures.

FIGURE 197

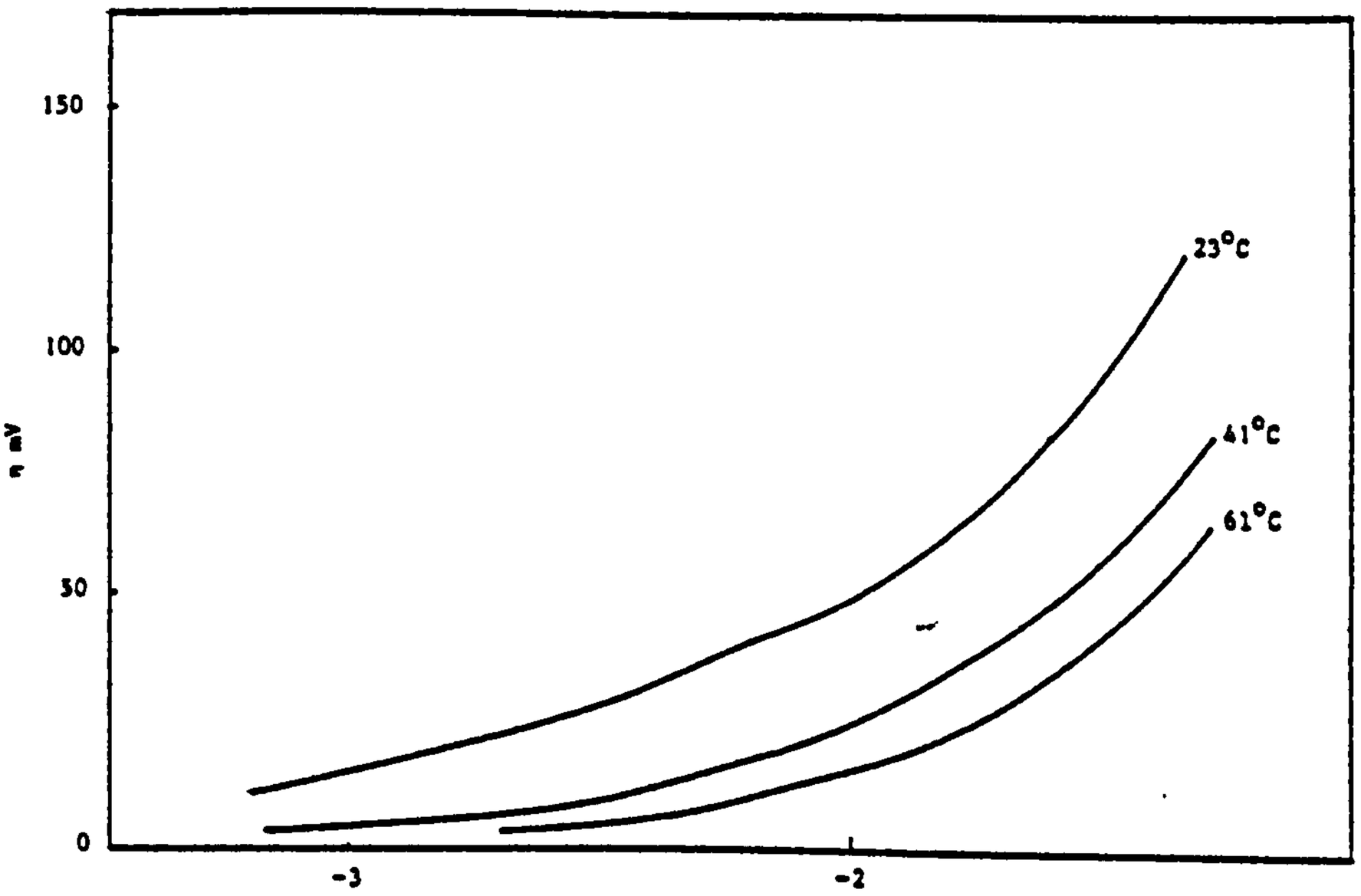

E vs log i curve for the reduction of βPbO_2 in 48% HBF_4 at different temperatures. The βPbO_2 electrode polarised at a sweep rate of 0.5mV sec^{-1} from its rest potential.

FIGURE 198

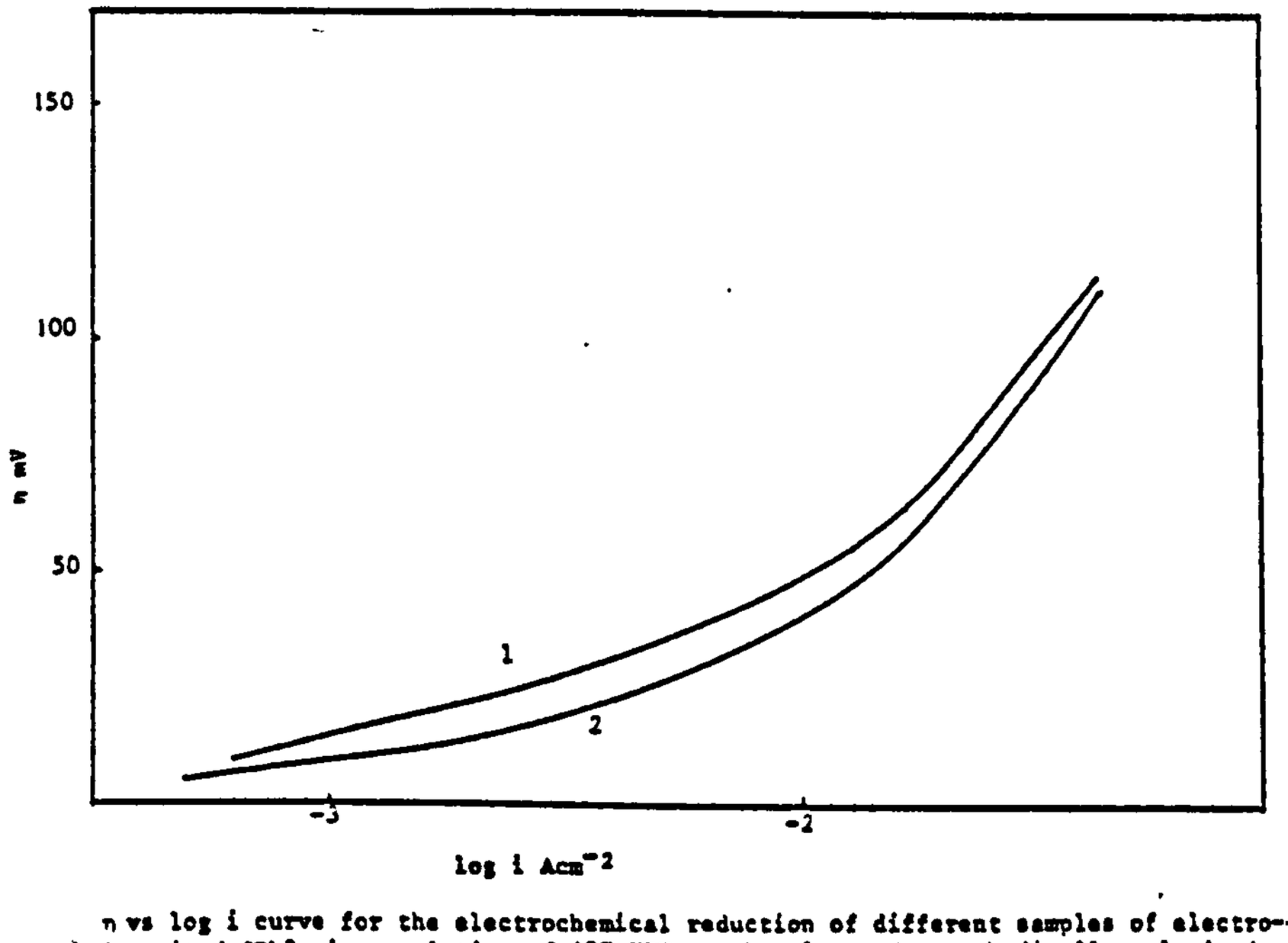

η vs log i curve for the electrochemical reduction of different samples of electrodeposited βPbO_2 in a solution of 48% HBF_4 , the electrodes cathodically polarised at a sweep rate of 5mV sec^{-1} .

1 = Sample of βPbO_2 electrodeposited onto Ni at 2A dm^{-2} from a solution of 360 gl^{-1} $Pb(NO_3)_2$.

2 = Sample of βPbO_2 electrodeposited at 2A dm^{-2} from a solution of 360 gl^{-1} $Pb(NO_3)_2$ heated to 250°C for ½ an hour.

FIGURE 199

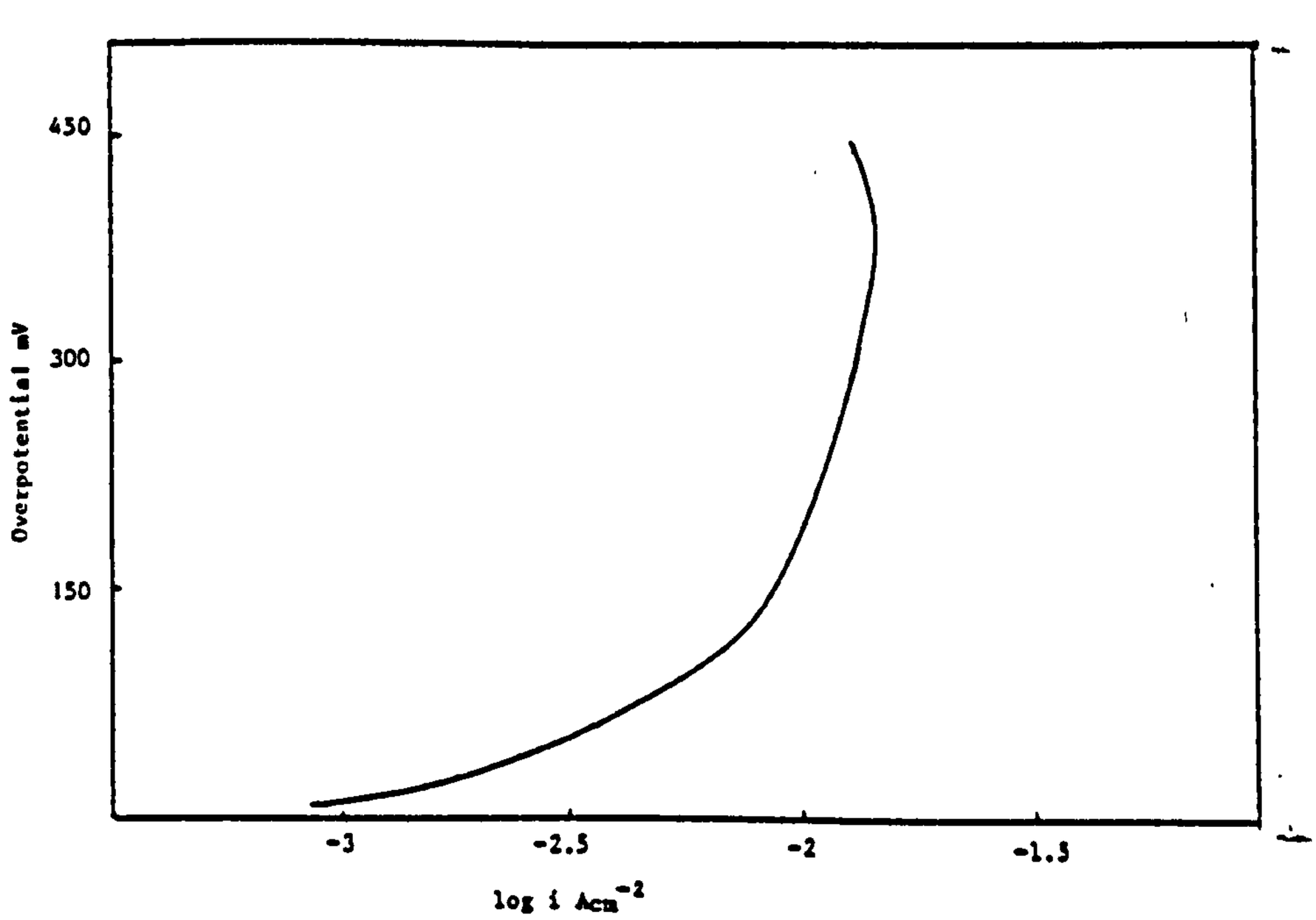

η vs log i curve for a sample of βPbO_2 electrodeposited in Ni heated to a temperature of 250°C for ½ hr, then cathodically polarised at a sweep rate of 5mV sec^{-1} in a solution of 48% HBF_4 .

FIGURE 200

The calculated activation energy for β-PbO_2 reduction from the above data is 35 kJ $mole^{-1}$ from the plot of E vs log i and 42 kJ $mole^{-1}$ from the linear relationship between η and i.

The polarisation curve for β-PbO_2 heated to 250°C for 30 min was found to be different from that of non heat-treated PbO_2, at slow sweep speeds (see Fig. 199).

A polarisation curve for PbO_2 heated to 250°C for 30 min and polarised at 5 mV sec^{-1} in 48% HBF_4 is shown in Fig. 200 from which a value of i_o of 6 x 10^{-4} Acm^{-2} was determined (from extrapolation of the E vs log i curve).

The value of E_{rest} for PbO_2 at 23°C was + 1.565 V, at 41°C, + 1.554 V and at 61°C, + 1.550 V.

3.4.5 Electrochemical impedance measurements on Pb and PbO_2 in HBF_4

3.4.5.1 Pb in 48% HBF_4

A plot of Z' vs Z" for a Pb electrode in 48% HBF_4 at the rest potential of -0.29 V and at 25°C is shown in Fig. 201.

The value of R_{ct} was found to be 8.83 ohms cm^2 for the high frequency semi-circle which corresponds to a value for i_o of 1.45 x 10^{-3} Acm^{-2}. A plot of Z" vs w yields a double layer capacitance of 68 μF cm^{-2} in the high frequency semi-circle with the value for w_{max} found to be 1039 Hz. This equates to a time constant of 1.53 x 10^{-4} sec for this system.

The low frequency region below 78 Hz does not indicate the existence of any mass transfer controlled process, with a plot of Z' vs Z" essentially linear, although a possible semi-circle arc is visible.

The Z' vs Z" plot for a Pb electrode anodically polarised at an initial current density of 0.86 Adm^{-2} and maintained at a fixed potential of -0.23 V is shown in Fig. 202.

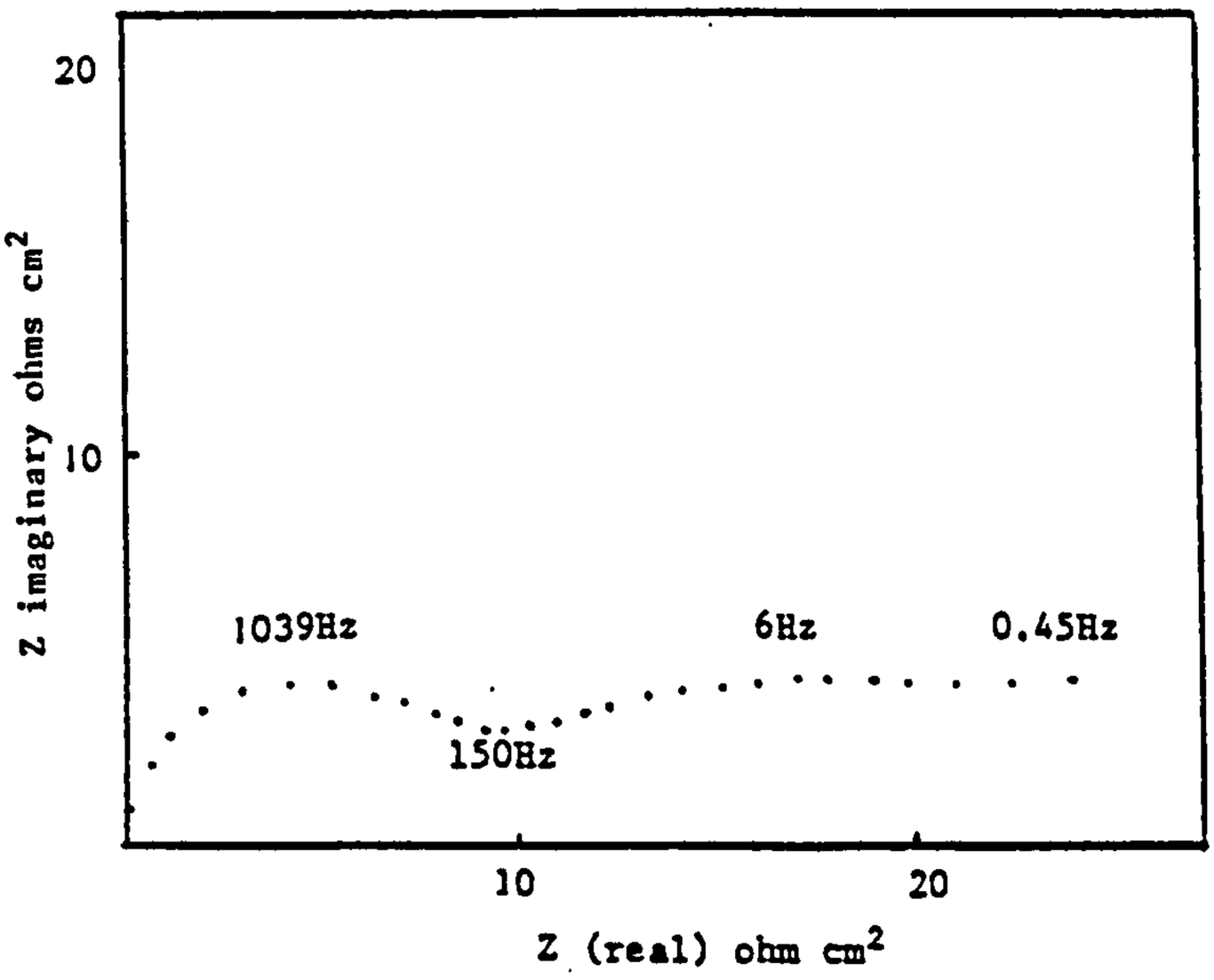

Z real vs Z imaginary for a Pb electrode held at its rest potential of -0.289 7 vs SHE in a 48% HBF_4 solution at 25°C.

FIGURE 201

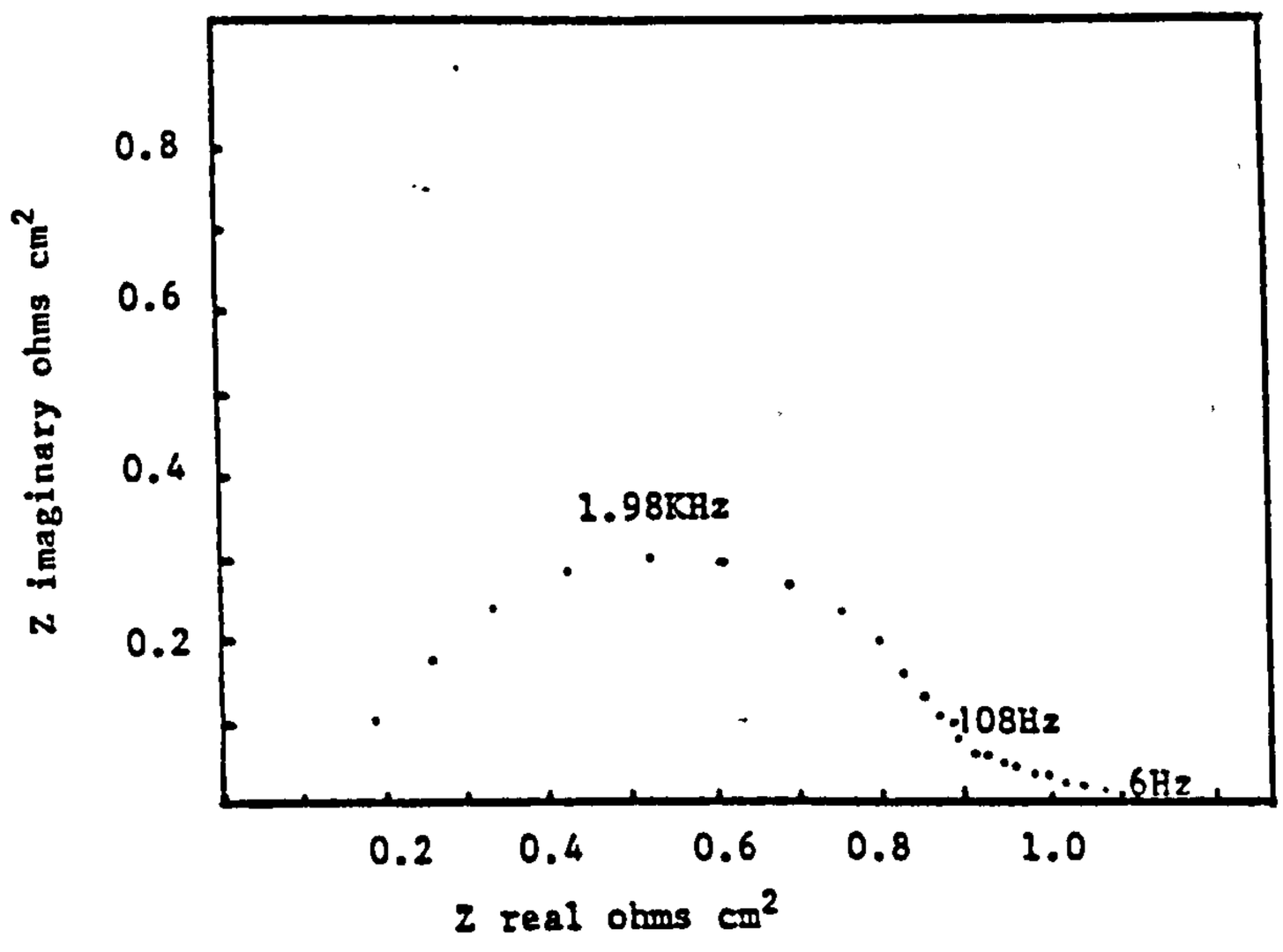

Z real vs Z imaginary for a Pb electrode held a fixed anodic potential of -0.23V in a solution 48% HBF_4, current density 0.8Adm^{-2}.

FIGURE 202

The value of R_{ct} is 0.7 ohms cm^2 and the value of C_{dl} determined from a plot of Z" vs w is 4.7 $\mu F cm^{-2}$ with the value for w_{max} found to be 1983 Hz.

3.4.5.2 Impedance measurements on β-PbO_2 electrodes in 48% HBF_4

Studies were also undertaken to determine the impedance characteristics of PbO_2 electrodes in 48% HBF_4. Samples of commercially prepared PbO_2 that exhibited both good and bad adhesion onto a Ni foil substrate, together with a sample of PbO_2 obtained under laboratory controlled conditions by electrodeposition at 2 Adm^{-2} from a solution of 360 gl^{-1} $Pb(NO_3)_2$ at 50°C were studied. In addition a section of the PbO_2 electrode obtained under laboratory conditions was heated in a furnace to 250°C for 30 minutes and its impedance characteristics were also determined.

PbO_2 electrodeposited onto Ni electrodes was immersed in 48% HBF_4 and allowed to reach an equilibrium potential. The electrode was then maintained at the rest potential. However because of the nature of the surface under investigation, self corrosion of the PbO_2 deposit did occur at pores in the PbO_2 coating and it was not always possible to maintain the electrode at an equilibrium condition i.e no net current flow. As a result the values of R_{ct} for different specimens were subject to some degree of variation. A plot of Z' vs Z" for a PbO_2 electrode on Ni foil that exhibited good adhesion of PbO_2 held at a potential of +1.61 Volts is shown in Fig. 203. The value of R_{ct} was determined as 160 ohm cm^2 which corresponds to a value for i_o of 8×10^{-5} Acm^{-2}. The value of C_{dl} in the frequency range 754 to 108 Hz was measured as 70 $\mu F\ cm^{-2}$, with the value for w_{max} 1.18 Hz.

The mean value for i_o for 3 samples of β-PbO_2 on Ni foil that exhibited good adhesion was 6×10^{-5} A cm^{-2} with a mean value of R_s of 1.07 ohms cm^2 (where R_s = series resistance).

The Z' vs Z" plots for samples of commercially prepared PbO_2 electrodeposited onto Ni foil that exhibited bad adhesion of electrodeposited PbO_2 are shown in Figs. 204 and 205. Each experiment was carried out at a rest potential of +1.556 and +1.568 V respectively.

The value of R_{ct} obtained from Fig. 204 was found to be 290 ohms cm^2 which corresponds to a value for i_o of 4.3×10^{-5} Acm^{-2} and that for C_{dl} was found to be 68 $\mu F\ cm^{-2}$ in the frequency range 1455 to 57 Hz. The values for R_{ct} obtained from the Z' vs Z" plot shown in Fig. 205 is 550 ohms cm^2, equivalent to a value for i_o of 2.3×10^{-5} Acm^{-2}, the value for C_{dl} was found to be 134 μFcm^{-2} in the same frequency range and the value of w_{max} 0.86 Hz.

The mean value of i_o for commercially prepared samples of PbO_2 onto Ni that exhibited bad adhesion was 3.4×10^{-5} Acm^{-2} with a mean value for R_s of 1.71 ohms cm^2.

The Z' vs Z" plot for a β-PbO_2 electrode in 48% HBF_4, prepared in the laboratory by electrodeposition at 2 Adm^{-2} from a solution of 360 gl^{-1} $Pb(NO_3)_2$ at 50°C onto an etched Ni surface is shown in Fig. 206. The electrode was maintained at its rest potential of + 1.556 V. A value for R_{ct} of 350 ohms cm^2 was measured which corresponds to a value for i_o of 3.6×10^{-5} Acm^{-2}, the value of C_{dl} was found to be 40 $\mu F\ cm^{-2}$ with w_{max} of 0.171 Hz and R_s of 1.31 ohms cm^2.

The Z' vs Z" plot in a solution of 48% HBF_4 for a sample of PbO_2 electrodeposited onto a Ni foil substrate yet heated to 250°C for 30 min is shown in Fig. 207.

The value of R_{ct} in this instance was found to be 66 ohm cm^2 corresponding to a value for i_o of 1.9×10^{-4} Acm^{-2}. with the value of C_{dl} in the frequency range 1983 Hz to 395 Hz, 12 μFcm^{-2} whilst in the frequency range 395 Hz to 21 Hz a value of 1300 $\mu F\ cm^{-2}$ was obtained, the value of w_{max} was

2.256 Hz. A Z' vs Z" plot for a similar specimen gave a value for R_{ct} of 37 ohms cm^2 corresponding to a value for i_o of 3.4×10^{-4} Acm^{-2} when the specimen was maintained at a potential of +1.531 V. The value for C_{dl} was found to be 495 $\mu F\ cm^{-2}$ in the frequency range 149.8 to 0.32 Hz and 234 $\mu F\ cm^{-2}$ in the range 1039 to 207 Hz.

3.4.5.3 Impedance characteristics for PbO_2 cathodically polarised at 0.5 Adm^{-2} in 48% HBF_4 at room temperature

The Z' vs Z" curve for a sample of β-PbO_2 electrodeposited onto a Ni foil that exhibited good adhesion, then cathodically polarised at an initial current density of 0.5 Adm^{-2} in 48% HBF_4 and maintained at a fixed potential of + 1.530 V is shown in Fig. 208. The value of R_{ct} was measured as 2.8 ohms cm^2, with the value for C_{dl} 869 μFcm^{-2} in the frequency range 395 to 56 Hz, and the value of w_{max} 56.9 Hz.

A similar curve, yet for a sample of commercially prepared PbO_2 that exhibited bad adhesion on a Ni foil substrate is shown in Fig. 209 for a sample polarised at an initial current density of 0.5 Adm^{-2} in 48% HBF_4 to a fixed potential of 1.504 V. The value for R_{ct} on this sample was found to be 3.8 ohms cm^2 whilst that for a different specimen was 3.4 ohm cm^2. The values of C_{dl} were found to be 630 μFcm^{-2} in the frequency range 545.9 to 56.99 Hz and 945 $\mu F\ cm^{-2}$ in the frequency range 41.25 to 0.0648 Hz, the value of w max was 56.9 Hz.

Cathodic polarisation of a sample of PbO_2 which had been heated to 250°C at an initial current density of 0.5 Adm^{-2} in a solution of 48% HBF_4 resulted in a Z' vs Z" plot shown in Fig. 210. The value of R_{ct} was measured as 2.3 ohm cm^2 with the values of C_{dl} again frequency dependent. A value of 870 $\mu F\ cm^{-2}$ was measured in the range 545 Hz to 56 Hz and 1200 $\mu F\ cm^{-2}$ in the frequency range 41 to 0.089 Hz, the value of w_{max} was 56.9 Hz.

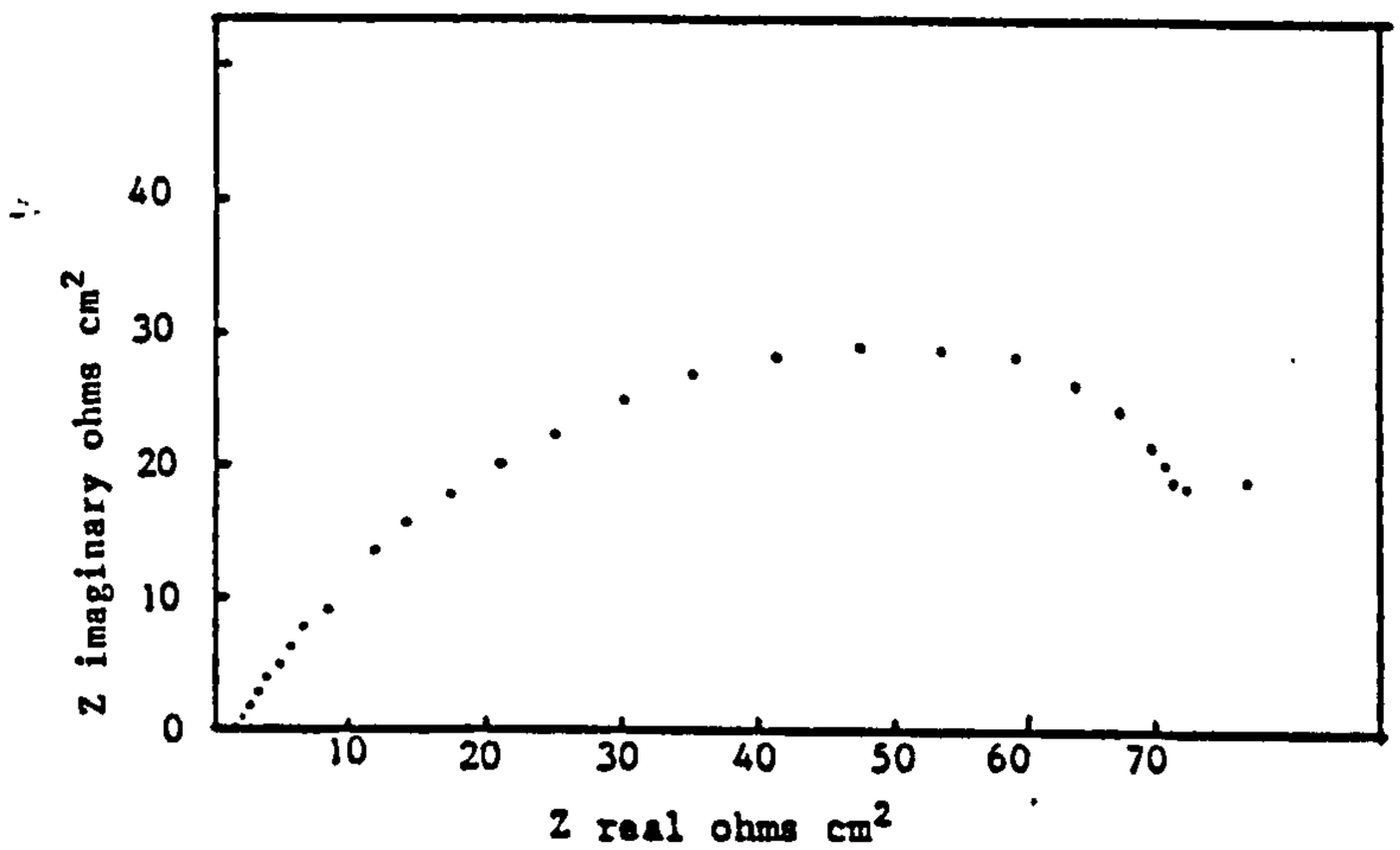

Z real versus Z imaginary for a sample of PbO_2 electrodeposited onto Ni 200. The specimen exhibited good adhesion in the bend test. The electrode maintained at its rest potential of 1.610V vs SHE in 48% HBF_4 at 25°C.

FIGURE 203

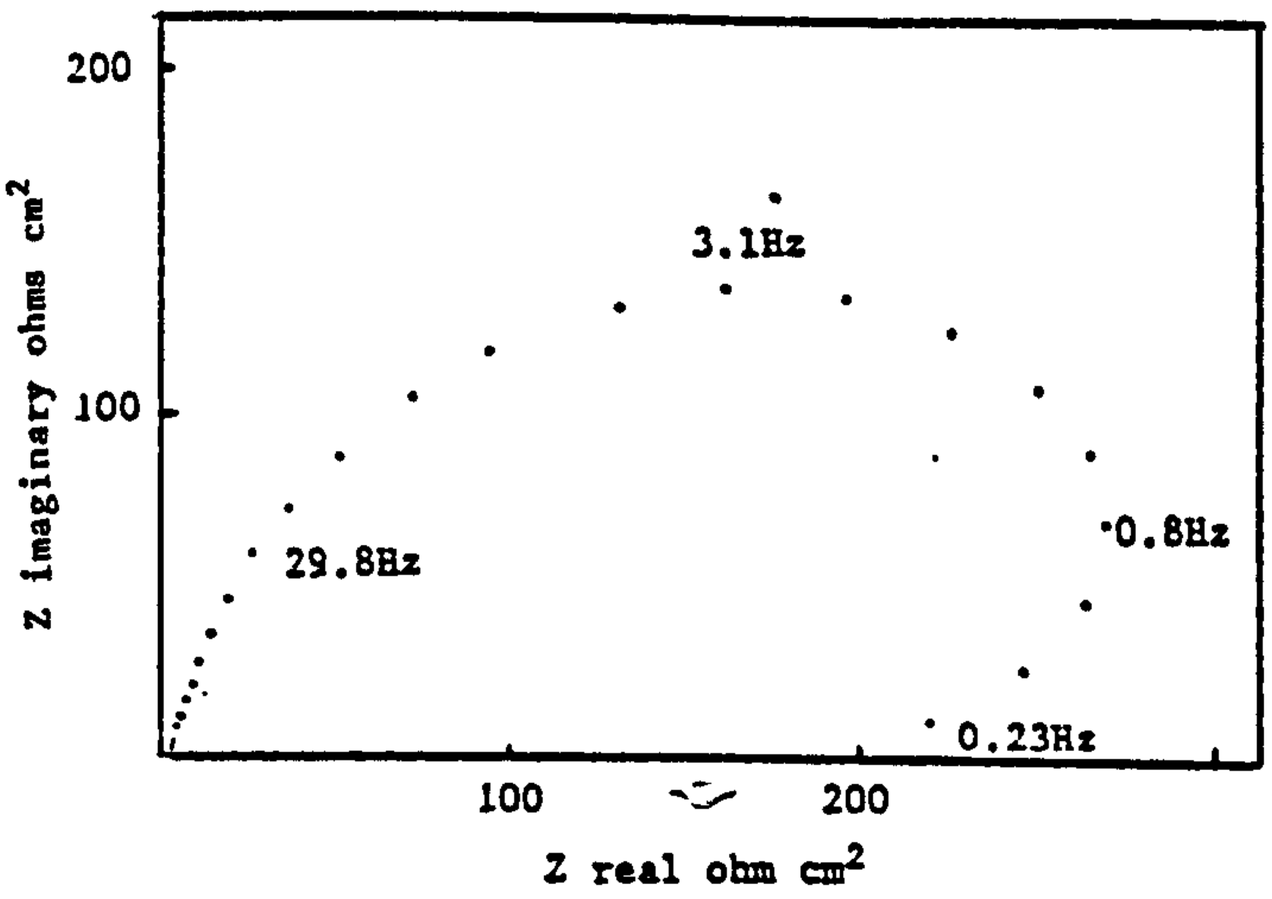

Z real vs Z imaginary for a PbO_2 electrodeposited onto Ni 270 foil in 48% HBF_4 . The sample exhibiting bad adhesion in the adhesion bend test. The electrode maintained at +1.556 V vs SHE.

FIGURE 204

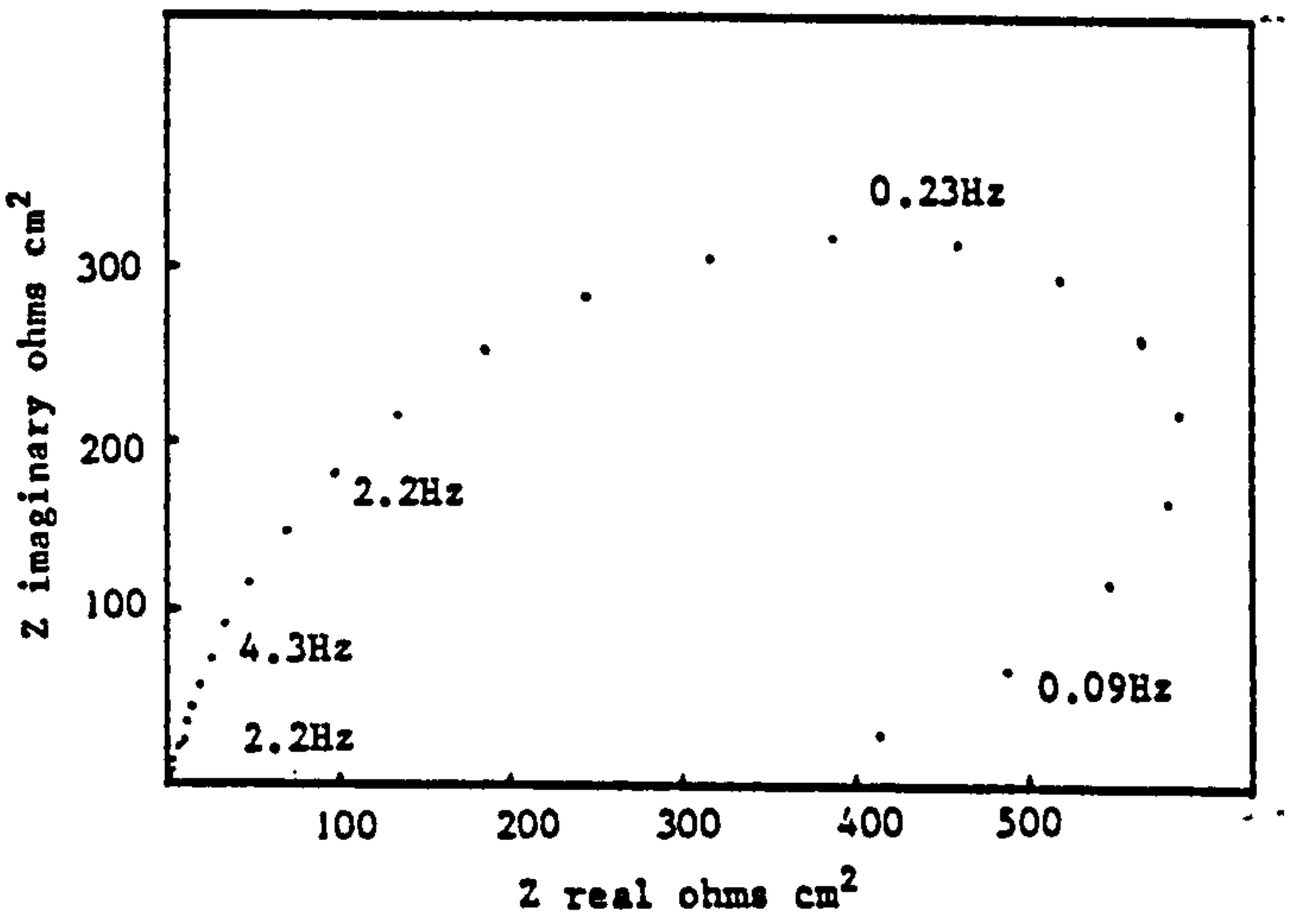

Z real vs Z imaginary for $1bO_2$ electro-deposited onto Ni270 that exhibited poor adhesion for the PbO deposit. The electrode maintained at a rest potential of 1.568V vs SHE.

FIGURE 205

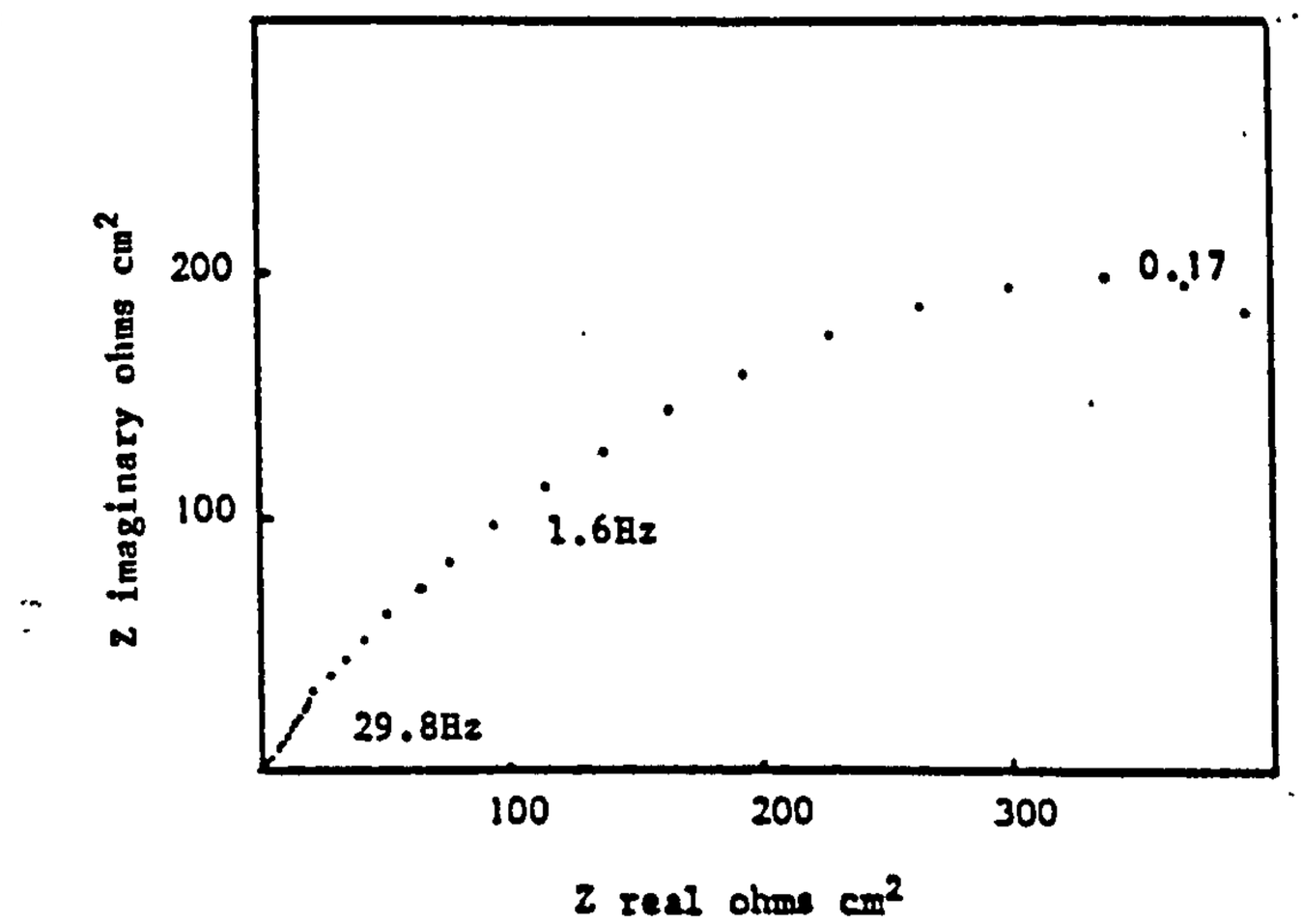

Z real vs Z imaginary for PbO_2 electro-deposited onto Ni200 at 2 Adm^{-2} from a 360 gl^{-1} $Pb(NO_3)_2$ solution. The electrode maintained at its rest potential of 1.556V vs SHE in a solution of 48% HBF_4 .

FIGURE 206

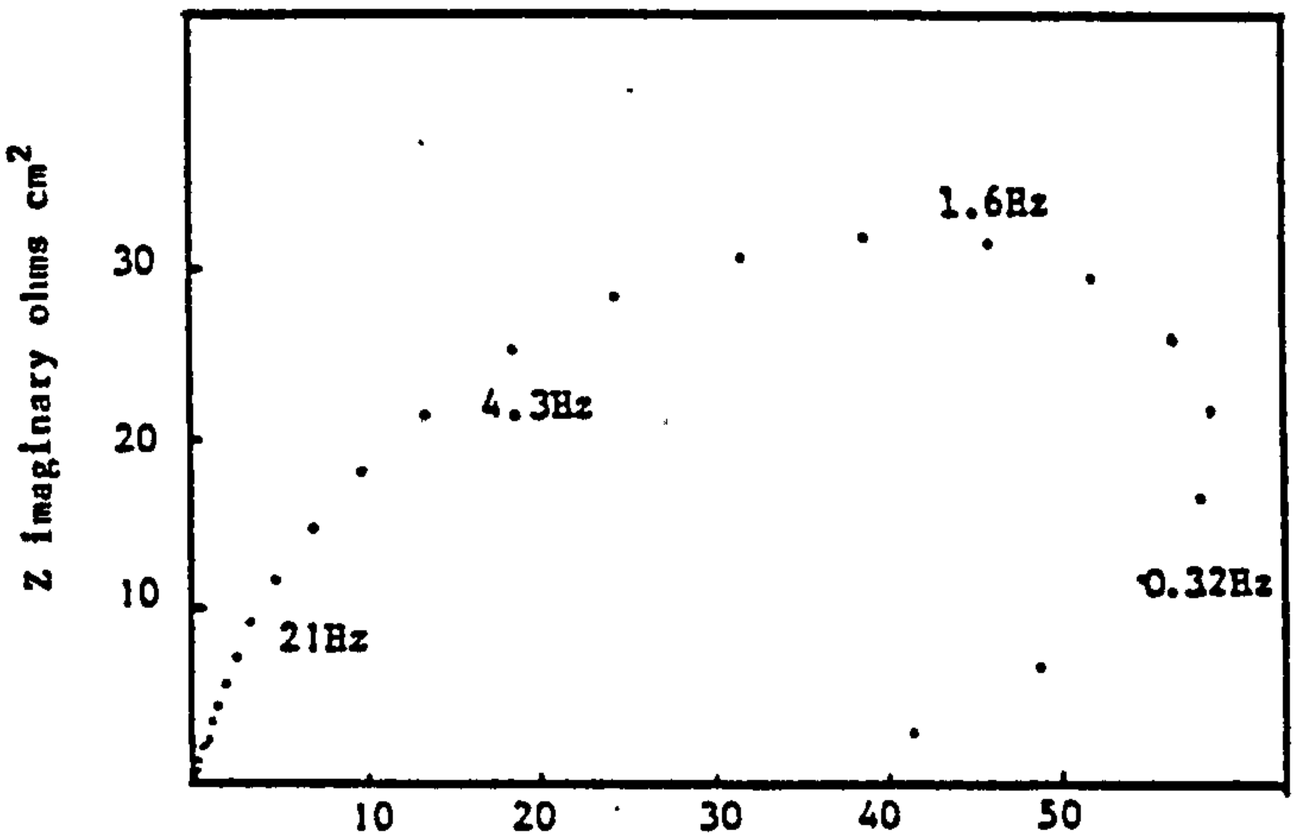

Z real vs Z imaginary for PbO_2 electrodeposited onto Ni 200 foil, then heat treated at 250°C for ½ hour. The electrode maintained at its rest potential in 48% HBF_4 .

FIGURE 207

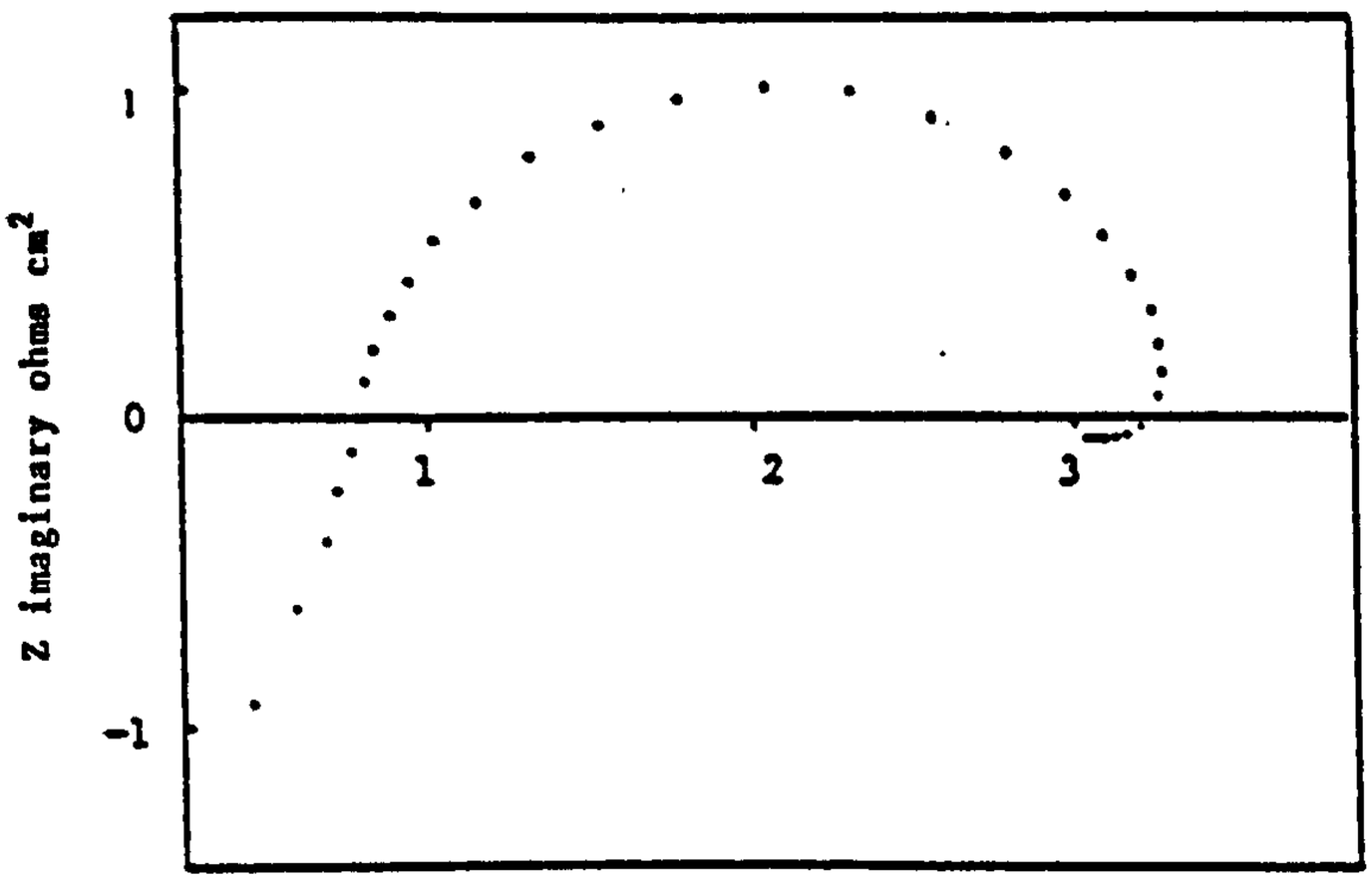

Z real vs Z imaginary for PbO_2 electrodeposited onto Ni200 under laboratory conditions. The electrode cathodically polarised to a potential of 1.505V vs SHE in 48% HBF_4 at 25°C.

FIGURE 208

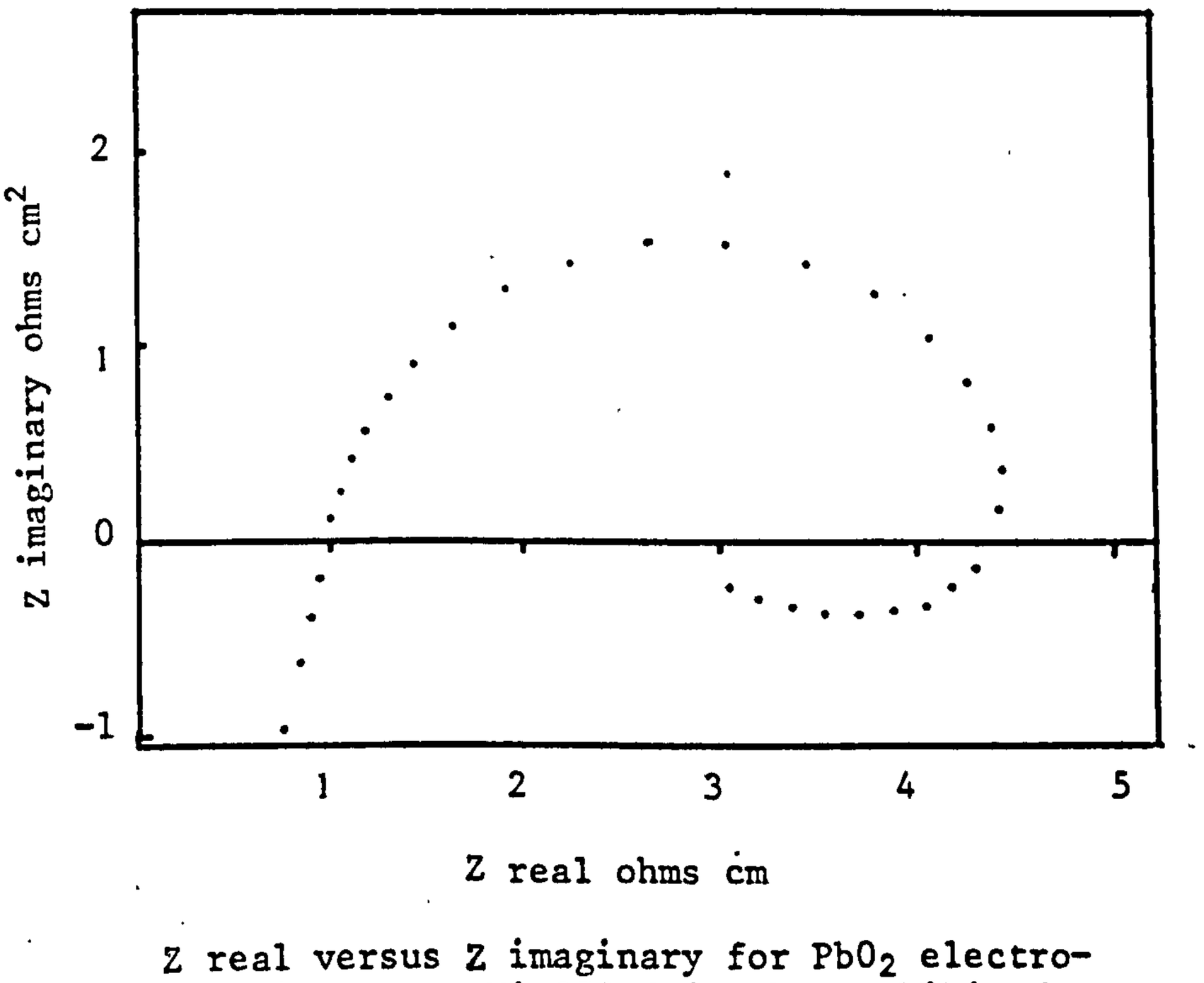

Z real versus Z imaginary for PbO_2 electrodeposited onto Ni 270 foil that exhibited bad adhesion when subjected to an adhesion bend test. The PbO_2 electrode cathodically polarised to +1.502 V vs SHE in a 48% HBF_4 solution, current 0.5Adm^{-2} .

FIGURE 209

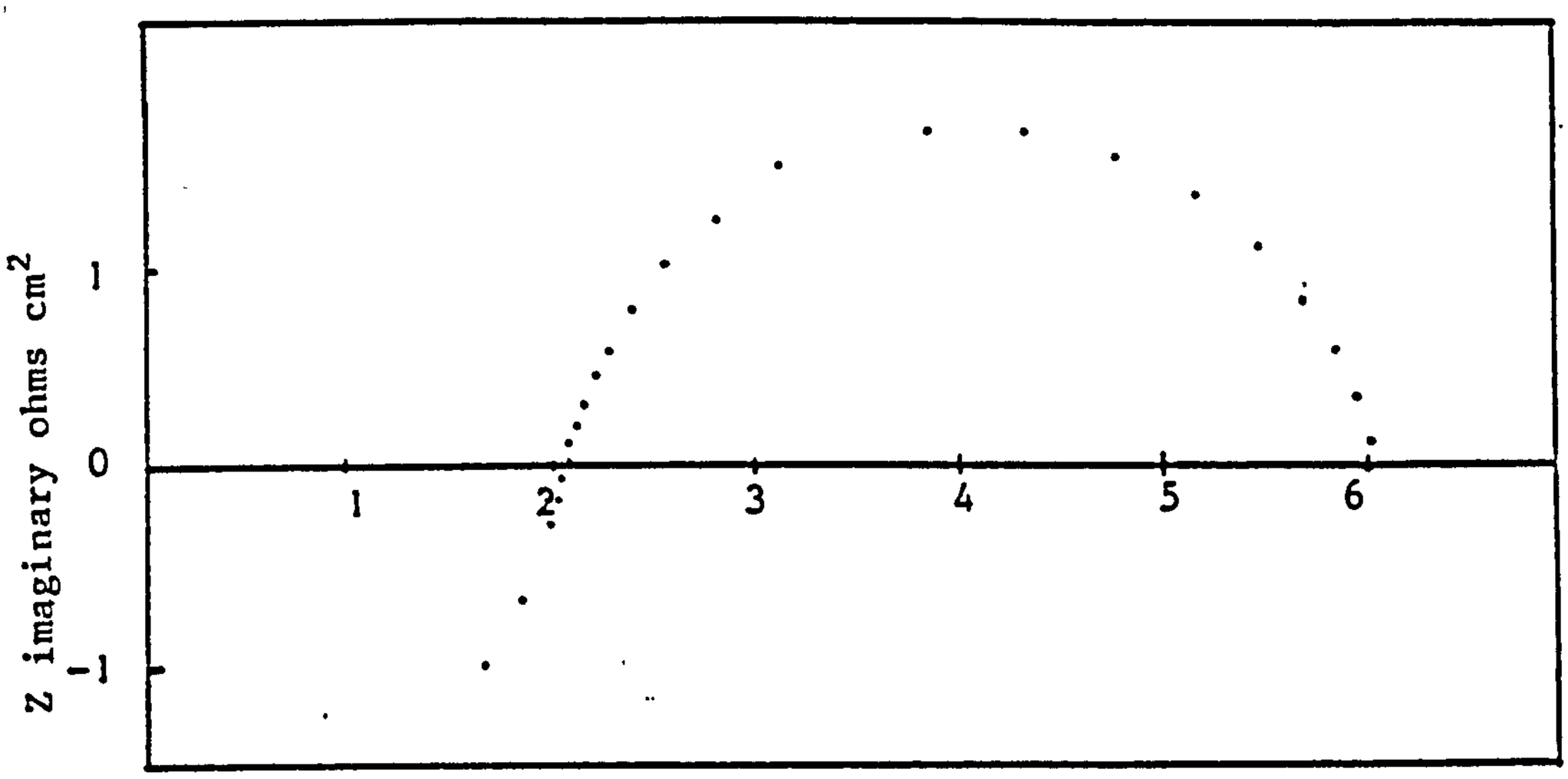

Z real vs Z imaginary for PbO electrodeposited onto Ni 200 heated to 250°C for ½ hr then polarised to 1.505V vs SHE in 48% HBF_4 at 25°C.

FIGURE 210

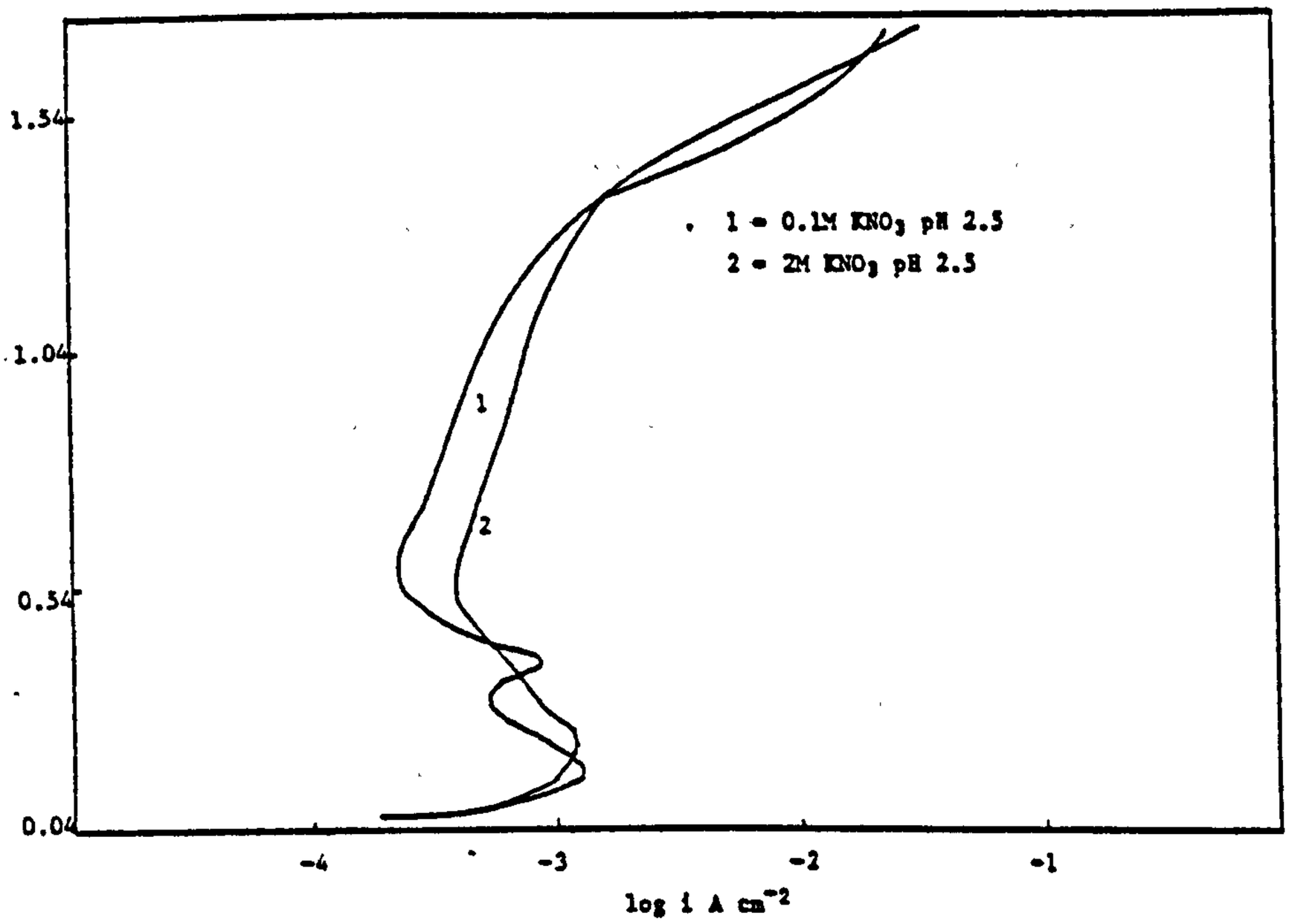

E vs log i curve for a Ni electrode anodically polarised at a sweep rate of 10 mV sec^{-1} in solutions of different KNO_3 concentrations each solution pH 2.5.

FIGURE 211

3.5 Passivity of Ni in NO_3^- solutions

3.5.1 Introduction

Ni, passivated in a NO_3 solution acts as the inert substrate for PbO_2 deposition from $Pb(NO_3)_2$ solutions in the production of lead acid primary batteries. To aid the understanding of the problem of the adhesion of PbO_2 onto nickel and the addition of selected additives to $Pb(NO_3)_2$ plating solutions. It was considered necessary to investigate the passivity of Ni in NO_3^- solutions, with and without certain anions and organic complexing agents.

Cyclic voltammetry and linear potential sweep studies were undertaken with these objectives in mind. Experiments were conducted to investigate the effect of pH, $[NO_3^-]$ and selected anion concentrations on nickel passivity from NO_3^- solutions. This work was also undertaken to supplement the relatively small amount of information on Ni passivation in NO_3^- solutions available in the literature (see Section 1.6).

3.5.2 The effect of NO_3^- concentration on Ni passivity

The effect of KNO_3 concentration, in the range 2M to 0.1M KNO_3 in a solution of constant pH, on the passivity of Ni was investigated.

The E vs logi curve for a Ni electrode polarised at a sweep rate of 10 mV sec^{-1} in two different NO_3^- concentrations is shown in Fig. 211. The most noticeable effect is the appearance of a second passivation peak (a) at + 0.390 V in 0.1M KNO_3 solutions, whilst at higher concentrations (2M) this peak is absent. A decrease in the NO_3^- concentration makes the second passivation peak more apparent.

The values of i_{pp}, E_{pp}, and the minimum value of i_{pass} with change in NO_3 concentration for a KNO_3 solution of pH 2.5 are given in Table 73, for a sample of high purity Ni polarised at 10 mV sec^{-1}.

TABLE 73

The effect of NO_3^- concentration on the anodic polarisation of Ni at 10 mV sec^{-1} in a solution of pH 2.5 at 25°C.

KNO_3 concentration moles litre $^{-1}$	i_{pp} (minimum value) Adm^{-2}	i_{pass} Adm^{-2}	E_{pp} Volts
2	0.136	0.400	+ 0.193
1	0.146	0.216	+ 0.185
0.5	0.125	0.210	+ 0.178
0.1	0.120	0.210	+ 0.163

N.B The values quoted are the mean results of 3 separate determinations.

From Table 73 it can be seen that i_{pass} is not significantly affected by NO_3^- concentration and indeed only at high NO_3^- concentrations was a variation the minimum value of i_{pass} detected.

The value of i_{pp} in 1M KNO_3 was found to be slightly higher than in other solutions and this is attributed to the difficulties in reproducing a suitable Ni surface rather than a genuine phenomenon. The value of i_{pp} appears to be almost independent of NO_3^- concentration.

3.5.3 The effect of pH on Ni passivity

To investigate the effect of pH on Ni passivity in a solution of constant NO_3^- concentration a solution of 1M KNO_3 was used as the test electrolyte and the pH adjusted to the required value with either HNO_3 or KOH.

The Ni electrode was polarised at 10 mV sec^{-1} from its' rest potential and the resultant current continuously recorded. The current necessary to cause passivation of the Ni electrode was found to be pH dependent, with an essentially linear relationship between log i_{pp} and pH recorded (see Fig. 212).

The following relationship was observed :

$$\log i = KpH + \log i_o$$

where K = constant

log i = i_{pp} at a given pH

log i_o = i_{pp} at pH 0.

For a Ni electrode polarised at 10 mV sec^{-1} in a 1M KNO_3 solution the value of K was found to be - 0.96 and log i_o - 0.15 Acm^{-2}

The time of immersion prior to anodic polarisation was found to be important, particularly in low pH solutions, to achieve reproducible results. Some scatter of results was recorded even with constant immersion times e.g for a 1M KNO_3 solution at pH 2.0 the values of i_{pp} from 3 separate anodic polarisations were 0.43, 0.62 and 0.56 Adm^{-2}.

A Tafel constant of 45 mV per decade was recorded in solutions of pH 1 and 120 mV per decade in pH 4 solutions.

The effect of pH on the nature of the E vs log i curve for two different pH solutions is shown in Fig. 213, whilst the values of E_{pass}, and i_{pp} for Ni polarised in 1 M KNO_3 at selected pH's are presented in Table 74.

A graph of E_{pp} versus pH (Fig. 214) was found to be linear in the pH range 2.5 to 0.7, at values of pH 2.5 and above no sharp easily discernable passivation peak could be detected.

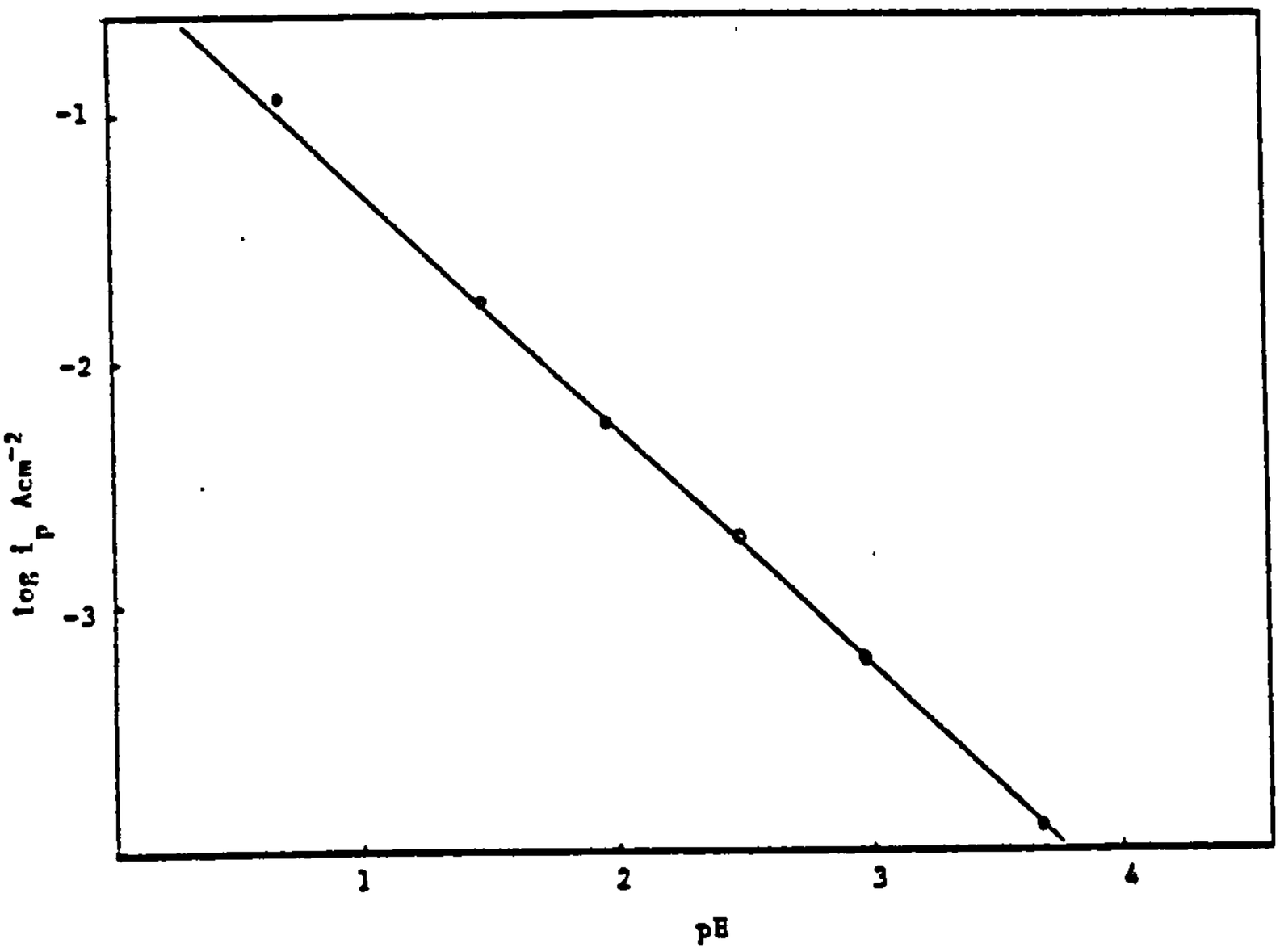

A graph of log i_p vs pH for Ni anodically polarised at 10 mV sec^{-1} in a solution of 1M KNO_3 .

FIGURE 212

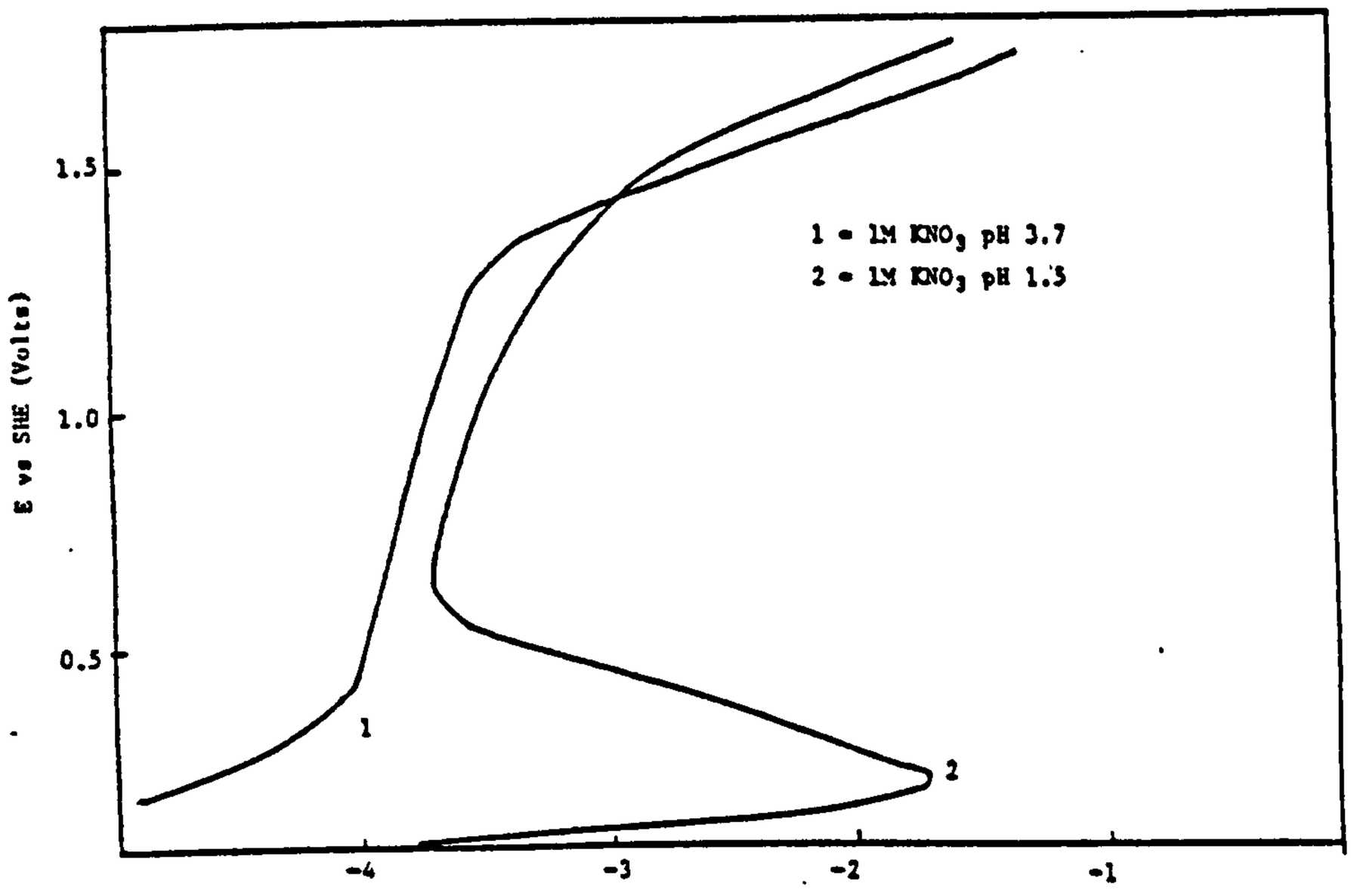

E vs log i curve for a Ni electrode anodically polarised at 10 mV sec^{-1} in a solution of 1M KNO_3 at different pH's, pH adjusted by the addition of HNO_3

FIGURE 213

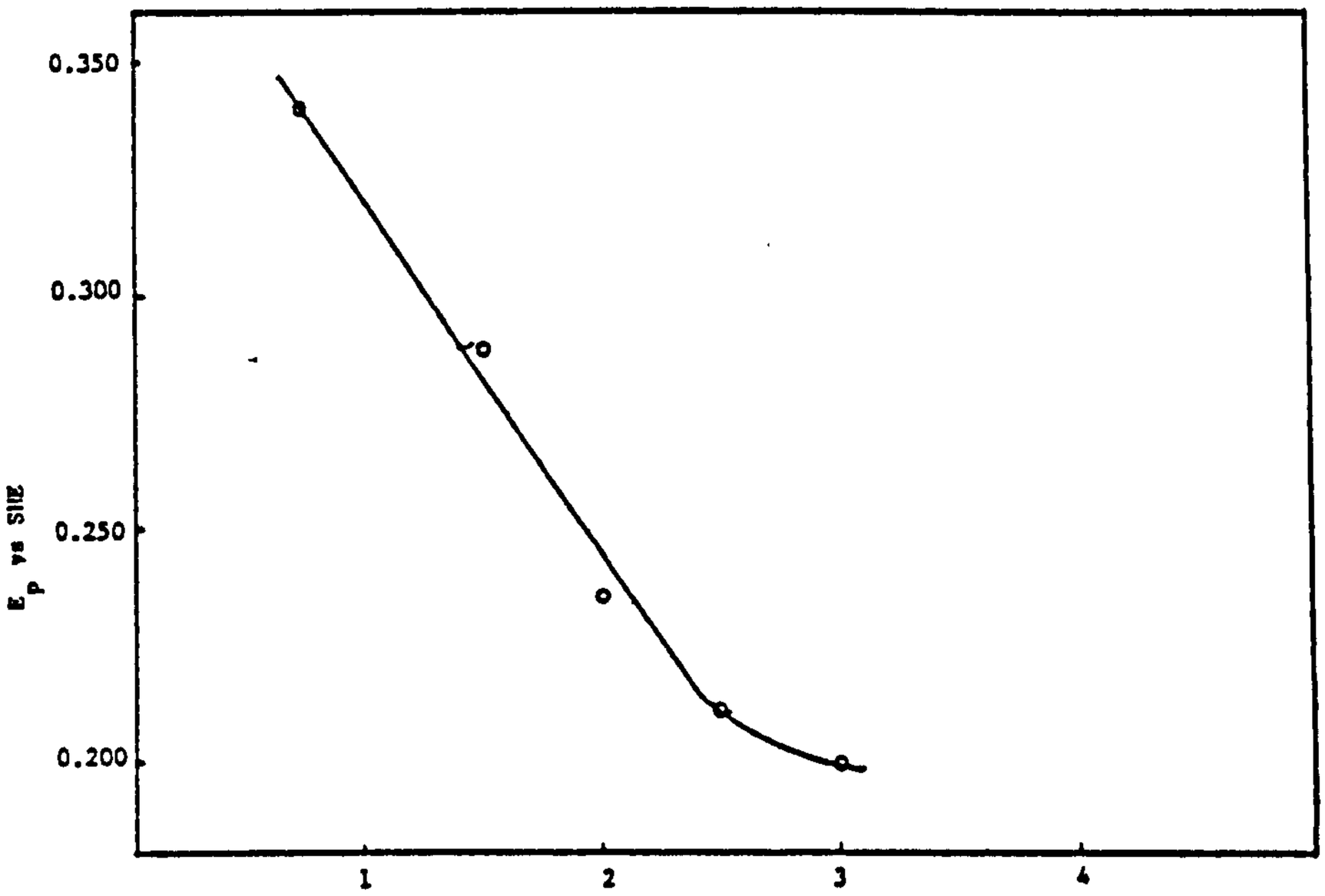

A graph of E_{pp} vs pH for a Ni electrode anodically polarised at a sweep rate of 10mV sec^{-1} in a solution of 1M KNO_3 of different pH, pH adjusted with HNO_3.

FIGURE 214

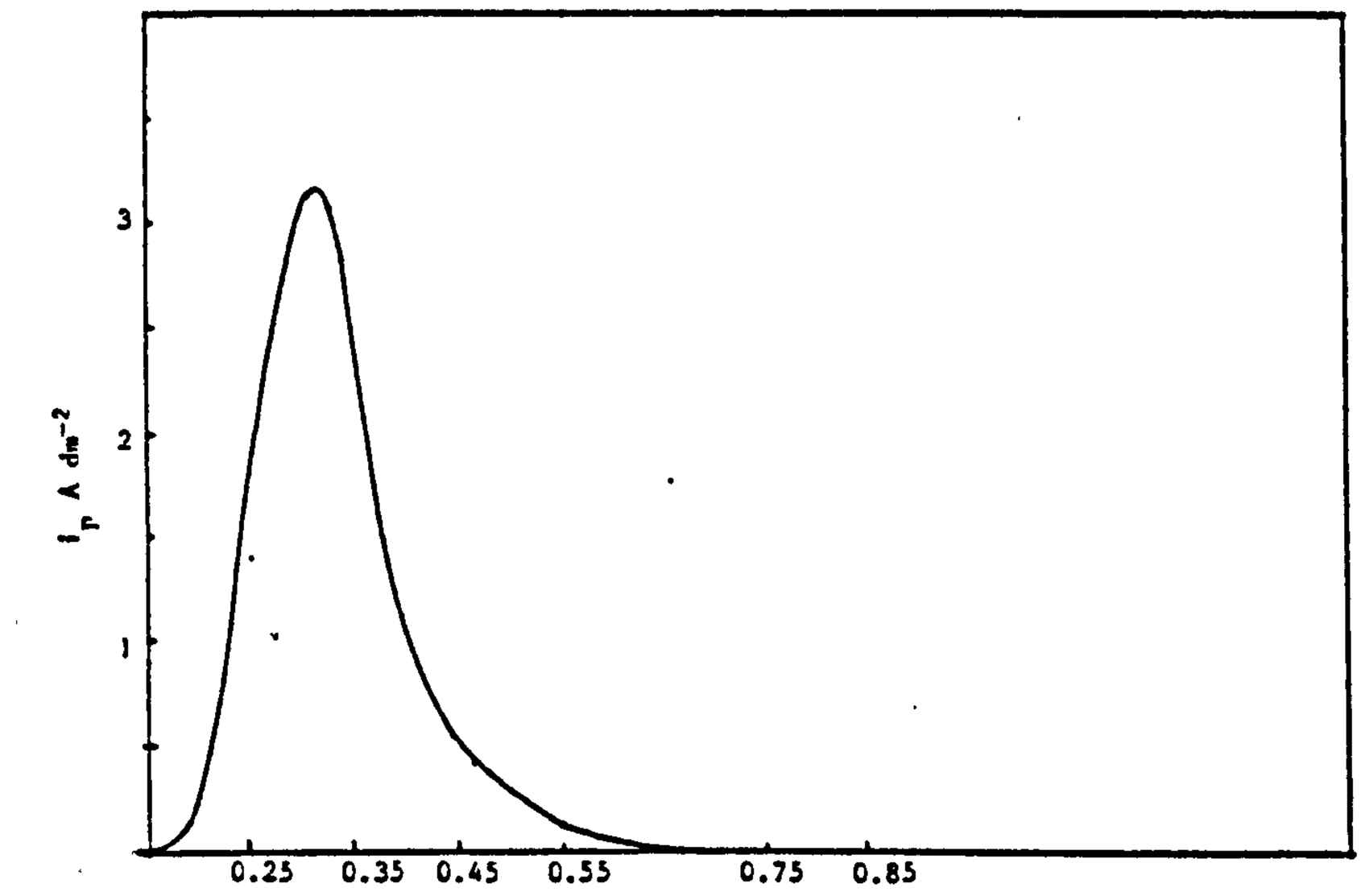

E vs i curve for a Ni electrode anodically polarised at a sweep rate of 10mV sec^{-1} in a solution of 1M KNO_3 pH 1.05 at 25°C.

FIGURE 215

TABLE 74

Values of E_{pp}, i_{pass} and i_{pp} for a sample of high purity Ni anodically polarised at 10 mV sec^{-1} in 1M KNO_3 solutions of different pH at 25°C

pH	$i_{critical}$ Adm^{-2}	i_{pass} (minimum value) Adm^{-2}	E_{pp} Volts
3.7	0.012	-	-
3.0	0.058	0.0168	+ 0.200
2.5	0.187	0.0192	+ 0.210
2.0	0.55	0.0155	+ 0.235
1.5	1.79	0.0199	+ 0.288
0.7	11.4	0.0240	+ 0.340

The following relationship between E_p and pH was observed :

$$E_p = E_o - KpH$$

where E_o = Passivation potential in solution of pH 0

K = Constant

E_p = Passivation potential at a given pH

For a Ni electrode polarised at 10 mV sec^{-1} it was found that

$$E_p = 0.390 - 0.080\ pH$$

Difficulty in obtaining consistent results for a Ni electrode in NO_3^- solutions meant that a plot of (d logi/d pH) at constant potential exhibited too great a degree of scatter, primarily because of variation in the rest potential. However, a plot of d logi/d pH at constant overpotential namely 50mV exhibited a slope of 0.95.

The values of i_{corr} for Ni dissolution in NO_3^- solutions also varied with pH e.g in a solution of pH 1.5 a value of 2×10^{-4} Acm^{-2} was obtained whilst in a solution of pH 3.7 the value was 4×10^{-6} Acm^{-2}.

3.5.4 Cyclic voltammetry studies on Ni passivation in 1M KNO_3

Cyclic voltammograms for nickel anodically polarised at different sweep rates in a 1M KNO_3 solution at selected pH's show the existence of two diffferent passivation peaks.

In a solution of low pH the voltammogram at a sweep rate of 10mv sec^{-1} indicates the presence of one passivaton peak at +0.315 V and a value of i_{pp} of 3.2 Adm^{-2} (see Fig. 215). The variation of i_{pp} with sweep rate (v) was investigated in this solution and a linear relationship between i_p and $v^{1/2}$ observed (see Fig. 216). However, the results were difficult to reproduce in low pH solutions and at least four (4) separate determinations were carried out to determine the mean value. At higher sweep rates (250 mV sec^{-1}) the appearance of a second passivation peak was detected at + 0.600 V indicating the possibility of two different oxides even in low pH solutions (see Fig. 217).

The magnitude of i_{pp} was dependent upon both sweep rate and pH and the appearance of a second passivation peak with increase in solution pH was clearly visible as can be seen from Fig. 218 for the same experiment carried out in 1M KNO_3 pH 1.72. Indeed as the solution pH is increased still further to pH 2.6, the relative intensities of the two passivation peaks also increases at a given sweep rate (see Figs. 219 and 220). Until at pH 4 only one passivation peak is visible (see Fig. 221) and only at low sweep rates can a clear value of E_{pp} be obtained.

A linear relationship between i_{pp} and $v^{1/2}$ for the formation of both nickel oxides was observed at pH's 1.72 and 2.6 (see Figs. 222 and 223). Slope (a) is for the formation of the first passivation peak whilst (b) relates to the formation of the

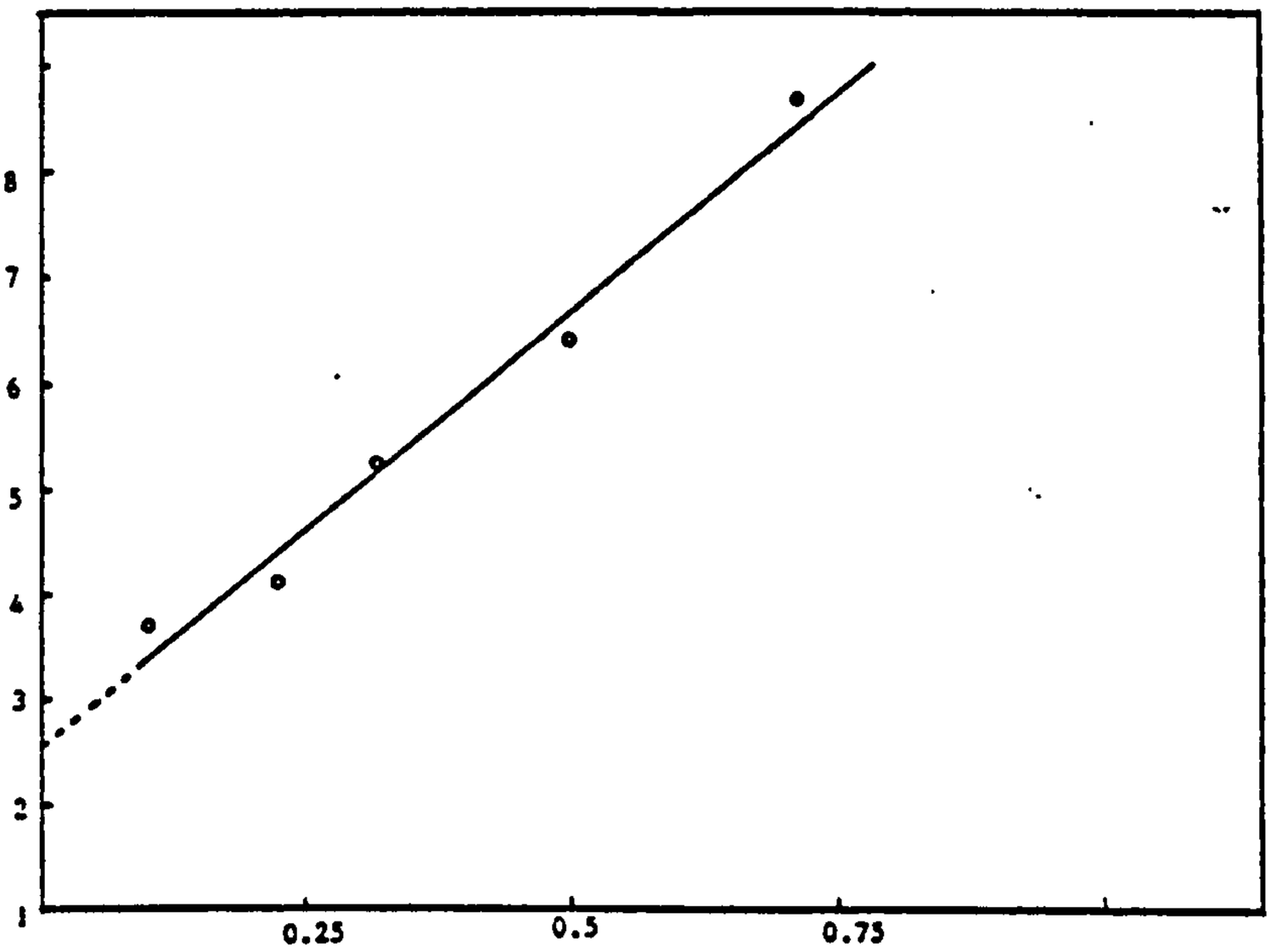

A plot of i_p vs $v^{\frac{1}{2}}$ for a Ni electrode anodically polarised in a solution of 1M KNO_3 pH 1.0

FIGURE 216

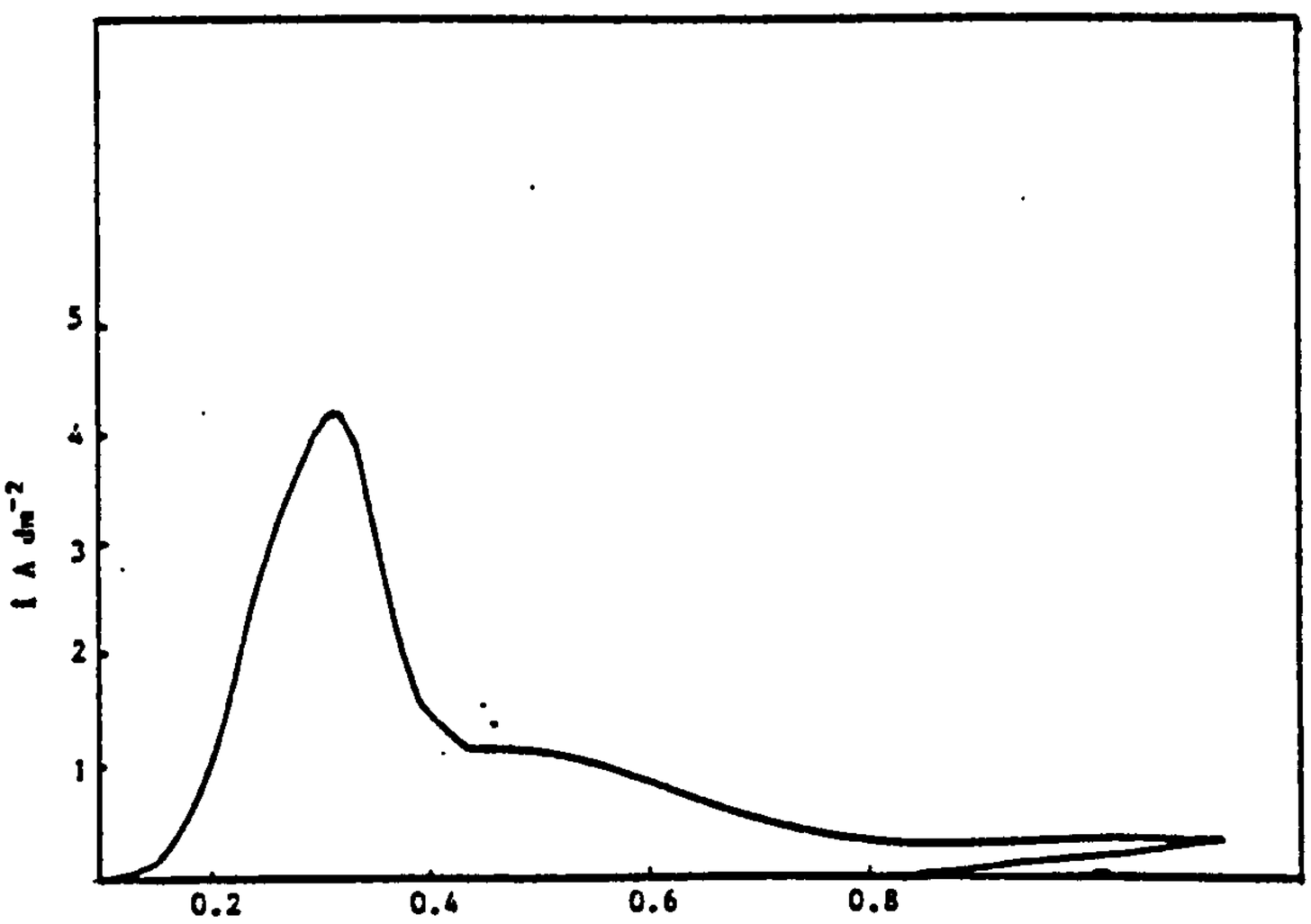

A graph of E vs i for the anodic polarisation of a Ni electrode at a sweep rate of 250 mV sec^{-1} in a solution of 1M KNO_3 pH 1.0. pH adjusted with HNO_3.

FIGURE 217

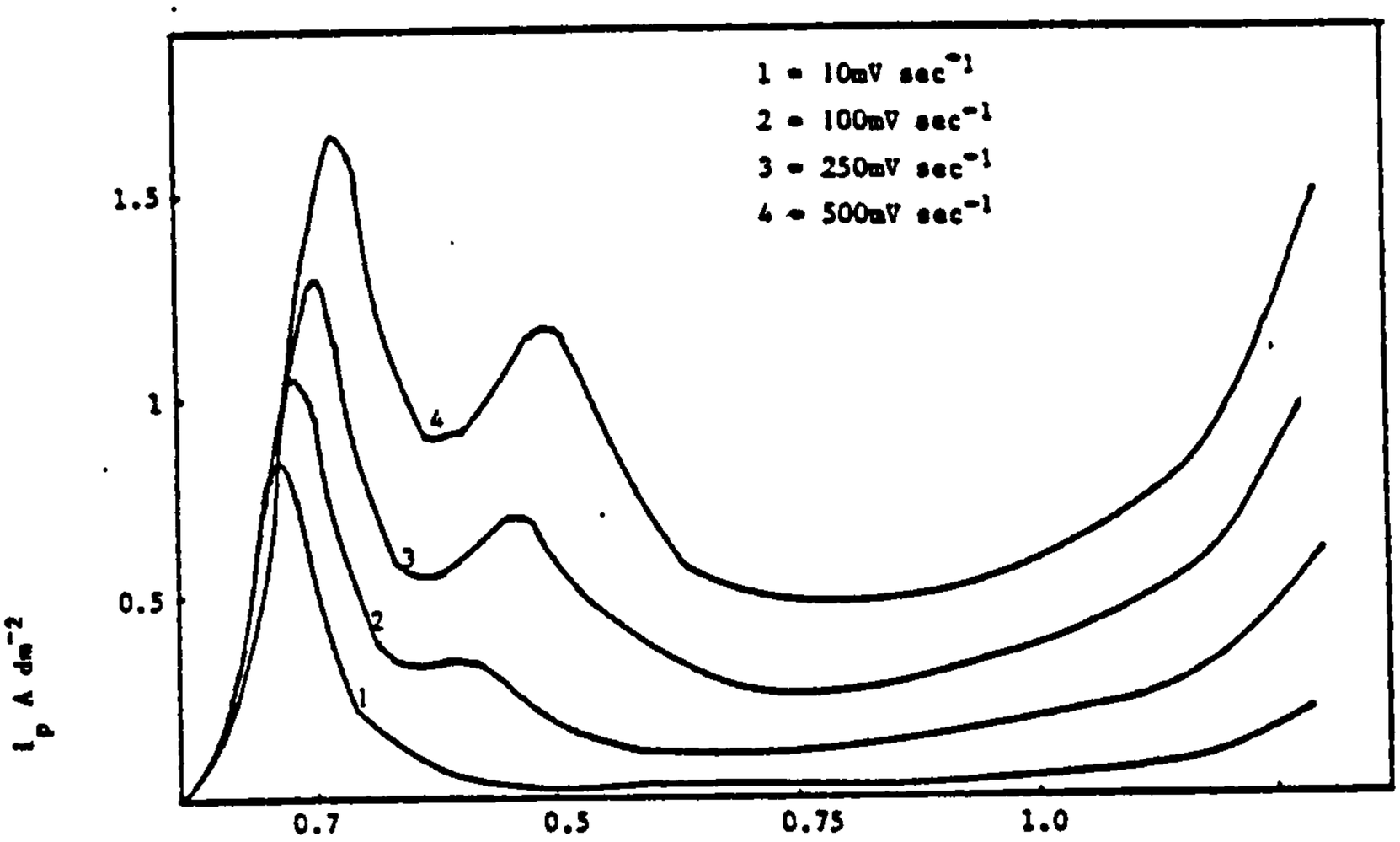

E vs i curves for a Ni electrode anodically polarised from its rest potential in a 1M KNO_3 solution pH 1.72 at different sweep rates.

FIGURE 218

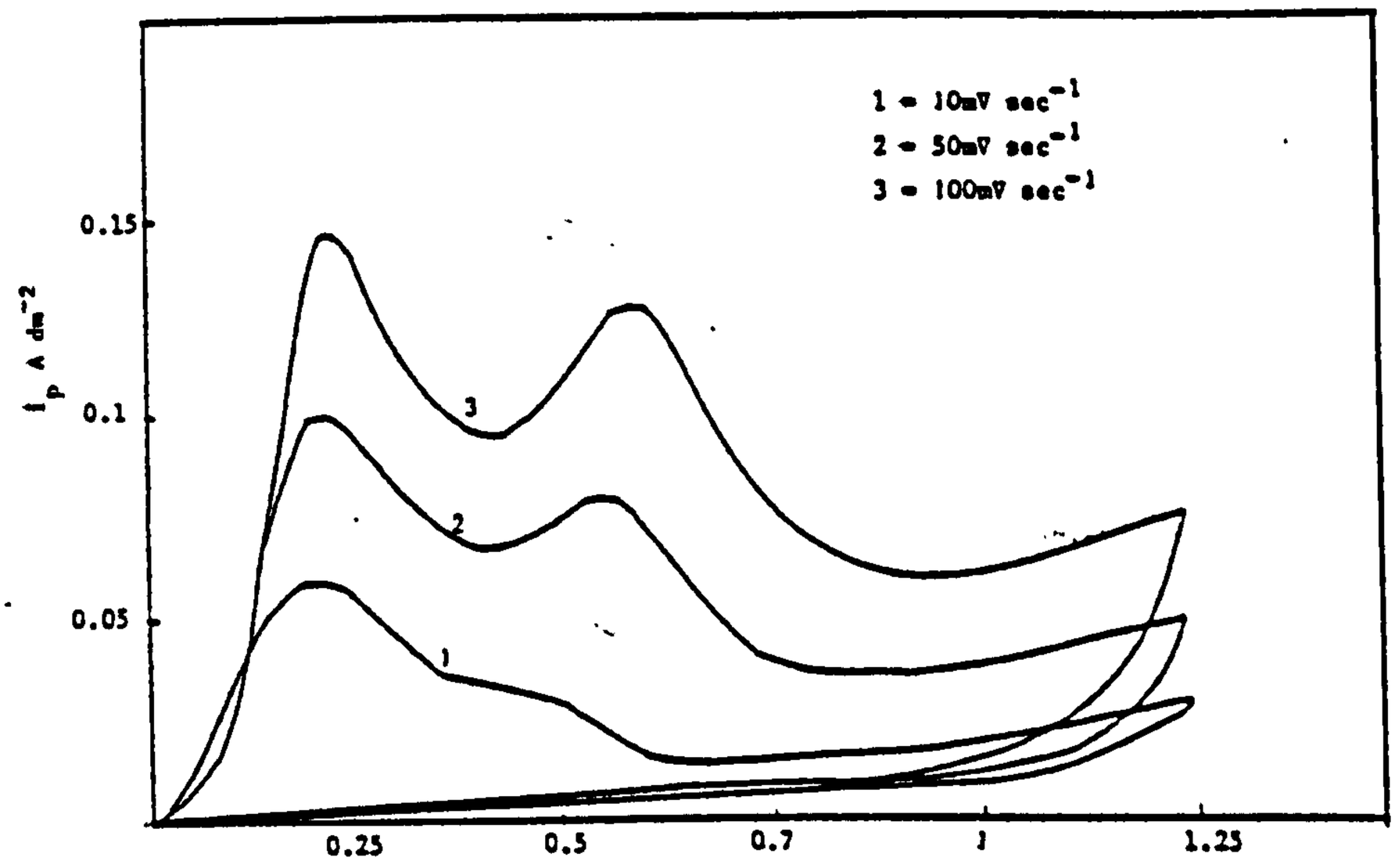

E vs i curve for a Ni electrode anodically polarised from its rest potential in a 1M KNO_3 solution pH 2.56 at different sweep rates.

FIGURE 219

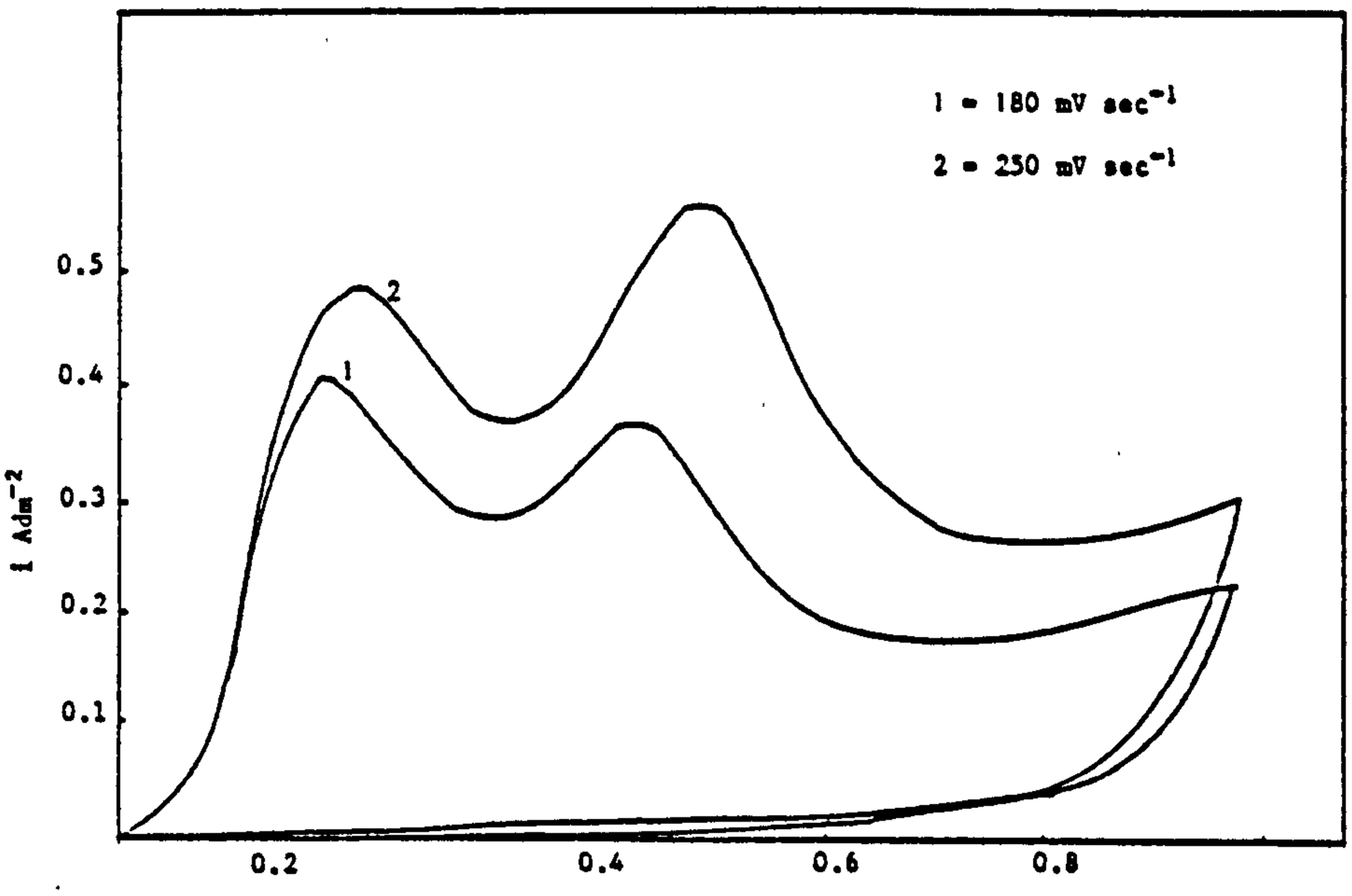

E vs i curve for a Ni electrode anodically polarised from its rest potential in 1M KNO_3 pH 2.56 at selected sweep rates.

FIGURE 220

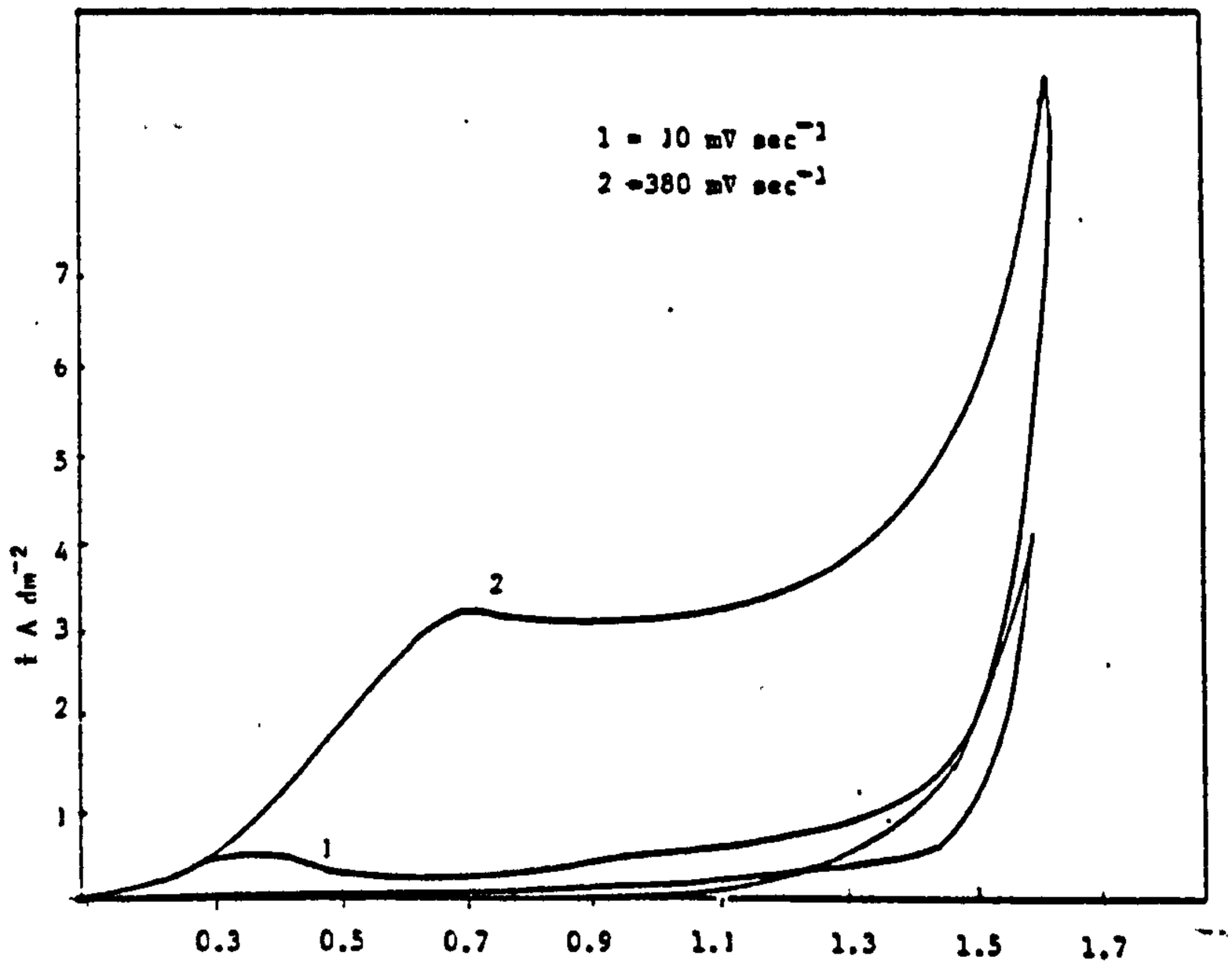

A graph of E vs i for a Ni electrode anodically polarised at different sweep rates in a 1M KNO_3 solution pH 4.1.

FIGURE 221

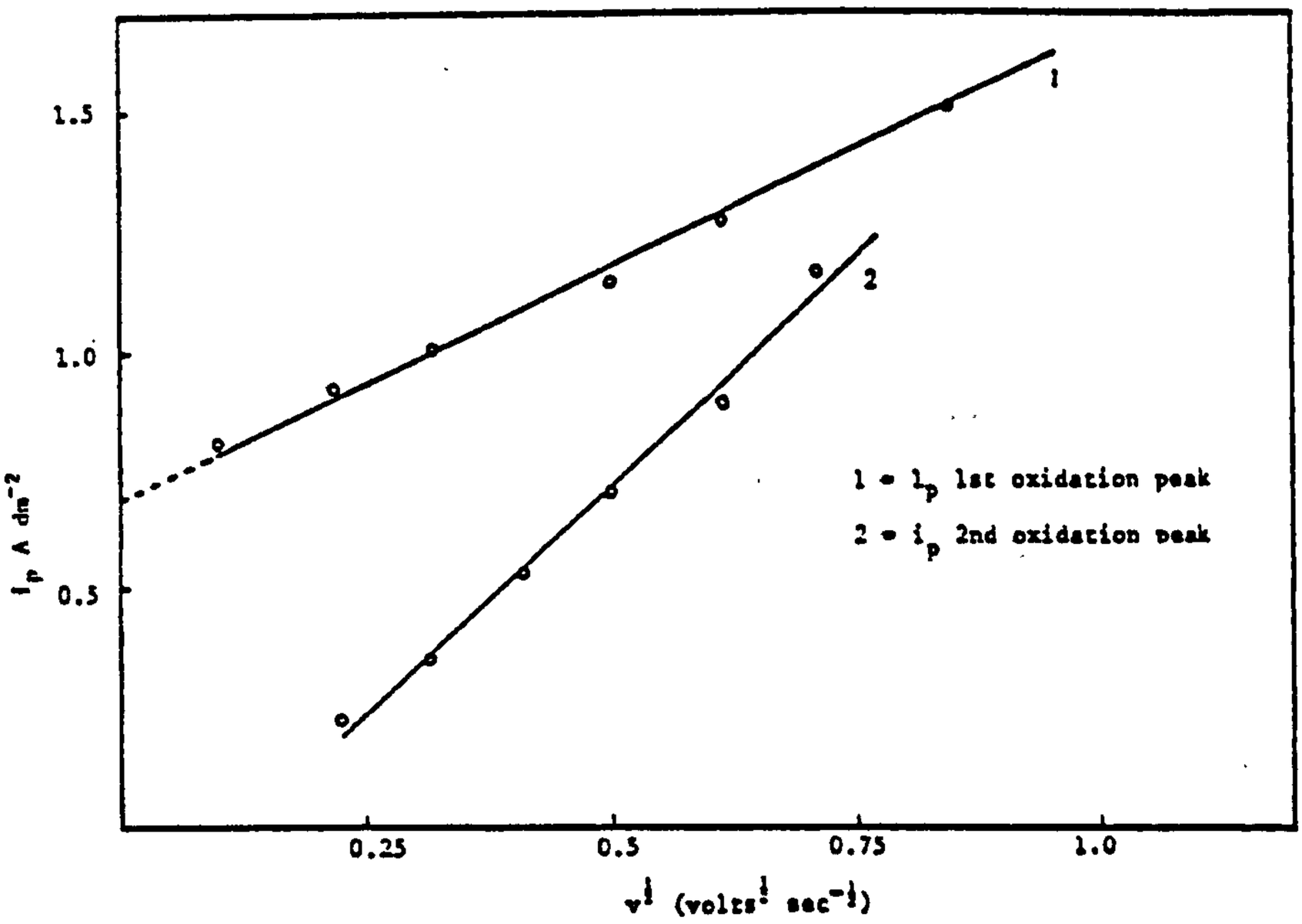

A graph of i_p vs $v^{\frac{1}{2}}$ for a Ni electrode anodically polarised in a 1M KNO_3 solution pH 1.72.

FIGURE 222

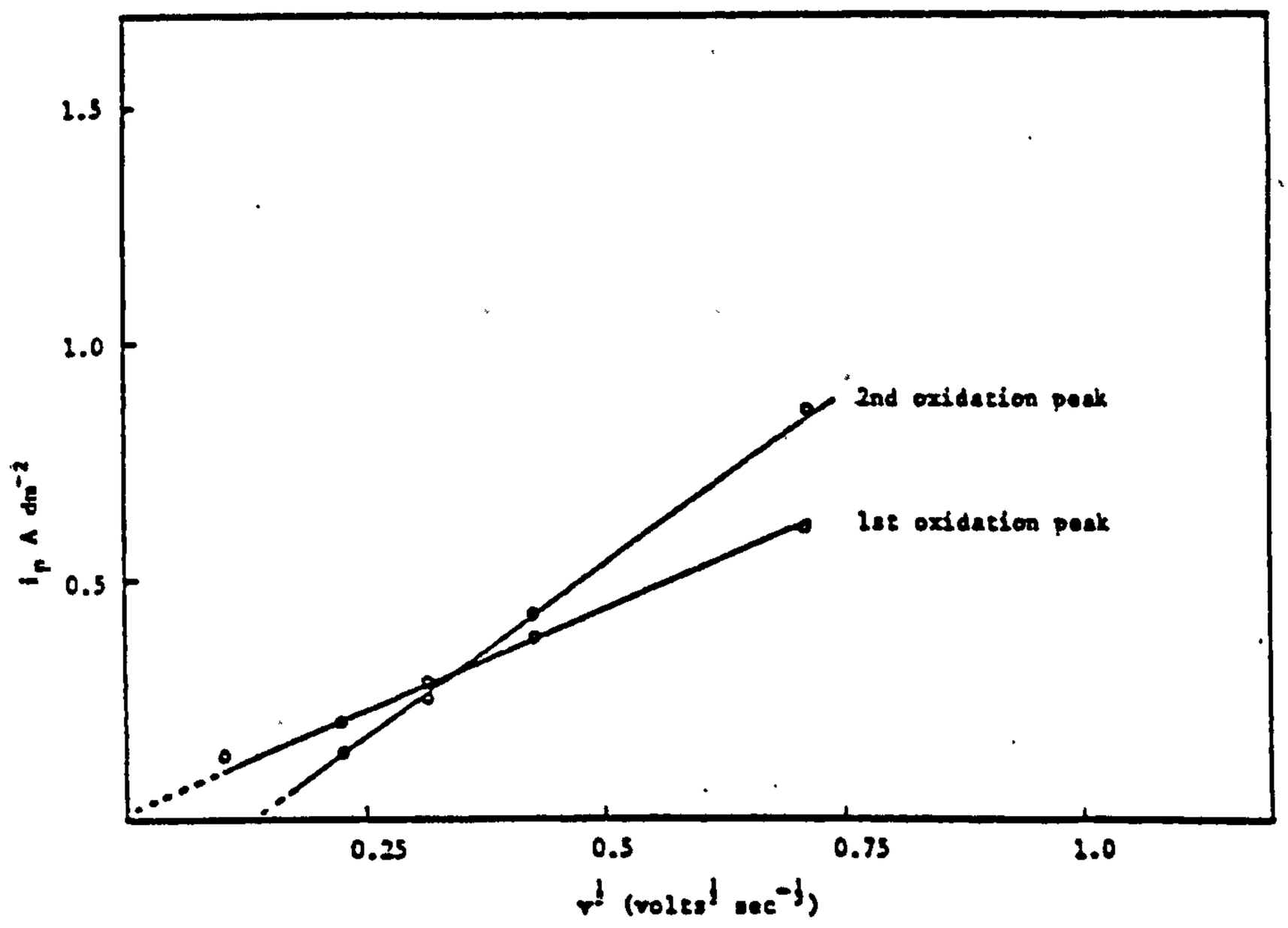

A graph of i_p vs $v^{\frac{1}{2}}$ for a Ni electrode anodically polarised in a solution of 1M KNO_3 pH 2.56.

FIGURE 223

second passivation peak. In pH4 solutions a linear relationship between i_p and $v^{1/2}$ was observed but only one for passivation peak present, see Fig. 224.

In the case of these solutions it was found difficult to identify the passivation peaks at high sweep speeds with a graph of i_p vs $v^{1/2}$ only linear up to sweep speeds of 100mV sec^{-1} (see Fig. 224).

The relationship between i_p and $v^{1/2}$ has been explained by Muller (320) (assuming the film formation process to be under ohmic resistance control).

The expression for peak current is :

$$i_p = (nF\rho K)^{1/2} A_o (1 - 0_p) \quad v^{1/2}$$
$$M$$

where n = number of electrons involved in charge transfer

F = Faradays constant

K = Specific conductivity of the solution inside pores

ρ = film density

M = molecular weight

0_p = fraction of initial electrode surface (A_o) covered

A similar relationship is found to exist between passivation potential E_{pp} and sweep rate and is given by :

$$E_p = E_o + (nFK)^{1/2} \quad d + \quad A_o (1- 0_p) v^{1/2}$$

where R = resistance of external circuity

d = film thickness

E_o = minimum potential for film formation

A linear relationship between E_{pp} and $v^{1/2}$ was observed (see Figs. 225, 226 and 227) and the values of E_{pp} in solutions of different pH are given in Table 75.

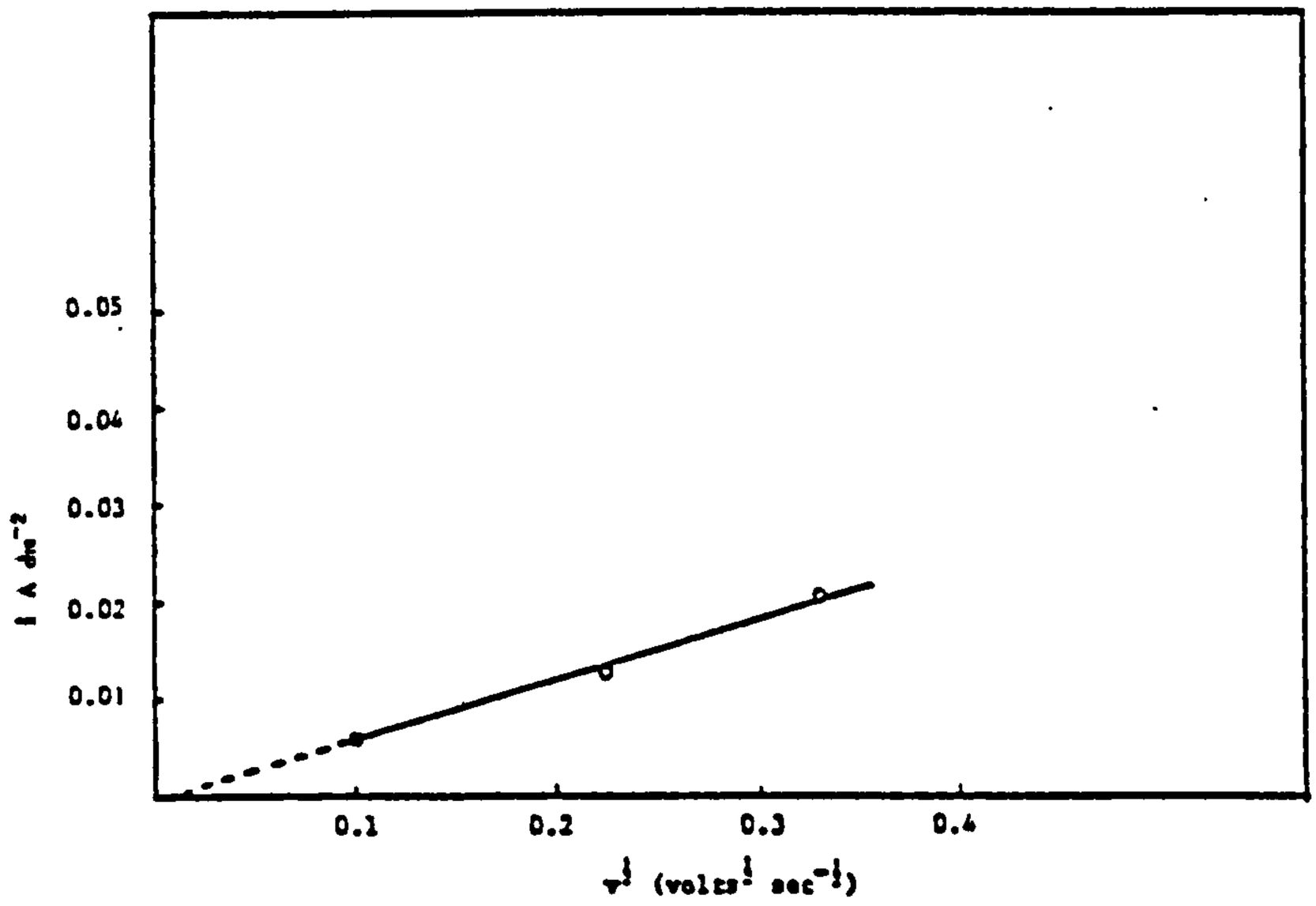

A graph of i_p vs $v^{\frac{1}{2}}$ for a Ni electrode anodically polarised in a solution of 1M KNO_3 pH4.

FIGURE 224

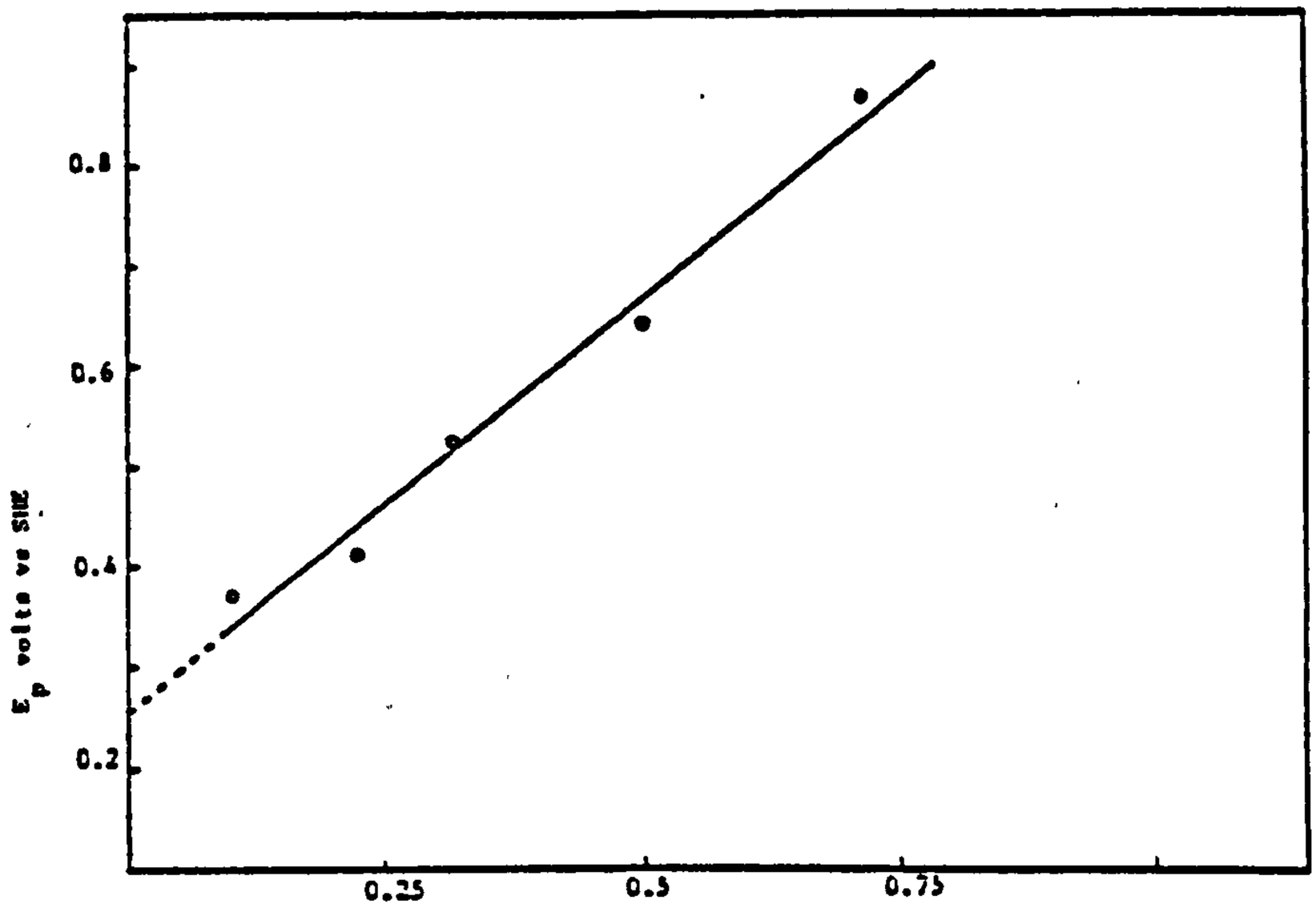

A graph of E_p vs $v^{\frac{1}{2}}$ for a Ni electrode anodically polarised in a 1M KNO_3 solution pH1.

FIGURE 225

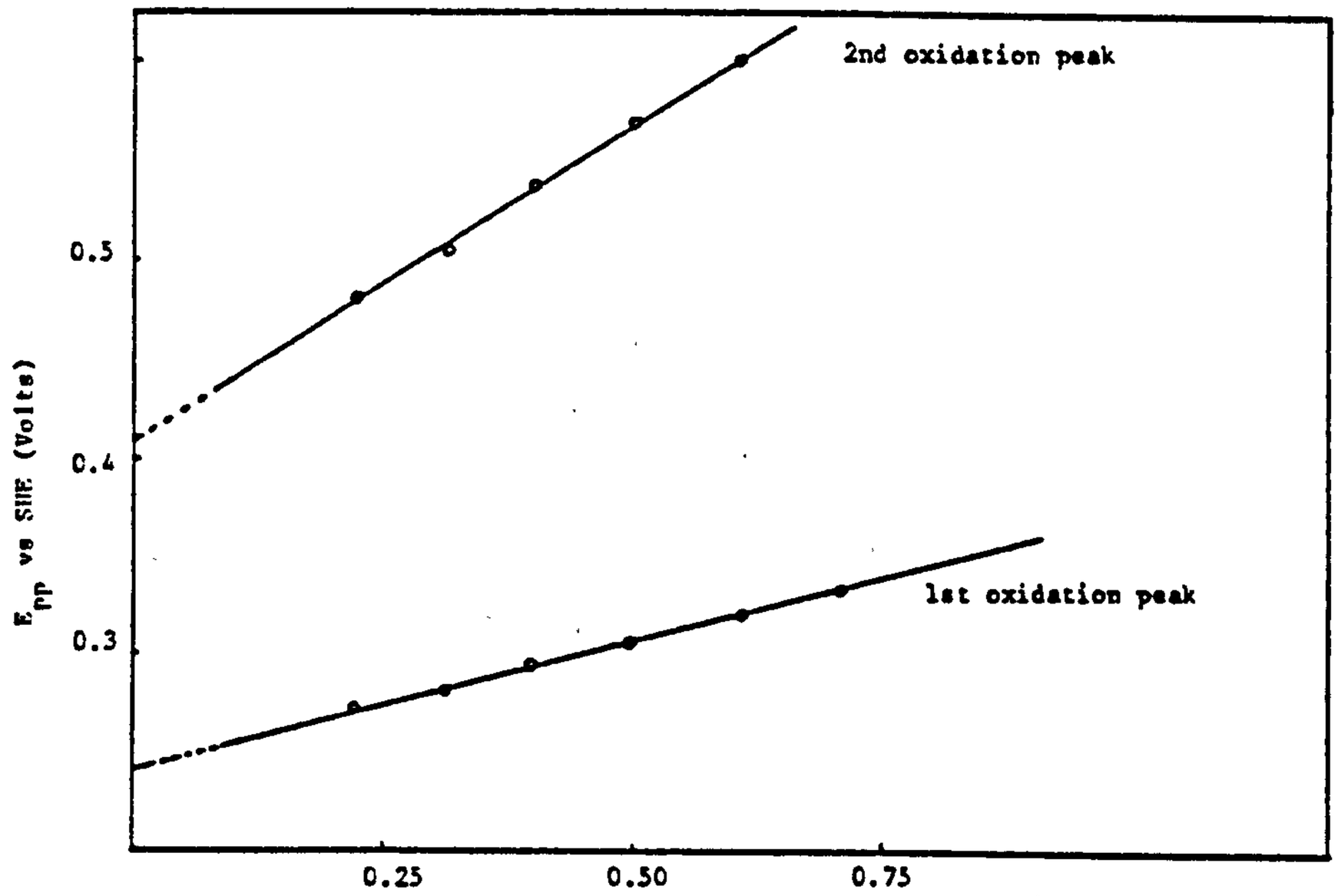

A graph of E_{pp} vs $v^{\frac{1}{2}}$ for the two oxidation peaks observed when a Ni electrode was anodically polarised in a solution of 1M KNO_3 pH 1.76.

FIGURE 226

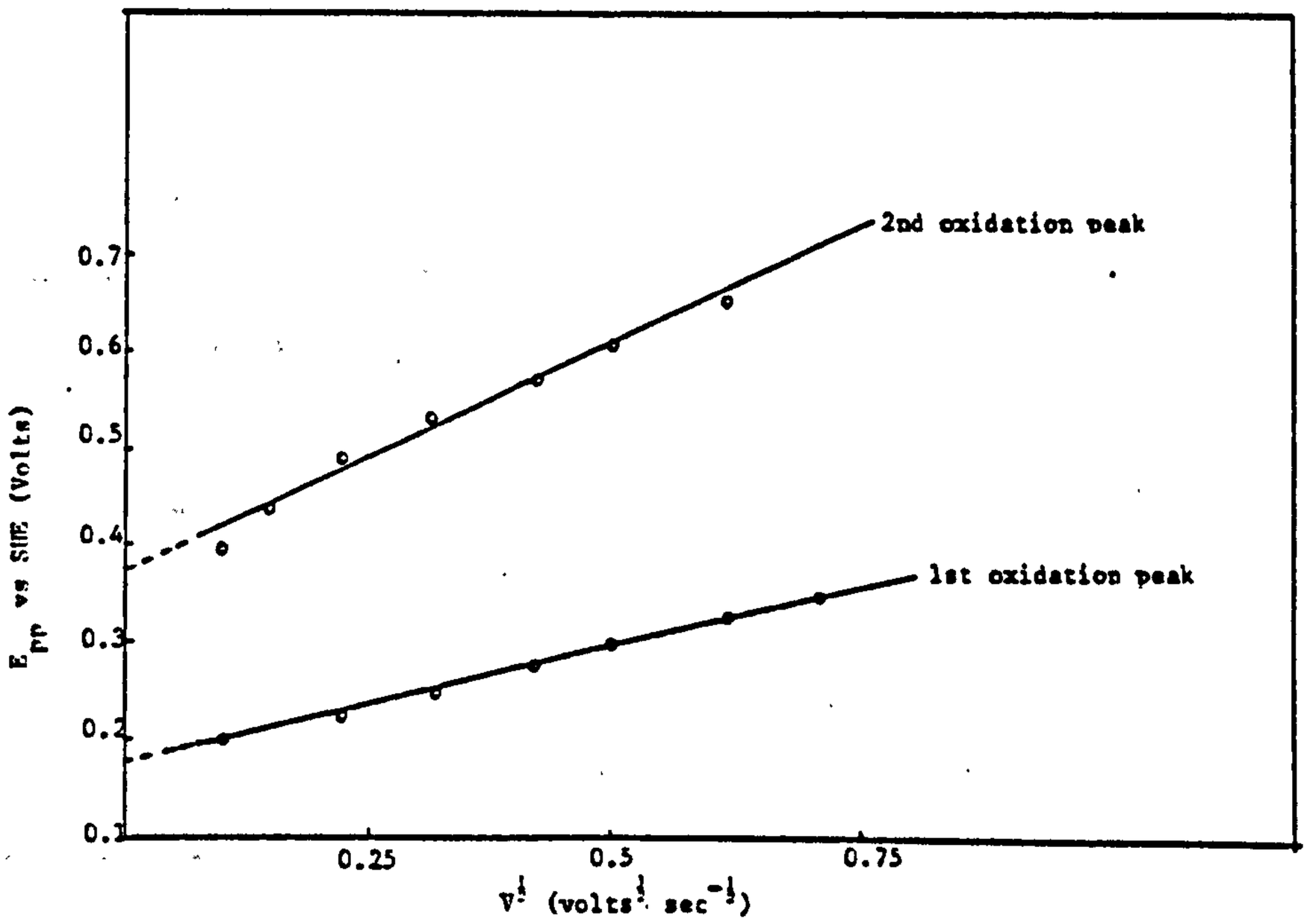

A graph of E_{pp} vs $v^{\frac{1}{2}}$ for a Ni electrode anodically polarised in a solution of 1M KNO_3 pH 2.56.

FIGURE 227

A linear relationship between E_{pp} vs pH was observed as is evident from Fig 228, from which it was possible to determine a value of E_o for the respective oxides.

The value of E_o for the first oxidation peak was found to follow the relationship.

$$E_{pp} = 0.34 - 0.065 \text{ pH}$$

Whilst for the value of E_{pp} for the second oxidation peak was found to obey the following relationship;

$$E_{pp} = 0.50 - 0.057 \text{ pH}$$

The above values for E_o are each based on the results of 3 separate experiments and should only be considered to give an indication of E_o and not be used as accurate values. Further work would be necessary before any statistical significance can be applied to these results.

TABLE 75

Variation of E_o with pH for a Ni electrode anodically polarised in a 1M KNO_3 solution at different pH's

pH of 1M KNO_3 solution	Value of E_{pp} (Volts)	
	1st passivation peak	2nd passivation peak
1	0.272	-
1.76	0.242	0.415
2.56	0.175	0.375
4.00	-	0.275

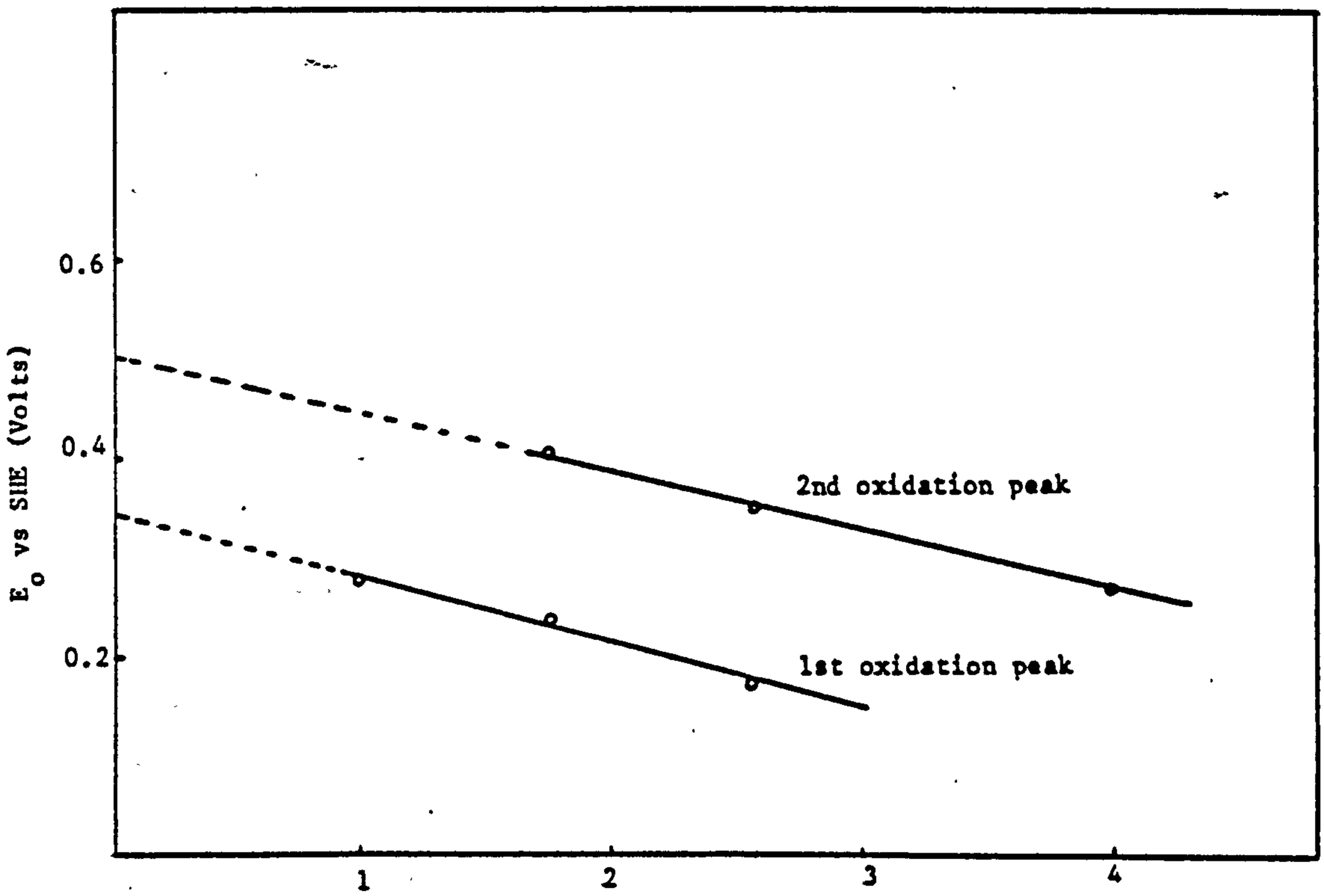

A graph of E_o vs pH for the anodic polarisation of a Ni electrode in a solution of 1M KNO_3. The values of E_o at a given pH obtained by extrapolation of the graphs of E_{pp} vs $v^{\frac{1}{2}}$ to zero sweep rate.

FIGURE 228

The value of E_o for a 1M KNO_3 solution of pH4 is + 0.275 V for the first oxidation peak this was found to fit onto the E_o vs pH plot for the second passivation peak obtained from other solutions (see Fig. 228).

The Tafel slope for Ni dissolution was also found to be pH dependent in 1M KNO_3 with values of approximately 120 mV per decade in pH 4 solution 65mV in pH 2.56, 55mV per decade in pH 1.76 and 45 mV per decade for solutions of pH 1, all values were obtained at sweep rate of 10 mV sec^{-1}.

3.5.5 Effect of the addition of selected anions on Ni passivity in NO_3^- solutions

The concentration of foreign anions in a stock solution of 1M KNO_3 of pH's 1, 2.5 and 4 was altered to see what effect, if any, small concentrations of impurity anion had on Ni passivity in nitrate solutions.

The anions selected for these studies were BF_4^-, F^-, $NH_2SO_3^-$, SiF_6^{2-}, sodium gluconate and sodium ethylenediamine tetra acetic acid all of which are used in Pb plating solutions with the exception of F^- which is used as a grain refining agent in PbO_2 deposition.

All the anions studied were found to effect both the active and passive dissolution of Ni to varying degress. The inorganic anions particularly BF_4^- and F^- were found to decrease the range of Ni passivity however an increase in the organic anion concentration actually reduced the values of i_{pp} at a given pH.

3.5.5.1 The effect of sodium ethylenediaminetetraacetic acid (Na EDTA) on Ni passivity in NO_3^- solutions

Na EDTA has a limited solubility in 1M KNO_3 solutions and when added altered the pH to approximately 2. The pH of each solution was then adjusted with KOH or HNO_3 depending upon the required pH.

As can be seen from Figs. 229, 230, 231 increase in the Na EDTA concentration had a significant effect on the value of i_{pp} and reduced the values of i_{pass} in the potential range up to + 1.1 V.

This can be seen in Table 76 where the values of i_{pp} for a Ni electrode in solutions of 1M KNO_3 of different pH and with selected concentrations of Na EDTA are given

In a 1M KNO_3 solution pH 1 increase in the Na EDTA was found to decrease the free corrosion rate from 7×10^{-5} Acm^{-2} in the absence of Na EDTA, to 1.8×10^{-5} Acm^{-2} with 0.001 M Na EDTA and to 4×10^{-6} Acm^{-2} with 0.005 M Na EDTA.

TABLE 76

Variation of i_{pp} for a Ni electrode anodically polarised at 5 mV sec^{-1} in 1M KNO_3 solutions of different pH, with selected Na EDTA concentrations

pH of 1M KNO_3 solution	Value of i_{pp} (Adm^{-2}) for Ni dissolution in 1M KNO_3 containing selected Na EDTA concentrations at different pH's		
	OM Na EDTA	0.001 M Na EDTA	0.005 M Na EDTA
1	2.4	1:5	0.11
2.5	0.17	0.11	0.0044
4	0.0078	0.0044	0.0037

An increase in transpassive dissolution was observed with increase in Na EDTA concentration, with a peak current detected at + 1.4 Volts at pH1, + 1.35 volts at pH 2.5 and + 1.3 volts at pH 4 for 1M KNO_3 all with 0.005M Na EDTA additions. This apparent transpassive dissolution region is attributed to anodic oxidation of the ethlyenediaminetetra-acetic acid.

The value of the Tafel slope for Ni dissolution in the active region of approximately 45mV per decade was found to be essentially independent of EDTA concentration, only in low pH solutions.

However, in the active region for Ni dissolution the current density at a given potential was found to be dependent upon EDTA concentration, increase in EDTA concentration reducing the current density at a given potential. An insufficient number of values were obtained to produce an accurate value of the d log i/d [NaEDTA] at constant potential, although initial results indicate a slope of -1.5. The value of E_{pp} did also decrease but not significantly with increase in EDTA concentration e.g from +0.355 V at OM EDTA, to + 0.320 V at 0.001M and 0.005M EDTA in 1M KNO_3 solutions of pH1.

In a solution of 0.005M NaEDTA + 1M KNO_3, pH1 a second passivation peak was visible at approximatley +0.055V vs SHE. In pH 2.5 solutions the nature of the E vs log i altered with increase in NaEDTA and for a solution of 0.005M NaEDTA + 1M KNO_3 pH 2.5 the first oxidation peak was absent and only a passivation peak at +0.058 V was recorded. The active dissolution of Ni was visibly affected by an increase in NaEDTA concentration with the value of the Tafel constant in the 0.005M NaEDTA solution recorded as 430 mV per decade.

In pH4 solutions NaEDTA still appeared to affect the anodic dissolution of Ni although not to such an appreciable extent as in the low pH solutions and had only a limited effect in reducing the value for $i_{passive}$. The value of E_{pp} was also found to increase with NaEDTA from 0.32V in 1M KNO_3 to 0.5V in 1M KNO_3 + 0.005M NaEDTA.

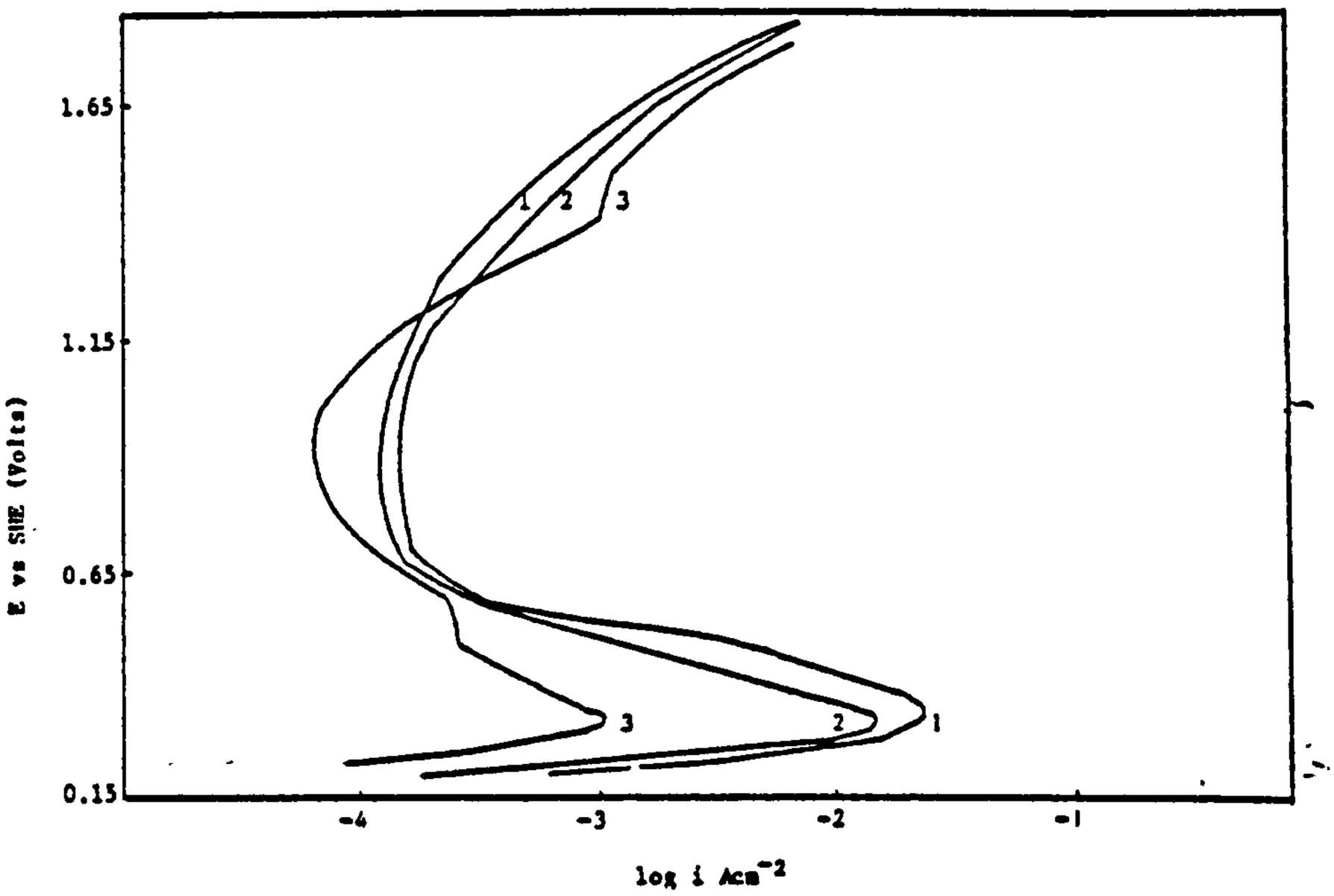

E vs log i curve for a Ni electrode anodically polarised at a sweep rate of 5 mV sec^{-1} in a solution of 1M KNO_3 pH 1.0 containing different concentrations of sodium ethylene damine-tetracetic acid (Na EDTA)

1 = 0 Na EDTA 2 = 0.00M Na EDTA 3 = 0.005M Na EDTA

FIGURE 229

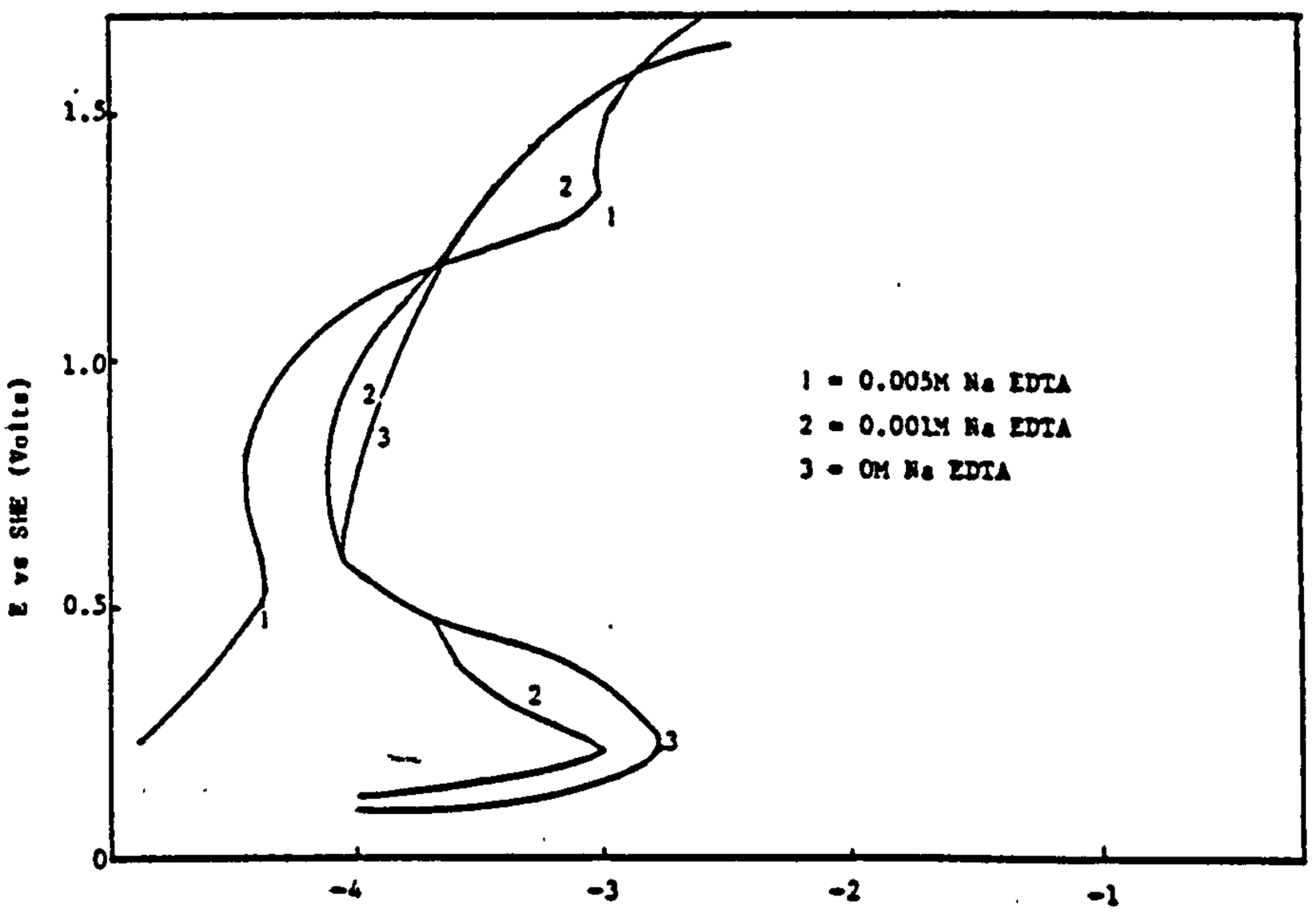

E vs log i curves for a Ni electrode anodically polarised at a sweep rate of 5mV sec^{-1} in a 1M KNO_3 solution pH 2.5 with and without sodium ethylene diamine tetra acetic acid (Na EDTA) additions.

FIGURE 230

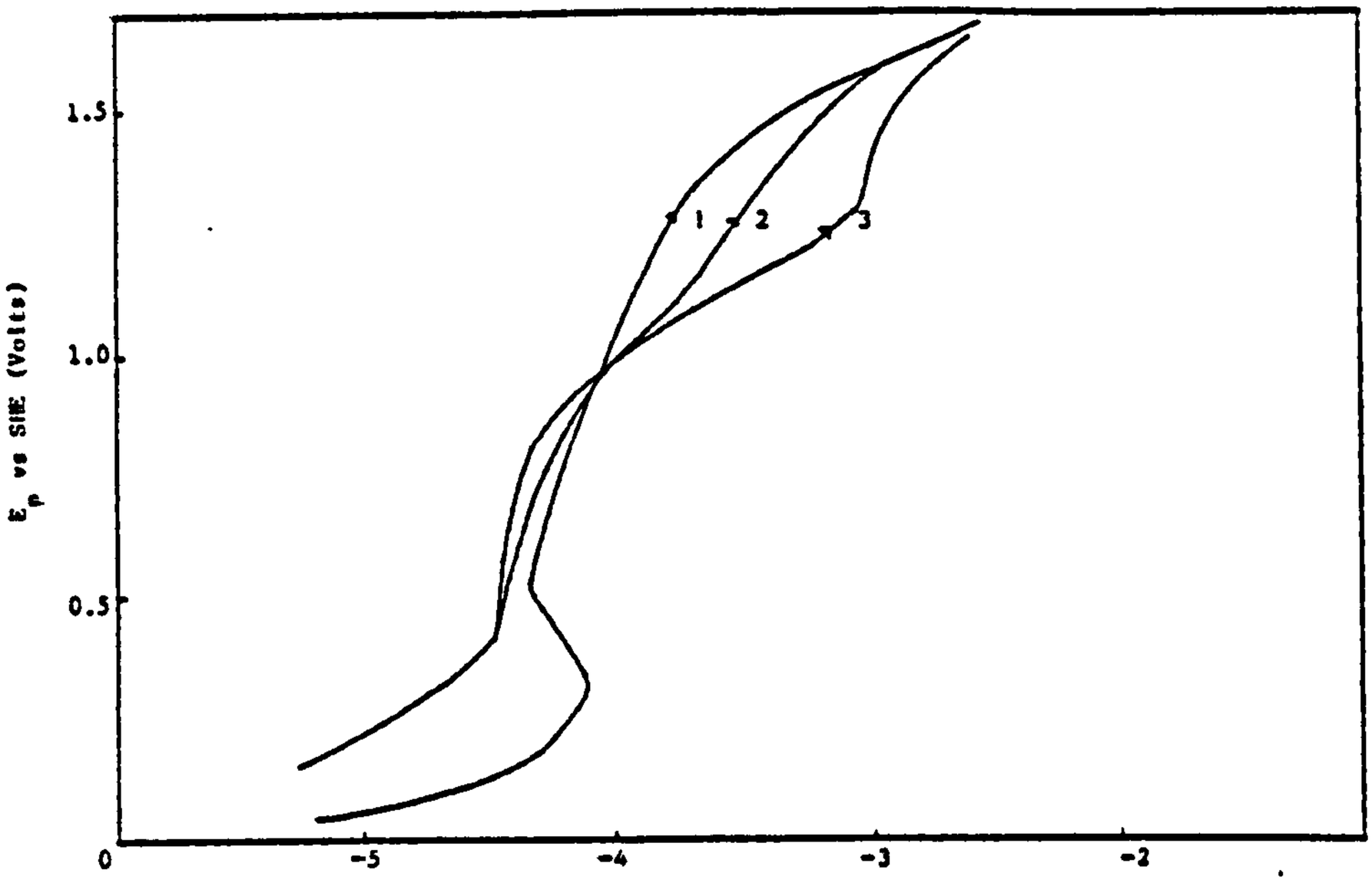

E vs log i curve for a Ni electrode anodically polarised at 5mV sec^{-1} in a solution of 1M KNO pH 4.0 containing different concentrations of sodium ethylenediamine-tetracetic acid (NaEDTA).

1 = No Na EDTA 2 = 0.001M Na EDTA 3 = 0.005M Na EDTA

FIGURE 231

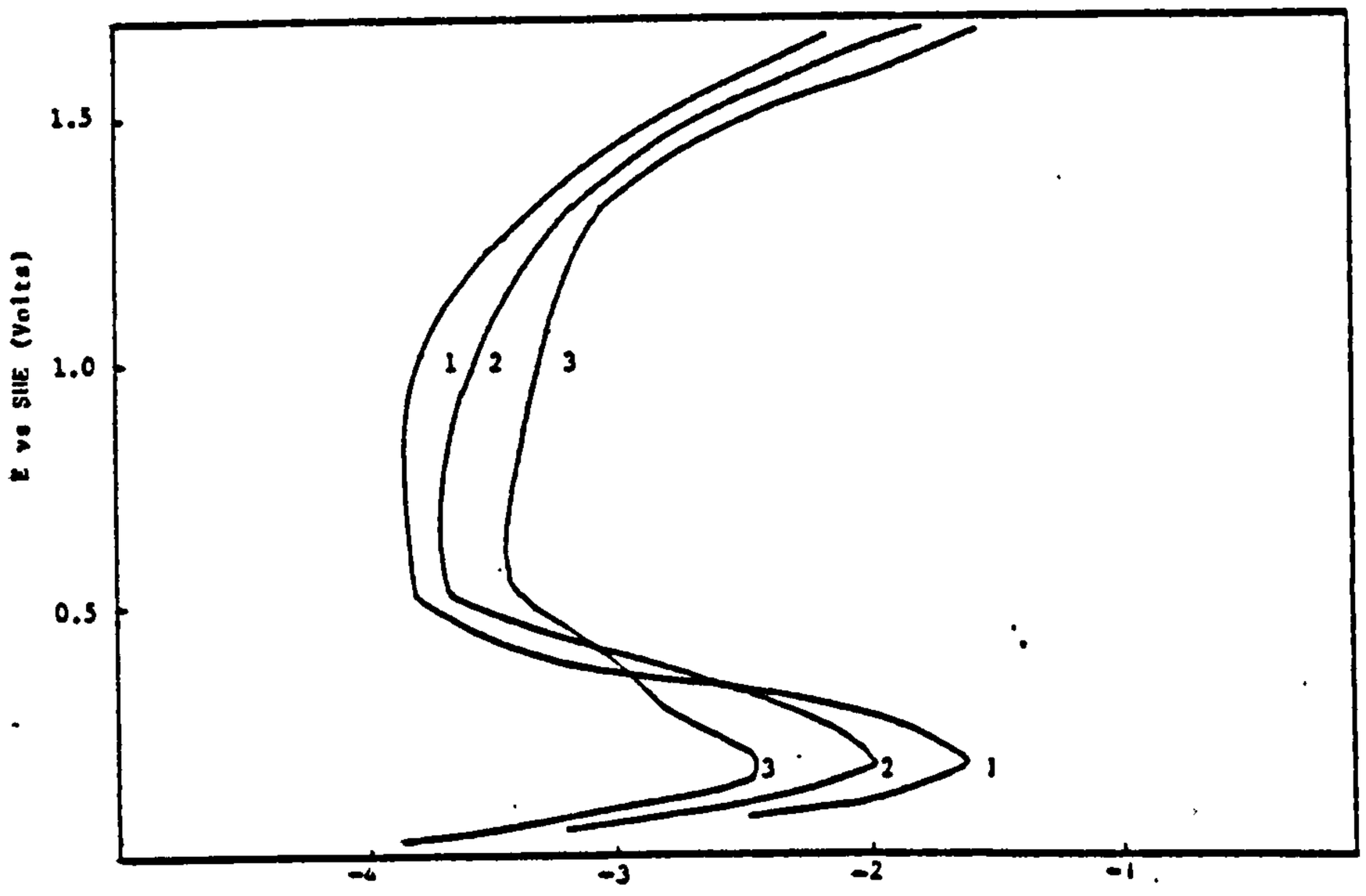

E vs log i for a Ni electrode anodically polarised at a sweep rate of 5mV sec^{-1} in a solution of 1M KNO pH 1.0 containing different concentrations of sodium gluconate

1 = 0.M sodium gluconate 2 = 0.05M sodium gluconate 3 = 1M sodium gluconate

FIGURE 232

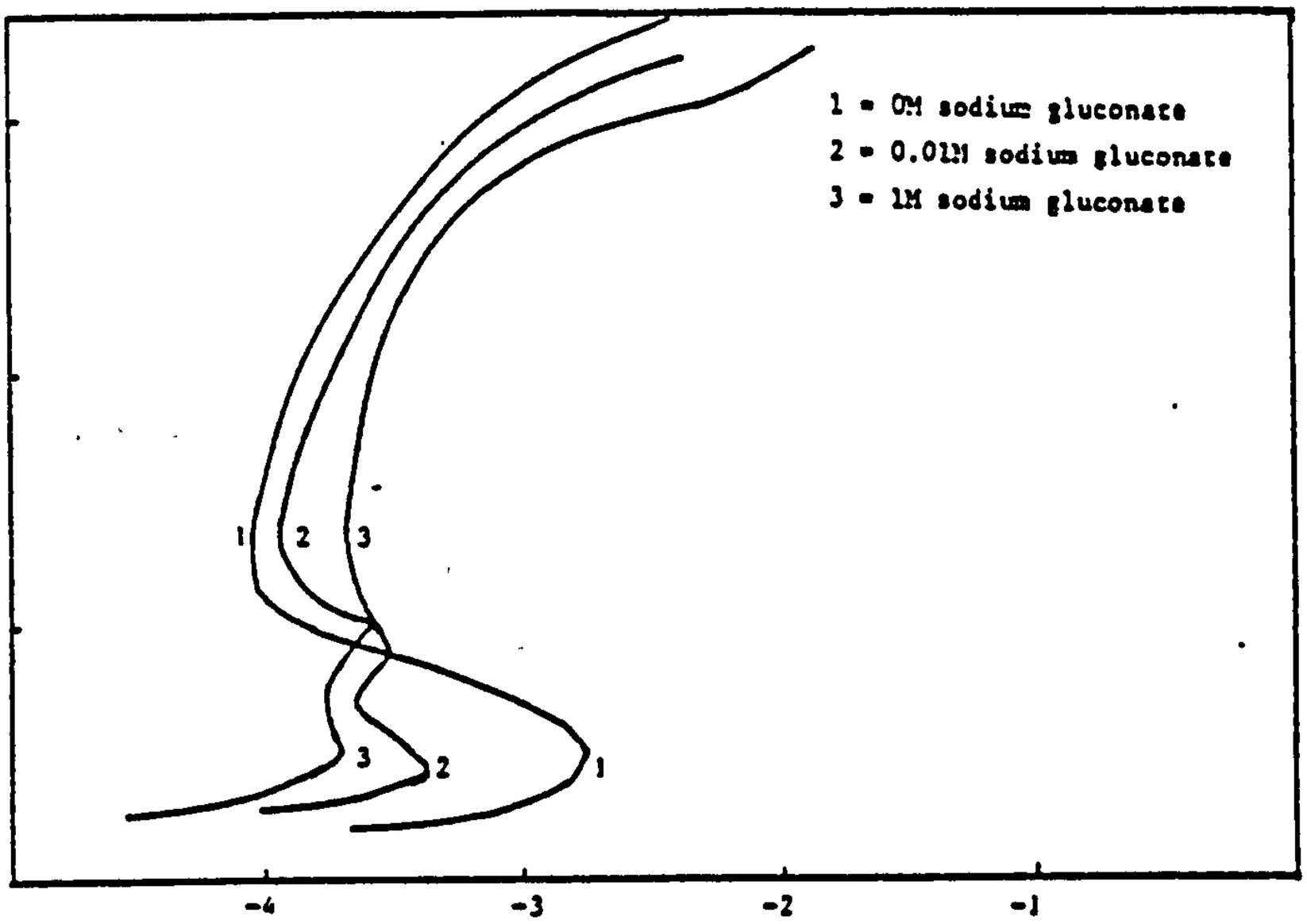

E vs log i for a Ni electrode anodically polarised at a sweep rate of 5mV sec^{-1} in a solution of 1M KNO_3 plus sodium gluconate pH 2.5.

FIGURE 233

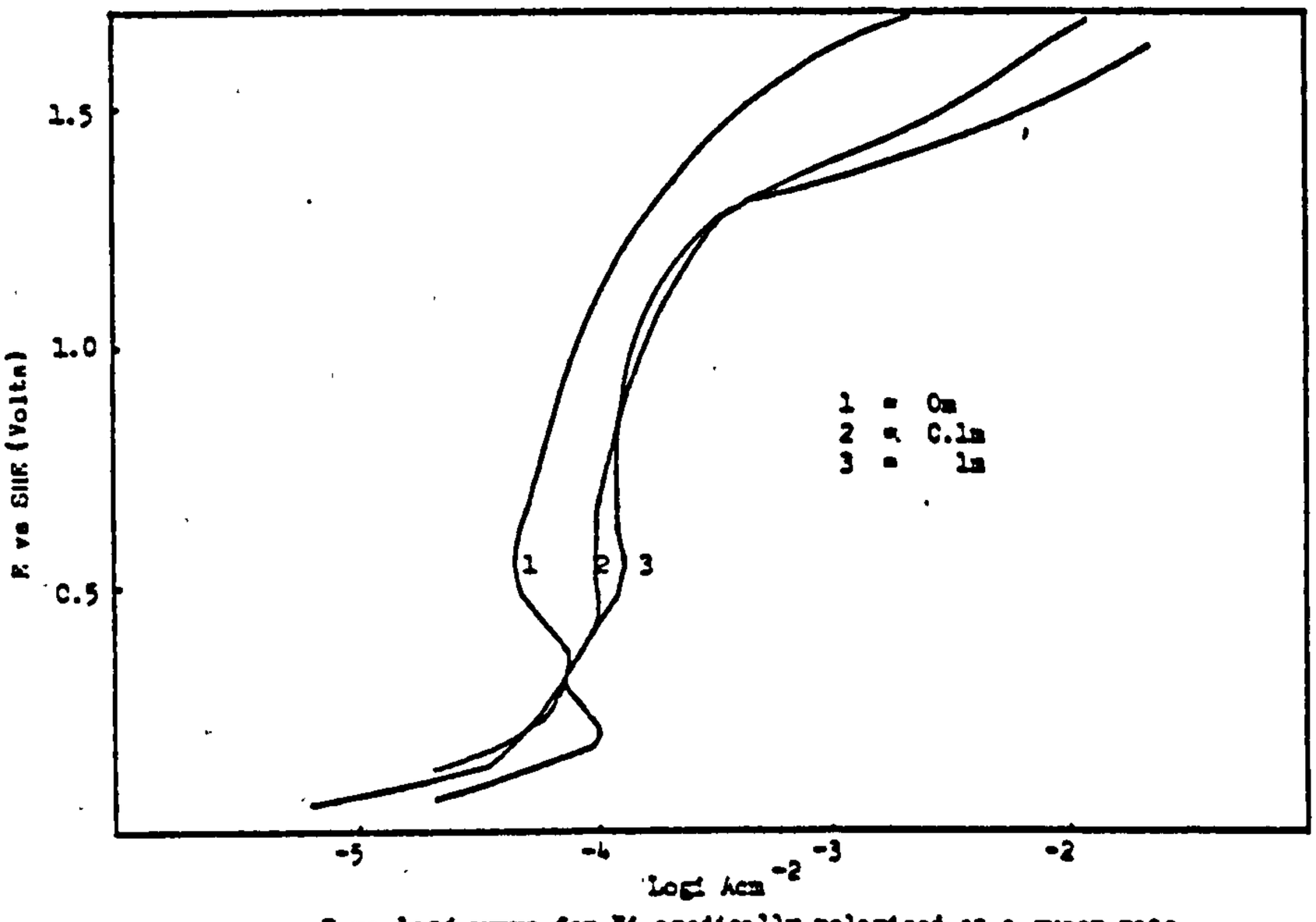

E vs log i curve for Ni anodically polarised at a sweep rate of 5mVsec^{-1} in a solution of 1M KNC, pH 4.0 containing selected concentrationsof Na gluconate.

FIGURE 234

3.5.5.2 The effect of sodium gluconate on Ni passivity in NO_3^- solutions

The effect of the addition of sodium gluconate to 1M KNO_3 solutions on Ni passivity was similar to that of EDTA, in that the rate of active dissolution of Ni decreased, with increase in concentration of sodium gluconate, although not to the same extent as with Na EDTA (see Figures 232 ,233, 234).

A graph of log i vs log [sodium gluconate] at constant potential yields a slope of +0.2 ± 0.05 for the active dissolution of Ni in a supporting electrolyte of 1M KNO_3, pH1.

In 1M KNO_3, pH 2.5 at high sodium gluconate concentrations, the presence of two passivation peaks was observed presumably due to the formation of higher valent nickel oxides, the second passivation peak occuring at +0.470V for 1M KNO_3 + 0.01M sodium gluconate and +0.530V for 1M KNO_3 + 1M sodium gluconate.

The rate of dissolution in the passive region was also found to be dependent upon potential and the concentration of sodium gluconate.

In high pH solutions (pH4) no reduction in the active dissolution of Ni was observed with increase in concentration of sodium gluconate, unlike the rate of passive dissolution which increased with increase in concentration of sodium gluconate (see Fig. 234).

The effect of sodium gluconate concentration on selected parameters for the anodic polarisation of Ni in 1M KNO_3 pH1 at 10mV sec^{-1} is given in Table 77.

3.5.5.3 Effect of NaF additions on Ni passivity in 1M KNO_3

NaF was found to effect both the active and passive dissolution of Ni (see Figs. 235, 236 and 237).

TABLE 77

The variation of E_{pp}, i_{pp} and minimum value of i_{pass} for the anodic polarisaton of Ni in 1M KNO_3 pH1 with different concentrations of sodium gluconate. The Ni electrode polarised at 10mV sec^{-1} from its rest potential at 25°C

Concentration sodium gluconate moles $litre^{-1}$	i_{pp} Adm^{-2}	E_{pass} Volts	i_{pass} Adm^{-2}	b mV $decade^{-1}$
0	2.4	+ 0.335	0.015	45
0.001	2.3	+ 0.335	0.016	45
0.05	1.03	+ 0.330	0.0204	55
0.1				
0.5	0.55	+ 0.310	0.030	50
1	0.36	+ 0.310	0.036	55

TABLE 78

The effect on NaF concentration on the values of i_{pp} for Ni dissolution in 1M KNO_3 pH1. The Ni electrode polarised at 10 mV sec^{-1} from its rest potential

Concentration of NaF moles $litre^{-1}$	i_{pp} for Ni dissolution in 1M KNO_3, pH1 Adm^{-2}
0	2.4
0.005	2.6
0.01	2.7
0.05	3.2
0.1 (saturated)	3.34

In a solution of 1M KNO_3 at pH 1 the rate of nickel dissolution was found to be independent of $[F^-]$ with a Tafel slope of approximately 50 mV per decade recorded. The value of E_{pp} was that recorded for a non flouride containing solution, at a sweep rate of 5 mV sec^{-1} i.e +0.350 V, although i_{pp} was found to increase slightly with increase in F^- concentration (see Table 78).

However, in a solution of 1M KNO_3 pH4 the rate of nickel dissolution was found to be dependent on $[F^-]$ with the slope of d log i/d log $[F^-]$ approximately equal to 1.

Passive film formation was more susceptible to increase in $[F^-]$ concentration. Indeed in high pH solutions the active to passive transition region is absent at high NaF concentrations, with no passivation peak detectable until + 0.850 V. The passiviation potential E_{pp} increases with an increase in NaF concentration.

In the active dissolution region for Ni a slope of log i (at constant potential) versus log $[F^-]$ of $+1 \pm 0.3$ was recorded, whilst at a potential of +0.7 V a slope of + 1.2 for log i vs $[F^-]$ was recorded. A large degree of scatter of the results was recorded, and the figures given above are only representative of observed trends.

The values of Tafel coefficient observed in pH 4 solutions were, 90mV per decade for non fluoride containing solution, 180 mV for 0.01M NaF and 55 mV per decade at 0.05M NaF. In contrast to solutions of low pH where no variation in Tafel slope was observed i.e at pH's 1 and 2.5, where a value of 45 to 50 mV per decade was observed.

3.5.5.4 The effect of $NaBF_4$ additions on the passivity of Ni in NO_3^- solutions

As with NaF, $NaBF_4$ additions affected both the active and passive transition regions for Ni in NO_3^- solutions (see Figs. 238, 239, 240).

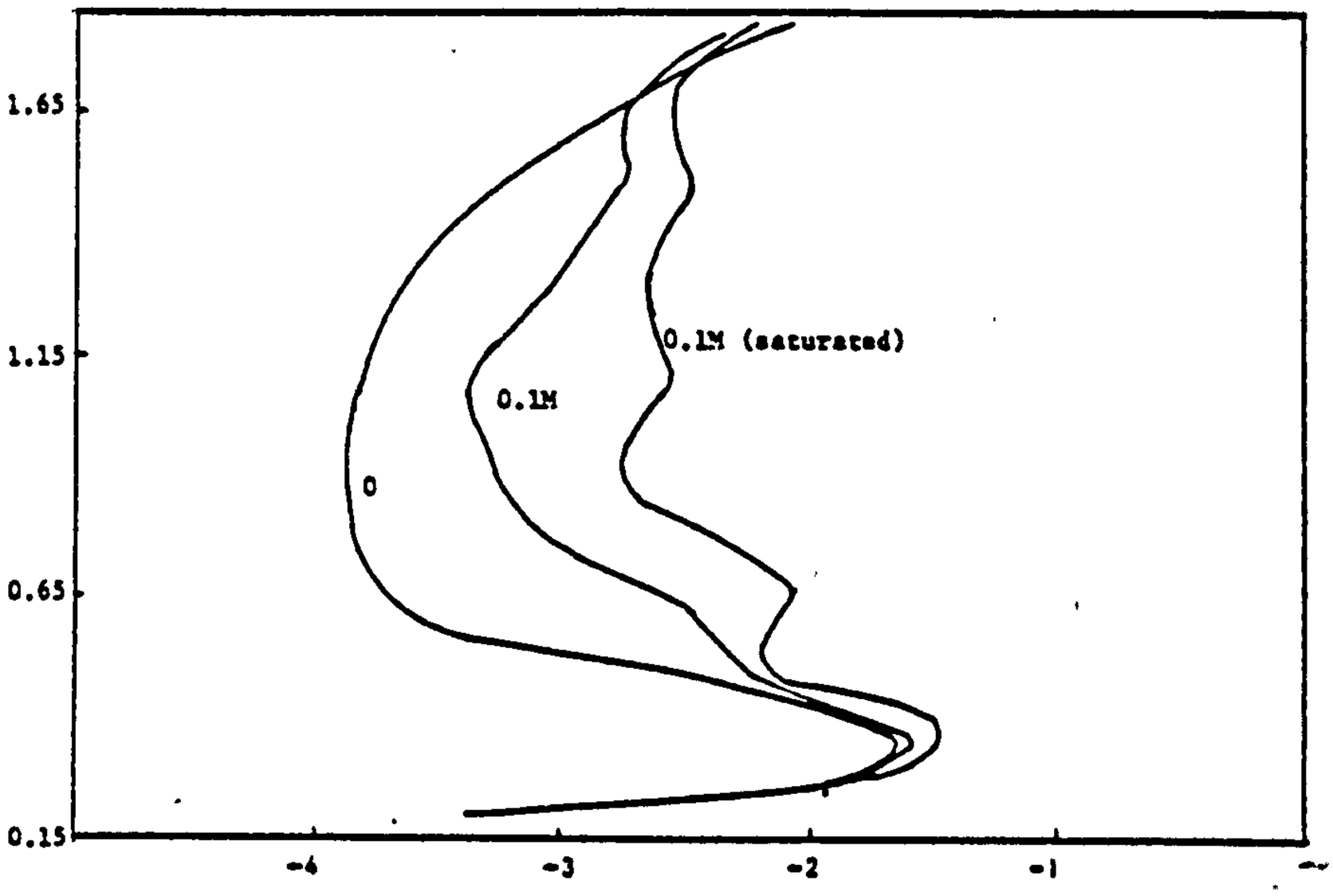

E vs log i curves for a Ni electrode anodically polarised at a sweep rate of 5mV sec^{-1} in a solution of 1M KNO_3 pH 1.0 with different concentrations of NaF.

FIGURE 235

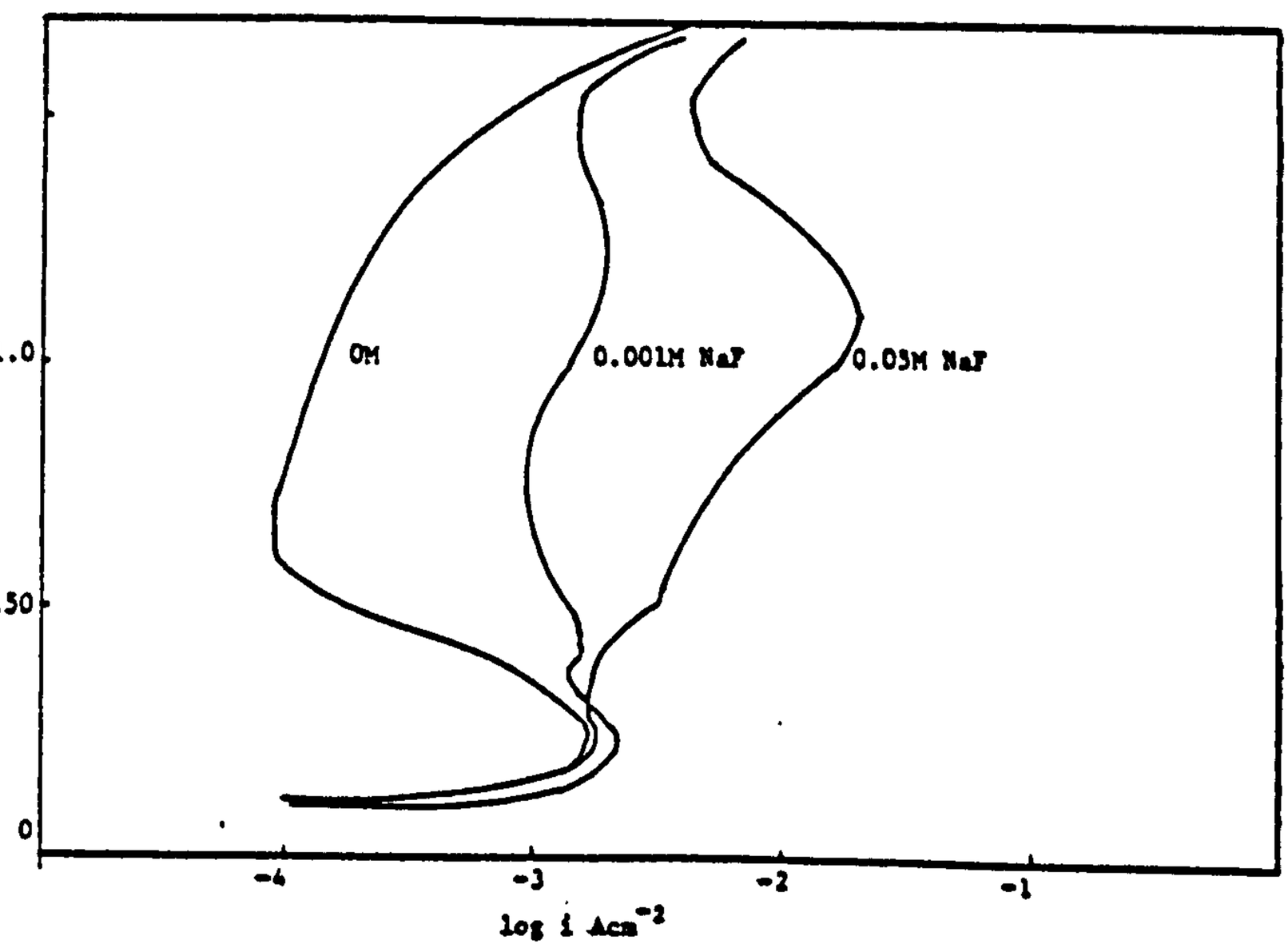

E vs log i curves for Ni electrode anodically polarised at a sweep rate of 5 mV sec^{-1} in a solution of 1M KNO_3 pH 2.5 with different NaF concentrations.

FIGURE 236

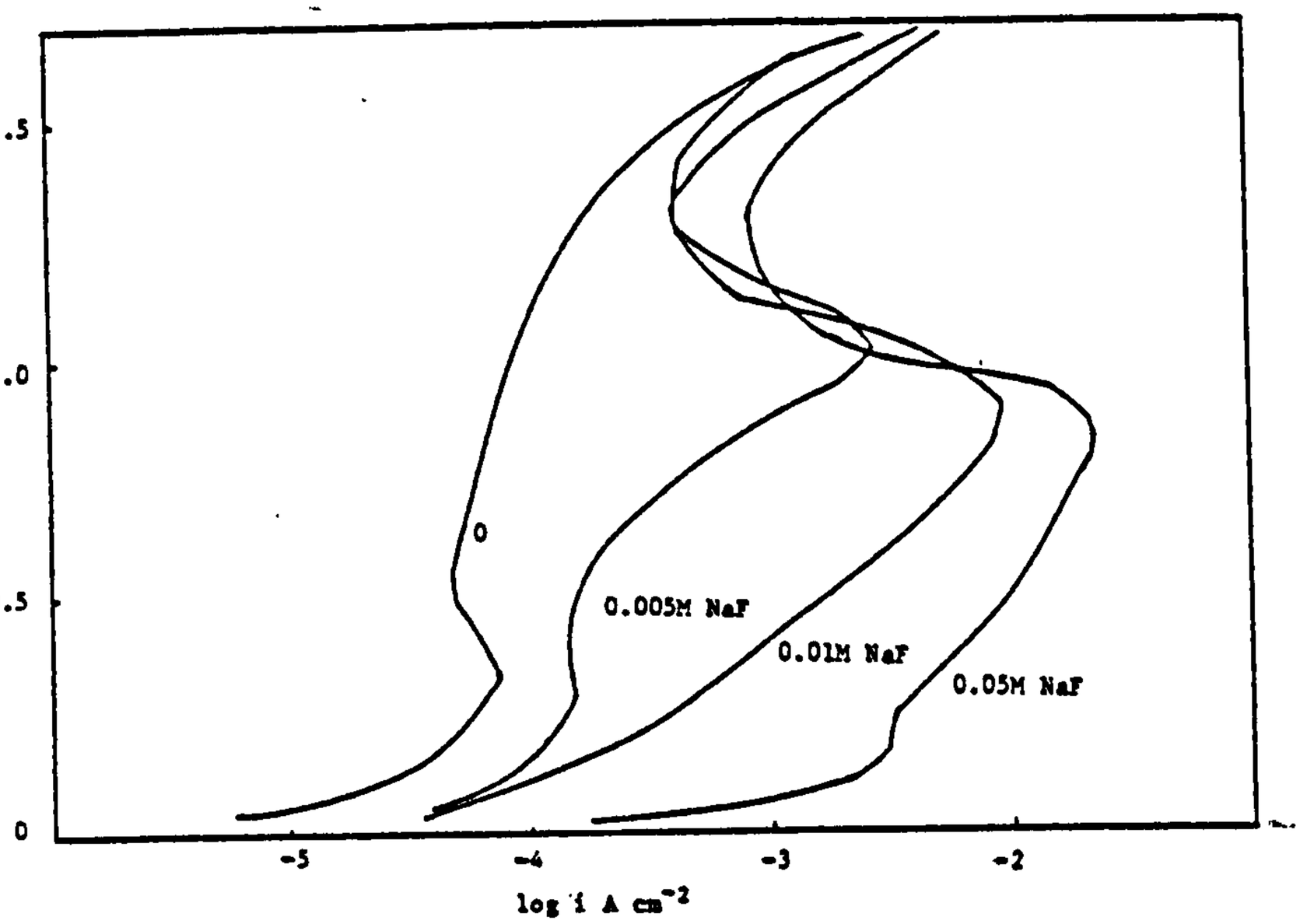

E vs log i curves for a Ni electrode anodically polarised at a sweep rate of 5mV sec^{-1} in a solution of 1M KNO_3 pH4 plus selected concentrations of NaF.

FIGURE 237

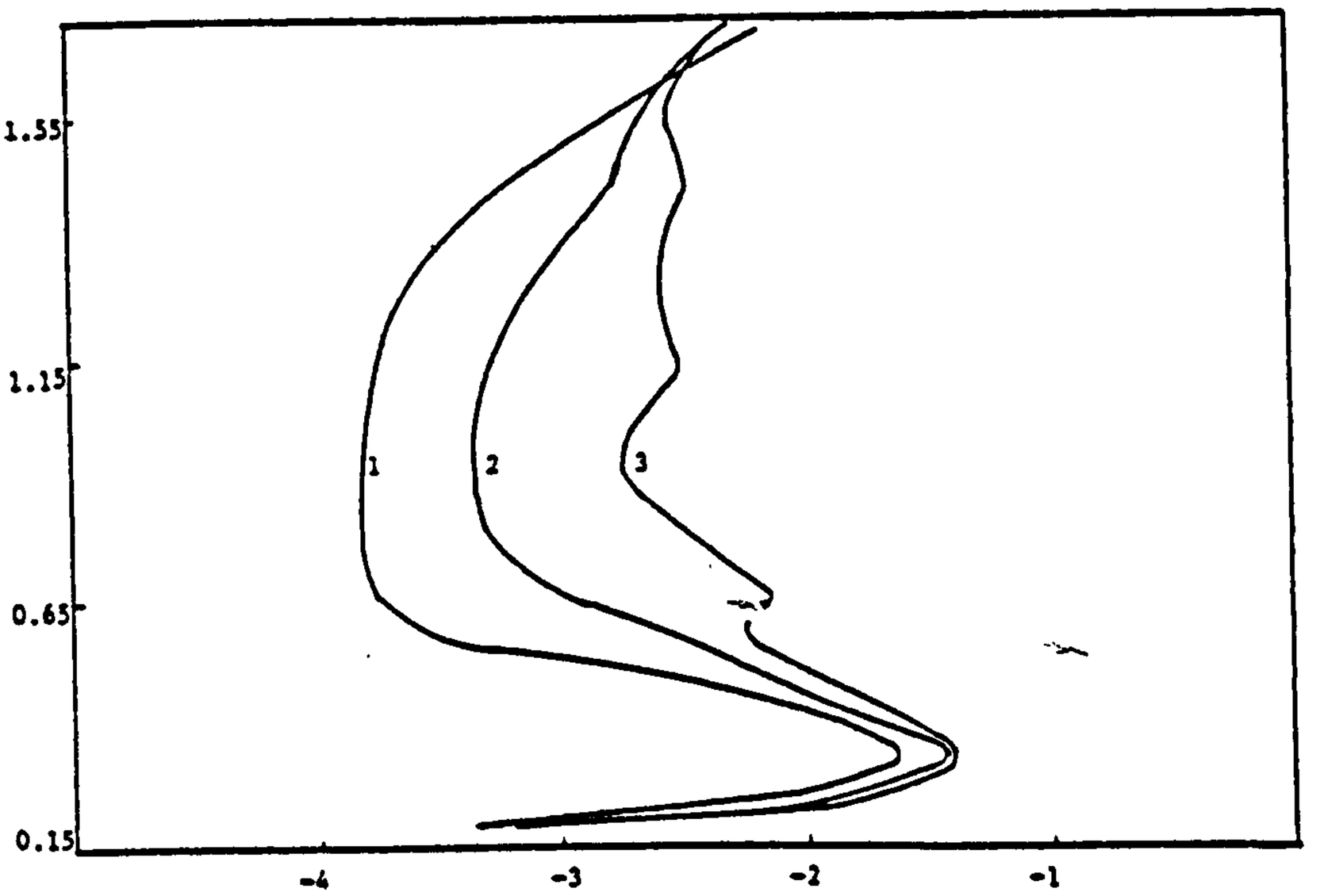

A graph of E vs log i for the anodic polarisation of a Ni electrode at a sweep rate of 5mV sec^{-1} in a solution of 1M KNO_3 pH 1.0 containing different Na BF_4 concentrations.

1 = No $NaBF_4$ 2 = 0 005M $NaBF_4$
3 = 0.1M M $NaBF_4$ (supersaturated)

FIGURE 238

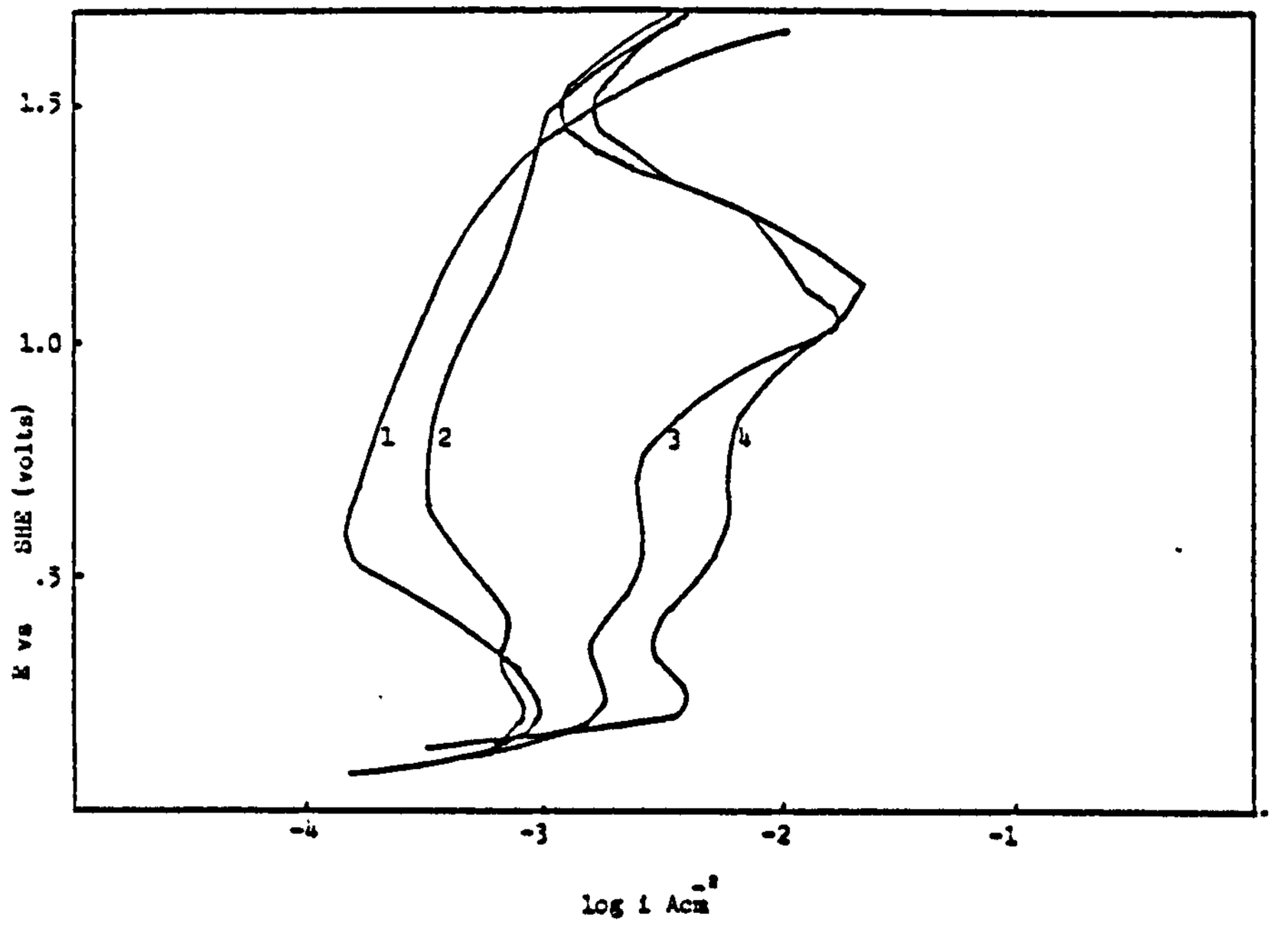

E vs log i curve for a Ni electrode anodically polarised at a sweep rate of 5mV sec^{-1} in a solution of 1M KNO, pH 2.5 containing different concentrations of $NaBF_4$ 1=0M, 2=0.005M, 3=0.01M, 4=0.1M (saturated).

FIGURE 239

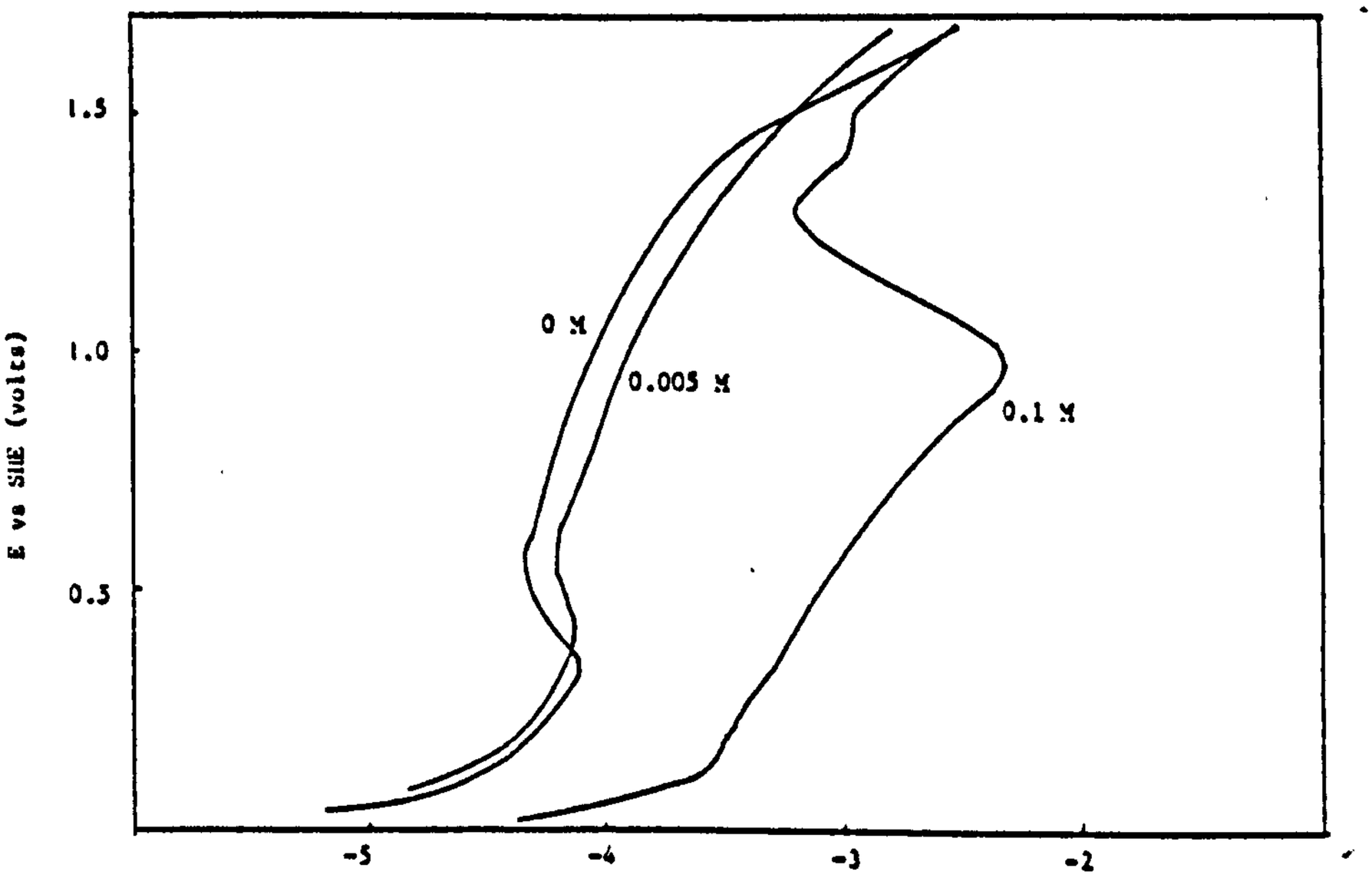

The E vs log i curves for the anodic polarisation of a Ni electrode at a sweep rate of 5 mV sec^{-1} in a solution of 1M KNO_3 pH4 containing different concentrations of $Na\ BF_4$.

FIGURE 240

The current density at any given potential in the active region was dependent upon the $NaBF_4$ concentration. The value of E_{pp} was essentially the same as for the non additive solution i.e +0.330 V however a slight increase in Tafel slope from 45 mV per decade to 50 mV per decade was detected, as was an increase in the value of i_{pp} from 2.4 Adm^{-2} in the absence of $NaBF_4$, to 4 Adm^{-2} with an addition of 0.1M $NaBF_4$. A secondary passivation peak at +0.650 V was also recorded, presumably due to the formation of a higher valent nickel oxide.

In solutions of pH 2.5 an increase in $NaBF_4$ concentration resulted in an increase in i_{pp} whilst the values for E_{pass} remained essentially the same (Fig. 239).

TABLE 79

The variation of E_{pass}, i_{pass} and i_{pp} on the addition of different concentratons of $NaBF_4$ to a solution of 1M KNO_3 pH 2.5. The Ni electrode polarised at a sweep rate of 10 mV sec^{-1} from its rest potential at 25°C

$NaBF_4$ Concentration moles $litre^{-1}$	E_{pass} Volts	i_{pp} Adm^{-2}	i_{pass} (minimum) Adm^2	b mV per decade
0	0.250	0.14	0.009	60
0.005	0.210	0.10	0.033	-
0.01	0.240	0.18	0.15	-
0.1M (saturated)	0.240	0.39	0.27	60

As can be seen from Table 79 only at $NaBF_4$ concentrations in excess of 0.1M was any significant variation observed in the values of i_{pp}. It was also found difficult to achieve reproducable values of i_{pp}, as the results above indicate.

In the case of high concentration $NaBF_4$ solutions a secondary passivation peak at +1.05 Volts was observed, the current for which is greater than the primary value of i_{pp} at 0.24V e.g 1.7 Adm^{-2} for 0.01M $NaBF_4$ and 2.3 Adm^{-2} for 0.1M $NaBF_4$ additions to 1M KNO_3. After the formation of the secondary passivation peak the current density decreases rapidly until oxygen evolution commences. The current density in the passive region is influenced by both the potential and the anion concentration (see Table 80).

TABLE 80

The variation of current density with potential in the passive region for dissolution of the passive film on a Ni electrode polarised at 10 mV sec^{-1} in a 1M KNO_3 solution pH4 containing selected concentrations of $NaBF_4$

$NaBF_4$ concentration moles $litre^{-1}$	Current density (Adm^{-2}) at a given potential (Volts versus SHE)					
	+0.5	+0.6	+0.7	+0.8	+0.9	+1.0
0	0.0165	0.0089	0.0098	0.011	0.0126	0.0148
0.001	0.023	0.018	0.018	0.019	0.022	0.028
0.005	0.053	0.037	0.033	0.035	0.038	0.046
0.01	0.24	0.25	0.24	0.30	0.53	1.26
0.1	0.46	0.57	0.60	0.64	0.79	1.45

In solutions of pH4 only concentrations greater than 0.005M NaBF had any significant effect on passivity (Fig. 240). However, in the case of a super saturated solution of $NaBF_4$ (0.1M) no active to passive transition region could be detected only a secondary passivation peak observed at +0.950 V.

3.5.4.5 The effect of $NaNH_2SO_3$ on Ni passivity in NO_3^- solutions

$NaNH_2SO_3$ additions were not found to significantly effect either the active or passive dissolution of Ni in nitrate solutions as can be seen from Figs. 241, 242 and 243.

Indeed at solutions of pH 4 a gradual reduction in both i_{pp} and i_{pass} with increase in Na NH_2SO_3 concentration was observed.

3.5.4.6 The effect of Na_2SiF_6 on Ni dissolution in NO_3^- solutions

Na_2 SiF_6 was found to be insoluble in solutions of pH greater than 2.5 and it was found difficult to maintain the pH of the Na_2SiF_6 containing solutions within set limits, particularly at pH 2.5 (see Fig. 243). The low value of i_{pp} i.e lower than i_{pp} for the none additive solution may well be due to pH variations although this would need verification in any future work. In solutions of lower pH Na_2SiF_6 had only a limited solubility but was found to increase both the active and passive dissolution of nickel (see Fig. 244).

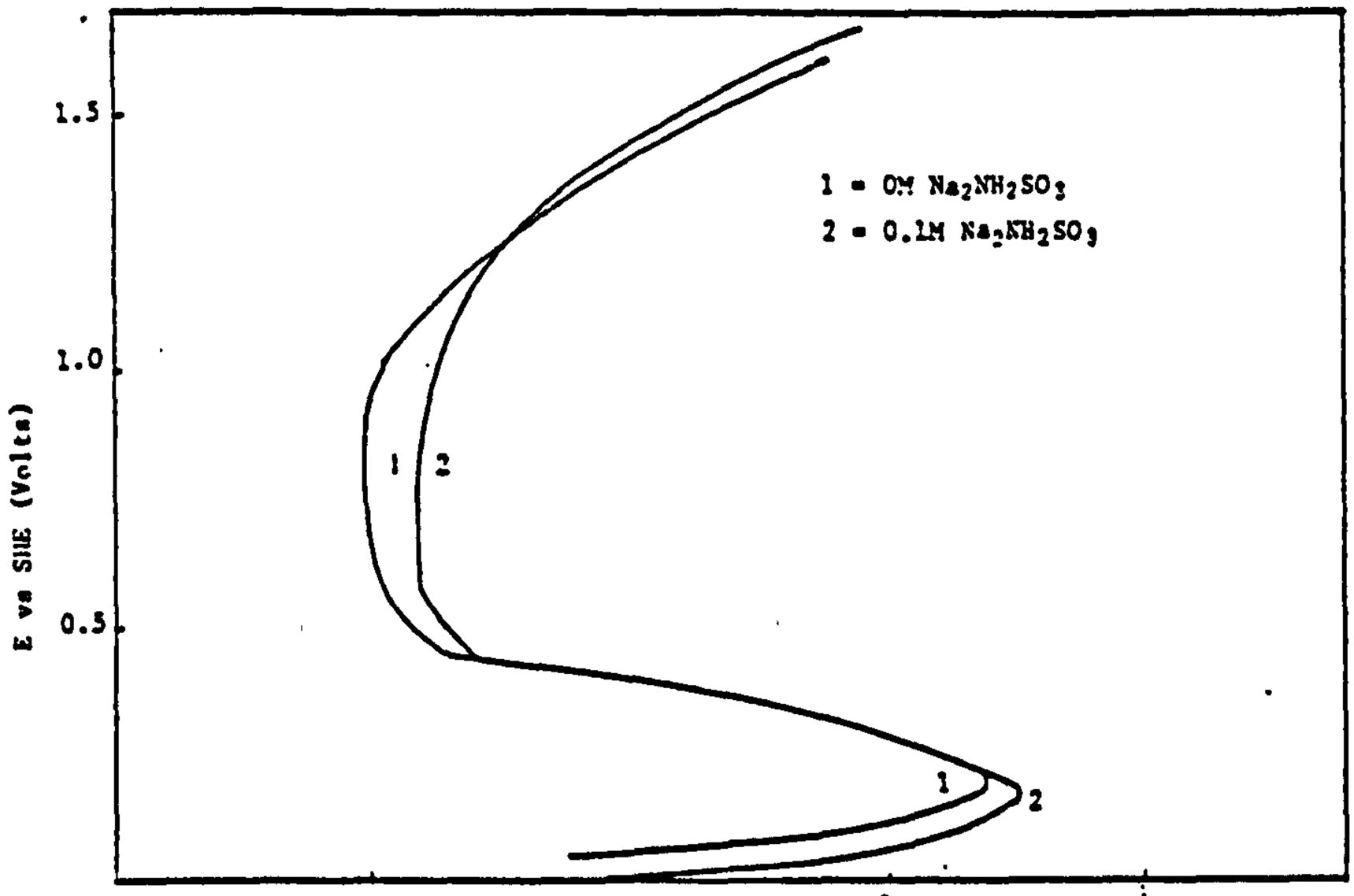

E vs log i curve for a Ni electrode anodically polarised at 5 mV sec^{-1} in a solution of 1M KNO_3 pH 1 containing selected concentrations of $Na\ NH_2SO_3$.

FIGURE 241

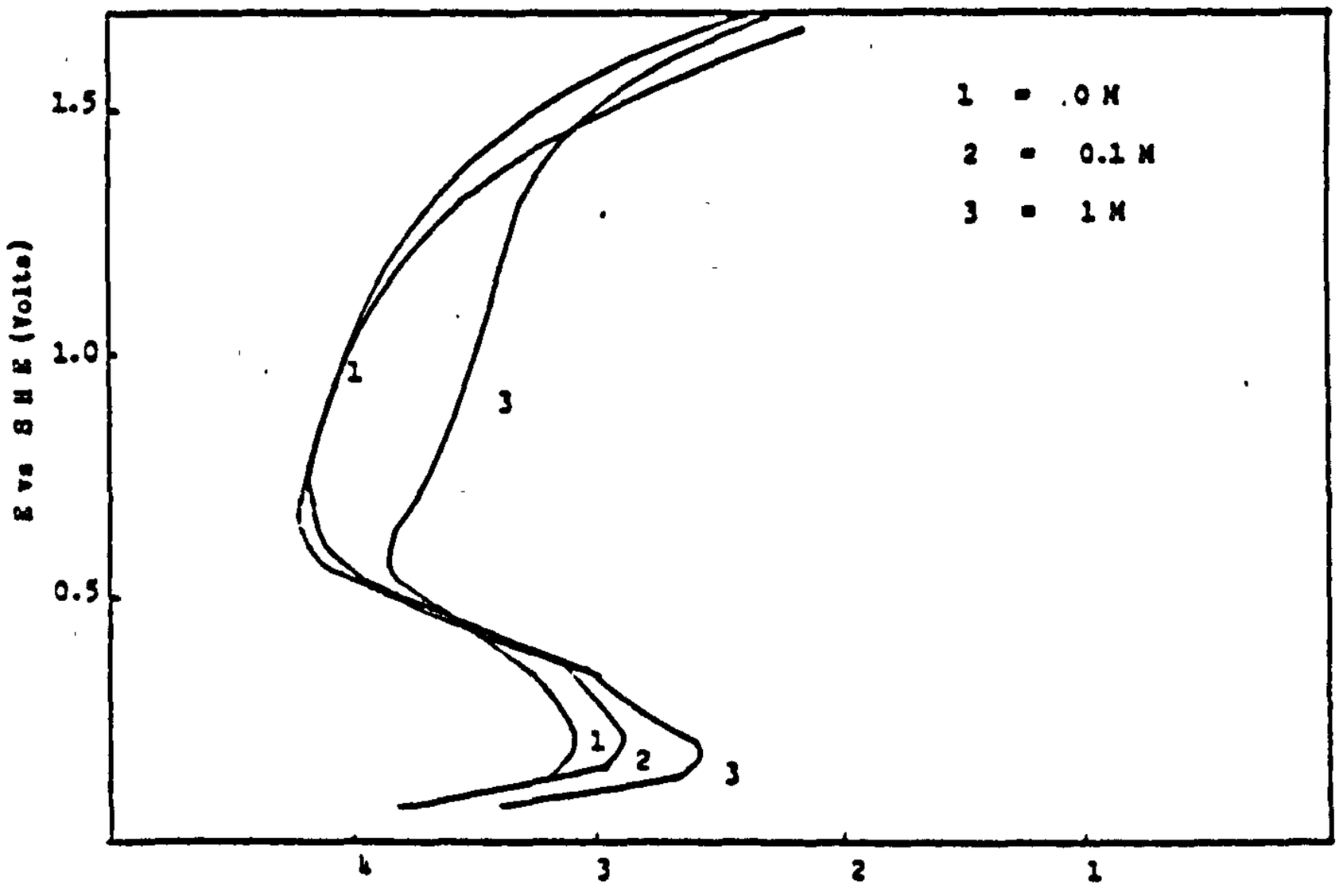

E vs log i curve for a Ni electrode anodically polarised at a sweep rate of 5 mV sec^{-1} in 1 M KNO_3 pH 2.5 containing different concentrations of $NaNH_2SO_3$

FIGURE 242

MISSING

PAGES

NOT

AVAILABLE

4 DISCUSSION

4.1 The simultaneous electrodeposition of Pb and PbO_2 from $Pb(NO_3)_2$ solutions

At present there is no proven scientific method of predicting the performance of specific addition agents from their chemical composition. Therefore, the initial selection of addition agents for use in Pb deposition from $Pb(NO_3)_2$ solutions was more of an empirical than a scientific nature. An extensive literature search was conducted to determine those organic addition agents that may give suitable improvements in Pb and PbO_2 electrodeposits obtained from $Pb(NO_3)_2$ plating solutions and addition agents found from this study were selected for investigation.

A preliminary study into the effect of a few selected individual addition agents on the properties of Pb and PbO_2 electrodeposits obtained from a 360 gl^{-1} $Pb(NO_3)_2$ solution was conducted. The additives investigated were described in Section 3.1, and all showed some improvement in surface coverage of the Ni foil substrate by the Pb deposit, when compared to the deposit obtained from an additive free solution, but not to any appreciable extent. Some additives notably resorcinol and hydroquinone were found to significantly reduce the current efficency for PbO_2 formation because they were oxidised at the PbO_2 anode. Whilst others particularly gelatin and peptone when added to a 360 gl^{-1} $Pb(NO_3)_2$ solution at room temperature, gave little improvement in the Pb deposit properties and produced PbO_2 deposits with a tendency to detach themselves from the Ni substrate.

Indeed, electrodeposition of PbO_2 at a relatively low current density (0.5 Adm^{-2}) from $Pb(NO_3)_2$ solutions containing peptone was found to produce a fine grained, highly reflective PbO_2 deposit. The subsequent deposit was however found to exhibit a poor adhesion to the Ni foil substrate and therefore could not satisfy the requirements for the active material used in the $Pb/HBF_4/PbO_2$ primary battery.

The use of individual addition agents was found to be unsuccessful and further work was concentrated on studies of binary combinations of addition agents. The additive found to be one of the most successful in terms of achieving improved Pb surface coverage was Triton X100. Further stuides utilising this addition agent in combination with a second addition agent e.g anthraquinone-2-monosulphonic acid, anthraquinone-2,6-disulphonic acid, 1,4 napthoquinone, anthraquinone-1,5-disulphonic acid, 2-butyne-1,4-diol or 1-napthol-4-sulphonic acid, gave a considerable improvement in the nature of the Pb deposit, its surface coverage over the Ni foil substrate and adherence without significantly affecting the nature of the PbO_2 deposit.

In order to quantify the effect of different addition agent combinations on the extent of surface coverage on the Ni foil substrate, a porosity test suitable for Pb electrodeposited onto Ni was developed. The 'porosity test' described in Section 2.1.2 provided numerical values of the porosity index or the relative percentage of exposed Ni on each sample of Pb electrodeposited onto Ni. This enabled a quantitative evaluation of the improvement in Pb surface coverage brought about by each addition agent combination to be made.

The reproducibility of the porosity results on certain samples was poor but this was thought to be associated with variations in the Pb porosity over the bulk sample rather than some inherent defect in the technique. Thus, the variation in the porosity values on a given sample could be associated with differences in the deposition c.d over the substrate surface or even the nature of the etched nickel surface.

A number of specimens were taken from each sample of Pb electrodeposited onto Ni, so that a mean value of porosity could be obtained. The results of porosity were expressed in terms of exposed Ni surface area.

The latter statement, the expression of porosity results in terms of the exposed Ni surface area, is only true for highly porous coatings where the value for E_{pp} (coated nickel) is the same as the value of E_{pp} for etched nickel in the test solution.

However, on coatings with a low porosity the value of E_{pp} (coated nickel) was found to be considerably lower than that for the uncoated etched nickel substrate. Thus, dividing i_{pp} (electrodeposited coating) by i_{pp} (etched Ni) will not give a true representation of the exposed Ni surface area, because each of these i_{pp} values was obtained at a different potential. As the potential for primary passivation (E_{pp}) decreases so will the value of i_{pp} (etched nickel). For this reason the value of exposed surface area on low porosity coatings may in actual fact be lower than the values quoted. Nevertheless, since this technique was primarily developed to assess the relative merits of individual addition agents in improving Pb surface coverage from $Pb(NO_3)_2$ solutions rather than determine the true exposed surface area, no adjustments to the values of exposed surface area were made. The porosity results should therefore be considered as a porosity index rather true exposed Ni surface areas.

The measurement of the polarisation resistance for the coated electrodes close to the rest potential may also give an accurate value for the true exposed surface area i.e the value of dV/di for a coated electrode anodically polarised at a low over-potential (30mV) from its rest potential. However, no work was carried out to perfect this technique. Although it may be worthy of investigation in future work.

Porosity measurements were used to determine the optimum deposition parameters for Pb electrodeposited from $Pb(NO_3)_2$ plating solutions considered to show the most promise, by studying the effect of $Pb(NO_3)_2$ concentration, additive concentration and current density on the porosity of the Pb deposit.

The most successful additive combination to $Pb(NO_3)_2$ solutions in terms of achieving the minimum Pb porosity on the Ni substrate was found to be 3 gl^{-1} Triton X100, plus 0.1 gl^{-1} anthraquinone-2-monosulphonic acid. The porosity of the Pb deposit of a given thickness remained almost constant in the concentration range 270 gl^{-1} to 100 gl^{-1}, $Pb(NO_3)_2$ at 0.1 to 0.21%, whilst at a higher concentration, namely 360 gl^{-1} $Pb(NO_3)_2$ the value of porosity increased to 3.4%. This marked increase in porosity over a small concentration range may be related to difficulty in ensuring complete solubility of the additive anthraquinone-2-sulphonic acid.

The concentration of Triton X100 should be maintained at 3 gl^{-1} to obtain the lowest value porosities i.e best surface coverage of the Ni substrate. The effect of increase in Triton X100 concentration above 3 gl^{-1} on the values of the Pb porosity was not investigated.

Most experiments particularly with the anthraquinone-2-monosulphonic acid Triton X100 system were conducted at a Triton X100 concentration level of 2 gl^{-1}. Further improvements in the nature of the Pb deposit may therefore be obtained at higher Triton X100 concentrations.

In the case of the use of other additive combinations namely 3 gl^{-1} Pluronic L64 plus 0.1 gl^{-1} anthraquinone-2-monosulphonic acid, and 3 gl^{-1} BRIJ35 plus 0.1 gl^{-1} anthraquinone-2-monosulphonic acid, the porosity of the Pb coating decreased with decrease in $Pb(NO_3)_2$ concentration. Although the Pb deposit porosity from these solutions was marginally greater than with the Triton X100 system.

The optimum current density for the 3 gl^{-1} Triton X100 plus 0.1 gl^{-1} anthraquinone-2-monosulphonic acid additive system was found to be 3 Adm^{-2} although suitable values of Pb porosity were obtained in the current density range 1 to 5 Adm^{-2}, at a $Pb(NO_3)_2$ concentration of 360 gl^{-1}.

The $Pb(NO_3)_2$ solutions utilising Triton X100 and anthraquinone-2-monosulphonic acid as addition agents were however unsuitable for producing Pb deposits from room temperature $Pb(NO_3)_2$ solutions, because on the edges of the substrate dendritic Pb deposits were formed at a current density of 2 Adm^{-2}. To obtain Pb deposits from room temperature $Pb(NO_3)_2$ plating solutions it was found necessary to use an alternative additive combination. The additives found to give the best results were tannic acid and Wafex. It was also necessary to add HNO_3 to the $Pb(NO_3)_2$ solution to ensure complete solubility of the tannic acid. The low solution pH created by the addition of HNO_3 meant that this additive combination could not be used for the simultaneous electrodeposition of Pb and PbO_2, since the Ni anode would not remain inert in such a solution.

A good coverage of the nickel substrate with the Pb deposit is obtained from the Wafex plus tannic acid bath as is evident from the porosity values (see Section 3.1.2.4) and SEM photographs (Section 3.1.4). These solutions could be used for room temperature electrodeposition of Pb from $Pb(NO_3)_2$ solutions.

The studies on the effect of addition agents on the nature of the Pb and PbO_2 deposit obtained from $Pb(NO_3)_2$ solutions were primarily concentrated on the Pb deposit. As it was shown that selected addition agents had a greater effect on the Pb deposit and hardly affected the properties of the PbO_2 deposit.

As the major requirement of the present studies was to produce active material that satisfied the requirements for the $Pb/HBF_4/PbO_2$ primary battery, simultaneous electrodeposits were prepared and then evaluated for use as active material in the $Pb/HBF_4/PbO_2$ battery. This work concentrated on comparing the discharge properties of conventional active plate material with Pb and PbO_2 material obtained by simultaneous electrodeposition from various plating solutions.

The deposits from the simultaneous plating solutions, although of equivalent thickness to the Pb and PbO_2 deposits obtained using the standard commercial process were shown to have inferior discharge properties in 48% HBF_4. The cell voltage at room temperature remained constant for only the first 100 seconds of discharge at a c.d of 5.5 Adm^{-2}, whilst the cell voltage for the conventional Pb and PbO_2 deposits of similar thickness, remained constant for approximately the first 220 seconds of discharge. No major differences in the discharge properties at room temperature for the Pb and PbO_2 deposits obtained from different simultaneous plating solutions, based on the following addition agents (a) 2 gl^{-1} Triton X100 plus 0.1 gl^{-1} anthraquinone-2-monosulphonic acid, (b) 2 gl^{-1} Pluronic L64 plus 0.1 gl^{-1} anthraquinone-2-monosulphonic acid and (c) 3 gl^{-1} Triton X100 plus 1.5 gl^{-1} butyne 1,4 diol were observed.

The deposits from the simultaneous plating solutions also exhibited inferior discharge properties at elevated temperature when compared to Pb and PbO_2 deposits obtained from conventional plating solutions. The Pb and PbO_2 deposits from the Triton X100, anthraquinone-2-monosulphonic acid solution maintaining a constant cell voltage for between 110 to 140 seconds at a discharge c.d of 5.9 Adm^{-2} at 60°C whilst the deposits from the butyne diol, Triton X100 bath would only maintain a constant cell voltage for between 50 to 80 seconds, These figures should be compared with conventionally produced Pb and PbO_2 deposits where the cell voltage remained constant for some 200 to 220 seconds, again all deposits were of an equivalent thickness

The deposits from the Triton X100, anthraquinone-2-monosulphonic acid bath were found to exhibit the best discharge properties of any simultaneous Pb and PbO_2 deposit at 60°C.

Tests have confirmed that it is the nature of the Pb not the PbO_2 deposit that produces the relatively short operational life for $Pb/HBF_4/PbO_2$ batteries constructed from material produced

from the simultaneous plating solutions. The "fall off" in cell voltage with time for the deposits obtained from the simultaneous plating solutions is attributed to the gradual detachment or undermining of the Pb deposit produced from these solutions, thus reducing the effective Pb anode area, rather than the organic plating additives producing a highly stressed PbO_2 deposit that readily detaches itself from the substrate surface (see Fig. 26). The poor coulombic efficiency of the simultaneous deposits is therefore associated with the Pb not the PbO_2 electrode. The reduction in coulombic efficiency of the Pb anode in the deposits from the simultaneous bath may be brought about by either a decrease in the level of adhesion of these deposits, their larger grain size or high porosity. The assumption that it is not the PbO_2 deposit from the simultaneous baths that causes the "fall off" in cell voltage with time is supported by the fact that the coulombic efficiency of the PbO_2 deposits obtained from a $Pb(NO_3)_2$ plating solution containing the additives Triton X100 and anthraquinone-2-monosulphonic acid was not different to that from the additive free solution.

However, PbO_2 deposits produced from $Pb(NO_3)_2$ solutions containing CETB as an addition agent did exhibit a reduced coulombic efficiency when used as the cathodic material in the $Pb/HBF_4/PbO_2$ primary battery. Thus some organic additives do appear to affect the coulombic efficiency of the PbO_2 electrodeposit in HBF_4.

Results obtained from pilot plant trials have confirmed that the operational life of $Pb/HBF_4/PbO_2$ batteries produced from active material obtained by simultaneous electrodeposition from additive containing $Pb(NO_3)_2$ solutions can be improved by utilising thicker Pb and PbO_2 deposits i.e. plating for longer periods. Thus, deposits of Pb and PbO_2 can be produced from a number of simultaneous plating solutions based on $Pb(NO_3)_2$ plus selected addition agents, that satisfy all the basic requirements for the $Pb/HBF_4/PbO_2$ fuse battery. As the other major requirements of the Pb and PbO_2 deposits i.e activation time and adhesion were unaffected by the additive combinations

used in the simultaneous plating solutions. Furthermore, it may be possible to obtain improved discharge characteristics for Pb and PbO_2 deposits obtained by simultaneous electrodeposition from lower concentration $Pb(NO_3)_2$ solutions, since these produce lower porosity Pb deposits.

The X-ray diffraction pattern for the bulk samples of PbO_2 obtained by electrodeposition from a 360 gl^{-1} $Pb(NO_3)_2$ solution at a c.d of 1 Adm^{-2} and temperature of 50^oC reveals that the deposit formed was a mixture of α and β -PbO_2, not β -PbO_2 as is generally believed. This result however supports the observations made by Bone (308) and Rusin (309) that PbO_2 deposits from near neutral pH, $Pb(NO_3)_2$ solutions are not pure deposits of PbO_2 but a mixture of α and β .

Bone reports that PbO_2 electrodeposited from a 0.125 M $Pb(NO_3)_2$ solution at 85^oC and at a c.d. of 0.21 Adm^{-2} is predominantly β -PbO_2 with traces of α -PbO_2, whilst the PbO_2 deposit obtained by electrodeposition from $Pb(NO_3)_2$ at a c.d of 0.1 Adm^{-2} dissolved in concentrated HNO_3 is only β -PbO_2. Rusin (309) studied the effect of the concentration of the $Pb(NO_3)_2$ solution and c.d for electrodeposition and found that at a low c.d β -PbO_2 is formed yet at high c.ds α-PbO_2 is formed, with mixtures of α and β -PbO_2 formed at intermediate current densities e.g in a 300 gl^{-1} solution of $Pb(NO_3)_2$ at a c.d of 1 Adm^{-2} he observed that the PbO_2 deposit consisted of a mixture of α and β -PbO_2.

A limited study on the effect of certain addition agents on the X-ray diffraction pattern for PbO_2 deposits obtained by electrodeposition from $Pb(NO_3)_2$ solutions containing selected addition agents was also undertaken. In the case of the PbO_2 deposit obtained from a $Pb(NO_3)_2$ solution containing 1 gl^{-1} CETB only a single α -PbO_2 reflection (less than 2%) from the (111) plane was observed and the deposit found to be predominantly β -PbO_2. The relative proportions of α to β -PbO_2 were found to differ from the non additive and additive containing $Pb(NO_3)_2$ solutions e.g. when Wafex was used as an addition agent, the deposit exhibited a high degree of preferred orientation and only a limited α- PbO_2 content.

The effect of addition agents on the nature of the PbO_2 deposit would be worthy of further investigation, especially additives such as peptone and 6,8 diphenylamine which produce very small grained, highly reflective PbO_2 deposits.

4.1.1 The anodic oxidation of selected organic addition agents

The discussion in this section is aimed at highlighting those additives that may be susceptible to anodic oxidation as well as describing the chemical structure of addition agents that have hitherto only been referred to by their proprietary names.

Electrochemical studies on the anodic oxidation of possible additives for use in simultaneous plating solutions, have revealed that some additives are clearly unstable over the potential range at which deposition of PbO_2 would occur in a simultaneous plating solution.

Indeed, the marked decrease in Pb deposit properties with time on pilot plant studies, further supports the fact that decomposition of addition agents does occur, thus decreasing the effective addition agent concentration with plating time.

Triton X100, one of the most successful addition agents for Pb and PbO_2 deposition has been shown to undergo electrochemical oxidation. The cyclic voltammogram for a Pt electrode polarised in a supporting electrolyte of 0.2M Na_2SO_4 pH2 containing 1 gl^{-1} Triton X100, showed a current peak (i_p) at +1.65V vs SHE with oxidation appearing to commence at a lower potential i.e. +1.2 V. The value of E_o obtained from a plot of E_{pp} vs $v^{1/2}$ was found to be 1.63V.

Triton X100 is a non ionic surface active agent formed by the reaction of octyl phenol with ethylene oxide, the product described as an alkyl aryl poly ether alcohol. The chemical formula for the Triton X100 series of chemicals is given as :

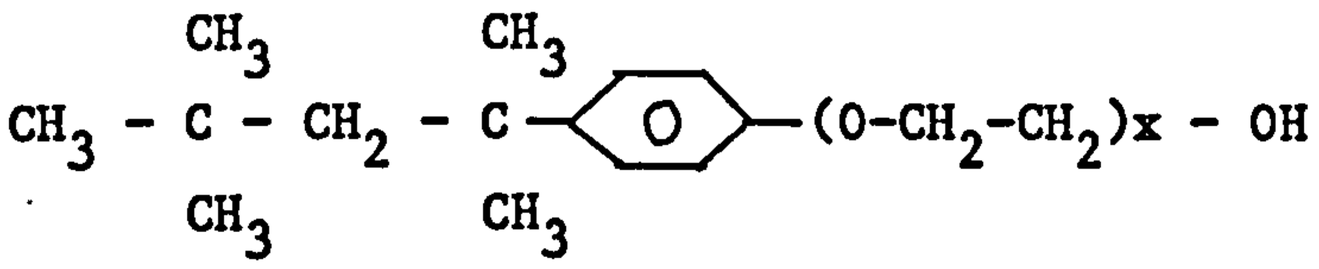

Where x = 9-10 for Triton X100

x = 7-8 for Triton X114

The anodic degradation of Triton X100 is believed to be by the oxidation of the primary OH group to either the corresponding aldehyde or carboxylic acid. Some workers (310) have shown that the anodic oxidation of aliphatic alcohols occurs at potentials greater than +0.8V and that at high current densities only carboxylic acids are produced. Indeed, an increase in the alcohol chain length, from C2 to C7 was shown to result in a reduction in current efficiency for aldehyde production. In the case of the anodic oxidation of propyl alcohol oxidised at 1 to 5 Adm^{-2} on a Pt electrode in a H_2SO_4 solution the yield was 60% propionaldelyde and 40% propionic acid, whilst at higher current densities propyl propionate was formed. This therefore indicates that the possible products from the oxidation of Triton X100 could be the corresponding aldelyde, carboxylic acid or a mixture of these, with the high chain length of the aliphatic alcohol in Triton X100 favouring oxidation to the carboxylic acid.

Attempts to identify the decomposition products of Triton X100 and other additives were not conclusive. U.V analysis of solutions of Triton X100 oxidised in 3M H_2SO_4 on Pt electrode, at a current density of 2 Adm^{-2}, could not identify any decomposition products, even though a colour change was visible. The reason for this is that the only absorbtion peak detected for Triton X100 and other surfactants, in the U.V region, at 283 μm, corresponds to that for the aromatic ring system. The fact that no reduction in intensity of this peak was detected shows no decomposition of the aromatic ring system occurs as a result of anodic oxidation. The absorbtion peak for the hydroxyl group was outside the U.V range and no change in hydroxyl intensity could be detected with this technique.

Infra red analysis of the ether extract from a simultaneous plating solution of 360 gl^{-1} $Pb(NO_3)_2$, 3 gl^{-1} Triton X100 plus 1.5 gl^{-1} butyne-1,4-diol could also not identify any decomposition products. However, with this technique the difficulty in ensuring complete removal of ether made identification of the infra red absorbtion spectrum difficult. N.M.R analysis of both the aqueous and CCl_4 extract from this plating solution could also not detect the presence of any new compounds. Nevertheless, whilst these analytical techniques were unable to identify any decomposition products, this does not mean that none were formed.

On the contrary, the individual quantitative analysis for Triton X100 and butyne 1,4 diol does show a decrease in both additive concentrations with time for a simultaneous Pb and PbO_2 plating solution based on these addition agents. The decrease in additive concentration with time is further confirmed by the reduction in the Pb deposit properties with prolonged operation of the plating solution.

Ideally chromatographic analysis of the organic extract from the plating solution, either HPLC or thin film could have been used to identify the decomposition products. However, this technique could not be made available and more detailed work to analyse the decomposition products should be carried out in future work.

Both the gravimetric and colorimetric methods of analysis for Triton X100, show that the Triton X100 content of a simultaneous plating solution falls rapidly during the first 250 amp hours plating at 2.4 Adm^{-2}, then remains at a relatively constant value. The colorimetric method of analysis was found to exhibit a greater degree of accuracy and is recommended for any future analytical work.

The limiting value of Triton X100 concentration after 2000 amp hours plating is not thought to be due to any equilibrium between the formation of the oxidation product(s) of Triton X100 at the PbO_2 anode and the reduction of these compounds at the Pb

electrode. Since the cyclic voltammogram for the anodic polarisation of Triton X100 did not exhibit any reduction peak, indicative of the fact that the oxidation of Triton X100 is an irreversible process. But that at Triton X100 concentrations below 1 gl^{-1} the additive is non oxidised at any appreciable rate, at a PbO_2 plating current density of 2.4 Adm^{-2}.

The method used to analyse for butyne 1,4 diol relied upon the determination of the Triton X100 content by a separate method, followed by a determination of the total quantity of oxidisable material present in solution. From a knowledge of the quantity of $KMnO_4$ required to oxidise Triton X100 it was possible to determine the butyne 1,4 diol concentration.

This method of analysis is however complicated by the fact that during the plating process NO_2^- ions are formed at the Pb cathode, from the reduction of NO_3^-. The presence of NO_2 ions in solution will introduce a source of error since $KMnO_4$ will also oxidise NO_2^- to NO_3^- and therefore the calculated value of butyne 1,4 diol concentration may well be higher than the actual value. In practice the relatively high pH (low H^+ concentration) of the $Pb(NO_3)_2$ plating solution i.e pH4, results in the formation of only a small quantity of NO_2^- during the plating process.

In the case of a non additive $Pb(NO_3)_2$ solution it is found, in an operational plating solution that 200ml of 30% H_2O_2 is required to oxidised all the NO_2^- produced after $7m^2$ of Ni foil has been plated, from a 1600 litre solution of 360 gl^{-1} $Pb(NO_3)_2$ at a current density of 2.4 Adm^{-2}. Since it takes 2 hours to plate $1m^2$ of foil at this current density, this equates to 500 amp hours plating producing 2.4×10^{-4} M NO_2^- which would require 1.19×10^{-3} M of $KMnO_4$ for complete oxidation of the NO_2^-. Since 7.2×10^{-2} M $KMnO_4$ is required to oxidise 1g of butyne 1,4 diol, this corresponds to an approximate error of 2%, in the analysis of a 1 gl^{-1} solution of butyne 1,4 diol after 500 amp hours plating. Assuming a linear rate for NO_2^- formation based on the foregoing

information, the values of butyne 1,4 diol concentration can be adjusted to take into account the estimated NO_2^- concentration and these are given in Table 81.

TABLE 81

The effect of $[NO_2^-]$ on the measured values of butyne 1,4 diol as determined by oxidation with $KMnO_4$

Amp Hours plating at 2.4 Adm^{-2}	Butyne 1,4 diol concentration gl^{-1}	
	Measured value	value adjusted to take into account NO_2^- in the solution
0	1.9	1.9
250	1.3	1.3
500	1	1
750	0.4	0.4
1250	0.6	0.55
1900	0.6	0.5

As can be seen from Table 81 the calculated NO_2^- concentration had only a negligible effect on the measured values of butyne 1,4 diol concentration, the error only significant after extended plating times. In view of the experimental errors involved in determining the end point of the $KMnO_4$ and $K_4Fe(CN)_6$ titration and the Triton X100 concentration by a separate method. The error introduced by NO_2^- can be considered to be insignificant. In addition, the rate of formation of NO_2^- may also be affected by the presence of the addition agents in the solution and may well be reduced from that in a non additive containing solution (see Section 3.2.2.6).

Butyne 1,4 diol is liable to oxidation and other workers have reported that the oxidation of butyne 1,4 diol at a PbO_2 electrode in H_2SO_4 at a c.d. of 10 Adm^{-2} yields 74% butyne 1,4 dicarboxylic acid (312). Although Wolf (313) reports a yield of 95% butyne 1,4 dicarboxylic acid under slightly different conditions. The proposed reaction scheme is as follows:

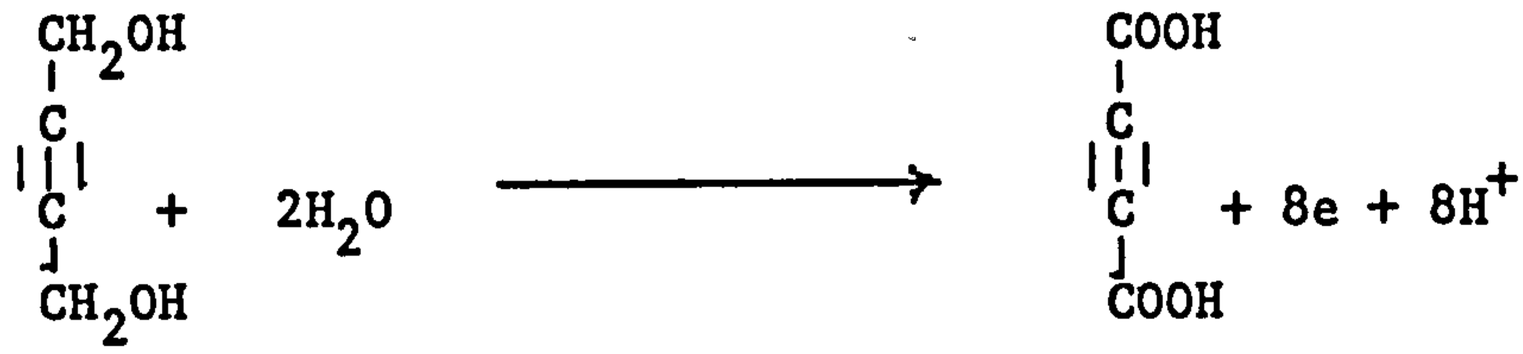

The cyclic voltammogram for a solution of 1 gl^{-1} butyne 1,4 diol in a supporting electrolyte of 0.2M Na_2SO_4 pH2 does not show a clear easily definable current peak (i_p) on anodic oxidation. There was however a slight variation in the E vs i curve for this solution (Fig. 56) when compared to a non additive containing solution of 0.2M Na_2SO_4 (Fig. 55) with a larger c.d. observed in the potential range between +1.1 and +1.2 volts, possibly due to oxidation of butyne, 1,4 diol. No reduction peak was observed. The decrease in c.d. at +2.0 V at a constant sweep rate with increase in butyne 1,4 diol concentration is thought to be due to strong adsorbtion of this additive on the Pt electrode, increasing the oxygen overvoltage.

Other surface active agents namely Pluronic L64 and BRIJ35 were also found to be suitable for use in simultaneous plating solutions and work was undertaken to determine the electrochemical stability of these additives. The Pluronic range of non ionic surface active agents are condensation products of ethylene oxide with polypropylene glycols and are represented by the following formula.

$$H\ (O\text{-}CH_2\text{-}CH_2)_a\ (O\text{-}CH_3\text{-}CH_2)_b(O\text{-}CH_2\text{-}CH_2)_a - OH$$

Pluronic L64 is a liquid (L), and the number 64 signifies, 6 for the base polypropylene glycol and 4 for the percentage of ethylene oxide i.e 40 to 49%. Pluronic L64 has a cloud point of 58°C, which explains why solutions of $Pb(NO_3)_2$ containing this additive heated to above 55°C appeared cloudy.

MISSING

PAGES

NOT

AVAILABLE

From a study of the chemical structure of Pluronic L64 it would appear that there are two labile primary alcohol groups which would be susceptible to anodic oxidation, either to the corresponding aldehyde or carboxylic acid.

The cyclic voltammogram for a solution of 5 gl^{-1} Pluronic L64 in 0.2M Na_2SO_4 exhibited no discernable current peak (i_p) on anodic polarisation. However, the E vs log i curve for a solution of 1 gl^{-1} Pluronic L64 in 0.2M Na_2SO_4 when compared to that for a non additive containing solution shows a higher value of i at a given potential (see Fig. 48).

This effect is considered to indicate that oxidation of this additive also occurs at a similar potential to that observed for Triton X100 i.e about +1.6V. However, no diffusion limited supply of Pluronic L64 to the Pt electrode was observed.

The decrease in current at a given potential with increase in Pluronic concentration may be explained by adsorbtion of the additive on the Pt electrode, blocking off the active sites for oxygen evolution.

In the case of the addition of BRIJ 35 to the test electrolyte, there was no significant reduction in current at any given potential with increase in surfactant concentration. Although a hysteresis effect on repeated cycling was observed, a phenomenum not recorded with any of the other addition agents.

BRIJ35 is a non-ionic surfactant, polyethylene oxide lauryl ether of chemical formula.

$$C_{11}H_{23}O - [CH_2 - CH_2 - O]_n - CH_2\ CH_2\ OH$$

where n = 23

As with Triton X100 and Pluronic L64 this addition agent also contains a labile primary alcohol group which may be subject to oxidation. The ether group is essentially electro-inactive, with the anodic oxidation of ethers generally proceeding by the production of an intermediate species in the supporting elec

trolyte. In the case of the oxidation of aqueous diethyl ether solutions in $HClO_4$, the diethyl ether is unattacked and oxygen evolution is the only reaction which occurs. However, in a non aqueous $HClO_4$ solution diethyl ether is oxidised to yield 30% acetaldehyde (314).

All surface active agents were found to significantly increase the oxygen overvoltage in 0.2M Na_2SO_4 solutions (see Table 59), in particular the Triton X100 series of compounds, quaternary ammonium compounds such as CETB (cetyltrimethyl-ammonium bromide), Hyamine and BRIJ35. However, the reduction in oxygen over-voltage was not directly related to the present studies and was therefore not investigated in any detail. The increase in oxygen overvoltage is thought to be due to adsorption of these additives on the Pt surface blocking off active sites for oxygen evolution and thus reducing the effective anode area.

Other additives were also investigated for their susceptibility to anodic oxidation in aqueous solutions.

Hydroquinone an additive used in proprietary $Pb(BF_4)_2$ plating solutions, is readily oxidised at low anodic potentials. The values of i_p and E_p from a cyclic voltammogram for hydro-quinone in 0.2M Na_2SO_4 were found to be dependent upon concentration and sweep rate, oxidation commencing at about +0.7V for a 0.5 gl^{-1} solution of hydroquinone in the test electrolyte. The value of E_p (oxidation) at a sweep rate of 10 mV sec^{-1} was found to be +0.83 Volts and a reduction peak visible at +0.38V. Similar results were also recorded for resorcinol containing solutions with this additive shown to be readily oxidised at low anodic potentials.

In the case of the additive anthraquinone-2-monosulphonic acid sodium salt, no decomposition peaks could be observed even though the current observed at a given voltage was greater than in the case of the non additive solution. This may be due to either a reduction in the oxygen overvoltage on addition of this additive, or the oxidation of anthraquinone.

Literature reports (315) show that 9,10 anthraquinone is liable to oxidation at +1.44V in a CH_3CN, $EtNClO_4$ solution on a Pt electrode, to yield a mixture of hydroxylated anthraquinones. The following reaction mechanism may therefore apply to the oxidation of anthraquinone-2-monosulphonic acid.

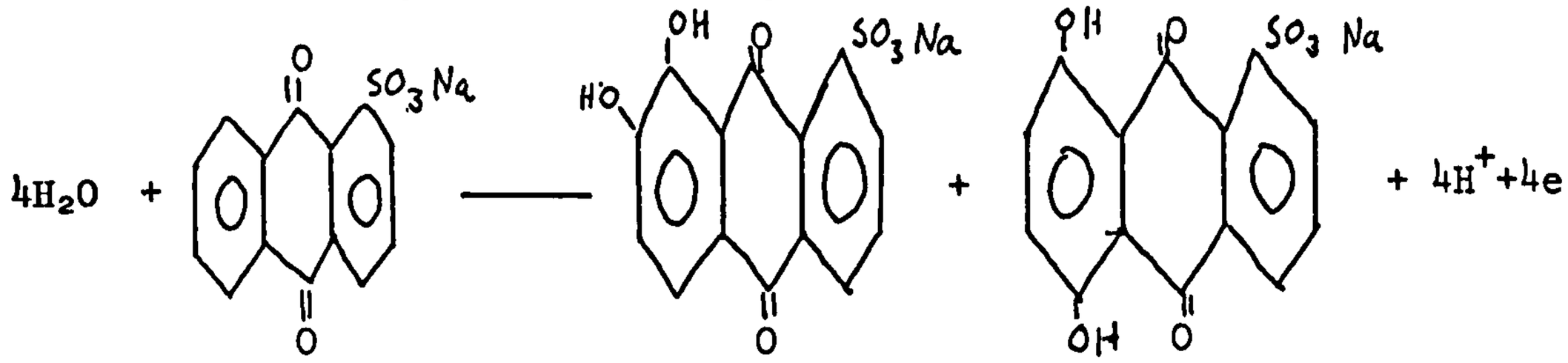

No information on the reversibility of the above process could be obtained.

Anthraquinone may be reduced, a process which is pH dependent and occurs at -0.4V for anthraquinone-2-monosulphonic acid in a caustic ethanol solution (316).

In the potential range overwhich a simultaneous plating solution based on $Pb(NO_3)_2$ operates, reduction of anthraquinone should not occur. Since the cathode potential will not become lower than the potential for Pb deposition.

The results of the cyclic voltammogram for the anodic oxidation of CETB containing solutions, showed quite clearly that this additive is subject to oxidation and that the process is reversible. This should not result in a loss of addition agent concentration with time during the plating process, if the reaction is totally reversible, as reduction may take place at the cathode.

CETB exhibited two oxidation peaks, one at +1.2V and the other at +1.4V, with reduction peaks visible at +1.1V and +0.55V. The reduction of the Pt oxide film can also be seen at +0.25 V.

Examination of the literature revealed little information on the anodic oxidation of quaternary ammonium salts (314), with the studies on their electrochemical activity concentrating on the cathodic reduction not the anodic oxidation. The fact that two distinct oxidation peaks, were observed in the case of CETB indicates two possible reactions occur yet in the case of Hyamine a proprietary quaternary ammonium salt, only one oxidation peak was detected at approximately +1.6V.

CETB has the chemical structure given below :

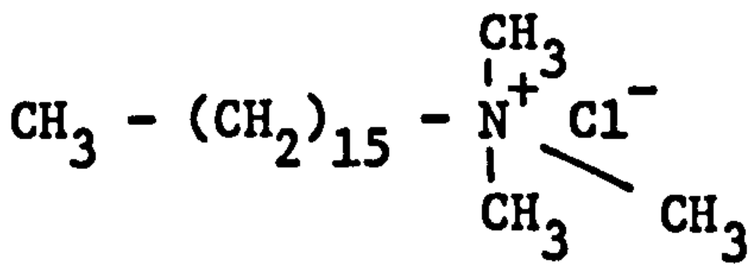

The above chemical formula shows no apparent labile groups, with the potential at which oxidation occurs too low to be due to chlorine evolution. Decomposition of the quaternary ammonium ion must occur, although the nature of the product formed may only be speculated upon at this stage.

The same would apply to Hyamine (diisobutylphenoxy ethyldimethyl-benzyl ammonium chloride) the chemical formula of which is given below.

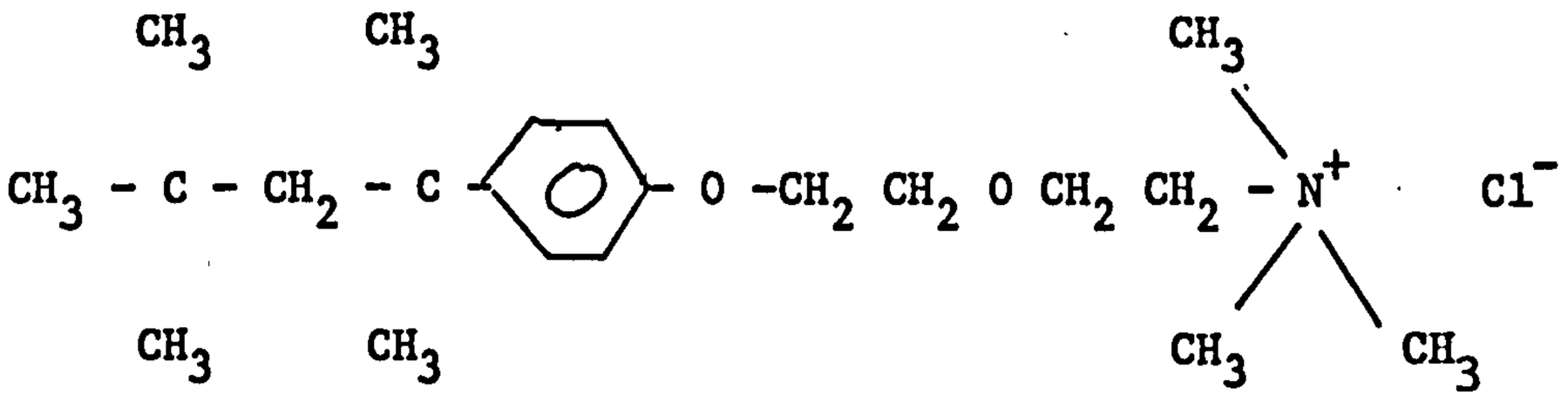

Some of the other addition agents studied also exhibited oxidation peaks e.g 1-naphthol-4-sulphonic acid which is presumably oxidised to 1-naphthoquinone-4-sulphonic acid. Tannic acid also contains a mixture of naturally occurring products that are susceptible to oxidation. Though interest in tannic acid as a plating additive for simultaneous electrodeposition of Pb and

PbO_2 is purely academic, since this additive is only soluble in $Pb(NO_3)_2$ solutions when HNO_3 is added. Ni would not remain inactive when anodically polarised in such a solution and can not therefore be used as a substrate for PbO_2 deposition.

Wafex is a sodium lignosulphonate i.e a sulphonate extract from wood and of unknown chemical formula and may contain groups liable to oxidation. Although no current peak was observed in the cyclic voltammogram for these solutions, a colour change was observed after electrolysis of the Wafex containing solutions, indicative of oxidation of this additive.

4.2 The electrochemistry of Pb deposition from $Pb(NO_3)_2$ solutions

The effect of the addition of certain organic chemicals to $Pb(NO_3)_2$ solutions on the nature of the E vs log i curves for Pb deposition in static solutions can be seen in Figs. 61-64. The addition agents appear to inhibit the Pb deposition reaction by increasing the overpotential necessary to achieve a given current density and in the case of certain addition agents, a diffusion limited current density is obtained under static conditions. The E vs log i curves for Pb deposition were only found to be useful indications as to the effectiveness of individual addition agents but did not provide detailed information on the mechanism whereby different addition agents affect either the kinetics for Pb deposition or the rate of diffusion of Pb^{2+} ions to the electrode surface. To investigate these parameters additional electrochemical techniques were used.

The diffusion limited supply of Pb^{2+} ions to the electrode surface, particularly at low Pb^{2+} concentrations (0.01M) when specific surfactants were added to $Pb(NO_3)_2$ solutions can be seen by comparing Fig. 73 with Figs. 74 to 78. These graphs show that the nature of the E vs i curve for Pb deposition can be affected by different addition agents, as these appear to control the rate of mass transport of Pb^{2+} ions to the electrode surface i.e. a diffusion limited supply of Pb^{2+} ions is

visible. This effect is also apparent in higher Pb^{2+} concentration solutions although not to the same extent, compare Fig. 65 with Figs. 66-72. Furthermore, in the additive containing 0.1M $Pb(NO_3)_2$ solutions a limiting current is only visible in static solutions.

The diffusion coefficients for Pb^{2+} ions near the reversible potential in solutions with and without surface active agents were determined using the rotating disc technique to ascertain if these chemicals had any effect on the measured value of the diffusion coefficient D_o. The usual procedure to extract a value of D_o is from the slope of a plot of i vs $w^{1/2}$, which according to equation a) should be a straight line.

$$i = 0.62\ n\ F\ D^{2/3}\ v^{-1/6}\ w^{1/2}\ C_b \qquad a)$$

This equation assumes that the surface concentration of Pb^{2+} ions is zero and that the reaction is under diffusional control. At low overpotentials this will not be the case e.g at an applied cathodic overpotential of 10 mV for a Pb electrode in 0.1M $Pb(NO_3)_2$ the surface Pb^{2+} concentration calculated from the Nernst equation assuming unit activity for Pb^{2+} ions will be 0.046M, at 20 mV it will be 0.021M, 30 mV 0.0096M and at 50 mV 0.00205M. Therefore, only at high overpotentials will the surface concentration of Pb^{2+} approach zero.

Values for the diffusion coefficient for metal ions in an ideal electrolyte are determined at potentials remote from the rest potential where the reaction is under diffusion control and in solutions of low metal ion concentration. The present studies were concerned with investigations on the metal deposition reaction in practical plating solutions i.e with a relatively high $Pb(NO_3)_2$ concentration. At cathodic overpotentials greater than 30mV in 0.1M $Pb(NO_3)_2$ solutions and at high rotational speeds dendritic deposits of Pb formed on the electrode surface. These dendritics changed the nature of the surface under investigation and as a result the current density at a given overpotential did not remain constant.

This inability to control the substrate surface necessitated the selection of a low potential range over which the diffusion coefficient could be determined. Values for the diffusion coefficient have been calculated assuming both a surface concentration of zero Pb^{2+} ions and on the thermodynamic concentration of Pb^{2+} ions on the metal surface (calculated from the Nernst equation). The values of D_o extracted from plots of i_d vs $w^{1/2}$ at a given potential were straight lines, although only over a limited electrode rotation speed as is evident from Figs 82-86.

The values of diffusion coefficient determined in this way were found to be potential dependent.

The values of D_o at a given potential were also calculated from the slope of the 1/i vs $1/w^{-1/2}$ plots i.e the Levich equation based on mixed diffusion and kinetic control as given in equation 6, Section 3.2.2. The results obtained for the diffusion coefficient using the two methods can be seen by a comparison of Tables 45 and 46 with 47A and 48A.

A large difference in the value of D using the Levich equation a) and the Levich equation with mixed diffusional control has also been reported by Quickenden and Jiang (317) for copper deposition. They concluded that the Levich equation based on diffusion control only gives the correct value of D_o over a narrow potential range when the deposition process is strictly under diffusion control. The mixed form of the Levich equation they have shown provides values of D_o that give good agreement with values obtained from other techniques. The values of D_o also remain constant over a wide potential range i.e D_o is essentially independent of potential.

The results from the present studies show that the value of D_o determined from the i vs $w^{1/2}$ plots may vary with overpotential, whereas those obtained from the graph of 1/i vs $1/w^{1/2}$ do not show the same degree of variation. This variation is not thought to be solely associated with the fact

that the concentration of Pb^{2+} ions at the electrode surface is above zero at low overpotentials. Particularly, since at a cathodic overpotential of 30mV and above the values of D_o obtained from the i vs $w^{1/2}$ plots do not vary significantly when they are adjusted to take into account the true surface concentration i.e with the concentration term used in the Levich equation being $(C_b - C_s)$ not C_b. The plots of i vs $w^{1/2}$ were also only linear over a limited rotational speed when compared to plots of 1/i vs $1/w^{1/2}$ which were linear over the whole rotational range studied.

The $1/i$ vs $1/w^{1/2}$ graph takes into account the diffusion process in the presence of kinetic control and it appears that this equation is applicable to the determination of the diffusion coefficient for Pb^{2+} at low overpotentials. Furthermore the values of D_o determined using the mixed diffusion control form of the Levich equation do not exhibit a marked variation with overpotential as those obtained from the i vs $w^{1/2}$ plots and in the non-additive solutions the values of D_o remain constant within the limits of experimental error at 20 and 30mV in 0.1M $Pb(NO_3)_2$ and 30 and 50 mV in 0.01M $Pb(NO_3)_2$ with values of 1.45×10^{-5} and 1.24×10^{-5} cm^2 sec^{-1} respectively.

The surface active agents BRIJ 35, Triton X100 and Pluronic L64 all reduced the value of D_o from that in the non additive solution in both 0.1 and 0.01M $Pb(NO_3)_2$ as determined from the plots of i vs $w^{1/2}$ with Triton X100 showing the greatest reduction in the apparent value of D_o particularly in 0.01M $Pb(NO_3)_2$ solutions.

However, the values of D_o determined from plots of $1/i$ vs $1/w^{1/2}$ did not show the same trend as those for $Pb(NO_3)_2$ solutions containing addition agents with the values of D_o not noticeably different between the additive and the non-additive solutions, except in the case of anthraquinone-2-monosulphonic acid.

In the case of the latter additive the variation in D_o with overpotential was greater than for any of the other addition agents studied. This, it is thought, is associated with the fact that this additive forms a complex at the Pb surface which reduces the activity of Pb^{2+} to below the Nernstian value for Pb^{2+} at a given overpotential.

The additive anthraquinone-2-monosulphonic acid must modify, Pb^{2+} concentration within the boundary layer adjacent to the Pb electrode. Since the value of D_o was calculated on the basis of the Nernstian concentration of Pb^{2+} however if anthraquinone-2-sulphonic acid complexes the Pb^{2+} at the electrode surface a lower concentration term for $C_b - C_s$ would be used. Indeed, at low overpotentials the concentration of Pb^{2+} in anthraquinone-2-monosulphonic acid containing solutions may well be lower than the Nernstian value because of the complexing power of this addition agent. Then only at high overpotentials when the Pb^{2+} concentration approaches zero will a similar diffusion coefficient to that in the additive-free $Pb(NO_3)_2$ solutions be recorded for anthraquinone-2-sulphonic acid containing solutions.

In static 0.1M $Pb(NO_3)_2$ solutions a limiting current density for Pb deposition is visible in additive containing solutions but not in additive free solutions. However, on rotation of the Pb electrode in additive containing solutions no limiting current was observed and the nature of the E vs i curve as well as the value of i_o for Pb deposition were not noticeably different from the non-additive containing solution. Addition agents have been shown not to affect the diffusion coefficient for Pb deposition and therefore it is not a reduction in the diffusion coefficient that causes the limiting current. One possible explanation would be that in additive free $Pb(NO_3)_2$ solutions dendritic deposits of Pb are formed and a diffusion limited current is not visible because of the rapidly changing electrode surface area.

The addition agents it is thought change the morphology of the Pb deposit and prevent the formation of Pb dendrites or growth spirals. This provides a relatively flat yet constant surface area on which the Pb^{2+} deposition reaction can occur and a limited current density for deposition is observed. Indeed, one would expect a limiting current density in low concentration Pb^{2+} solutions if the morphology of the deposit did not change i.e no dendritic growths occurred. The addition agents are thought to prevent the formation of dendritic growths and thus enable the diffusion limited supply of Pb^{2+} to become apparent.

On rotation of the electrode surface the rate of supply of Pb^{2+} ions to the electrode surface increases. In 0.1M $Pb(NO_3)_2$ solutions the addition agent concentration is sufficiently low and cannot diffuse to the electrode surface at a sufficient extent to inhibit the growth process.

The main objective of the 1/i vs $1/w^{1/2}$ plots was to determine the kinetically controlled current at a given overpotential and determine if selected addition agents had any effect on the kinetics for Pb deposition. Since the greater the value of the intercept on the 1/i axis the more kinetically hindered the process. If a sufficiently large overpotential range was studied it would have also been possible to determine i_o and (the charge transfer coefficient) but this was not the case in the present studies since the formation of Pb dendrites limited the overpotential range over which measurements could be made.

Only tannic acid appeared to significantly influence the kinetics for Pb deposition in 0.1M $Pb(NO_3)_2$ solutions, yet in 0.01M $Pb(NO_3)_2$ solutions Triton X100 and anthraquinone-2-mono sulphonic had a significant effect on the kinetics for Pb deposition. Why Triton X100 should only have a significant effect on the kinetics for Pb deposition in low Pb concentration solutions is not readily apparent. It may be that this additive adsorbs at the energetically favoured sites for Pb deposition i.e the kink sites. Thus, in the high concentration solutions the rate of diffusion of Pb^{2+} to the electrode surface exceeds that

for Triton X100, so that whilst the Triton X100 may absorb at certain sites it is rapidly incorporated in the deposit as it grows. In low concentration Pb solutions the concentration of Pb^{2+} approaches that of the additive and it is the rate of diffusion of the additive to the growing surface that could govern the kinetics of the growth process. The additive although incorporated in the growing deposit still diffuses to the Pb surface at a sufficient rate to maintain a high enough concentration on the growing surface, to adsorb at specific sites and inhibit the growth process.

4.2.1 Pb nucleation from $Pb(NO_3)_2$ solutions

The initial stages of Pb deposition from $Pb(NO_3)_2$ solutions at selected overpotentials have been studied using the pulse potentiostatic technique and can be seen in Fig. 116 whilst the effect of different additive concentrations on the i vs t curve can be seen in Fig. 117.

The initially high current density observed in all instances is a result of charging of the double layer capacitance and this decreases rapidly with time.

The deposition of Pb has been studied by a number of workers. Palmisano et al (212) report a linear relationship between i and $t^{1/2}$, which Astley (214) has shown corresponds to 3 dimensional nucleation followed by hemi-spherical growth. A similar current versus time relationship for Pb deposition from $Pb(NO_3)_2$ solutions was also found in the present studies for both additive and non additive containing solutions (see Figs. 118, 119, and 120). The current versus time dependence given by Astley (214) and associated with instantaneous 3D nucleation followed by hemi-spherical growth was :

$$i = \frac{F\, N_o \pi\, M^{\frac{1}{2}}\, (2D_o)^{3/2} C^{3/2}\, t^{1/2}}{\rho^{\frac{1}{2}}}$$

The significance of all units is given in Section 1.5.7.

This equation would predict a zero intercept for the i vs $t^{1/2}$ plot with no dependence upon overpotential. In practice at low overpotentials an intercept on the $t^{1/2}$ axis is observed (Fig 118, 119). This intercept on the time axis has also been observed by Palmisano (212) who explained it in terms of an induction period before nucleation proceeds. The addition of Wafex and CETB to $Pb(NO_3)_2$ solutions appeared to increase the induction period (at a given overpotential) whilst with the additive combination Triton X100 and anthraquinone-2-mono sulphonic acid an intercept on the current axis for the i vs $t^{1/2}$ plot was obtained and no induction period reported.

Fleischmann et al (213) in their studies on the effect of additives on Ni deposition have also reported an increase in the induction period prior to nucleation of the 3D growth centres and showed that the additive pyridine increased the induction period but did not affect the rate of growth of the Pb nuclei. This was the phenonenon observed with the addition of the additives CETB and Wafex to $Pb(NO_3)_2$ plating solutions i.e the induction period for nuclei formation increased at a given overpotential but the rate of growth of the nuclei was unaffected.

The additive combination Triton X100 and anthraquinone-2-monosulphonic acid, does appear to affect the rate of nuclei growth as is evident from the slope of the i vs $t^{1/2}$ plot, yet it did not produce any induction period for nuclei formation.

The gradients of the i vs $t^{1/2}$ curve also enabled a calculation of N_o the number of nucleation sites to be performed (see Table 82), using the equation given by Astley. The additive Wafex does not appear to have any significant effect on reducing the number of nuclei formed at a given overpotential yet the additive combination Triton X100 plus anthraquinone-2-monosulphonic reduced the number of nuclei formed at a given potential i.e these addition agents inhibited the formation of Pb nuclei. It should be remembered that at low overpotential the surface Pb^{2+} concentration will not be zero and that the values quoted in Table 82 do not take this into account. The reason for the

intercept on the current axis for Pb deposition from a Triton X100, anthraquinone-2-monosulphonic acid solution is not fully understood at this stage and it would require more detailed studies to determine the reason for the absence of any induction period.

TABLE 82

Gradient of i vs $t^{1/2}$ curve for 0.1M $Pb(NO_3)_2$ solutions selected containing addition agents and the number of nuclei calculated from equation proposed by Astley and Hills (214).

Solution Composition	Gradient at given potentials (A cm^{-2} $sec^{1/2}$)				Number of nucleation sites at given potentials (N_o cm^{-2} x 10^7)			
	0.165V	0.180V	0.20V	0.22V	0.165V	0.180V	0.20V	0.22V
0.1M $Pb(NO_3)_2$	0.47	1.67	2.91	-	1.10	3.82	6.81	-
0.1M $Pb(NO_3)_2$ +0.5 gl^{-1} Wafex	0.18	2.09	2.91	-	0.42	4.89	6.81	-
0.1M $Pb(NO_3)_2$ + 1 gl^{-1} Triton X100 +0.1 gl^{-1} anthra-quinone-2-mono sulphonic acid	-	0.33	0.76	1.53	-	0.77	1.78	3.58

4.2.2 Cyclic voltammetry and electrochemical impedance studies

The cyclic voltammetry studies on the polarisation of a Pt electrode in 0.1M $Pb(NO_3)_2$ solutions with and without addition agents all indicate a diffusion limited supply of Pb^{2+} ions to the electrode surface. For a reversible process the value of E_p should be independent of sweep rate however, this was not found to be the case. A linear relationship between E_p and $v^{1/2}$ was observed (Fig. 111), extrapolation of which to zero sweep rate is $v^{1/2} = 0$ gave values of E_p at zero sweep rate. It was interesting to note that the value of E_p at $v^{1/2} = 0$ for the non-additive containing solution was higher than for the additive containing solutions.

The values of E_p for the non-additive solution taken at higher sweep rates when extrapolation to zero sweep rate on the plot of $v^{1/2}$ did yield a lower value of E_p. The high values of E_p at low sweep rates may be associated with the system under investigation e.g that dendritic deposits of Pb have sufficient time to form a low sweep rate and these can change the nature of the surface under investigation, effectively reducing any diffusion effects. The linear relationship between E_p and $v^{1/2}$ may be explained in a similar manner to that for metal passivation (see Section 3.5.4), where partial film formation takes place. The relationship between potential and sweep rate is worthy of further investigation.

The nature of E vs i curves at different sweep rates is dependent upon the addition agent. In the case of the additive free solution a diffusion limited peak E_p is visible followed by a rapidly rising current, presumably due to dendritic growth. The addition agents all inhibit this rising current to varying extents and with certain additives e.g BRIJ35 (Fig. 107) and Tannic acid (Fig. 109), the rapidily rising current after E_p is not visible.

The results of experiments on the activation energy for Pb deposition show an activation energy for Pb dissolution of 7 kJ $mole^{-1}$, similar to the value of 5 kJ $mole^{-1}$ reported by

Haruyama (216). Both values of activation energy were determined on a cold worked surface not subjected to any anneal and this could explain why these low values of activation energy are low in comparison to the results of Hampson and Larkin (217) where a value of 12 kJ mole^{-1} was reported.

The values of the exchange current density for Pb^{2+} deposition from $Pb(NO_3)_2$ solutions determined from the rotating disc and cyclic voltammetry techniques are lower than the reported literature values. However, this is more than likely due to diffusion effects which limit these techniques to measurements of electrochemical reactions with a low exchange current density. The results of work using the electrochemical impedance technique, although limited in quantity do provide values of i_o that correspond to those reported by other workers (204, 205, 216, 217).

The Z' vs Z" plot for 0.05M $Pb(NO_3)_2$ with and without Triton X100 do not show any marked difference. The same value for double layer capacitance is obtained in both solutions and similar values of i_o recorded. Only the Warburg impedance in the low frequency spectrum is different between the two solutions with Triton X100 appearing to reduce the diffusion coefficient for Pb^{2+} diffusion. The same value of double layer capacitance between the two solutions is also indicative of little adsorption of the Triton X100.

The addition of the additive anthraquinone-2-sulphonic acid to a solution of 0.05M $Pb(NO_3)_2$ + 1 gl^{-1} Triton markedly reduces the exchange current density for the Pb deposition process and shows a high double layer capacitance 170 μF cm^{-2} indicative of strong adsorption and possibly some other factor. A similar effect is seen with the use of tannic acid as an addition agent.

The effect of rotational speed on the Z' vs Z" curves in tannic acid and Wafex containing solutions was not investigated in the present studies but would warrant further investigation to study if the rate of diffusion of addition agents has an effect on the

charge transfer process. Although it is apparent in static solutions that anthraquinone-2-sulphonic acid can considerably reduced the measured value of i_o.

4.2.3 The nitrate reduction process on a Pb cathode

In $Pb(NO_3)_2$ solutions four cathodic processes may take place 1) Pb deposition, 2) hydrogen evolution 3) oxygen reduction and 4) nitrate reduction, whilst in an additive containing solution a fifth process namely reduction of the additive may also occur, depending upon the additive and the electrode potential.

The nitrate reduction process may proceed via one of two possible mechanisms (319, 328). In weakly acidic solutions and in the absence of a catalyst nitrite formation will be favoured

$$NO_3^- + 2H^+ + 2e \longrightarrow NO_2^- + H_2O \qquad 1)$$

Whilst in strongly acidic solutions reduction of nitrate ions may occur via reaction 2)

$$NO_3^- + 9H^+ + 8e \longrightarrow 3H_2O + NH_3 \qquad 2)$$

In the $Pb(NO_3)_2$ plating solution used for the commercial production of PbO_2 for primary $Pb/HBF_4/PbO_2$ batteries it is the nitrite formation reaction which is favoured. This is evident by the yellow colour observed with prolonged operation of the plating solution, which is due to the formation of a weak complex of the type $Pb[Pb(NO_2)_4]$.

The work carried out in the present studies revealed that the nitrate reduction current density is small in comparison to that for Pb deposition at a given potential, particularly in high pH solutions although in acidified $Pb(NO_3)_2$ solutions the NO_3 reduction current may be significant e.g in 0.1M $Pb(NO_3)_2$ + 1M KNO_3 pH2 the ratio of the nitrate reduction current density to that for Pb deposition at a c.d of 5 Adm^{-2} is approximately 0.1% whilst in pH 0.7 solutions it may be approximately 5%.

Triton X100 when added to a 1M KNO_3 solution has been shown to reduce the rate of NO_3^- reduction at a given potential and pH, from that in the additive free solution. This is thought to be due to the strong adsorbtion of Triton X100 on the Pb electrode hindering the diffusion H^+ ions to the electrode surface. Only at high overpotentials will the rate of diffusion of H^+ ions to the electrode surface control the overall rate. If the Triton X100 absorbed on the Pb surface reduced the number of active sites for NO_3^- reduction this kinetic effect should be apparent at low overpotentials but this was not observed.. The mechanism whereby Triton X100 inhibits the reduction of NO_3^- should be the subject of further studies.

It may well be that the additive combination Triton X100 plus anthraquinone-2-monosulphonic acid in a simultaneous plating solution would reduce the rate of nitrate reduction in comparison to that for the non-additive solution. This could be confirmed by separate colorimetric analysis for nitrite ions.

Indeed in a non-additive containing $Pb(NO_3)_2$ solution oxidation of the nitrite ions is carried out by the addition of H_2O_2. Since the nitrite ions formed at the cathode can reduce the current efficiency for PbO_2 formation. The oxidation of nitrite to nitrate by the use of H_2O_2 in a simultaneous plating solution would also result in the oxidation of the organic plating additives and therefore necessitate the addition of fresh organic addition agents. The exhausted organic addition agent could be dissolved in an immiscible organic solvent which would then be decanted off prior to the use of fresh addition agents. Alternatively the organic addition agents could be removed from the plating solution prior to the use of H_2O_2 to remove the NO_2^-.

The removal of NO_2^- ions from the simultaneous solution would be necessary to maintain the efficency for PbO_2 formation. However, in a simultaneous plating solution the frequency of H_2O_2 additions may have to be reduced.

4.2.4 Electrodeposition of PbO_2 from $Pb(NO_3)_2$ in additive containing solutions.

The addition of certain organic addition agents to $Pb(NO_3)_2$ solutions has been shown to affect the nature of the E vs i curve for PbO_2 electrodeposited from these solutions (see Figs. 132-139, 144-153).

Organic addition agents inhibit the nucleation of the PbO_2 deposit at a given potential as can be seen in Table 56. The increase in overpotential necessary before nucleation of PbO_2 takes place was dependent upon the nature of the addition agent with tannic acid, peptone and diphenylamine exhibiting the greatest effect. The nucleation of PbO_2 onto an inert substrate was first studied by Fleischmann and Liler (170) however, little work has since been reported, especially on the effect of organic addition agents. Gilroy and Stevens (173) have studied the effect of F^- on the nucleation and growth of PbO_2 electrodeposits from $Pb(NO_3)_2$ solutions. F^- ions they found reduced the number of nuclei and the growth rate at a given potential. The morphology of the PbO_2 deposit was also studied.

The mechanism proposed by Gilroy whereby F^- ions inhibited nucleation was that they re-adsorbed on the substrate surface and prevented the formation of a pre-adsorbed layer and thus reduced the density of viable nuclei. The F^- ion adsorption onto the surfaces of the growing crystal could inhibit its growth. The slower growth of PbO_2 nuclei in the presence F^-, Gilroy and Stevens considered produces conditions amenable to progressive nucleation.

Cyclic voltammetry studies do not provide detailed information on the growth of the PbO_2 deposits. However, from separate plating experiments the use of selected organic addition agents did reduce the grain size for the PbO_2 deposit (see Section 3.1.5.3). They were even found to affect the crystallographic composition of the deposit (see Section 3.1).

The fact that certain addition agents appear to inhibit the nucleation step is evident by the increase in potential necessary before deposition can occur. The addition agents would then behave in a similar manner to F^- ions in reducing the number of nuclei formed at a given potential. The growth of the nuclei would then be inhibited. Furthermore, because of the small grain size observed with certain addition agents it is probable that progressive nucleation of the PbO_2 takes place. This would need to be confirmed by separate studies and coupled with the manner in which addition agents affect the deposit morphology.

At low sweep speeds (50 mV sec^{-1}) in an additive free solution a nucleation peak for PbO_2 deposition onto Pt is visible Fig. 131 and on subsequent scans when the nucleation of PbO_2 takes place it occurs on what is essentially a PbO_2 surface yet at a lower potential.

In solutions containing Triton X100 a small anodic current density is visible at potentials greater than 1.3V. A similar effect was also apparent with butyne-1,4-diol. This is thought to be due to oxidation of these additives.

A plot of i_p vs $v^{1/2}$ for all $Pb(NO_3)_2$ solutions was found to be linear, although the slope and intercept were dependent upon the nature of the addition agent. In the additive containing solutions an intercept on the i_p axis of zero was invariably obtained whilst for the non-additive solution a positive intercept was recorded.

The values of $E_p - E_{p/2}$ for a non-additive solution were found to be essentially constant upto sweep rates of 190 mV sec^{-1} above this the value of E_p - Ep/2 was found to increase. This may be associated with the experimental technique e.g the position of the reference electorde and errors in potential measurement because of the ohmic potential created by current flow in the electrolyte.

For a reversible reaction the value of $E_p - E_{p/2}$ is a constant independent of sweep rate and is denoted by the following equation

$$E_p - E_{p/2} = 2.2RT/nF$$ where all units have their usual significance

$$E_p - E_{p/2} = 0.056.5/n \text{ at } 25^{\circ}C$$

The value of $E_p - E_{p/2}$ over the sweep range 20 to 140 mV sec^{-1} was 0.115V. Thus n is equal to 0.5. The theoretical value of n for the formation of PbO_2 from $Pb(NO_3)_2$ solution is 2.

For the non-additive containing solution, the values of $E_p - E_{p/2}$ were not constant and lower than for the non-additive solution.

The first peak for the deposition of PbO_2 is indicative of a diffusion dependent reversible process, where the following relationship between i_p and v was observed

$$i_p = (2.69 \times 10^5)\, n^{3/2}\, D^{1/2}\, v^{1/2}\, C_o$$

The value of D_o for Pb^{2+} obtained from the graph of i_p vs $v^{1/2}$ was 2.6×10^{-6} cm^{-2} sec^{-1} for the non-additive solution.

The rapidily rising current with increase in overpotential is thought to be associated with the concurrent process of oxygen evolution. The magnitude of i_p was invariably greater for the solutions containing the surface active agents BRIJ35, Pluronic L64 and Triton X100. This may be because these addition agents alter the boundary conditions at the electrode interface i.e. modify the diffusion layer thickness. These additives do also appear to reduce the rate of the oxygen evolution reaction.

The nucleation peak observed on the second scan occurs at a lower potential than the first and is due to deposition of PbO_2 onto a PbO_2 substrate. The surface concentration of Pb^{2+} ions on this second scan will also be greater than in the bulk solution because of the reduction of PbO_2 in the first scan. This higher Pb^{2+} concentration will also explain the lower potential at which PbO_2 deposition takes place.

At fast sweep rates (250 mV sec^{-1}) the first passivation peak is absent when certain additives are used (Fig. 152, 153). Because insufficent time has elapsed to create a diffusion limited supply and the higher overpotential required before nucleation can take place. The potential for the first and second passivation peak also approaches the same value because the reduction of PbO_2 at fast sweep speeds occurs at too fast a rate to cause a large increase in the Pb^{2+} concentration. In the tannic acid solution, a passivation peak is visible for the second potential scan, because growth of the PbO_2 deposit is not inhibited since nuclei will be present from the first scan, at which PbO_2 deposition can take place.

This work was not carried out as an exhaustive study on PbO_2 deposition but has highlighted areas for further research.

4.3 The varying degrees of adhesion of electrodeposited PbO_2 onto Ni foil

Earlier work by Ramanathan (192) carried out in these laboratories has shown that the Ni foils that exhibited 'poor' adhesion of PbO_2 were invariably Ni200, whilst those foils that exhibited 'good' adhesion for electrodeposited PbO_2 were invariably Ni270. No definite conclusions as to the reason for this were proposed by Ramanathan, although he did observe the formation of a brown film on Ni200 after anodic etching in 30% H_2SO_4. The removal of which was shown to improve the levels of adhesion, but not to any great extent.

However, in the present studies the opposite was found to occur i.e it was the samples of the high purity Ni270 foil that

exhibited 'poor' levels of adhesion for electrodeposited PbO_2, whilst the Ni200 foil samples exhibited good adhesion. This latter observation was further supported by tests carried out on commercially prepared samples of battery plate material, which confirmed that it was the Ni270 not the Ni200 foils that exhibited a low level of adhesion for electrodeposited PbO_2.

The chemical composition of all samples used as substrates for PbO_2 deposition was determined, the results from which (Section 3.3.1) confirmed that all samples of Ni foil that exhibited poor levels of adhesion did conform to the specification for Ni270, whilst the foils which exhibited good adhesion were Ni200. Ramanathan did not undertake a separate chemical analysis in his studies to confirm that the foils under examination conformed to a particular specification. However, from the electron micrographs of the etched foil surfaces and the electrochemical polarisation curves he reports, it would appear that the Ni samples which Ramanathan investigated which exhibited poor levels of adhesion were indeed Ni200 and those that exhibited good levels of adhesion were Ni270.

The fact that both Ni200 and Ni270 foils have now been shown to exhibit poor levels of adhesion, infers that minor variations in the chemical content between the different foils cannot explain the problem of the poor adhesion for electrodeposited PbO_2 onto certain foil samples.

The most noticeable visual difference between the 'good' and 'bad' adhesion foils in the present studies was a variation in the etch pattern over the foil surface after anodic etching in 30% H_2SO_4. In the case of the Ni200 foils the surface was uniformly etched, as is evident from Fig 74P. However, all Ni270 foils exhibited a non uniform etch pattern, with certain areas of the foil clearly unaffected by the etching operation. The reason for the non uniform etch on the Ni270 foils was not readily apparent, although a number of possibilities did exist (a) surface contamination (b) variations in the chemical composition of the foils over relatively small areas or (c) variations in the degree of preferred orientation.

Results from the XRFS analysis could not detect any variation in chemical content between the etched and unetched areas neither did the Back Reflection X-ray diffraction patterns show any evidence of preferred orientation in any of the Ni foil specimens, which could account for enhanced rates of metal dissolution on certain areas of the foil.

The most likely explanation for the random etch pattern on certain Ni270 foils is surface contamination, either from lubricating oils used in the rolling process or from the presence of an oxide film. The work carried out using an Auger spectrophotometer together with ion beam etching (Section 3.4.6) has shown that the Ni270 foil that exhibited poor levels of adhesion had a considerably thicker oxide film in the as received state, than the Ni200 foil, 400A^{o} as opposed to 200A^{o}. Auger and XPS work was also used to determine if any differences between the etched and unetched areas of a Ni270 foil could be detected but this work was not conclusive. Indeed, although a slightly higher oxygen level was detected in the etched areas of the foil, this could presumably be due to the larger exposed surface area of the etched area and also the presence of some residual SO_4 from the anodic etching solution. Thus, this work did not enable any direct differences in surface contamination between the etched and unetched areas to be detected.

The most interesting aspect of the XPS studies is the high oxide film thickness found on the Ni270 samples (see Fig. 158). The formation of which is thought to occur during the rolling process.

The production of Ni foil involves the gradual reduction in width of a slab of Ni until the required foil thickness is obtained. This process involves a number of successive rolling operations and interstage anneals, to produce foils of the required hardness and surface finish. The maximum interstage anneal temperature is 1000^{o}C but this will be reduced as the strip is rolled

thinner to a minimum of 700°C. Pickling of the hot worked material is then carried out after the anneal in a warm nitric acid/ferric chloride solution. Annealed material will be soft and have a matt surface finish but brightness is retained if dry hydrogen is used as the protective atmosphere. The degree of polish on the work rolls will also control the level of surface brightness.

It is thought that the oxide contamination of the Ni foil takes place when the foil surface is at a sufficient temperature for thermal oxidation to occur. It may be associated with the fact that insufficient time is allowed to reduce the oxide film during the interstage anneal when a reducing atmosphere is used or even the lack of a reducing atmosphere. The ingress of air into the reducing atmosphere used for the interstage anneals may also result in oxidation of the Ni foil.

A variation in the oxide thickness over the specimen surface could account for the uneven etch pattern observed. This may be associated with inadequate cover of the hot foil surface with lubricating oils or incomplete removal of the oils prior to the interstage anneals resulting only in the exposure of certain areas of the Ni foil to the oxidising atmosphere.

Some of the Ni270 foil samples did appear to be covered with a interference film and were of a dull matt appearance, where as the Ni200 foils all had a bright surface finish, which is generally achieved by passing the foil through highly polished cylindrical rollers and the use of hydrogen as a reducing atmosphere to remove any oxide film formation in the interstage anneals.

Analysis of the tensile test results show that the Ni200 foil studied had not been extensively work hardened after its final interstage anneal, as evident from the high elongation before failure, (see Table 64) in comparison to the Ni270 sample. An examination of the hardness readings would indicate that the Ni200 foil is in the quarter to half hard condition whilst the

Ni270 foils are in the spring hard condition. The exact cause of the higher oxide contamination on Ni270 can only be postulated at this stage without further details on the rolling procedure, from the manufacturers. However, results would indicate that the Ni270 foils had been subjected to a greater degree of cold work than the Ni200 foils and thus received to a larger number rolling passes following the interstage anneal. This could result in a greater degree of surface contamination on the Ni270 foils.

Furthermore, from the surface finish obtained on the Ni270 foils and the results of the Auger analysis it would be reasonable to infer that a reducing atmosphere may not have been used in the interstage anneals on these foil samples.

The presence of an oxide film has been shown to have a detrimental effect on the adhesion of electrodeposited coatings and thus every effort should be made to ensure that a thick oxide film is absent from the Ni foil surface used as the substrate for PbO_2 deposition. The foils should have a bright oil free surface which would be achieved by reducing the number of rolling operations following the interstage anneal, the use of a reducing atmosphere in the interstage anneal and using rolls with a smooth surface finish.

Ramanathan states the hardness condition of the Ni200 and Ni270 foils he studied but not their surface condition. It is however interesting to note that whilst the S.E.M photographs presented in his Thesis were limited in quantity, one low magnification view of an etched Ni200 surface did appear to exhibit the uneven etch pattern found in the present studies on Ni270 foils. Therefore whilst Ramanathan did not report the appearance of an uneven etch pattern this does not necessarily mean that this did not occur on the Ni200 samples he examined but merely that he may not have attached any significance to this observation. Thus, the poor adhesion of PbO_2 onto Ni200 observed by Ramanathan may possibly be due to the surface finish of the foils used in his investigations.

Further evidence for the fact that oxide contamination of the Ni surface is responsible for the non-uniform etch pattern is that a sample of Ni270 that exhibited a random etch pattern after anodic etching in a solution of 30% H_2SO_4, when heated to 800°C under vacuum for half an hour then subjected to the anodic etching operation exhibited a smooth uniformly etched, yet faceted surface (see Fig. 94P). At this temperature and pressure NiO is thermodynamically unstable and will revert to its base metal. Thus no surface oxide film would be present.

The Ni foils treated in this way do not form suitable substrates for PbO_2 deposition since the resultant PbO_2 deposits are poorly adherent. Thus whilst it would appear that the presence of an oxide film on the Ni substrate has a detrimental effect on the adhesion of electrodeposited PbO_2, the nature of the substrate surface would also appear to be equally as important. A smooth faceted surface without any etch pits, as is obtained by annealing the Ni270 foil at 800°C would not aid the mechanical keying of the PbO_2 deposit, as subsequent adhesion tests have shown (see Fig. 73P).

The etch patterns for Ni200 and Ni270 foils are noticeably different as is evident from the scanning electron micrographs (Figs. 76P - 95P).

In the case of the Ni200 foils elongated etch pits orientated in the rolling direction were visible, with some undermining of the Ni surface by small pits radiating out from the centre of the large individual etch pits. The number of etch pits per unit area and their size varied over the foil surface but no relatively large areas could be seen that were unaffected by the etching operation. Only the area of the Ni foil in the immediate vicinity of the etch pit was unaffected by the etching process.

The nature of etched surface on Ni270 foils varied for individual specimens. On a heavily work hardened Ni270 sample etch pits similar to those seen on the Ni200 samples were visible. The etch pits were again elongated in the direction of rolling but

were rounded and the area in the immediate vicinity of certain etch pits was affected by the etching operation. However, large areas of the Ni foil had a relatively small density of etch pits when compared to other areas on the same foil e.g compare Fig 85P with Fig 86P. The nature of the etched surface on other Ni270 foils was different and some large areas were again clearly unaffected by the etching process whilst other areas of the foils were well etched. In the etched areas no clearly definable etch pits were visible, merely a rough well etched surface with no preferred orientation in the direction of rolling.

The etching proces is an essential pre-requisite in achieving a good Ni substrate suitable for the electrodeposition of an adherent PbO_2 deposit. The increase in surface area brought about by the etching process provides a clean, rough surface onto which the PbO_2 deposit may "key". Double layer capacitance measurements (Section 3.3.5) show that the surface area of the Ni200 foils is increased by approximately 1.5 times with anodic etching and that reproducible results for the double layer capacitance on this foil could be obtained. The results of similar measurements on Ni270 foils did not show the same degree of reproducibility, the values for double layer capacitance varying as would be expected varied with the extent to which the foil surface had been etched and on the source of the Ni270 foil.

Ramanathan in his work on the capacitance determinations on etched Ni foil did not report any variation in the reproducibility of his results and obtained values for increase in surface area on anodic etching, (measured at -0.16 V i.e the point of zero charge) of 1.7 times for Ni270 foil and 1.5 times for Ni200 etched at 2.5 Adm^{-2} for 10 min. Furthermore, in his discussion on the double layer capacitance results Ramanathan (192) states, that at a low c.d. the Ni200 surface was only etched in certain areas and a high c.d. was necessary before a more uniform etch pattern was observed. A phenomenon which he did not report on the Ni270 samples studied. This provides further evidence for the fact that the Ni200 foils Ramanathan used for his studies <u>did</u> exhibit the uneven etching characteristics that have been found on Ni270 foils used during the course of the present investigation.

An examination of certain bend test adhesion failure specimens was also undertaken to try to ascertain the adhesion failure mechanism. The tip of bend test failure specimens over which the PbO_2 had been detached does not show any exposed Ni surface, but a very thin PbO_2 coating, as is evident from Figs 63P and 64P. Cracks were visible in the coating which ran parallel to the centre of the bend, with the space between each parallel line of cracks increasing with distance from the centre of the bend. This indicates that the adhesion failure is cohesive, since it occurs not at the PbO_2/Ni interface but in the PbO_2 deposit close to the interface. Furthermore, when such failures occur the PbO_2 deposit is invariably detached along the whole length of the bend not at a few isolated locations.

In the samples of PbO_2 electrodeposited onto Ni200 foils that exhibited good levels of adhesion. The PbO_2 deposit at the centre of the bend was seen to have cracked but these cracks had not resulted in the detachment of the PbO_2 deposit (see Figs. 71P and 72P).

When the bend test is used the base on the Ni foil at the centre of the bend is subjected to a compressive stress, whilst the PbO_2 deposit is subjected to a tensile stress. The strain exerted on the PbO_2 deposit is at its greatest on the PbO_2 deposit surface. PbO_2 is a very brittle material and will fracture when a strain is applied to it and this explains the cracks visible on the deposit surface after the bend test on both 'good' and 'bad' adhesion failure specimens.

The adhesive failures observed are a function of the state of the substrate surface, preferred orientation in the PbO_2 deposit, the presence an oxide film and the forces acting on the PbO_2 deposit at the Ni/PbO_2 interface. The reasons why the failure of the bend test adhesion specimen failures is invariably cohesive not adhesive, why oxide contamination should cause a cohesive failure and why failure occurs along the whole length of the bend and at a few locations are not readily apparent.

4.3.1 The electrochemical properties of Ni200 and Ni270 in H_2SO_4 and $Pb(NO_3)_2$ solutions

Electrochemical studies on different samples of Ni200 and Ni270 foil show that Ni200 is electrochemically more active than Ni270. This is evident from Fig 198 which shows that the value of i_{pp} in a solution of 360 gl^{-1} $Pb(NO_3)_2$ at a given pH is higher for the Ni200 than the Ni270 foils.

High values of i_{pp} for a Ni200 electrode anodically polarised in a $NiSO_4$ electrolyte in comparison to the values for a high purity Ni electrode have also been reported by Di Bari and Petrocelli (256). They showed in their studies that minor impurity levels of selected elements had a greater effect on the anodic polarisation curve than the degree of cold work since these catalyse the electron transfer process. Therefore since Ni200 has a higher impurity content than Ni270 it is not surprising that differences in the value of i_{pp} and E_{pp} between the two foils were observed. The anodic polarisation curves for different samples of Ni200 and Ni270 did not reveal any unexpected variations that would possibly explain the variation in the levels of adhesion of PbO_2.

The specimen area used for the polarisation studies was small and it was difficult to obtain reproducible results for the E vs log i curves for the different samples particularly the Ni270 specimens, where large variations in both i_{pp} and E_{pp} were observed. A phenomenon which is thought to be associated with a greater degree of surface contamination on the Ni270 samples.

The values of E_{pp} recorded indicate that film passivation is due to the formation of Ni_3O_4 not NiO, with an increase in temperature increasing the primary passivation potential for Ni270 but having little effect on the value of E_{pp} for Ni200. Variations in the degree of work hardening and foil composition also appeared to have a slight effect on the values of E_{pp} and i_{pp}.

Work conducted to measure the change in dissolution current with time for different samples of Ni etched in H_2SO_4 at a constant potential did reveal that reproducibility of the results from this work was difficult to achieve, presumably due to the nature of the surface under investigation.

Samples of Ni200 all exhibited a rapidly rising current with time for the first 50 to 100 seconds, at a constant potential after which time the current density reduced. An induction period prior to the rapidly rising current was visible.

However, all samples of Ni270 investigated exhibited a very small induction period, followed by a rising current density. The current density at a given potential was also invariably lower for all Ni270 foils examined with the exception of one, than for the Ni200 foil. Anealing of a Ni270 sample produced a similar i vs t curve to that obtained with Ni200 foils except that the initial induction period was very short and a greater degree of reproducibility was achieved.

An E vs i curve for an Ni200 and Ni270 electrode polarised from its rest potential at 700 mV sec^{-1} in 360 gl^{-1} $Pb(NO_3)_2$, shows that Ni200 is more active but also that the nature of the electrochemically formed film is different, with the value of i_{pp} for the second passivation peak apparently greater for the Ni270 sample. The polarisation at fast sweep speeds was conducted to simulate the effects of a practical plating solution where a rapid current perturbation is applied to the Ni substrate.

4.4 The thermal decomposition of PbO_2 and electrochemical properties of Pb and PbO_2 in 48% HBF_4

The work on the thermal decomposition of PbO_2 and electrochemical properties of Pb and PbO_2 in 48% HBF_4 was undertaken to ascertain the reason for the improved activation times of heat treated PbO_2 when compared to the unheat-treated deposits.

The improvement in activation time by heat treatment of electrodeposited PbO_2 at 250°C for 30 min was first reported by Smith (9) and is the subject of a British Patent (21). However, no definite explanation for the improved activation times has so far been proposed. The objective of the present studies was to attempt to explain this phenomenon.

4.4.1 The thermal decomposition of PbO_2

A limited amount of research has been reported in the literature into the thermal decomposition of PbO_2 and some conflicting information is given, particularly on the temperature at which the decomposition of PbO_2 commences.

The initial work on the thermal decomposition of PbO_2 was therefore concentrated on thermodynamic calculations to determine the theoretical temperatures at which decomposition of PbO_2, to its lower oxides could occur. This would enable an accurate assessment of the results obtained from the present studies to be made. A graph of ΔG vs temperature for PbO_2 decomposition to its different oxides is shown in Fig. 182.

The dissociation of PbO_2 to Pb_3O_4 has been calculated to be theoretically possible at temperatures above 204°C at an oxygen partial pressure of 0.21 atm. The temperature may vary slightly depending upon the source used to obtain the value for free energy value and also on the nature of the PbO_2 deposit i.e whether α or β -PbO_2, since the different crystalline forms have different free energies of formation.

Nishimura et al (321) have shown that decomposition of β -PbO_2 occurs at 250°C and also report an unexplained phase change or thermal decomposition reaction at approximately 180°C but could not detect any change in crystal structure of the β -PbO_2 heated to this temperature. Alexandrov (323) found that heating rate affected the apparent temperature at which decomposition occured, but noted that at temperatures below 280°C no phase change of PbO_2 took place with decomposition of PbO_2 only commencing at 290°C. The formation of Pb_3O_4 did not occur until 490°C.

Ruetschi and Cahn (324) have also carried out work on the thermal decomposition of α and β-PbO_2. They report that α-PbO_2 decomposes at lower temperatures than β-PbO_2, with rapid decomposition appearing to commence at temperatures in excess of 250°C for α-PbO_2 and 310°C for β-PbO_2. Ruetschi and Cahan also quote values for the free energy difference G between the α and β oxides but it should be pointed out that the low value of ΔG (1.6 kJ $mole^{-1}$) would not explain the reason for the apparently large difference in dissociation temperature, they observed. Butler and Copp (325) also report that β-PbO_2 remains stable up to 293°C with only a slight loss of weight whilst in the temperature range 293°C to 343°C and α-PbO_x oxide is formed, above 359°C this converts to β-PbO_x then decomposes to Pb_3O_4 above 374°C.

In the present studies the change in the diffraction pattern of PbO_2 reported by Nishimura at 250°C was not observed and this is further supported by the very small weight loss with time recorded on heating PbO_2 at this temperature. The small variations in relative intensities observed for electrodeposited PbO_2 heated to 250°C are considered to be due to small changes in the degree of preferred orientation the PbO_2 grain size, brought about by heating the electrodeposited coating.

Bagshaw (326) has shown that electrodeposited PbO_2 does exhibit a considerable degree of preferred orientation.

Heat treatment of electrodeposited PbO_2 at 300°C for 24 hours was still not found to effect the nature of the X-ray diffraction pattern obtained and no new reflections could be detected. However,separate weight loss measurements did show that decomposition of PbO_2 with time did occur at 300°C. After 8 hours exposure at 300°C the total Pb_3O_4 content would be approximately 9% and the presence of the PbO_x compound formed should be detected by X-ray studies. The reason why no new compound could be detected is not readily apparent.

At 350°C new reflection peaks were visible, as was evident from Figs. 191 - 194, either attributable to the formation Pb_3O_4 or a PbO_x oxide. As Alexandrov reports that at 360°C $PbO_{1.54}$ is formed and that Pb_3O_4 is not formed until 374°C.

Heating PbO_2 to temperatures in excess of 350°C and upto 500°C the weight loss vs time curve appeared to reach a maximum value then cease. At 460°C the weight loss vs time curve approached the theoretical value of 44.6 mg per gram of PbO_2 for conversion to Pb_3O_4, whilst at 506°C the weight loss of 53mg per gram of PbO_2 is in excess of theoretical value for conversion to Pb_3O_4 and conversion to PbO must take place at this temperature.

Therefore whilst decomposition of PbO_2 at 250°C is thermodynamically possible. The rate of decomposition is extremely low. The changes in internal stress that occur by heating electrodeposited PbO_2 are therefore thought to be mainly associated with recrystalisation of the PbO_2 deposit, loss of incorporated hydroxyl ions although the thermal decomposition of PbO_2 to PbO_x and incorporation of this in the deposits may also be a contributing factor.

Smith (9) reports that the pH of the $Pb(NO_3)_2$ solution from which PbO_2 is deposited is an important factor in determining the voltage rise time of the PbO_2 deposit. At the anode a high concentration of H^+ will build up from the formation of PbO_2 i.e by the reaction $Pb^{2+} + 2H_2O \longrightarrow PbO_2 + 4H^+ + 2e$. Therefore, the pH at the anode will be lower than in the bulk solution. The pH at the anode solution interface will be governed by c.d. temperature and rate of diffusion of H^+ ions into the bulk solution away from the growing PbO_2 deposit. Agitation of the PbO_2 anode during deposition will increase the rate of diffusion of H^+ ions and thus increase the pH at the electrode solution interface. Work was carried out to determine if agitation of the anode during PbO_2 deposition did produce PbO_2 deposits with a superior activation time.

A PbO_2 deposit with an improved activation time was obtained by rotating the anode during electrodeposition at 500 rpm. This gives further support to the fact that the solution pH is an important factor in determining the PbO_2 deposit performance, a fact already reported by Smith who noted that PbO_2 electrodeposited from a $Pb(NO_3)_2$ solution of pH 3.9 had a faster activation time than PbO_2 from a pH 3.2 solution.

The increase in activation time may be associated with the fact that there is a higher percentage of α-PbO_2 in the PbO_2 deposit formed in solutions of a high pH. Other work (313) has indicated that the pH of the $Pb(NO_3)_2$ solution from which the PbO_2 is deposited does determine the crystallographic composition of the PbO_2. Therefore, since α-PbO_2 has a higher exchange current density i_o for PbO_2 reduction in HBF_4 than β-PbO_2, any increase in the -PbO_2 content could affect the value of i_o for electrodeposited PbO_2. Because the exchange current density can be shown to affect the voltage rise time of the PbO_2 deposit it is proposed that the modification of the α to β PbO_2 ratio on solution agitation explains the reason for the improved activation time.

4.4.2 The anodic dissolution of Pb and cathodic reduction of PbO_2 in HBF_4

A limited investigation into the anodic dissolution of Pb and cathodic reduction of PbO_2 in 48% HBF_4 was carried out primarily to aid the understanding of the improved activation times for the $Pb/HBF_4/PbO_2$ battery brought about by heat treatment of the electrodeposited PbO_2 cathode. The information from these studies was also thought to be useful in providing supplementary information on the performance of the $Pb/HBF_4/PbO_2$ battery.

The exchange current density for Pb dissolution was determined using three different techniques extrapolation of the E vs log i curve to zero overpotential, determination of the linear portion of the η vs i curve and electrochemical impendance studies to determine the charge transfer resistance, at room temperature.

The mean value of i_o obtained from two polarisation data experiments at room temperature was 1.35 x 10^{-3} Acm^{-2} whilst that using the impedance technique was 1.45 x 10^{-3} Acm^{-2}. All values show a close agreement between each other. No value of i_o for Pb dissolution in HBF_4 could be found in the literature although Haruyama (216) reports a value of i_o for Pb dissolution in $HClO_4$ of 3 x 10^{-1} Acm^{-2}.

The activation energy for Pb dissolution determined from the polarisation data shows a good agreement, even though there was some variation in the values for i_o obtained from the extrapolation of the E vs log i curve and from the linear portion of the η vs i graph. The mean value of activation energy from the two techniques was determined as 26.7 kJ $mole^{-1}$. Although it should be stressed that only 3 values of i_o were used to determine the activation energy. More detailed work would be required to give an accurate value for i_o and the activation energy for Pb dissolution in 48% HBF_4.

The values of i_o for PbO_2 reduction did not show such a good correlation between the different techniques as those for Pb dissolution. The mean value of i_o determined from the polarisation studies was 3.8 x 10^{-4} Acm^{-2} at 23°C whilst the value of i_o from the impedance studies depended upon the nature of the PbO_2 electrode with the highest value recorded being 8 x 10^{-5} Acm^{-2}.

The value of the activation energy for the PbO_2 reduction also showed a considerable variation between the two techniques. Hampson (177, 178) reports values for the reduction of PbO_2 in 3M $HClO_4$ of 9.6 x 10^{-5} Acm^{-2} with the value decreasing with decrease in Pb^{2+} concentration. The activation energy he also found was dependent upon the crystalline form of PbO_2 investigated either α or β and a value of 31 kJ $mole^{-1}$ for PbO_2 reduction was reported. This compares to the mean value of 38.5 kJ $mole^{-1}$ obtained in the present studies.

The activation energy for Pb dissolution enabled a calculation for the value of i_o for Pb dissolution at -32^oC, the temperature at which the activation time experiments are conducted. The value of i_o at -32^oC was calculated to be 1.2×10^{-4} Acm^{-2}.

The value of i_o for PbO_2 reduction at -32^oC was then extrapolated from the Arrhenius plot and a value of 9×10^{-6} Acm^{-2} calculated at -32^oC. The value of C_{dl} was also found to vary depending upon the nature of the PbO_2 electrode but a typical value was 70 μFcm^{-2}, comparable with the value of 68 $\mu F\ cm^{-2}$ for the Pb electrode.

It was also interesting to note that the bad adhesion PbO_2 deposits always exhibited a lower series resistance (R_s) than the bad adhesion foils. As the foil samples were of a similar size the higher series resistance on the bad adhesion foils could be associated with a higher contact resistance at the Ni/PbO_2 interface, possibly associated with a thicker oxide film on the bad adhesion foils.

The C_{dl} for the heat treated PbO_2 electrodes was found to be higher than for conventional PbO_2 electrodes, see Section 3.4.5.2). This is attributable to the reactive nature of this electrode and difficulty in maintaining it at its true rest potential during the course of the impedance measurements which could result in the formation of an adsorbed film giving misleading values for double layer capacitance.

Cathodic polarisation of the PbO_2 electrode actually increased the measure value of C_{dl} to approximately 880 μFcm^{-2}.

The purpose of measuring the activation energy for the cathodic reduction of PbO_2 reduction and the anodic dissolution of Pb in HBF_4 was so that the various parameters for the equivalent circuit in the $Pb/HBF_4/PbO_2$ battery can be determined at the temperature at which the activation time experiments was conducted.

This battery can be represented in terms of its electrical analogue

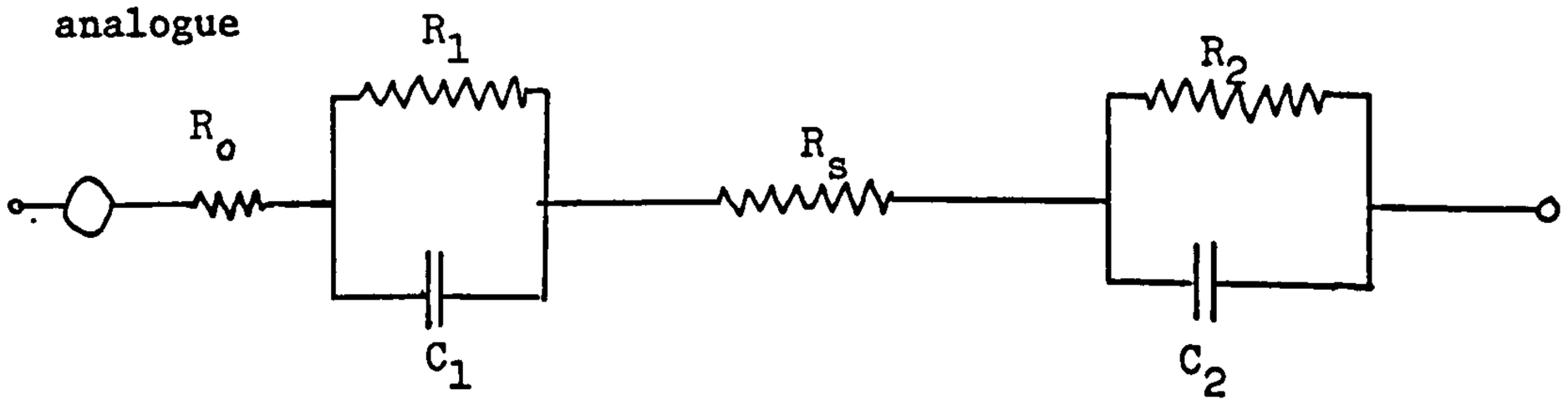

where R_o = The contact resistance between PbO_2 and Ni interface (ohms cm^2)

R_1 = Charge transfer resistance for the PbO_2 electrode (ohms cm^2)

C_1 = PbO_2 double layer capacitance (μFcm^2)

R_s = Solution resistance (ohms)

R_2 = Charge transfer resistance for the Pb electrode (ohms cm^2)

C_2 = Pb double layer capacitance ($\mu F\ cm^{-2}$)

○ = Represents a voltage source i.e the cell e.m.f.

N.B. No Warburg impedances have been shown although these would be present.

This circuit like any other capacitive circuit will have a time constant, which will govern the time taken for the voltage to reach a given value and to discharge.

When the $Pb/HBF_4/PbO_2$ is activated the values of R_1 and R_2 will be high but as current is drawn from the battery the charge transfer resistances will decrease and so will the cell impedance.

For the ease of calculation and because the time, temperature and potential dependence of the double layer capacitance are unknown. The capacitance has been assumed to be independent of potential over the time scale in which the experiments were conducted. Although the capacitance of a Pb electrode decreases as current is drawn to 4.8 μFcm^{-2} which is associated with the formation of a $Pb(BF_4)_2$ film on the Pb surface, whilst the capacitance of the PbO_2 electrode increases. The reason for the increase in capacitance of the PbO_2 electrode is not fully understood.

The process of film formation is thought to take some time to take place may not to occur to any significant extent during the first few hundred milliseconds of discharge so as to affect the value of the double layer capacitance and thus the time constant for the $Pb/HBF_4/PbO_2$.

Although it should be stressed that the values of the double layer capicitance were determined under equilibrium conditions and whether these values would be the apparent double layer capacitances during the initial activation period for both the Pb and PbO_2 electrodes is not known.

The voltage across a capacitor at a time t is given by the equation

$$V_t = V_o (1 - e^{t/cR}) \qquad a)$$

where V_o = Initial voltage
V = Voltage at time t
C = capacitance μFcm^{-2}
R = resistance ohms

During the initial stages of activation the value of R for the Faradaic impedance will be high, however as current passes through the electrode the value of R will decrease. Thus R will not be constant during the discharge process. The cell voltage will initially be required to charge the double layer capacitance C_{dl}, which discharges through the Faradaic impedance i.e PbO_2 reduction and Pb dissolution take place.

Thus, there will be two competing processes charging and discharging of the double layer capacitance. The time constant for charging the double layer capacitance will be CR_s where C is the total of all capacitances and R_s is the series resistance i.e the resistance of the electrolyte, the internal electrode resistance, e.t.c a nominal value for which is 10 ohms at -32^oC. The value of the charge transfer resistance for both the Pb and PbO_2 electrode will only affect the time constant for the discharge process not the charging process.

The Pb electrode does not dictate the time constant for the $Pb/HBF_4/PbO_2$ battery since the charge transfer resistance for the Pb dissolution process is considerably lower than that for the corresponding cathodic process of PbO_2 reduction i.e it has a lower time constant.

From the Tafel equation neglecting the reverse reaction the overvoltage for the reduction of PbO_2 will be :

$$i = i_o e^{-\alpha z F \eta / RT} \qquad b)$$

However η will vary with time according to equation a) above, therefore

$$i = i_o e^{-\alpha z F \eta_f (1 - e^{t/CR})} \qquad c)$$

where η_t = overpotential at time t

η_f = final overpotential

At a cell voltage of 1.32V this equates to an anodic and cathodic current density of $1.32/56 = 2.36\ Adm^{-2}$ with a load resistance of 56 ohms. The resistivity of HBF_4 at -32^oC has been calculated as 9 ohm cm and with an electrode spacing of 0.5 cm, this corresponds to an electrolyte resistance of 4.5 ohms at this temperature.

From equation b) inserting the values of i_o at -32^oC and using a value of 0.5. This equates to an anodic overvoltage of 0.112V for Pb dissolution and a cathodic overvoltage of 0.165V for PbO_2 reduction.

The voltage rise time phenomenon can therefore be related to exchange current density for the slowest half cell reaction. Heat treatment of electrodeposited $-PbO_2$ has been shown to more than double the exchange current densitiy for PbO_2 reduction. Thus the value of i_o at -32^oC will be higher than for heat-treated PbO_2, than the non heat-treated approximately 2.4 times at $2.2 \times 10^{-5}\ Acm^{-2}$.

The rapid voltage rise over the initial activation period is considered to be due to cell charging which has a low time constant whilst the slower slope is explained by the discharge process. The slow variation in cell voltage after initial activation may also be due to a slow diffusion process.

At high electrolyte temperatures the charge transfer resistances for the Pb and PbO_2 electrodes and the internal resistance will be considerably lower and this would also explain the virtually instantaneous activation time observed.

The higher exchange current density for heat-treated PbO_2 would decrease the activation polarisation loss and result in a higher cell voltage. This increase in exchange density for the PbO_2 reduction process would explain higher cell voltage recorded for heat-treated PbO_2.

Further work would be needed to develop this idea and put it on a detailed mathematical and theoretical basis. The foregoing discussion is merely intended to put forward the idea that the improvement in activation times is related to the increase in exchange current density.

4.5 Nickel Passivity in NO_3^- solutions

Most research into nickel dissolution has been conducted in H_2SO_4 rather than HNO_3 solutions. The main reason for this is the strong oxidising power of the NO_3^- ion and the difficulty therefore in producing a clean oxide free metal surface. It is also not possible to cathodically pre-treat the nickel electrode in NO_3^- solutions because this will result in the formation of NO_2^- ions will be oxidised when the nickel electrode is anodically polarised. These factors mean that NO_3^- solutions do not provide a convenient medium in which to carry out studies on metal dissolution and are therefore rarely used for such investigations.

The present research has shown that Ni dissolution in NO_3^- solutions is pH dependent with a value for (d log i_{pp}/dpH) of 0.96. This result tends to support the theory that Ni dissolution does occur via a complex metal ion intermediate in which OH^- is involved.

The nature of the E vs i curve for Ni dissolution in KNO_3 was also found to be dependent upon both pH and sweep rate. In solutions of 1M KNO_3 pH1 only one passivation peak was observed at low sweep rates, whilst in solutions of pH 2.6 two passivation peaks were observed the second peak becoming more apparent with increase in sweep rate. In 1M KNO_3 pH4 only one passivation peak was observed. A plot of E_{pp} vs $v^{1/2}$ gave a straight line and enabled the value of E_{pp} at zero sweep rate to be extrapolated (see Figs. 225 to 227). A plot of E_{pp} at v = 0 versus pH (Fig 228) indicates two different oxide films are formed. A result observed by other workers on Ni passivity, in different solutions (267, 268, 269, 272).

De Gromoboy and Shreir (272) state that the passivation peaks they observed in Na_2SO_4 solutions were due to the reversible potential for different Ni oxides (Ni/Ni_xO_y).

The thermodynamic values for the different Ni/Ni_xO_y oxides calculated from the data given by Cowan and Staehle (285), using the equation $\Delta G_o = -E_o zF$ are :

$$Ni + H_2O \text{ ----- } NiO + 2H^+ + 2e$$
$$E_p = 0.116 - 0.059\ pH \qquad 1)$$

$$3Ni + 4H_2O \text{ ----- } Ni_3O_4 + 8H^+ + 8e$$
$$E_p = 0.307 - 0.059\ pH \qquad 2)$$

$$2Ni + 3H_2O \text{ ----- } Ni_2O_3 + 6H^+ + 6e$$
$$E_p = 0.419 - 0.059\ pH \qquad 3)$$

All the above values for E_o (the passivation potential in pH0 solutions) are quoted at 298 ^oK.

Fig 228 gives the value of E_o for the first oxidation peak as 0.34 Volts, however it should be stressed that this value was obtained from the measurement of E_{pp} at only 3 different pH values and therefore a certain degree of experimental error may exist. Further work would therefore be necessary to confirm an accurate value for E_o but from the value obtained it would appear that the 1st oxidation peak on the E vs i curves for Ni dissolution in acidic NO_3 solutions does appear to conform to the value for E_o for the formation of Ni_3O_4 and this is the value that has been reported by other workers in different solutions (267, 268). The second oxidation peak may be due to the formation of Ni_2O_3 from Ni however the value of E_o of +0.50V observed in the present studies was 0.08V higher than the value of E_o calculated from thermodynamics (see equation 3).

A value similar to 0.50V recorded in the present studies namely 0.48V has been reported by Sato and Okamoto (277) for Ni dissolution H_2SO_4 with a pH dependence of 60mV per decade (the pH dependence observed in the present studies). They initially considered this value to be due to the reversible potential for the reaction:

$$3NiO + H_2O \text{ ----- } Ni_3O_4 + 2H^+ + 2e \qquad 4)$$

Or when the concentration of nickel ions in solution is high to the reaction:

$$3NiOH^+ + H_2O \text{ ----- } Ni_3O_4 + 5H^+ + 2e \qquad 5)$$

However, from thermodynamic calculations they have shown that the value of E_o for reaction 4) would follow the relationship $E_p = 0.876-0.059pH$ whilst for reaction 5) the relationship would be $E_p = 1.44-0.0885pH$ based on the value for $NiOH^+$ quoted by Sato and Okamato (277). Thus, thermodynamic calculations show that the reactions initially proposed by Sato and Okamato do not correspond with the observed passivation potentials.

They therefore postulated an alternative reaction for the production of a higher oxide film namely :

$$3NiOH^{+} + OH^{-} \text{ —— } Ni_3O_4 + 4H^{+} + 2e \qquad 6)$$

$$E_p = 0.725 - \frac{3RT}{ZF} \ln [NiOH^{+}] + \frac{5RT}{ZF} \ln [H^{+}] \qquad 7)$$

The concentration of $NiOH^{+}$ in the vicinity of the electrode surface they considered would be maintained about the saturation value for $NiOH^{+}$ at high potentials owing to the precipitation of NiO, so that the value of E_o for this oxide formation potential they calculated from equation 4) and the value of the solubility product for NiO (K_w):

$$E_p = E_o - \frac{3RT}{ZF} \ln K_w + \frac{RT}{F} \ln [H^{+}] \qquad 8)$$

$$= 0.480 - 0.059pH \text{ at } 25^{o}C$$

Infact using the thermodynamic values given by Sato and Okamoto a recalculation of the value of E_o shows that the actual value is 0.487 V not the value 0.480 V, they report.

Thus, the oxidation peak observed in the current studies at +0.50V could theoretically correspond to passivation of the Ni electrode with Ni_3O_4 by two separate mechanisms. Rather than by passivation of the Ni surface by Ni_3O_4 followed by oxidation of the exposed Ni to Ni_2O_3, since whilst the latter reaction is thermodynamically possible the value of E_o for this reaction is much lower than the value of E_o determined in practice.

The formation of Ni_3O_4 by reaction 2 appears to be favoured acid solutions

As is evident by the fact that only one oxidation peak is visible at a relatively low pH, whilst in higher pH solutions, namely pH4 reaction 6 may be the predominant reaction.

The two reactions competing with each other at intermediate pH's.

Passivation has not been shown to take place by NiO formation in NO_3 solutions, a result which is in agreement with other workers (254). In acid solutions, in particular the dissolution rate of $NiOH^+$ is so large that the NiO formation does not contribute to passivation.

The rate of reaction 6) Sato and Okamoto state is given by the equation

$$i = k[NiOH^+] \ [OH^-] \exp^{-\alpha z F \eta / RT}$$

Thus reaction 6 is not favoured in low pH solutions because of the low concentration of $[OH^-]$, even though a relatively high $[NiOH^+]$ may be present.

The concentration of NO_3^- also appears to affect the nature of the E vs log i curve as is evident from Fig 211. In a 0.1M KNO_3 solution of pH 2.5, a Ni electrode anodically polarised at a low sweep rate showed the presence of two passivation peaks, whilst in a high concentration solution i.e. 2M KNO_3 only 1 oxidation peak was visible. Variations in the NO_3^- concentration did not appear to significantly affect the rate of active dissolution of Ni.

The presence of the second oxidation peak in a low NO_3 concentration could be explained by a process of competitive adsorbtion at the electrode surface, with the NO_3^- ions in high concentration solutions displacing the OH^- ions at the electrode surface and thus reducing the rate of reaction 6). Although at this stage it appears that the concentration of NO_3 does affect the relative mechanisms for passivation, the reason for this is not readily understood and further work on this subject would be necessary.

The value of E_{pass} also varied with NO_3 concentration a phenomenum which would not be anticipated if the anion did not take part in the dissolution process.

The linear variation of i_p with $v^{1/2}$ for metal passivation has been explained by Muller assuming film formation to be under ohmic control With similar results reported by Kapusta and Hackerman (326) on tin passivation in alkaline solutions. Nevertheless for the passivation reaction to be under ohmic resistance control as explained by Muller (320) and observed by Kapusta and Hackerman. A graph of i_p vs $v^{1/2}$ would give an intercept on the current axis of $i_p = 0$ at $v^{1/2} = 0$. This was only found to be the case in high pH solutions, namely pH 4 and in a lower pH solution 2.6 for the formation of the first Ni oxidation peak. In solutions of pH lower than 2.6 a positive intercept for i_p at $v^{1/2} = 0$ was observed for the 1st oxidation peak the value of which decreased with increase in pH. Whilst in low pH solutions a negative intercept for the second oxidation peak was oberved which became less positive until at pH4 the value of i_p ($v^{1/2} = 0$) was equal to zero.

In low pH solutions, passivation of the Ni surface may not be under simple ohmic resistance control, since at the primary passivation potential nett dissolution takes place. The negative intercepts for the 2nd oxidation peak are thought to be due to the fact that the value of i_p measured for the second oxidation peak, at its passivation potential, is the sum of the true passivation current for the second oxidation peak (i_{p2}) plus the background current for the first oxidation peak at this potential (i_{p1}) i.e i_p measured = $i_{p2} + i_{p1}$. At the same potential as i_{p2}, for the second oxidation peak, the value of i_{p1} approaches zero only in high pH solutions and a plot of i_p vs $v^{1/2}$ will intercept on the current axis at zero. The value of i_{p1} will also be greater in low pH solutions and will also vary with sweep rate to a different extent to i_{p2}. The sum of these two factors it is thought accounts for the negative intercept observed on the i_p vs $v^{1/2}$ graphs (see Figs. 222 and 223).

The effect of various anion additions to 1M KNO_3 solutions on both the passivity and anodic dissolution of Ni has been studied. This work was carried out to determine whether selected inorganic anions can be added to NO_3^- solutions without adversely affecting Ni passivity and thus ascertain their suitability for use in simultaneous Pb and PbO_2 plating solutions.

The most interesting aspect of this work was found to be the decrease in the value of i_{pp} for Ni dissolution with increase in concentration of sodium ethylenediaminetetracetic acid (Na EDTA) and sodium gluconate, although the latter additive was not as effective as the former in this respect.

Na EDTA appears to reduce the free corrosion rate of Ni in 1M KNO_3 at a given pH and also affect the rate of active dissolution of Ni, as is evident from Fig. 229 in low pH solutions, whilst in higher pH solutions namely pH 2.5 the nature of the oxide film formed appears to alter (see Fig 230). In that in a solution of 0.005M Na EDTA + 1M KNO_3 the first passivation peak does not occur till 0.58V vs SHE.

The EDTA or gluconate ions appear to interfere with the passivation mechanism possibly by forming a $NiOH^+$ complex at the electrode interface, thus reducing the activity of $NiOH^+$ ions. At a low $NiOH^+$ concentration the value of i at a given potential will decrease. Because the complexing power of EDTA is greater than gluconate, the former additive will have a greater effect on the Ni dissolution process. Thus passivation of the Ni electrode will occur at the same potential yet the current density necessary to achieve this potential will decrease.

In 1M KNO_3 solutions, pH4, the inhibitive effect of Na EDTA is not as great since at this potential the formation of the Ni_3O_4 film is controlled by the OH^- concentration rather than $NiOH^+$ concentration. Although in 1M KNO_3, pH 2.5, the addition of Na EDTA appears to favour the formation of Ni_3O_4 by the second passivation mechanism i.e. reaction 6.

The apparent transpassive dissolution seen in 0.005M Na EDTA, 1M KNO_3 solutions at approximately +1.3V is essentially pH independent and therefore not thought to be associated with the formation of a higher valent oxide but the oxidation of EDTA.

The mechanism whereby the organic complexing agents affect the rate of dissolution can only be postulated at this stage.

Nickel dissolves anodically via a soluble intermediate

$Ni + OH^-$	$NiOH + e$	a)
$NiOH$	$NiOH^+ + e$	b)
$NiOH^+ + H^+$	$Ni^{2+} + H_2O$	c)

The rate of reaction will be governed by the rate determined step which Sato and Okamoto proposed is reaction a), but changes to reaction c) with increase in pH.

$$i = K[NiOH^+]\,[H^+]\,\exp^{-\alpha z F\eta/RT}$$

In F^- and BF_4^- a NiF^+ complex may also be formed and may account for the enhanced rates of dissolution.

The active dissolution of Ni was only found to be markedly affected by F^- in high pH solutions, namely pH4. A similar effect was also observed with BF_4^- and SiF_6^{2-} ions.

However, the most significant effect of these anions was seen to be on the passivity of Ni in NO_3^- solutions not its active dissolution.

In 1M KNO_3 solutions pH1 supersaturated with NaF a number of secondary passivation peaks were recorded, the first at +0.65V, the second at + 1.125V and the third transpassive peak at +1.5V.

Lochel et al (298 to 299) in studies on the passivity of Ni in $HClO_4$ solutions containing F^- also observed that the dissolution of Ni in the passive region was dependent on F^- concentration. A passivation peak at 1.1V was observed which they associated with the deposition NiF_2 over the oxide film, yet they did not report the presence of any additional passivation peaks. Similar passivation potentials to those reported by Lochel were observed for the anodic polarisation of a Ni electrode in a 1M KNO_3 + 0.1M $NaBF_4$ solution, pH1.

The primary passivation peak is associated with formation of Ni_3O_4, although the thickness of the oxide film will possibly be lower than in the additive free solutions. The secondary passivation peak at +0.65V observed in the present studies could be associated with the formation of Ni_3O_4 by reaction 6 described earlier or formation of Ni_3O_4 by a similar mechanism. The transpassive dissolution potential at +1.1V has been associated with the formation of NiF_2 and in BF_4 solutions may be due to the formation of $Ni(BF_4)_2$. Whilst the passivation potential at 1.5V only visible in low pH solutions may be the redox potential for the oxidation of Ni_2O_3 or Ni^{2+} to NiO_2. The transfer of Ni^{2+} into the electrolyte is catalysed by the presence of F^-, BF_4^- and SiF_6^{2-} as is evident from the increase in the passive dissolution of Ni (see Figs. 235-240).

Lochel et al consider the reaction proceeds by the following reaction

$$Ni_{ox} + HF_{aq} \longrightarrow NiF_{ad} + H_{aq}$$

$$NiF_{ad} \text{ —} NiF_{aq}$$

$$NiF_{aq} + 3HF \text{ —} NiF_4^{2-} + 3H_{aq} + 2e$$

They also deduced that the reaction order for Ni dissolution with respect to HF is 1.6.

MacDougal et al in their studies on Ni dissolution in F^- containing solutions, discuss breakdown of the NiO film and explain the increase in dissolution rate with temperature is due to an increase in the number of nucleation sites for film breakdown and of accelerating lateral growth.

In high pH solutions no active to passive transition appears to occur until +0.95V, and this passivation potential is dependent upon both pH and $NaBF_4$ or NaF concentration.

The sulphamate ion did not appear to have any effect on the active dissolution of Ni nor its passivity. Thus NH_2SO_3 can be used as additive to $Pb(NO_3)_2$ plating solutions without markedly affecting the inertness of the Ni anode, yet BF_4^{2-}, F^- and SiF_6^{2-} may only be added in very low concentrations.

4.6 General Discussion

Nitrate based plating solutions are rarely used for metal deposition because of the reduction of the nitrate ion at the cathode and the consequent decrease in the cathodic current efficiency. Furthermore, in the case of $Pb(NO_3)_2$ solutions, without additives dendritic deposits of Pb are produced.

The production of smooth, relatively pore free electrodeposits of Pb from $Pb(NO_3)_2$ plating solutions has however, now been shown to be possible by the careful selection of addition agents. Such addition agents cannot at present produce Pb deposits of grain size and porosity equivalent to those obtained from the more conventional $Pb(BF_4)_2$ plating solutions. Although with further research it may be possible to produce further improvements in the nature of the Pb deposit from $Pb(NO_3)_2$ solutions.

It is not considered that the $Pb(NO_3)_2$ plating solutions developed in the present studies will gain any commercial significance and replace the $Pb(BF_4)_2$ solutions. However, in applications such as the electrorefining of Pb where high speed deposition is required or in the simultaneous electrodeposition of Pb and PbO_2 in which $Pb(NO_3)_2$ is the only practical

electrolyte, the $Pb(NO_3)_2$ bath may gain acceptance. In the former example it should be noted that it may not be possible to plate non dendritic Pb deposits from $Pb(NO_3)_2$ solutions at fast flow rates because the addition agents may not be effective in dynamic solutions.

The prime objective of the present studies was not to produce Pb deposits from $Pb(NO_3)_2$ that would be equal to Pb deposits from other plating solutions but to produce Pb deposits that would be acceptable for use in the $Pb/HBF_4/PbO_2$ battery. This has been achieved and it has been shown that it is possible to produce smooth Pb deposits from $Pb(NO_3)_2$ solutions without affecting the nature of PbO_2 deposit formed on an inert anode. The Pb deposit obtained from this solution does not exhibit similar discharge properties to the Pb deposit from $Pb(BF_4)_2$ solutions of an equivalent thickness. The exact reason for this is not readily apparent but may be associated with a combination of large grain size, a poor throwing power from $Pb(NO_3)_2$ solution, small levels of porosity and a lower level of adhesion of the Pb deposit from $Pb(NO_3)_2$ solutions. $Pb/HBF_4/PbO_2$ batteries of the required cell life can however be produced from the material obtained by the simultaneous electrodeposition of Pb and PbO_2 by utilising thicker Pb deposits.

The difficulty in using a simultaneous plating solution for the formation of Pb and PbO_2 battery plate material in a bipolar cell arrangement is that a regular and careful control of the addition agent composition should be maintained because oxidation of the addition agents at the PbO_2 anode will take place. Thus, whilst it is now possible to obtain bipolar battery plate material in one continuous plating operation using a simultaneous plating solution i.e., the number of operations involved is reduced and the process can be made semi-automatic. The deposit properties from such a process are susceptible to small variations in addition agent concentration and a method will have to be perfected to maintain the addition agent concentration within specified limits. Nevertheless, this problem could be overcome and simultaneous plating solutions could be used to produce $Pb/Ni/PbO_2$ battery material on a continuous basis with the inherent cost savings that this would involve.

The production of simultaneous electrodeposits of Pb and PbO_2 on Ni would not be commercially viable unless the problem of the high reject rate for battery plate material due to poor adhesion of the PbO_2 deposit onto different Ni substrate could be solved. A considerable research effort has been conducted to investigate the possible reasons for the adhesion failures observed particularly in respect of any variations in the substrate condition between the 'good' and 'bad' adhesion foils. The major conclusion is that it is the nature of the Ni foil surface that dictates the level of adhesion of electrodeposited PbO_2, with foils with a bright surface (i.e low oxide film thickness) invariably exhibiting good levels of adhesion. The cold rolling of the Ni foil prior to anodic etching is however an important factor in producing the etch pits on the Ni surface since in the absence of any etching process low levels of adhesion on the Ni foil are obtained.

The work conducted during the course of the present studies has highlighted areas for future work, in particular the effect of addition agents on the growth of electrodeposits. Despite the importance of addition agents to most commerical plating solutions there appears to have been little fundamental research carried out on the mode of addition agent action e.g the rate of diffusion of addition agents to the electrode surface, the incorporation of addition agents in the electrodeposit or mechanism whereby they affect the kinetics for the growth process.

5 CONCLUSIONS

1) Deposits of Pb and PbO_2 suitable for use in the primary $Pb/HBF_4/PbO_2$ battery can be obtained by simultaneous electrodeposition from $Pb(NO_3)_2$ solutions containing selected organic addition agents.

2) With careful selection of addition agents it is possible to electrodeposit Pb from $Pb(NO_3)_2$ solutions over a wide current density and $Pb(NO_3)_2$ concentration range. The deposits obtained from these solutions have a higher porosity and grain size than deposits from $Pb(BF_4)_2$ plating solutions.

   The deposition of Pb from $Pb(NO_3)_2$ solutions can be carried out at room temperature and 50°C from these solutions.

   The addition agent combination found suitable for room temperature electrodeposition of Pb from $Pb(NO_3)_2$ solutions was tannic acid and Wafex, whilst for the simultaneous electrodeposition of Pb and PbO_2 at 50°C the most effective additive combination was Triton X100 plus anthraquinone-2-monosulphonic acid.

3) Anodic oxidation of Triton X100 and similar chemicals does take place at the PbO_2 anode and in order to maintain the Pb deposit properties from $Pb(NO_3)_2$ plating solutions it is necessary to replenish the $Pb(NO_3)_2$ plating solution with fresh addition agents after prolonged periods of plating.

4) The Pb deposit obtained from $Pb(NO_3)_2$ solutions is not as effective an anode material in the $Pb/HBF_4/PbO_2$ battery as that obtained from a conventional $Pb(BF_4)_2$ plating solution, after an equivalent deposition time. The desired cell life can however be obtained by utilising Pb deposits from $Pb(NO_3)_2$ solutions of a greater thickness than those from $Pb(BF_4)_2$ plating solutions.

5) The addition of peptone to $Pb(NO_3)_2$ solutions produces highly reflective PbO_2 electrodeposits, when PbO_2 is deposited at a low current density.

6) Certain organic addition agents notably peptone, diphenylamine and 1-nitroso-naphthalene-3,6-disulphonic acid can considerably reduce the grain size of PbO_2 electrodeposited from $Pb(NO_3)_2$ solutions, whilst others affect the to PbO_2 ratio in the resultant PbO_2 deposit.

7) The anodic polarisation of a Pb plated Ni substrate in H_2SO_4 solutions can be used to provide a quantitative method of assessing the porosity of Pb electrodeposited onto Ni.

8) The PbO_2 deposit obtained from a 360 gl^{-1} $Pb(NO_3)_2$ solution of pH4 at 1 Adm^{-2} consists of a mixture of α and β-PbO_2 but is predominantly β - PbO_2.

9) Certain organic chemicals when added to 0.2M Na_2SO_4 solutions markedly increase the oxygen overvoltage on a Pt electrode.

10) The additives Triton X100, BRIJ 35 and Pluronic L64 inhibit the diffusion of Pb^{2+} ions to the electrode surface in static solutions, whilst the additive anthraquinone-2-monosulphonic acid reduces the exchange current density for the Pb deposition process.

Triton X100 affects the kinetics of the Pb deposition process only at a low Pb^{2+} concentration but does not significantly affect the diffusion coefficient for Pb^{2+} ions in $Pb(NO_3)_2$ solutions.

11) Triton X100 and anthraquinone-2-monosulphonic acid when added to a $Pb(NO_3)_2$ solution inhibit the nucleation of Pb electrodeposits at a given potential.

12) Organic additives in $Pb(NO_3)_2$ solutions increase the anodic overpotential for the formation of PbO_2 onto a Pt substrate.

13) Poor adhesion of PbO_2 can be obtained on both Ni200 and Ni270 foil substrates.

The surface condition of the Ni foil substrate is an important factor in controlling the levels of adhesion, with Ni200 foils with a bright surface finish exhibiting a better level of adhesion than Ni270 foils with a matt surface finish.

14) Ni foils that exhibited a random etch pattern on anodic etching in 30% H_2SO_4 invariably exhibited a low level of adhesion for PbO_2 electrodeposits.

15) The failure of the PbO_2 deposit in the adhesion bend test is cohesive not adhesive with failure occuring in the PbO_2 electrodeposit adjacent to the PbO_2/Ni interface.

Annealing Ni foil at 800°C under vacuum so as to remove any oxide film failed to produce a substrate that exhibited a good level of adhesion for electrodeposited PbO_2.

16) PbO_2 can theoretically decompose to a lower oxide at temperatures in excess of 204°C.

17) The improvement in the voltage rise time for electrodeposited PbO_2 in HBF by heating the deposit to 250°C for 1/2 hour is associated with the accompanying increase this brings about in the exchange current density for, the cathodic reduction of PbO_2.

18) Improved activation times for electrodeposited PbO_2 may also be brought about by the agitation of the plating solution used to electrodeposit PbO_2.

19) The passivation of Ni in NO_3^- solutions occurs by the formation of Ni_3O_4 via one of two possible mechanisms dependent upon the solution pH.

20) The addition of the organic complexing agents sodium ethylenediamine tetraacetic acid and sodium gluconate to a KNO_3 solution will reduce the rate of active Ni dissolution particularly in solutions of low pH.

The free corrosion rate of Ni in KNO_3 solutions will also be decreased by the addition of these additives.

21) BF_4^{2-}, F^-, and SiF_6^{2-} ions when added to KNO_3 solutions will decrease the passivity of Ni.

6 RECOMMENDATIONS FOR FUTURE WORK

1) Pb and PbO_2 electrodeposits of different thicknesses are simultaneously electrodeposited from a solution of 360 gl^{-1} $Pb(NO_3)_2$, 3 gl^{-1} Triton X100 plus 0.1 gl^{-1} anthraquinone -2-monosulphonic acid. The discharge properties of these deposits in 48% HBF_4 at room temperature and 60°C are then measured, so that the optimum deposit thicknesses required to give the desired operational life for the $Pb/HBF_4/PbO_2$ battery can be determined.

   The discharge properties of active material produced from lower Pb^{2+} concentration solutions are also measured.

2) An investigation into the effect of multiple combinations of addition agents and pH on the nature and properties of both the Pb and PbO_2 deposits obtained from $Pb(NO_3)_2$ solutions be undertaken. Since in the present studies only the effect of binary combinations of addition agents has been studied rather than that of tertiary or even ternary combinations of addition agents.

   The additives recommended for further investigation are Triton X100, BRIJ35, Pluronic L64, anthraquinone-2-monosulphonic acid butyne 1,4 diol, 1,4 naphthoquinone and anthraquinone-2,6-disulphonic acid.

   This work is considered essential if further improvements in the properties of the Pb deposit obtained by electrodeposition from $Pb(NO_3)_2$ solutions are to be achieved.

   As it may be that a simultaneous plating solution based on a combination of Triton X100, BRIJ 35, anthraquinone-2-monosulphonic acid, and 1,4 naphthoquinone could well produce improved deposits of both Pb and PbO_2 from $Pb(NO_3)_2$ solutions.

3) Further investigations into the room temperature deposition of Pb from $Pb(NO_3)_2$ solutions containing tannic acid and Wafex as addition agents are conducted. This work should also be aimed at studying the effect of multiple combinations of addition agents on the Pb deposit properties e.g the effect of tannic acid and Wafex, plus either anthraquinone-2-monosulphonic acid and/or 1,4 napthoquinone.

4) Studies are carried out on the effect of pH and the addition of various organic addition agents to $Pb(NO_3)_2$ solutions on the crystal structure of PbO_2 electrodeposited from these solutions and on the nature of the PbO_2 deposit obtained.

5) Conduct detailed work on the electrodeposition of Pb from $Pb(NO_3)_2$ solutions using the electrochemical impedance and pulse potentiostatic techniques. The factors worthy of investigation are a) the effect of pH, b) the determination of exchange current density at selected $Pb(NO_3)_2$ concentrations and temperatures c) the effect of various addition agents.

6) Studies on the mechanism whereby certain organic addition agents affect the nucleation and deposition of PbO_2 from $Pb(NO_3)_2$ solutions.

7) Samples of Ni270 are obtained with a bright surface finish and in the quarter to half hard condition, so that the degree of adhesion of PbO_2 electrodeposited onto these foils can be measured. This would verify the proposal made earlier that it is the surface condition of the as received Ni foil that controls the level of adhesion not it's chemical composition.

8) Further investigations are carried out into the effect of the internal stress of electrodeposited PbO_2 on the exchange current density for PbO_2 reduction in acid solutions.

9) The effect of sodium ethylenediaminetetraacetic acid (NaEDTA) and other similar complexing agents on the active dissolution and anodic passivation of Ni in HNO_3, H_2SO_4 and other acidic solutions is studied. In addition it is further recommended that studies on the mechanism of Ni passivity in HNO_3 solutions are conducted to supplement the work already reported. In particular the reason for the two passivation peaks on a Ni electrode anodically polarised NO_3^- solutions.

10) The voltage rise time phenomenon is studied from a theoretical view point.

APPENDIX 1

Linear polarisation of a Pb electrode at 1mV sec^{-1} in a 0.1M $Pb(NO_3)_2$ + 0.01M HNO_3 solution with and without selected addition agents

Additive	Additive Concentration gl^{-1}	Overpotential (mV) at selected current densities (Adm^{-2})				
		0.1 Adm^{-2}	1 Adm^{-2}	2 Adm^{-2}	5 Adm^{-2}	10 Adm^{-2}
None	-	2.45	29	61	157	188
Pluronic L64	0.5	3	36	82	770	-
Triton X100	0.5	2.6	35	78	705	800
BRIJ 35	0.5	3	37	80	571	762
Pluronic F68	0.5	3	32	70	220	261
	2	3	33	71	247	296
Tween 80	0.5	3.5	40	96	230	266
Polyoxy-ethylene oxide	0.5	3	36	77	202	260
Cetyltri-methyl ammonium bromide	0.5	2.5	32	69	223	271
	2	14	37	77	167	212
Aloin	1	2.4	27	59	420	497
	2	2.6	31	51	466	557
Tannic Acid	0.5	6	53	143	335	370
	2	8.2	59	179	441	498
Humic acid	0.5	8	47	83	195	238

Additive	Additive Concentration gl^{-1}	Overpotential (mV) at selected current densities (Adm^{-2})				
		0.1 Adm^{-2}	1 Adm^{-2}	2 Adm^{-2}	5 Adm^{-2}	10 Adm^{-2}
Gelatin	0.5	3.3	35	72	230	261
Peptone	0.5	2.6	31	63	196	228
Hydroquinone	0.5	2.9	33	72	182	224
	2	2.9	35	78	210	257
Resorcinol	1	2.8	34	73	198	241
Itaconic acid	0.5	2.5	32	67	164	202
	2	2.5	33	70	166	209
Araquad	0.5	4.5	48	128	238	300
Empigen BAC	0.5	3	37	83	330	372
Wannin	0.5	3.6	31	58	180	206
	2	42	32	59	222	255
Wafex	0.5	4.3	36	69	199	232
	2	5.6	42	70	230	259
Serla Soln.	0.5	4.4	37	71	202	244
	2	4.2	36	65	233	272
Lignosol	0.5	5.1	40	80	212	245
	2	5.8	35	77	238	271
Hyamine	0.5	3	39	86	323	371

Additive	Additive Concentration gl^{-1}	Overpotential (mV) at selected current densities (Adm^{-2})				
		0.1 Adm^{-2}	1 Adm^{-2}	2 Adm^{-2}	5 Adm^{-2}	10 Adm^{-2}
anthraquinone 2 sulphonic acid	0.5	6.9	56	110	334	372
Ascorbic acid	0.5	3	36	77	175	223
	2	3.3	36	77	175	221
mallic acid	0.5	2.5	31	69	168	207
Coumarin	0.5	2.5	29	59	159	198
	2	2.5	29	60	182	221
Oil of Cloves	0.5	4.0	37	75	215	255
	2	4.8	49	93	330	373
antipyrine	0.5	3.4	32	65	157	193
	2	3	34	70	167	209
hexamine	0.5	2.8	31	69	160	197
	2	3	33	69	102	200
glycine	0.5	3	35	75	173	219
	2	3.5	39	84	189	242
2-cystine	0.5	3.5	36	76	174	224
	2	3.5	39	79	181	226
2-napthylamine 6,8 disulphonic acid	2	3.5	29	64	191	220
napthalene-1,5-disulphonic acid	0.5	2.3	26	59	167	196
	2	2.5	29	63	183	215

Additive	Additive Concentration gl^{-1}	Overpotential (mV) at selected current densities (Adm^{-2})				
		0.1 Adm^{-2}	1 Adm^{-2}	2 Adm^{-2}	5 Adm^{-2}	10 Adm^{-2}
p-cresol	0.5	7	73	121	215	294
Diphenyl-amine	0.5	3.7	47	126	223	263
Allylgly-cidyl ether	2	2.9	27	62	163	205
Crotonal-dehyde	0.5	4	39	81	178	229
2-napthyla-mine-1,5-disulphonic	0.5	3.3	31	66	184	214
napthalene 1,3,6 trisul phonic acid	0.5	3.3	34	72	188	232
Eugenol	0.5	3.9	38	75	220	273
2 hydroxy benzoyl alcohol	0.5	3.1	35	73	229	262
	2	3.1	36	83	307	332
1,5 dihy-droxy napthalene	0.5	4.4	44	80	301	342
pyrogallol	0.5	4.1	39	76	272	311
	2	5.1	42	97	284	322
butyne 1,4 diol	0.5	2.8	32	68	168	205
	2	3	33	68	171	210
butadiene sulphone	0.5	2.7	29	63	162	190
	2	2.6	30	63	153	185

Additive	Additive Concentration gl^{-1}	Overpotential (mV) at selected current densities (Adm^{-2})				
		0.1 Adm^{-2}	1 Adm^{-2}	2 Adm^{-2}	5 Adm^{-2}	10 Adm^{-2}
Camphor disulphonic acid	0.5	2.8	31	66	157	191
	2	3	31	63	155	189
aceptophe-none	0.5	3.5	38	87	192	244
quinoline	0.5	3.5	37	82	185	230
1 napthol 2 napthol disulphonic acid	0.5	3.5	37	79	205	249
1-napthol	0.5	5	39	73	301	340
1,4 naptho-quinone	0.5	4	41	77	304	343

5-0570 MINOR CORRECTION

d	3.07	2.95	2.74	5.893	PbO(YELLOW)
I/I$_1$	100	31	28	6	LEAD (II) OXIDE (MASSICOT)

Rad. CuKα_1 λ 1.5405 Filter Ni
Dia. Cut off Coll.
I/I$_1$ G. C. DIFFRACTOMETER d corr. abs.?
Ref. SWANSON AND FUYAT, NBS CIRCULAR 539, Vol. II

Sys. ORTHORHOMBIC S.G. C^{5}_{2v} - P$bn2_1$
a$_o$ 5.489 b$_o$ 4.755 c$_o$ 5.891 A 1.154 C 1.239
α β γ Z 4
Ref. IBID.

ε n=β γ Sign
2V D 9.642 mp Color YELLOW
Ref.

SAMPLE FROM NAT. LEAD CO. SPECT. ANAL.: <0.01% Bi,Fe; <0.001% Al,Ag,Cu,Mg,Si,Ca
X-RAY PATTERN AT 27°C
REPLACES 1-0824, 3-0610, 3-0599, 3-0600

d Å	I/I$_1$	hkl	d Å	I/I$_1$	hkl
5.893	6	001	1.363	<1	114
3.067	100	111	1.325	1	223
2.946	31	002	1.297	2	204
2.744	28	200	1.289	3	313
2.493	<1	201	1.252	3	024
2.377	20	020	1.244	2	402
2.278	<1	112	1.203	4	133
2.203	<1	211	1.188	3	040,420
2.008	12	202	1.174	4	331
1.963	2	003	1.139	2	224
1.850	14	212,022	1.120	2	115
1.797	14	220	1.102	4	242,422
1.724	15	113	1.091	2	240
1.640	13	311			
1.596	<1	203			
1.534	9	222			
1.514	8	213			
1.474	11	131,004			
1.408	<1	321			
1.372	1	400			

5-0561 MAJOR CORRECTION

d	3.12	2.81	1.97	5.018	PbO(RED)
I/I$_1$	100	62	37	8	LEAD II OXIDE (LITHARGE)

Rad. CuKα_1 λ 1.5405 Filter Ni
Dia. Cut off Coll.
I/I$_1$ G. C. DIFFRACTOMETER d corr. abs.?
Ref. SWANSON AND FUYAT, NBS CIRCULAR 539, Vol. II

Sys. TETRAGONAL S.G. D^{9}_{4h} - P4/nmm
a$_o$ 3.9729 b$_o$ c$_o$ 5.0192 A C 1.263
α β γ Z 2
Ref. IBID.

ε n=β 2.665 γ 2.535(Li) Sign
2V D 9.355 mp (Li) Color RED
Ref.

SAMPLE FROM NAT. LEAD CO. SPECT. ANAL.: <0.01% Bi,Cu,Fe,Si; <0.001% Ca,Mg.
X-RAY PATTERN AT 27°C
REPLACES 3-0561, 3-0573, 1-0796, 1-0797

d Å	I/I$_1$	hkl	d Å	I/I$_1$	hkl
5.018	8	001	1.0410	2	304
3.115	100	101	1.0386	<1	303
2.809	62	110	1.0294	<1	314
2.510	18	002	0.9738	1	401,105
2.124	1	102	.9462	1	411,115
1.988	8	200	.9365	3	330,224
1.972	37	112	.9200	3	331,223
1.675	24	211			
1.558	6	202			
1.842	11	103			
1.438	2	113			
1.405	3	220			
1.282	2	301,300			
1.256	3	310			
1.226	4	222			
1.219	3	311,213			
1.1977	<1	104			
1.1462	2	114			
1.1232	2	312			
1.0768	2	321,223			

2-0539 MAJOR CORRECTION

1943 d 2-0547	3.18	1.95	1.66	3.18	Pb_2O_3
I/I$_1$ 2-0539	100	100	100	100	LEAD OXIDE

Rad. CuK λ Filter Ni
Dia. Cut off Coll.
I/I$_1$ VISUAL d corr. abs.?
Ref. A. BARONI, GAZZ. CHIM. ITAL. 68, 391(1938)

Sys. CUBIC S.G.
a$_o$ 5.50 b$_o$ c$_o$ A C
α β γ Z 2
Ref. Wy48

ε n=β ω γ Sign
2V D 9.925 mp Color
Ref. C.C.

D.T. 370 (HCP)
Wy48 GIVES MONOCLINIC: A_o = 7.03
c_o = 3.93
β = 82°
a_o = 5.62

d Å	I/I$_1$	hkl	d Å	I/I$_1$	hkl
3.18	100	111			
2.75	70	200			
1.95	100	220			
1.66	100	311			
1.58	80	222			
1.2[illegible]	90	331			
1.23	70	420			
1.12	80	422			
1.06	90	511,333			
0.931	90	531			
.918	70	600,442			
.868	70	620			
.840	70	533			
.828	70	622			

4-0850 MINOR CORRECTION

d 4-0834	2.03	1.76	1.25	2.034	Ni
I/I$_1$ 4-0830	100	42	21	100	Nickel

Rad. CuKα λ 1.5405 Filter Ni
Dia. Cut off Coll.
I/I$_1$ G. C. Diffractometer d corr. abs.?
Ref. Swanson and Tatge, JC Fel. Reports, NBS 1951

Sys. Cubic S.G. O_h^5 - Fm3m
a_o 3.5238 b_o c_o A C
α β γ Z 4
Ref. Ibid.

ε ω=β ξ γ Sign
2V Dx 8.907 mp Color
Ref.

Spectrographic analysis shows <0.01% each of Mn, Si and Ca.
At 26°C
To replace 1-1258, 1-1260, 1-1266, 1-1272, 3-1043, 3-1051

d Å	I/I$_1$	hkl	d Å	I/I$_1$	hkl
2.034	100	111			
1.762	42	200			
1.246	21	220			
1.0624	20	311			
1.0172	7	222			
0.8810	4	400			
.8084	14	331			
.7880	13	420			

4-0686 MAJOR CORRECTION

d 4-0678	2.86	2.48	1.45	2.855	Pb
I/I$_1$ 4-0686	100	50	32	100	Lead (Lead)

Rad. CuKα$_1$ λ 1.5405 Filter Ni
Dia. Cut off Coll.
I/I$_1$ G. C. Diffractometer d corr. abs.?
Ref. Swanson and Tatge, JC Fel. Reports, NBS (1953)

Sys. Cubic S.G. O_h^5 - Fm3m
a_o 4.9506 b_o c_o A C
α β γ Z 4
Ref. Ibid.

ε ω=β ξ γ Sign
2V Dx 11.341 mp Color
Ref. Ibid.

Spectrographic analysis shows faint traces of Bi and Mg. Purity >99.999%
At 20°C
To replace 1-0995, 3-1156, 2-0811, 1-0972, 2-0799 and 3-1153

d Å	I/I$_1$	hkl	d Å	I/I$_1$	hkl
2.855	100	111			
2.473	50	200			
1.750	31	220			
1.493	32	311			
1.429	9	222			
1.238	2	400			
1.1359	10	331			
1.1069	7	420			
1.0105	6	422			
0.9526	5	511			
.8752	1	440			
.8369	9	531			
.8251	4	600			

REFERENCES

1) M Barak, Chem Ind UK, Vol 20, pp871-876 (1976)

2) M A Dasoyan, J A Aguf, Current Theory on Lead Acid Batteries, pub by Technicopy Ltd England (1979).

3) C Faure, Patent Specs, France 139, 258 (1880), 141 057 (1881); UK 129 (1881).

4) B. Ravid, Paper presented at 2nd ERA Battery Seminar and Exhibition Royal Garden Hotel, London, 3rd and 4th October. (1979)

5) G.D. MacDonald, E Y Weissman, T S Roemer, J. Electrochem Soc Vol 116 (6), pp660-663 (1972).

6) A.N. Dey, N. Hamilton, J Applied Electrochemisty, Vol 12, pp33-40 (1982)

7) T J Kilduff, E F Horsey, 24th Annual Proceedings Power Sources Symposium, May (1970)

8) J W Paulson, Lead abstracts 280-0411 and 01047.

9) J F Smith, Transactions Institute of Metal Finishing, Vol 53, p83, (1975).

10) W E Casson, T Keiley, Proceeding 12th Int Power Sources Symposium, Brighton (1980)

11) R Jasinski, High Energy Batteries, Plenum Press New York, p209 (1967).

12) F C Turril, W C Kirchberger, Proceedings 24th Annual Power Sources Conference p36, (1970)

13) M A Barron, Proceedings 23rd Annual Power Sources Conference, p134 (1969)

14) E D MacDonald, E Y Weissman, E R Dettwiler, J Electrochem Soc, Vol 120, p660 (1973).

15) Chemistry and Physics, Rubber Handbook (1976).

16) N A Hampson, C J Bushrod; J Appl Electrochem, Vol 4 pp1-6 (1974).

17) J C White, W H Powers, R L McMurtric, R T Pierce Jr, Trans Electrochem Soc, Vol 91, p73 (1947).

18) N E Bagshaw, J Power Sources 7, Proc 11th Int Symposium Brighton p677, (1978).

19) N A Hampson, P C Jones, R F Phillips, Can J Chem, Vol 45, p2045 (1967).

20) S Haruyama, J Electrochem Soc Japan, Vol 35, p62, (1967).

21) J F Smith, British Patent 1340914.

22) W G Darland, US Patent 3,033,908, May (1962).

23) US Patent, 3,033,908 Union Carbide Corporation (1959).

24) J.E Curtis, T J Sinclair, J Power Sources, Vol 3, pp267-276 (1978).

25) A T Kuhn, The Electrochemistry of lead, London Academic Press (1979)

26) F.W Beck, Bundesministerium fur Forschung und Technologie Report No FBT 77-78 published Dec 1977. Title "The Development of Electrochemical Storage batteries with improved energy density".

27) C A Smith, Finishing Industries, pp29-32 Oct (1977).

28) J S Woodrich, British Patent 943, (1842).

29) A Smee, Elements of Electrometallurgy published Longman and Brown 3rd edition (1851).

30) H Fontaine, "Electrolysis" published by E and F Spon (1885).

31) C Leuchs, German Patent, 38,193 (1886).

32) A Betts, US Patent 679,824 (1901).

33) A Betts, US Patents 713,278-9 (1902).

34) R L Seth, Electroplating and Metal Finishing, pp5-10, Feb (1972).

35) G Buss, Metall, Vol 17 part 6, pp567-571, (1963).

36) E Rabinowicz, M Imai and V Santos, "Friction and Wear at Elevated Temperatures" Report No RTD-TDR-63-4272 part 5 Contract AF 33 (616)-7648. Massachusetts Institute of Technology Dec (1963).

37) A K Graham, H L Pinkerton, Plating, Vol 54, pp367-377, (1967).

38) J W Dini, J R Helms, Metal Finishing, August, pp53-55, (1969).

39) E Raub, W Blum : "The Electrodeposition of Pb-Sn alloys" Metalloberflaecher, Vol 9A(4) pp54-57 (1955).

40) W Hoffman, lead and lead alloys, properties and technology, 2nd Rev, Springer - Verlag, Berlin (1970)

41) J E Stareck, E J Seyb, A C Tulumello, Plating, Vol 42, part 11, pp1395-1402, (1955).

42) C E Heussner, A R Balden, Plating Vol 35, part 7, pp719-723, (1948).

43) A W Hothersall, J Inst Metals, Symposium on Internal Stress in Metals and Alloys, preprint No 1082 (1947).

44) R Walker, Mettallurgica, pp131-135, October (1968).

45) M. Ya Popereka, Russian Journal of Physical Chemistry, Vol 39, part 6, p705-709 (1965).

also Zh Fiz Khimi, Vol 39, part 6, pp1321-1327 (1965).

46) H Safranek, C H Layer, Transactions Institute of Metal Finishing, Vol 40, pp249-258, (1963).

47) F A Lowenheim, "Modern Electroplating", John Wiley and Sons, 2nd Edition pp242-257. (1963).

48) A K Graham, H L Pinkerton, Transactions Institute of Metal Finishing, Vol 40, pp249-258. (1963).

49) J W Dini, J R Helms, J Electrochem Soc, Vol 117, No 2, pp269-272, (1970).

50) H J Wiesner, W P Frey, R R Vandervoort, E L Raymond, Plating, pp358-361 and pp362-368, April (1970).

51) A Betts, "Lead Electrorefining by Electrolysis" John Wiley and sons, New York (1908).

52) H Reeve, Transacttions American Electrochem Soc, Vol 35, p389, (1919).

53) A Gray, Steel, Vol 115 (22), p78 (1944).

54) R Piontelli, J Electrochem Soc, Vol 94, p106 (1948).

55) F Mathers, R Forney, Trans Electrochem Soc, Vol 76, p371, (1939).

56) A Levin, V F Lazerev, V A Makjin, Zh Prikl Dhim, Vol 38(7), pp1569-74, (1965).

57) B A Shenoi, R Subramanian, K S Inira, Electroplating and Metal Finishing, pp399-402 Dec (1968).

58) T L Rama Char, J Vaid, Metal Finishing, p44-40 Dec (1961).

59) F Cambell, J A Von Fraunhoffer, Surface Tech, Vol 5, pp235-284, (1977).

60) F Salt, Electroplating, Vol 9, p3, (1956).

61) British Patent 786, 418 (1953).

62) V Sree, T Rama Char; Plating, Vol 1, p50, (1961).

63) V Sree, T L Rama Char, Bull India Section Electrochem Soc, Vol 9, p59 (1960).

64) V Sree, J Sci Industries Res, Vol 18A, p478-483, Oct (1959).

65) J Vaid, T L Rama Char, J Electrochem Soc, Vol 104, No 7, p460-461, (1957).

66) J Vaid, T L Rama Char; Proc 41st Indian Science Congress, part 3 p86, (1954).

67) O V Izbekova, O K Kudra, V I Suprunchuk, Proc Metals, Vol 6, pp555-6, (1970).

68) R Walker, S Thorley; Metal Finishing, p30-34, Jan (1976).

69) H Gatos, F C Mathers, J Electrochem Soc, Vol 102, p554 (1955)

70) F C Mathers, J Suttle; J Electrochem Soc, Vol 93, p47, (1948)

71) F C Mathers, J C Griess Jr; J Electrochem Soc, Vol 94, p461, (1948).

72) A Uenc, K Okubo, Kinzoku Hyomen Gijutsu, Vol 15, p216 (1964).

73) T A Loveland, US Patent 2, 466, 600, (1949).

74) W Machu, M Lofty Ali el Sayed Badawy; Werkstoffe Korrosion, Vol 14, p939 (1963) and Vol 15, p8, (1964).

75) T K Zotova, V P Artamonov; Zash Metall, Vol 11, p113, (1975).

76) F C Mathers, Trans Electrochem Soc, Vol 17, p261, (1910).

77) M Schloetter "Die Korrosion Metallischer Werkstoffe" Vol 3 p393, pub Hirzel, Leipzig (1940).

78) L Peraldo Birelli, C Ramagnani; Electrochim Metal, Vol 4, p140, (1969).

79) R Henri, US Patent (1956).

80) G Hansel, Elektrie, Vol 17, p264, (1962).

81) G A Emelyanenko, E Y Bairharova, T A Koretskaya; Ukr Khim Zh, Vol 35, p22, (1969).

82) R L Seth, Electroplating and Metal Finishing, Vol 25, p5-10, Feb (1972).

83) N T Kudryavstev, V G Solokhina, V Ya Mattis, Zhur Prikl Khim Vol 29, p236-41, (1956).

84) F C Mathers, A McKinney; Trans American Electrochem Soc, Vol 15, p131-138, (1915).

85) D N Gritsan, D Shun; USSR Patent, 111,483 (1959).

86) D N Gritsan, G V Pentsova, T M Volskaya, USSR Patent (1965).

87) H V K Udupa, K C Narasimham, P S Gomathi, Plating and Surface Finishing p1150-1154, Dec (1975).

88) B I Skirstymonskaya, J Appl Chem USSR, Vol 31 p395, (1958).

89) P Renich, Trans Kansas Acad Sci, Vol 48, p169, (1945).

90) M Loshkarev, J Applied Chem (USSR), Vol 21, p589, (1949).

91) G Kiryakov, Kokl Akad Nauk USSR, Vol 94, p1097 (1954).

92) G Kiryakov, I Korchmarck, Izv Akad Nauk Kaz SSR Ser Khim, Vol 54, No 8, (1954).

93) A K Graham, H L Pinkerton, Plating, Vol 50, p139-446, (1963).

94) A K Graham, H L Pinkerton; Plating, Vol 49, (10), pp1071-75, (1962).

95) W Blum, Trans Electrochem Soc, Vol 17, p261, (1920).

96) M B Diggin, Metal Finishing, Vol 41, pp418, (1943).

97) J W Dini, J R Helms, Metal Finishing, August pp 53-55 (1969).

98) H J Weisner, Plating, Vol 57, (4), pp358-368, (1970).

99) I Rajagopal, K.S Rajim, Metal Finishing USA, Vol 76, (12), pp51-55 (1978).

100) E.I Du Pont, (De Nemours and Co Ltd), UK Patent 595, 148 (1947).

101) A Gray, British Patent, 570,287 (1945).

102) J Nachtman, US Patent, 2,446,716 (1948).

103) British Patent, 1,251,290 July (1969).

104) US Patent, 3,554,864 Aug (1968).

105) F C Smyers, US Patent, 2,827,410 (1958).

106) F C Mathers, US Patent, 2,664,393 (1953).

107) K S Indira, K V K Udupa; Metal Finishing Vol 71 (6) p53, (1973).

108) P Belyaev, I Korroziya, S Borha, Chem Abst 36, 4031 (1942).

109) A Liger, US Patent, 2,474,092 (1947).

110) J Booe, US Patent 2,545,566 (1951).

111) N Dohi, M Kamon; US Patent 3,905,878 (1975).

112) W Rosenberg, W E Eckles US Patent 3,875,029 (1975).

113) G F Hsa, US Patent, 3,785,939 (1974).

114) F Passal, British Patent 1,411,970 (1975).

115) Kenvert International Corporation UK Patent 1,368,318 (1974).

116) A J Paris, A Szcur, Plating p878 July (1967).

117) E Richards, Metal Finishing, Vol 51 (2), p59 (1953).

118) N Spiliotis, Metal Finishing Guide Book Directory, Finishing Publications New York, p267 (1967).

119) B B Joffe, Metal Finishing USA, Vol 60 (5), p54-60, (1962).

120) "Symposium on Properties, Test and Performance of Electrodeposited Metallic Coatings" A.S.T.M Spec Tech Pub No 197 p97, (1957).

121) A K Graham, "Electroplating Engineering Handbook" 3rd Edition, p263 Military Specification L-13808 and M1L-F-14072 USA. (1962)

122) M Clarke "The properties of electrodeposits, their measurement and significance Chapter 8. (1975) The Electrochemical Society, Princeton NJ.

123) L Weisberg, A K Graham, Trans Electrochem Soc, Vol 80 p 509 (1941).

124) M Clarke, J M Leeds, Transactions Institute of Metal Finishing, Vol 46, p81-86, (1968).

125) D J MacNaughton; Trans Faraday Soc, Vol 126, No 111, part 8, pp465-480 (1930).

126) U.R Evans, S.C Shome, J Electrodepositors Tech Soc, Vol 26, p137 (1950).

127) R J Morrisey, J Electrochem Soc, Vol 117, 742, (1970).

128) M Clarke "Porosity in electrodeposited coatings" Micromethods Wakefield (1966).

129) "Lead Chemicals" published by International Lead Zinc Research Organisation.

130) P Ruetschi, J Sklarchak, R J Angstadt; Electrochim Acta, Vol 8, p333-342, (1963).

131) N E Bagshaw, R L Clark, B Halliwell; J Appl Chem, Vol 16, p150-84, (1966).

132) H Bode "Lead Acid Batteries" Sponsored by the Electrochemical Society Inc, J Wiley and Sons (1977).

133) H Bode, E Voss, Z Elektrochem, Vol 60, pp1053-56, (1956).

134) P Chartier, Thesis Strasbourg, Ber Bunsenges Phys Chem, Vol 68, pp404-410. (1964)

135) A I Salawski, J D Konridschow, Tolkatschew Kokl Acad Nauk USSR, Vol 75, p559-562 (1950).

136) S Ikari, S Yoshizawa, S Okada; J Electrochem Soc Japan
Vol 27, (1959) E 186-189, (1959)
E 223-227
E 247-250

137) V H Dobson, J Electrochem Soc, Vol 108 pp401-405, and 406-412. (1961)

138) D Spahrbier, Dissertation, Stuttgart (1960).

139) M Ya Popereka, Acta Mettalurica (1964).

140) U R Evans; "Corrrosion and oxidation of metals", Chapter 15 p632 (1960).

141) C J Bushrod, N A Hampson; British Corrosion Journal, Vol 6, May (1971).

142) Y Shibaski, Bull Facility of Engineering Yokahama National University, Vol 2, p69, (1953) Vol 3, p77, (1954) Vol 4, p85, (1955) Vol 5, p149, (1956).

143) K Nishihara, M Kurachi, M Hayashi, I Mem Fac Eng Kyoto University Japan, Vol 32, part 2, p285-295, (1970).

144) N E Bagshaw, R L Clarke, B Halliwell, J Appl Chem Vol 6, p 180, (1960).

145) K S A Gnanasekaran, K C Narasimaham, H V K Udupa; Electrochim Acta, Vol 15, pp1615-1622, (1970).

146) D R Gabe, J M West; Transactions Institute of Metal Finishing, Vol 40, p6-12, (1963).

147) D J MacNaughton, A W Hothershall, Trans Faraday Soc, Vol 24, p387, (1928).

148) K P McAllister, L L Shreir, 1st Interim report, Intrinsic stress in electrodeposited PbO_2 City of London Polytechnic. (April 1976) (unpublished)

149) K P McAllister, L L Shreir, 2nd Intermin report, Intrinsic Stress in PbO_2 electrodeposits (March 1977)

150) K P McAllister, L L Shreir, 3rd Intermin report, Intrinsic Stress in PbO_2 electrodeposits (Sept 1977)

151) K P McAllister, L L Shreir, 4th Intermin report, Intrinsic Stress in PbO_2 electrodeposits (May 1978)

152) K P McAllister, L L Shreir, 5th Intermin report, Intrinsic Stress in PbO_2 electrodeposits (Oct 1978)

153) G G Stoney, Proc Royal Soc, A, Vol 82, p172, (1909).

154) S Vasundra, K C Narasimham, H V K Udupa; Electrochim Acta, Vol 16, pp1301-1310, (1971).

155) K.S.A Gnanasekaran, K C Narasimham, H V K Udupa, J Appl Electrochemistry, Vol 6, p189-198, (1976).

156) N G Bakhchisaraitsyan, K G Samoskenkova, E P Grechina, Tr Mosk Khim Teknol Inst, Vol 54, p156. (1967).

157) D J Leikis, E K Venstrem, Proc Akad Sci USSR (PhysChem Section) English Trans, Vol 112, p17, (1957).

158) B D Kabanov, I.G Kiseleva, D I Leikis, Dokl Akad Nauk (USSR) Vol 99, p805, (1954).

159) V H Volgina, Electrokhimiya, Vol 9, p1038, (1973).

160) U B Thomas, J Electrochem Soc, Vol 94 (21), p42-49, (1948).

161) W Mindt, J Electrochem Soc, Vol 116 (8), p1076-1080, (1967).

162) T Katz, Ann Chim, Vol 5, p5, (1950).

163) P Ruetschi, B D Cahan, J Electrochem Soc, Vol 105, p369, (1958).

164) J P Carr, N A Hampson, Chem Reviews Vol 72, (6) p679, (1972).

165) G H Kelsall, "A review of electrodeposited lead dioxide anode preparation" published by The Electricity Research Council (1977).

166) M Pourbaix "Atlas of Electrochemical Equilibria in Aqueous solutions", Pergamon Press, Brussels (1966).

167) G W Vinal "Storage Batteries" J Wiley and Sons New York, (1965).

168) J Burbank, A Simon, E Willihnganz; Advance Electrochemistry Electrochem Eng, Vol 8, p157, (1971).

169) J A Duisman, W F Giaugue, J Phys Chem Vol 72 (2), p562, (1968).

170) M Fleischmann, M Liler, Trans Faraday Soc, Vol 54, p1370, (1958).

171) M Fleischmann, H R Thirsk, Electrochim Acta, Vol 1, p146, (1959).

172) M Fleischmann, H R Thirsk, Trans Faraday Soc, Vol 51, p71, (1955).

173) D Gilroy, R Stevens, J Appl Electrochem, Vol 10, p511-525, (1980).

174) M Fleischmann, H R Thirsk, I M Tordesillas; Trans Faraday Soc, Vol 58, p1865, (1962).

175) H A Laitinen, N A Watkins; J Electrochem Soc, Vol 123, p804 (1976).

176) F Beck, J Electroanalytical Chem, Vol 65, p231, (1975).

177) N A Hampson, P C Jones, R F Philips; Canadian J Chem, Vol 45, p2039-2044, (1967).

178) N A Hampson, P C Jones, R F Philips, Canadian J Chem, Vol 45, p2045-2049, (1967).

179) N A Hampson, P C Jones, R F Philips, Canadian J Chem, Vol 47, p2171-2179 (1969) and ibid, Vol 46, p1325 - 1335, (1968).

180) N A Hampson, C J Bushrod; Transactions Institute of Metal Finishing, Vol 48, p131-132, (1970).

181) V F Lazarev, N V Babkova, A I Levin, Izr Vyssh Uchebn Zaved Khim Tekhnol, Vol 18, part 8, p1336, (1975).

182) A T Kuhn, Chem Ind, p867, 16th Oct, (1976).

183) F D Gibson, B B Halker, R L Thayer, British Patent 1,159,241 (1966).

184) I Osuga, S Fujii, K Sayino, T Sekine; J Electrochem Soc, Vol 116, part 2 (1969).

185) M Nayalingham, P Govinda Rao, C J Raju, K L Narasimham, S Sampath, H V K Udupa; Chem Ing Tech, Vol 41, p1301, (1969).

186) W White, R Roy, J American Ceramic Soc, Vol 47, p242 (1964).

187) K C Narasimham, H Udupa, J Appl Electrochem, Vol 6, p189, (1976).

188) K C Narasimham, H Udupa, Can J Chem, Vol 53, p3327, (1978).

189) Y Shibaski; J Electrochem Soc, Vol 105, p624, (1958).

190) D Wabner, Habil Thesis, Munich (1976).

191) US Bureau of Mines report 1.811 "Lead dioxide plated Ti anodes", L W Higley, D W Dresset (1976).

192) L V Ramanathan Phd, Thesis "The Adhesion of Electrodeposited PbO_2 to Nickel substrates" City of London Polytechnic (1977).

193) G Bowman "Private Communication" (1982).

194) J F Smith "Private Communication" (1982).

195) S S Voyutski Adhesives Age, Vol 5, p30, (1962).

196) B V Derjaguin, N A Krotova, Doklady Akad Nauk (USSR), Vol 61, 849, (1948).

197) B J Briscoe, D Tabor Faraday Discussions of the Chem Soc "Surface forces in Friction and Adhesion, Vol 2, (7) (1972).

198) K L Mittal "Critical appraisal of the methods of measuring adhesion of electrodeposited coatings"

199) J O'M Bockris, G A Razumney "Fundamental Aspects of Electrocrystallisation, Plenun Press, New York (1967).

200) B E Conway, J O'M Bockris, Electrochim Acta, Vol 3, p340, (1961).

201) H Gerischer, Z Elektrochem, Vol 62, p256 (1958).

202) V I Chernenko; Yu E Udovenko, Vol 13 (9), p1120-1123, (1977).

203) E.M Strochkova; K V Rybalka, D I Leikis, Elektrokhimya, Vol 11, 336, (1975).

204) W Lorenz, Z Phys Chem (Frankfurt), Vol 19, 377 (1959).

205) P Delahay, J Phys Chem, Vol 66, p2208, (1962).

206) W H Reinmuth, Analytical Chem, Vol 34, pp1272, (1962).

207) V I Chernenko, K I Litovchenko, Sov Electrochemistry, Vol 10, p567, (1974).

208) F Miyashita, E Miyataui, Technol Reports Kansai Univ (Japan) Vol 16, pp87-89, (1977).

209) C A Snavely, J Electrochem Soc, Vol 94, p537 (1947) and Vol 97, p466 (1950).

210) M Fleischman, H R Thirsk, Electrochim Acta, Vol 2, pp22-49, (1960).

211) H R Thirsk, J Harrison; A Guide to the Study of Electrode Kinetics, Academic Press (1972).

212) F Palmisano, E Desimoni, L Sabbatini, E Torsi, J Appl Electrochemistry, Vol 9, pp517-525, (1979).

213) M Y Abyaneh, M Berkem, M Fleischmann, Transactions of the Institue of Metal Finishing, Vol 60, p114 (1982).

214) D J Astley, J A Harrison, H R Thirks, J Electroanalytical Chem, Vol 19, p325, (1968).

215) E Hills, I Montenegro, B Scharifker, J Applied Electrochemistry, Vol 10, p807-809, (1980).

216) S Haruyuma, J Electrochem Soc Japan, Vol 35, p62, (1967).

217) N A Hampson, D Larkin, Trans Faraday Soc, p1660 (1969).

218) J E B Randles, Trans Symposium Electrode Processes (1950), Edited Yeager p213, (1961).

219) G J Hills, D J Schiffrin, J Thompson, Electrochim Acta, Vol 19, p657-670 (1974).

220) G J Hills, D J Schiffrin, J Thompson, Electrochim Acta, Vol 19, p671-680 (1974).

221) G A Gunawardena, G J Hills, I Montenegro; Electrochim Acta, Vol 23, pp693-697, (1978).

222) J A Harrison, R P J Hill, J Thompson, Electroanalytical Chemistry, Vol 44, pp445-455, (1973).

223) R Adzic, E Yeager, B D Cahan; J Electrochem Soc, Vol 121, No 4, pp474-484, (1974).

224) E Schmidt, N Wurtlich; J Electroanalytical Chem, Vol 28, p349, (1970).

225) J M Keen, J P Farr, J Electrochem Soc, Vol 109 (8), pp668-678 (1962).

226) L P Bicelli, G Poli, Electrochim Acta, Vol 11, pp289-296, (1966).

227) S Itoh, N Yamazoe, T Seiyama, Surface Technology, Vol 5, p27-42 (1977).

228) G Wranglen, Electrochim Acta, Vol 2, pp130-246 (1960).

229) F Ogburn, C Bechtoldt, J B Morris, A De Koranyi; J Electrochem Soc, Vol 112 (6), p574-577, (1965).

230) R Walker, Structure and Properties of Electrodeposited Metals, International Metallurgical Reviews, Review 148, Vol 19 (1974)..

231) O Volk, H Fischer, Electrochim Acta, Vol 5, p112, (1961).

232) J O M Bockris, M Green, D A J Swinkels; J Electrochem Soc, Vol 111, p743 (1964).

233) B B Damaskin, B N Afanasev, Electrokhimya, Vol 13, No8, p1094-1117 (1977).

234) A K Vijh, J P Randin, Surface Tech Vol 5, p257-269, (1977).

235) J K Prall, L L Shreir, Transactions Institute of Metal Finishing, Vol 41, p29, (1964).

236) J Edwards, Transactions Institute of Metal Finishing, Vol 41, p169, (1964).

237) "Corrosion of Nickel and Nickel Base ALloys" Edited by Wayne Z Friend, pub J Wiley and Sons (1980).

238) N Sato, G Okamato, J Electrochem Soc, Vol 111, p 897, (1964).

239) K F Heusler, L Gaiser, Electrochim Acta, Vol 13, p59, (1968).

240) R C V Piatti, A J Arvia, J Podesta, Electrochim Acta, Vol 14, p541, (1969).

241) R C V Piatti, J J Podex, A J Arvia, An Asoc Quim Argentina, Vol 57, p71, (1969).

242) K Schwabe, C H Voigt, J Electrochem Soc, Vol 113, p886, (1966).

243) G T Burstein, G A Wright, Electrochim Acta, Vol 20, pp95-99, (1975).

244) M L Kronberg, J C Banter, E Yeager, F Hovorka, J Electrochem Soc, Vol 110, p1007 (1963).

245) F Ovari, A L Rotingan, Elektrochimiya, Vol 6, p516, (1970).

246) G E Lopovok, M Kolotyrikin, Zashch Met, Vol 2, p527, (1966).

247) G Trabanelli, Zucchi, A Betti, Corrosion Sci, Vol 7, p423, (1967).

248) Y M Kolotyrkin, J Electrochem Soc, Vol 108, p209, (1961).

249) E Stupnisek Lisac, M Karsulin, Electrochim Acta, Vol 29 (10), pp1339-1343, (1984).

250) H G Feller, M Kesten, H J Ratzer Scheibe, 5th International Congress on Metallic Corrosion, Tokyo, Japan, (May 1972).

251) H G Feller, S J Krupski, Zeitschrifte Fur Metallkunde, Vol 65 (5), p401 - 407 (1974).

252) M Zamin, H B Ives, Corrosion Vol 29, (8), p319-324 (1973)

253) P Sury, Corrosion Sci, Vol 16, pp879-901, (1976).

254) T Touscek, Coll Czech Chem Commun, Vol 31, p3083, (1966).

255) T P Hoar, Transactions Institute Metal Finishing, Vol 39, p166-171, (1962)

256) E A Di Bari, J V Petrocelli, J Electrochem Soc, Vol 112 (1), p99, (1965).

257) B MacDougall, M Cohen, J Electrochem Soc, Vol 122 (3), p383, (1975).

258) S Shimodaira, K Hashimoto, Corrosion Engineering, Vol 15, p279-285 (1966).

259) H Worch, Werkstoffe und Korrosion, Vol 124 (10), p872-880, (1973).

260) A T Vagramyan; L A Uvarov, Dokl Akad Nauk USSR, Vol 146 (9), p1520, (1962).

261) A T Vagramyan, L A Uvarov Dokl Akad Nauk USSR, Vol 146, pp635 (1962).

262) A T Vagramyan, A Zhamagortsyam, Dokl Akad Nauk USSR, Vol 148, p301, (1964).

263) A T Vagramyan, A Zhamagortsyam, Zasheh Metal, Vol 5, p74, (1969).

264) A T Vagramyan, A Zhamagortsyam, Elektrockhimiya Vol 6, p733, (1970). and ibid 6, 755 (1970).

265) R M Latanison, R W Staehle, Acta Met, Vol 17 p307, (1969)

266) A J Bard "Encloypedia of Electrochemistry of the Elements", pub Decker, Vol 3 (1975).

267) R Raub, A Disam, Metalloberflache, Vol 15, p193, (1961).

268) N D Greene, "First International Congress on Corrosion", Butterworths, p113, London (1963).

269) N Sato, G Okamato, J Electrochem Soc Japan, Vol 27, p125, (1959).

270) J Osterwald, H H Uhlig, J Electrochem Soc, Vol 108, p515 (1961).

271) A K Hug, A Rosenberg, A C Murkides, J Electrochem Soc, Vol 111, p278, (1964).

272) T S De Gromoboy, L L Shreir, Electrochim Acta, Vol 11, p895, (1966).

273) H J Ratzer-Scheibe, H G Feller, Zeitschrifte Fur Metallkunde, Vol 63 (6), pp351-355 (1972).

274) K Schwabe, G Dietz, Z Elecktrochem, Vol 62, p751, (1958).

275) K J Vetter, K Arnold Z Elektrochem, Vol 64, p407, (1960).

277) K J Vetter, K Arnold, Z Elektrochem, Vol 64, p244, (1960).

277) N Sato, G Okamato, J Electrochem Soc, Vol 110, p605, (1963).

278) J A Ammar, S Darwish, Electrochim Acta Vol 12, p225, (1967).

279) K J Vetter, J Electrochem Soc, Vol 110, p598 ,(1963).

280) H Uhlig, H G Feller, J Electrochem Soc, Vol 107, p865, (1960).

281) I A Ammar, S Darwish, Electrochim Acta, Vol 11, p1541, (1966).

282) I A Ammar, S Darwish, Electrochim Acta, Vol 13, p781, (1968).

283) M C Petit, A Jouanneau Electrocheim Acta, Vol 15, p1325 (1970).

284) T Ishikawa, G Okamoto, Electrochim Acta, Vol 9, p1259, (1964).

285) R L Cowan, R W Staehle, J Electrochem Soc, Vol 118, p557, (1971).

286) J W Schultze, M M Lohrengel, D Ross, Electrochim Acta, Vol 28, (7), p973 - 984, (1984).

287) U Ebersbach, K Schwabe, U Ritter, Electrochem Acta, Vol 12, p927, (1967).

288) U Ebersbach, K Schwabe, P Koenig, Electrochim Acta, Vol 14, p773, (1969).

289) J O'M Bockris, A K N Reddy, B Rao, J Electrochem Soc, Vol 113, p1133, (1966).

290) W F K Wynne Jones, G W D Briggs, Electrochim Acta, Vol 7, p241, (1962).

291) J Postelthwaite, L K Freese, Corrosion, Vol 23, p109, (1967).

292) G Truempler, R Keller, Helvs Chim Acta, Vol 44, p1691, (1961).

293) D L Prion, K Noble, Dept Engineering University Califormia, Los Angeles, Rep 66-37 (1966).

294) A Desterat, I Epelboin, M Froment, M Keddam, P H Moret Electrochim Acta, Vol 8, p433, (1963).

295) M Okayama, S Haruyama, Corrosion Sci, Vol 14, pp1-4, (1974).

296) I A Ammar, S Darwish, S Riad, Electrochim Acta, Vol 13, p1875, (1969).

297) B MacDougall, J Electrochem Soc, Vol 127 (4), p798, (1980).

298) B Lochel, H H Strehblow, M Sakashita, J Electrochem Soc, Vol 131 (3), p522-529 (1984)

299) B Lochel, H H Strehblow, J Electrochem Soc, Vol 121, pp713-23 (1984)

300) C J Chatfield, L L Shreir, Electrochim Acta Vol 14, pp1015-1023 (1969).

301) A Barber, C C T Chinnick, P A Lincoln, Analyst 81, pp18-25 (1956).

302) J R Weber, E F Degner, K S Bahjat, Analytical Chem, Vol 19 (1), pp32-34 (1947).

303) N Schonfeldt, J Am Oil Chemists Soc, Vol 32, pp77-79 (1955).

304) M Nelkon, P Parker, "Advanced Level Physics" 3rd Edition (1971).

305) E G Gagnon, J Electrochem Soc, Vol 120, p251, (1973) and ibid Vol 121, p512, (1974).

306) R Deplanque, L L Shreir, 1st Report on the Simultaneous Electrodeposition of PbO_2 and Pb, City of London Polytechnic, August (1979).

307) D R Gabe, A Samel, J Applied Electrochemistry, p193 (1984).

308) A Bone, PhD Thesis, Durham University (1960).

309) A I Rusin, Z I Zhivitova, Yu M Shutova, K M Soluv'eva, Zhurnal Prikladnoi Khimii, Vol 41 (12) pp2614-2619 (1970).

310) K I Kryschenko, M Y Fioshin, I A Arbruts Kayu, M D Gol'dshtein, Soviet Electrochem, Vol 5, p761 (1969).

311) T Berzins, P Delahay, J Am Chem Soc, Vol 75 p555 (1953).

312) L Katz, M E Chiddix, U S Patent, 3,352,766 (1967).

313) V Wolf, U S Patent, 2,786,022 (1957).

314) M Baizer, "Organic Electrochemisty" pub Marcel Dekker, New York (1973).

315) M Ashraf, J B Headridge, Talanta, Vol 16, p1436 (1969).

316) B Mooney, H Stonehill, J Chem Soc America, Vol 1 (1967).

317) T I Quickenden, X Jiang, Electrochim Acta, Vol 29 pp693-700 (1984).

318) J W Johnson, C K Wu, W J James, Corrosion Science, Vol 8, p309 - 315 (1968).

319) D Pletcher, Z Poorabed, Electrochim Acta, Vol 24, pp1253-1256 (1979).

320) W J Mueller, Trans Faraday Soc, Vol 27, p 737 (1931).

321) N Nishimura, T Higashiyama, S Yamamoto, S Hasegawa, Rep Res Lab for Surface Science, Okayama Univ Japan, Vol 3, pp223-230 (1971).

322) Smith, Basic Chemical Thermodynamics,

323) V V Alexandrov, J Thermal Analysis, Vol 13 p205 (1978).

324) P Reutschi, B D Cahan, J Electrochem Soc, Vol 105, (7), p369-376 (1958).

325) E Butler, J L Copp, J Chem Soc p725 (1956).

326) J Bagshaw, J Applied Chem, Vol 16, p175 (1966).

327) S D Kapusta, N Hackerman, Electrochim Acta, Vol 25, pp 1625-1639, (1980).

328) C J Bushrod, N A Hampson, British Corrosion J, Vol 6 May (1971).